ADVANCES IN 3D HABITAT MAPPING OF MARINE ECOSYSTEM ECOLOGY AND CONSERVATION

EDITED BY: Renata Ferrari, Manuel Gonzalez-Rivero, Javier Xavier Leon, John H. R. Burns, Will F. Figueira, Stuart A. Sandin and Andrew J. Davies

PUBLISHED IN: Frontiers in Marine Science

frontiers Research Topics

ISSN 1664-8714
ISBN 978-2-88974-485-5
DOI 10.3389/978-2-88974-485-5

About Frontiers

Frontiers is more than just an open-access publisher of scholarly articles: it is a pioneering approach to the world of academia, radically improving the way scholarly research is managed. The grand vision of Frontiers is a world where all people have an equal opportunity to seek, share and generate knowledge. Frontiers provides immediate and permanent online open access to all its publications, but this alone is not enough to realize our grand goals.

Frontiers Journal Series

The Frontiers Journal Series is a multi-tier and interdisciplinary set of open-access, online journals, promising a paradigm shift from the current review, selection and dissemination processes in academic publishing. All Frontiers journals are driven by researchers for researchers; therefore, they constitute a service to the scholarly community. At the same time, the Frontiers Journal Series operates on a revolutionary invention, the tiered publishing system, initially addressing specific communities of scholars, and gradually climbing up to broader public understanding, thus serving the interests of the lay society, too.

Dedication to Quality

Each Frontiers article is a landmark of the highest quality, thanks to genuinely collaborative interactions between authors and review editors, who include some of the world's best academicians. Research must be certified by peers before entering a stream of knowledge that may eventually reach the public - and shape society; therefore, Frontiers only applies the most rigorous and unbiased reviews.
Frontiers revolutionizes research publishing by freely delivering the most outstanding research, evaluated with no bias from both the academic and social point of view. By applying the most advanced information technologies, Frontiers is catapulting scholarly publishing into a new generation.

What are Frontiers Research Topics?

Frontiers Research Topics are very popular trademarks of the Frontiers Journals Series: they are collections of at least ten articles, all centered on a particular subject. With their unique mix of varied contributions from Original Research to Review Articles, Frontiers Research Topics unify the most influential researchers, the latest key findings and historical advances in a hot research area! Find out more on how to host your own Frontiers Research Topic or contribute to one as an author by contacting the Frontiers Editorial Office: frontiersin.org/about/contact

ADVANCES IN 3D HABITAT MAPPING OF MARINE ECOSYSTEM ECOLOGY AND CONSERVATION

Topic Editors:
Renata Ferrari, Australian Institute of Marine Science (AIMS), Australia
Manuel Gonzalez-Rivero, Australian Institute of Marine Science (AIMS), Australia
Javier Xavier Leon, University of the Sunshine Coast, Australia
John H. R. Burns, University of Hawaii at Hilo, United States
Will F. Figueira, The University of Sydney, Australia
Stuart A. Sandin, University of California, United States
Andrew J. Davies, University of Rhode Island, United States

Citation: Ferrari, R., Gonzalez-Rivero, M., Leon, J. X., Burns, J. H. R., Figueira, W. F., Sandin, S. A., Davies, A. J., eds. (2022). Advances in 3D Habitat Mapping of Marine Ecosystem Ecology and Conservation. Lausanne: Frontiers Media SA. doi: 10.3389/978-2-88974-485-5

Table of Contents

frontiers in Marine Science

EDITORIAL
published: 21 January 2022
doi: 10.3389/fmars.2021.827430

Editorial: Advances in 3D Habitat Mapping of Marine Ecosystem Ecology and Conservation

Renata Ferrari[1], Javier X. Leon[2], Andrew J. Davies[3], John H. R. Burns[4], Stuart A. Sandin[5], Will F. Figueira[6] and Manuel Gonzalez-Rivero[1]*

[1] Australian Institute of Marine Science, Townsville, QLD, Australia, [2] School of Science, Technology and Engineering, University of the Sunshine Coast, Maroochydore, QLD, Australia, [3] University of Rhode Island, Kingston, RI, United States, [4] MEGA Lab, University of Hawaii at Hilo, Hilo, HI, United States, [5] Scripps Institution of Oceanography, University of California, San Diego, San Diego, CA, United States, [6] Faculty of Science, School of Life and Environmental Sciences, The University of Sydney, Sydney, NSW, Australia

Keywords: 3D structural complexity, photogrammetry, rugosity, standardization, error reporting, cross-platform, marine ecology, structure-from-motion

OPEN ACCESS

Edited by:
Wei-Bo Chen, National Science and Technology Center for Disaster Reduction (NCDR), Taiwan

Reviewed by:
Lida Teneva, Independent Researcher, Sacramento, United States

****Correspondence:***
Renata Ferrari
R.FerrariLegorreta@aims.gov.au

Specialty section:
This article was submitted to Ocean Solutions, a section of the journal Frontiers in Marine Science

Received: *02 December 2021*
Accepted: *21 December 2021*
Published: *21 January 2022*

Citation:
Ferrari R, Leon JX, Davies AJ, Burns JHR, Sandin SA, Figueira WF and Gonzalez-Rivero M (2022) Editorial: Advances in 3D Habitat Mapping of Marine Ecosystem Ecology and Conservation. Front. Mar. Sci. 8:827430. doi: 10.3389/fmars.2021.827430

Editorial on the Research Topic

Advances in 3D Habitat Mapping of Marine Ecosystem Ecology and Conservation

Advances in 3D technology have enabled low-cost and accurate measurements of habitat structure and organism size in both terrestrial and marine environments. However, there is still a need for guidance on how to apply novel 3D technologies for marine ecology and conservation. Multiple teams from around the world are leading the application of 3D photogrammetry in marine ecosystems. The widespread adoption of 3D methodologies produces a growing need for agreed standards to assess the quality of 3D data (e.g., error metrics). Similarly, standardized techniques where possible, will ensure collaboration and compatibility of 3D data across space and time.

This Research Topic is a first step toward the standardization of methods and communication of the state of the field to the wider audience in marine science and conservation using or considering the use of 3D technologies. The Topic provides relevant information that: (1) defines standard methods for the application of 3D technologies to marine ecosystem ecology and conservation, (2) advances fundamental marine ecological and conservation knowledge relevant to the habitat structure of marine ecosystems; and (3) highlights knowledge gaps and directions to move toward a high-resolution 3D map of the world's oceans.

The Research Topic focuses on the use of high-resolution 3D reconstructions of underwater ecosystems. It includes 13 articles, of which six are original research articles, one is a perspective, and six are methodological advances. Most of the original research articles also included a methodological validation or comparison. The geographic scope of this Research Topic ranges from the Caribbean to Greenland to the Pacific Islands and Australasia. Nine articles were conducted in coral reefs, three in temperate rocky reefs, and one on a deep-sea cliff, which highlights the versatility of 3D technologies. The diverse group of articles explored the relationship between habitat features, benthic and fish abundance, health, diversity, the potential of reef scape genomics, and the effectiveness of marine protection. A range of equipment from action cameras and DSLRs, to machine vision cameras, underwater robots, and echo-sounders were used to generate 3D

reconstructions, emphasizing how a broad range of 3D technologies can benefit a wide variety of end users and applications. Similarly, the breath of the research published in this Research Topic captured 3D reconstructions of sub-millimeter resolutions, as well as 3D maps across large spatial extents.

KEY FINDINGS IN ORIGINAL RESEARCH ARTICLES

Advancing Fundamental Marine Ecological and Conservation Knowledge

Across large spatial extents, 3D technologies were used to characterize structural complexity and investigate its drivers and representation within marine parks. Asner et al. mapped reef rugosity (2 and 6 m resolution) to 22 m depth throughout the eight main Hawaiian Islands, and found rugosity was mainly driven by water depth and reef slope. Mayorga-Martínez et al. mapped slope, aspect, curvature, rugosity, and ruggedness (2.5 m resolution) for three submerged banks and two emerging reefs in the Southwestern Gulf of Mexico and found structural complexity increased with depth and was underrepresented within marine parks.

Three-dimensional technologies were used to investigate the relationship of surface rugosity and more traditional metrics of ecosystem health and state at the scale surveys are routinely conducted (hundreds of squared meters). Urbina-Berreto et al. explored the relationship between structural complexity and coral cover on reef slopes and lava-flows and found sites with the highest coral cover also had the highest structural complexity. Monfort et al. investigated the relationship between fish assemblages and surface rugosity in Mediterranean shallow rocky reefs and found total fish abundance and species richness increased with surface rugosity. Kanki et al. investigated the relationships between the prevalence of four benthic sessile organisms (ascidian, barnacle, polychaete, and articulated coralline algae) and terrain variables derived from 3D maps of the seafloor (cm resolution, 4 m^2 extent). Filter-feeders were more abundant on vertical and/or high faces above the seafloor, likely due to higher current velocities. In contrast, algae occurred at various heights and on gentle slopes suitable for photosynthesis.

At colony scales, Richaume et al. investigated the effect of longevity of no-take zones on populations of red coral (*Corallium rubrum*) in France, by using photogrammetry to measure morphometrics. They found after 5-years under protection red coral colonies were taller and had more branches inside no-take zones, the difference persisted after 40 years. Million et al. explored relationships between linear extension and growth metrics in the staghorn coral (*Acropora cervicornis*) using photogrammetry. They found growth in higher order metrics was not a linear function of growth in branch length and concluded the use of early growth to predict future performance of corals is limited.

Methodological Enhancements Over Traditional Metrics

Several studies independently compared traditional methods with photogrammetry, unanimously concluding that metrics derived using 3D technologies are comparable to traditional metrics. Specifically, several studies agreed that photogrammetric methods can provide data with higher precision, lower error, extraction of additional and useful metrics, and improved representativeness. Limitations of 3D technologies included its effectiveness for species-level taxonomic identification, a requirement for initial investment and a steep learning curve. However,

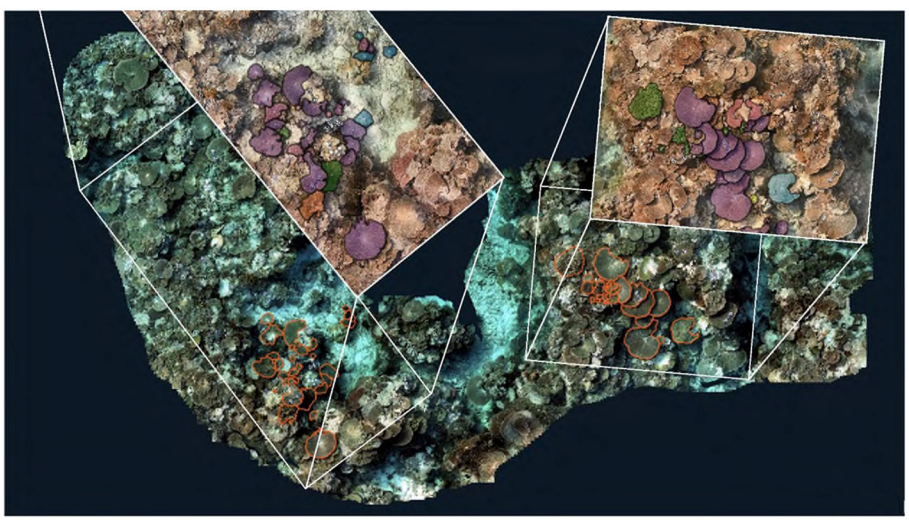

FIGURE 1 | Example of two datasets collected with different platforms over the same area of a coral reef. The larger dataset was collected using action cameras and has a ground sampling distance of approximately 1 cm, the smaller excerpts were collected with a digital single-lens reflex camera and has a ground sampling distance of approximately 1 mm.

photogrammetric methods were also regarded as more efficient once established.

Million et al. developed a photogrammetry processing pipeline for fragments of staghorn coral. 3D models were built with Agisoft Metashape, which was automated to run on a high-performance computing system to serially process models. They showed photogrammetry is an information rich method for quantifying colony-level morphometrics and is compatible with field measurements. Couch et al. compared data from in-water surveys to photogrammetry-derived metrics for assessing coral demography, bleaching, and diversity. They concluded most metrics did not vary significantly between methods regardless of the habitat type or depth, and that photogrammetry offers a unique opportunity to quantify and mitigate inter-observer error rigorously. Urbina-Berreto et al. compared field and digital estimates of coral cover using the Line Intercept Transect (LIT) method and found *in situ* estimates were higher than digitized estimates. They also performed surface analyses on the orthomosaics to quantify coral cover and found these yielded the most precise estimates. They concluded surface analysis was the most efficient method and outperformed other methods in terms of data outputs and representativeness of the ecosystem. Conley and Hollander found no significant difference in surface area measurements derived using traditional methods (wax dipping, geometrical calculation, and buoyant weight) and photogrammetry. They used this to characterize the relationship between buoyant weight and surface area over time for the coral species *Stylophora pistillata*.

Several studies published in this Research Topic presented 3D approaches to derive novel metrics, maximize limited bottom-time, and explore difficult-to-access environments. Kanki et al. proposed a new photogrammetric method to 3D map the seafloor (cm resolution, 4 m^2 extent) and quantify terrain variables and the prevalence of sessile organisms. Macedo Cruz de Oliveira et al. compared methods for classification of marine organisms from photogrammetric reconstructions of cold-water coral habitats, and found 3D support vector machine outperformed other methods, but each method explored has advantages for specific applications. Van Audenhaege et al. demonstrated a novel approach for mapping and classifying vertical habitats (e.g., cliffs, drop-offs) that are difficult to access and challenging to study. Hatcher et al. developed and tested a new mapping platform (SQUID-5), capable of 2.5D mapping complex coral reef habitats (between 3 and 9 m of depth) and is capable of measuring changes in the morphology and location of seafloor features over time (∼3 cm resolution) without pre-existing ground controls. Finally, Bongaerts et al. discussed the potential of "reef-scape genomics" that uses recent advances in underwater 3D technology to enable spatially explicit molecular ecology studies on coral reefs.

Challenges as We Move Toward a 3D Map of the World's Oceans

Future applications of 3D mapping, based on photogrammetry or other technologies, should meet standard requirements that allow comparisons across environments, sensors, and processing approaches and ensure a robust assessment of the product's quality and uncertainties. Following the recommendations by James et al., we suggest that: (1) the selection of sensors and methods is clearly described and justified as fit for purpose, (2) error reporting includes both the performance of the model fitting and, importantly, the quality of the 3D product is assessed using independent measurements, and (3) uncertainties (e.g., in bias or precision) are explicitly acknowledged and managed, especially when performing change detection analyses.

Despite the important contribution of this Research Topic toward a future 3D map of the world's oceans, several important questions remain unanswered. Especially in regard to good practices when scaling across datasets of different spatial resolutions (e.g., grain size) and extents (e.g., window size), defining the key parameters to compare datasets from different sources (e.g., echosounder vs. cameras), and the potential and limitations of machine learning for automatic segmentation and classification of 3D data (**Figure 1**).

AUTHOR CONTRIBUTIONS

RF conceived the Research Topic, invited guest editors, read all articles, summarized, analyzed the research findings across the Research Topic, and wrote this editorial. All other authors reviewed manuscript and contributed equally to editing and reviewing several articles submitted for publication in Research Topic.

ACKNOWLEDGMENTS

We appreciate the help of Tiny Remmers Barry to source the panels for the figure used in this editorial and to the authors of all articles published in this Research Topic. RF and MG-R were funded through the Reef Restoration and Adaptation Program and other internal projects within the Australian Institute of Marine Science. AD was supported by the USDA National Institute of Food and Agriculture, Hatch Formula project accession no. 1017848.

Conflict of Interest: The authors declare that the research was conducted in the absence of any commercial or financial relationships that could be construed as a potential conflict of interest.

Publisher's Note: All claims expressed in this article are solely those of the authors and do not necessarily represent those of their affiliated organizations, or those of the publisher, the editors and the reviewers. Any product that may be evaluated in this article, or claim that may be made by its manufacturer, is not guaranteed or endorsed by the publisher.

frontiers in Marine Science

METHODS
published: 26 June 2020
doi: 10.3389/fmars.2020.00525

Accurate Bathymetric Maps From Underwater Digital Imagery Without Ground Control

Gerald A. Hatcher[1], Jonathan A. Warrick[1], Andrew C. Ritchie[1], Evan T. Dailey[1], David G. Zawada[2], Christine Kranenburg[2] and Kimberly K. Yates[2]*

[1] Pacific Coastal and Marine Science Center, United States Geological Survey, Santa Cruz, CA, United States, [2] St. Petersburg Coastal and Marine Science Center, United States Geological Survey, St. Petersburg, FL, United States

Structure-from-Motion (SfM) photogrammetry can be used with digital underwater photographs to generate high-resolution bathymetry and orthomosaics with millimeter-to-centimeter scale resolution at relatively low cost. Although these products are useful for assessing species diversity and health, they have additional utility for quantifying benthic community structure, such as coral growth and fine-scale elevation change over time, if accurate length scales and georeferencing are included. This georeferencing is commonly provided with "ground control," such as pre-installed seafloor benchmarks or identifiable "static" features, which can be difficult and time consuming to install, survey, and maintain. To address these challenges, we developed the SfM Quantitative Underwater Imaging Device with Five Cameras (SQUID-5), a towed surface vehicle with an onboard survey-grade Global Navigation Satellite System (GNSS) and five rigidly mounted downward-looking cameras with overlapping views of the seafloor. The cameras are tightly synchronized with both the GNSS and each other to collect quintet photo sets and record the precise location of every collection event. The system was field tested in July 2019 in the U.S. Florida Keys, in water depths ranging from 3 to 9 m over a variety of bottom types. Surveying accuracy was assessed using pre-installed stations with known coordinates, machined scale bars, and two independent surveys of a site to evaluate repeatability. Under a range of sea conditions, ambient lighting, and water clarity, we were able to map living and senile coral reef habitats and sand waves at mm-scale resolution. Data were processed using best practice SfM techniques without ground control and local measurement errors of horizontal and vertical scales were consistently sub-millimeter, equivalent to 0.013% RMSE relative to water depth. Survey-to-survey repeatability RMSE was on the order of 3 cm without georeferencing but could be improved to several millimeters with the incorporation of one or more non-surveyed marker points. We demonstrate that the SQUID-5 platform can map complex coral reef and other seafloor habitats and measure mm-to-cm scale changes in the morphology and location of seafloor features over time without pre-existing ground control.

Keywords: underwater photogrammetry, Structure-from-Motion, synchronized cameras, coral reef, digital surface model, orthomosaic, post processed kinematic GNSS, ground control

OPEN ACCESS

Edited by:
Tim Wilhelm Nattkemper, Bielefeld University, Germany

Reviewed by:
Alessandra Savini, University of Milano-Bicocca, Italy
Carl J. Legleiter, United States Geological Survey (USGS), United States
Antoine Collin, Université Paris Sciences et Lettres, France

****Correspondence:***
Gerald A. Hatcher
ghatcher@usgs.gov

Specialty section:
This article was submitted to Ocean Observation, a section of the journal Frontiers in Marine Science

Received: *09 March 2020*
Accepted: *09 June 2020*
Published: *26 June 2020*

Citation:
Hatcher GA, Warrick JA, Ritchie AC, Dailey ET, Zawada DG, Kranenburg C and Yates KK (2020) Accurate Bathymetric Maps From Underwater Digital Imagery Without Ground Control. Front. Mar. Sci. 7:525. doi: 10.3389/fmars.2020.00525

INTRODUCTION

Benthic ecosystems throughout the world have been stressed by human impacts, including land-based pollution, overharvesting, coastal engineering, ocean acidification, and climate change (Hughes, 1994; Edinger et al., 1998; Kleypas and Yates, 2009; Storlazzi et al., 2015; Toth et al., 2015; Prouty et al., 2017; Takesue and Storlazzi, 2019). It is critical, therefore, to develop accurate geospatial inventories of benthic systems and track structural and compositional changes over time. An important element of monitoring benthic habitats is the development of accurate maps of species distribution, health, and diversity in relation to seafloor composition characteristics such as reef, rock, rubble, and sand (Burns et al., 2016; Raoult et al., 2017; Magel et al., 2019). Additionally, accurate measurements of the three-dimensional (3D) structure of reefs and changes in reef elevation over time advances understanding of reef hydrodynamics, growth, and erosion (Kuffner et al., 2019).

New opportunities to map accurately and at high resolution have been made possible by advancements in Structure-from-Motion (SfM) photogrammetry, which include feature identification and matching in photos; bundle adjustment computations of camera positions, orientations, and lens distortions; multi-view stereo techniques; GPU and network-based computing. When combined, these techniques can rapidly produce high-density, three-dimensional point clouds with associated color information from source photos (Matthews, 2008; Westoby et al., 2012; Fonstad et al., 2013). With the addition of high-quality digital cameras to novel photographing platforms including drones, and digital sources of historical photos, a resurgence of photogrammetric mapping for natural resource management has occurred during the past decade (Chirayath and Earle, 2016; Storlazzi et al., 2016; Casella et al., 2017; Pizarro et al., 2017; Warrick et al., 2017).

Structure-from-Motion photogrammetry was initially developed and applied to terrestrial settings, but it has also become an important tool for creating three dimensional models of underwater bathymetry and habitats (Li et al., 1997; Cocito et al., 2003; Burns et al., 2015, 2016; Leon et al., 2015; Storlazzi et al., 2016; Ferrari et al., 2017; Pizarro et al., 2017; House et al., 2018; Chirayath and Instrella, 2019; Price et al., 2019). In certain applications underwater SfM products have several benefits over more traditional sonar and lidar bathymetric maps. Perhaps the most important of these advantages is the incorporation of color imagery into the final products, which can be used to identify benthic features and characteristics, including substrate type and a diversity of marine species (Burns et al., 2016; Chirayath and Instrella, 2019; Magel et al., 2019). These SfM-based products also enable the development of accurate micro-roughness maps for studies of flow distribution and sediment re-suspension (Rogers et al., 2018; Pomeroy et al., 2019).

Several underwater SfM techniques exist, including photographing the seafloor from both above and below the water surface (Burns et al., 2015; Leon et al., 2015; Massot-Campos and Oliver-Codina, 2015; Chirayath and Earle, 2016; Raoult et al., 2016; Storlazzi et al., 2016; Casella et al., 2017; Pizarro et al., 2017; Raber and Schill, 2019). However, consistent with terrestrial SfM mapping, bathymetric SfM products will be optimized when best practices and accurate ancillary data are included in the workflow (Matthews, 2008). Additionally, the use of multiple cameras with different perspectives can increase the likelihood of obtaining accurate photogrammetry products (Raber and Schill, 2019). Notable factors for optimizing SfM workflows include: a stable camera and lens that can be accurately modeled by lens calibration equations; adequate photograph resolution, clarity, and overlap geometry; and high-accuracy photo positions and/or ground control, which can be used to scale and georeference SfM products (Matthews, 2008; Pizarro et al., 2017). Applied to underwater SfM, these best practices include the use of a camera with a global (not rolling) shutter, a fixed lens with constant aperture and focus settings, a lens and sensor with geometries that are not affected by camera power cycles, underwater housings that – when combined with the camera system – can be adequately modeled by lens calibration equations, adequate spatial distribution of seafloor ground control with surveyed coordinates, and accurate camera positions for each photo. Unfortunately, it can be difficult to develop an underwater ground control network for seafloor settings owing to the challenge of deploying and accurately surveying a proper constellation of markers (Casella et al., 2017; Neyer et al., 2018). These difficulties have made accurately scaled, repeatable and georeferenced bathymetric maps largely unattainable, thereby necessitating co-registration methods to map change with SfM (Burns et al., 2015; Neyer et al., 2018; Magel et al., 2019).

Here we describe, test, and evaluate a new underwater SfM mapping system that incorporates many of the photogrammetric principles mentioned above to map shallow benthic settings, such as coral reefs, without surveyed ground control points. Important elements of this system include: integration of multiple cameras and a survey-grade Global Navigation Satellite System (GNSS), high precision temporal coupling across all measurements, low distortion camera housings, a rigid frame to ensure constant camera-to-GNSS antenna geometry, and a sufficiently small system to ship to remote locations and operate from small vessels. We tested this system in diverse locations of the Florida Keys Reef Tract (**Figure 1**) and evaluated the geospatial accuracy of SfM products by comparing with known locations of previously surveyed human-made seafloor structures visible in the SfM reconstructions and with multiple independent surveys of a single site to test repeatability. Accuracy of local small-scale measurements from the SfM maps was assessed by imaging precision-machined 3D scale bars that were temporarily placed on the seabed in the survey area. Our results were used to evaluate the quality of mapping products generated over different benthic settings, including live reef, senile reef, reef rubble, and sand. We use these results to comment on the potential application of similar systems for generating accurate high-resolution surveys of complex seafloor structure and composition and measuring changes over time.

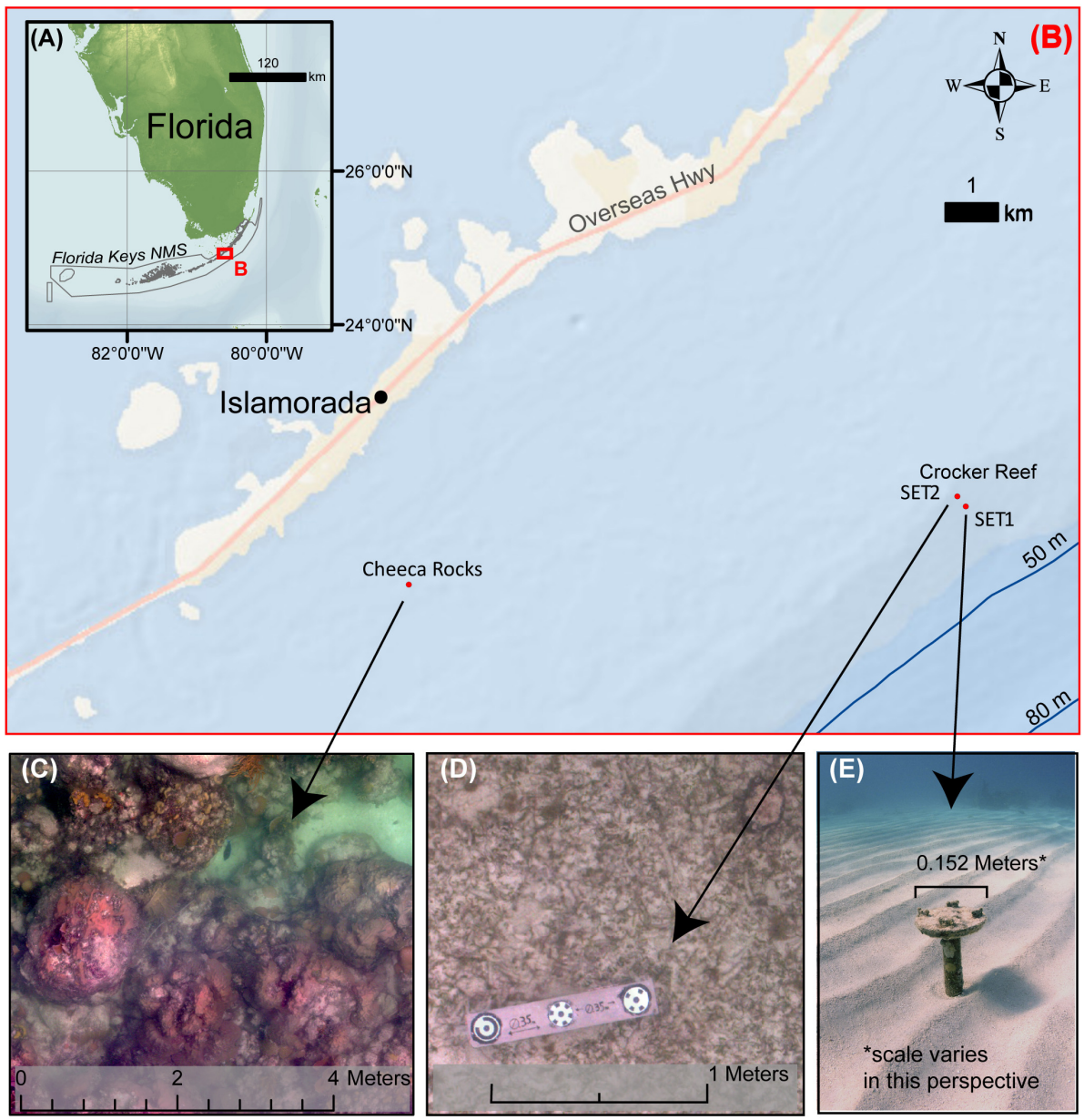

FIGURE 1 | (A) Geographic location of fieldwork in the U.S. Florida Keys, global bathymetry (GEBCO), with operation area outlined. **(B)** Larger scale map of field site showing the locations of Surface Elevation Table (SET) stations and the Cheeca Rocks reef site location. **(C)** Example of the Cheeca Rocks coral reef orthomosaic generated from imagery collected using SQUID-5 (depth ranges from ~2.5 m to over 4.5 m). **(D)** Sample of orthomosaic generated above SET station 2 from SQUID-5 imagery with scalebar and circular encoded targets attached (water depth ~ 3.6 m). **(E)** Perspective photo of SET station 1 with protective cover plate installed showing sandy seabed and ripples typical at the site.

METHODS

Instrumentation

During development of our underwater photogrammetry device, which is termed the SfM Quantitative Underwater Imaging Device with Five Cameras (SQUID-5; **Figures 2**, **3**), several physical design goals were established, including the ability to hand deploy from a small vessel, easy disassembly and reassembly for shipping, structural rigidity, acceptable towing behavior in sea conditions of 1.5 m or less non-breaking surface waves from moderate swell, and survey speeds of 1.5 m/s or slower. The SfM analysis we intended required the design to incorporate precise synchronization between image capture and associated geospatial location of the image measured by the onboard GNSS. Additionally, early prototype testing on land suggested that a design with three or more cameras could both function in continuous mapping mode and allow for the generation of a complete 3D scene at every collection instance

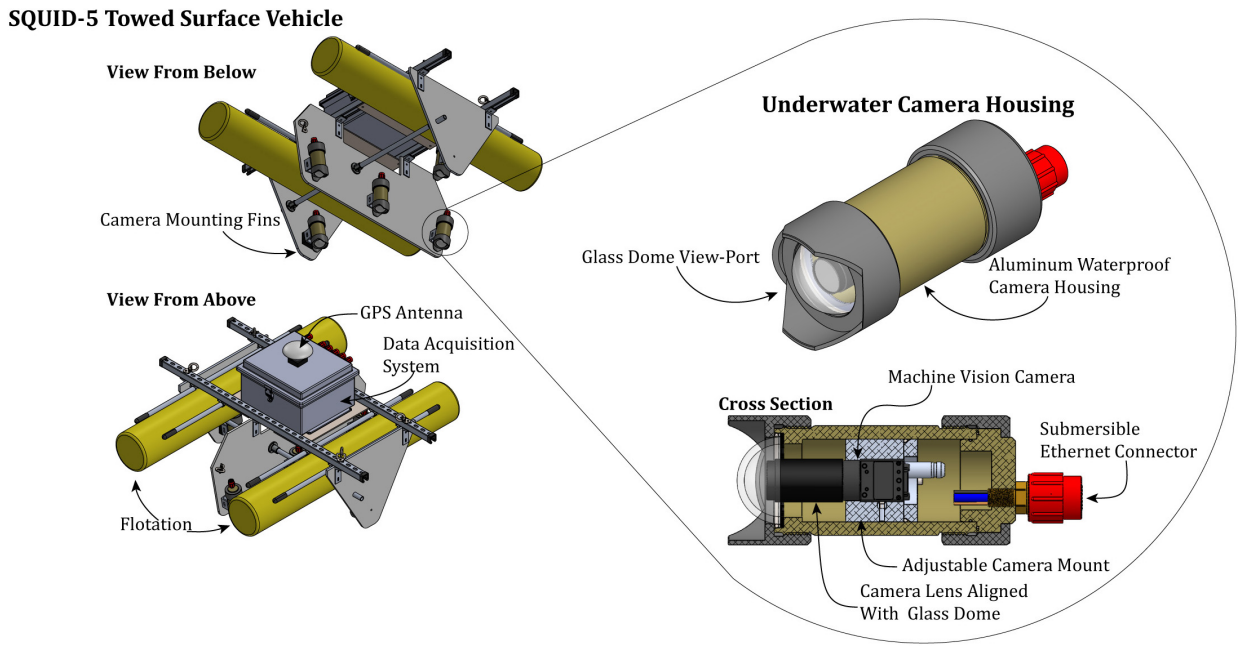

FIGURE 2 | Diagram of the SQUID-5 towed surface vehicle and the waterproof camera housings with labeled components. The camera mounting mechanism aligns the camera axially with the dome and allows the camera to be adjusted fore and aft to accommodate various lens types and enable alignment with the glass port radius of curvature for minimal distortion.

if the cameras were synchronized, fixed equidistant from each other at a spacing approximately 25% of their distance to the target surface, and oriented toward a central target point for maximum imagery overlap. Here we focus on the continuous mapping mode; the latter topic (scenes at each instance) will be addressed in future work. That noted, continuous mapping from multiple instances of three or more synchronized cameras appears to be advantageous because moving features – such as sand ripples, algae, fish, and debris – are collected at the same instant, which improves the reconstruction of these objects and reduces noise. A minimum of three overlapping images from slightly different perspectives is generally required to generate a 3D surface with SfM (Ullman, 1979). We built SQUID-5 conservatively by incorporating five cameras, each at different locations and view angles, to account for the fact that some imagery would likely be unusable. We correctly anticipated that a small camera vehicle towed on the open ocean surface would occasionally be oriented at an extreme angle relative to the seafloor due to surface wave action causing imagery from one or more cameras to be too oblique, and that the system would occasionally pass over debris or bubbles floating just below the surface, temporarily obscuring one or more camera views. The SQUID-5 design is summarized below, and further details including the system diagram and details of equipment and components can be found in the System Engineering **Supplementary Material**.

SQUID-5 Towed Surface Vehicle

We built SQUID-5 with a central downward-looking camera and four cameras orthogonally spaced roughly 0.5 m from the central camera (**Figure 2**). The camera orientation can be easily adjusted, and two setups were used during our operations. On the first deployment of the first day in the Crocker Reef area, we tested a setup intended to be used for efficient area mapping by creating a large across-track image footprint on the seabed, orienting port and starboard cameras 10° outward from the center camera's field of view (FOV). This geometry still maintains approximately 100% overlap between the forward, center, and trailing cameras, and approximately 30% across track image overlap between the port, center and starboard cameras in 3.0 m of water. For the remainder of the fieldwork we maintained a camera orientation with all cameras pointed inward toward the center camera's FOV resulting in nearly 100% overlap between all five cameras in 3.0 m of water.

The overall dimensions and weight of SQUID-5 enable it to be hand-carried, deployed, and retrieved by two people (System Engineering **Supplementary Material**). Structural support is provided by widely available aluminum strut channels and aluminum honeycomb panels, which combine to minimize flexure under loading. A fiberglass waterproof container is mounted atop SQUID-5 to contain the acquisition computer and provide a GNSS antenna mounting location (**Figure 2**). Buoyancy is created by two inflatable pontoons of urethane-coated canvas. The cameras are mounted to the lower portion of the honeycomb panels approximately 0.3 m below the water surface to minimize bubbles caused by towing turbulence (**Figure 3**). The mass of the aluminum camera housings mounted well below the vehicle's center of buoyancy creates a stable arrangement for towing in seas with wave heights up to 1.5 m.

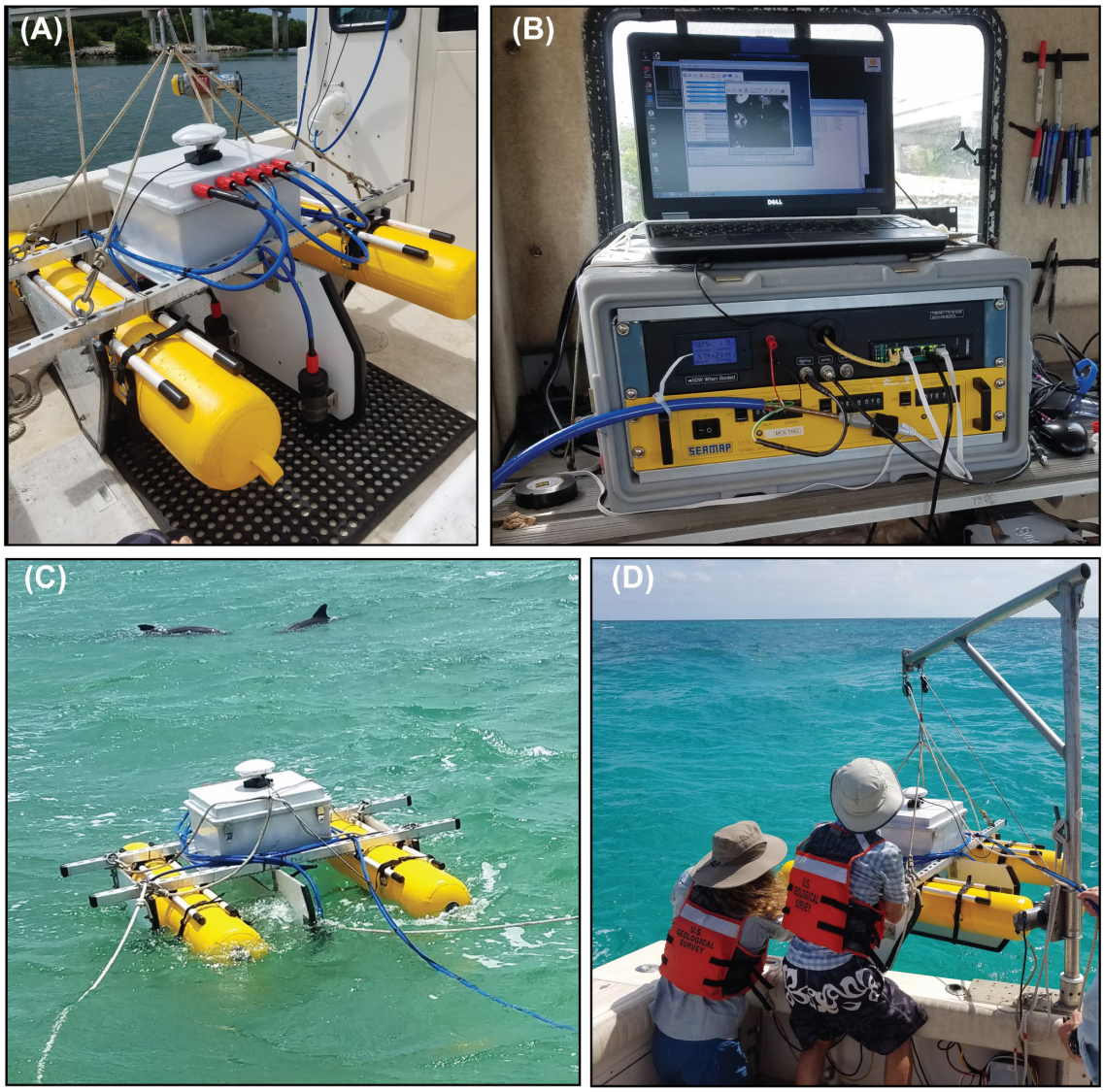

FIGURE 3 | Photographs of field operations with the SQUID-5 towed surface vehicle: **(A)** the vehicle on the deck of the support vessel rigged for deployment; **(B)** the control station onboard the support vessel consisting of laptop, power supply, NTP time server, Ethernet hub, power supply, and trigger signal generating electronics; **(C)** the towed surface vehicle in operation; and **(D)** launch and recovery of the SQUID-5.

Cameras and Housings

Performance criteria for the SQUID-5 required cameras and lenses with high quality optics and a reliable high-quality image sensor with stable performance, small size, and reasonable cost. We selected 5.0 MP (2448 × 2048 pixels) FLIR Systems Blackfly S Gigabit Ethernet (GigE) machine vision cameras, which have a global shutter, 3.45 μm sensor pixel size, 24-bit color, and up to seven frames-per-second capture speeds. Additionally, the small size and symmetry of these cameras (approximately a 30 mm cube) simplified the design and fabrication of waterproof housings (**Figure 2**). Several lens options existed for these cameras, and we chose the Fujinon HF6XA-5M 6 mm fixed focal length lens, which has a 74.7° horizontal FOV and a 58.1° vertical FOV. At a design target of 3.0 m above the seafloor, an image from this camera and lens captured 4.57 m horizontally (across-track) and 3.34 m vertically (along-track), with a ground sample distance (GSD) of ∼1.725 mm at nadir (Matthews, 2008; Newman, 2008). Since the camera housings were built using glass dome viewports (see below), these GSD estimates were not significantly affected by water refraction of light. During data collection, the focus and aperture settings were fixed, while camera gain and shutter speed were adjusted as needed for each collection area using custom camera control software developed for this project.

Custom underwater camera housings were designed and built for SQUID-5 to minimize optical distortions and accommodate a range of lens options (**Figure 2**). Hemispheric BK7 glass domes were used for the camera viewport to minimize variations in focal

length, FOV, radial and chromatic distortion, all of which are known limitations of flat ports in underwater photogrammetry (Nocerino et al., 2016). In addition, the hemispherical dome enabled the option of a more wide-angle lens if needed and increased the focus depth-of-field by approximately 33% for the same aperture setting over the flat port alternative (Menna et al., 2016). Cameras were mounted in the housings such that the camera lens nodal point was aligned with the center of the dome radius. With our chosen aperture of $f5.6$, the underwater focus depth-of-field was approximately 1 m to ∞.

GNSS and Camera Positioning

Positions of the cameras during each image capture instance were referenced to survey-grade GNSS measurements from a Trimble R7 GNSS receiver with a Trimble Zephyr-2 GNSS antenna mounted atop the SQUID-5 towed surface vehicle (**Figure 2**). Raw GNSS data were processed against base station data from a continuously operating reference station (CORS) in the Florida Permanent Reference Network (FPRN). The CORS station used (FLPK) was within 10 km of all survey sites and provided 1-hertz dual-frequency GPS and GLONASS data. The raw base and rover data were combined with precision ephemeris data and post-processed in Novatel's Grafnav (v. 8.80) software suite, resulting in trajectories with RMS errors of 1.7 cm horizontal and 3.8 cm vertical. Timestamps from each trigger event were then imported into Grafnav and the interpolated antenna positions exported. All data are referenced to the NAD83 (2011) coordinate system and exported as both geographic and projected (UTM Zone 17N) coordinates, with both ellipsoid and orthometric (NAVD88 GEOID 12B) heights.

The existing CORS network was used for Post Processed Kinematic (PPK) GNSS position refinement out of convenience but it was not required. A similar level of accuracy is possible without the existence of the CORS network (or any other) by installing a temporary GNSS base station 24 h prior to the mapping fieldwork to refine its locally measured location. Once the base location is established it can then be used to record data continuously and simultaneously during the mapping fieldwork for later use in refinement of the mobile GNSS's position data through post processing. The error of the mobile GNSS PPK locations are a function of distance from the base station, therefore the baseline distance should be minimized. Although the single baseline distance can acceptable to a distance of 30 km (Allahyari et al., 2018).

To translate the single PPK GNSS antenna position to individual camera locations, offset distances from the nodal point of each camera to the GNSS antenna phase center were measured using SfM. This included photographing SQUID-5 in the laboratory with machined scale bars temporarily mounted on the vehicle. Seventy-four photos from multiple angles were used to develop a SfM point cloud with point spacing less than 1 mm. Distance measurements from the cameras to the GNSS antenna were calculated in each camera sensor frame of reference using CloudCompare (version 2.10.2) and were included as initial estimates of the GNSS lever arm distances in the SfM analyses.

System Synchronization

To ensure images were collected at the same instant that GNSS location events were recorded, we used an electronic signal generator which triggered each system simultaneously through a shared voltage pulse (10-volt square wave) from the support vessel (see details in System Engineering **Supplementary Material**). Manufacturer's specifications suggested that signal propagation delays should be less than 50 μs for the cameras and less than 1 μs for the GNSS. Therefore, maximum uncertainty in the relative position caused by timing errors during image capture was approximately 0.08 mm at a maximum survey speed of 3.0 knots (∼1.5 m/s), which is well below the PPK GNSS horizontal uncertainty of approximately 1.7 cm and was therefore considered negligible.

Data Acquisition

The acquisition computer was located directly on the tow vehicle in a waterproof housing (**Figure 2**). It was remotely controlled with a second computer located on the support vessel using Microsoft's Remote Desktop application over a wired network connection (**Figure 3**). Both the control and acquisition computer system clock times were maintained using a GPS-based network time protocol (NTP) server located on the support vessel. To facilitate a rapid rate of data collection, four 2 TB solid-state hard drives were installed in the acquisition computer and configured as a high speed striped (RAID 0) array for a total storage capacity of approximately 8 TB and a sustainable write speed of over 300 MB per second. Each camera was connected directly to the data acquisition computer via its own dedicated GigE port.

Study Site

The Florida Keys Reef Tract parallels the 240-km-long Florida Keys island chain and extends from southeast of Miami to the Dry Tortugas in the Gulf of Mexico (Lidz et al., 2008). This barrier reef is approximately 6–7 km wide and numerous patch reefs are located in a shallow lagoon at water depths of approximately 3–6 m. The Florida Keys have a microtidal environment with tides less than 1 m. Field operations were conducted at Crocker Reef and Cheeca Rocks, both within the Florida Keys National Marine Sanctuary. These sites were chosen for their diversity of benthic settings, ease of access from a small boat, and history of scientific investigations, including previously installed Surface Elevation Table (SET) stations (**Figure 1**). Crocker Reef is a barrier reef located approximately 11 km east of the town of Islamorada, Florida, and is primarily a senile reef characterized by eroding coral reef topography, extensive bare sand, coral rubble, and seagrass habitat with average water depths less than 10 m. Two pre-installed SET stations were located at the Crocker Reef sites (**Figures 1D,E**). Cheeca Rocks is a small patch reef located approximately 2.5 km southeast of Islamorada, Florida, within a Sanctuary Preservation Area of the Florida Keys National Marine Sanctuary with complex topography. No pre-installed ground controls were located at Cheeca Rocks. Water depths at this study site were approximately 2–5 m as measured by the support vessel's echo sounder.

TABLE 1 | Coordinates of the Crocker Reef Surface Elevation Table (SET) stations as measured by a survey-grade Global Navigation Satellite System (GNSS).

Site name	Northing, easting, depth[1] (m)	Uncertainty[2] (m)
SET1	2754981.878, 547830.459, −4.120	*RMSE:* 0.058 m (H), 0.041 m (V) *Max:* 0.096 m (H), 0.050 m (V)
SET2	2755156.748, 547682.200, −3.603	*RMSE:* 0.036 m (H), 0.041 m (V) *Max*: 0.055 m (H), 0.050 m (V)

[1]Measurements are to the center of the top of the SET station using GNSS, antennae rods, and a plumb line held in place with a bottom-mounted tripod and are reported in UTM 17N, NAD83(2011) GEOID12A1. [2]Horizontal (H) and vertical (V) uncertainties were calculated from the combination of GNSS measurement uncertainties and positional uncertainties introduced by the plumb line and antennae rods. "Reasonable" uncertainties ("RMSE") were computed by adding in quadrature assuming independent errors. "Max" uncertainties were computed by summation assuming dependent errors.

The SET stations were installed at the site in August of 2014 by the USGS Coastal and Marine Science Center of St. Petersburg, FL, United States, for the purpose of tracking relative change in the seafloor bed elevation over time using a portable leveling device (Lynch et al., 2015). To ensure stability, the SET stations were fixed in place by drilling vertically to the depth of the Pleistocene layer, driving an aluminum rod into the hole until firm resistance, trimming the rod to length, attaching and leveling the SET station cap, and cementing the rod in place. Once installed, the locations of the SET stations were measured with a survey-grade GNSS by temporarily erecting a tripod directly above the station using a bubble level and weighted line to align and center a GNSS antenna mast over the center of the SET station caps. For maximum possible accuracy, the antenna locations were further refined in post-processing to correct for local atmospheric effects using data simultaneously collected with a nearby land-based stationary GNSS. Finally, antenna positions were translated to the SET station cap positions by applying offsets measured while the tripod was in place (**Table 1**). The uncertainties of these measurements were approximately 6 cm horizontally and 4 cm vertically, owing to the imprecision of the leveling devices and the accuracy of the GNSS measurements (**Table 1**).

It is important to recognize that the significance of the pre-installed SET stations with known geo-spatial coordinates located within the study site was only that they provided a means to measure the geo-spatial accuracy of seafloor data products generated using data from SQUID-5 and SfM. The SET station locations were not used as ground control during SfM processing. Geo-spatial SET station locations were measured independently using the newly generated SQUID-5 bathymetric data products and then compared to the previously GNSS surveyed coordinates from 2014. This is described further in the section "Accuracy Assessments of SfM Products".

Field Operations

Seafloor imagery and associated geo-locations were collected with SQUID-5 during small boat operations based out of Islamorada, Florida, on July 11–13, 2019 (**Figure 1**). The USGS *R/V Sallenger* (8-m long Parker 2530 with enclosed cabin) was used as the host vessel with real-time acquisition and monitoring set up inside the cabin (**Figure 3B**). A second team of USGS science personnel used another small boat, the USGS *R/V Halimeda* (8-m long, modified Oceans Formula with an open deck), to attach circular encoded targets to SET stations and deploy a three-dimensional scale bar, both of which were used for data validation (**Figure 4**).

The primary purpose of the field experiment was to evaluate SQUID-5's capabilities and limitations. Therefore, our focus at the two SET stations was to acquire data in order to assess data accuracy, precision, and reproducibility. The Cheeca Rocks site was selected to evaluate system performance and its ability to resolve complex benthic features over a high relief area (**Figure 1C**). Data from several adjacent passes at all three locations were combined to create seamless maps of several hundred square meters, demonstrating the potential for mapping larger areas of contiguous reef at both sites (**Figures 5–8**). Notably, SQUID-5 is a tool intended to map relatively small areas but at very high resolution when compared with more traditional mapping technologies such as sonar or airborne lidar. For example, mapping a 100 m × 200 m area of seafloor in 3 m of water depth would require an estimated 2.5 h of boat operations. This estimate assumes only 50% efficiency during collection in order to allow for vessel turns and the difficulty of navigating a vessel along tightly spaced survey lines.

To achieve optimal SfM results, our image collection rate was selected such that sequential images had at least 60% overlap and angular change between features in sequential images would not exceed 15° (Matthews, 2008). As detailed in the Optimal Image Spacing **Supplementary Material**, the limiting factor for our wide-angle lens selection was the 15° angular change maximum, and, considering a target distance of 3 m, we calculated that a 2 Hz collection rate at a maximum survey speed of 3.0 knots (∼1.5 m/s) would adequately meet this requirement. Actual operating conditions commonly included survey speeds of 1.5–2 knots (∼0.8–1 m/s) and imagery collection at 2 Hz (**Table 2**). However, the vehicle was occasionally allowed to drift slowly over features of interest to evaluate the effects of greater photo densities. Over the course of fieldwork, sea state ranged from calm to over 1 m wind chop. Water clarity at both SET stations was such that the seabed was clearly visible in all the imagery. Turbid conditions at Cheeca Rocks made it difficult to clearly discern the seafloor in many images collected in water depths greater than approximately 4 m. Ambient lighting ranged between partly cloudy and overcast, which limited the effects of light ray caustics that can inhibit photogrammetric reconstructions (Agrafiotis et al., 2018).

SfM Analyses

The SfM processing was done with Agisoft Metashape software (version 1.5.2, build 8432) using general single-collection

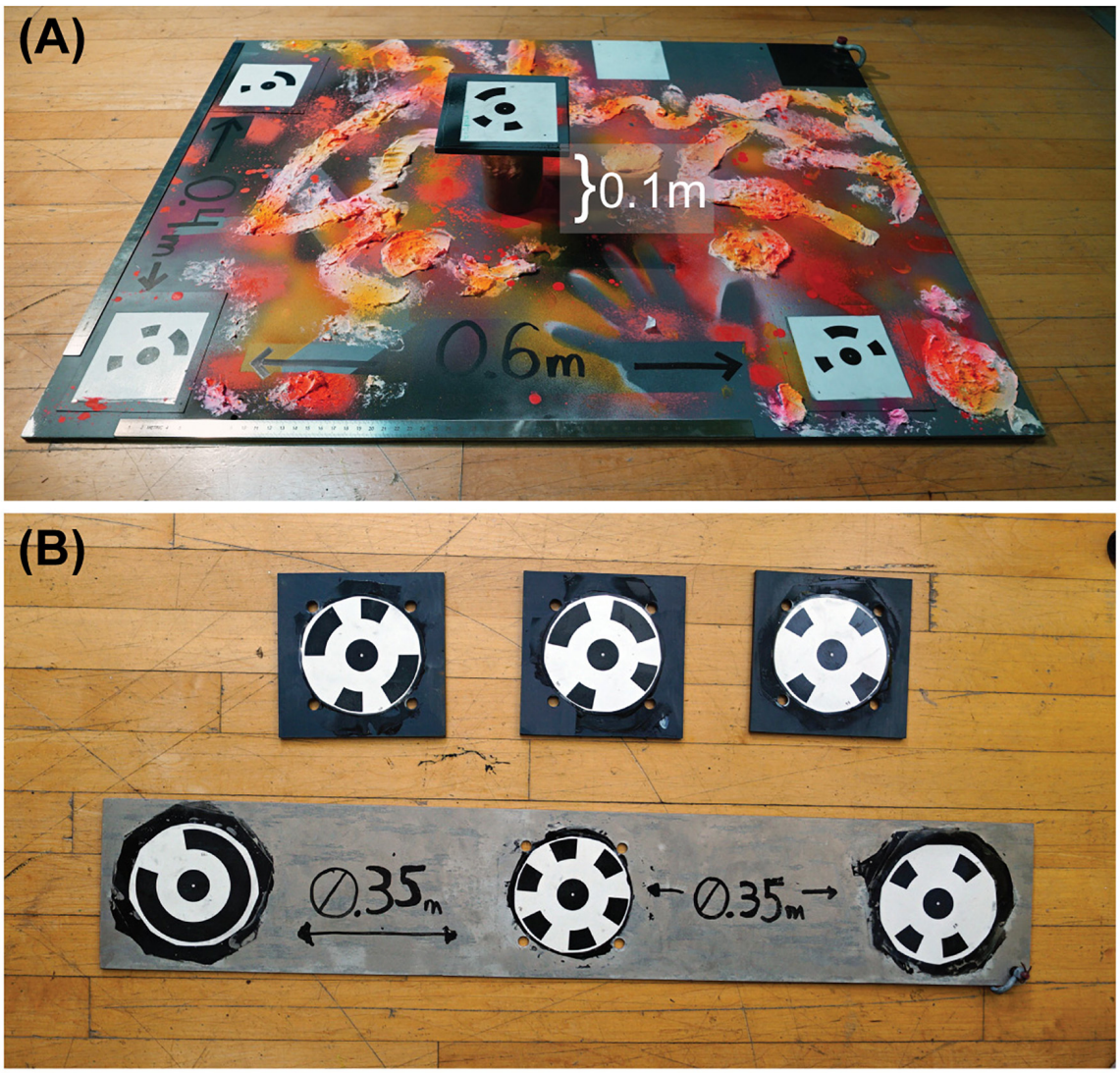

FIGURE 4 | Machined scale bars and targets for accuracy assessment during field operations: **(A)** submersible camera calibration plate including precisely positioned circular encoded targets in three dimensions, painted with texture to assist Structure-from-Motion (SfM) photogrammetry reconstruction of the plate and with black and white squares for exposure and color balance adjustment; **(B)** individual circular encoded targets and a linear scale bar for mounting precisely to the Surface Elevation Table (SET) stations.

techniques. The SfM analyses were performed in a manner to maximize seabed returns and limit errors from insufficient or excessive photo coverage. Higher photo densities from drifting at slow speeds resulted in overly noisy SfM point clouds, largely from the small separation distances between photos with respect to water depth. To minimize these errors, the complete photo sets of each study area were subsampled such that minimum GNSS measured spacings between independent collection instances were at least 0.75 m (see Optimal Image Spacing **Supplementary Material**). This data reduction step dramatically reduced the noise in the final SfM products.

For each survey site, the subsampled photo quintets were combined with GNSS positions and camera-to-GNSS-antennae distance vectors (lever arm offsets) and aligned with independent lens models derived for each camera using camera-specific image subsets within Metashape. The computed camera positions and lens models were then refined using three statistical tools (reconstruction uncertainty, projection accuracy, and reprojection error) in Metashape to eliminate poorly constructed tie points. With trial and error, we found that threshold values of 20, 8, and 0.4 (entered as unit less parameters) for these statistical tools, respectively, resulted in good alignment and adequately dense tie point distributions in both high-relief reef settings and relatively flat sandy areas.

Once the photo alignment and lens models were optimized, dense point clouds were generated with Metashape using high point density and moderate filtering settings. Dense point clouds were used to generate digital surface models (DSMs) and photo

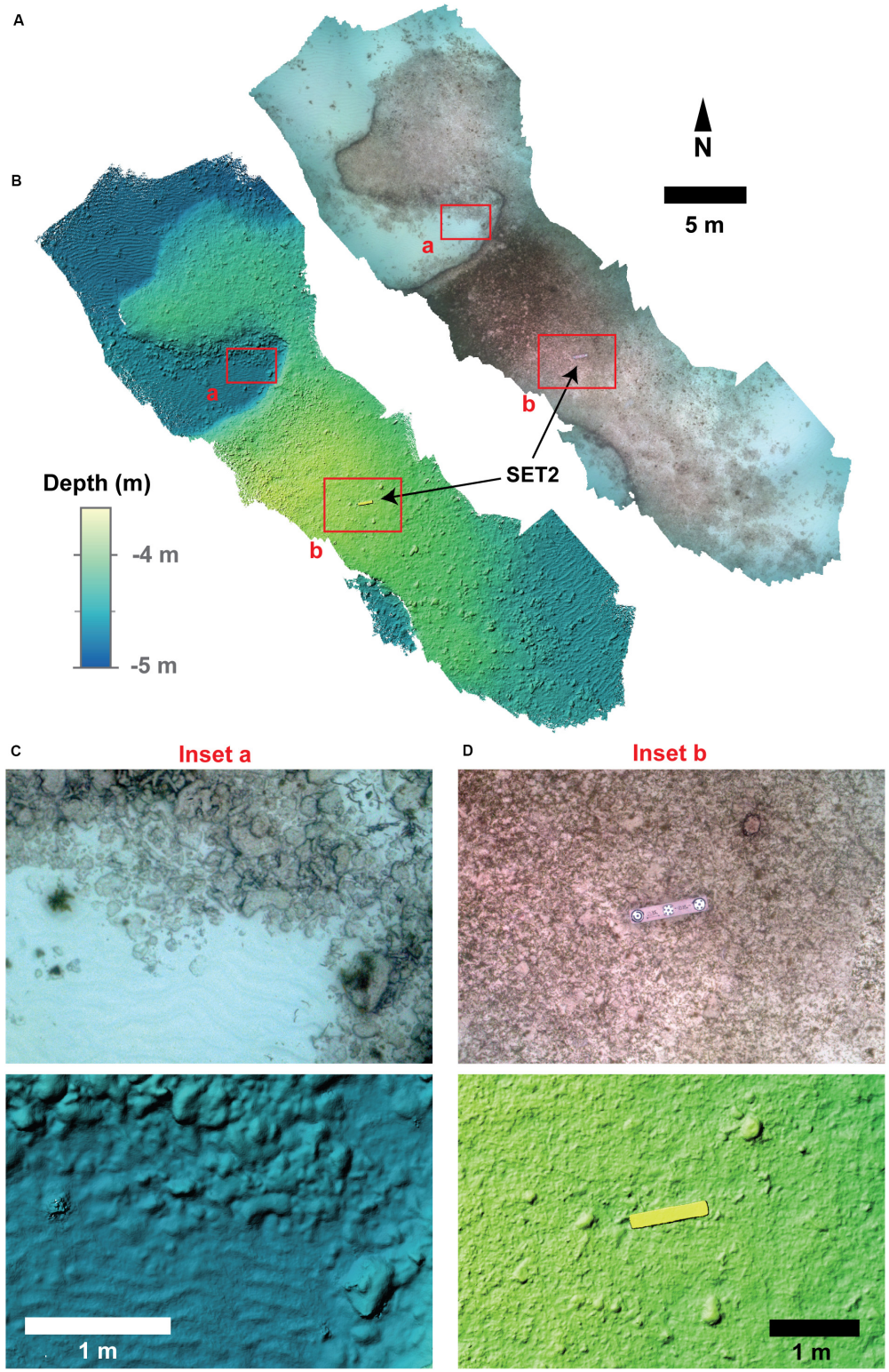

FIGURE 5 | (A,B) Mapped orthomosaic and bathymetry obtained from three survey passes of the Surface Elevation Table (SET) station 2 site with the SQUID-5 system. The shaded relief bathymetry is shown for a digital surface model (DSM) derived from the Structure-from-Motion (SfM) dense point cloud. The spatial resolution of the photo mosaic and DSM are 2.1 mm and 4.1 mm, respectively. **(C,D)** Highlights of the benthic maps of the site, including sand, rubble, eelgrass and the scale bar mounted on the SET station 2 monument.

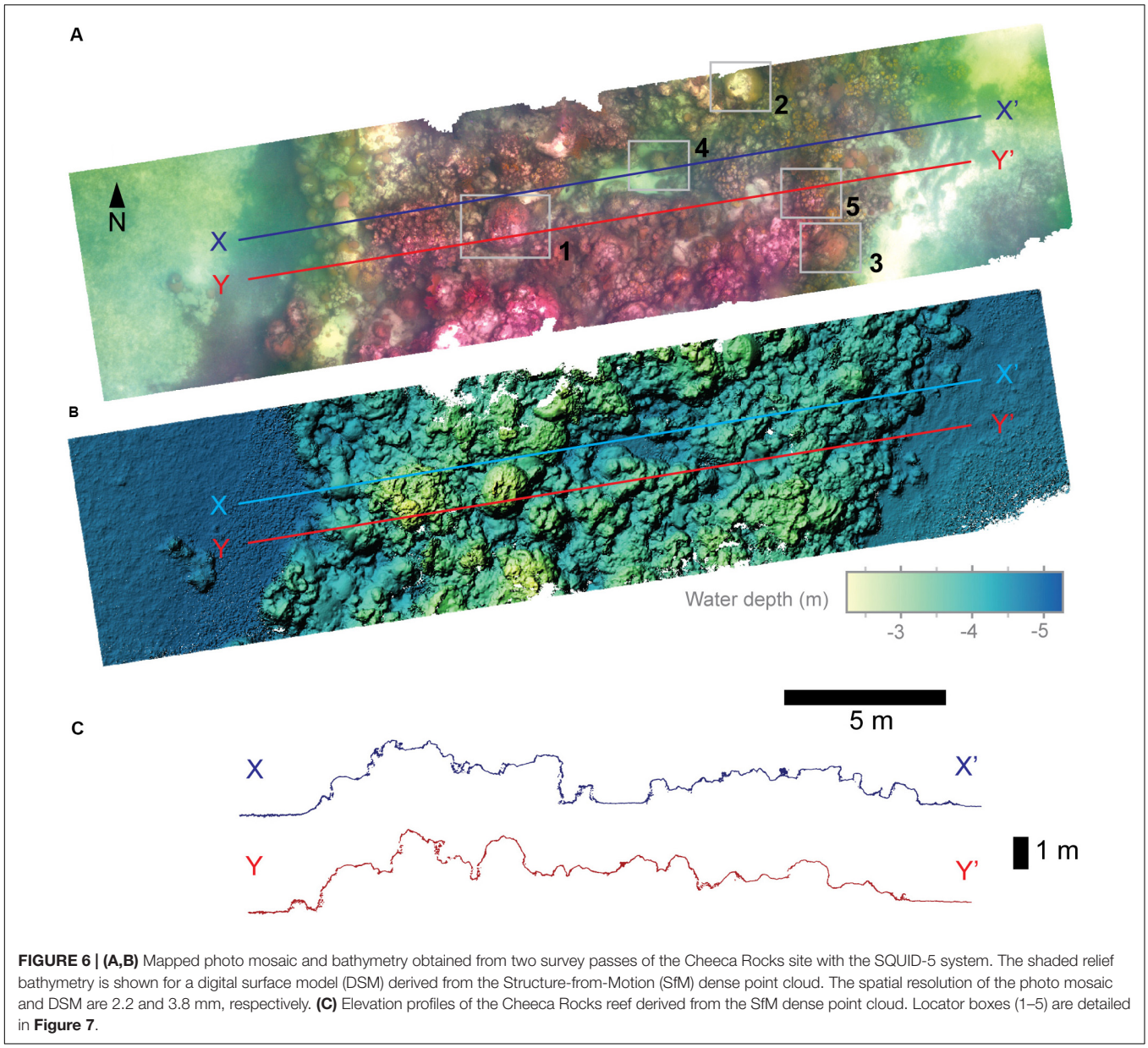

FIGURE 6 | (A,B) Mapped photo mosaic and bathymetry obtained from two survey passes of the Cheeca Rocks site with the SQUID-5 system. The shaded relief bathymetry is shown for a digital surface model (DSM) derived from the Structure-from-Motion (SfM) dense point cloud. The spatial resolution of the photo mosaic and DSM are 2.2 and 3.8 mm, respectively. **(C)** Elevation profiles of the Cheeca Rocks reef derived from the SfM dense point cloud. Locator boxes (1–5) are detailed in **Figure 7**.

orthomosaics for each study site using the Metashape default cell spacing, which ranged between 3.8 and 4.1 mm for the DSMs and 2.0 and 2.2 mm for the orthomosaics. The DSM and orthomosaic products were generated primarily for visualization, whereas most of the analyses were based on the high-density point clouds. For the SET station 1 site, two independent surveys were conducted using different SQUID-5 camera orientations and on different dates to evaluate the reproducibility of the data at this site.

Accuracy Assessment

Accuracies of the resulting data were evaluated for both local-scale measurements (decimeter to meter) and georeferenced map products. Linear measurements in the SfM point clouds, which included both horizontal and vertical directions, were compared with precisely measured dimensions of scale bars placed in two study sites (**Figures 1D**, **4**, **5D**). Printed targets were physically attached to the scale bars at precise spacings with submillimeter accuracies. The targets were detected in imagery with algorithms available in Metashape or manually identified in photos where the detection algorithms did not select them, and then Metashape was used to calculate distances between targets.

Three-dimensional georeferenced point accuracies were evaluated by comparing SfM-derived positions and elevations of the two SET stations with their previously measured GNSS-surveyed positions and elevations acquired at their time of installation in 2014. At SET station 1, two independent SfM measurements were made with SQUID-5 using different camera set-ups and on separate days (**Table 2**). SET station 2 was mapped on a single survey day.

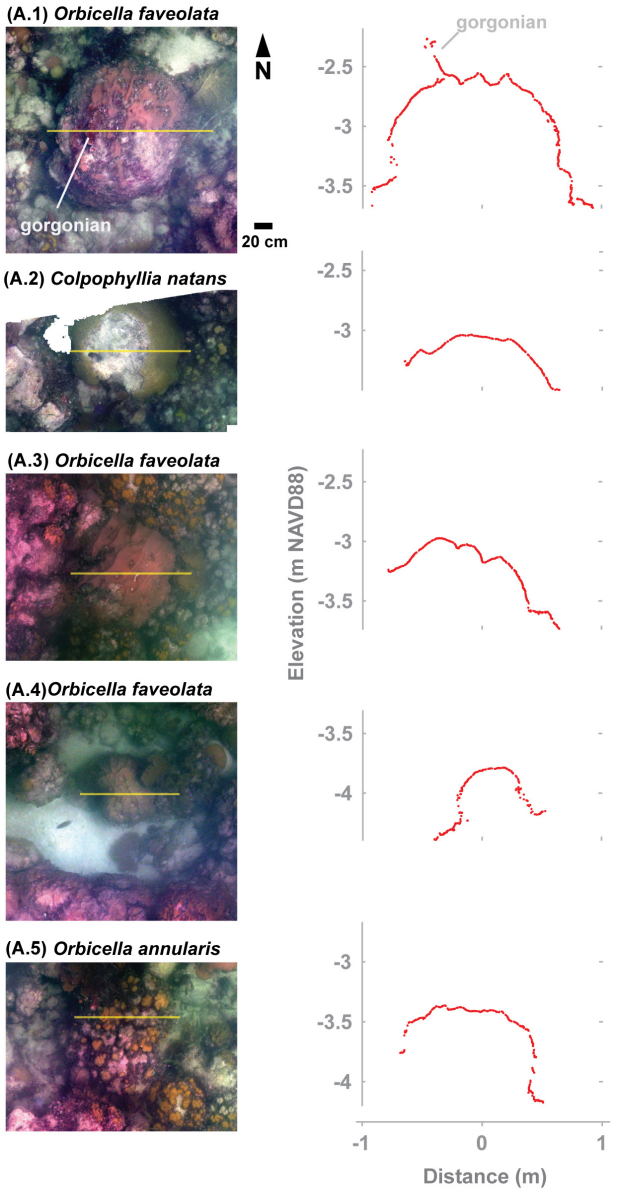

FIGURE 7 | Photo mosaics and elevation profiles for several coral heads mapped at the Cheeca Rocks site and highlighted by locator boxes 1–5 shown in **Figure 6A**. Coral species include Mountainous Star Coral (*Orbicella faveolata*), Boulder Brain Coral (*Colpophyllia natans*), and Boulder Star Coral (*Orbicella annularis*). The profile in **(A)** includes a sea fan, or gorgonian (*Gorgonia ventalina*). Profiles were derived from the original Structure-from-Motion (SfM) point cloud using all points within ±1 mm of the profile transect.

The reproducibility of the SfM bathymetric surfaces was assessed with two independent surveys of the SET station 1 site. An area of overlap, which was roughly 20 m by 10 m and included elevated sessile reef and sandy regions with pieces of reef rubble, was obtained in both surveys and analyzed for differences. The reef and rubble were assumed to be stationary between the two surveys, such that they were used in direct point cloud-to-point cloud comparisons. All cloud-to-cloud comparisons were made within CloudCompare using the Multiscale Model to Model Cloud Comparison (M3C2) algorithm, which computes total and directional differences normal to the local surface of one of the point clouds (Lague et al., 2013).

The results of the overlapping surveys were assessed both by using the uncorrected, or raw, SfM output of both surveys and by correcting offsets between the SfM point clouds using locations on hard features that were assumed to be fixed to remove biases. Three bias correction techniques were used: (i) three-dimensional translation of a point cloud by northing, easting and vertical constants derived from comparisons of a single, easily identified point on the ridged structure of the reef ("single-point bias correction"), (ii) three-dimensional translation and rotation of a point cloud using differences in three points easily identified on the reef and in the rubble area ("three-point bias correction"), and (iii) use of the positions of three points on the reef and rubble as SfM markers for a second reprocessing generating a complete reanalysis with the SfM technique ("three-point iterative SfM correction").

RESULTS

Benthic SfM Products

With SQUID-5 we collected photo quintets and associated GNSS positions that were used with SfM processing to generate point clouds, surface models, and orthomosaics (Warrick et al., 2020) of complex seafloor structure that included biotic and abiotic components of benthic habitat such as coral heads, rubble, and sandy ripples (**Figures 5**, **6**, **8**). To verify the capability for multi-pass seamless area mapping with SQUID-5, data from three survey passes of the SET station 2 site were processed simultaneously to generate nearly continuous point cloud, elevation, and photo mosaic products for an area approximately 500 m^2 (**Figures 5A,B**). Close examination of these data reveal that the SfM products characterized the 3D extension of reef, rubble, sand ripples, benthic organisms, and the scale bar placed atop the SET station 2 (**Figures 5C,D**).

The ability of SQUID-5 to capture details of complex topography can be seen by examining profiles of SfM data collected at Cheeca Rocks, which includes live coral, sand flats, and vertical-to-overhanging slopes (**Figure 6A** inlay 1, 4, and 5). This site was mapped in detail using the 2.2 mm resolution photo mosaic and millimeter-scale point cloud (**Figure 7**). Profiles of the point clouds through these coral heads reveal detailed topographic information on the coral surfaces and can detect other centimeter or sub-meter scale benthic organisms such as gorgonians (**Figure 7A.1**). Vertical to overhanging sections of the coral heads were commonly less well resolved and more highly variable than the uppermost surfaces, indicating these areas are more challenging to map and illustrating a limitation of surface-towed cameras for SfM methods.

Lastly, two independent multiple-pass surveys were conducted approximately 24 h apart on the SET station 1 site and revealed a broad sandy plain and a senile reef (**Figure 8**). We did not attempt to repeat the same survey lines on the

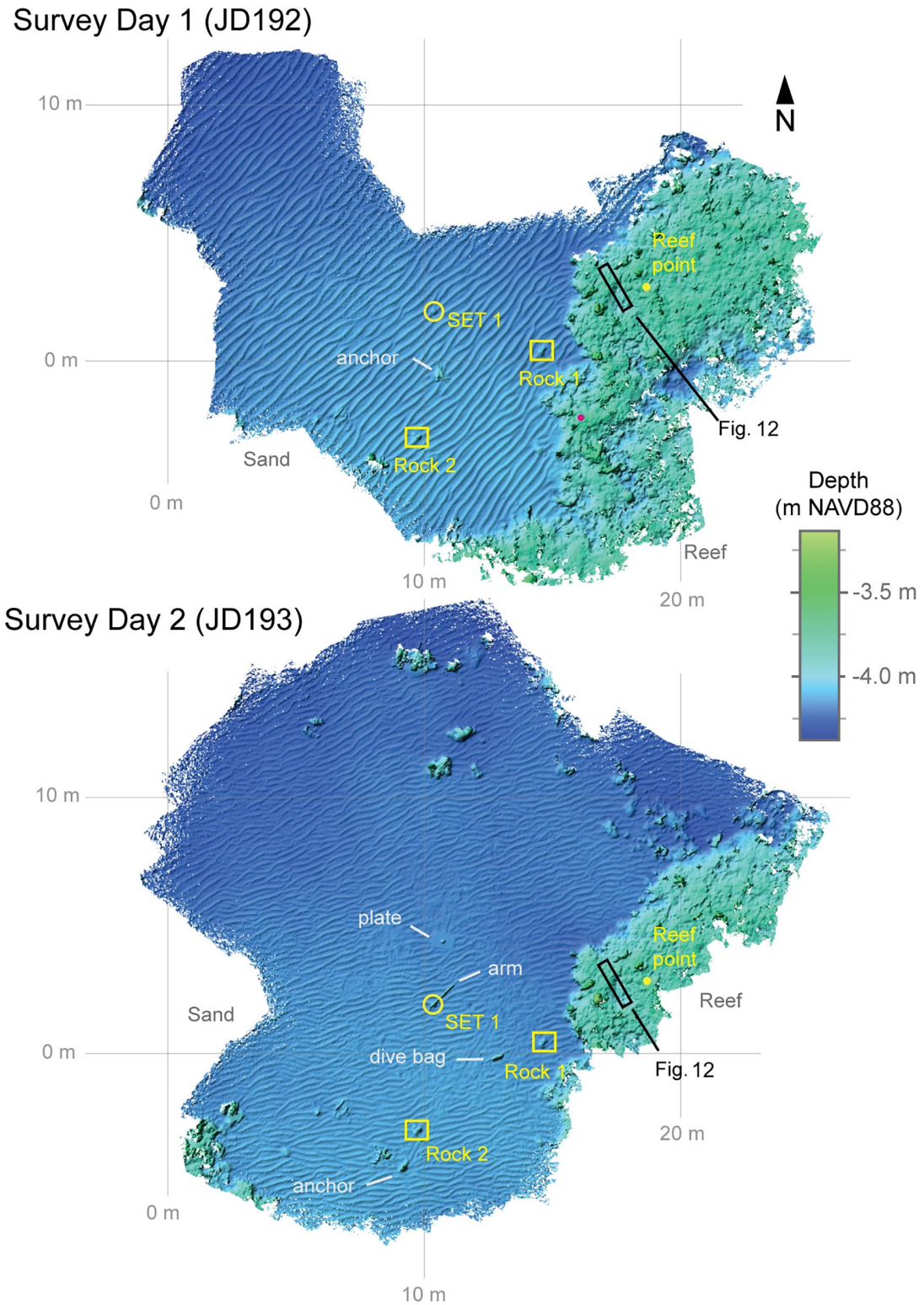

FIGURE 8 | Mapped bathymetry obtained from several survey passes of the Surface Elevation Table (SET) station 1 site with the SQUID-5 system. Survey data from 2 days were collected and processed independently with our Structure-from-Motion (SfM) workflow. Shaded relief bathymetry is shown for the DSMs with spatial resolutions of 3.9 and 4.1 mm, respectively. The wavelength (approximately 0.3–0.5 m) and amplitude (approximately 0.02–0.04 m) of the sand ripples were similar between surveys; however, an approximately 40° change in orientation and complexity increase are readily observed. Locations of several features used for the analyses are labeled. Field crews were conducting SET measurements during the second survey day, as shown by the dive bag, anchor, and measurement tool arm on the SET site.

TABLE 2 | Environmental conditions and system settings used at each survey site.

Calendar day, site name	System settings [gain, exposure, collect rate]	Operating conditions [water depth, survey speed, lighting, sea state]
CD192, SET1[1]	0 dB, 2000 μs, 2 Hz	3.2–5.4 m, 1.5–2 kts, neutral overcast, ∼0.5–1.5 m wind waves
CD193, SET1	5 dB, 2000 μs, 2 Hz	3.4–4.2 m, 1.5–2 kts, neutral overcast, ∼0.3 m wind waves
CD193, SET2	10 dB, 2000 μs, 2 Hz	3.4–4.2 m, 1.5–2 kts, neutral overcast, ∼0.3 m wind waves
CD194, Cheeca Rocks	10 dB, 2000 μs, 2 Hz	2.4–5.2 m, 1.8–2.5 kts, neutral overcast, ∼0.5–1.0 m wind waves

[1]CD192 SET1 was the only collection with port and starboard cameras pointed 10° outward from the center camera. In all others the port and starboard cameras were aimed 10° inward toward the center camera.

TABLE 3 | Comparisons of SfM distance measurements using no ground control with machined scales placed on the seafloor.

Measurement location	Actual distance (m)	SfM distance (m)	Error (m)	Error relative to water depth (%)
Plate, Axis A	0.4000	0.3997	0.0003	0.007%
Plate, Axis B	0.6000	0.5997	0.0003	0.008%
Plate, Axis C	0.7211	0.7209	0.0002	0.006%
Plate, Vertical Axis	0.1003	0.1002	0.0001	0.002%
Scale Bar, Left Side[1]	0.3500	0.3506	−0.0006	−0.016%
Scale Bar, Right Side[1]	0.3500	0.3491	0.0009	0.024%
		Mean	0.0002	0.005%
		St. Dev.	0.0005	0.013%
		Range	−0.0015	−0.04%

[1]Lower accuracies reported for the scale bar are most likely because of fewer passes that were all similarly oriented, resulting in a smaller number of unique camera perspectives than were collected at the scale plate location.

2 days, so the total area covered differed. However, substantial changes were observed in the area intersected by both surveys, most markedly in the orientation and complexity of the sand ripples, which were likely caused by time-dependent changes in ocean waves (**Figure 8**). For example, the orientation of the sand ripples rotated clockwise by 15–40° with the greatest amount of rotation occurring adjacent to the reef, and the wavelength and amplitude of the ripples decreased by approximately 25 and 40%, respectively. The ripples on the second day of surveying were disturbed slightly from dive crew operations, as noted by the diver bag, calibration plate, marker buoy anchor and associated drag marks, and the measurement arm attached to the SET station (**Figure 8**). Hard features, including bedrock and a portion of the reef, were mapped during both survey dates and showed little change, which suggests that they can be used to measure differences in the SfM point clouds as detailed below.

Accuracy Assessments of SfM Products

Measurements of the 3D scale bars generated with the SfM techniques differed from the actual values of the machined scale bars by less than 1 mm (scale length ranged from 10 cm to over 72 cm and the mean difference was 0.2 mm with a standard deviation of 0.5 mm; **Table 3**). Scaling by the water depth of each measurement, these errors ranged between 0.016 and 0.024% of water depth (**Table 3**). Thus, the SQUID-5 reliably produced sub-millimeter measurement accuracy both vertically and horizontally over distances of 10 s of centimeters on the seafloor.

The SfM-based position estimates of the SET station geo-spatial locations were within approximately 3 cm of the total uncertainty of coordinates previously acquired using GNSS surveys (**Figure 9**). As described in Section "Study Site," prior SET station location measurements were collected using a survey GNSS attached to a tripod that was temporarily erected on the seafloor and extended above the water surface directly above the SET stations. Positional differences between the two measurements were greater in the horizontal directions than the vertical, which reflects greater error in the horizontal positions of the original GNSS surveys, owing to the difficulty of precisely leveling a tripod with a total height greater than 4 m in the open coastal ocean environment. The two independent measurements of the geo-spatial position of SET station 1 by our SfM methods produced results that differed by only 0.98 and 0.83 cm in the horizontal and vertical directions, respectively, which suggests that position reproducibility of this SET station was on the order of a centimeter (**Figure 9A**).

A more thorough analysis of reproducibility was conducted by comparing three areas of hard substrate at the SET station 1 site: two rocks in the sand and the overlapping portion of the reef contained in both data sets (**Figure 10**). Comparing the raw SfM output from the two independent surveys reveals that the sandy areas had complex changes associated with the reorganization of the ripples, but that the reef area had more spatially consistent offsets of roughly 1–4 cm, which increased toward the northwest (**Figure 10A**). These offsets were reduced markedly with the three bias correction techniques, approaching values less than 1 cm (**Figures 10B–D**). The single-point bias correction continued to have a positive slope in the computed offset (**Figure 10B**), whereas the three-point correction techniques had limited slope in the offsets (**Figures 10C,D**).

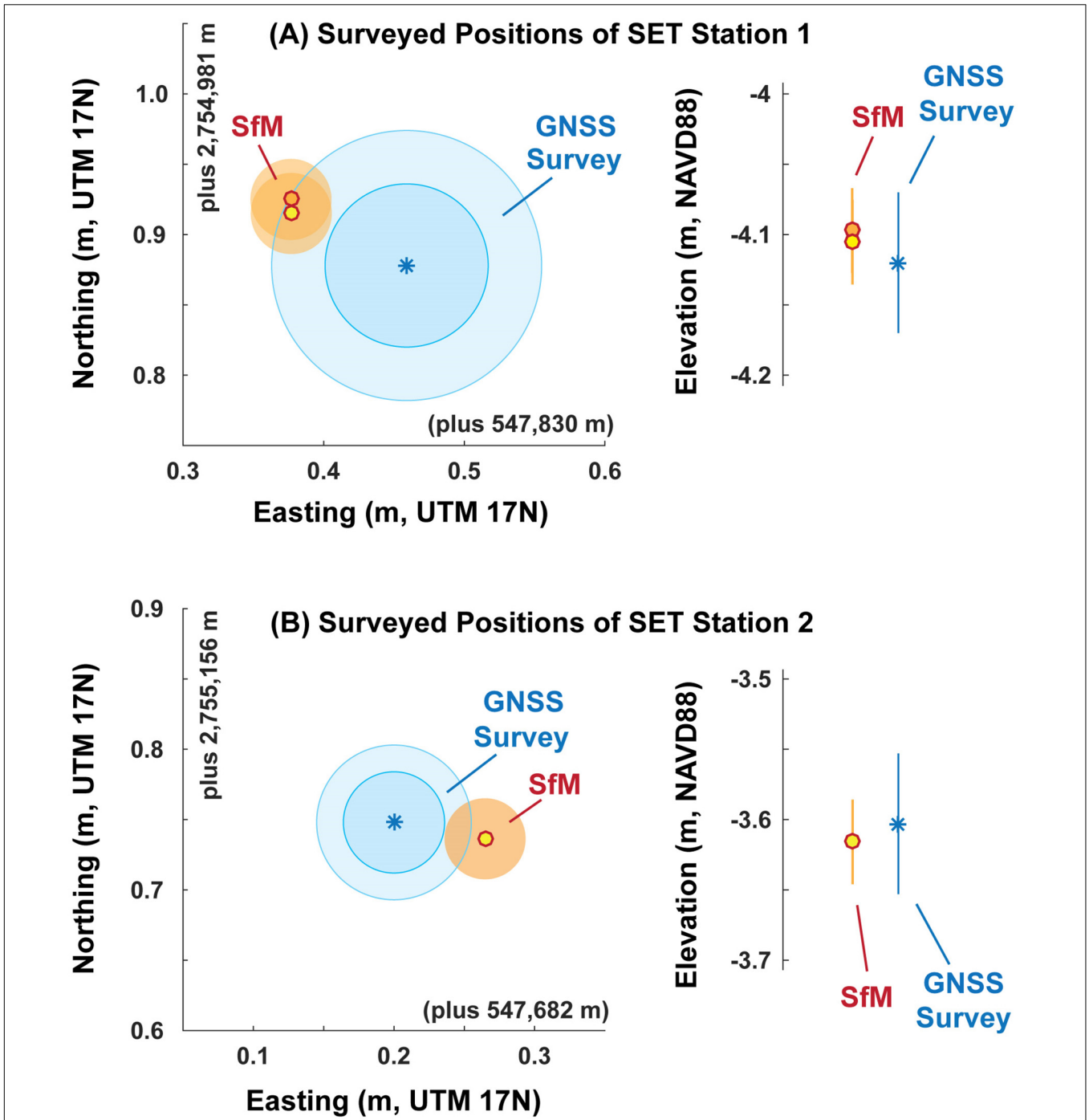

FIGURE 9 | Comparison of the measured positions of the Surface Elevation Table (SET) stations 1 and 2 (shown in **A,B** respectively) from field-based Global Navigation Satellite System (GNSS) and Structure-from-Motion (SfM) with the SQUID-5 system. Greater uncertainty exists for the GNSS measurements owing to the leveling techniques during scuba conditions, and both "reasonable" and "max" uncertainties are shown for the GNSS measurements (see **Table 1**). Uncertainty of the SfM measurements assumed to be 3 cm, which is equivalent to the approximate uncertainty of the survey-grade GNSS measurement.

A summary of the effect of the bias correction techniques shows that corrections dramatically reduced offsets between the two SfM surveys (**Figure 11**). For the raw SfM output, the mean difference of the three stationary areas ranged between 4 and 19 mm, and the variance of these differences ranged between 7 and 15 mm (**Figure 11**). The single-point bias correction shifted the overall errors closer to zero and brought variance to 4–8 mm. The smallest differences were measured for the two three-point correction techniques, which resulted in mean errors that

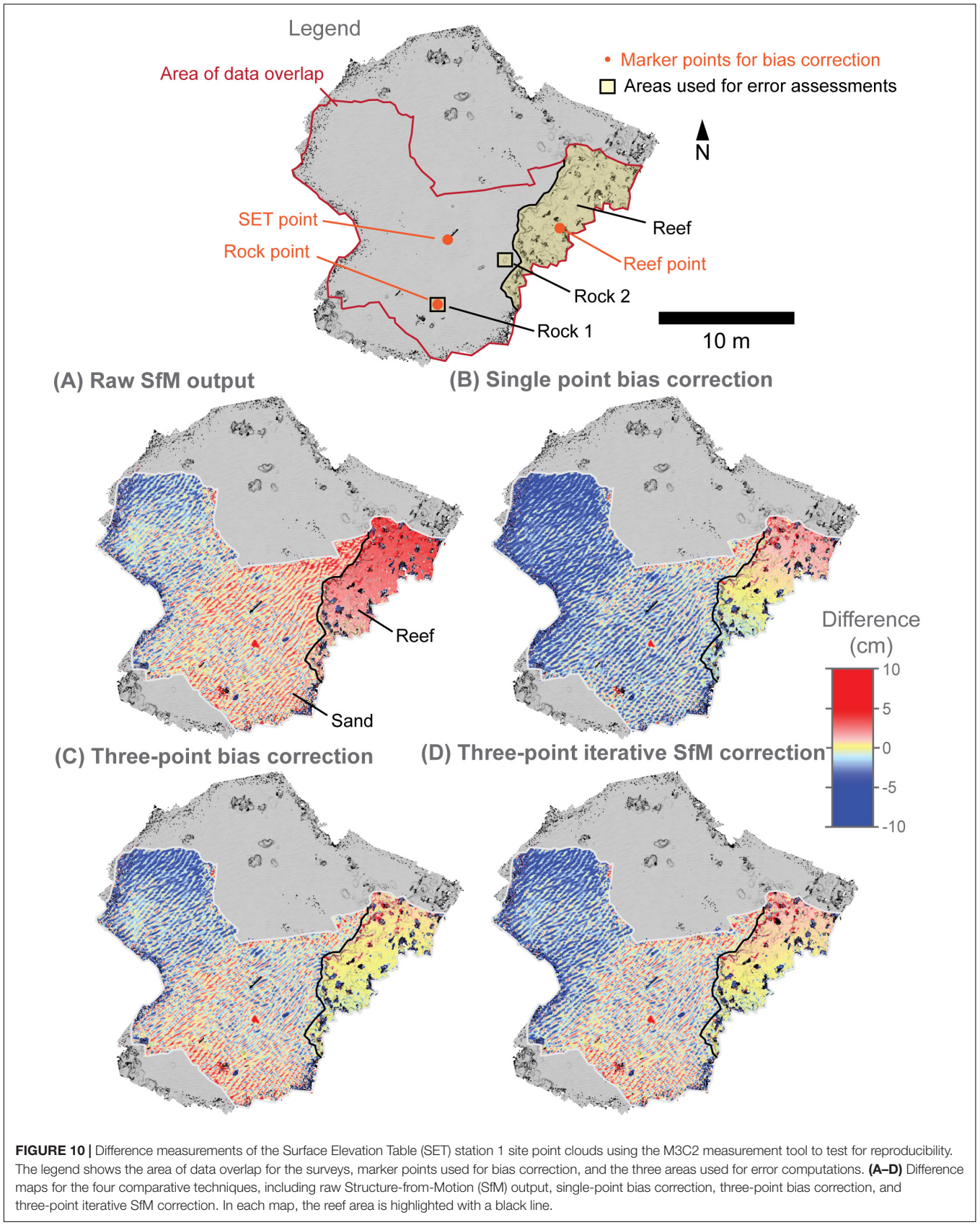

FIGURE 10 | Difference measurements of the Surface Elevation Table (SET) station 1 site point clouds using the M3C2 measurement tool to test for reproducibility. The legend shows the area of data overlap for the surveys, marker points used for bias correction, and the three areas used for error computations. **(A–D)** Difference maps for the four comparative techniques, including raw Structure-from-Motion (SfM) output, single-point bias correction, three-point bias correction, and three-point iterative SfM correction. In each map, the reef area is highlighted with a black line.

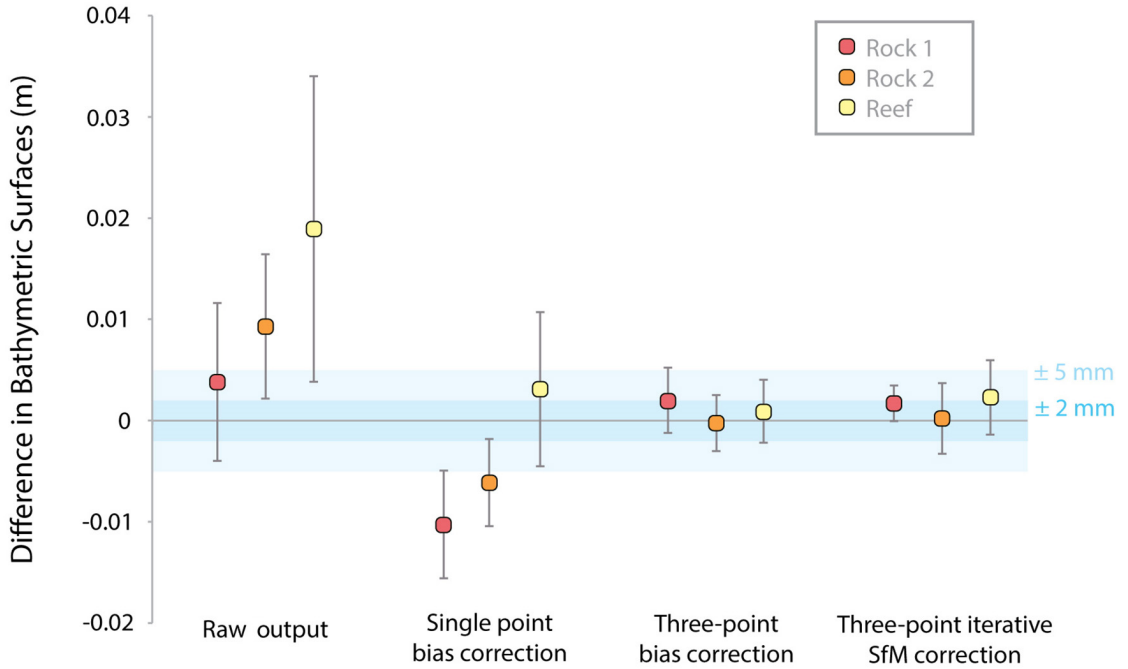

FIGURE 11 | Summaries of the differences in stationary objects at the Surface Elevation Table (SET) station 1 site during the two surveys. Three different objects were used for measurements, the locations of which are shown in **Figure 10**, and four comparative techniques were used as detailed in the text. Differences computed from M3C2 measurements of the point clouds, and the mean and standard deviation of the measurements are shown with the point and error bars, respectively. Shading highlights differences that are ± 5 mm and ± 2 mm.

were consistently within 2 mm and variances that were 2–4 mm (**Figure 11**).

An example of the differences for the three-point bias correction technique is shown for a 2 m by 0.4 m transect of the SET station 1 reef that is complex and greater than 1 m away from the reef marker point (**Figure 12**). The shaded-relief bathymetries from the two surveys are quite similar, with an elevated region on the northern end that contains live coral and a depression near the southern end with some sand (**Figures 12A–C**). Differences in this bathymetry are generally low, with a mean and variance of 0.8 and 3.1 mm, respectively (**Figures 12D,E**). Differences in excess of several millimeters are apparent in a few locations, including an area with plausible actual change resulting from sand movement and two areas with overhangs that were reconstructed differently by the SfM algorithms but likely had no actual change (**Figure 12D**). This subset of the reef reveals that repeatability can be achieved with an uncertainty of a few millimeters for reef tops and flats, but that uncertainty increases in difficult to measure areas, such as overhangs.

DISCUSSION

A multi-camera SfM system was successfully developed and used for surveying benthic habitat of the Florida Keys, resulting in millimeter-scale resolution, ∼0.01% linear measurement uncertainty as a function of depth, and mm-to-cm scale positional accuracy, all without any independent, pre-existing ground control. Synchronization between the SfM cameras and the survey-grade GNSS allowed for detailed three-dimensional point clouds of reefs and surrounding areas that were confirmed to be accurate using linear scales, three-dimensional positions, and repeatability of mapped surfaces. Over live coral heads, the resulting SfM point clouds were dense and uniform except on steep or overhanging surfaces, where data densities dropped and became noisy (**Figure 7**). Combined, these capabilities will allow for highly accurate measurements of change on the tops and exposed sides of corals, rock outcrops, or other benthic structures, but less accurate measurements within steep to overhanging sides and edges of these features.

Repeatability of the mapping output was improved greatly with the addition of markers to remove biases from the raw SfM output (**Figure 11**). Because many benthic settings, such as coral reefs, are continually changing with time from growth and degradation, stationary marker points should be installed and used at future mapping sites to achieve millimeter-scale change detection over annual to decadal scales. These markers do not need to be surveyed – position and scale information for the SfM products can be derived from the tightly coupled survey-grade GNSS data – but the markers must be stationary through time and easily identified in photos. Multiple markers provide significant benefits over single markers, as shown by the differences between single-point and three-point corrections (**Figures 11**, **12**). The SET stations, with their potential to incorporate installation of

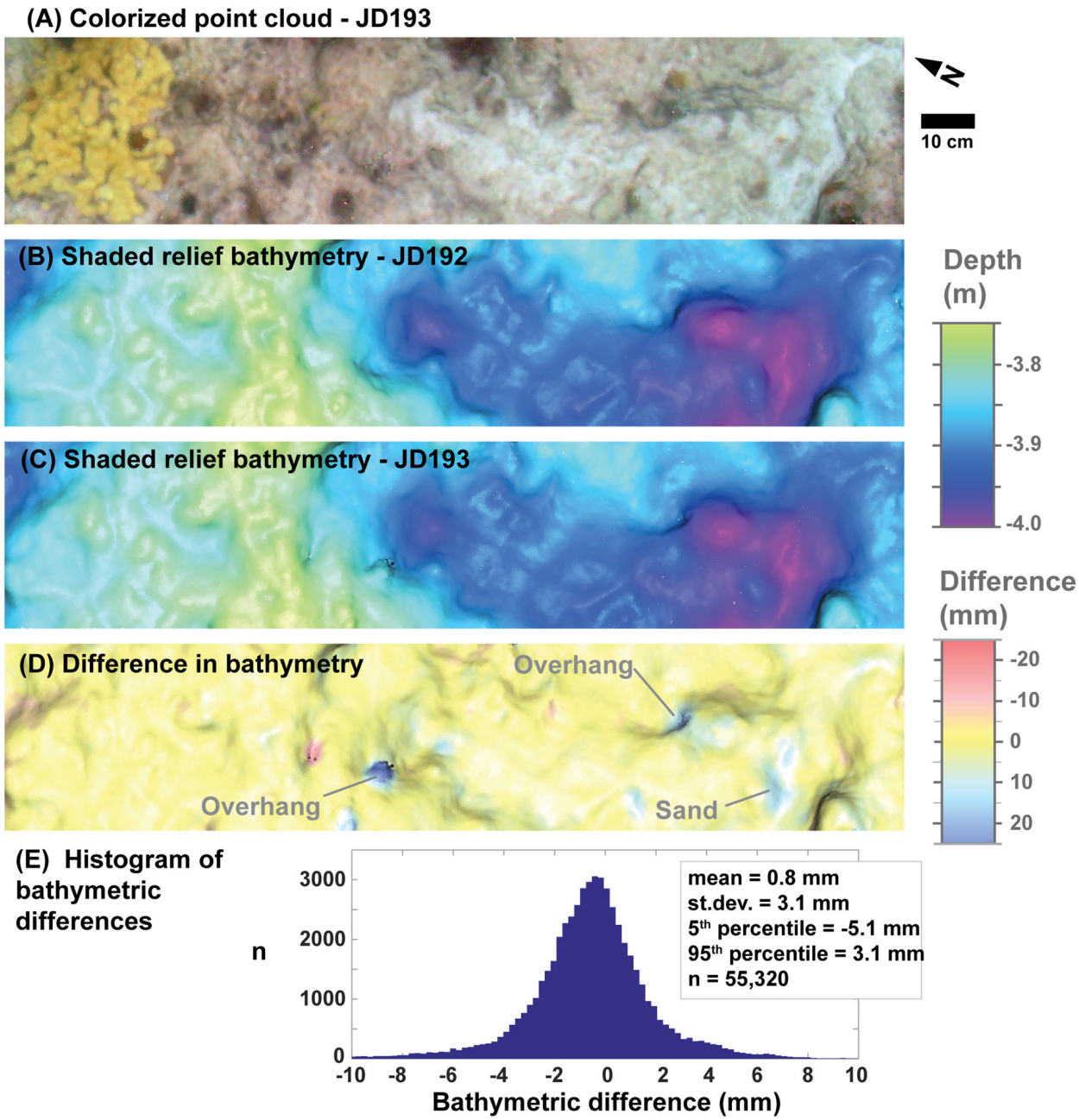

FIGURE 12 | Survey-to-survey differences for a 2 m by 0.4 m section of the Surface Elevation Table (SET) station 1 site reef chosen for its spatial complexity and lack of bryozoans. Location of this inset is shown in **Figure 8**. **(A)** True color map of the point cloud showing live coral on the northern end of the transect and a depression with sand on the southern end. **(B,C)** Shaded relief of the bathymetric point clouds. **(D)** Difference between the two point clouds using the M3C2 measurement tool. Features with the greatest difference values are highlighted and described. **(E)** A histogram of the M3C2 difference measurements for this transect, including summary statistics of the distribution.

circular encoded targets, provide a good example of marker stations for future SfM studies (**Figures 1D,E**). Without markers, change measurements using the SQUID-5 system will only be resolvable to several centimeters, which is ultimately related to the GNSS positional accuracy of the system (**Figure 11**).

These results exceeded previous accuracies and change detection limits reported by other SfM mapping efforts of shallow benthic settings. For example, Neyer et al. (2018) achieved centimeter to multiple-centimeter accuracy in their SfM change detection analyses for a coral reef in Moorea from SCUBA divers with handheld cameras, but only with a multitude of ground

control points that required field work that was "exhausting and time-consuming." Other studies have achieved multiple-centimeter to decimeter change detection limits using ground control, which can adequately detect massive loss resulting from storm events or other impacts that exceed several centimeters to decimeters (e.g., Burns et al., 2016; Magel et al., 2019), but will not be adequate to measure slower rates of coral growth or erosion. Many of the previous techniques have used co-registration techniques, such as the iterative closest point (ICP) registration method to co-align two or more SfM point clouds (Burns et al., 2015; Neyer et al., 2018; Magel et al., 2019). While the ICP algorithms provide good registration results, these methods also assume no change has occurred between surveys in an area of interest. These are commonly good assumptions over time scales that coral growth, reef erosion, or sediment transport are insignificant, but the ICP techniques will prove inadequate for longer time scales, such as years to decades, during which the entire reef structure might change from organism growth or substrate erosion. As such, surveying and registration techniques that allow for wholesale changes of the reef will be needed, and the examples provided here using the SQUID-5 system provide models for these efforts.

Although we were successful in measuring multiple shallow reef settings, our results with SQUID-5 were limited by factors that make underwater SfM analyses universally challenging (Neyer et al., 2018; Raber and Schill, 2019). For example, results were functionally and quantitatively dependent on sea state, water clarity, and ambient lighting conditions, which must be good but not, necessarily, perfect. Additionally, the SQUID-5 system required specialized computer equipment and the capability to manage, store, and process very large volumes of data. This was achieved with a small support vessel towing the SQUID-5, which confined mapping operations to settings where a small vessel could be safely navigated while towing. For these reasons, a more compact and autonomous system could make the methodology proven by SQUID-5 suitable for a wider diversity of applications (Raber and Schill, 2019).

Several additional improvements and developments could make the SQUID-5 system more useful. For example, deeper water operations may be possible by combining the SQUID-5 towed surface vehicle imagery with unregistered imagery collected concurrently via diver or deep towed camera systems. This approach potentially could result in georeferenced SfM products with millimeter-scale resolution and accuracies at depths that exceed 10 m. Additionally, color corrections in the original imagery or in the orthomosaic products based on depth and distance information, using machine learning (Akkaynak and Treibitz, 2019), could aid species identification and characterization. The SfM products shown in this work exhibit somewhat unnatural coloration due to the absorption properties of seawater and an incorrect white balance setting on the cameras during the fieldwork. However, subtle color differences of features are easily discernible and with the appropriate white balance adjustment and color correction algorithms we will be able to use color as an additional tool for species and feature identification with SQUID-5 in future work. Problems with wave focused ambient light could be reduced or eliminated through the addition of synchronized strobes, especially for nighttime operations.

CONCLUSION

Benthic studies of the seafloor and ecosystems, such as coral reefs, have been fundamentally improved with recent developments in underwater SfM photogrammetry (Magel et al., 2019). Here we describe significant improvements to these techniques through the development of a closely synchronous, multi-camera system with survey-grade GNSS. The SQUID-5 system produces high-resolution SfM point clouds and associated products with highly accurate scaling and positioning without the need for independently surveyed or scaled ground control. The Florida Keys case study illustrates that advancements achieved by the SQUID-5 in imagery quality and precise geolocation allow for efficient mapping and surficial seabed change detection (on the scale of millimeters to centimeters) and at the same time eliminate much of the labor-intensive requirement of field operations to install and survey ground control.

DATA AVAILABILITY STATEMENT

The datasets generated for this study can be found in the publicly accessible repository https://doi.org/10.5066/P9V7K7EG.

AUTHOR CONTRIBUTIONS

GH led the engineering, bench testing, and fabrication of SQUID-5 hardware, electronics and control software, compiled co-author input, was responsible the majority of text concerning system development and field operations, and wrote the **Supplementary Material**. JW contributed most of the text detailing data analysis and describing the results. JW and AR created the SfM workflow, created the SfM data products, and the error analysis. AR and CK were responsible for preliminary in-the-field SfM processing used for data quality assessment and guiding the fieldwork. ED created the real-time data acquisition quality control python scripts. CK was responsible for all the GNSS data corrections including establishing the temporary base station and PPK post processing. CK contributed the GNSS processing description to the manuscript. DZ and KY have established long-term fieldwork experiments currently operating in the area of this fieldwork and so provided expert guidance during experimental design, planning and operations, contributed to the text describing field site characteristics, and provided the invaluable contributions from the perspective of coral reef scientists during manuscript revisions. GH, AR, ED, DZ, CK, and KY were all critical participants in the fieldwork operation. All authors contributed to the article and approved the submitted version.

FUNDING

Funding has been provided by the following U.S. Geological Survey sources: (1) The Coastal and Marine Hazards and

Resources Program through the Remote Sensing Coastal Change project; (2) The Ecosystem Processes Impacting Coastal Change Project; and (3) The Hurricane and Wildfire Supplemental Task.

ACKNOWLEDGMENTS

Any use of trade, firm, or product names is for descriptive purposes only and does not imply endorsement by the U.S. Government. We would like to thank the other members of the USGS fieldwork team Mitchell Lemon, Zachery Fehr, and Hunter Wilcox for their invaluable boat handling and diving assistance during the Florida fieldwork. We thank USGS Summer Intern Emily Regan for her unyielding enthusiasm and assistance during early prototype development, construction and testing and Andrew Pomeroy (University of Western Australia) for assistance with proof of concept validation. Finally, we also thank personnel on the US Coast Guard Station Islamorada for providing secure boat launch and docking facilities and The Florida Keys National Marine Sanctuary for approving the permits required to conduct this fieldwork.

SUPPLEMENTARY MATERIAL

The Supplementary Material for this article can be found online at: https://www.frontiersin.org/articles/10.3389/fmars.2020.00525/full#supplementary-material

REFERENCES

Agrafiotis, P., Skarlatos, D., Forbes, T., Poullis, C., Skamantzari, M., and Georgopoulos, A. (2018). "Underwater photogrammetry in very shallow waters: main challenges and caustics effect removal," in *ISPRS - International Archives of the Photogrammetry, Remote Sensing and Spatial Information Sciences (Copernicus GmbH)*, (Heipke: ISPRS), 15–22. doi: 10.5194/isprs-archives-XLII-2-15-2018

Akkaynak, D., and Treibitz, T. (2019). "Sea-Thru: a method for removing water from underwater images," in *Proceedings / CVPR, IEEE Computer Society Conference on Computer Vision and Pattern Recognition. IEEE Computer Society Conference on Computer Vision and Pattern Recognition*, Long Beach, CA, 1682–1691.

Allahyari, M., Olsen, M., Gillins, D., and Dennis, M. (2018). Tale of two RTNs: Rigorous evaluation of real-time network GNSS observations. *J. Surv. Eng.* 144:5018001. doi: 10.1061/(ASCE)SU.1943-5428.0000249

Burns, J. H. R., Delparte, D., Gates, R. D., and Takabayashi, M. (2015). Integrating structure-from-motion photogrammetry with geospatial software as a novel technique for quantifying 3D ecological characteristics of coral reefs. *PeerJ* 3:e1077. doi: 10.7717/peerj.1077

Burns, J. H. R., Delparte, D., Kapono, L., Belt, M., Gates, R. D., and Takabayashi, M. (2016). Assessing the impact of acute disturbances on the structure and composition of a coral community using innovative 3D reconstruction techniques. *Methods Oceanogr.* 15–16, 49–59. doi: 10.1016/j.mio.2016.04.001

Casella, E., Collin, A., Harris, D., Ferse, S., Bejarano, S., Parravicini, V., et al. (2017). Mapping coral reefs using consumer-grade drones and structure from motion photogrammetry techniques. *Coral Reefs* 36, 269–275. doi: 10.1007/s00338-016-1522-0

Chirayath, V., and Earle, S. A. (2016). Drones that see through waves – preliminary results from airborne fluid lensing for centimetre-scale aquatic conservation. *Aqu. Conserv.* 26, 237–250. doi: 10.1002/aqc.2654

Chirayath, V., and Instrella, R. (2019). Fluid lensing and machine learning for centimeter-resolution airborne assessment of coral reefs in American Samoa. *Remote Sens. Environ.* 235, 111475. doi: 10.1016/j.rse.2019.111475

Cocito, S., Sgorbini, S., Peirano, A., and Valle, M. (2003). 3-D reconstruction of biological objects using underwater video technique and image processing. *J. Exp. Mar. Biol. Ecol.* 297, 57–70. doi: 10.1016/S0022-0981(03)00369-1

Edinger, E. N., Jompa, J., Limmon, G. V., Widjatmoko, W., and Risk, M. J. (1998). Reef degradation and coral biodiversity in Indonesia: Effects of land-based pollution, destructive fishing practices and changes over time. *Mar. Pollut. Bull.* 36, 617–630. doi: 10.1016/S0025-326X(98)00047-2

Ferrari, R., Figueira, W. F., Pratchett, M. S., Boube, T., Adam, A., Kobelkowsky-Vidrio, T., et al. (2017). 3D photogrammetry quantifies growth and external erosion of individual coral colonies and skeletons. *Sci. Rep.* 7, 1–9. doi: 10.1038/s41598-017-16408-z

Fonstad, M. A., Dietrich, J. T., Courville, B. C., Jensen, J. L., and Carbonneau, P. E. (2013). Topographic structure from motion: a new development in photogrammetric measurement. *Earth Surf. Process. Landf.* 38, 421–430. doi: 10.1002/esp.3366

House, J. E., Brambilla, V., Bidaut, L. M., Christie, A. P., Pizarro, O., Madin, J. S., et al. (2018). Moving to 3D: relationships between coral planar area, surface area and volume. *PeerJ* 6:e4280. doi: 10.7717/peerj.4280

Hughes, T. P. (1994). Catastrophes, phase shifts, and large-scale degradation of a caribbean coral reef. *Science* 265, 1547–1551. doi: 10.1126/science.265.5178.1547

Kleypas, J. A., and Yates, K. K. (2009). Coral reefs and ocean acidification. *Oceanography* 22, 108–117. doi: 10.5670/oceanog.2009.101

Kuffner, I. B., Toth, L. T., Hudson, J. H., Goodwin, W. B., Stathakopoulos, A., Bartlett, L. A., et al. (2019). Improving estimates of coral reef construction and erosion with in situ measurements. *Limnol. Oceanogr.* 64, 2283–2294. doi: 10.1002/lno.11184

Lague, D., Brodu, N., and Leroux, J. (2013). Accurate 3D comparison of complex topography with terrestrial laser scanner: Application to the Rangitikei canyon (NZ). *ISPRS J. Photogram. Remote Sens.* 82, 10–26. doi: 10.1016/j.isprsjprs.2013.04.009

Leon, J. X., Roelfsema, C. M., Saunders, M. I., and Phinn, S. R. (2015). Measuring coral reef terrain roughness using 'Structure-from-Motion' close-range photogrammetry. *Geomorphology* 242, 21–28. doi: 10.1016/j.geomorph.2015.01.030

Li, R., Li, H., Zou, W., Smith, R. G., and Curran, T. A. (1997). Quantitative photogrammetric analysis of digital underwater video imagery. *IEEE J. Oceanic Eng.* 22, 364–375. doi: 10.1109/48.585955

Lidz, B. H., Brock, J. C., and Nagle, D. B. (2008). Utility of Shallow-Water ATRIS Images in Defining Biogeologic Processes and Self-Similarity in Skeletal Scleractinia, Florida Reefs. *J. Coast. Res.* 245, 1320–1330. doi: 10.2112/08-1049.1

Lynch, J., Hensel, P., and Cahoon, D. R. (2015). *The Surface Elevation Table and Marker Horizon Technique: A Protocol for Monitoring Wetland Elevation Dynamics*. Reston, VA: USGS.

Magel, J. M. T., Burns, J. H. R., Gates, R. D., and Baum, J. K. (2019). Effects of bleaching-associated mass coral mortality on reef structural complexity across a gradient of local disturbance. *Sci. Rep.* 9, 1–12. doi: 10.1038/s41598-018-37713-1

Massot-Campos, M., and Oliver-Codina, G. (2015). Optical sensors and methods for underwater 3D reconstruction. *Sensors* 15, 31525–31557. doi: 10.3390/s151229864

Matthews, N. (2008). *Aerial and Close-Range Photogrammetric Technology: Providing Resource Documentation, Interpretation, and Preservation*. Washington, D.C: U.S. Department of the Interior, Bureau of Land Management.

Menna, F., Nocerino, E., Fassi, F., and Remondino, F. (2016). Geometric and Optic Characterization of a Hemispherical Dome Port for Underwater Photogrammetry. *Sensors* 16:48. doi: 10.3390/s16010048

Newman, K. J. (2008). Trends for digital aerial mapping cameras. *Int. Arch. Photogram. Rem. Sens. Spatial. Info Sci.* 28, 551–554.

Neyer, F., Nocerino, E., and Gruen, A. (2018). Monitoring Coral Growth: The Dichotomy Between Underwater Photogrammetry and Geodetic Control

Network. *Int. Arch. Photogramm. Remote Sens. Spatial Inf. Sci.* 2, 759–766. doi: 10.5194/isprs-archives-XLII-2-759-2018

Nocerino, E., Menna, F., Fassi, F., and Remondino, F. (2016). Underwater Calibration of Dome Port Pressure Housings. *ISPRS Int. Arch. Photogram. Rem. Sens. Spat. Inform. Sci.* 34, 127–134. doi: 10.5194/isprs-archives-XL-3-W4-127-2016

Pizarro, O., Friedman, A., Bryson, M., Williams, S. B., and Madin, J. (2017). A simple, fast, and repeatable survey method for underwater visual 3D benthic mapping and monitoring. *Ecol. Evol.* 7, 1770–1782. doi: 10.1002/ece3.2701

Pomeroy, A., Storlazzi, C. D., Rosenberger, K. J., Hatcher, G., and Warrick, J. A. (2019). Integrating structure from motion, numerical modelling and field measurements to understand carbonate sediment transport in coral reef canopies. *Proc. Coast. Sediments* 2019, 959–969. doi: 10.1142/9789811204487_0083

Price, D. M., Robert, K., Callaway, A., Lo Iacono, C., Hall, R. A., and Huvenne, V. A. I (2019). Using 3D photogrammetry from ROV video to quantify cold-water coral reef structural complexity and investigate its influence on biodiversity and community assemblage. *Coral Reefs* 38, 1007–1021. doi: 10.1007/s00338-019-01827-3

Prouty, N. G., Cohen, A., Yates, K. K., Storlazzi, C. D., Swarzenski, P. W., and White, D. (2017). Vulnerability of coral reefs to bioerosion from land-based sources of pollution. *J. Geophys. Res.* 122, 9319–9331. doi: 10.1002/2017JC013264

Raber, G. T., and Schill, S. R. (2019). Reef rover: a low-cost small autonomous unmanned surface vehicle (usv) for mapping and monitoring coral reefs. *Drones* 3:38. doi: 10.3390/drones3020038

Raoult, V., David, P. A., Dupont, S. F., Mathewson, C. P., O'Neill, S. J., Powell, N. N., et al. (2016). GoProsTM as an underwater photogrammetry tool for citizen science. *PeerJ* 4:e1960. doi: 10.7717/peerj.1960

Raoult, V., Reid-Anderson, S., Ferri, A., and Williamson, J. E. (2017). How reliable is structure from motion (sfm) over time and between observers? A case study using coral reef bommies. *Remote Sens.* 9:740. doi: 10.3390/rs9070740

Rogers, J. S., Maticka, S. A., Chirayath, V., Woodson, C. B., Alonso, J. J., and Monismith, S. G. (2018). Connecting Flow over Complex Terrain to Hydrodynamic Roughness on a Coral Reef. *J. Phys. Oceanogr.* 48, 1567–1587. doi: 10.1175/JPO-D-18-0013.1

Storlazzi, C. D., Dartnell, P., Hatcher, G. A., and Gibbs, A. E. (2016). End of the chain? Rugosity and fine-scale bathymetry from existing underwater digital imagery using structure-from-motion (SfM) technology. *Coral Reefs* 35, 889–894. doi: 10.1007/s00338-016-1462-8

Storlazzi, C. D., Elias, E. P. L., and Berkowitz, P. (2015). Many atolls may be uninhabitable within decades due to climate change. *Scie. Rep.* 5:14546. doi: 10.1038/srep14546

Takesue, R. K., and Storlazzi, C. D. (2019). Geochemical sourcing of runoff from a young volcanic watershed to an impacted coral reef in Pelekane Bay. Hawaii. *Sci. Total Environ.* 649, 353–363. doi: 10.1016/j.scitotenv.2018.08.282

Toth, L. T., Aronson, R. B., Cobb, K. M., Cheng, H., Edwards, R. L., Grothe, P. R., et al. (2015). Climatic and biotic thresholds of coral-reef shutdown. *Nat. Clim. Change* 5, 369–374. doi: 10.1038/nclimate2541

Ullman, S. (1979). The interpretation of structure from motion. *Proc. R. Soc. Lond. B. Biol. Sci.* 203, 405–426. doi: 10.1098/rspb.1979.0006

Warrick, J. A., Ritchie, A. C., Adelman, G., Adelman, K., and Limber, P. W. (2017). New Techniques to Measure Cliff Change from Historical Oblique Aerial Photographs and Structure-from-Motion Photogrammetry. *J. Coast. Res.* 331, 39–55. doi: 10.2112/JCOASTRES-D-16-00095.1

Warrick, J. A., Ritchie, A. C., Dailey, E. T., Hatcher, G. A., Kranenburg, C., Zawada, D. G., et al. (2020). *SQUID-5 Structure-From-Motion Point Clouds, Bathymetric Maps, Orthomosaics, and Underwater Photos of Coral Reefs in Florida, 2019. U.S. Geological Survey data Release*. Reston, VA: USGS, doi: 10.5066/P9V7K7EG

Westoby, M. J., Brasington, J., Glasser, N. F., Hambrey, M. J., and Reynolds, J. M. (2012). 'Structure-from-Motion' photogrammetry: A low-cost, effective tool for geoscience applications. *Geomorphology* 179, 300–314. doi: 10.1016/j.geomorph.2012.08.021

Conflict of Interest: The authors declare that the research was conducted in the absence of any commercial or financial relationships that could be construed as a potential conflict of interest.

frontiers in Marine Science

ORIGINAL RESEARCH
published: 11 February 2021
doi: 10.3389/fmars.2021.631842

Abiotic and Human Drivers of Reef Habitat Complexity Throughout the Main Hawaiian Islands

Gregory P. Asner, Nicholas R. Vaughn, Shawna A. Foo, Ethan Shafron, Joseph Heckler and Roberta E. Martin*

Center for Global Discovery and Conservation Science, Arizona State University, Tempe, AZ, United States

Reef rugosity, a metric of three-dimensional habitat complexity, is a central determinant of reef condition and multi-trophic occupancy including corals, fishes and invertebrates. As a result, spatially explicit information on reef rugosity is needed for conservation and management activities ranging from fisheries to coral protection and restoration. Across archipelagos comprising islands of varying geologic stage and age, rugosity naturally varies at multiple spatial scales based on island emergence, subsidence, and erosion. Reef rugosity may also be changing due to human impacts on corals such as marine heatwaves and nearshore coastal development. Using a new high-resolution, large-area mapping technique based on airborne imaging spectroscopy, we mapped the rugosity of reefs to 22 m depth throughout the eight Main Hawaiian Islands. We quantified inter- and intra-island variation in reef rugosity at fine (2 m) and coarse (6 m) spatial resolutions, and tested potential abiotic and human drivers of rugosity patterns. We found that water depth and reef slope remain the dominant drivers of fine- and coarse-scale rugosity, but nearshore development is a secondary driver of rugosity. Our results and maps can be used by fisheries management and reef conservations to track geologic versus human impacts on reefs, design effective marine managed areas, and execute activities to improve reef resilience.

Keywords: bathymetry, coral reef, Hawai'i, imaging spectroscopy, reef structure, rugosity

OPEN ACCESS

Edited by:
Javier Xavier Leon, University of the Sunshine Coast, Australia

Reviewed by:
Xinming Lei, South China Sea Institute of Oceanology (CAS), China
Kostantinos Stamoulis, Seascape Solutions, United States

****Correspondence:***
Gregory P. Asner
gregasner@asu.edu

Specialty section:
This article was submitted to Coral Reef Research, a section of the journal Frontiers in Marine Science

Received: *21 November 2020*
Accepted: *22 January 2021*
Published: *11 February 2021*

Citation:
Asner GP, Vaughn NR, Foo SA, Shafron E, Heckler J and Martin RE (2021) Abiotic and Human Drivers of Reef Habitat Complexity Throughout the Main Hawaiian Islands. Front. Mar. Sci. 8:631842. doi: 10.3389/fmars.2021.631842

INTRODUCTION

Habitat complexity is the three-dimensional (3D) structure of the physical environment with which organisms interact and is a key influencer of the distribution of marine biota. Habitat complexity can affect a variety of ecological functions such as by providing prey protection from predators, surfaces for coral settlement and growth, and different microhabitats to support a variety of species. Habitat complexity interacts with other environmental factors such as light, temperature and wave action to generate a wide range of ecological conditions (Sebens, 1991).

On coral reefs, 3D habitat complexity is a determinant of reef fish assemblages, where fish abundance, biomass, and richness are often positively correlated with complexity (Cinner et al., 2009; Graham et al., 2009). Yet the direction and strength of this relationship does vary, and studies can also show mixed connectivity between reef complexity and fish stocks (Jennings et al., 1996; Harborne et al., 2012). Coral cover is also often positively correlated with reef complexity (Alvarez-Filip et al., 2009; Graham and Nash, 2012). Correspondingly, negative relationships between

complexity and algal cover often exist, perhaps indirectly reflecting the role of reef complexity in predicting reef fish and resulting herbivory (Graham and Nash, 2012). However, 3D habitat complexity is not only driven by coral cover, but also by benthic geomorphology at a range of scales from small boulder and erosion-deposition zones to large subsurface geologic structures.

The Main Hawaiian Islands (MHIs) are an important case-in-point, varying widely in geologic age from less than a few years old on Hawai'i Island to more than six million years old on Ni'ihau (Neall and Trewick, 2008). Island age is accompanied by stage of accretion and subsidence, processes that generate enormous inter- and intra-island variation in reef extent associated with benthic substrate availability (Asner et al., 2020b). Younger islands such as Hawai'i contain vast fringing reefs dominated by rock substrates (i.e., lava beds, massive boulders, rock fields) that define much of the reef rugosity, but with embayments and coves co-dominated by geology and coral growth. In contrast, older islands such as Kaua'i and O'ahu contain reefs defined by geologic subsidence and erosional surfaces, with broad expanses of both sandy bottom and calcareous reef substrate.

Overlain on this geologic template, water motion and light penetration decrease with increasing depth, and wave-sheltered areas show the greatest Holocene reef accretion (Grigg, 1998). Generally, optimal reef growth occurs between 10 and 20 m depth in the MHI, reflecting a trade-off between wave-induced stress and decreased light availability (Storlazzi et al., 2005). In areas of greatest wave power, turf algae and crustose coralline algae dominate due to more wave-tolerant, flatter morphologies. On the other hand, low wave power regions are dominated by hard corals and macroalgae with structures more vulnerable to dislodgement (Engelen et al., 2005; Madin et al., 2014; Gove et al., 2015).

Reef complexity varies over multiple spatial scales (Mumby et al., 2004). Measurements of complexity aim to quantify the vertical variation of the benthic surface in relation to the two-dimensional (2D) surface of the same area, and therefore complexity metrics are dependent upon the resolution of the mapping technique. Larger grid or pixel sizes of bathymetric maps result in complexity values describing broader geological features in comparison to smaller pixel sizes that represent specific coral colonies, rock outcrops and other fine-scale features. Presently, the spatial scale at which biophysical drivers influence fish or invertebrate assemblages is poorly known (Purkis et al., 2008; Aston et al., 2019), and a multi-scale assessment of reef complexity would improve our understanding of habitat across a range of scales relevant to a wide range of ecological processes (Harborne et al., 2006; Williams et al., 2015).

Over the past several decades, there has been a rapid increase in the diversity of methods used to quantify 3D habitat complexity, where various techniques are aimed at quantifying complexity at specific scales and spatial resolutions. Studies focusing on colony-level measures most commonly use a chain-and-tape method to estimate rugosity, an index of habitat complexity. Rugosity is estimated by calculating the ratio of chain length laid across the bottom reef profile to the linear distance of the transect (Risk, 1972). Complexity has also been estimated visually by scoring a range of structural variables (Gratwicke and Speight, 2005). Modern methods of assessing habitat complexity include 3D computer models, which are generated from images via structure-from-motion photogrammetry, allowing quantification of complexity metrics such as surface rugosity among fractal dimension, total surface area and surface height (Burns et al., 2015; Figueira et al., 2015). Field techniques, however, can be time-consuming and typically operate over limited areas (<0.25 ha; Lechene et al., 2019).

Remote sensing methods–primarily acoustic imaging and light detection and ranging (LiDAR)–have allowed estimations of reef complexity over areas of much greater extent. More than 50 years ago, sound navigation and ranging (SONAR) revolutionized reef mapping over large areas by providing moderate resolution information (Moravec and Elfes, 1985). Subsequent LiDAR-derived rugosity measures of reef at 4–5 m spatial resolution have been correlated with *in situ* measures of reef rugosity (Wedding et al., 2008). However, measurements of habitat complexity coarser than 10 m did not show significant relationships with *in situ* rugosity, but they still provided relevant information at broader geographic scales (Wedding et al., 2008). Similarly, reef rugosity estimated though acoustic methods showed relationships with fish at kernel sizes less than 40 m, with the most significant relationships with species richness at a resolution finer than 8 m (Purkis et al., 2008). More recently, airborne imaging spectroscopy has opened up access to large-area bathymetric and reef rugosity mapping at resolutions of 0.4 m (Asner et al., 2020a).

Throughout the Hawaiian Islands, it is not known how environmental and physical factors compare with human influences in shaping 3D habitat complexity (Wedding et al., 2018). Understanding controls over spatial patterns of complexity is relevant to creating effective marine managed areas, where planning can benefit fish assemblages, protect essential fish habit and enhance recruitment (Grober-Dunsmore et al., 2007). This is especially important for coastal communities that heavily rely on ecosystem services from reef fish populations. Furthermore, protecting locations with greater reef complexity should be a management priority as they have increased resilience to coral bleaching and enhanced recovery through larger fish populations (Graham and Nash, 2012; Rogers et al., 2014). Considering the wealth of research linking reef complexity and reef fish, rapid methods that can document rugosity at broader geographic scales are of great value. Here we use a new airborne mapping technique to report on how 3D habitat complexity varies at fine and coarse spatial resolutions within and between each Main Hawaiian Island. We undertook this study without a specific focus on live corals, which was largely covered in Asner et al. (2020b). In that earlier paper, we determined the geographic distribution of live corals, but we were unable to associate live coral cover broadly with rugosity due to extremes in island age, geologic stage, and erosional processes. As a result, in the present submission, we determined the geographic distribution of fine- and coarse-scale rugosity surfaces in order to assess on the relative importance of multiple abiotic environmental as well as

human factors potentially affecting reef complexity at intra- and inter-island scales.

MATERIALS AND METHODS

Bathymetric Mapping

Using data collected by the Global Airborne Observatory (Asner et al., 2012), we mapped benthic depth at 2 m spatial resolution throughout the eight MHI. We selected 2 m mapping resolution as a practical trade-off between time and cost of mapping the vast area of the MHI, while simultaneously achieving sufficient resolution to resolve fine-scale variation in reef structure that incorporates larger coral colonies and basaltic rock outcrops (see Asner et al., 2020a). The GAO collected data from multiple coaligned instruments, two of which were used for bathymetric and rugosity mapping: a high-fidelity visible-to-shortwave infrared (VSWIR) imaging spectrometer and a dual-beam LiDAR scanner (Asner et al., 2012). Data from the spectrometer were used to model benthic depth using the deep learning methodology described, tested and validated in Asner et al. (2020a).

The VSWIR spectrometer and LiDAR data were collected between January 2 and February 4, 2019. To maximize data consistency, daily airborne operations were performed from 0830 to 1100 local time. Collection location could change during each flight day and was actively managed based on need, cloud cover, and windspeeds to provide both the most efficient use of time and the best conditions for spectroscopic seafloor measurements. During flight, instrument settings were set for the planned nominal flight altitude of 2 km above the sea surface. Flightlines were spaced to achieve 50% overlap in VSWIR spectrometer coverage. Aircraft ground speed was 130–140 kt. LiDAR pulse frequency was set to 200 kHz (100 kHz per laser) and scan frequency was 34 Hz with a field of view of 38°, allowing 2° of buffer on each side of the spectrometer field of view of 34°, achieving a nominal pulse density of more than 4 pulses m^{-2}. The radiance data from the spectrometer are collected in 427 spectral channels covering the 350–2500 nm wavelength range in 5 nm increments. Using a modified version of the ATREM model (Gao and Goetz, 1990; Thompson et al., 2017), we retrieved ocean surface reflectance from the at-sensor radiance data. The reflectance data for each flight line were passed through the model described in Asner et al. (2020a) to retrieve estimated depth in meters after masking out problematic regions (clouds, waves, and regions of excessive solar glint) from the data. Because water absorbs nearly all infrared light, land surface objects were filtered from analysis using a reflectance threshold at the 890–910 nm wavelength.

Orthorectification of the spectrometer data was a multi-step process. During flight GPS timing data were collected during flight by both instruments, and this timing location was used to link the data to a precise flight trajectory built from corrected and interpolated data from the onboard positioning and orientation system (POS). With a LiDAR-derived digital surface model (DSM) and a known position and orientation of the sensor at each sample, the 3-dimensional position of each spectrometer pixel was ray-traced to the sea surface level. However, to accurately map the location of each pixel on the ocean floor, we needed to account for estimated depth (d) and the refraction of light at the ocean surface. For each pixel, observation angle from zenith at the water surface, ϕ_a, is known and with standard refractive indices of 1.33000 for water and 1.00029 for air, Snell's refraction formula can be used to compute the angle after crossing the water surface boundary as $\phi_b = \sin^{-1}(0.75210 \sin \phi_a)$. This angle can be traced down to the ocean floor to retrieve the 3-dimensional ocean floor location for each pixel.

We took advantage of the 50% overlap in flight lines to build smooth depth mosaics by reducing sharp transitions between flight lines. For each group of flight lines making up a single region of coastline, the process for mosaicking followed these steps:

(1) Record pixel id, flight line id, depth, and observation zenith angle for up to 5000 (randomly sampled, if more than 5000 are available) pixels that have overlapping flightlines.
(2) For each pixel id, compute the mean and range of measured depth across all overlapping flightlines in addition to the view zenith angle for each flightline.
(3) Compute the mean observation zenith angle for each flight line id and subtract this value from all angle values in the flight line (center the values at 0).
(4) Filter out pixel ids where range $>$ 5.0 m from analysis, as they are likely to be affected by noisy depth retrieval.
(5) For each flight line with valid pixels in overlap area, set up a linear regression with pixel mean depth as dependent variable and terms for intercept, line depth, and mean-centered line observation zenith angle. The fitted coefficients are saved for later use.
(6) Correct all pixel values for each flight line using the linear transformation from the regression fit.
(7) For each mosaic pixel id collect the corrected depths from all overlapping flight lines and compute mean depth.

This was done for each coastal region for each of Niʻihau (one region), Kauaʻi (four regions), Oʻahu (four regions), Molokaʻi, Lanaʻi, Kahoʻolawe (each one region), Maui (four regions), and Hawaiʻi (11 regions). These individual regions were then hand-mosaicked into whole-island maps of depth, with the exception of Hawaiʻi which was broken into four quadrants due to size limitations.

Multi-Resolution Rugosity

We computed island-wide maps of rugosity at two resolutions using the "planar" rugosity metric (Jenness, 2004) on the GAO benthic depth maps (**Figure 1**). Missing data of less than two pixels in width were filled using an inverse-distance weighted average of the three nearest neighboring pixels. Fine-scale rugosity was computed using a 3 $\times$ 3 pixel (6 $\times$ 6 m) moving window on the original 2 m resolution bathymetric maps (**Figure 1b**). This resolution seeks high frequency changes on the seafloor arising from coral colonies, rocks, and other bottom features that generate local habitat variability. Coarse-scale rugosity was computed by first down-sampling the 2 m depth

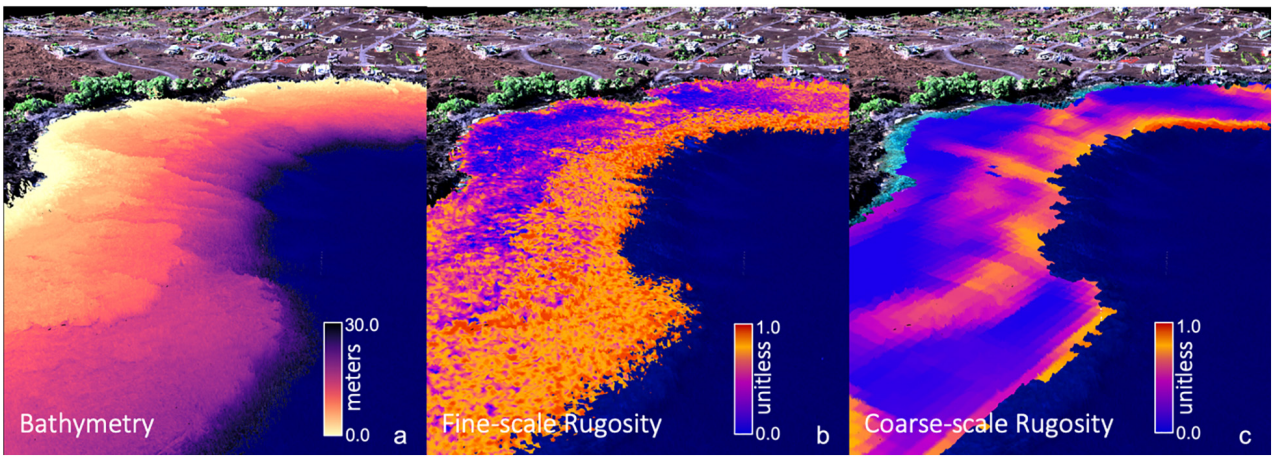

FIGURE 1 | Global Airborne Observatory (GAO) mapping of three-dimensional **(a)** reef bathymetry, **(b)** fine-scale rugosity, and **(c)** coarse-scale rugosity for an embayment along the coast of Hawai'i Island. Water depth and fine-scale rugosity were mapped at 2 m spatial resolution. Coarse-scale rugosity was mapped at 6 m resolution. Background provides 3D coastline terrain, vegetation and infrastructure as visual reference.

maps to 6 m resolution using a mean filter. The planar rugosity metric was then computed using a 9 × 9 pixel (54.0 × 54.0 m) moving window on the 6 m depth maps. Coarse-scale rugosity is responsive to variations in larger terrain features resulting from geologic, reef-scale accretion and subsidence processes. Previous testing at other resolutions indicated that a 9 × 9 pixel coarse-scale rugosity product gives the best detail for geologic features while removing fine-scale "noise" from corals and rock boulders (**Figure 1c**). These two resolutions of rugosity were computed for each of the individual island depth maps. Because the distribution of rugosity (r) is heavily skewed to the right because of occasional noise pixels, and the units of the output are not meaningful, we transformed raw rugosity values to have an approximate uniform [0,1] distribution T by sorting the n individual values across the map and assigning the value of transformed rugosity $T(r_i) = \frac{\text{float}(\text{rank}(r_i))}{n}$. Thus, for the island-scale fine and coarse rugosity maps, low transformed rugosity values will be near-zero, mid-range values will be near 0.5, and extreme values will never be more than 1.0.

Geospatial Analyses

We assessed the spatial patterning of fine and coarse rugosity both between and within the MHIs using empirical variograms. To overcome computer memory and time limits, we broke the rugosity maps for each island into a grid of 1 × 1 km cells, made up of 500 × 500 pixels for fine rugosity and 167 × 167 pixels for coarse rugosity. Because of the additive nature of the variogram variances, we could compute one for each island using sample-size weighted averages of the individual lag variances across grid cells into a single variogram. This methodology provided the additional benefit of generating information about the variation in spatial patterning within each island.

For each grid cell, the associated square region was extracted from the rugosity map along with a buffer of 500 m (250 pixels for fine-scale maps and 83 pixels for coarse-scale maps) on all sides. The empirical variogram for each grid cell was computed with the GeoStats package (Hoffimann, 2018) in the Julia programming language (Bezanson et al., 2012), using 40 lag steps and a maximum lag of 500 m. A variogram model was fit to the empirical variogram for each grid cell, with the fitting software iterating over eight model forms to find the optimal form as well as the associated optimal estimates for the model parameters: sill, nugget, and range parameters. By storing the sill, nugget, and range value for each parcel, we were able to aggregate these into a 1 × 1 km resolution map of each parameter for each island. The island-wide empirical variogram was computed as a weighted average of the variograms from all grid cells, where the weight for each cell was the number of valid rugosity observations separated by the given lag distance within that cell.

Land-Sea Driver Modeling

We used multiple land-sea environmental maps available for the MHI to assess the relative importance of environmental and human factors that may contribute to the mapped distribution of fine- and coarse-scale rugosity (**Table 1**). For example, reef depth, slope, and distance to coastline vary with island geologic stage, thereby affecting erosion, subsidence, and other factors known to shape larger benthic structures (Fletcher et al., 2008; Gove et al., 2015). Abiotic drivers also play a role in shaping rugosity, either via physical impacts of waves and wind action (Li et al., 2016), or via the impacts of temperature on calcareous organisms like corals that contribute to rugosity (Ignatov, 2010; Wedding et al., 2018). Finally, nearshore development may have an effect on reef rugosity via sedimentation and/or removal of reef structures (Center for International Earth Science Information Network-Ciesin, 2018). We checked for driver variable co-variance and utilized a combination of drivers each with less than 50% correlation.

While the GAO fine- and coarse-scale rugosity maps have a resolution of 2 and 6 m, respectively, many of the environmental maps in **Table 1** are provided only at resolutions of 30 m or

TABLE 1 | Summary statistics for the two mapped rugosity scales as well as 11 factors used in the land-sea driver modeling assessment.

Name	Units	Source	Minimum	Mean	Maximum	Std. Dev.
Fine-scale Rugosity	–	GAO (1–3)	0	0.5	1	0.29
Coarse-scale Rugosity	–	GAO (1–3)	0	0.5	1	0.29
Depth	m	GAO (1, 2)	0	7.5	19.7	4.6
Slope	–	GAO (1, 2)	−4.74	0	6.29	0.74
Distance from coast	M	HI DOP†	1	46.8	208.1	37.6
Average Windspeed	$m\ s^{-1}$	NOAA (13)	0.7	5.1	6.7	1.2
Windwardness	–	NOAA (13)	−1	0.05	1	0.67
Average Wave Power	$kW\ m^{-1}$	OTP (6, 7)	0	9.7	40.8	8.2
Maximum Wave Power	$kW\ m^{-1}$	OTP (6, 7)	0	54.1	350.6	61.9
Nearshore Development	–	OTP (6, 9)	0	0.04	1	0.08
Average SST	°C	OTP (6, 10)	25.1	25.4	26.1	0.2
Maximum SST	°C	OTP (6, 10)	26.1	27	28.3	0.4
Total Effluent	$gal\ km^{-2}\ d^{-1}$	OTP (6)	0	4962.4	118544.3	9957.8

These land-sea drivers were selected based on availability and known role in shaping geological and biological reef conditions. †From coastline data downloaded from the Hawai'i Department of Planning (https://planning.hawaii.gov/gis). GAO, global airborne observatory; OTP, ocean tipping points.

coarser. The GAO rugosity maps were therefore coarsened to 30 m resolution using a mean filter, because we determined this resolution to sufficiently balance the finer and coarser datasets in this analysis. Similarly, all input factors were resampled to match this resolution, using cubic spline interpolation for maps requiring upscaling and a mean filter for maps requiring downscaling. These input factor maps included the GAO bathymetry map used to compute rugosity, as well as slope computed from the 30 m depth map.

We sought to analyze the relative importance and influence of each of these factors on each of the two scales of rugosity at two levels: once separately for each individual island and once for all islands combined. By separating these analyses, we assessed whether drivers of rugosity differ by island while simultaneously revealing general patterns that apply to all islands. We randomly selected 80,000 pixels from the 30 m resampled maps for each individual island and, separately, randomly selected 100,000 pixels across all islands. Modeling was carried out using a Random Forest Machine Learning (RFML) approach (Breiman, 2001) with the Scikit-Learn python package version 0.22.1 (Pedregosa et al., 2011). Optimal settings for the RFML metaparameters defining the number of trees in the forest ("nest") were discovered through a grid search approach separately for each island (**Table 2**). We manually specified several metaparameters: four as the maximum tree depth, 1 as the minimum number of samples per leaf, two as the minimum number of samples per split, and four as the maximum number of features scanned at each split. All other meta parameters were left at the default settings. The final model was a descriptive machine learning model, fit to better understand the system rather than be applied to any new data. Because the risk of overfitting is negligible in these circumstances, the idea of parsimony is not applicable and no model simplification procedure was required. With the RF model-fitting procedure, unimportant factors are simply not selected as splitting criteria for many of the node splits that make up each component regression tree. Thus, these factors will have little influence over model capacity to fit the data, and this lack of influence will show as low values in any following assessments of individual factor importance.

TABLE 2 | Optimized random forest metaparameters used in each individual and combined model from the land-sea driver modeling along with resulting fit statistics, R-squared and Mean square error (MSE), as estimated by the cross-validation fitting procedure.

Island	Scale	Num. Trees	CV R^2	CV MSE	Full Dataset R^2
All Combined	Fine	2000	0.86	0.00037	0.96
	Coarse	4000	0.72	0.02078	0.93
Hawai'i	Fine	3500	0.88	0.00024	0.97
	Coarse	3000	0.78	0.01632	0.94
Maui	Fine	2500	0.91	0.00029	0.98
	Coarse	4000	0.82	0.01343	0.95
Kaho'olawe	Fine	2500	0.73	0.00607	0.93
	Coarse	2500	0.84	0.00780	0.96
Lana'i	Fine	2500	0.90	0.00027	0.97
	Coarse	2000	0.82	0.01272	0.95
Moloka'i	Fine	2500	0.95	0.00021	0.99
	Coarse	1500	0.92	0.00066	0.98
O'ahu	Fine	2500	0.94	0.00014	0.98
	Coarse	1500	0.78	0.01735	0.94
Kaua'i	Fine	2500	0.91	0.00020	0.98
	Coarse	2000	0.79	0.01460	0.94
Ni'ihau	Fine	3000	0.93	0.00014	0.98
	Coarse	2000	0.74	0.02038	0.93

The R-squared value after fitting the model to the full dataset is shown as baseline R^2 used in the permutation importance procedure.

We assessed the importance of each variable using a permutation-based, correlation coefficient (R^2)-reduction metric. To reduce the complexity of the permutation procedure, the baseline R^2 value used for this analysis was first obtained by re-fitting the final model for each island and rugosity scale using the full dataset (no train/test split) and comparing the predictions of this full model against the map value of rugosity for all samples in the dataset (**Table 2**). Next, the following permutation

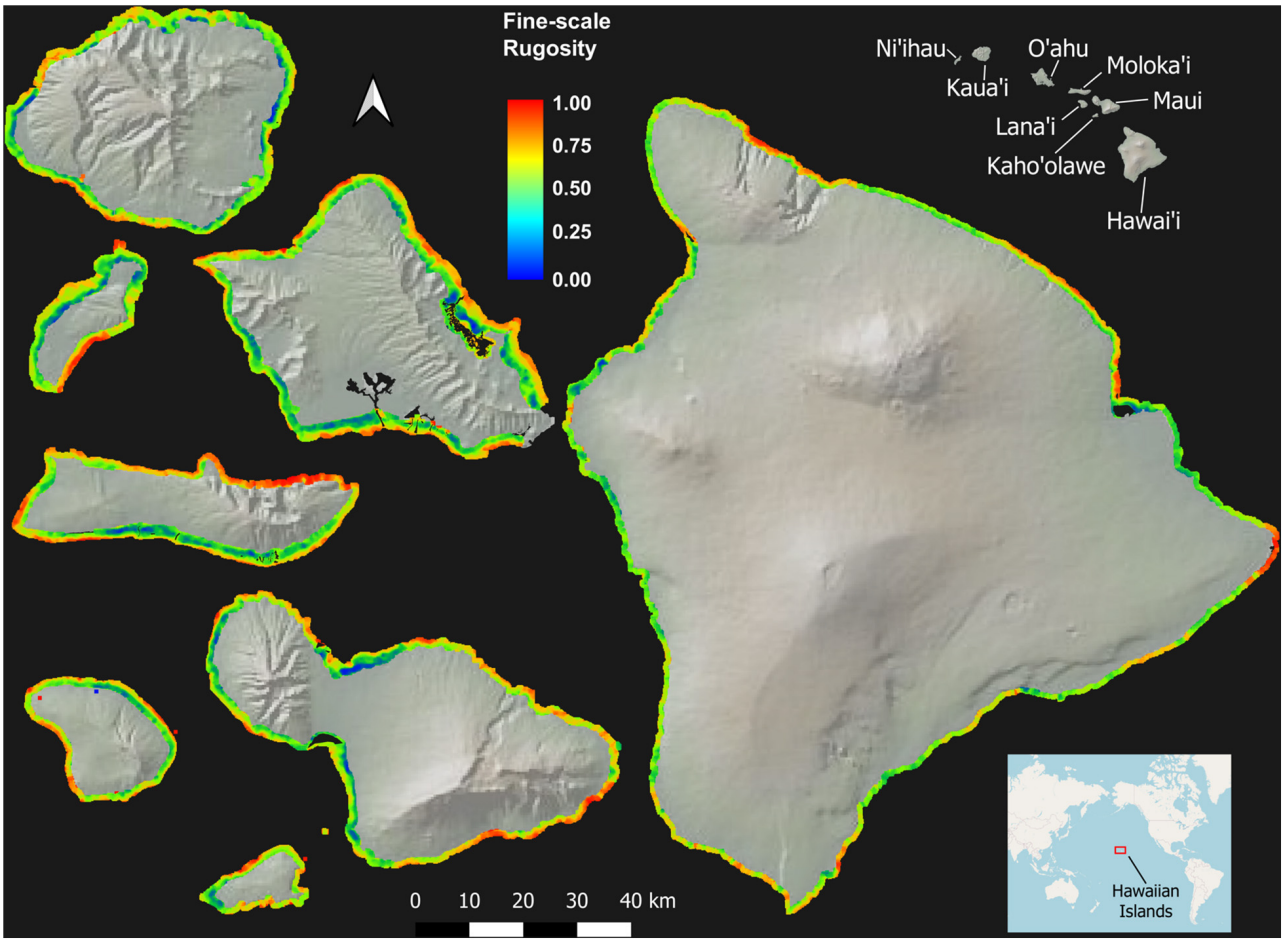

FIGURE 2 | Fine-scale rugosity of the eight Main Hawaiian Islands at 2 m spatial resolution to a depth of 22 m. Values are relative from 0.0 to 1.0. Coarse-scale rugosity is provided in **Appendix Figure A1**.

importance analysis was performed for each of the island-level models and the combined models at each scale of rugosity: For each input variable and for each of five iterations, the values for this variable were randomly shuffled, keeping values of all other variables intact. During each iteration, predictions were again obtained using the model on the full dataset containing the permuted variable, and we retained the difference between the original R^2 and the R^2 computed from this permutation. The five difference values were averaged for each variable to get a single importance value, where larger positive values indicate greater reduction in R^2 and, equivalently, greater variable importance.

In addition to the importance of each variable, we measured the marginal trends between each of the input variables and modeled rugosity values. These trends help understand why and how the individual input variables are important, a difficult task considering the high dimensionality of these systems. As with the importance analysis, this analysis was done for each input variable for each of the models in **Table 2**. For each model trained with the full dataset, the predicted rugosity values for the entire dataset were computed and stored. Next, the full range of each input variable was split into 100 equally sized bins based on percentiles of the input variable. For each of these partitions, the mean model-predicted rugosity value was computed along with the median value of the input variable within the partition. Plotting the predicted rugosity against median input variable values provides a view of rugosity response relative to the variable, inclusive of all correlations with other variables in the model. Where importance can inform as to how strongly rugosity shifts with a variable, the marginal plots can show whether the relationship is positive or negative and linear or curvilinear.

RESULTS

Inter-Island Reef Rugosity

Across the MHI, the total shallow reef area mapped was 98,344 ha, covering about 95% of all known reefs to a depth of 22 m **Figure 2** and **Appendix Figure A1**). On a whole-island basis, Hawai'i and Kaho'olawe contained reefs with the greatest 3D habitat complexity, with relative rugosity values in the 0.8–0.9 range (**Table 3**). O'ahu had the lowest reef complexity overall, at

0.55 or nearly half that of the structurally most complex island-scale reefs. Fine- and coarse-scale rugosity roughly tracked one another at the island level.

Geospatial Variation in Reef Complexity

Despite strong inter-island differences in 3D habitat complexity, any given local reef area displayed a wide range of rugosity values (**Figure 3** and **Appendix Figure A2**). Sandy areas with low rugosity are shown in blue, while highly complex coral and rock reef patches are expressed in yellow to red colors. Relative to shoreline, the location and spatial distribution of high-rugosity benthic surfaces was highly variable, although rugosity can be seen to broadly increase with distance to shore (**Figure 3**).

At the individual island level, both fine- and coarse-scale rugosity values were non-normally distributed (**Figure 4**). Hawai'i and Kaho'olawe were highly skewed in the positive direction, indicating the widespread presence of structurally complex benthic surfaces. Field observations indicated that these

TABLE 3 | Mean fine-scale and coarse-scale rugosity, and the total reef mapping area, of each island in the Main Hawaiian Islands.

Island	Fine-scale rugosity	Coarse-scale rugosity	Mapped area (ha)
Hawai'i	0.81	0.87	13,277
Maui	0.72	0.77	13,993
Kaho'olawe	0.85	0.88	1,408
Lana'i	0.74	0.77	3,662
Moloka'i	0.73	0.72	13,523
O'ahu	0.54	0.56	29,838
Kaua'i	0.65	0.65	14,661
Ni'ihau	0.73	0.64	7,983

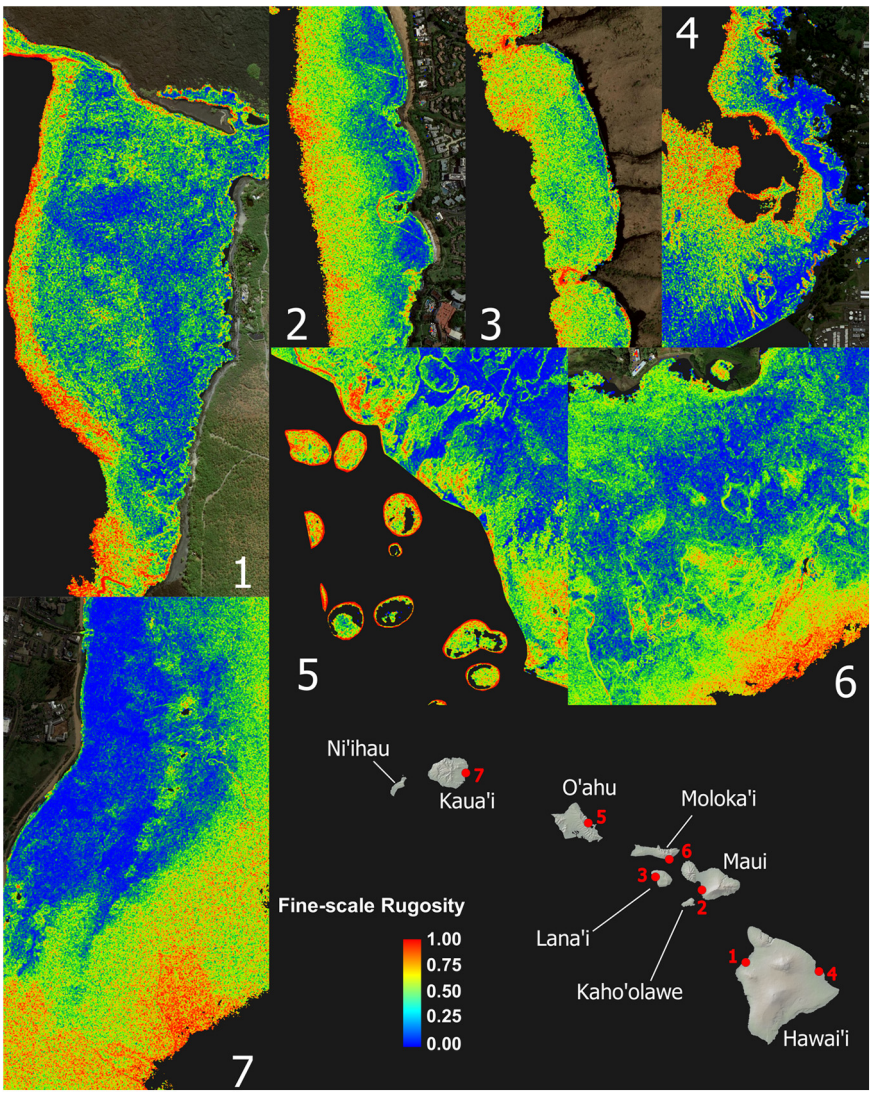

FIGURE 3 | Zoom images from maps shown in **Figure 2** demonstrating high spatial frequency variation and pattern in the fine-scale rugosity. These seven example reefs encompass the range of conditions among high-rugosity sites. Coarse-scale rugosity is provided in **Appendix Figure A2**.

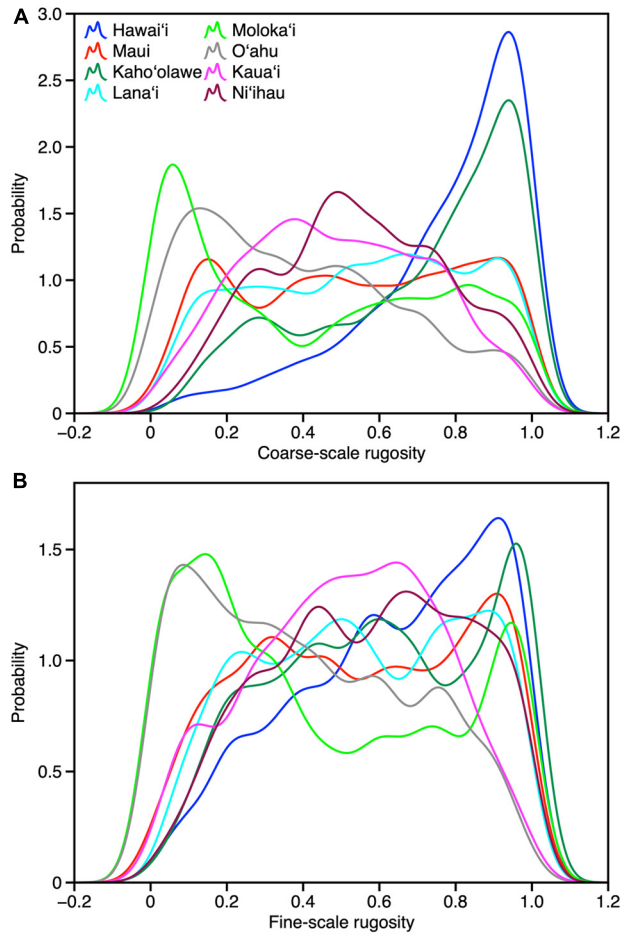

FIGURE 4 | Frequency distributions of **(A)** coarse-scale and **(B)** fine-scale rugosity by island.

areas are dominated by rock and/or coral. By contrast, O'ahu was largely comprised of low-rugosity substrate, with few rocks and coral colonies, and large swaths of sand- and algal-covered surfaces (see Asner et al., 2020b). These contrasting distributions are both an expression of island age, size, and stage as well as how much live coral can be found in each reef ecosystem. Notably, Moloka'i displayed a bi-modal rugosity distribution, with high values dominating the windward north coast and lower values found along the leeward south coast (**Figure 2**).

Reef rugosity showed a highly variable spatial arrangement at intra- and inter-island scales (**Figure 5** and **Appendix Figure 3**). Variogram-range maps reveal that, on geologically older islands such as Ni'ihau, Kaua'i and O'ahu, reef rugosity mostly varied at low spatial frequency, often more than 100 m, indicated by high variogram-range values (**Figure 5a** and **Appendix Figure 3a**). However, this background condition was punctuated by reef locations with relatively high spatial frequency changes in rugosity. By contrast, on geologically younger islands such as Hawai'i, Lana'i and Maui, low variogram-range values indicated high-frequency variability in rugosity over large tracks of reef. Variogram-sills represent the baseline variation in rugosity between areas on an island that are far enough apart to lack any shared local environmental controls. Again, geologically older islands were largely uniform (**Figure 5b** and **Appendix Figure 3b**), whereas younger islands were far more variable. Overall, based on island-level semi-variograms, Lana'i and Hawai'i were among the most variable in terms of fine- or coarse-scale rugosity (**Figure 5c** and **Appendix Figure 3c**).

Drivers of Habitat Complexity

Machine learning analyses revealed a heirarchical set of contributors to the spatial variability of fine- and coarse-scale rugosity throughout the MHI (**Figure 6**). Fine and coarse models accounted for 86 and 73%, respectively, of the overall mapped geospatial variation, indicating that the driver variables used in the model were appropriate in assessing rugosity at both resolutions. Water depth and reef slope exerted the strongest influences on the spatial variation in rugosity as evidenced in model permutation reduction R^2-values of up to 0.88 and 0.69, respectively, among all islands combined for fine- and/or coarse-scale rugosity (**Figure 6**). Secondarily, nearshore development and distance from coast exerted a detectable effect (R^2 up to 0.31). Other variables such as sea surface temperature, wind speed, total land effluent, and substrate age accounted for far less variation in rugosity ($R^2 < 0.11$).

There was a wide inter-island range of influence of each major driver on 3D habitat complexity. First, depth was far more important than reef slope in driving fine-scale rugosity, but depth alone ranged in relative importance from low on Hawai'i to extremely high on O'ahu (**Figure 6a**). In contrast, reef slope effect on fine-scale rugosity was minimal on Ni'ihau but much higher on Hawai'i. For coarse-scale rugosity, slope exerted the greatest influence on Hawai'i and the lowest on Ni'ihau and O'ahu (**Figure 6b**). The opposite was true for water depth. Here we note the apparent positive relationship between nearshore development and reef rugosity off Ni'ihau: Investigation of the mapping data indicated a highly localized spatial correlation between a small area of development and reef presence and rugosity relative to other sandy and cliff-like access points to the coastline.

Examination of model partial dependency indicated that water depth and reef slope had a positive linear relationship with fine-scale rugosity at the scale of the eight MHI (**Figure 7**). However, coarse-scale rugosity showed an asymptotic relationship with depth and slope (**Appendix Figure 4**). Moreover, while average fine-scale rugosity across all islands was fairly flat relative to distance to coast and all other factors (**Figure 7**), distance and wave power did show relationships with coarse-scale rugosity (**Appendix Figure 4**). We note an especially poor relationship between sea surface temperature and rugosity at either resolution.

DISCUSSION

Reef complexity, as indicated by maps of rugosity at 2 and 6 m resolutions, revealed a nested set of 3D habitat patterns across and within the eight MHIs. Coarse-scale rugosity was largely driven by reef slope and secondarily by depth; the opposite was

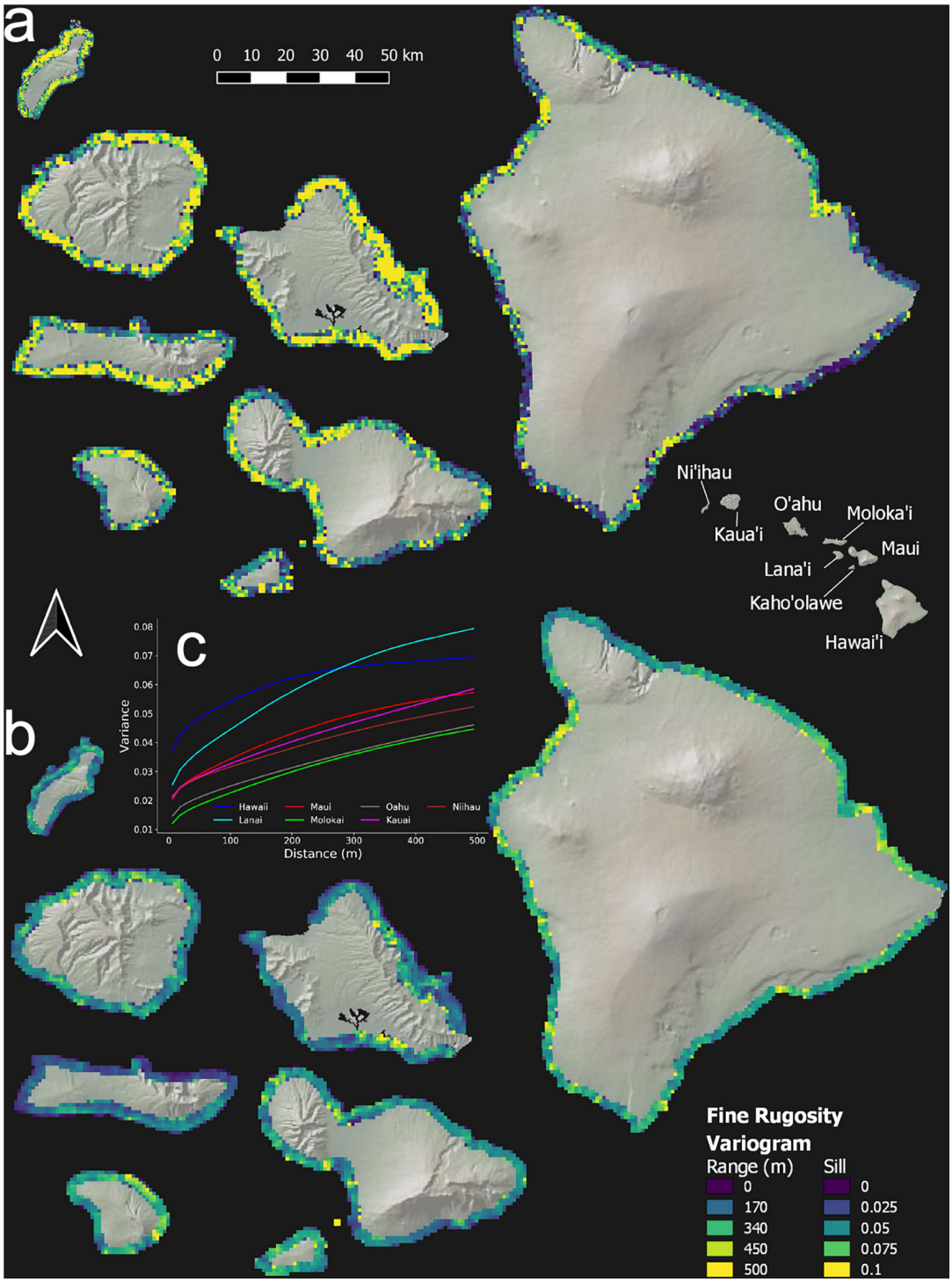

FIGURE 5 | Geospatial variation in fine-scale rugosity for the eight main Hawaiian Islands. Semi-variogram **(a)** range and **(b)** sill are shown at the top and bottom, respectively. **(c)** Island-scale semi-variograms in the inset graph. Coarse-scale rugosity is provided in **Appendix Figure A3**.

true for fine-scale rugosity (**Figure 6**). Taken together, these two indicators suggest that geologic stage dominates the broader habitat structure of reefs across the archipelago. Younger islands harbor reefs on steep basaltic slopes, often with rapid drop-offs to extreme depths (Fletcher et al., 2008). During their formation via lava flows, these rock-dominated reefs resemble complex canyon, spire, tube, and spur-and-groove type patterns. As islands age, subside and undergo surficial erosional processes, nearshore

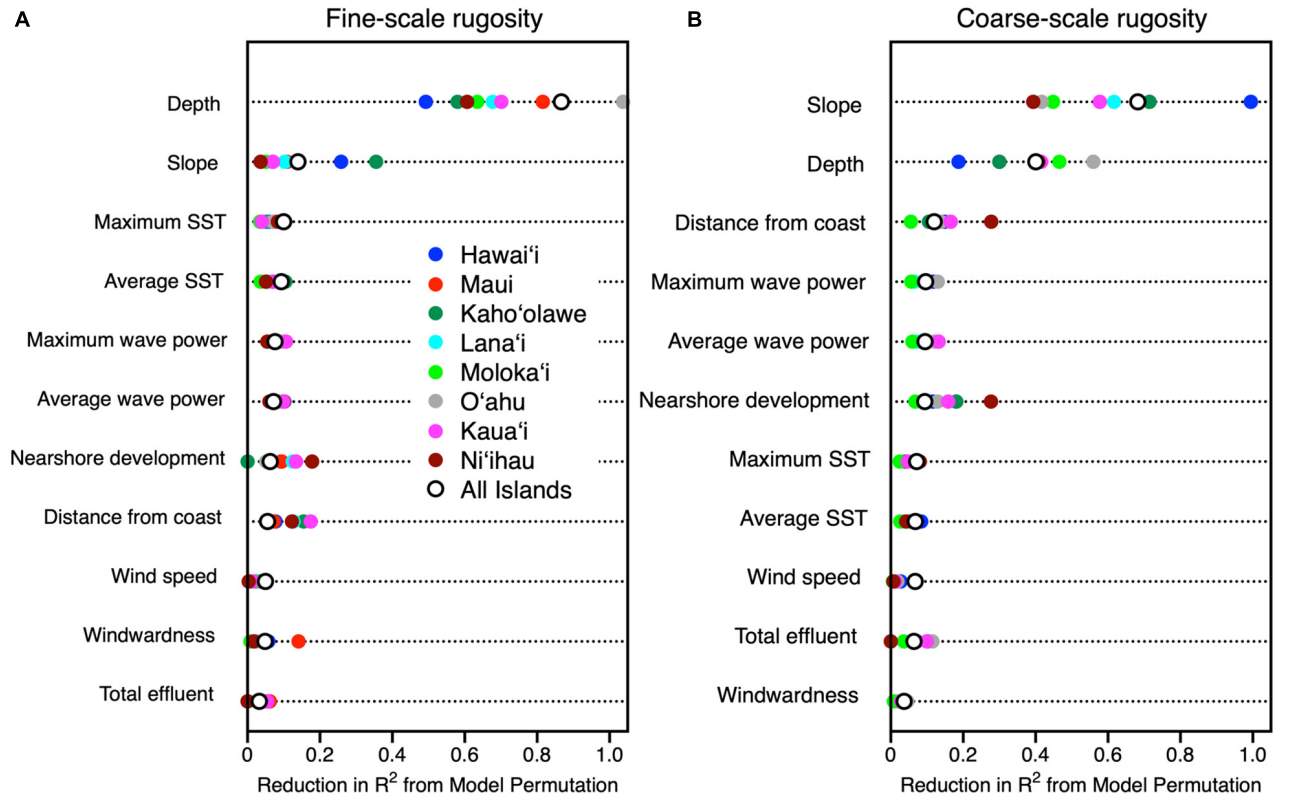

FIGURE 6 | Relative importance of potential contributing variables evaluated using machine learning to drive spatial variation in **(A)** fine-scale and **(B)** coarse-scale reef rugosity throughout the eight Main Hawaiian Islands. Colored dots indicate relative importance by island, and open circles indicate relative importance for all islands combined.

shallow (<22 m depth) slopes become smoother (Fletcher et al., 2008), are reduced in rugosity, and show weakening relationships with coarse-scale rugosity (**Figure 6**).

In contrast to coarse-scale rugosity, the distribution and patterning of fine-scale features were far more driven by water depth than by reef slope (**Figure 6**), where inter-island differences in rugosity track differently with island age and stage. For example, the youngest island, Hawai'i, has the steepest nearshore slopes, where depth has relatively little effect on fine-scale rugosity as compared to O'ahu. For the latter, fine-scale rugosity tracks water depth, largely due to the prevalent role of live coral along forereef locations in the 15+ m range (see Asner et al., 2020b). Shallower inshore areas on O'ahu are largely devoid of rock or coral needed to drive fine-scale rugosity patterns. It is notable that spatial variation in fine-scale rugosity peaks in the middle-aged islands associated with the conglomerate geologic structure of Maui Nui (**Figure 5**), comprised of the islands of Maui, Lana'i, Kaho'olawe, and Moloka'i (Price and Elliott-Fisk, 2004). On these islands, reefs undergo large spatially explicit swings in fine-scale rugosity, which we hypothesize to be associated with highly variable coral habitat conditions moderated by substrate availability, currents, depth, and other sub-regional factors (Asner et al., 2020b). Such high-frequency variability in fine-scale rugosity is far less prevalent on older (Kaua'i, O'ahu) and younger (Hawai'i) islands (**Figure 5**).

Overlain on these geologically driven patterns, there may be an emerging set of 3D habitat conditions associated with nearshore development and other direct human impacts, but the signal remains variable by island (**Figure 6**). On islands with developed land-based infrastructure like O'ahu, fine-scale rugosity appears suppressed in areas of nearshore development (**Figure 7**), perhaps related to the suppression of live coral cover in these locations (Asner et al., 2020b). On other less developed islands like Hawai'i, fine-scale rugosity was positively related to nearshore development, perhaps because the relationship between land and reef patterns has not yet been sufficiently altered (Wedding et al., 2018). Repeat flights are required to identify areas with changing rugosity for subsequent mitigation actions related to nearshore development.

Beyond the drivers of reef complexity, our rugosity maps have revealed a nested set of patterns ranging in scale from local to archipelago. In a recent study across the MHI, the rugosity maps presented here were a primary determinant of resource fish, herbivore fish, and total fish biomass (Donovan et al., 2020). They also showed that the recovery potential for reef fish was strongly mediated by reef rugosity. These findings amplify both the importance of high-resolution reef complexity mapping and monitoring as well as the way that management can integrate habitat mapping into plans and actions to protect and restore reef fisheries (Nowlis and Friedlander, 2005; Wedding et al., 2008).

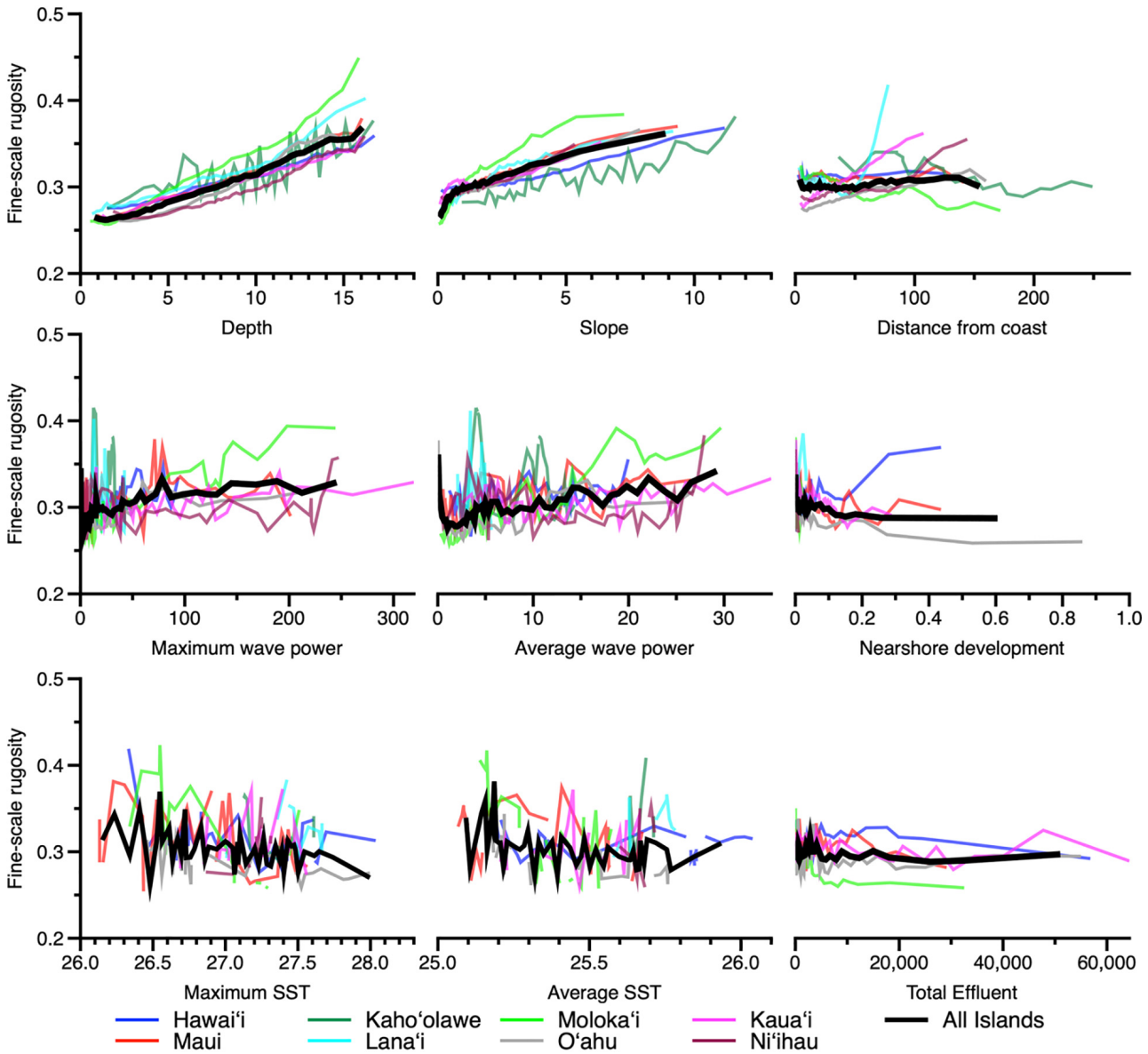

FIGURE 7 | Partial dependence plots indicating the relationship between fine-scale rugosity and the top nine variables presented in **Figure 6**. Colored lines indicate relationships by island, and thick black lines indicate relationships for all islands combined. Coarse-scale rugosity is provided in **Appendix Figure A4**.

Two major limits to our study involve spatial resolution and maximum achieved depth. In our companion study describing the methods and validation for mapping 3D habitat complexity used here, Asner et al. (2020a) found that rugosity maps could be generated at 40–60 cm resolution, thereby revealing the location of smaller coral colonies and rock outcrops. These smaller features may be key to understanding a host of other reef patterns and processes such as fish and invertebrate dynamics, coral larval settlement, and disease (Hata et al., 2017; Eggertsen et al., 2020). The current study cannot resolve these ultra-fine rugosity issues due to the practicalities of mapping an entire archipelago at high altitude and thus lower (2 m) spatial resolution.

Our maximum achieved mapping depth was 22 m (72 fsw). While much of the biological diversity of Hawaiian reefs is contained within our mappable depth range, critically important habitat in the lower euphotic and mesophotic zones are missed by our current approach (Rooney et al., 2010; Baldwin et al., 2018). While we continue to push the limits of spectroscopy-based depth and rugosity mapping, with some indications of 30 m penetrability in clear waters (G.P. Asner, *unpub. data*), this is not likely to become operational in the near future due to the limits of solar photon flux at such depths paired with limits of our high-fidelity imaging spectrometers. While these current spectrometer-based approaches are limited to a very few manned aircraft platforms, the technology is downsizing

and could become UAV (drone) based in the coming years. Additionally, these types of high-fidelity spectrometers are being prepared for low Earth orbit, such as the NASA Surface Biology and Geology mission (Schneider et al., 2019). Although the planned spatial resolution of 30 m will remain coarse for reef applications, the quality of the spectroscopic measurement will be analogous to the airborne capability today, perhaps allowing for coarse-scale rugosity mapping worldwide with the ecological fidelity proven here at an archipelago scale.

We found that water depth and reef slope are dominant drivers of both fine- and coarse-scale rugosity, where the greatest variation in rugosity occurred on middle-aged islands (e.g., Maui) in comparison to young and older islands (e.g., Hawai'i, Kaua'i). Nearshore development is an emerging secondary driver of decreasing rugosity, for example on O'ahu, the most highly developed island. Our rugosity maps are a tool that can be used by fisheries management and reef practitioners to prioritize areas for conservation and to design marine managed areas for greater resilience and recovery potential.

DATA AVAILABILITY STATEMENT

The datasets presented in this study can be found in online repositories. The names of the repository/repositories and accession number(s) can be found in Asner et al. (2020c).

AUTHOR CONTRIBUTIONS

GA conceived and funded the study, collected the data, provided the analysis, and wrote the manuscript. NV and JH collected the data, provided the analysis, and contributed to the writing of the manuscript. SF, ES, and RM provided the analysis and contributed to the writing of the manuscript. All authors contributed to the article and approved the submitted version.

FUNDING

This study was supported by the Lenfest Ocean Program and The Battery Foundation. The Global Airborne Observatory is made possible with support of private foundations, visionary individuals, and Arizona State University.

SUPPLEMENTARY MATERIAL

The Supplementary Material for this article can be found online at: https://www.frontiersin.org/articles/10.3389/fmars.2021.631842/full#supplementary-material

REFERENCES

Alvarez-Filip, L., Dulvy, N. K., Gill, J. A., Côté, I. M., and Watkinson, A. R. (2009). Flattening of Caribbean coral reefs: region-wide declines in architectural complexity. *Proc. R. Soc. B* 276, 3019–3025. doi: 10.1098/rspb.2009.0339

Asner, G. P., Knapp, D. E., Boardman, J., Green, R. O., Kennedy-Bowdoin, T., Eastwood, M., et al. (2012). Carnegie Airborne Observatory-2: Increasing science data dimensionality via high-fidelity multi-sensor fusion. *Remote Sens. Environ.* 124, 454–465. doi: 10.1016/j.rse.2012.06.012

Asner, G. P., Vaughn, N. R., Balzotti, C., Brodrick, P. G., and Heckler, J. (2020a). High-resolution reef bathymetry and coral habitat complexity from airborne imaging spectroscopy. *Remote Sens.* 12:310. doi: 10.3390/rs12020310

Asner, G. P., Vaughn, N. R., Heckler, J., Knapp, D. E., Balzotti, C., Shafron, E., et al. (2020b). Large-scale mapping of live corals to guide reef conservation. *Proc. Natl. Acad. Sci.* 117, 33711–33718. doi: 10.1073/pnas.2017628117

Asner, G. P., Vaughn, N. R., and Heckler, J. (2020c). Global airborne observatory: hawaiian islands reef rugosity 2019+2020 (Version 1.0) [Data set]. *Zenodo*. doi: 10.5281/zenodo.4294332

Aston, E. A., Williams, G. J., Green, J. A. M., Davies, A. J., Wedding, L. M., Gove, J. M., et al. (2019). Scale-dependent spatial patterns in benthic communities around a tropical island seascape. *Ecography* 42, 578–590. doi: 10.1111/ecog.04097

Baldwin, C. C., Tornabene, L., and Robertson, D. R. (2018). Below the mesophotic. *Sci. Reports* 8:4920.

Bezanson, J., Karpinski, S., Shah, V. B., and Edelman, A. (2012). Julia: A Fast Dynamic Language for Technical Computing. *ArXiv* 2012, 1209.51451.

Breiman, L. (2001). Random forests. *Machine Learn.* 45, 5–32.

Burns, J., Delparte, D., Gates, R., and Takabayashi, M. (2015). Integrating structure-from-motion photogrammetry with geospatial software as a novel technique for quantifying 3D ecological characteristics of coral reefs. *PeerJ.* 3:e1077. doi: 10.7717/peerj.1077

Center for International Earth Science Information Network-Ciesin, C. U. (2018). "Gridded Population of the World, Version 4 (GPWv4): Population Count," in *NASA Socioeconomic Data and Applications Center (SEDAC)*, (Palisades, NY: Columbia University).

Cinner, J. E., Mcclanahan, T. R., Daw, T. M., Graham, N. A. J., Maina, J., Wilson, S. K., et al. (2009). Linking social and ecological systems to sustain coral reef fisheries. *Curr. Biol.* 19, 206–212. doi: 10.1016/j.cub.2008.11.055

Donovan, M. K., Counsell, C. W. W., Lecky, J., and Donahue, M. J. (2020). *Estimating indicators and reference points in support of effectively managing nearshore marine resources in Hawai'i, Report by* Hawai: Monitoring and Reporting Collaborative.

Eggertsen, M., Chacin, D. H., Van Lier, J., Eggertsen, L., Fulton, C. J., Wilson, S., et al. (2020). Seascape configuration and fine-scale habitat complexity shape parrotfish distribution and function across a coral reef lagoon. *Diversity* 12:391. doi: 10.3390/d12100391

Engelen, A. H., Åberg, P., Olsen, J. L., Stam, W. T., and Breeman, A. M. (2005). Effects of wave exposure and depth on biomass, density and fertility of the fucoid seaweed Sargassum polyceratium (Phaeophyta. *Sargassaceae). Eur. J. Phycol.* 40, 149–158. doi: 10.1080/09670260500109210

Figueira, W., Ferrari, R., Weatherby, E., Porter, A., Hawes, S., and Byrne, M. (2015). Accuracy and precision of habitat structural complexity metrics derived from underwater photogrammetry. *Remote Sens.* 7, 16883–16900. doi: 10.3390/rs71215859

Fletcher, C. H., Bochicchio, C., Conger, C. L., Engels, M. S., Feirstein, E. J., Frazer, N., et al. (2008). "Geology of Hawaii Reefs," in *Coral Reefs of the USA*, eds B. M. Riegl and R. E. Dodge (Dordrecht: Springer Netherlands), 435–487.

Gao, B.-C., and Goetz, A. F. H. (1990). Column atmospheric water vapor and vegetation liquid water retrievals from airborne imaging spectrometer data. *J. Geophys. Res.* 95, 3549–3564. doi: 10.1029/jd095id04p03549

Gove, J., Williams, G., Mcmanus, M., Clark, S., Ehses, J. S., and Wedding, L. (2015). Coral reef benthic regimes exhibit non-linear threshold responses to natural physical drivers. *Mar. Ecol. Prog. Series* 522, 33–48. doi: 10.3354/meps11118

Graham, N. A. J., and Nash, K. L. (2012). The importance of structural complexity in coral reef ecosystems. *Coral Reefs* 32, 315–326. doi: 10.1007/s00338-012-0984-y

Graham, N. A. J., Wilson, S. K., Pratchett, M. S., Polunin, N. V. C., and Spalding, M. D. (2009). Coral mortality versus structural collapse as drivers of corallivorous butterflyfish decline. *Biodiver. Conserv.* 18, 3325–3336. doi: 10.1007/s10531-009-9633-3

Gratwicke, B., and Speight, M. R. (2005). The relationship between fish species richness, abundance and habitat complexity in a range of shallow tropical marine habitats. *J.Fish Biol.* 66, 650–667. doi: 10.1111/j.0022-1112.2005.00629.x

Grigg, R. W. (1998). Holocene coral reef accretion in Hawaii: a function of wave exposure and sea level history. *Coral Reefs* 17, 263–272. doi: 10.1007/s003380050127

Grober-Dunsmore, R., Frazer, T. K., Lindberg, W. J., and Beets, J. (2007). Reef fish and habitat relationships in a Caribbean seascape: the importance of reef context. *Coral Reefs* 26, 201–216. doi: 10.1007/s00338-006-0180-z

Harborne, A. R., Mumby, P. J., and Ferrari, R. (2012). The effectiveness of different meso-scale rugosity metrics for predicting intra-habitat variation in coral-reef fish assemblages. *Environ. Biol. Fishes* 94, 431–442. doi: 10.1007/s10641-011-9956-2

Harborne, A. R., Mumby, P. J., Żychaluk, K., Hedley, J. D., and Blackwell, P. G. (2006). Modeling the beta diversity of coral reefs. *Ecology* 87, 2871–2881.

Hata, T., Madin, J. S., Cumbo, V. R., Denny, M., Figueiredo, J., Harii, S., et al. (2017). Coral larvae are poor swimmers and require fine-scale reef structure to settle. *Sci. Reports* 7:2249.

Hoffimann, J. (2018). GeoStats.jl – High-performance geostatistics in Julia. *J. Open Source Software* 3:692. doi: 10.21105/joss.00692

Ignatov, A. (2010). *GOES-R Advanced Baseline Imager (ABI) algorithm theoretical basis document for sea surface temperature*. Washington, D.C: NOAA NESDIS Center for Satellite Applications and Research.

Jenness, J. S. (2004). Calculating landscape surface area from digital elevation models. *Wildlife Soc. Bulletin* 32, 829–839. doi: 10.2193/0091-7648(2004)032[0829:clsafd]2.0.co;2

Jennings, S., Boullé, D. P., and Polunin, N. V. C. (1996). Habitat correlates of the distribution and biomass of Seychelles' reef fishes. *Env. Biol. Fishes* 46, 15–25. doi: 10.1007/bf00001693

Lechene, M. A. A., Haberstroh, A. J., Byrne, M., Figueira, W., and Ferrari, R. (2019). Optimising sampling strategies in coral reefs using large-area mosaics. *Remote Sens.* 11:2907. doi: 10.3390/rs11242907

Li, N., Cheung, K. F., Stopa, J. E., Hsiao, F., Chen, Y.-L., Vega, L., et al. (2016). Thirty-four years of Hawaii wave hindcast from downscaling of climate forecast system reanalysis. *Ocean Model.* 100, 78–95. doi: 10.1016/j.ocemod.2016.02.001

Madin, J. S., Baird, A. H., Dornelas, M., and Connolly, S. R. (2014). Mechanical vulnerability explains size-dependent mortality of reef corals. *Ecol. Lett.* 17, 1008–1015. doi: 10.1111/ele.12306

Moravec, H., and Elfes, A. (1985). "High resolution maps from wide angle sonar," in *Proceedings of the 1985 IEEE International Conference on Robotics and Automation*. Missouri. 116–121.

Mumby, P. J., Skirving, W., Strong, A. E., Hardy, J. T., Ledrew, E. F., Hochberg, E. J., et al. (2004). Remote sensing of coral reefs and their physical environment. *Mar. Pollut. Bull.* 48, 219–228.

Neall, V. E., and Trewick, S. A. (2008). The age and origin of the Pacific islands: a geological overview. *Philosoph. Transac. R. Soc. B* 363, 3293–3308. doi: 10.1098/rstb.2008.0119

Nowlis, J. S., and Friedlander, A. (2005). *Marine reserve function and design for fisheries management*. Washington, D.C: Island Press.

Pedregosa, F., Varoquaux, G., Gramfort, A., Michel, V., Thirion, B., Grisel, O., et al. (2011). Scikit-learn: Machine learning in Python. *J. Machine Learn. Res.* 12, 2825–2830.

Price, J. P., and Elliott-Fisk, D. (2004). Topographic History of the Maui Nui Complex, Hawai'i, and Its Implications for Biogeography. *Pacific Sci.* 58, 27–45. doi: 10.1353/psc.2004.0008

Purkis, S. J., Graham, N. A. J., and Riegl, B. M. (2008). Predictability of reef fish diversity and abundance using remote sensing data in Diego Garcia (Chagos Archipelago). *Coral Reefs* 27, 167–178. doi: 10.1007/s00338-007-0306-y

Risk, M. J. (1972). Fish diversity on a coral reef in the Virgin Islands. *Atoll Res. Bull* 153, 1–7. doi: 10.5479/si.00775630.153.1

Rogers, A., Blanchard, J., and Mumby, P. (2014). Vulnerability of Coral Reef Fisheries to a Loss of Structural Complexity. *Curr. Biol.* 24, 1000–1005. doi: 10.1016/j.cub.2014.03.026

Rooney, J., Donham, E., Montgomery, A., Spalding, H., Parrish, F., Boland, R., et al. (2010). Mesophotic coral ecosystems in the Hawaiian Archipelago. *Coral Reefs* 29, 361–367. doi: 10.1007/s00338-010-0596-3

Schneider, F. D., Ferraz, A., and Schimel, D. (2019). Watching Earth's interconnected systems at work. *Eos*, 100. doi: 10.1029/2019EO136205

Sebens, K. P. (1991). "Habitat structure and community dynamics in marine benthic systems," in *Habitat Structure: The physical arrangement of objects in space*, eds S. S. Bell, E. D. Mccoy, and H. R. Mushinsky (Dordrecht: Springer Netherlands), 211–234. doi: 10.1007/978-94-011-3076-9_11

Storlazzi, C. D., Brown, E. K., Field, M. E., Rodgers, K., and Jokiel, P. L. (2005). A model for wave control on coral breakage and species distribution in the Hawaiian Islands. *Coral Reefs* 24, 43–55. doi: 10.1007/s00338-004-0430-x

Thompson, D. R., Hochberg, E. J., Asner, G. P., Green, R. O., Knapp, D. E., Gao, B.-C., et al. (2017). Airborne mapping of benthic reflectance spectra with Bayesian linear mixtures. *Remote Sens. Environ.* 200, 18–30. doi: 10.1016/j.rse.2017.07.030

Wedding, L. M., Friedlander, A. M., Mcgranaghan, M., Yost, R. S., and Monaco, M. E. (2008). Using bathymetric lidar to define nearshore benthic habitat complexity: Implications for management of reef fish assemblages in Hawaii. *Remote Sens. Environ.* 112, 4159–4165. doi: 10.1016/j.rse.2008.01.025

Wedding, L. M., Lecky, J., Gove, J. M., Walecka, H. R., Donovan, M. K., Williams, G. J., et al. (2018). Advancing the integration of spatial data to map human and natural drivers on coral reefs. *PLoS One* 13:e0204760.doi: 10.1371/journal.pone.0204760

Williams, G. J., Gove, J. M., Eynaud, Y., Zgliczynski, B. J., and Sandin, S. A. (2015). Local human impacts decouple natural biophysical relationships on Pacific coral reefs. *Ecography* 38, 751–761. doi: 10.1111/ecog.01353

Conflict of Interest: The authors declare that the research was conducted in the absence of any commercial or financial relationships that could be construed as a potential conflict of interest.

frontiers in Marine Science

CORRECTION
published: 17 March 2021
doi: 10.3389/fmars.2021.671048

Corrigendum: Abiotic and Human Drivers of Reef Habitat Complexity Throughout the Main Hawaiian Islands

Gregory P. Asner, Nicholas R. Vaughn, Shawna A. Foo, Ethan Shafron, Joseph Heckler and Roberta E. Martin*

Center for Global Discovery and Conservation Science, Arizona State University, Tempe, AZ, United States

Keywords: bathymetry, coral reef, Hawai'i, imaging spectroscopy, reef structure, rugosity

OPEN ACCESS

Approved by:
Frontiers Editorial Office, Frontiers Media SA, Switzerland

****Correspondence:***
Gregory P. Asner
gregasner@asu.edu

Specialty section:
This article was submitted to Coral Reef Research, a section of the journal Frontiers in Marine Science

Received: *22 February 2021*
Accepted: *03 March 2021*
Published: *17 March 2021*

Citation:
Asner GP, Vaughn NR, Foo SA, Shafron E, Heckler J and Martin RE (2021) Corrigendum: Abiotic and Human Drivers of Reef Habitat Complexity Throughout the Main Hawaiian Islands. Front. Mar. Sci. 8:671048. doi: 10.3389/fmars.2021.671048

A Corrigendum on

Abiotic and Human Drivers of Reef Habitat Complexity Throughout the Main Hawaiian Islands
by Asner, G. P., Vaughn, N. R., Foo, S. A., Shafron, E., Heckler, J., and Martin, R. E. (2021). Front. Mar. Sci. 8:631842. doi: 10.3389/fmars.2021.631842

Ethan Shafron was not included as an author in the published article. The corrected Author Contributions Statement appears below.

The authors apologize for this error and state that this does not change the scientific conclusions of the article in any way. The original article has been updated.

AUTHOR CONTRIBUTIONS

GA conceived and funded the study, collected the data, provided the analysis, and wrote the manuscript. NV and JH collected the data, provided the analysis, and contributed to the writing of the manuscript. SF, ES, and RM provided the analysis and contributed to the writing of the manuscript. All authors contributed to the article and approved the submitted version.

frontiers in Marine Science

ORIGINAL RESEARCH
published: 22 March 2021
doi: 10.3389/fmars.2021.640713

3D Classification of Cold-Water Coral Reefs: A Comparison of Classification Techniques for 3D Reconstructions of Cold-Water Coral Reefs and Seabed

Larissa Macedo Cruz de Oliveira[1], Aaron Lim[1,2], Luis A. Conti[3] and Andrew J. Wheeler[1,4]*

[1] School of Biological, Earth and Environmental Sciences, Environmental Research Institute, University College Cork, Cork, Ireland, [2] Green Rebel Marine, Crosshaven Boatyard, Crosshaven, Ireland, [3] Escola de Artes, Ciências e Humanidades, Universidade de São Paulo, São Paulo, Brazil, [4] Irish Centre for Research in Applied Geosciences, Marine and Renewable Energy Institute, University College Cork, Cork, Ireland

OPEN ACCESS

Edited by:
Andrew J. Davies, The University of Rhode Island, United States

Reviewed by:
Katleen Robert, Memorial University of Newfoundland, Canada
Charles Alan Jacoby, St. Johns River Water Management District, United States

***Correspondence:**
Larissa Macedo Cruz de Oliveira
Larissa.oliveira@ucc.ie

Specialty section:
This article was submitted to Coral Reef Research, a section of the journal Frontiers in Marine Science

Received: *11 December 2020*
Accepted: *17 February 2021*
Published: *22 March 2021*

Citation:
de Oliveira LMC, Lim A, Conti LA and Wheeler AJ (2021) 3D Classification of Cold-Water Coral Reefs: A Comparison of Classification Techniques for 3D Reconstructions of Cold-Water Coral Reefs and Seabed. Front. Mar. Sci. 8:640713. doi: 10.3389/fmars.2021.640713

Cold-water coral (CWC) reefs are complex structural habitats that are considered biodiversity "hotspots" in deep-sea environments and are subject to several climate and anthropogenic threats. As three-dimensional structural habitats, there is a need for robust and accessible technologies to enable more accurate reef assessments. Photogrammetry derived from remotely operated vehicle video data is an effective and non-destructive method that creates high-resolution reconstructions of CWC habitats. Here, three classification workflows [Multiscale Geometrical Classification (MGC), Colour and Geometrical Classification (CGC) and Object-Based Image Classification(OBIA)] are presented and applied to photogrammetric reconstructions of CWC habitats in the Porcupine Bank Canyon, NE Atlantic. In total, six point clouds, orthomosaics, and digital elevation models, generated from structure-from-motion photogrammetry, are used to evaluate each classification workflow. Our results show that 3D Multiscale Geometrical Classification outperforms the Colour and Geometrical Classification method. However, each method has advantages for specific applications pertinent to the wider marine scientific community. Results suggest that advancing from commonly employed 2D image analysis techniques to 3D photogrammetric classification methods is advantageous and provides a more realistic representation of CWC habitat composition.

Keywords: cold-water corals, 3D photogrammetry, structure-from-motion, remotely operated vehicles, object-based classification, 3D image classification

INTRODUCTION

Azooxanthallate scleractinian corals, such as *Lophelia pertusa* (synonymised to *Desmophyllum pertusum* in Addamo et al., 2016) and *Madrepora oculata*, are recognised by their three-dimensional branching morphology and framework building capacity (Mortensen et al., 1995; Roberts, 2002; Jonsson et al., 2004; Costello et al., 2005; Wheeler et al., 2005a, 2007b; Gass and Roberts, 2006;

Guinan et al., 2009). In suitable environmental conditions, these cold-water coral (CWC) species can form structural habitats such as small coral patches (Wilson, 1979a), reefs (Masson et al., 2003; Roberts et al., 2006b; Victorero et al., 2016; Lim et al., 2018), and giant carbonate mounds (Hovland and Thomsen, 1997; Mienis et al., 2006; Wheeler et al., 2007a; Freiwald et al., 2011; Huvenne et al., 2011) that can reach up to 400 m above the seabed. The presence of reef-forming CWC colonies has been documented in a range of settings from fjords (Fosså et al., 2006) to continental shelfs, slopes (Wilson, 1979b; Mortensen et al., 1995; Wheeler et al., 2005c; Leverette and Metaxas, 2006; Mienis et al., 2006) to seamounts and submarine canyons (Huvenne et al., 2011; Appah et al., 2020) throughout the North Atlantic, Indian, and Pacific oceans and the Mediterranean Sea (de Mol et al., 2005; Freiwald and Roberts, 2005; Wheeler et al., 2007a,b; Roberts et al., 2009; Freiwald et al., 2011; Lim et al., 2018).

Cold-water coral environments are commonly considered marine biodiversity "hotspots" as they can harbour increased biodiversity and biomass relative to their surrounding areas (Jonsson et al., 2004; Wheeler et al., 2007a; Fanelli et al., 2017). Despite being among the world's most important reservoirs of marine biodiversity (Freiwald et al., 2011), CWC reefs are also susceptible to environmental changes and threats such as temperature and salinity changes, as well as anthropogenic activities (Roberts et al., 2006a; Wheeler et al., 2007a; Orejas et al., 2009; Huvenne et al., 2016), e.g., bottom trawling (Wheeler et al., 2005b), mining (Savini et al., 2014), and oil and gas exploration (Roberts, 2002; Gass and Roberts, 2006; Barbosa et al., 2019). Several studies have affirmed that CWC reefs are declining rapidly in response to high rates of environmental change (Lim et al., 2018; Boolukos et al., 2019) and ocean acidification (Turley et al., 2007; Findlay et al., 2013). Consequently, there is a need for CWC reef assessments that quantify variations in temperature, salinity, food supply, and growth rates combined with measurements of structural complexity and biodiversity. It is therefore essential to understand these environments and to assign priority areas for protection (Ferrari et al., 2018; Appah et al., 2020).

Three-dimensional structures enhance small-scale spatial variability and play a major role in species biodiversity and nutrient cycling (Graham and Nash, 2013; Pizarro et al., 2017; Lim et al., 2018). The use of multibeam echosounders (MBES) can provide sub-metre pixel resolution bathymetric coverages of submarine canyons (Huvenne et al., 2011; Robert et al., 2017) and CWC environments (De Clippele et al., 2017; Lim et al., 2017). However, there is a lack of studies at a centimetric resolution (King et al., 2018; Anelli et al., 2019; Price et al., 2019) that reveal the complexity of coral frameworks. The analysis of these environments usually relies on 1D or 2D estimates of coral cover and distribution that can potentially disregard important changes in reef habitats as they may not integrate accurate vertical or volumetric information (Courtney et al., 2007; Goatley and Bellwood, 2011; House et al., 2018). Therefore, there is an increasing demand for the development of novel techniques for measuring coral reef environments in 3D (Burns et al., 2015a,b; House et al., 2018; Fukunaga et al., 2019). This demand has been mitigated with the use of novel mapping techniques such as structure-from-motion (SfM) photogrammetry (Cocito et al., 2003; Burns et al., 2015b; Storlazzi et al., 2016; Robert et al., 2017; Price et al., 2019) which is becoming progressively more common since the introduction of remotely operated vehicles (ROVs) (Kwasnitschka et al., 2013; Lim et al., 2020). Increasing access to computer processing power, high-resolution digital imagery, and recent developments in image processing software has led to a considerably higher number of studies utilising photogrammetry for seabed habitat mapping (Storlazzi et al., 2016; Pizarro et al., 2017; Hopkinson et al., 2020). SfM photogrammetry is considered a time- and cost-effective method for seabed mapping that allows high-resolution environment reconstruction (Burns et al., 2015a,b; Storlazzi et al., 2016; Robert et al., 2017; House et al., 2018). SfM utilises multiple overlapping images at various angles to reconstruct 3D models of complex scenes. To this end, SfM uses a scale-invariant feature transform (SIFT) algorithm to extract corresponding image features from an offset of images captured sequentially along the camera transect (Lowe, 1999). These calculations of overlapping imagery can be used to reconstruct 3D point cloud models of the photographed surface or scene (Carrivick et al., 2016). Moreover, the use of ROV video data has a number of benefits when compared to traditional sampling methods given that it is non-destructive and can have a wide spatial coverage (Guinan et al., 2009; Bennecke et al., 2016; De Clippele et al., 2017; Young, 2017).

The increase of data derived from SfM mapping has led to the necessity for new tools and techniques to aid time-effective and high-quality analysis of large areas (Storlazzi et al., 2016; Pizarro et al., 2017; Young et al., 2018; Marre et al., 2019). As technology advances, datasets are also becoming larger which, in turn, leads to a need for automated processing with faster, more precise, and accurate classification outputs (Brodu and Lague, 2012; Weinmann et al., 2015). Currently, this need has been achieved by integrating machine learning (ML) with mapping techniques to achieve automated meaningful pattern detection from multi-thematic datasets. ML has been widely used in remote sensing (Pal, 2005; Mountrakis et al., 2011), archaeology (Menna et al., 2018; Lambers et al., 2019), and to predict fish abundances (Young, 2018). Studies have shown optimal results on the application of ML for satellite, aerial, and terrestrial imagery (Wang et al., 2015; Pirotti and Tonion, 2019). Classification studies using LiDAR data performed in Walton et al. (2016) and Weidner et al. (2019) are also good examples. However, there is still a scientific gap between ML and marine surveying for seabed classification due to the costly computational nature of ML methods and the time-intensive annotation of marine datasets which usually requires expert knowledge (Shihavuddin et al., 2013; Marburg and Bigham, 2016; Hopkinson et al., 2020). This gap is emphasised when we consider the use of 3D data. Even though existing ML models such as neural networks (NNs) have shown promising results on 3D reconstructions of single objects, there is still room for improvement for the classification of complex 3D scenes (Weinmann et al., 2015; Roynard et al., 2018), especially in the case of marine habitats (Gómez-ríos et al., 2018; Hopkinson et al., 2020). Challenges related to the complexity derived from variability of point density, non-uniform point structure, and size of the dataset still cause difficulties when

developing and applying new methodologies for 3D point cloud classification (Weinmann et al., 2013). In the specific case of coral reefs, difficulties in detecting coral shape, colour, and texture have also been reported (Gómez-ríos et al., 2018; King et al., 2018; Hopkinson et al., 2020) especially as corals tend to occur in colonies and can have similar features.

In this study, we assess three different image classification techniques embedded in image analysis software and evaluate both the performance and results when using 3D data. We also compare their resource requirements and information outputs. The usability and the computing power required to process and analyse data were also taken into account. In a wider scenario, this study aims to show novel applications of ML for seabed mapping of submarine canyons and CWC reefs. Furthermore, we provide a classification workflow created for these environments and evaluate the limitations and advantages of using 3D data in comparison to 2D. For the first time, the techniques were applied to the CWC reefs in the Porcupine Bank Canyon (PBC), NE Atlantic. As such, this paper contributes to the wider scientific community using existing image processing software for 3D classification of deep-sea environments.

MATERIALS AND METHODS

Three classification workflows applied to underwater photogrammetric reconstructions of CWC habitats in the PBC are analysed. The methods range from a relatively straightforward appraisal to ones of increased complexity in terms of computational requirements and user knowledge. Herein, we describe data acquisition, processing, and the workflow of the applied methods.

Study Area

Submarine canyons offer a variety of CWC habitats including vertical habitats (Huvenne et al., 2011; De Clippele et al., 2017; Robert et al., 2017). The three methodologies presented herein were applied to CWC habitats in the PBC, located approximately 300 km southwest of Ireland (**Figure 1**). The canyon is located between the Porcupine Seabight to the southeast and the Rockall Trough to the west (Wheeler et al., 2005a). Measuring 63 km in length, the PBC is one of the largest submarine canyons on Ireland's western margin. Since 2016, the PBC has been designated as a special area of conservation (SAC) (n°003001) by the European Union Habitats Directive (2016), and therefore no fishing or other exploratory activities are allowed in the area.

The PBC is a tectonically controlled (Shannon, 1991), asymmetrical canyon with two branching heads separated by a ridge and exiting separately into the Rockall Trough (Appah et al., 2020; Lim et al., 2020). A steep, ∼700 m high, cliff face exists at the southeast margin of the canyon with exposed bedrock. This bedrock contrasts with the sediment-dominant slope on the northwest margin that extends to the canyon base (Dorschel et al., 2010; Appah et al., 2020; Lim et al., 2020). Giant carbonate mounds of up to 100 m high (Wheeler et al., 2005a) are concentrated along the edges of the canyons or associated with fault systems existing around the canyon head, leading to escarpments of up to 60 m high (Mazzini et al., 2012).

The PBC is influenced by strong currents along the mound tops and flanks, water column stratification, enhanced bottom currents, and upwelling (Mazzini et al., 2012). Unprecedented current speeds of 114 cm s^{-1} have been recorded within the PBC, which is the highest current speed ever recorded in a CWC habitat (Lim et al., 2020). Data from conductivity-temperature-depth (CTD) measurements show that the region is mainly influenced by the eastern north atlantic water (ENAW) down to 800 m water depth flowing northerly (Lim et al., 2020) with the labrador sea water (LSW) below 1100 m depth (Appah et al., 2020). Mediterranean outflow water (MOW) also flows through the canyon between 800 and 1100 m water depth (Appah et al., 2020; Lim et al., 2020). It is suggested that current regimes influence the distribution of benthic fauna throughout the canyon and that CWC habitats in the PBC can tolerate considerably high current speeds (Lim et al., 2020). High biodiversity including actively growing and well-developed coral colonies is found at depths of 600–1000 m where the ENAW and MOW occur, while poorly developed coral colonies were related to the LSW (Appah et al., 2020). The main framework forming CWC in the canyon is *L. pertusa* (syn. *D. pertusum*), and the other most common coral species were black corals *Stichopathes* cf. *abyssicola* and *Leiopathes glaberrima* and sponges *Aphrocallistes beatrix* and *Hexadella dedritifera* (Appah et al., 2020).

Video Survey and Data Collection

The video data used in this survey were acquired during research cruises CE19008 (Lim et al., 2019b) and CE19014 (Lim et al., 2019a) from 13rd to 23rd of May of 2019 and 25th to 31st of July of 2019, respectively. Video data were collected using the *Holland 1* ROV, although the methodologies compared in this paper could be applied to towed-camera or diver surveys. The ROV is equipped with 11 camera systems of which two were used as data sources for analysis in this paper: an HDTV camera (HD Insite mini-Zeus with HD SDI fibre output), and a Kongsberg OE 14–208 digital stills camera. Two deep-sea power lasers spaced at 10 cm were used for scaling. Positioning data were recorded with a Sonardyne Ranger 2 ultra short baseline (USBL) beacon and corrected by an IXBlue doppler velocity logger (DVL) (Lim et al., 2020). ROV video data were acquired at a height of ∼2 m above the seabed with a survey speed of <0.2 knots at locations in the PBC. High-definition video data (1080p) were acquired at 50 fps and stored as *.mov files. The areas selected for reconstruction were based on the distribution and variety of CWC habitats such as small individual coral colonies, coral colonies on rock outcrops, coral gardens, and mounds.

3D Reconstruction Using Structure-From-Motion (SfM) Photogrammetry

Remotely operated vehicle video data, digital stills, and camera positioning information were used to produce the 3D reconstructions in this study. One frame per second was extracted

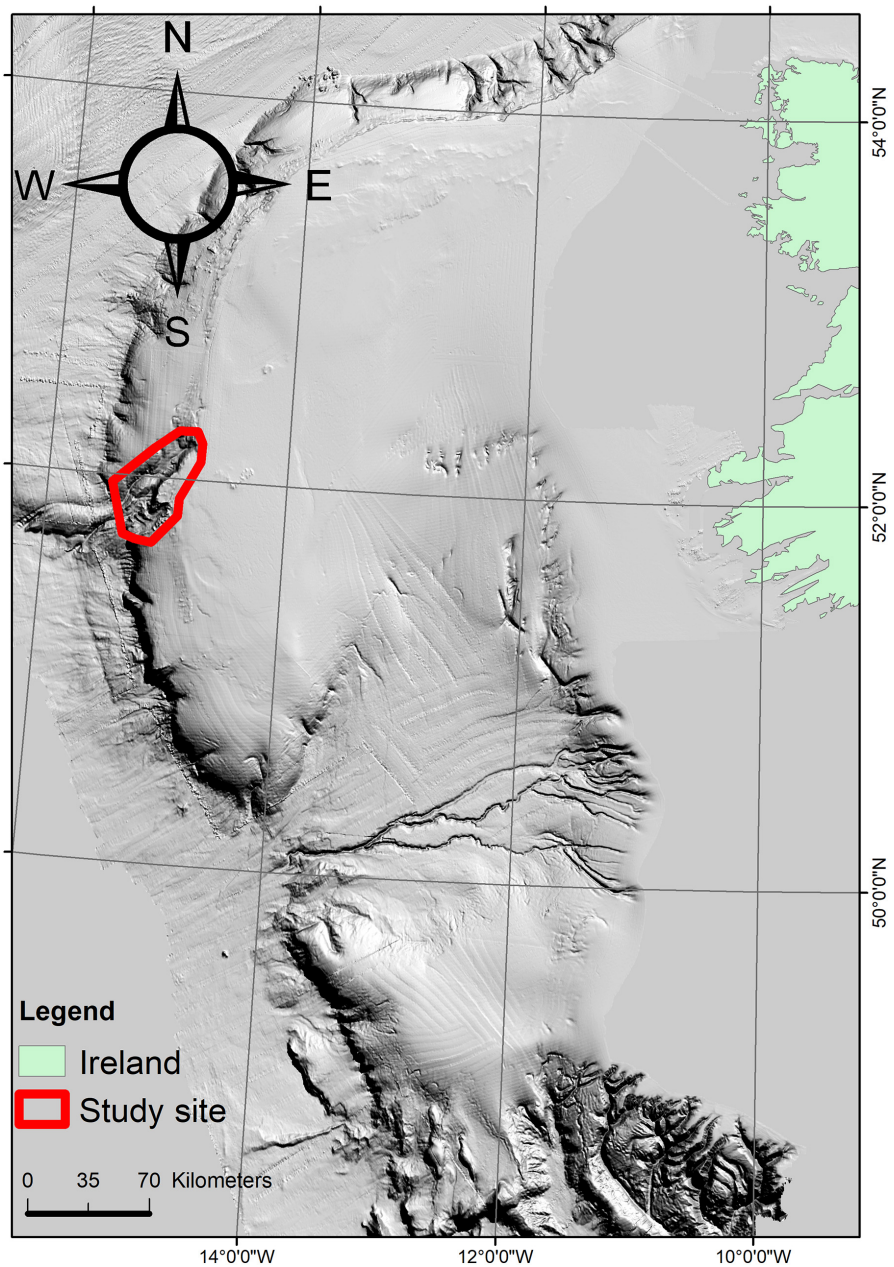

FIGURE 1 | Study site (in red)—The Porcupine Bank Canyon study area on the Irish continental margin west of Ireland.

from the raw video data with Blender (version 2.78). The frames were imported into Agisoft Metashape Professional v1.6, and each frame was georeferenced with its relative USBL positioning data. The lasers from the HD camera were utilised to scale features during the reconstruction process. The workflow for model rendering was carried out as detailed in Agisoft (2019) using an Intel I7 hexa core, 16 GB of RAM, and NVIDIA GTX1070 (8 GB) graphics card. The overall workflow and data outputs are shown in **Figure 2**. Dense clouds were used in method 1–MGC [section "Method 1–Multiscale Geometrical Classification (MGC)"] and method 2–CGC [section "Method 2–Colour and Geometrical Classification (CGC)"], while the orthomosaics were used for method 3–OBIA [section "Method 3–2D Object-Based Image Analysis (OBIA)"].

Classification Methods

Method 1–Multiscale Geometrical Classification (MGC)

An MGC approach was utilised in this study to perform a binary classification of our 3D CWC reef reconstructions. We utilised Canupo (Brodu and Lague, 2012), a support

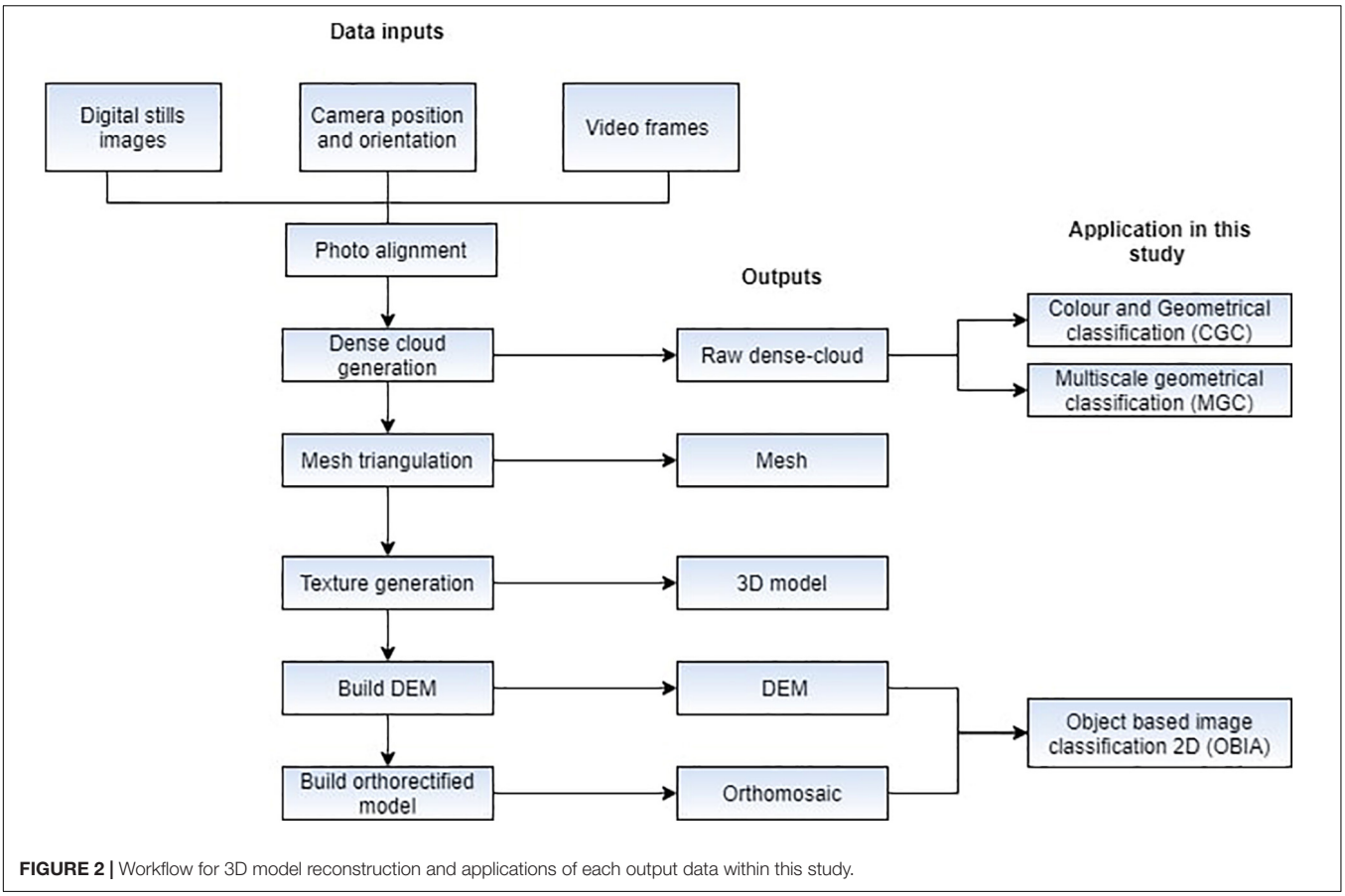

FIGURE 2 | Workflow for 3D model reconstruction and applications of each output data within this study.

vector machine (SVM) classification algorithm implemented in the open-source software CloudCompare (Girardeau-Montaut, 2011). This method was chosen due to its solid workflow for classification of point clouds applicable to natural environments (Brodu and Lague, 2012). As this technique uses dimensionality (computation of vector dispersion for each point relative to a neighbourhood of points) as a parameter for classification, it provides flexibility when applied to data derived from different sources as geometrical measurements are not dependent on the instrument used (Brodu and Lague, 2012). Therefore, these SVM-based classifiers can be reutilised by other users with point cloud data derived from different sources, e.g., terrestrial or airborne laser scanning. Another reason for choosing a dimensionality-based classifier is the limited separability of RGB component spectral signatures in underwater photogrammetry.

The multiscale classification technique used here computes the degree to which each neighbourhood of points can be examined as single-, two-, or three-dimensional aspects by identifying the principal components of the point coordinates in the given neighbourhood (Brodu and Lague, 2012). This method is defined as a multiscale classification because it calculates these statistics for each core point in the scene at a spherical neighbourhood of different sizes, referred to as scales parameters. As such, this method generates a feature vector that can distinguish between semantic objects (Maxwell et al., 2018; Weidner et al., 2019), such as coral and bedrock. The computation of neighbourhoods defined by each scale gives the classifier a multi-scale refining property (Brodu and Lague, 2012; Weidner et al., 2019). The final product of this process is defined herein as a multiscale classifier that is applied to the test dataset. Here, the neighbourhood sizes were chosen to include a range from coral frameworks to differing rock sizes so that small-scale objects would also be captured in large-scale sizes.

As this technique is a semi-automated classification that employs a probabilistic approach, it is essential to build classifiers based on samples of features of interest from a training dataset, i.e., live and dead corals. Entire dense clouds were manually segmented into objects of interest and divided in two classes: "coral" and "seabed." The class "coral" consisted of hard and soft coral colonies and frameworks. The class seabed consisted of the remainder, i.e., seafloor and other benthic organisms (e.g., coral rubble, echinoderms, sponges, etc.). The segmentation process was repeated on each axis (X, Y, and Z) to avoid single view bias.

Scale parameters used for the multiscale descriptors were based on the variance of object size within the scene. Ten initial scales with steps of 0.1 or 0.005 were chosen based on an empirical analysis of the data, combining the evaluation of features to be identified with a trial-and-error approach. The maximum number of core points (MNCPs) value is the number of randomly sub-sampled points that will be used for computations on the scene data. The higher the MNCP value,

the greater the number of computations. Thus, an increase in the number of scales and core points was directly related to the ability to discriminate and the processing power required to train the classifier. The performance of each classifier was quantified by the Balanced Accuracy (*ba*) value which is defined by the equation:

$$ba = \frac{1}{2}(a_{c1} + a_{c2})$$

Where each class accuracy (a_{c1} and a_{c2}) is defined as $a_{c1} = {tc_{c1}}/{(tc_{c1} + fc_{c2})}$ and $a_{c2} = {tc_{c2}}/{(tc_{c2} + fc_{c1})}$ (tc_{c1}–truly classified class 1, tc_{c2}–truly classified class 2, fc_{c1}–falsely classified class 1, and fc_{c2}–falsely classified class 2). For each sample, the classifier assigns a distance, *d*, from the separation line of the classifier and the measure of separability is calculated by the Fisher Discriminant Ratio (*fdr*) described in Sergios and Konstantinos (2008) which is defined as:

$$fdr = {(\mu_2 - \mu_1)^2}/{\nu_1 + \nu_2}$$

where μ_2 and μ_1 and ν_1 and ν_2 are the mean and the variance of the aforementioned distance *d* for each class 1 and 2. The *fdr* is used to assess the class separability, i.e., how well the classes are separated. Therefore, a high *ba* value indicates that the trained classifier has a good recognition performance, whereas a high *fdr* indicates that the classes are well separated in a plane of maximal separability. The classifier quality is directly proportional to *ba* and *fdr* values. The higher the values, the better the classifier can identify and classify objects into two classes. Further details can be found in Brodu and Lague (2012).

The dataset consisted of eight dense-clouds that were split into training and testing sets. The training set was used for training the classifier, which was then applied onto the unseen testing set. Each classifier was trained with a combination of segments from a single dense-cloud or two different dense-clouds, referred to here as source-clouds. The testing dataset composed by the remainder of the dataset after excluding the dense-clouds was used to train the classifier. The classifiers with the highest *ba* and *fdr* values were applied to the testing dataset to evaluate their robustness and reproducibility, i.e., their ability to be applied to analogous environments. Initially, no confidence threshold was set for the classification. Therefore, all points were classified as either coral or seabed. After a visual inspection of preliminary results, a confidence threshold was set to arbitrary values 0.5 or 0.9 and the classifier was executed again. The confidence threshold allows class labels to be assigned only if the results exceed that value; otherwise, the point is left unclassified. If more than 30% of the points were left unclassified, the classifier was retrained with a different number of scales and core points (**Supplementary Figure 1**). This threshold was set to reassure classification quality in a trial-and-error approach (Weidner et al., 2019). Hence, higher values will result in less generalisation and more complex decision boundaries (Maxwell et al., 2018). Studies in terrestrial point clouds for rock slope classification have chosen the confidence threshold based on up to 15% of unclassified points (Weidner et al., 2019). A 30% confidence threshold was chosen for this study due to the point cloud density differences and the classes of objects to be addressed.

Method 2–Colour and Geometrical Classification (CGC)

The second classification workflow is based on the use of colour and geometrical feature information following the work of Becker et al. (2018) which has shown satisfactory results for ground classification point clouds surveys using unmanned aerial vehicles (UAVs) (Klápště et al., 2018).

The use of geometrical features for semantic classification has brought positive results in several terrestrial data studies (Weinmann et al., 2015; Hackel et al., 2016). In addition to geometrical features, the use of colour information in the classification process of point clouds provides a significant increase in prediction accuracy (Lichti, 2005; Becker et al., 2018). For underwater photogrammetry, the use of colour has been advised as a way to include important image spectral information (Beijbom et al., 2012; Bryson et al., 2013, 2015, 2016). However, its importance is questionable as there are interactions between the colour spectrum and water column, e.g., the red colour channel is attenuated with distance from camera (Carlevaris-Bianco et al., 2010; Beijbom et al., 2012; Bryson et al., 2013).

Here, the same training set of dense point clouds was classified using the supervised multiclass classification algorithm implemented in Agisoft Metashape (**Supplementary Figure 2**). This automatic multiclass classification approach associates geometric and colour features that are fed into the Gradient Boosted Tree (GBT) algorithm to predict the class of each point in the point cloud. GBT utilises colour features computed from the colour values of each point and the average colour values of its neighbouring points.

Geometrical features used in the algorithm were previously presented in Becker et al. (2018). For each point, its neighbouring points are computed and the set is used to build a local 3D structure covariance tensor which summarises the predominant direction of the slope gradients in the neighbourhood of a point. The eigenvalues and corresponding eigenvectors are used to compute the local geometric features, for instance, ominivariance, eigentropy, anisotropy, planarity, linearity, surface variation, verticality, and scatter. These features, which originate from the 3D covariance matrix of nearest neighbours of each point, can be used to describe the local 3D structure and dimensionality (Weinmann et al., 2013). Further information about the algorithm can be found in Becker et al. (2018). This technique provides a supervised classification which is pre-trained using terrestrial datasets. The dense clouds were classified with the GBT classifier into ground (seabed) and low vegetation (corals).

Method 3–2D Object-Based Image Analysis (OBIA)

As a baseline method, object image classification was utilised to analyse the range of information that 2D data classification can provide in comparison to the 3D data. Object-based analysis techniques have been widely applied across different remote sensing areas, especially for marine studies (Conti et al., 2019;

Lim et al., 2020), aerial imagery (Zhang et al., 2010), and land cover mapping (Benz et al., 2004).

For this classification method, the georeferenced orthomosaics, DEM, and slope from the training set were used. Slope was derived from the DEM in ArcGIS Spatial Analyst toolbox. Slope, DEM, and the orthomosaics derived from the point cloud processing were imported into eCognition Developer (Trimble Germany GmbH, 2019) and segmented using the multi-resolution segmentation algorithm (Benz et al., 2004) at a pixel level using different layer weights for RGB, DEM, and slope layers. This segmentation approach merges pixels of similar values into objects based on relative homogeneity criterion. The homogeneity criterion measures how homogeneous an image object is in relation to itself and it is calculated as a combination of spectral and shape criteria (Trimble, 2018). The shape ratio determines to what extent the shape influences the segmentation compared to colour. The compactness is a weighting value that affects the compactness of the objects in relation to smoothness created during the segmentation. These ratios are obtained by calculating primary object features, shape, and colour, with heterogeneity calculations, i.e., standard deviation (Benz et al., 2004). Layer weight values control the emphasis given to colour and shape during the heterogeneity calculation (Koop et al., 2021) as it increases the weight of a layer based on the heterogeneity. The weight parameters adapt the heterogeneity definition to the application in order to get suitable segmentation output for image data (Benz et al., 2004). The layer weight values used were chosen following Lim et al. (2020). The scale parameter is considered the most effective parameter (Benz et al., 2004; Kavzoglu and Yildiz, 2014) and is used to control the average image object size in relation to the whole scene, the higher the value, the larger the objects will be. Scale parameters, shape, and compactness thresholds were set for each model individually, following a trial-and-error approach.

After the segmentation, each model was manually classified by an expert. The simplified process is defined in the workflow in **Supplementary Figure 3**.

Ground Truthing

To assess classification performance, dense cloud datasets were manually annotated. These points were then compared to the classification outputs from the MGC and CGC methods. Classification accuracy was calculated in Python with the ML library Scikit-learn (Pedregosa et al., 2011).

The accuracy score was calculated by summing the true positives and true negatives of all classes and dividing by the total number of annotated points (true positives, false positives, true negatives, and false negatives). The balanced accuracy was calculated as the arithmetic mean of sensitivity (true positive rate) and specificity (true negative rate) of each class. These metrics were chosen because they take into account the class imbalance, i.e., classes do not have the same number of samples, which is typical of seabed imagery datasets. Failure to do so would accidentally inflate the performance of classifiers (Akbani et al., 2004; Brodersen et al., 2010).

RESULTS

3D Reconstructions

A total of eight 3D reconstructions were produced using 3681 images. Dense clouds were composed of a total of 165,356,594 points. The average reconstruction length was 19.73 m and depths ranged from 595 to 1001 m, with average depth of 732.57 m. Mean total error (i.e., root-mean-square error for *X*, *Y*, and *Z* coordinates for all the cameras) was 13.015. Continuous video acquisition along the ROV transects was not regularly possible because of variations in ROV height and speed. High current speeds at the PBC and the presence of particles in suspension in water column (marine snow) also impacted the ROV video transect and consequently the video quality in some areas. Low-quality data were rejected prior to reconstruction. Despite the presence of a few gaps in the surface, the reconstructions showed medium scale features (>10 cm) such as coral branches, coral rubble, and some benthic species with distinction. However, fine scale features (<5 cm) such as individual coral polyps and encrusted algae were not easily visible.

Coral and Seabed Distribution in the Porcupine Bank Canyon

The dense clouds were manually annotated by an expert and segmented into classes: coral and seabed. The percentage distribution of the coral and seabed samples from the annotated test set showed an average of 7.19% coral and 92.81% seabed. Models A, B, and C, located on the upper part of the PBC, showed higher percentages of coral (>10%) and sediment-dominated facies with dropstones (**Figure 3**). Models D, E, and F, located on the canyon flank ridge, showed lower percentages of coral (<5%), predominance of bedrock with occasional sediment-dominated facies in areas proximal to the eastern side of the flank (Model F; **Figure 3**).

Multiscale Geometrical Classification (MGC)

A total of 11 SVM classifiers were built based on different combinations of annotated samples from the training dataset (Part 1 of **Supplementary Figure 1**). Overall classifier training results had an average *ba* of 89.85%, and *fdr* ratio of 4.27. Classifier 6 presented the best *ba* and *fdr* with values of 99.8 and 8.98%, respectively (**Figure 4**). The training was performed with 20,000 core points and 10 scales with a minimum of 0.1, maximum of 1, and step of 0.2. Classifiers trained with classes from two different source clouds hence, different environments, presented higher *ba* and *fdr* ratios than classifiers trained with one single cloud source.

The classifier that presented the best performance (classifier 6 on **Figure 4**) was applied to the testing dataset (see Part 2 of **Supplementary Figure 1**). As this classifier was trained with two different source clouds, these were excluded from the test set, which was composed of the remainder of the dataset, i.e., six manually annotated dense clouds. Average accuracy and balanced accuracy scores were 68.2 and 74.7%, respectively. Two

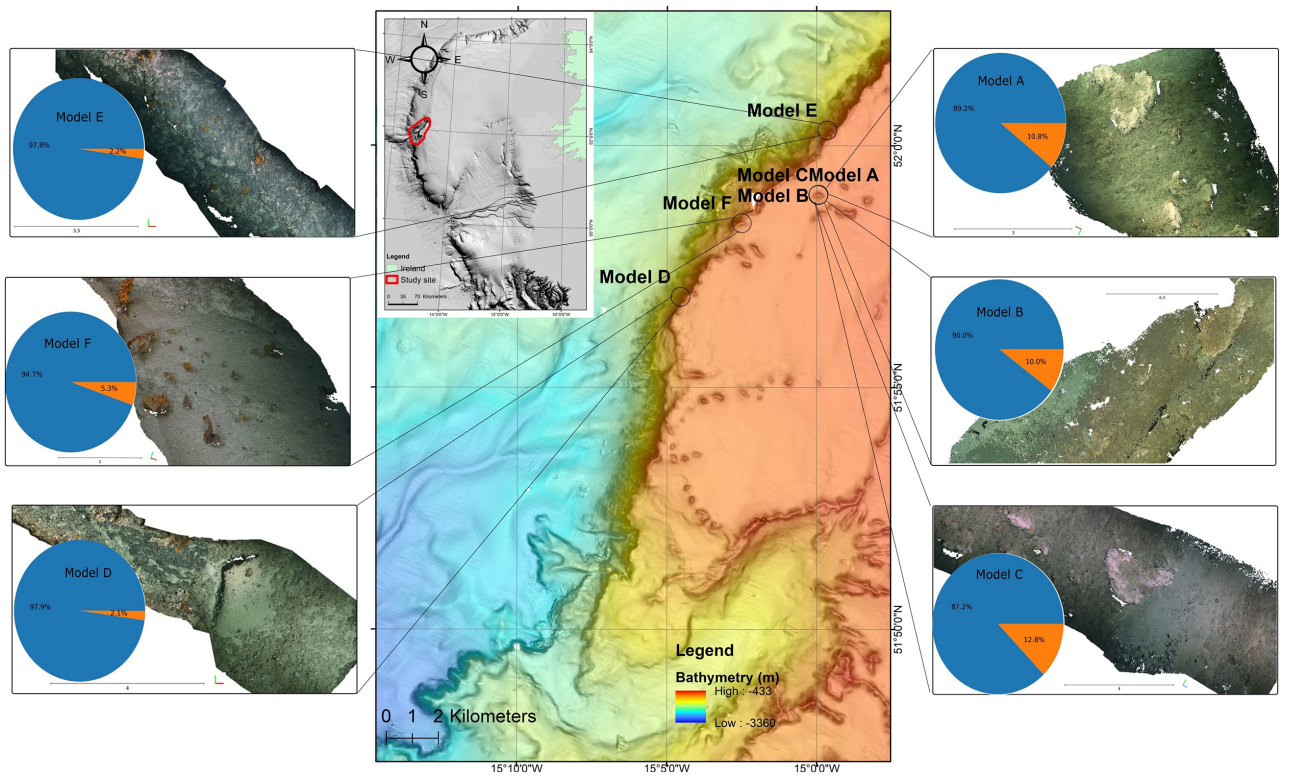

FIGURE 3 | Map showing the location of the Porcupine Bank Canyon on the Irish continental shelf and the location of each SfM reconstructed dense cloud produced in this study and its respective class distribution with manual annotation. Blue represents seabed and orange represents coral.

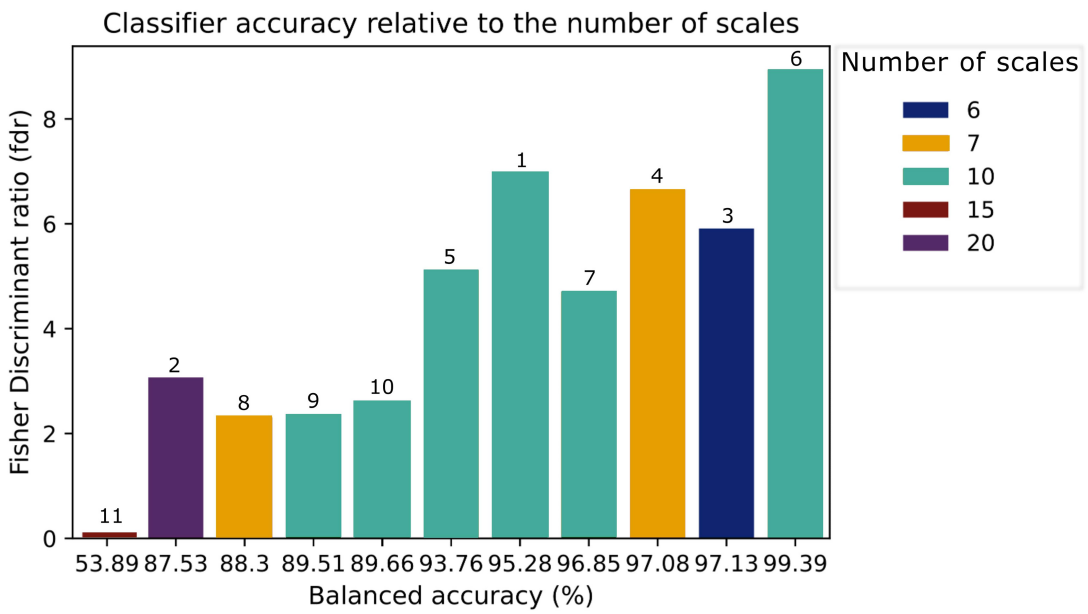

FIGURE 4 | Classifier accuracy in relation to the number of scales. The classifier ID is placed on the top of each bar. In the MGC method, scale is defined as the neighbourhood size of pixels to which the classifiers compute each metrics.

models presented accuracy scores above 80% and two models above 60% (**Figure 5**). Models which presented an accuracy score above 80% shared a similar coral distribution pattern. This pattern is represented by the vertical elongation of the coral branches through the *Z*-axis, i.e., height information, which can be accurately determined using 3D information (**Figure 6**-Model F).

Colour and Geometrical Classification (CGC)

The average classification accuracy score using the colour and geometrical classification method was approximately 67.9% with an average balanced accuracy of 58.1%. The classification output resulting from this method is shown in **Figure 7**. From the six models analysed on our testing dataset, two models presented accuracy scores below 60%. The remainder presented accuracy scores above 70%, ranging from 75 to 95% (**Figure 8**).

Object-Based Image Classification (OBIA)

The OBIA method was performed on the orthomosaics, respective DEMs, and calculated slopes of the same dataset. The average classification accuracy was approximately 100%. This result is to be expected because all orthomosaics were manually classified (**Figure 9**) and an adequate manual classification, when repeated by an expert, is expected to have the same outcome.

DISCUSSION

This study compares classification methods of 3D point clouds and 2D images. The workflow involved annotation of datasets, training of classifiers (MGC method), evaluation of the classification output, and the analysis of 3D and 2D-derived information from CWC environments. Studies have shown that overall accuracy is widely used for both OBIA and pixel-based classification accuracy assessments (Ye et al., 2018). Recent developments in accuracy assessment techniques have indicated redundancies in metrics such as standard Kappa indices (Foody, 1992; Pontius and Millones, 2011; Ye et al., 2018; Verma et al., 2020). The use of a Kappa score (Cohen, 1960) as a metric compares the observed accuracy to random accuracy; therefore, it is considered questionable to create a classification map (Foody, 2008; Pontius and Millones, 2011). Although there is substantial discussion on the appropriate

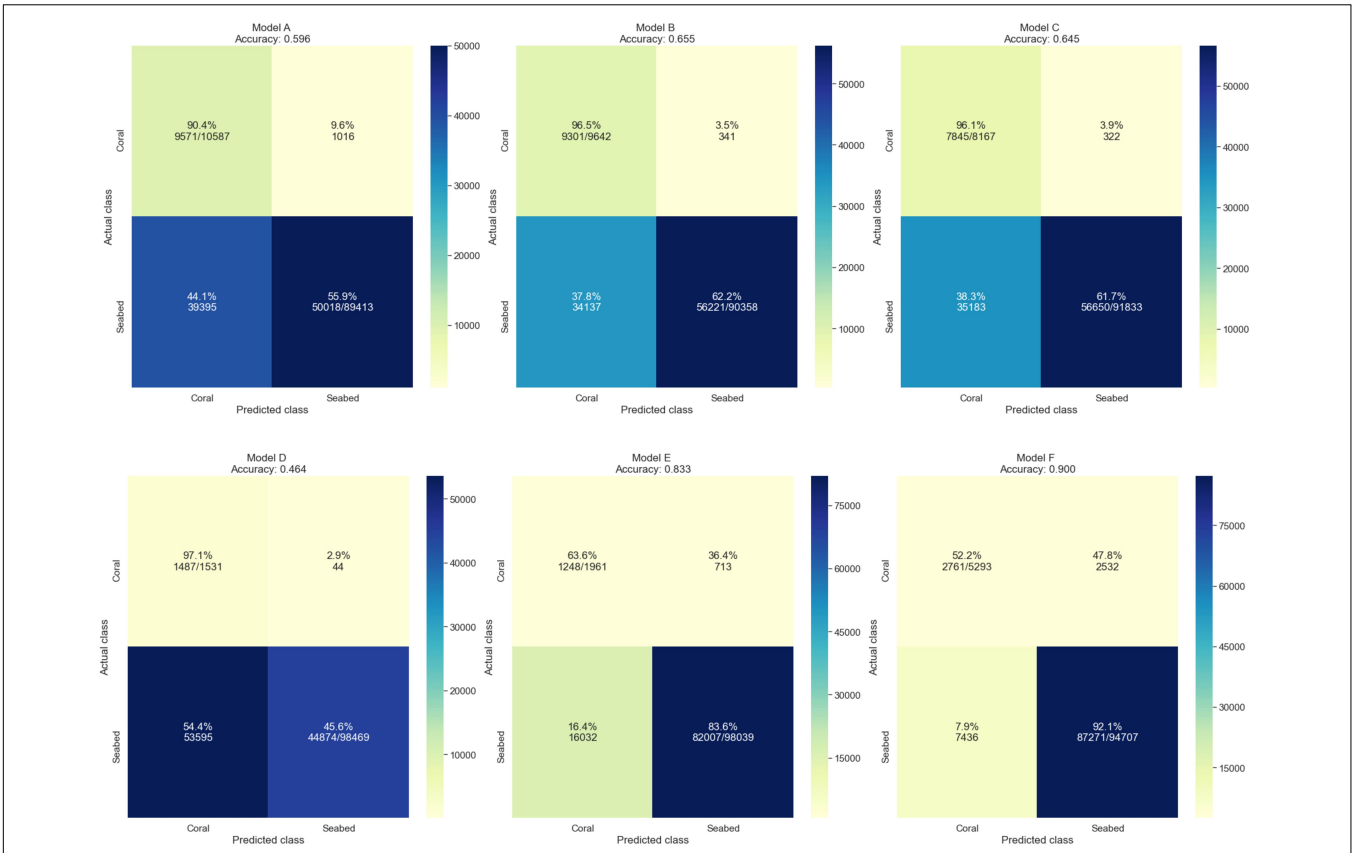

FIGURE 5 | Confusion matrices representing the MGC classification results for each dense cloud reconstruction. Confusion matrices show the accuracy score and the relationship between the referenced data and the classification. The "Actual class" on the *y*-axis refers to the manually annotated data, whereas the "Predicted class" on the *x*-axis relates to the classification output. The main diagonal of the matrices lists the correctly classified percentage of points per class. The colour scale bar on the right of each confusion matrix represents the number of points.

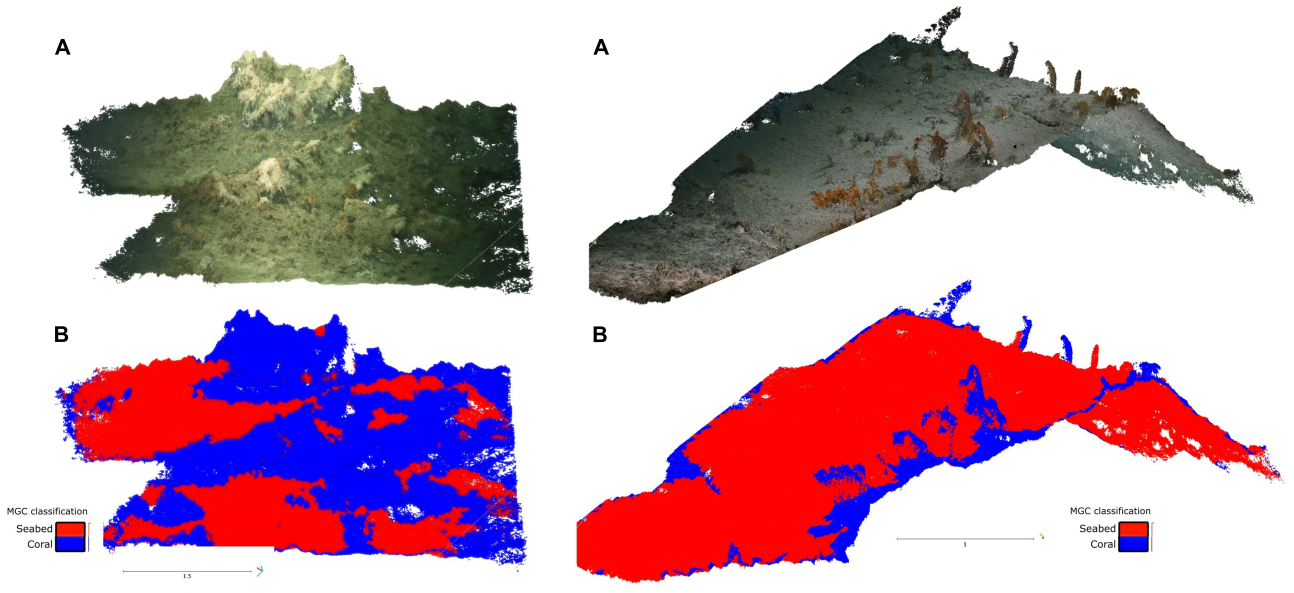

FIGURE 6 | Model F – Results of classification using the MGC method – **(A)** Dense cloud **(B)** Classification output. Model with predominance of black corals (Leiopathes sp.) Red is seabed and blue is coral. **Model A** – Results of classification using the MGC method – **(A)** Dense cloud **(B)** Classification output. Model with predominance of coral rubble patterns. Red is seabed and blue is coral.

metrics for image classification (Congalton, 1991; Banko, 1998; Foody, 2008; Ye et al., 2018), the confusion matrices presented here are a neutral representation of the true positives and true negatives of the classification.

The class distribution of the test data showed more abundance of corals on areas located on the eastern canyon flank. Reconstructions from sites located proximal to the canyon axis, towards the west, presented fewer coral features than sites located on the eastern canyon flank, as also described in previous studies (Appah et al., 2020; Lim et al., 2020). Appah et al. (2020) show that benthic taxa mean percentage coverage is twice as high in the flank as in adjacent areas, such as north towards the canyon head and the southern part of the canyon. Lim et al. (2020) provide a high-resolution habitat suitability correlation with current speeds, photogrammetry, and coral distribution in the PBC, showing that the variation in coral habitats does not follow a specific pattern, for example, from south to north. This result was also observed in reconstructions from areas located proximal to the canyon flank ridge (models D, E, and F), where the percentage of coral did not present any major increase or decrease following the north–south trend.

Classification Results

The *ba* and *fdr* ratios obtained for method MGC indicate that classifiers were influenced by the diversity of point sources used during the training process. Classifiers that were trained with two different dense clouds showed higher *ba* and *fdr* than classifiers trained with a single dense cloud. This suggests that training data with different datasets including those with habitat variability, e.g., different ratios of coral, seabed, and seabed facies, have a positive impact on the classifier performance, as also seen by Mountrakis et al. (2011), Brodu and Lague (2012), and Weidner et al. (2019) in terrestrial data studies. Interestingly, classifier accuracy results (*ba* and *fdr* ratios) showed that increasing the number of scales did not directly impact the quality of the classifier, as increasing the scale past a certain number did not necessarily lead to an increase in accuracy (see **Figure 4**). Thus, incorporating a great number of scales to build a classifier aiming to address a variety of seabed features in the classification computation did not show an improvement on the classifier performance and it can increase the computational complexity required to train the classifier. The process of incorporating multiple scales to acquire the best combination of scales thereby allowing the maximum separability between two classes is constructed automatically and as such, it can tend to overfit. SVM model overfitting can happen by maximising the margin and minimising the training error, which is typical of not only SVMs but also general kernel-based functions (Mountrakis et al., 2011).

Dense clouds that shared a similar coral distribution pattern, such as individual coral colonies with high vertical elongation and low presence of coral rubble as shown in Model F (**Figure 6**), had high accuracy scores (>80%). In contrast, models with lower accuracy results (<60%) (**Figure 6**-Model A) originated from areas with less defined feature boundaries such as coral rubble.

The colour and geometrical classification algorithm applied in the CGC method did not show any definite patterns concerning the structural complexity of the environment. Even though the classification outputs showed that coral

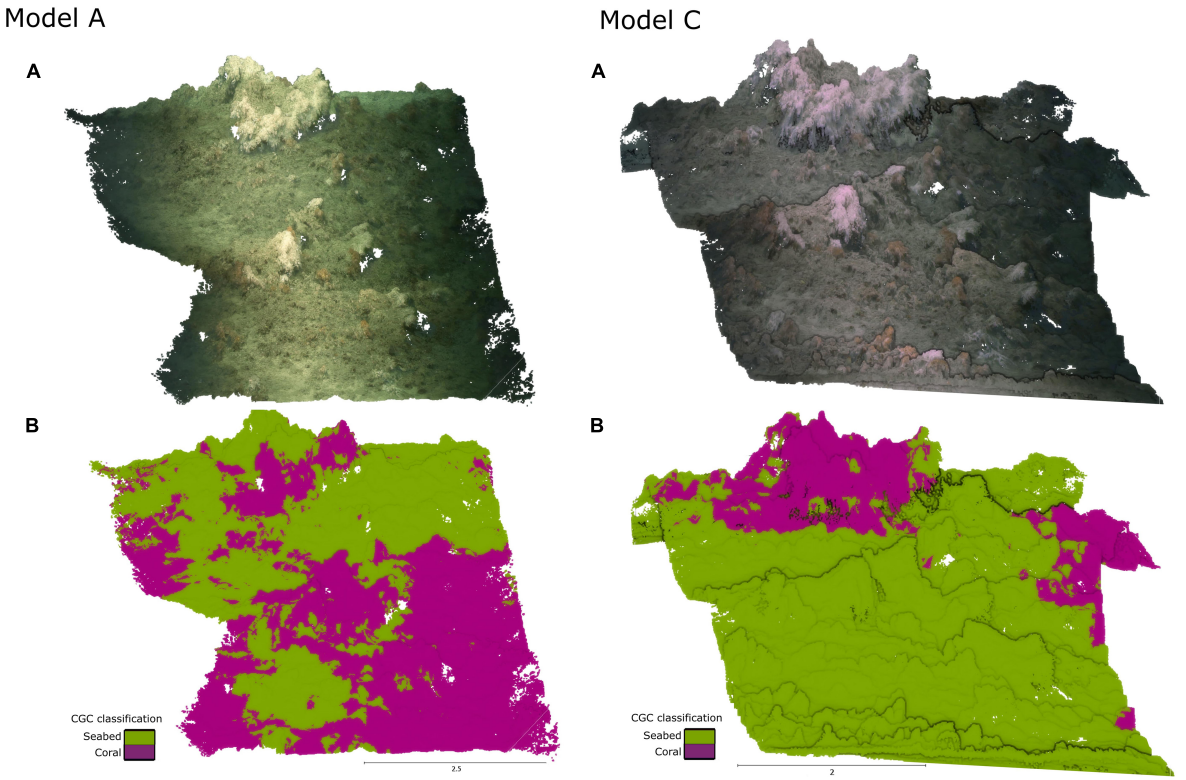

FIGURE 7 | Results of classification using CGC method—**(A)** Dense cloud and **(B)** classification output with CGC method.

colonies and patches tended to be misclassified in non-flat areas, the classifier resulted in different behaviours when applied to dense-cloud reconstructions of similar environments (**Figure 7**). In previous studies, the algorithm performed well for the detection of buildings and roads, but it misclassified vegetation and ground, especially in datasets containing hills and non-flat surfaces (Becker et al., 2018) meaning that terrain variations could have influenced object detection. Performance results showed that, although accuracy scores were >60% for the majority of the models, the visual assessment of the predicted output was not in accordance with the high values, as the classification results did not reflect the real objects clearly. Therefore, this result suggests that the high accuracy score may have been derived from the class imbalance in the test dataset, given that the seabed is more dominant than the coral class. Thus, the balanced accuracy provided a better representation of the overall performance. These results may also reflect the similarity of RGB spectral signatures as previously mentioned here and discussed in Lichti (2005), Beijbom et al. (2012), and Hopkinson et al. (2020). It is also possible that the performance of the CGC classifier may improve if there was an intermediary step that allowed training with seafloor and coral data within Agisoft Metashape. Nevertheless, the minimal user input required for this method, since pre-training is not necessary, makes it suitable for fast identification of seabed distribution.

In relation to the OBIA method, the automated segmentation performed better in small-scale orthomosaics (<4 m) where corals and rubble were easily distinguishable. In large-scale models (>8 m), the segmentation tended to under or over-segment, resulting in a poor differentiation in coral and seabed classes, specifically between coral patches and coral rubble (**Figure 9**). A benefit of utilising object-based techniques applied to classification tasks is the automatic segmentation process, which in the workflow shown herein (**Supplementary Figure 3**) can be faster and more accurate than manual segmentation for annotation of datasets. However, although orthomosaics and DEMs provide height information that is useful for larger scale models, they can be limiting for high-resolution analyses. Conversely, 3D metrics derived from vector dispersion and triangulation in dense clouds provide more detailed information for characterising individual coral colonies and benthic species (Fukunaga and Burns, 2020). Thus, the use of 2D metrics for detailed habitat analysis can lead to lack of discernment when detecting seabed features, e.g., coral branches, coral rubble, and sand ripples as also noted by Hopkinson et al. (2020).

Comparison Within 3D Classifications

Accuracy results (**Table 1**) suggest that models behaved similarly when 3D methods are used (MGC and CGC). Models that obtained an accuracy score of >60% with the MGC method also obtained a comparable result for the CGC method. Occasionally, MGC tended to ignore coral, while

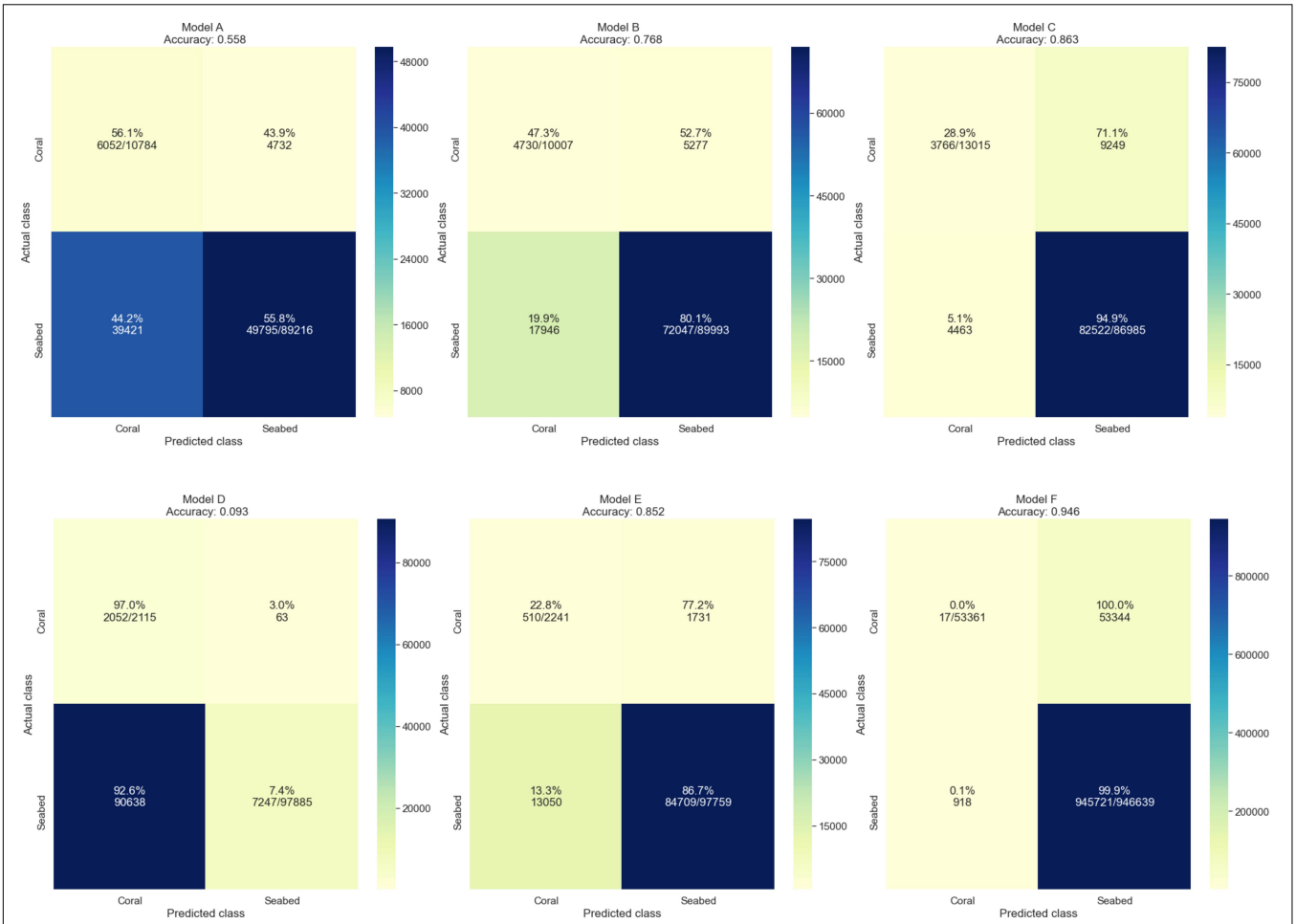

FIGURE 8 | Confusion matrices representing the CGC classification results for each dense cloud reconstruction. The "Actual class" on the *y*-axis refers to the manually annotated data, whereas the "Predicted class" on the *x*-axis relates to the classification output. The main diagonal of the matrices lists the correctly classified percentage of points per class. The colour scale bar on the right of each confusion matrix represents the number of points.

CGC tended to overclassify such objects. Both CGC and MGC appeared to be susceptible to object occlusion and canopy effects created by objects. This occlusion was recognised by a classification pattern occurring not only on the object itself (e.g., coral) but also on the shade it created, producing an elongated pattern behind the object consistent with its shadow (**Figures 6**, **7**).

In support of this observation, challenges related to the partial occlusion of objects and lighting artefacts have been addressed in other studies (Singh et al., 2004; Gracias and Negahdaripour, 2005). Lighting artefacts such as light scattering, colour shifts, and blurring related to the data acquisition can be considered a bottleneck which impacts the overall model resolution and hence the classification output (Bryson et al., 2015, 2016, 2017). This difficulty can be addressed with the use of image enhancement methods, e.g., texture delighting and colour filtering that can diminish object occlusion artefacts (Bryson et al., 2015). In the overall outputs, the canopy effect pattern was more evident in the CGC method. Furthermore, dense cloud models with a low RGB variability hence, similar RGB values for coral and seabed, resulted in slightly different classification outputs with the CGC method not being able to recognise seabed as compared to the method MGC. As previously mentioned, the classifier in the CGC method also seemed to take into consideration terrain surface variations. Conversely, the geometrical approach and the resistance to shadow effects of the MGC provided a degree of variability and heterogeneity in the class characteristics. As such, MGC appears more suitable for the classification of CWC because (a) it addressed coral colonies and coral patches more

TABLE 1 | Accuracy metrics for Method 1–Multiscale Geometrical Classification (MGC), Method 2–Colour and Geometrical Classification (CGC), and Method 3–Object-based Image Classification (OBIA).

Accuracy/method	MGC	CGC	OBIA
Balanced accuracy	0.74	0.66	1
Accuracy score	0.68	0.56	1

The values represent the average from the results on the testing set.

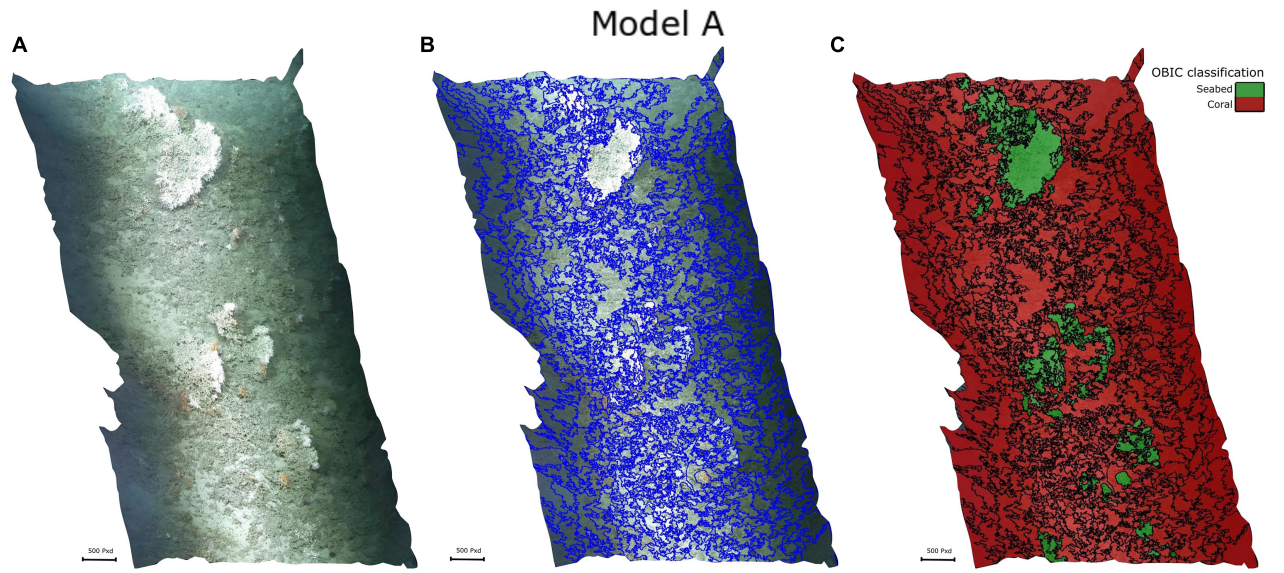

FIGURE 9 | Results of classification using OBIA method—**(A)** Orthomosaic, **(B)** output of the multi-resolution automated segmentation, and **(C)** manual classification.

accurately, (b) it was able to identify seabed coverage in all 3D reconstructions, and (c) it can be reapplied to classify similar coral reef environments. As a preliminary study, the results showed herein provide important insights towards the advancement on the venue of 3D classification as an accessible and informative approach.

Cost and Data-Loss Related to Representing 3D Objects as 2D

With the exception of the CGC method, all methods required similar amounts of data processing, which was mainly allocated to segmentation, labelling, and parameter-tuning, e.g., manual segmentation and labelling in MGC and manual classification in the OBIA method. Even though visual classification output did not fully delineate areas where coral rubble and gradational boundaries were present, the CGC method provided more accurate results when applied to models where objects have well-defined boundaries and sharp edges such as man-made objects (Becker et al., 2018). Conversely, the MGC method is more appropriate for complex scenes with high environmental variability (Brodu and Lague, 2012). One important aspect that should be considered in the MGC application is the amount of training data required to train the classifier. As for most of the classification methods, training data size and availability should be evaluated prior to choosing the methodology to be followed as it directly impacts the performance of the classifier (Lu and Weng, 2007; Maxwell et al., 2018; Zurowietz et al., 2018).

Similarly, the abundance of coral rubble and octocorals must be considered when choosing the classification method as they are subject to underwater colour and intensity distortions (Beijbom et al., 2012; Bryson et al., 2013). Such features present similar values within the intensity range and tend to exhibit wave-length attenuation when reconstructed (Bryson et al., 2013). Attention is drawn to coral rubble features as they present undefined boundary features which hinders their detection. Previous studies have also highlighted the difficulties of automatically classifying coral rubble in images (Beijbom et al., 2012) and 3D models (Hopkinson et al., 2020). Coral rubble occurs due to the coral exposure for extensive periods which lead to abrasion and bioerosion of coral framework (Titschack et al., 2015). High proportions of coral rubble may be indicative of high current speeds in the area (Lim et al., 2020). In contrast, the segmentation utilised in the OBIA method successfully distinguished coral rubble from sediment. This observation agrees with previous studies that have shown that orthomosaics can be useful for high-resolution habitat mapping of large areas (Lim et al., 2017; Conti et al., 2019). Although coral rubble was not included as a class on our framework, this observation can be useful for future studies.

Representing 3D objects in a 2D space may potentially lead to data bias due to misrepresentation of the object in the feature space and the use of metrics that disregard

TABLE 2 | Percentage of class distribution results from the manual annotation for each habitat and each class in 2D and 3D.

	3D dense cloud		OBIA	
	Coral	Seabed	Coral	Seabed
Model A	10.8%	89.2%	9.3%	90.7%
Model B	10.0%	90.0%	6.9%	93.1%
Model C	12.8%	87.2%	8.4%	91.6%
Model D	2.1%	97.9%	5.5%	94.5%
Model E	2.2%	97.8%	4.5%	95.5%
Model F	5.3%	94.7%	7.7%	92.3%
Average	7.2%	92.8%	7.1%	92.9%

its multidimensionality factors. In this study, two manual annotation schemes were used to provide a baseline and ground-truth for accuracy calculation. Annotations were performed by an expert in dense-clouds (3D) and orthomosaics for each 3D reconstruction. **Table 2** shows the percentage distribution of classes of each model in each manual annotation schemes: 3D dense cloud annotation and OBIA manual classification.

Class distribution results for each method (**Table 2**) show that there is a higher distribution of coral class within the 3D dense-cloud annotation in comparison to the OBIA method in 50% of the models. When such variation happens, there is a difference of up to 4.45% in the percentage of coral with a mean of 3.02%. Conversely, in models where the distribution of coral class is higher in the OBIA methods, the difference is only up to 3.39%, with a mean of 2.75%.

The average class distribution for the 3D dense cloud was 7.2% coral and 92.8% seabed as opposed to 7.1% coral and 92.9% seabed in the OBIA method. The average of the difference between class distributions was 0.2%. These results show that there is potentially an impact of at least a magnitude order of a tenth of the value in using 2D methods to represent objects that are naturally 3D structures. Although these values may not appear significant in the overall scheme, they have the potential to impact studies whose aims are derived from habitat mapping at a sub-centimetre resolution and a more significant impact when applied over large areas.

Scleractinian corals are naturally vertical-orientated features that, when mapped using 2D metrics, may give a small contribution in the percentage coverage. The 3D branching framework of CWC can increase sediment baffling with reefs or around colonies by offering a resistance to currents, for example (Mienis et al., 2019; Lim et al., 2020). However, the vertical structure of corals would be taken into account in overall biomass estimates if mapped in 3D. Furthermore, calculation of biomass considering all aspects of the environment is extremely relevant to understanding coral reef metabolism and overall environmental dynamics (McKinnon et al., 2011; Burns et al., 2015a, 2019; Price et al., 2019; Hopkinson et al., 2020). In comparison to 2D metrics, the use of multiscale dimensionality features that describe the local geometry of each point in relation to the entire scene makes 3D classification more suitable for the analysis of real complex scenarios at higher resolutions. Thus, advancing from commonly employed 2D image analysis techniques to 3D methods could provide more realistic representations of coral reefs and submarine environments (Fisher et al., 2007; Anelli et al., 2019).

Main Advantages and Disadvantages of the 3D Workflows Identified Within This Study

Three-dimensional reconstructions provide rich, non-destructive ecological and structural habitat information (Burns et al., 2015b; Figueira et al., 2015; Pizarro et al., 2017; Price et al., 2019), serving as a valuable tool for monitoring growth rates and assessing impacts of environmental disturbances (Bennecke et al., 2016; Marre et al., 2019). The use of SfM can also increase versatility and repeatability of reef surveys (Storlazzi et al., 2016; Bayley et al., 2019; Lim et al., 2020) as it can provide accurate quantifications for habitat coverage as well as coral orientation analyses (Lim et al., 2020). The 3D reconstructions produced in this study can complement recent studies (e.g., Appah et al., 2020; Lim et al., 2020) by providing an object of comparison for spatio-temporal changes in the PBC. The workflows applied herein yield the identification and quantification of CWC distribution at high resolutions.

In contrast, monitoring seabed habitats through 3D reconstruction require centimetric to milimetric resolutions and corresponding accuracies (Marre et al., 2019). High-resolution 3D models require significant data resources (storage and processing power) (Bayley and Mogg, 2020; Hopkinson et al., 2020; Mohamed et al., 2020). Therefore, it is important to highlight the constraints associated with manipulating 3D data. In many cases, it is necessary to develop sub-sampling processes to analyse large batches of data without compromising data resolution. The computer resources and methods available to manipulate and analyse 3D data from marine environments at larger scales could be further improved (Bryson et al., 2017; Robert et al., 2017). The 3D-based workflows described herein demonstrate that most off-the-shelf algorithms need to be adapted for seabed classification and mapping.

The use of SfM for seabed mapping requires consideration of a number of variables to determine the feasibility and accuracy of each study (Burns et al., 2015a; Bayley and Mogg, 2020). For example, environmental conditions such as visibility, swell variations, changes in camera altitude, and ROV speed can impact the survey design, hence, the video quality (Mohamed et al., 2018; Anelli et al., 2019; Marre et al., 2019). Factors related to HD video acquisition and processing such as camera position, lens, light attenuation, calibration, image overlap, and software options can affect the results of 3D reconstructions (Marre et al., 2019; Rossi et al., 2020). Furthermore, high-resolution reconstruction of models can take up to 12 h of processing and a considerable amount of HD video footage (Robert et al., 2017). A regular laptop computer may face limitations to process the resulting models, which can be over 10 GB in size (Robert et al., 2017).

CONCLUSION

Cold-water corals significantly contribute to deep-sea biodiversity due to their 3D structure and reef-building capacity. Submarine canyons act as conduits for sediments, nutrients, and organic matter supporting high biomass communities (Nittrouer and Wright, 1994; Puig and Palanques, 1998; Harris and Whiteway, 2011). There is an increasing demand for new methods able to efficiently capture fine-scale changes in these environments. SfM can contribute to more precise structural analysis of CWC habitats while also providing grounds for temporal and volumetric change detection in CWC reefs. This study describes three classification methods applied to CWC reefs within the PBC SAC in the North East Atlantic. The workflows described provide an original and not yet

applied methodology for the classification of 3D reconstructed marine environments at the PBC. The dataset consisted of 3D reconstructed point clouds, respective orthomosaics, DEMs, and associated terrain variables of CWC environments. The classification workflows designed for 3D point clouds showed a similar accuracy, even though visual results had different outputs and had a different level of robustness. The balanced accuracy and accuracy scores averaged 67.2% for the 3D methods. The study defines methodologies that are compatible with off-the-shelf commercial software with high-resolution data. Furthermore, the execution of the methods was fast and appeared suitable for the wider deep-sea research community who have access to the SfM point cloud data. Executing more complex frameworks is possible at the expense of computation power and time resources. Future research should involve the application of unsupervised learning with use of geometrical features and application of other ML algorithms for supervised learning. The use of more robust classification methods and higher resolution 3D reconstructions will aid the inclusion of more classes, especially of objects with irregular contour boundaries.

DATA AVAILABILITY STATEMENT

The raw data supporting the conclusions of this article will be made available by the authors, without undue reservation.

AUTHOR CONTRIBUTIONS

All authors contributed to the conceptualisation, writing, review, and editing of the manuscript, and read and agreed to the published version of the manuscript. LO and AL: methodology, investigation, data curation, and project administration. LO: formal analysis, writing—original draft preparation, and visualisation. AL and AW: resources. AL, LC, and AW: supervision. AL, AW, and LO: funding acquisition.

FUNDING

This research was funded by Science Foundation Ireland, grant number: 16/IA/4528 and Irish Research Council, grant number: GOIPG/2020/1659. The APC was funded by Science Foundation Ireland. AL was supported by the European Union's Horizon 2020 Research and Innovation Program "iAtlantic" project, grant number: 818123. LC was supported by São Paulo Research Foundation (Fundação de Amparo à Pesquisa do Estado de São Paulo – FAPESP), grant number: 2017/19649-8.

ACKNOWLEDGMENTS

The authors would like to thank the Science Foundation Ireland, Geological Survey Ireland, and Marine Institute who funded this work through the MMMonKey_Pro (grant number 16/IA/4528) and the Irish Research Council for funding the first author's Ph.D. research project ASMaT (grant number: GOIPG/2020/1659). Especial thanks goes to Marine Institute for funding the ship time on RV Celtic Explorer under the 2018 and 2019 Ship Time Program of the National Development scheme and the shipboard party of RV Celtic Explorer and ROV Holland 1 for their support with data acquisition.

SUPPLEMENTARY MATERIAL

The Supplementary Material for this article can be found online at: https://www.frontiersin.org/articles/10.3389/fmars.2021.640713/full#supplementary-material

REFERENCES

Addamo, A. M., Vertino, A., Stolarski, J., García-Jiménez, R., Taviani, M., and Machordom, A. (2016). Merging scleractinian genera: the overwhelming genetic similarity between solitary Desmophyllum and colonial Lophelia. *BMC Evol. Biol.* 16:1–17. doi: 10.1186/s12862-016-0654-8

Agisoft (2019). *Agisoft Metashape User Manual. 160*. Available online at: https://www.agisoft.com/pdf/metashape-pro_1_5_en.pdf (accessed March 12, 2020).

Akbani, R., Kwek, S., and Japkowicz, N. (2004). "Applying support vector machines to imbalanced datasets," in *Proceedings of the 15th European Conference on Machine Learning*, Berlin, 39–50.

Anelli, M., Julitta, T., Fallati, L., Galli, P., Rossini, M., and Colombo, R. (2019). Towards new applications of underwater photogrammetry for investigating coral reef morphology and habitat complexity in the Myeik Archipelago. *Myanmar. Geocar. Int.* 34, 459–472. doi: 10.1080/10106049.2017.1408703

Appah, J. K. M., Lim, A., Harris, K., O'Riordan, R., O'Reilly, L., and Wheeler, A. J. (2020). Are non-reef habitats as important to benthic diversity and composition as coral reef and rubble habitats in submarine canyons? Analysis of controls on benthic megafauna distribution in the porcupine bank Canyon, NE Atlantic. *Front. Mar. Sci.* 7:831. doi: 10.3389/fmars.2020.571820

Banko, G. (1998). *A Review of Assessing the Accuracy of and of Methods Including Remote Sensing Data in Forest Inventory. Internation Institute for Applied Systems Analysis, Interim Report IT-98-081*. Laxenburg: Internation Institute for Applied Systems Analysis.

Barbosa, R. V., Davies, A. J., and Sumida, P. Y. G. (2019). Habitat suitability and environmental niche comparison of cold-water coral species along the Brazilian continental margin. *Deep Sea Res. Part I* 155:103147. doi: 10.1016/j.dsr.2019.103147

Bayley, D. T. I., and Mogg, A. O. M. (2020). A protocol for the large−scale analysis of reefs using structure from motion photogrammetry. *Methods Ecol. Evolut.* 11, 1410–1420. doi: 10.1111/2041-210x.13476

Bayley, D. T. I., Mogg, A. O. M., Koldewey, H., and Purvis, A. (2019). Capturing complexity: field-testing the use of "structure from motion" derived virtual models to replicate standard measures of reef physical structure. *PeerJ* 2019:6540. doi: 10.7717/peerj.6540

Becker, C., Rosinskaya, E., Häni, N., d'Angelo, E., and Strecha, C. (2018). Classification of aerial photogrammetric 3D point clouds. *Photogramm. Eng. Remote Sens.* 84, 287–295. doi: 10.14358/PERS.84.5.287

Beijbom, O., Edmunds, P. J., Kline, D. I., Mitchell, B. G., and Kriegman, D. (2012). "Automated annotation of coral reef survey images," in. *Proceedings of the IEEE Computer Society Conference on Computer Vision and Pattern Recognition*, Washington, DC, 1170–1177. doi: 10.1109/CVPR.2012.6247798

Bennecke, S., Kwasnitschka, T., Metaxas, A., and Dullo, W. C. (2016). In situ growth rates of deep-water octocorals determined from 3D photogrammetric reconstructions. *Coral Reefs* 35, 1227–1239. doi: 10.1007/s00338-016-1471-7

Benz, U. C., Hofmann, P., Willhauck, G., Lingenfelder, I., and Heynen, M. (2004). Multi-resolution, object-oriented fuzzy analysis of remote sensing data for GIS-ready information. *ISPRS J. Photogramm. Remote Sens.* 58, 239–258. doi: 10.1016/j.isprsjprs.2003.10.002

Boolukos, C. M., Lim, A., O'Riordan, R. M., and Wheeler, A. J. (2019). Cold-water corals in decline – A temporal (4 year) species abundance and biodiversity appraisal of complete photomosaiced cold-water coral reef on the Irish Margin. *Deep Sea Res. Part I Oceanogr. Res Pap.* 146, 44–54. doi: 10.1016/j.dsr.2019.03.004

Brodersen, K. H., Ong, C. S., Stephan, K. E., and Buhmann, J. M. (2010). "The balanced accuracy and its posterior distribution," in *Proceedings of the International Conference on Pattern Recognition*, Istanbul, 3121–3124. doi: 10.1109/ICPR.2010.764

Brodu, N., and Lague, D. (2012). 3D terrestrial LiDAR data classification of complex natural scenes using a multi-scale dimensionality criterion: applications in geomorphology. *ISPRS J. Photogramm. Remote Sens.* 68, 121–134. doi: 10.1016/j.isprsjprs.2012.01.006

Bryson, M., Ferrari, R., Figueira, W., Pizarro, O., Madin, J., Williams, S., et al. (2017). Characterization of measurement errors using structure-from-motion and photogrammetry to measure marine habitat structural complexity. *Ecol. Evol.* 7, 5669–5681. doi: 10.1002/ece3.3127

Bryson, M., Johnson-Roberson, M., Pizarro, O., and Williams, S. (2016). "Colour-Consistent structure-from-motion models using underwater imagery," in *Proceedings of the Robotics: Science and System*, Sydney, NSW. doi: 10.15607/rss.2012.viii.005

Bryson, M., Johnson-Roberson, M., Pizarro, O., and Williams, S. B. (2013). Colour-consistent structure-from-motion models using underwater imagery. *Robotics* 8, 33–40. doi: 10.7551/mitpress/9816.003.0010

Bryson, M., Johnson-Roberson, M., Pizarro, O., and Williams, S. B. (2015). True color correction of autonomous underwater vehicle imagery. *J. Field Robot.* 33, 1–17. doi: 10.1002/rob.21638

Burns, J. H. R., Delparte, D., Gates, R. D., and Takabayashi, M. (2015a). Integrating structure-from-motion photogrammetry with geospatial software as a novel technique for quantifying 3D ecological characteristics of coral reefs. *PeerJ* 2015:1077. doi: 10.7717/peerj.1077

Burns, J. H. R., Delparte, D., Gates, R. D., and Takabayashi, M. (2015b). Utilizing underwater three-dimensional modeling to enhance ecological and biological studies of coral reefs. *Int. Arch. Photogramm. Remote Sens. Spatial Inf. Sci.* 40, 61–66. doi: 10.5194/isprsarchives-XL-5-W5-61-2015

Burns, J. H. R., Fukunaga, A., Pascoe, K. H., Runyan, A., Craig, B. K., Talbot, J., et al. (2019). 3D habitat complexity of coral reefs in the northwestern hawaiian islands is driven by coral assemblage structure. *ISPRS Annal. Photogramm. Remote Sens. Spatial Inf. Sci.* 42, 61–67. doi: 10.5194/isprs-archives-XLII-2-W10-61-2019

Carlevaris-Bianco, N., Mohan, A., and Eustice, R. M. (2010). Initial results in underwater single image dehazing. *MTS/IEEE Seattle OCEANS* 2010, 1–8. doi: 10.1109/OCEANS.2010.5664428

Carrivick, J. L., Smith, M. W., and Quincey, D. J. (2016). *Structure from Motion in the Geosciences*. Hoboken, NJ: Wiley Blackwell.

Cocito, S., Sgorbini, S., Peirano, A., and Valle, M. (2003). 3-D reconstruction of biological objects using underwater video technique and image processing. *J. Exp. Mar. Biol. Ecol.* 297, 57–70. doi: 10.1016/S0022-0981(03)00369-1

Cohen, J. (1960). A coefficient of agreement for nominal scales. *Educ. Psychol. Measur.* 20, 37–46. doi: 10.1177/001316446002000104

Congalton, R. G. (1991). A review of assessing the accuracy of classifications of remotely sensed data. *Remote Sens. Environ.* 37, 35–46. doi: 10.1016/0034-4257(91)90048-B

Conti, L. A., Lim, A., and Wheeler, A. J. (2019). High resolution mapping of a cold water coral mound. *Sci. Rep.* 9:1016. doi: 10.1038/s41598-018-37725-x

Costello, M. J., McCrea, M., Freiwald, A., Lundälv, T., Jonsson, L., Bett, B. J., et al. (2005). "Role of cold-water *Lophelia pertusa* coral reefs as fish habitat in the NE Atlantic," in *Cold-Water Corals and Ecosystems*, eds A. Freiwald and J. M. Roberts (Berlin: Springer), 771–805. doi: 10.1007/3-540-27673-4_41

Courtney, L. A., Fisher, W. S., Raimondo, S., Oliver, L. M., and Davis, W. P. (2007). Estimating 3-dimensional colony surface area of field corals. *J. Exp. Mar. Biol. Ecol.* 351, 234–242. doi: 10.1016/j.jembe.2007.06.021

De Clippele, L. H., Gafeira, J., Robert, K., Hennige, S., Lavaleye, M. S., Duineveld, G. C. A., et al. (2017). Using novel acoustic and visual mapping tools to predict the small-scale spatial distribution of live biogenic reef framework in cold-water coral habitats. *Coral Reefs* 36, 255–268. doi: 10.1007/s00338-016-1519-8

de Mol, B., Henriet, J.-P., and Canals, M. (2005). Development of coral banks in Porcupine Seabight: do they have Mediterranean ancestors? *Cold Water Corals Ecosyst.* 5, 515–533. doi: 10.1007/3-540-27673-4_26

Dorschel, B., Wheeler, A. J., Monteys, X., and Verbruggen, K. (2010). *Atlas of the Deep-Water Seabed: Ireland*. Dordrecht: Springer Netherlands. doi: 10.1007/978-90-481-9376-9

European Union Habitats Directive (2016). *European Union Habitats (Porcupine Bank Canyon Special Area of Conservation 003001) Regulations 2016*. Available online at: http://www.irishstatutebook.ie/eli/2016/si/106/made/en/pdf (accessed October 25, 2020).

Fanelli, E., Delbono, I., Ivaldi, R., Pratellesi, M., Cocito, S., and Peirano, A. (2017). Cold-water coral *Madrepora oculata* in the eastern Ligurian Sea (NW Mediterranean): historical and recent findings. *Aquat. Conserv. Mar. Freshw. Ecosyst.* 27, 965–975. doi: 10.1002/aqc.2751

Ferrari, R., Marzinelli, E. M., Ayroza, C. R., Jordan, A., Figueira, W. F., Byrne, M., et al. (2018). Large-scale assessment of benthic communities across multiple marine protected areas using an autonomous underwater vehicle. *PLoS One* 13:e0193711. doi: 10.1371/journal.pone.0193711

Figueira, W., Ferrari, R., Weatherby, E., Porter, A., Hawes, S., and Byrne, M. (2015). Accuracy and precision of habitat structural complexity metrics derived from underwater photogrammetry. *Remote Sens.* 7, 16883–16900. doi: 10.3390/rs71215859

Findlay, H. S., Artioli, Y., Moreno Navas, J., Hennige, S. J., Wicks, L. C., Huvenne, V. A. I., et al. (2013). Tidal downwelling and implications for the carbon biogeochemistry of cold-water corals in relation to future ocean acidification and warming. *Glob. Change Biol.* 19, 2708–2719. doi: 10.1111/gcb.12256

Fisher, W. S., Davis, W. P., Quarles, R. L., Patrick, J., Campbell, J. G., Harris, P. S., et al. (2007). Characterizing coral condition using estimates of three-dimensional colony surface area. *Environ. Monitor. Assess.* 125, 347–360. doi: 10.1007/s10661-006-9527-8

Foody, G. M. (1992). On the compensation for chance agreement in image classification accuracy assessment. *Photogramm. Eng. Remote Sens.* 58, 1459–1460.

Foody, G. M. (2008). Harshness in image classification accuracy assessment. *Int. J. Remote Sens.* 29, 3137–3158. doi: 10.1080/01431160701442120

Fosså, J. H., Lindberg, B., Christensen, O., Lundälv, T., Svellingen, I., Mortensen, P. B., et al. (2006). "Mapping of *Lophelia* reefs in Norway: experiences and survey methods," in *Cold-Water Corals and Ecosystems*, eds A. Freiwald and J. M. Roberts (Heidelberg: Springer-Verlag), 359–391. doi: 10.1007/3-540-27673-4_18

Freiwald, A., Fosså, J. H., Grehan, A., Koslow, T., and Roberts, J. M. (2011). *Cold-water Coral Reefs: Out of Sight – no Longer out of Mind. UNEP-WCMC Biodiversity Series*. Cambridge: World Conservation Monitoring Centre. doi: 10.5962/bhl.title.45025

Freiwald, A., and Roberts, J. M. (2005). *Cold-Water Corals and Ecosystems*. Berlin: Springer. doi: 10.1007/3-540-27673-4

Fukunaga, A., and Burns, J. H. R. (2020). Metrics of coral reef structural complexity extracted from 3D mesh models and digital elevation models. *Remote Sens.* 12:2676. doi: 10.3390/RS12172676

Fukunaga, A., Burns, J. H. R., Craig, B. K., and Kosaki, R. K. (2019). Integrating three-dimensional benthic habitat characterization techniques into ecological monitoring of coral reefs. *J. Mar. Sci. Eng.* 7:27. doi: 10.3390/jmse7020027

Gass, S. E., and Roberts, J. M. (2006). The occurrence of the cold-water coral *Lophelia pertusa* (Scleractinia) on oil and gas platforms in the North Sea: colony growth, recruitment and environmental controls on distribution. *Mar. Pollut. Bull.* 52, 549–559. doi: 10.1016/j.marpolbul.2005.10.002

Girardeau-Montaut, D. (2011). CloudCompare-Open Source Project. OpenSource Project. Paris, France.

Goatley, C. H. R., and Bellwood, D. R. (2011). The roles of dimensionality, canopies and complexity in ecosystem monitoring. *PLoS One* 6:e0027307. doi: 10.1371/journal.pone.0027307

Gómez-ríos, A., Tabik, S., Luengo, J., and Shihavuddin, A. S. M. (2018). Towards highly accurate coral texture images classification using deep convolutional neural networks and data augmentation towards highly accurate coral texture images classification using deep convolutional neural networks and data augmentation. *Exp. Syst. Appl.* 118, 315–328. doi: 10.1016/j.eswa.2018.10.010

Gracias, N., and Negahdaripour, S. (2005). Underwater mosaic creation using video sequences from different altitudes. *Proc. MTS/IEEE OCEANS* 2005:e1639933. doi: 10.1109/OCEANS.2005.1639933

Graham, N. A. J., and Nash, K. L. (2013). The importance of structural complexity in coral reef ecosystems. *Coral Reefs* 32, 315–326. doi: 10.1007/s00338-012-0984-y

Guinan, J., Grehan, A. J., Dolan, M. F. J., and Brown, C. (2009). Quantifying relationships between video observations of cold-water coral cover and seafloor features in rockall trough, west of Ireland. *Mar. Ecol. Prog. Ser.* 375, 125–138. doi: 10.3354/meps07739

Hackel, T., Wegner, J. D., and Schindler, K. (2016). Fast emantic segmentation of 3d point clouds with strongly varying density. *ISPRS Ann. Photogramm. Remote Sens. Spatial Inf. Sci.* 3, 177–184. doi: 10.5194/isprs-annals-III-3-177-2016

Harris, P. T., and Whiteway, T. (2011). Global distribution of large submarine canyons: geomorphic differences between active and passive continental margins. *Mar. Geol.* 285, 69–86. doi: 10.1016/j.margeo.2011.05.008

Hopkinson, B. M., King, A. C., Owen, D. P., Johnson-roberson, M., Long, M. H., and Bhandarkar, S. M. (2020). Automated classification of three-dimensional reconstructions of coral reefs using convolutional neural networks. *PLoS One* 15:e0230671. doi: 10.1371/journal.pone.0230671

House, J. E., Brambilla, V., Bidaut, L. M., Christie, A. P., Pizarro, O., Madin, J. S., et al. (2018). Moving to 3D: relationships between coral planar area, surface area and volume. *PeerJ* 6:e4280. doi: 10.7717/peerj.4280

Hovland, M., and Thomsen, E. (1997). Cold-water corals – Are they hydrocarbon seep related? *Mar. Geol.* 137, 159–164. doi: 10.1016/S0025-3227(96)00086-2

Huvenne, V. A. I., Bett, B. J., Masson, D. G., le Bas, T. P., and Wheeler, A. J. (2016). Effectiveness of a deep-sea cold-water coral Marine Protected Area, following eight years of fisheries closure. *Biol. Conserv.* 200, 60–69. doi: 10.1016/j.biocon.2016.05.030

Huvenne, V. A. I., Tyler, P. A., Masson, D. G., Fisher, E. H., Hauton, C., Hühnerbach, V., et al. (2011). A picture on the wall: innovative mapping reveals cold-water coral refuge in submarine canyon. *PLoS One* 6:e0028755. doi: 10.1371/journal.pone.0028755

Jonsson, L. G., Nilsson, P. G., Floruta, F., and Lundälv, T. (2004). Distributional patterns of macro- and megafauna associated with a reef of the cold-water coral *Lophelia pertusa* on the Swedish west coast. *Mar. Ecol. Progr. Ser.* 284, 163–171. doi: 10.3354/meps284163

Kavzoglu, T., and Yildiz, M. (2014). Parameter-Based performance analysis of object-based image analysis using aerial and Quikbird-2 images. *ISPRS Annal. Photogramm. Remote Sens. Spat. Inform. Sci.* 7, 31–37. doi: 10.5194/isprsannals-ii-7-31-2014

King, A., Bhandarkar, S. M., and Hopkinson, B. M. (2018). "A comparison of deep learning methods for semantic segmentation of coral reef survey images," in *Proceedings of the 2018 IEEE/CVF Conference on Computer Vision and Pattern Recognition Workshops (CVPRW)*, (Salt Lake City, UT: IEEE), 1475–14758. doi: 10.1109/CVPRW.2018.00188

Klápště, P., Urban, R., and Moudrı, V. (2018). "Ground classification of UAV image-based point clouds through different algorithms: open source vs commercial software," in *Proceedings of the 6th International Conference on "Small Unmanned Aerial Systems for Environmental Research*, Split, 15–18.

Koop, L., Snellen, M., and Simons, D. G. (2021). An object-based image analysis approach using bathymetry and bathymetric derivatives to classify the seafloor. *Geosciences* 11:45. doi: 10.3390/geosciences11020045

Kwasnitschka, T., Hansteen, T. H., Devey, C. W., and Kutterolf, S. (2013). Doing fieldwork on the seafloor: photogrammetric techniques to yield 3D visual models from ROV video. *Comput. Geosci.* 52, 218–226. doi: 10.1016/j.cageo.2012.10.008

Lambers, K., Verschoof-van der Vaart, W. B., and Bourgeois, Q. P. J. (2019). Integrating remote sensing, machine learning, and citizen science in dutch archaeological prospection. *Remote Sens.* 11, 1–20. doi: 10.3390/rs11070794

Leverette, T. L., and Metaxas, A. (2006). "Predicting habitat for two species of deep-water coral on the Canadian Atlantic continental shelf and slope," in *Cold-Water Corals and Ecosystems*, eds A. Freiwald and J. M. Roberts (Berlin: Springer-Verlag), 467–479. doi: 10.1007/3-540-27673-4_23

Lichti, D. D. (2005). Spectral filtering and classification of terrestrial laser scanner point clouds. *Photogramm. Rec.* 20, 218–240. doi: 10.1111/j.1477-9730.2005.00321.x

Lim, A., Huvenne, V. A. I., Vertino, A., Spezzaferri, S., and Wheeler, A. J. (2018). New insights on coral mound development from groundtruthed high-resolution ROV-mounted multibeam imaging. *Mar. Geol.* 403, 225–237. doi: 10.1016/j.margeo.2018.06.006

Lim, A., O'Reilly, L., Summer, G., Harris, K., Oliveira, L., O'Hanlon, Z., et al. (2019a). *Monitoring Changes in Submarine Canyon Coral Habitats - Leg 2 (MoCha_Scan I), survey (CE19014) of the Porcupine Bank Canyon*, *Cruise Report*. Cork, Ireland. Marine Institute. doi: 10.5281/zenodo.3819565

Lim, A., O'Reilly, L., Summer, G., Harris, K., Shine, A., Harman, L., et al. (2019b). *Monitoring Changes in Submarine Canyon Coral Habitats - Leg 1 (MoCha_Scan I), survey (CE19008) of the Porcupine Bank Canyon*, Cruise Report. Cork, Ireland. Marine Institute. doi: 10.5281/zenodo.3699111

Lim, A., Wheeler, A. J., and Arnaubec, A. (2017). High-resolution facies zonation within a cold-water coral mound: the case of the Piddington Mound, Porcupine Seabight, NE Atlantic. *Mar. Geol.* 390, 120–130. doi: 10.1016/j.margeo.2017.06.009

Lim, A., Wheeler, A. J., Price, D. M., O'Reilly, L., Harris, K., and Conti, L. (2020). Influence of benthic currents on cold-water coral habitats: a combined benthic monitoring and 3D photogrammetric investigation. *Sci. Rep.* 10:19433. doi: 10.1038/s41598-020-76446-y

Lowe, D. G., (1999). "Object recognition from local scale-invariant features," in *The Proceedings of the Seventh IEEE International Conference on Computer Vision*, 1150–1157. doi: 10.1109/ICCV.1999.790410

Lu, D., and Weng, Q. (2007). A survey of image classification methods and techniques for improving classification performance. *Int. J. Rem. Sens.* 28, 823–870. doi: 10.1080/01431160600746456

Marburg, A., and Bigham, K. (2016). "Deep learning for benthic fauna identification," in *Proceeding of the OCEANS 2016 MTS/IEEE Monterey, OCE 2016*, Monterey, CA. doi: 10.1109/OCEANS.2016.7761146

Marre, G., Holon, F., Luque, S., Boissery, P., and Deter, J. (2019). Monitoring marine habitats with photogrammetry: a cost-effective, accurate, precise and high-resolution reconstruction method. *Front. Mar. Sci.* 6:276. doi: 10.3389/fmars.2019.276

Masson, D. G., Bett, B. J., Billett, D. S. M., Jacobs, C. L., Wheeler, A. J., and Wynn, R. B. (2003). The origin of deep-water, coral-topped mounds in the northern Rockall Trough, Northeast Atlantic. *Mar. Geol.* 194, 159–180. doi: 10.1016/S0025-3227(02)00704-1

Maxwell, A. E., Warner, T. A., and Fang, F. (2018). Implementation of machine-learning classification in remote sensing: an applied review Implementation of machine-learning classification in remote sensing: an applied review. *Int. J. Remote Sens.* 39, 2784–2817. doi: 10.1080/01431161.2018.1433343

Mazzini, A., Akhmetzhanov, A., Monteys, X., and Ivanov, M. (2012). The Porcupine bank canyon coral mounds: oceanographic and topographic steering of deep-water carbonate mound development and associated phosphatic deposition. *Geo Mar. Lett.* 32, 205–225. doi: 10.1007/s00367-011-0257-8

McKinnon, D., He, H., Upcroft, B., and Smith, R. N. (2011). *Towards Automated and In-Situ, Near-Real Time 3-D Reconstruction of Coral Reef Environments*. Waikoloa, HI, USA.

Menna, F., Agrafiotis, P., and Georgopoulos, A. (2018). State of the art and applications in archaeological underwater 3D recording and mapping. *J. Cult. Herit.* 33, 231–248. doi: 10.1016/j.culher.2018.02.017

Mienis, F., Bouma, T., Witbaard, R., van Oevelen, D., and Duineveld, G. (2019). Experimental assessment of the effects of coldwater coral patches on water flow. *Mar. Ecol. Prog. Ser.* 609, 101–117. doi: 10.3354/meps12815

Mienis, F., van Weering, T., de Haas, H., de Stigter, H., Huvenne, V., and Wheeler, A. (2006). Carbonate mound development at the SW Rockall Trough margin based on high resolution TOBI and seismic recording. *Mar. Geol.* 233, 1–19. doi: 10.1016/j.margeo.2006.08.003

Mohamed, H., Nadaoka, K., and Nakamura, T. (2018). Assessment of machine learning algorithms for automatic benthic cover monitoring and mapping using towed underwater video camera and high-resolution satellite images. *Remote Sens.* 10:773. doi: 10.3390/rs10050773

Mohamed, H., Nadaoka, K., and Nakamura, T. (2020). Towards benthic habitat 3D mapping using machine learning algorithms and structures from motion photogrammetry. *Remote Sens.* 12:127. doi: 10.3390/rs12010127

Mortensen, P. B., Hovland, M., Brattegard, T., and Farestveit, R. (1995). Deep water bioherms of the scleractinian coral *Lophelia pertusa* (L.) at 64° n on

the norwegian shelf: Structure and associated megafauna. *Sarsia* 80, 145–158. doi: 10.1080/00364827.1995.10413586

Mountrakis, G., Im, J., and Ogole, C. (2011). Support vector machines in remote sensing: a review. *ISPRS J. Photogramm. Remote Sens.* 66, 247–259. doi: 10.1016/j.isprsjprs.2010.11.001

Nittrouer, C. A., and Wright, L. D. (1994). Transport of particles across continental shelves. *Rev. Geophys.* 32, 85–113. doi: 10.1029/93RG02603

Orejas, C., Gori, A., lo Iacono, C., Puig, P., Gili, J. M., and Dale, M. R. T. (2009). Cold-water corals in the Cap de Creus canyon, northwestern Mediterranean: spatial distribution, density and anthropogenic impact. *Mar. Ecol. Prog. Ser.* 397, 37–51. doi: 10.3354/meps08314

Pal, M. (2005). Random forest classifier for remote sensing classification. *Int. J. Remote Sens.* 26, 217–222. doi: 10.1080/01431160412331269698

Pedregosa, F., Varoquaux, G., Gramfort, A., Michel, V., Thirion, B., Grisel, O., et al. (2011). Scikit-learn: machine learning in python. *J. Mach. Learn. Res.* 12, 2825–2830.

Pirotti, F., and Tonion, F. (2019). Classification of aerial laser scanning point clouds using machine learning: a comparison between random forest and tensorflow. *Int. Arch. Photogramm. Remote Sens. Spat. Inform. Sci. ISPRS Arch.* 42, 1105–1111. doi: 10.5194/isprs-archives-XLII-2-W13-1105-2019

Pizarro, O., Friedman, A., Bryson, M., Williams, S. B., and Madin, J. (2017). A simple, fast, and repeatable survey method for underwater visual 3D benthic mapping and monitoring. *Ecol. Evol.* 7, 1770–1782. doi: 10.1002/ece3.2701

Pontius, R. G., and Millones, M. (2011). Death to Kappa: birth of quantity disagreement and allocation disagreement for accuracy assessment. *Int. J. Remote Sens.* 32, 4407–4429. doi: 10.1080/01431161.2011.552923

Price, D. M., Robert, K., Callaway, A., lo lacono, C., Hall, R. A., and Huvenne, V. A. I. (2019). Using 3D photogrammetry from ROV video to quantify cold-water coral reef structural complexity and investigate its influence on biodiversity and community assemblage. *Coral Reefs* 38, 1007–1021. doi: 10.1007/s00338-019-01827-3

Puig, P., and Palanques, A. (1998). Temporal variability and composition of settling particle fluxes on the Barcelona continental margin (Northwestern Mediterranean). *J. Marine Research* 56, 639–654. doi: 10.1357/002224098765213612

Robert, K., Huvenne, V. A. I., Georgiopoulou, A., Jones, D. O. B., Marsh, L., Carter, D. O. G., et al. (2017). New approaches to high-resolution mapping of marine vertical structures. *Sci. Rep.* 7, 1–14. doi: 10.1038/s41598-017-09382-z

Roberts, J. M. (2002). The occurrence of the coral *Lophelia pertusa* and other conspicuous epifauna around an oil platform in the North Sea. *Underw. Technol.* 25, 83–91. doi: 10.3723/175605402783219163

Roberts, J. M., Peppe, O. C., Dodds, L. A., Mercer, D. J., Thomson, W. T., Gage, J. D., et al. (2006a). "Monitoring environmental variability around cold-water coral reefs: the use of a benthic photolander and the potential of seafloor observatories," in *Cold-Water Corals and Ecosystems*, eds A. Freiwald and J. M. Roberts (Berlin: Springer-Verlag), 483–502. doi: 10.1007/3-540-27673-4_24

Roberts, J. M., Wheeler, A., Freiwald, A., and Stephen, C. (2009). *Cold-Water Corals: The Biology and Geology of Deep-Sea Coral Habitats*. Available online at: https://books.google.ie/books?id=L6X6UW7ZszIC&pg=PA310&lpg=PA310&dq=Roberts,+J.M.,+2002.+The+occurrence+of+the+coral+Lophelia+pertusa+and+other+conspicuous+epifauna+around+an+oil+platform+in+the+North+Sea.+Journal+of+the+Society+for+Underwater+Technology+25,+83%E2%80%9391&source=bl&ots=i5-YhZ3N-v&sig=ACfU3U0Deub73vpl53Hu_Mo_t33_YOLrkg&hl=en&sa=X&ved=2ahUKEwixt6uc38rsAhXRqHEKHTZkCg0Q6AEwB3oECAcQAg#v=onepage&q&f=false (accessed October 23, 2020).

Roberts, J. M., Wheeler, A. J., and Freiwald, A. (2006b). Reefs of the deep: the biology and geology of cold-water coral ecosystems. *Science* 312, 543–547.

Rossi, P., Castagnetti, C., Capra, A., Brooks, A. J., and Mancini, F. (2020). Detecting change in coral reef 3D structure using underwater photogrammetry: critical issues and performance metrics. *Appl. Geomat.* 12, 3–17. doi: 10.1007/s12518-019-00263-w

Roynard, X., Deschaud, J.-E., and Goulette, F. (2018). *Classification of Point Cloud Scenes with Multiscale Voxel Deep Network*. Available online at: http://arxiv.org/abs/1804.03583 (accessed March 10, 2020).

Savini, A., Vertino, A., Marchese, F., Beuck, L., and Freiwald, A. (2014). Mapping cold-water coral habitats at different scales within the Northern Ionian Sea (central Mediterranean): an assessment of coral coverage and associated vulnerability. *PLoS One* 9:e0087108. doi: 10.1371/journal.pone.0087108

Sergios, T., and Konstantinos, K. (2008). "Chapter 5 – Feature selection," in *Pattern Recognition*, ed. S. Theodoridis (Amsterdam: Elsevier Science & Technology), 280–282.

Shannon, P. M. (1991). The development of Irish offshore sedimentary basins. *J. Geol. Soc.* 148, 181–189. doi: 10.1144/gsjgs.148.1.0181

Shihavuddin, A. S. M., Gracias, N., Garcia, R., Gleason, A., and Gintert, B. (2013). Image-based coral reef classification and thematic mapping. *Remote Sens.* 5, 1809–1841. doi: 10.3390/rs5041809

Singh, H., Howland, J., and Pizarro, O. (2004). Advances in large-area photomosaicking. *J. Ocean. Eng.* 29, 872–886.

Storlazzi, C. D., Dartnell, P., Hatcher, G. A., and Gibbs, A. E. (2016). End of the chain? Rugosity and fine-scale bathymetry from existing underwater digital imagery using structure-from-motion (SfM) technology. *Coral Reefs* 35, 889–894. doi: 10.1007/s00338-016-1462-8

Titschack, J., Baum, D., de Pol-Holz, R., López Correa, M., Forster, N., Flögel, S., et al. (2015). Aggradation and carbonate accumulation of Holocene Norwegian cold-water coral reefs. *Sedimentology* 62, 1873–1898. doi: 10.1111/sed.12206

Trimble (2018). *Trimble Documentation: eCognition ®Developer User Guide*. Munich: Trimble Germany GmbH, 1–272.

Trimble Germany GmbH (2019). *Trimble eCognition Developer – For Windows Operating System – Reference Book. 9.5.1*. Munich: Trimble Germany GmbH.

Turley, C. M., Roberts, A. J. M., and Guinotte, A. J. M. (2007). Corals in deep-water: will the unseen hand of ocean acidification destroy cold-water ecosystems? *Coral Reefs* 26, 445–448. doi: 10.1007/s00338-007-0247-5

Verma, P., Raghubanshi, A., Srivastava, P. K., and Raghubanshi, A. S. (2020). Appraisal of kappa-based metrics and disagreement indices of accuracy assessment for parametric and nonparametric techniques used in LULC classification and change detection. *Model. Earth Syst. Environ.* 6, 1045–1059. doi: 10.1007/s40808-020-00740-x

Victorero, L., Blamart, D., Pons-Branchu, E., Mavrogordato, M. N., and Huvenne, V. A. I. (2016). Reconstruction of the formation history of the Darwin Mounds, N Rockall Trough: how the dynamics of a sandy contourite affected cold-water coral growth. *Mar. Geol.* 378, 186–195. doi: 10.1016/j.margeo.2015.12.001

Walton, G., Mills, G., Fotopoulos, G., Radovanovic, R., and Stancliffe, R. P. W. (2016). An approach for automated lithological classification of point clouds. *Geosphere* 12, 1833–1841. doi: 10.1130/GES01326.1

Wang, Z., Zhang, L., Fang, T., Mathiopoulos, P. T., Tong, X., Qu, H., et al. (2015). A multiscale and hierarchical feature extraction method for terrestrial laser scanning point cloud classification. *IEEE Transact. Geosci. Remote Sens.* 53, 2409–2425. doi: 10.1109/TGRS.2014.2359951

Weidner, L., Walton, G., and Kromer, R. (2019). Classification methods for point clouds in rock slope monitoring: a novel machine learning approach and comparative analysis. *Eng. Geol.* 263:105326. doi: 10.1016/j.enggeo.2019.105326

Weinmann, M., Jutzi, B., Hinz, S., and Mallet, C. (2015). Semantic point cloud interpretation based on optimal neighborhoods, relevant features and efficient classifiers. *ISPRS J. Photogramm. Remote Sens.* 105, 286–304. doi: 10.1016/j.isprsjprs.2015.01.016

Weinmann, M., Jutzi, B., and Mallet, C. (2013). Feature relevance assessment for the semantic interpretation of 3D point cloud data. *ISPRS Annal. Photogramm. Remote Sens. Spat. Inform. Sci.* 2, 313–318. doi: 10.5194/isprsannals-II-5-W2-313-2013

Wheeler, A. J., Beck, T., Thiede, J., Klages, M., Grehan, A., and Monteys, F. X. (2005a). "Deep-water coral mounds on the Porcupine Bank, Irish Margin: preliminary results from the Polarstern ARK-XIX/3a ROV cruise," in *Cold-Water Corals and Ecosystems*, eds A. Freiwald and J. M. Roberts (Berlin: Springer), 393–402. doi: 10.1007/3-540-27673-4_19

Wheeler, A. J., Bett, B. J., Billett, D. S. M., Masson, D. G., and Mayor, D. J. (2005b). The impact of demersal trawling on northeast Atlantic deepwater coral habitats: the case of the Darwin mounds, United Kingdom. *Am. Fisher. Soc. Sympos.* 41, 807–818.

Wheeler, A. J., Beyer, A., Freiwald, A., de Haas, H., Huvenne, V. A. I., Kozachenko, M., et al. (2007a). Morphology and environment of cold-water coral carbonate mounds on the NW European margin. *Int. J. Earth Sci.* 96, 37–56. doi: 10.1007/s00531-006-0130-6

Wheeler, A. J., Ferdelman, T., Freiwald, A., Hebbeln, D., and Henriet, J. P. (2007b). Cold-Water coral ecosystem functioning through time in the deep sea: the example of cold-water coral carbonate mounds in the northeast Atlantic (from IODP307 to EuroMARC - CARBONATE). *Geophys. Res. Abstr.* 9:11617.

Wheeler, A. J., Kozachenko, M., Beyer, A., Foubert, A., Huvenne, V. A. I., Klages, M., et al. (2005c). "Sedimentary processes and carbonate mounds in the Belgica Mound province, Porcupine Seabight, NE Atlantic," in *Cold-Water Corals and Ecosystems*, eds A. Freiwald and J. M. Roberts (Berlin: Springer), 571–603. doi: 10.1007/3-540-27673-4_28

Wilson, J. B. (1979a). Patch development of the deep-water coral *Lophelia Pertusa* (L.) on rockall Bank. *J. Mar. Biol. Associat. U. K.* 59, 165–177. doi: 10.1017/S0025315400046257

Wilson, J. B. (1979b). The distribution of the coral *Lophelia pertusa* (L.) [L.Prolifera (Pallas)] in the North-East Atlantic. *J. Mar. Biol. Associat. U. K.* 59, 149–164. doi: 10.1017/S0025315400046245

Ye, S., Pontius, R. G., and Rakshit, R. (2018). A review of accuracy assessment for object-based image analysis: from per-pixel to per-polygon approaches. *ISPRS J. Photogramm. Remote Sens.* 141, 137–147. doi: 10.1016/j.isprsjprs.2018.04.002

Young, G. C. (2017). *Three-Dimensional Modelling of Coral Reefs for Structural Complexity Analysis*. 184. Ph.D. Thesis, University of Oxford, Oxford.

Young, G. C. (2018). *Convolutional Neural Networks Predict Fish Abundance from Underlying Coral Reef Texture*, Vol. 41. Bristol: MarXiv, 345–362.

Young, G. C., Dey, S., Rogers, A. D., and Exton, D. (2018). Cost and time-effective method for multi-scale measures of rugosity, fractal dimension, and vector dispersion from coral reef 3D models. *PLoS One* 13:e0201847. doi: 10.1371/journal.pone.0201847

Zhang, Y., Maxwell, T., Tong, H., and Dey, V. (2010). "Development of a supervised software tool for automated determination of optimal segmentation parameters for ecognition," in *ISPRS TC VII Symposium XXXVIII*, 690–696. Vienna, Austria.

Zurowietz, M., Langenkämper, D., Hosking, B., Ruhl, H. A., and Nattkemper, T. W. (2018). MAIA-A machine learning assisted image annotation method for environmental monitoring and exploration. *PLoS One* 13:e0207498. doi: 10.1371/journal.pone.0207498

Conflict of Interest: The authors declare that the research was conducted in the absence of any commercial or financial relationships that could be construed as a potential conflict of interest.

frontiers in Marine Science

ORIGINAL RESEARCH
published: 29 March 2021
doi: 10.3389/fmars.2021.654950

A New Method for Investigating Relationships Between Distribution of Sessile Organisms and Multiple Terrain Variables by Photogrammetry of Subtidal Bedrocks

Takayuki Kanki[1], Kenta Nakamoto[1], Jun Hayakawa[1], Takashi Kitagawa[1] and Tomohiko Kawamura[2]*

[1] International Coastal Research Center, Atmosphere Ocean Research Institute, The University of Tokyo, Otuschi, Japan, [2] Atmosphere Ocean Research Institute, The University of Tokyo, Kashiwa, Japan

OPEN ACCESS

Edited by:
Javier Xavier Leon,
University of the Sunshine Coast,
Australia

Reviewed by:
Xihan Mu,
Beijing Normal University, China
Marilia Bueno,
State University of Campinas, Brazil
Hirokazu Abe,
Iwate Medical University, Japan
Giovanni Coletti,
Milano Bicocca University, Italy

***Correspondence:**
Takayuki Kanki
tkanki@aori.u-tokyo.ac.jp

Specialty section:
This article was submitted to Marine Ecosystem Ecology, a section of the journal Frontiers in Marine Science

Received: 18 January 2021
Accepted: 01 March 2021
Published: 29 March 2021

Citation:
Kanki T, Nakamoto K, Hayakawa J, Kitagawa T and Kawamura T (2021) A New Method for Investigating Relationships Between Distribution of Sessile Organisms and Multiple Terrain Variables by Photogrammetry of Subtidal Bedrocks. Front. Mar. Sci. 8:654950. doi: 10.3389/fmars.2021.654950

Previous studies of habitat suitability of sessile organisms on subtidal rocky substrata have been focused only one or two terrain attributes. In this study, we propose a new method to construct a centimeter resolution seafloor topographic model by using underwater photogrammetry to obtain multiple terrain variables and to investigate relationships between the distribution of sessile organisms and multiple terrain variables. Point cloud models of five square sections (11.3–25.5 m^2) of the bedrock surface of Otsuchi Bay were reconstructed with a 0.05 m resolution. Using the 0.01 m resolution point cloud models, five terrain variables were calculated on each face of the mesh models: height above seafloor, topological position index, slope, aspect, and ruggedness. The presence/absence data of four species of sessile organisms (ascidian *Halocynthia roretzi*, barnacle *Balanus trigonus*, polychaete *Paradexiospira nakamurai*, and articulated coralline algae *Pachyarthron cretaceum*) were located on the mesh models. *H. roretzi* and *B. trigonus* were more abundant on vertical and high faces above the seafloor, and *P. nakamurai* were more abundant at high faces above the surroundings. In high position where the current velocity increases, the three sessile animals may have an advantage for their suspension feeding. In contrast, *P. cretaceum*, unlike the other three sessile animal species, occurred at various heights and on gentle slope faces suitable for photosynthesis.

Keywords: topographic features, benthic communities, habitat suitability modeling, rocky shore ecology, Sanriku Coast

INTRODUCTION

Sessile organisms cannot move once they have settled, and therefore their distributions are greatly affected by the environmental conditions around the attachment substrates where they settled. For example, distributions of sessile organisms in shallow waters are affected by physical environmental factors, such as wave exposure (Sanford and Menge, 2001), flow velocity (Smith, 1946; Leichter and Witman, 1997; Thomason et al., 1998) and light intensity (Barnes et al., 1951;

Crisp and Barnes, 1954; Hirose and Kawamura, 2017), and also by biological factors, such as predation pressure (Paine, 1966) and competition (Ponti et al., 2014).

Other important factors influencing the distribution of sessile organisms are terrain attributes, such as height above the seafloor (Hughes, 1975), slope (Chabot and Bourget, 1988; Connell, 1999; Chiba and Noda, 2000; Knott et al., 2006; Perkol-Finkel et al., 2006; Lozano-Cortés and Zapata, 2014), aspect (Barnes et al., 1951; Crisp and Barnes, 1954), and ruggedness (Archambault and Bourget, 1996; Chiba and Noda, 2000; Johnson et al., 2003; Chase et al., 2016) of substrates. These terrain attributes may directly affect the distribution of sessile organisms, for example, through the selective behavior of larvae during settlement (Keough and Downes, 1982). Some terrain attributes indirectly affect the distribution of sessile organisms by modifying other physical or biological factors. For example, slope and aspect of the substrate surface have been reported to affect the light intensity (Connell, 1999) and the ruggedness of the substrate surface has been reported to influence vulnerability to predation (Johnson et al., 2003). Thus terrain variables directly and indirectly affect the distribution of sessile organisms.

Conventional studies about the distribution of sessile organisms in shallow coastal settings usually focus on one or two terrain variables, probably due to the difficulty in obtaining multiple terrain variables with SCUBA diving. For example, one method to measure the ruggedness of the seafloor is to divide the length of a rope crawling between two points on the seafloor by the length of a straight line between the two points. This method requires a lot of time and includes measurement errors due to the skill of measurers (Friedman et al., 2012).

A three-dimensional (3D) model of the seafloor topography is a powerful tool to obtain multiple terrain variables easily. At each point on a 3D model, multiple terrain variables, such as slope, aspect and ruggedness can be numerically calculated. There are two main methods to construct a 3D model of the seafloor topography, acoustic-based or optical-based. Conventionally, acoustic depth measurements using side-scan sonar or multi-beam sonar have been used for constructing 3D models of the seafloor (Robert et al., 2017). By integrating multiple terrain variables calculated by 3D models using acoustic methods and the distribution of sessile organisms obtained by ROV transects or dredge samplings, habitat suitability models have been constructed (Wilson et al., 2007; Dolan et al., 2008; Tong et al., 2013; Georgian et al., 2014; Smith et al., 2015; Miyamoto et al., 2017).

However, acoustic-based methods usually require very expensive equipment. Photogrammetry is an optical-based method to survey the topography by obtaining 3D structures from image sequences taken from various angles. In the Structure from Motion (SfM) algorithm, an orthodox method in photogrammetry, by matching features extracted from each image and bundle adjustment, the location of each image and the 3D structure of the subject can be estimated (Westoby et al., 2012). The equipment necessary for SfM photogrammetry is only a digital camera and a computer, so the photogrammetry method is cost-effective.

Unlike side-scan and multi-beam sonar, undersea photogrammetry is not suitable for large-scale surveys, but it can obtain details of seafloor topography at smaller scales than the acoustic-based method (Robert et al., 2017). SfM photogrammetry has become practical due to recent improvements in the computational power of personal computers. In recent years, SfM photogrammetry has been used in seafloor topographic surveying in shallow sea areas, such as coral reefs (Courtney et al., 2007; Burns et al., 2015; Leon et al., 2015; Pizarro et al., 2017; Bryson et al., 2017; Young et al., 2017; Agudo-Adriani et al., 2019; Bayley et al., 2019; Fallati et al., 2020) or oyster reefs in the intertidal zone (Kim et al., 2018).Photogrammetric surveying can obtain more accurate and objective terrain variables than field measurements (Friedman et al., 2012).Despite the possibility of applying photogrammetry to habitat suitability models, there is only one study that has investigated the relationships between the distribution of two species of sessile organisms and multiple terrain variables (slope and ruggedness) in the deep sea (Robert et al., 2017), and no surveys have been conducted in shallow waters.

Using multiple terrain variables obtained from high resolution 3D models of seafloor topography, it is possible to gather more accurate information (in comparison to analysis based on a single variable) on the distribution of sessile organisms. For example, the combination or the relative importance of variables determining distribution of each species cannot be detected using small number of terrain variables.

The purpose of this paper is establishing a method to elucidate relationships between distributions of sessile organisms and multiple terrain variables on subtidal rocky substrates. For this purpose, using underwater photogrammetry, we constructed 3D models of the bedrock surfaces on the subtidal rocky shore in Otsuchi Bay, Japan. Subsequently, we calculated multiple terrain variables from the 3D seafloor topographic models and investigated the effect of the multiple terrain variables to the distribution of sessile organisms.

MATERIALS AND METHODS

Study Site

We conducted the field survey on the subtidal rocky shore at Akahama in Otsuchi Bay, Japan (39°21′00″ N, 141°56′10″ E) (**Figure 1**). Otsuchi Bay is elongated in an east-west direction, and the bay entrance is on the east side. The study site is located on the central part of the north coast of the bay. The sea surface temperature ranged 3–25°C. The west wind is dominant in the winter and the wind in the summer is moderate (Otobe et al., 2009). The wave height is usually less than 1 m and the southwest wave direction is dominant (Komatsu and Tanaka, 2017).

Obtaining Image Sequences

At the study site, five sections (A01 to A05) were chosen from the part of the bedrock surface for obtaining image sequences. The horizontal projected areas of the five sections were 11.3–25.5″, and they were located at 1.5–5.0 m depth. For each section, 89–178 photos were taken from various angles using

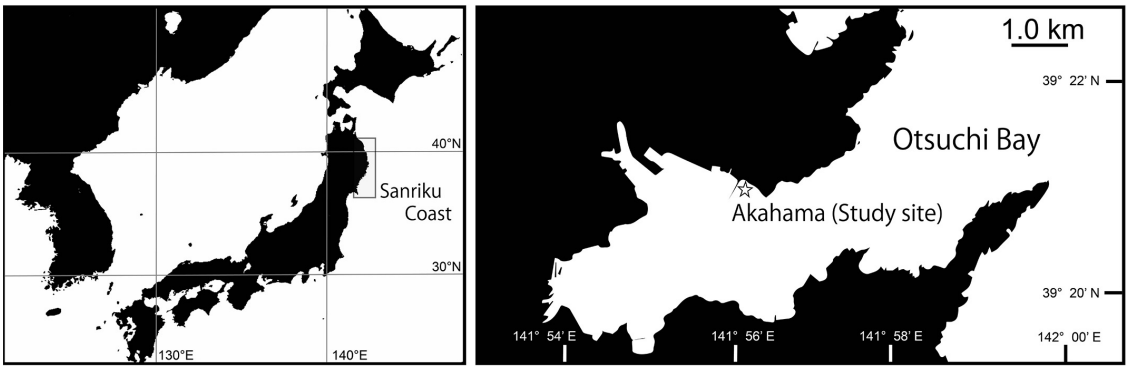

FIGURE 1 | The survey site was located on the subtidal rocky shore in Otsuchi Bay, Japan. The shaded area indicates the area of Sanriku Coast, and the star symbol indicates the location of the survey site.

SCUBA equipment (**Figures 2A–C**). Overlap rates between two consecutive photos were more than 70%. Photos were taken using a waterproof digital camera Tough TG-5 OLYMPUS with a wide-angle lens. The camera was set to the underwater wide mode, and no flash was used. Large seaweeds sway in the waves and veil the surface of the bedrocks so that the construction of 3D models was difficult when dense large seaweeds occur. In the study site, annual seaweeds *Ulva* spp., *Desmarestia virdis* (Müller) Lamouroux, 1813, and *Undaria pinnatifida* (Harvey) Suringar, 1872 dominated and they grew from winter to summer. Therefore, we conducted the field survey during November 2018 when large seaweeds were detached and the bedrock surface were exposed. Photographing was conducted at the daytime when the current was calm, the water clarity was high, and strong shadows did not occur.

On each bedrock surface for surveying, a reference point where the slope is 0 degree was found with a clinometer. At the reference point, the depth and azimuth were measured using a depth meter of the digital camera Tough TG-5 and an azimuth magnetic needle, respectively. In addition, for setting the size of the 3D models, a 20 cm square frame was placed at this point and a photograph was taken from a distance that can distinguish the location of the reference point on the 3D model.

3D Model Construction From Image Sequences

The 3D structure of each rock was reconstructed using the Visual SfM v0.5.26, an open-source software (Wu et al., 2011; Wu, 2013) that implements the Structure from Motion (SfM) algorithms. Visual SfM reconstructs the 3D structure from continuous overlapping image sequences (**Figure 2D**). Uploading the images to the Visual SfM, the tools Pairwise Matching, Reconstruct Sparse, and Reconstruct Dense were executed. The 3D model constructions were conducted using a HP Workstation with 32 GB memory and 1 GB GPU.

Meshing of the 3D Models

The obtained 3D point cloud models (**Figure 3**) were converted to 0.01 m resolution point cloud models and 0.05 m resolution mesh models. The 3D point cloud models constructed by Visual SfM were deployed using MeshLab 2016.12, an open-source software. The x-axis, y-axis, and z-axis directions were set to north, east, and vertical upward based on the value of the azimuth magnetometer taken at the reference point. The length 1.0 of the 3D models was set to 1.0 m based on the 20 cm square frame photograph taken at the reference point. The resolution of the obtained point cloud models differed both among rocks and within rocks because the quality of each image was different due to the variation of brightness.

The point cloud models were equalized to the 0.01 m and 0.05 m resolution models using the "Clustered Vertex Subsampling" tool setting "Cell size" as 0.01 and 0.05. The 0.05 m resolution point cloud models were converted to the triangular irregular network (TIN) mesh models using the "Surface Reconstruction: Ball Pivoting" tool (**Figure 2E**). In general, 3D point cloud models of seafloor topography are converted to raster models in which elevation values are stored for each grid of the x-y plane, but raster models are prone to be rough for the near-vertical plane due to rapid changes in elevation (Kemp, 2007). Therefore, TIN models were used in order to handle bedrock surfaces including near-vertical planes. The directions of the faces were calculated by the "Compute normal for point sets" tool. Some faces were incorrectly directed back from the actual front sides. The incorrectly directed faces were manually flipped in MeshLab.

Due to shadows in the photos and low resolution of the obtained 3D point cloud models, some areas in the 3D mesh models were missing. Because the missing areas were smaller than 10% of the total models and the number of sessile organisms on these areas was small, we ignored these areas and conducted the subsequent analysis.

Input of the Presence/Absence Data of Sessile Organisms

Four sessile species, a solitary ascidian *Halocynthia roretzi* (Drasche, 1884), a barnacle *Balanus trigonus* Darwin, 1854, a tube-forming polychaete *Paradexiospira nakamurai* Uchida, 1971, and an articulated coralline alga *Pachyarthron cretaceum* (Postels and Ruprecht) Manza, 1937 were dominant on the

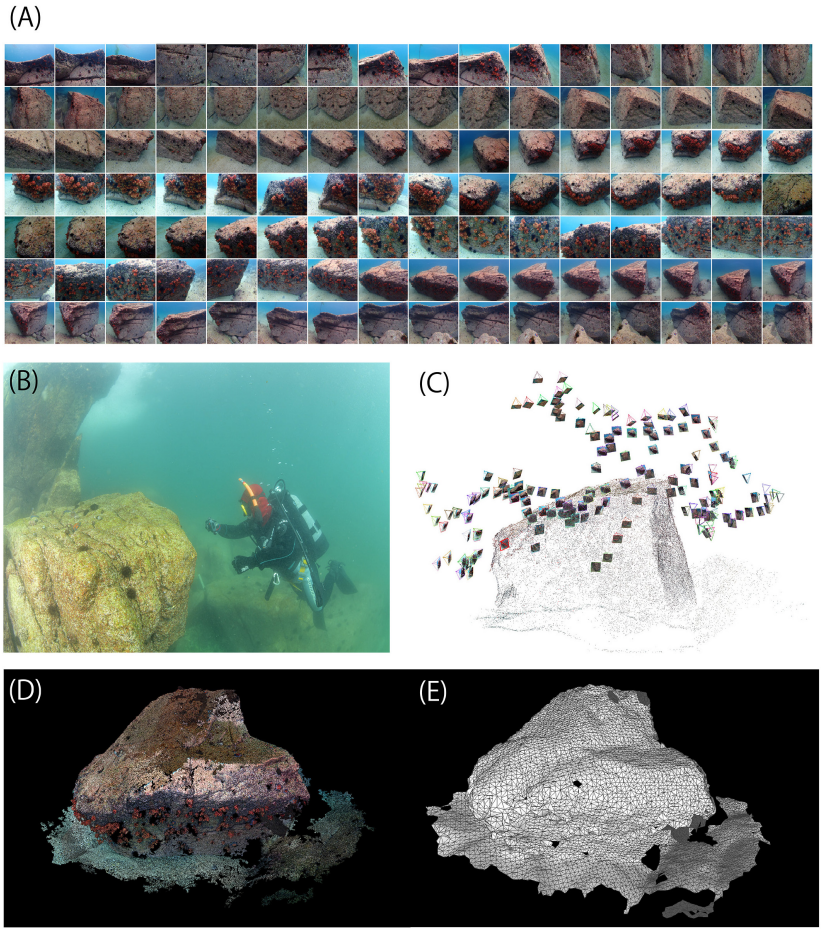

FIGURE 2 | Figures of the 3D seafloor topographic model construction process. **(A)** Image sequences of the section A01. **(B)** The scene of survey by SCUBA diving. **(C)** Locations of each photo estimated by Visual SfM. **(D)** The 3D point cloud model reconstructed from image sequences. **(E)** 0.05 m resolution mesh model translated by Meshlab.

surface of bedrock in the study site (**Figure 4**). Three sessile animals *H. roretzi*, *B. trigonus*, and *P. nakamurai* are suspension feeder.

In preliminary samplings, we caught and identified the sessile species dominated in the study site. Presence/absence data of each species were added to the 3D mesh models (**Figure 4**). Species and the location of each individual were identified from the photos which were also used for photogrammetry. In *H. roretzi* and *P. cretaceum*, as their diameters were larger than 5 cm, the presence data on a face of the two species is equivalent to the occurrence of one individual. In *P. nakamurai* and *B. trigonus*, as their diameters were smaller than 1 cm and they are gregarious species, the presence data on a face of the two species can include multiple individuals. This data included the location of dead individuals of *B. trigonus*, as the presence of the empty shell still indicates that the area was suitable for barnacle growth.

Calculating the Terrain Variables

On all the faces of each 0.05 m resolution mesh model, seven terrain variables; height above seafloor (as height), topological position index (as TPI), northness, eastness, 360 degrees azimuth (as aspect), as well as slope, and ruggedness were calculated based on the vertices of the 0.01 m resolution point cloud models (**Figure 5**). The vertices set of 0.01 m are denoted by $V_{0.01} = \{v_m | v_m \in R^3\}$ $(m = 1, ...m_{0.01})$. $v_m = (x_m, y_m, z_m)$ is the coordinates of the m-th vertice. $m_{0.01}$ is the number of vertices $V_{0.01}$. The vertices and faces set of the 0.05 m resolution mesh models are denoted by $V_{0.05} = \{v_{m'} | v_{m'} \in R^3\}$ $(m' = 1, ...m_{0.05})$ and $T_{0.05} = \{t_n \mid t_n \subset V_{0.05}\}$ $(n = 1, ...n_{0.05})$, respectively. $m_{0.05}$ is the number of vertices of the mesh model $V_{0.05}$, and $n_{0.05}$ is the number of the faces of the mesh model $T_{0.05}$. Because we used triangular faces, the elements of each face are represented as $t_n = (v_{1n}, v_{2n}, v_{3n})$, $(v_{in} \in V_{0.05})$, using three vertices that constitute the face. The following terrain variables were calculated by Python3.7.3.

Height Above Seafloor (Height)

Height is a parameter of the height above the seafloor. The seafloor was defined as the lowest z-value point in each mesh

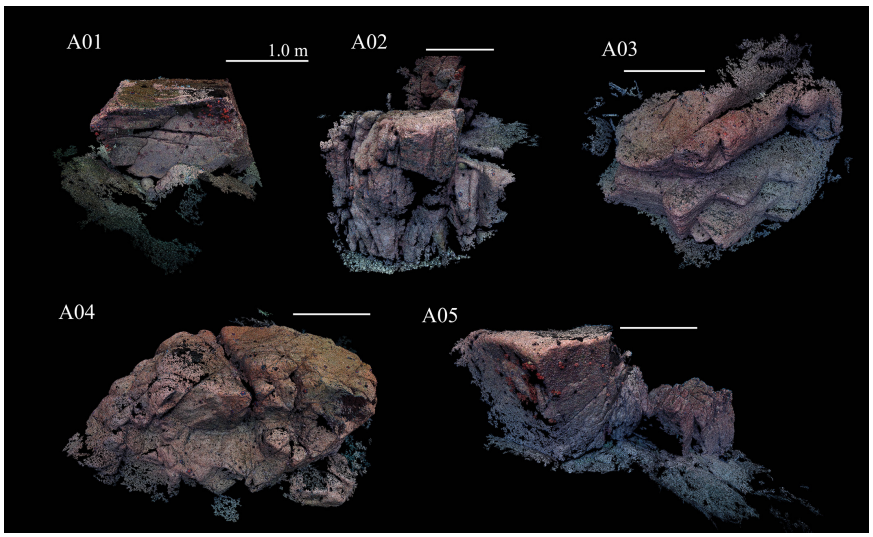

FIGURE 3 | 3D seafloor topographic models of the five sections of the subtidal rocky shores in Otsuchi Bay, Japan.

model. In each mesh model, the lowest z-value point is denoted by $min\,(z_m)$. The center of gravity coordinates on the target face t_n is denoted by $t_G = (x_G, y_G, z_G) = \frac{v_{1n}+v_{2n}+v_{3n}}{3}$. Height is calculated in meters as subtracting z_G with $min\,(z_m)$, i.e.:

$$Height = z_G - min\,(z_m)\ (m)$$

Topological Position Index (TPI)

TPI is an index of the height above or below the mean height of surroundings defined by a specific neighborhood (Weiss, 2001). A positive TPI value indicates the z-axis directional convex terrain, such as ridges or peaks. In contrast, a negative TPI value indicates the z-axis directionally recessed terrain, such as a valley or depression. TPI values near zero are either flat or constant slope areas. The vertices in the circle around t_G with radius R m are referred to as V_R. TPI is calculated in meters as subtracting z_G with the mean z-value of V_R, that is z_R i.e.:

$$TPI = z_G - mean(z_R)\ (m)$$

Northness, Eastness, and 360 Degrees Azimuth (Aspect)

360 degrees azimuth were splitted to northward component (northness) and eastward component (eastness). V_R was fit to the plane $D_R : ax + by + cz + d = 0$. The coefficients a, b, c, and d were calculated by the method of least squares of the V_R. Northness, Eastness, and 360 degrees azimuth (aspect) were calculated using the normal of the D_R. The normal of the D_R was denoted by $n_{D_R} = (n_x, n_y, n_z)$. The direction of the normal was specified with the front and back direction of the target face. Since the x-axis direction was specified as east, the y-axis direction as north,

$$Northness = 90 - cos^{-1}\left(\frac{n_x}{\sqrt{n_x^2 + n_y^2}}\right) \times \frac{180}{\pi}\ (degrees)$$

$$Eastness = 90 - cos^{-1}\left(\frac{n_y}{\sqrt{n_x^2 + n_y^2}}\right) \times \frac{180}{\pi}\ (degrees)$$

Northness and eastness take the value from -90 to 90. The combination of northness and eastness gives a 360 degrees azimuth. For example, (northness, eastness) = (90, 0) indicates that it is facing north, while (northness, eastness) = (−90, 0) indicates facing south. The 360 degrees azimuth were defined as 0 degrees north, 90 degrees east, 180 degrees south, and 270 degrees west.

$$Aspect = 180 - sgn\,(Eastness)\,(90 + Northness)$$

Slope

0 degree in slope indicates the horizontal plane, 90 degree indicates vertical plane, and 180 degree indicates overhang plane. Slope was also calculated using the normal of the D_R. Slope is calculated as the following equation:

$$Slope = \left(\frac{\pi}{2} - tan^{-1}\left(\frac{n_z}{\sqrt{n_x^2 + n_y^2}}\right)\right) \times \frac{180}{\pi}\ (degrees)$$

Ruggedness

Ruggedness was the parameter of the unevenness of the terrain. Ruggedenss was defined as the difference of the maximum height above or maximum depth below the plane D_R. Ruggedness was calculated in meters with the following equation:

$$Ruggedness = max(\left|n_{D_R} \cdot (v_i - \overline{v})\right|)\ (m)$$

v_i means the coordinates of the i-th vertex and $\overline{v}$ means the average coordinates of the V_R.

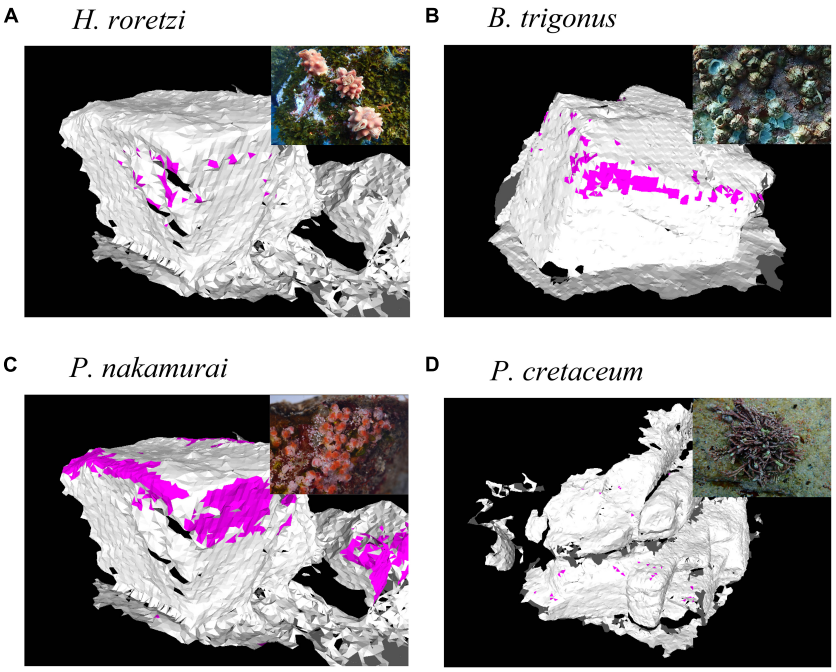

FIGURE 4 | Examples of occurrence data of sessile organisms. Colored faces indicate the faces each species occurred. **(A)** *Halocynthia roretzi*, **(B)** *Balanus trigonus*, **(C)** *Paradexiospira nakamurai*, **(D)** *Pachyarthron cretaceum*.

The small scale of the topographic survey resulted in 3D topographic models including the shape of the organisms themselves. This may have resulted in a significant error in the values of the terrain variables, especially in faces where large *H. roretzi* and seaweeds were present. A practicable solution for this problem is to take a sufficiently wide computational range of R to obtain the terrain variables. In this study, TPI, slope and aspect were calculated in the range of 0.10 m, and ruggedness was calculated in the range of 0.20 m for detecting a wide range of topographic changes. This allowed us to represent topographic changes on a scale larger than the size of the organisms surveyed in this research.

Statistical Analysis

Correlation Analysis Between Terrain Variables

The correlations between terrain variables (height, TPI, northness, eastness, slope, and ruggedness) were calculated by Pearson's linear correlation coefficient (LCC), and maximal information coefficient (MIC). MIC is the non-linear correlation coefficient based on the mutual information criteria between two variables. MIC can detect complex variable relationships, whereas LCC can detect only linear relationships (Speed, 2011).

In order to reduce the calculation time, the randomly 50% extracted data of terrain variables were used in calculating MIC. LCC and MIC were computed by Python 3.7.3 with the library scipy1.2.1, and minepy1.2.4, respectively.

Comparison of the Occurrence Conditions Among Species

For each variable (height, TPI, northness, eastness, slope, and ruggedness), the difference of occurrences pattern between species (including background data) was examined. Background data means the terrain variables obtained in the whole 3D models. As the normality of all the distributions was rejected by Shapiro-Wilk's test ($p < 0.01$) and therefore, the difference of occurrence pattern between species were examined by the multiple comparison with Mann-Whitney U test. As multiple comparisons were made, the significance level was reduced from 0.05 to 0.005 (=0.05/10) to adjust for 10 multiple comparisons (Bonferroni procedure). These statistical tests were conducted by the library scipy1.2.1 with Python3.7.3.

Contribution of Each Terrain Variable to Occurrence of Sessile Organisms

The contribution rate of each terrain variable for the four sessile organisms was estimated by the jackknife test with maximum entropy modeling which is the machine learning method for modeling species geographic distributions with presence-only datasets (Phillips et al., 2006). We used MaxEnt version 3.4.1, a software that implements the maximum entropy modeling for estimating the contribution rate of each parameter. MaxEnt was applied using linear features, quadratic features, and product features for each terrain variable. MaxEnt outputs the contribution rate of each terrain variable as the regularized training gain by the jackknife test. Simultaneously, the performance of the maximum entropy model was evaluated

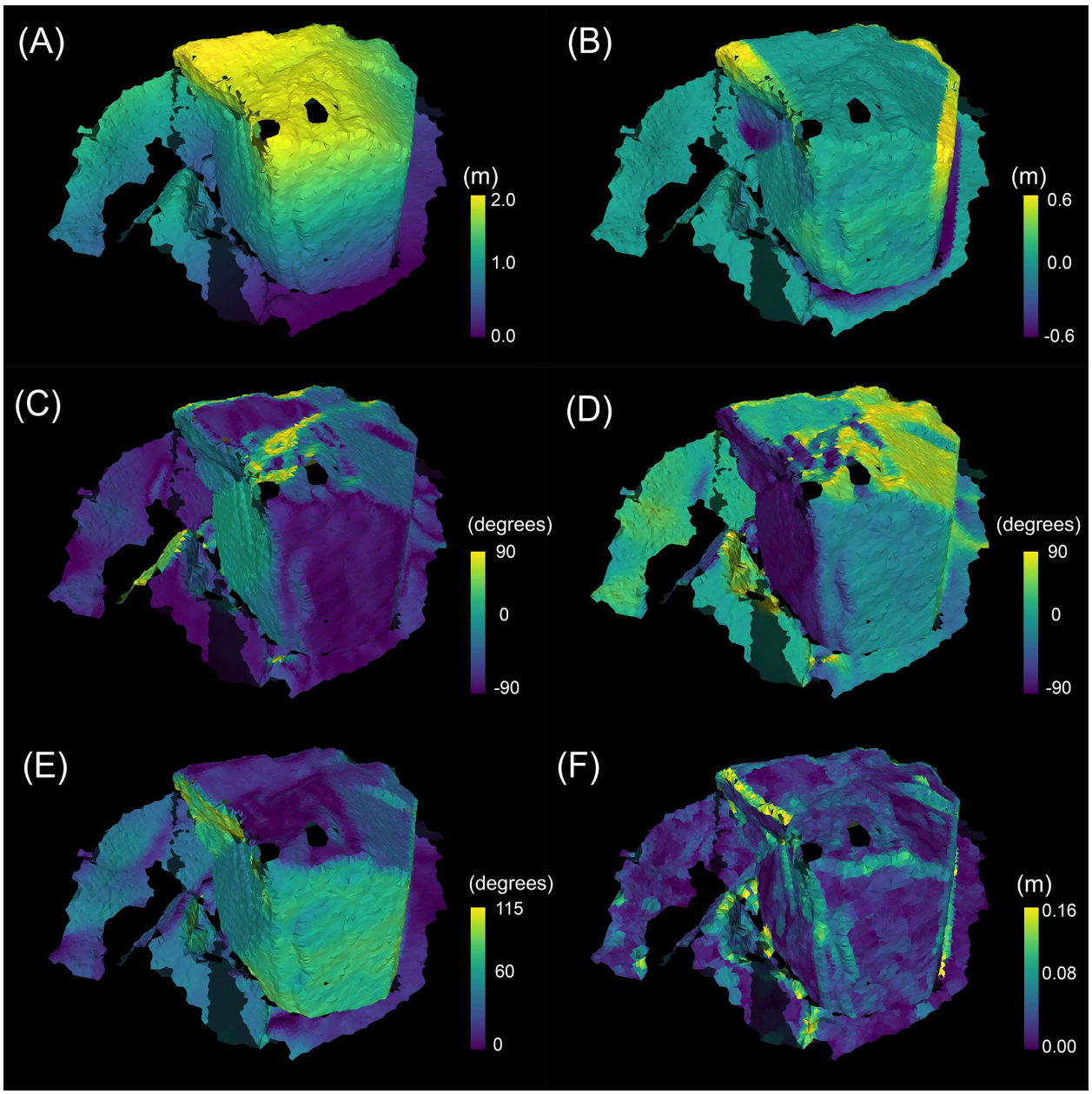

FIGURE 5 | The terrain variables calculated on the 3D mesh model of site A01. The brightness of the color indicates the magnitude of each variable. **(A)** height above the seafloor (height), **(B)** topological position index (TPI), **(C)** slope, **(D)** aspect (northness), **(E)** aspect (eastness), **(F)** ruggedness.

using the area under the curve (AUC) derived from the threshold independent receiver operating characteristics (ROC) curves.

RESULTS

3D Model Construction

Figure 3 shows the 3D models of the five sections of the bedrock surfaces constructed using photogrammetry. The point cloud models constructed using SfM (raw model) were composed of more than 1.5-million points (**Table 1**). The raw models were converted to 0.01 m resolution point cloud models composed of 290–520 thousand points and 0.05 m resolution mesh models composed of 13–42 thousand points and 25–42 thousand faces.

Correlation of Terrain Variables

Figure 6 shows the Pearson's linear correlation coefficients (LCC) and mutual information criteria (MIC) between terrain variables. Aspect is divided into northness and eastness. The maximal value of LCC was 0.45, which was recorded between height and TPI. The maximal value of MIC was 0.78 between northness and

TABLE 1 | Properties of the 3D models at five surveyed sections (A01–A05).

Section	area (m^2)	Number of photos	Vertice number of raw model	Vertice number of $V_{0.01}$	Vertice number of $V_{0.05}$	Mesh number of $T_{0.05}$
A01	11.3	177	6330690	310354	13427	23077
A02	13.2	146	5203103	340867	16350	27840
A03	25.5	134	3872837	520958	25216	42917
A04	12.9	89	1571033	294320	15125	25249
A05	14.0	178	4822436	333089	14954	26326

The column area(m^2) indicates the horizontal projected area of each surveyed sections.

eastness. The values of MIC were lower than 0.16 among height, TPI, slope, and ruggedness.

Species Occurrences

The total number of faces where at least one species of sessile organisms occurred was 9,522. *Paradexiospira nakamurai* was the dominant sessile organisms and occurred on 5,293 faces. The species compositions differed among the surveyed sections. *Halocynthia roretzi* occurred on all the surveyed sections, but the occurrences of *H. roretzi* was low on A02, A03, and A04. *Pachyarthron cretaceum* also occurred on all the surveyed sections. *Balanus trigonus* did not occur on A03 and A04, and *P. nakamurai* did not occur on A01 and A04 (**Table 2**).

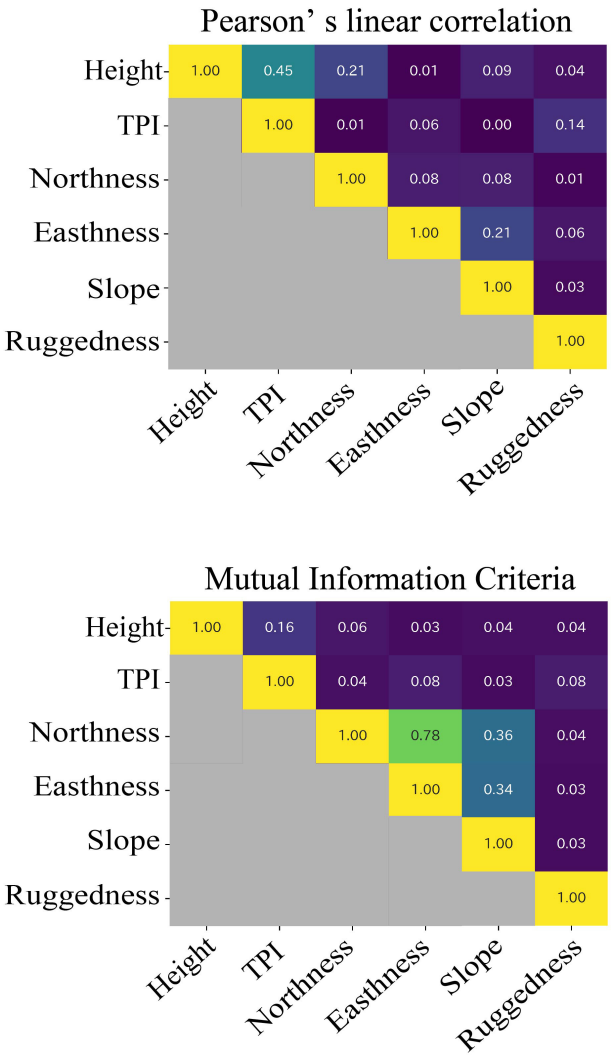

FIGURE 6 | Results of Pearson's linear correlation coefficients (LCC) and maximal information coefficients (MIC).

Species Distribution and Terrain Variables

Height

In all the surveyed bedrocks (background), the maximum value of the height was 3.9 m. More than 95% of *H. roretzi*, *B. trigonus*, and *P. nakamurai* occurred on 1.0–3.0 m height. *P. cretaceum* occurred on the surface areas higher than 0.3 m height, and 95% of them occurred at 0.5–3.0 m height. *P. cretaceum* distribution height range was wider than those of the three sessile animals (**Figure 7**). The median height where *P. nakamurai* occurred was 2.1 m, which was higher than values for the other species (**Figure 8**), and significant differences between *P. nakamurai* and the other species as well as background were detected by the multiple comparison with Mann-Whitney *U* test ($p < 0.005$, **Table 3**). For all species, the densities of occurrences showed similar patterns to the number of occurrences (**Figure 7**).

TPI

In all the surveyed bedrocks, TPI ranged -2.1 to 2.0. TPI distributed symmetrically from the center of 0.0 in all the surveyed bedrocks. More than 75% of *H. roretzi*, *B. trigonus*, and *P. nakamurai* occurred on the position with positive values of TPI. More than 80% of *P. cretaceum* occurred in the range -0.2 to 0.2 TPI (**Figure 7**). In all the species, the median TPIs where each species occurred was larger than the median TPI of the background (**Figure 8**), and significant difference between the four species and background was detected by the multiple comparison with Mann-Whitney *U* test ($p < 0.005$, **Table 3**). The densities of occurrences of *H. roretzi* showed similar patterns to the number of occurrences. Two peaks, around 0.0 and 1.0, were observed in the densities of occurrences of *B. trigonus*. In *P. nakamurai* and *P. cretaceum*, peaks were found around 1.0 and 0.5, respectively, in the densities of occurrences, which were larger than the mean values of the numbers of occurrences (**Figure 7**).

TABLE 2 | The numbers of faces on which each species occurred at each section (A01–A05) and surrounding bottoms.

Section	*H. roretzi*	*B. trigonus*	*P. nakamurai*	*P. cretaceum*	The surrounding bottom
A01	173	806	0	41	Sand bottom
A02	7	94	1705	20	Bedrock and pebble
A03	1	0	1171	32	Bedrock
A04	3	0	0	32	Bedrock and sand
A05	99	0	2417	12	Bedrock and sand

Aspect

In all the surveyed bedrocks, northeast faces were slightly dominant. The numbers of occurrences of *H. roretzi* were higher on northern faces, and that of *B. trigonus* was higher on northern and southwestern faces. Large numbers of *P. nakamurai* occurred on northeastern faces, and they rarely occurred on western faces. Most *P. cretaceum* occurred on southeastern faces (**Figure 7**). The median northness of the faces where *H. roretzi* occurred, and the median eastness of the faces where *P. nakamurai* occurred were higher than those of the other species (**Figure 8**). Significant differences between *H. roretzi* and the other species in northness were detected using the multiple comparison with Mann-Whitney *U* test ($p < 0.005$, **Table 3**). Significant differences between *P. nakamurai* and the other species in eastness were detected using the multiple comparison with Mann-Whitney *U* test ($p < 0.005$, **Table 3**). For all species, the densities of occurrences showed similar patterns to the numbers of occurrences (**Figure 7**).

Slope

In all the surveyed bedrocks, there were two peaks around near-horizontal approximately 30 and near-vertical approximately 90 degrees in the slope distribution. In terms of the three sessile animals, *H. roretzi*, *B. trigonus*, and *P. nakamurai*, there were peaks in the 70–100 degrees slope. *H. roretzi* distribution slope range was wider than those of *B. trigonus* and *P. nakamurai* (**Figure 7**). These species also occurred on an overhanging faces > 90 degrees. In *P. cretaceum*, there was a peak in the 10–20 degrees slope. No *P. cretaceum* occurred on the position with overhang faces >90 degrees (**Figure 7**). The median slope of the faces where *P. cretaceum* occurred was less than those of the other species (**Figure 8**). Significant differences between them were detected by the multiple comparison with Mann-Whitney *U* test ($p < 0.005$, **Table 3**). For all species, the densities of occurrences showed similar patterns to the numbers of occurrences (**Figure 7**).

Ruggedness

In all the surveyed bedrocks, the ruggedness ranged from 0.01 to 0.24 (**Figure 7**). *H. roretzi* and *P. nakamurai* occurred on higher ruggedness faces than *B. trigonus* and *P. cretaceum* (**Figure 8**). Significant differences between them were detected by the multiple comparison with Mann-Whitney *U* test ($p < 0.005$, **Table 3**). In *B. trigonus*, the peak of ruggedness (0.66–0.70) was the highest in all species. In *P. nakamurai*, the peak of the densities of occurrences was 0.14, which was higher than that of the numbers of occurrences. In the other three species, the densities of occurrences showed similar patterns to the number of occurrences (**Figure 7**).

The Combination of Multiple Conditions

The parallel coordinates were used to visualize the combinations of terrain variables with high occurrences and the interactions between variables (**Figure 9**). *H. roretzi* and *B. trigonus* were abundant in areas of more than 1.0 m height above the seafloor, on steep slopes of 45–120 degrees, and on various degrees of aspect and ruggedness. *P. nakamurai* was more abundant in areas of more than 1.0 m height above the seafloor and on various degrees of slope, aspect and ruggedness. *P. cretaceum* was more abundant on 0–60 degrees slope, southwestern faces, and various heights.

Contribution of Each Terrain Variable

For *H. roretzi* and *P. cretaceum*, the contribution of slope was the largest, followed by height in *H. roretzi*, and TPI in *P. cretaceum* (**Figure 10**). For *B. trigonus*, the contribution of TPI was the largest, followed by slope. For *P. cretaceum*, the contribution of height was the largest, followed by TPI. In *H. roretzi* and *B. trigonus*, the AUCs of training data were 0.922 and 0.897, respectively. In *P. cretaceum* and *P. nakamurai*, the AUCs of training data were 0.792 and 0.762, respectively, which were lower than those of other two species.

DISCUSSION

Seafloor Topographic Surveying Methods

In the present study, we succeeded in measuring multiple terrain variables of the subtidal rocky shore using underwater photogrammetry. In conventional field measurement methods, the ability to obtain detail of multiple terrain variables on a lot of points has been limited. Therefore, the relationships between the distribution of sessile organisms and terrain variables have been investigated only at the meter-scale with side-scan sonar or multibeam sonar (Wilson et al., 2007; Dolan et al., 2008; Tong et al., 2013; Georgian et al., 2014; Miyamoto et al., 2017). The resolution of the 3D seafloor topographic models obtained in the present study is much more detailed (0.05 meter-resolution) than those in the acoustic-based methods, which enabled us to investigate the distribution patterns of sessile organisms using more detailed scale of terrain variables.

To implement the photogrammetry method in other sites, it should be noted that the resolution of photos is affected by the

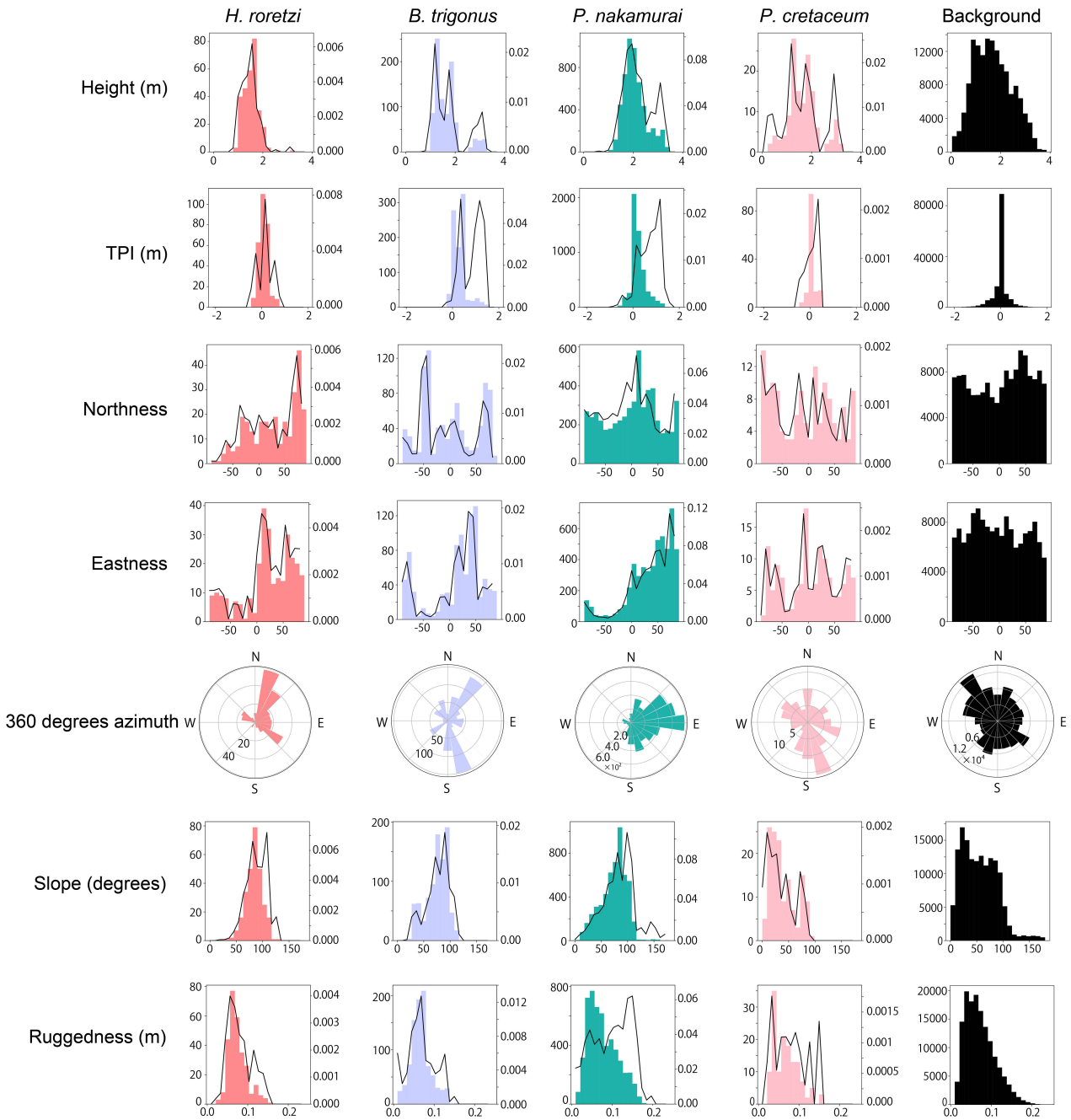

FIGURE 7 | Relationships between each terrain variable (height, TPI, northness, eastness, 360 degrees azimuth, slope, and ruggedness) and the occurrences of each species. For each parameter and each species, the number of occurrences is shown in histograms. Except for 360 degrees azimuth, the density of the occurrences was shown in line plots, which is the number of occurrences divided by the number of each bin of the background histogram. The horizontal axis refers to the value of each terrain variable, the left side of the vertical axis refers to the number of occurrences, and the right side of the vertical axis refer to the density of the occurrences which is the number of occurrences divided by the number of background in each bin. In aspects, the r direction refers to the number of occurrences and the θ direction refers to the aspect.

transparency of the water. At sites with insufficient brightness light, photos need to be taken using flash. In addition, to choose seasons when there are no large seaweeds swaying in the waves.

The photogrammetry method in the present study can measure terrain variables even on the entire model, resulting in an analysis of bedrock topography more accurate than those based on conventional field measurement methods. For example, in the study site, two peaks near horizontal and vertical slope were observed. This may indicate the topographic characteristics of the granite cliff (Dale, 1923), the fracture surface of which

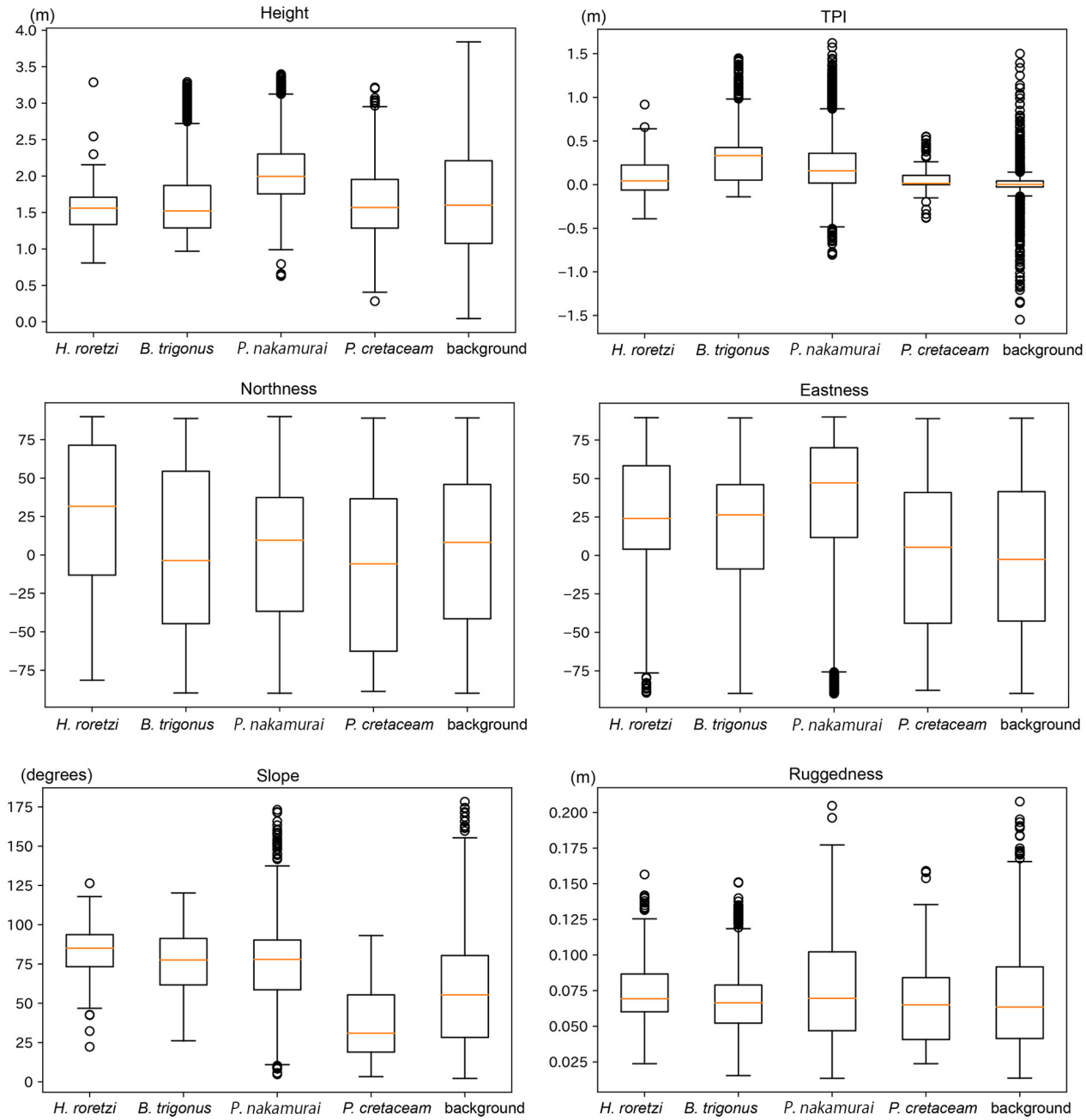

FIGURE 8 | Boxplots of terrain variables of the faces where each species occurred. Boxplots show the range (solid black lines), median (red lines), 25 and 75% quantiles (box), and outliers at 95% confidence (points).

is prone to plane orthogonally (cleavage), resulting in a block shaped bedrock (**Figure 7**).

Distribution patterns of each species based on 0.01 meter-scale terrain variables will be essential information for predicting what species occur on what kind of topographies (biological habitat mapping) in shallow marine rocky shores. In deep waters, biological habitat mapping has been conducted mainly for setting up the protect areas of cold-water corals from the bottom trawling fishery (Wilson et al., 2007; Dolan et al., 2008; Tong et al., 2013; Georgian et al., 2014; Miyamoto et al., 2017). In the shallow waters, the seafloor topography is often simplified by human activities. Topological simplifications significantly affect diversity and biomass of sessile organism communities (Perkol-Finkel et al., 2006). The species richness of sessile organisms often decreases on the artificial reefs of which the centimeter scale topography is simple (Loke and Todd, 2016). The communities of sessile organism play important roles for ecosystems on the subtidal rocky shore,

TABLE 3 | *P*-values of the multiple comparison with the Mann-Whitney test.

		Height	TPI	Northness	Eastness	Slope	Ruggedness
H. roretzi	vs. *B. trigonus*	0.009	**0**	**0**	0.12	**0**	**0**
	vs. *P. nakamurai*	**0**	**0**	**0**	**0**	**0**	0.274
	vs. *P. cretaceum*	0.048	0.29	**0**	**0.0004**	**0**	**0.0018**
	vs. background	0.006	**0**	**0**	**0**	**0**	**0.00064**
B. trigonus	vs. *P. nakamurai*	**0**	**0**	0.075	**0**	0.76	**0**
	vs. *P. cretaceum*	0.389	**0**	0.145	0.006	**0**	0.391
	vs. background	0.957	**0**	0.093	**0**	**0**	0.644
P. nakamurai	vs. *P. cretaceum*	**0**	**0**	0.051	**0**	**0**	0.005
	vs. background	**0**	**0**	0.114	**0**	**0**	**0**
P. cretaceum	vs. background	0.983	**0**	0.024	0.17	**0**	0.32

P-values less than 0.005 are shown in bold, and 0 indicates that the p-value was less than 1e-10.

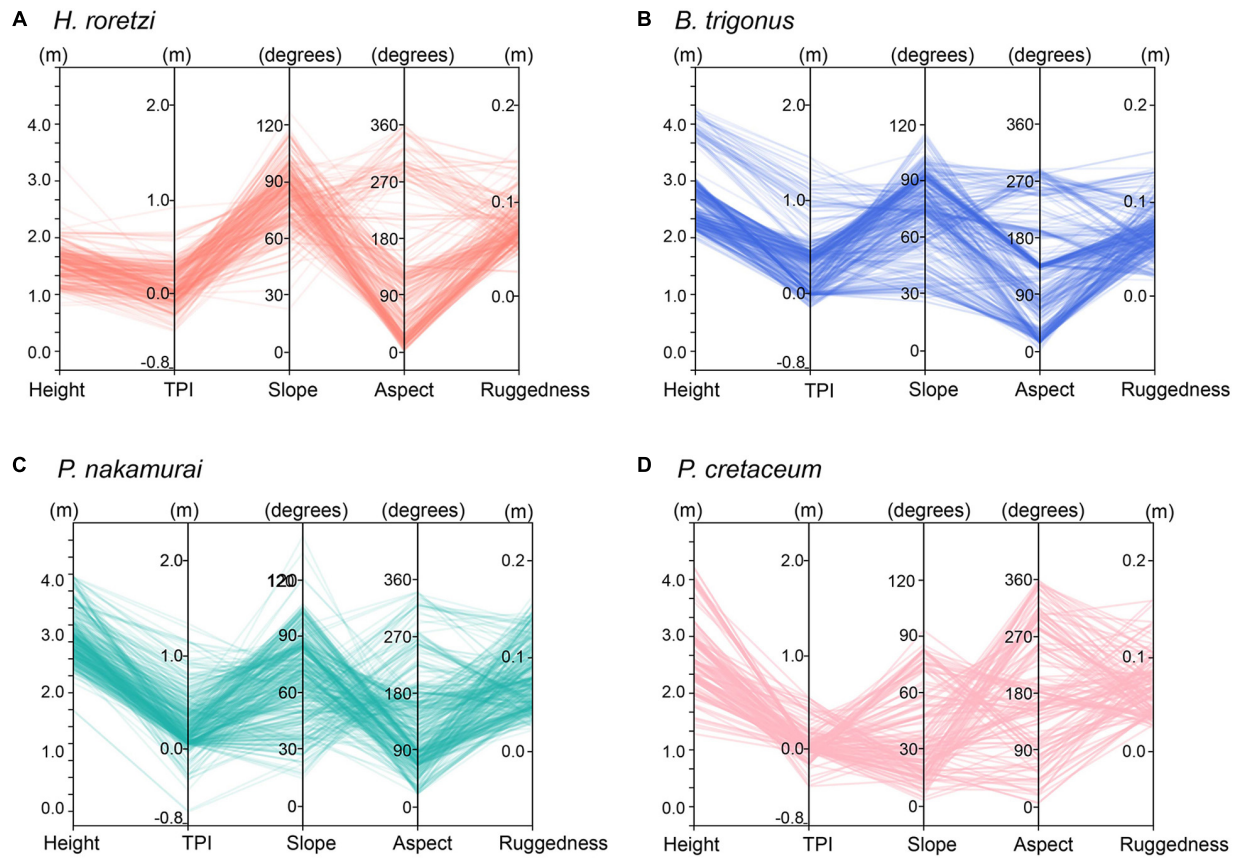

FIGURE 9 | Parallel coordinate graphs showing the combinations of terrain variables which each species of sessile organisms occurred [**(A)** *H. roretzi* **(B)** *B. trigonus* **(C)** *P. nakamurai* **(D)** *P. cretaceum*]. In parallel coordinates, each terrain variable at the location where an individual occurred is connected by a single plot. Respective lines indicate individual faces each species occurred. This allowed us to visualize not only the distribution of each terrain variable, but also the combinations of terrain variables with high occurrences.

such as habitat, food, spawning substrate, and shelter for other benthic organisms in coastal areas (Sarà, 1986). Seaweeds are also important as primary producers (Dean and Connell, 1987). Therefore, maintaining the biomass and the diversity of sessile organisms are important. To predict the decrease of sessile organisms by topographic alterations and to find the measures for conservation of the sessile organisms, the detailed scale habitat suitability modeling using photogrammetry may greatly contribute.

Habitat Suitability of Sessile Organisms

By analysis using multiple terrain variables, the combination of terrain variables of the faces on which each species occurred was elucidated. This enable more accurate distribution patterns

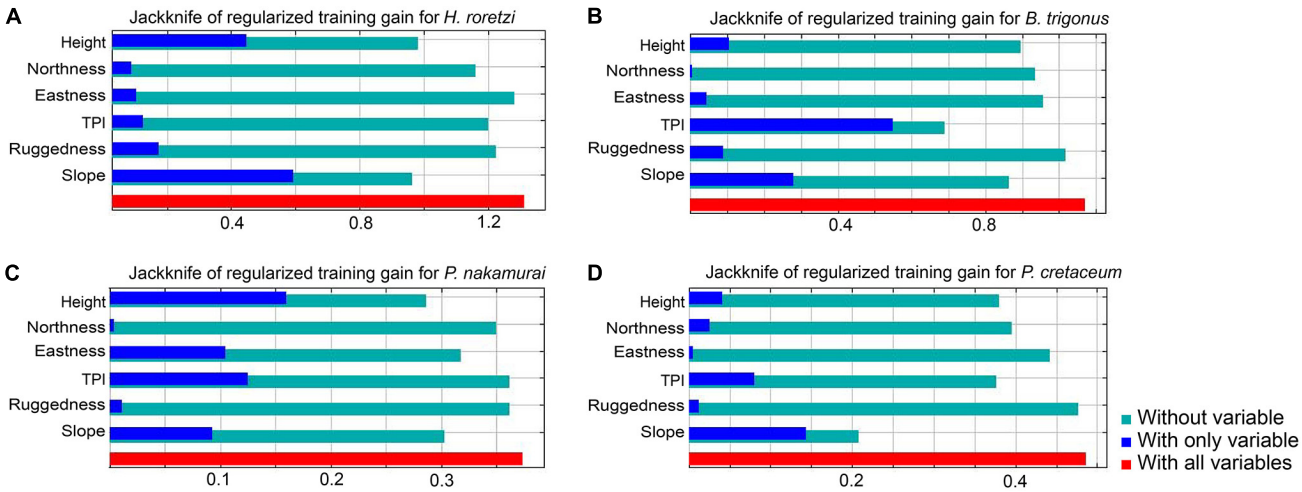

FIGURE 10 | Jacknife of regularized training gain for **(A)** *H. roretzi*, **(B)** *B. trigonus*, **(C)** *P. nakamurai*, **(D)** *P. cretaceum*. The lengths of the bars "With all variables" represent the full model accuracies with all parameters. Those of "Without variables" represent the model accuracies in which each variable was excluded. Those of "With only variables" represent the accuracies of the model in which only each variable was used, and effectively shows the contribution rate for explaining the presence or absence of the distribution.

of sessile organisms than those obtained in conventional studies focusing on one or two terrain variables. For example, occurrences of barnacles and ascidians were previously detected to be more on vertical planes than on horizontal planes (Wendt et al., 1989; Connell, 1999). The present study revealed that the number of the ascidian *Halocynthia roretzi* and the barnacle *Balanus trigonus* were large at high and vertical planes, and small at low positions, even on vertical planes.

The most important terrain variable for habitat preference varied with species. These variables were height (height above the seafloor and TPI) or slope. These variables may indicate the physical environment, such as light intensity and the current velocity. At steep slopes and high positions above the seafloor, the numbers of the three species of sessile animals (*H. roretzi*, *B. trigonus*, and the tube-forming polychaete *Paradexiospira nakamurai*) were higher than at low positions. Simulations and experiments of the currents around artificial reefs have shown that the presence of topographic abrupt changes cause contractions of the current flow and upwellings (Su et al., 2007; Liu and Su, 2013). In the case study on the artificial reefs about 20 m wide and 10 m high, the wake vortex flow arises behind the artificial reefs due to the contraction. Due to upwelling and backflow vortex, high densities of plankton have been shown to locally form on the upper part of the artificial reefs (Yanagi and Nakajima, 1991). Even on small, natural bedrocks in the subtidal rocky shore, since the depth which rapid becomes shallow is similar to that of the case study, the upwellings may arise and increase the food supply at high positions above the seafloor.

Therefore, on vertical planes at high positions, a large amount of particles may pass through due to the exposure to the contractions and the backflow vortex, which results in the favorable environment for suspension feeders. Conversely, at low positions on horizontal and vertical planes, obtaining food may be difficult for suspension feeders due to stagnant currents. Suspended materials close to the seafloor may also hinder feeding and growth of sessile suspension feeders (Robbins, 1983).

Most of *H. roretzi* occurred on north, vertical and middle height (lower than 2 m height) faces (**Figures 7**, **8**), therefore *H. roretzi* might prefer the place with low light intensity. In addition, the southwestern wave direction excelled in the study site. Therefore, the contraction frequently may occur on the north and vertical faces, and these faces might well be favorable environment for *H. roretzi* feeding. Most of *H. roretzi*, *B. trigonus*, and *P. nakamurai* occurred on high ruggedness convex and concave surfaces (**Figures 7**, **8**), which may function as refuges from predators like starfishes, sea urchins, and gastropods. In convex areas, the flow velocity increases due to the generation of turbulence. The feeding pressure on kelps by sea urchins is known to decrease in high current velocities (Kawamata, 2010). In concave areas, predators like large starfishes, sea urchins, and fish are prevented from access (Menge and Lubchenco, 1981). These phenomena may decrease the feeding pressure on sessile animals by predators in convex and concave areas. The articulated coralline alga, *Pachyarthron cretaceum* is not a suspension-feeder unlike the sessile animals, and therefore may occur even at lower heights and ruggedness faces than other suspension-feeding animals. More *P. cretaceum* occurred at a height over 1.0 m above the seafloor on southeastern near-horizontal faces, which will be suitable for their photosynthesis due to higher light intensities. Sea urchins more favorably prey on sessile animals than articulated coralline algae which have a low nutritional value for sea urchins (Endo et al., 2007). The low feeding pressure on *P. cretaceum* by sea urchins may be one of the factors allowing them to grow at low heights and ruggedness faces where the current velocities are moderate and feeding by sea urchins was minimal.

In order to detail the precise factors regulating the distribution of sessile organisms, elucidating how terrain variables are

specifically indicative of the physical and biological environments is needed. However, investigating the relationships between topographic conditions and physical environments is a frontier that has not been considered for rocky reef ecosystems, which could be carried by the development of numerical simulations and measurements of flow speed and light availability.

Although the distribution ranges were different among four sessile species, the occurrence conditions were similar and overlapped among three sessile animals *H. roretzi*, *B. trigonus*, and *P. nakamurai*. However, the number of occurrences at the peak of each species was much smaller than (less than 1/10) the number of background data. For example, the number of *P. nakamurai* occurrences peaked approximately 1,000 faces at 81–90 degrees, and the number of background data at 81–90 degrees was approximately 10,000 faces. Therefore, in the study site, there were surplus suitable habitat, suggesting that the sessile species were not under intense competition and they occurred in accordance with their habitat preferences.

In each terrain variable except TPI, the number and the density of occurrences showed similar patterns in all species. The peaks of the number of occurrences may indicate the suitable habitat conditions for each species. In TPI, for three sessile species except *H. roretzi*, the peaks of the density of occurrences were higher than those of the number of occurrences (**Figure 7**). Therefore, high TPI faces may be more suitable for the inhabitation of *B. trigonus*, *P. nakamurai*, and *P. cretaceum* than moderate TPI faces. High TPI faces may be under competition among those three species, and therefore, the number of occurrences may be higher on moderate TPI faces than on high TPI faces.

The species compositions of sessile organisms were different among the five sections of the bedrocks surface. The occurrences of *H. roretzi*, *B. trgionus*, and *P. nakamurai* became more concentrated in specific section of the bedrock surface. The communities of sessile organisms in the intertidal zone are known to be affected by the priority effect: when the substrate became vacant, the species of which a lot of larvae exist can settle on and dominate the substrates (Connell, 1961). The same effect may have caused biases of the species occurrences among sections. In addition, some species of barnacles have been reported to attach close to the adult individuals of the same species (Knight-Jones and Stevenson, 1950; Crisp and Meadows, 1962), which may result in the bias of the occurrences among sections.

In addition, the parameters not obtained in the photogrammetry method, such as the distance from the shore, distribution of the surrounding sediments or the terrain variables calculated on meter scales can possibility affect the species occurrences. For example, the distribution of *P. nakamurai* may be affected by aspects on a wider scales. The surveyed sections "A02," "A03," and "A05" were located on the east side of rocky shore of the study site, and therefore were composed of mainly east faces at the sufficiently larger scale than 0.1 m. *P. nakamurai* only occurred on these sections. Although the reason for this occurrence pattern is unknown, this may be related to the fact that east side of the rocky shore in the study site was susceptible to the effects of southwestern wave direction. Relationships between the surrounding sediment of each section and the species occurrence were not detected (**Table 2**). Although we focused only on centimeter-scale terrain variables in this study, coarse and broad scale topographic surveying by echo sounder is also necessary in order to investigate these wider scale environmental conditions. By combining narrow but detailed methods by photogrammetry and coarse but wide methods, we will get better ecological understandings about habitat suitability of various sessile organisms.

CONCLUSION

In the present study, 3D seafloor topographic models with 0.05 m resolution were constructed using photogrammetry on subtidal rocky shore, and the relationships between distributions of sessile organisms and multiple terrain variables calculated from the 3D models were successfully investigated.

Distributions of each species were found to be affected by multiple terrain variables, such as height, TPI, aspect, slope, and ruggedness. High height above the seafloor was important for the distributions of three species of sessile animals, and gentle slope was important for that of an articulated coralline alga, *P. cretaceum*. The light intensity and flow conditions controlled by these terrain variables might affect the distribution of each species.

As measuring the multiple terrain variables was difficult with conventional direct measurement methods, the effects of topography on the distribution of sessile organisms have not received much attention in spite of their underlying importance. In the present study, we developed a new method to investigate the relationships between the distribution of sessile organisms and multiple terrain variables, which can provide more accurate information of habitat suitable conditions for each species than the previous studies conducted on subtidal rocky shores.

DATA AVAILABILITY STATEMENT

The raw data supporting the conclusions of this article will be made available by the authors, without undue reservation, to any qualified researcher.

AUTHOR CONTRIBUTIONS

TKan conducted all the field survey and data analysis, also developed the analytical methods, and drafted the manuscript. JH planned the field surveys. KN joined the field surveys. KN and JH helped to draft the manuscript. TKit and TKaw supervised this study. All authors discussed the results and approved the submitted version of the manuscript.

FUNDING

This work was supported by the Sasakawa Scientific Research Grant (2018-7020) and the Tohoku Ecosystem-Associated Marine Sciences project.

ACKNOWLEDGMENTS

We greatly thank Masaaki Hirano, Takanori Suzuki, Nobuhiko Iwama, Naoya Otsuchi, Masafumi Kodama, and other members of International Coastal Research Center, Atmosphere and Ocean Research Institute, The University of Tokyo, Masato Hirose (Kitasato University), and Kaito Fukuda (Fukuda Marine Research Diving) for supporting surveying in Otsuchi Bay. We also thank Eijiroh Nishi (College of Education Yokohama National University) for supporting identification of polychaete.

REFERENCES

Agudo-Adriani, E. A., Cappelletto, J., Cavada-Blanco, F., and Cróquer, A. (2019). Structural complexity and benthic cover explain reef-scale variability of fish assemblages in Los Roques National Park, Venezuela. *Fron. Mar. Sci.* 6:690. doi: 10.3389/fmars.2019.00690

Archambault, P., and Bourget, E. (1996). Scales of coastal heterogeneity and benthic intertidal species richness, diversity and abundance. *Mar. Ecol. Prog. Ser.* 136, 111–121. doi: 10.3354/meps136111

Barnes, H., Crisp, D. J., and Powell, H. T. (1951). Observations on the orientation of some species of barnacles. *J. Anim. Ecol.* 20, 227–241. doi: 10.2307/1542

Bayley, D. T. I., Mogg, A. O. M., Koldewey, H., and Purvis, A. (2019). Capturing complexity: field-testing the use of 'structure from motion' derived virtual models to replicate standard measures of reef physical structure. *PeerJ* 7:e6540. doi: 10.7717/peerj.6540

Bryson, M., Ferrari, R., Figueira, W., Pizarro, O., Madin, J., Williams, S., et al. (2017). Characterization of measurement errors using structure-from-motion and photogrammetry to measure marine habitat structural complexity. *Ecol. Evol.* 7, 5669–5681. doi: 10.1002/ece3.3127

Burns, J. H. R., Delparte, D., Gates, R. D., and Takabayshi, M. (2015). Utilizing underwater three-dimensional modeling to enhance ecological and biological studies of coral reefs. *Int. Arch. Photogramm. Remote Sens. Spat. Inf. Sci.* XL-5/W5, 61–66. doi: 10.5194/isprsarchives-XL-5-W5-61-2015

Chabot, R., and Bourget, E. (1988). Influence of substratum heterogeneity and settled barnacle density of the settlement of cypris larvae. *Mar. Biol.* 97, 45–56. doi: 10.1007/BF00391244

Chase, A. L., Dijkstra, J. A., and Harris, L. G. (2016). The influence of substrate material on ascidian larval settlement. *Mar. Pollut. Bull.* 106, 35–42. doi: 10.1016/j.marpolbul.2016.03.049

Chiba, S., and Noda, T. (2000). Factors maintaining topography-related mosaic of barnacle and mussel on a rocky shore. *J. Mar. Biol. Assoc. U. K.* 80, 617–622. doi: 10.1017/S0025315400002435

Connell, J. H. (1961). The influence of interspecific competition and other factors on the distribution of the barnacle *Chthamalus Stellatu*. *Ecology* 42, 710–723. doi: 10.2307/1933500

Connell, S. D. (1999). Effects of surface orientation on the cover of epibiota. *Biofouling* 14, 219–226. doi: 10.1080/08927019909378413

Courtney, L. A., Fisher, W. S., Raimond, S., Oliver, L. M., and Davis, W. P. (2007). Estimating 3-dimensional colony surface area of field corals. *J. Exp. Mar. Biol. Ecol.* 351, 234–242. doi: 10.1016/j.jembe.2007.06.021

Crisp, D. J., and Barnes, H. (1954). The orientation and distribution of barnacles at settlement with particular reference to surface contour. *J. Anim. Ecol.* 23, 142–162. doi: 10.2307/1664

Crisp, D. J., and Meadows, P. S. (1962). The chemical basis of gregariousness in cirripedes. *Proc. R. Soc. B* 156, 500–520.

Dale, T. N. (1923). The Commercial granite of New England. *Bulletin* 738, 22–103. doi: 10.3133/b738

Dean, R. L., and Connell, J. H. (1987). Marine invertebrates in an algal succession. III. Mechanisms linking habitat complexity with diversity. *J. Exp. Mar. Biol. Ecol.* 109, 249–273. doi: 10.1016/0022-0981(87)90057-8

Dolan, M. F. J., Grehan, A. J., Guinan, C., and Brown, C. (2008). Modelling the local distribution of cold-water corals in relation to bathymetric variables: adding spatial context to deep-sea video data. *Deep Sea Res.* 55, 1564–1579. doi: 10.1016/j.dsr.2008.06.010

Endo, H., Nakabayashi, N., Agatsuma, Y., and Taniguchi, K. (2007). Food of the sea urchins *Strongylocentrotus nudus* and *Hemicentrotus pulcherrimus* associated with vertical distributions in fucoid beds and crustose coralline flats in northern Honshu, Japan. *Mar. Ecol. Prog. Ser.* 352, 125–135. doi: 10.3354/meps07121

Fallati, L., Saponari, L., Savini, A., Marchese, F., Corselli, C., and Galli, P. (2020). Multi-temporal UAV data and object-based image analysis (OBIA) for estimation of substrate changes in a post-bleaching scenario on a Maldivian reef. *Remote Sens.* 12:2093. doi: 10.3390/rs12132093

Friedman, A., Pizarro, O., Williams, S. B., and Johnson-Roberson, M. (2012). Multi-scale measures of rugosity, slope and aspect from benthic stereo image reconstructions. *PLoS One* 7:e50440. doi: 10.1371/journal.pone.0050440

Georgian, S. E., Shedd, W., and Cordes, E. E. (2014). High-resolution ecological niche modelling of the cold-water coral *Lophelia pertusa* in the Gulf of Mexico. *Mar. Ecol. Prog. Ser.* 506, 145–161. doi: 10.3354/meps10816

Hirose, M., and Kawamura, T. (2017). Distribution and seasonality of sessile organisms on settlement panels submerged in Otsuchi Bay. *Coast. Mar. Sci.* 40, 66–81. doi: 10.15083/00074036

Hughes, R. G. (1975). The distribution of epizoites on the hydroid *Nemertesia antennina* (L.). *J. Mar. Biol. Assoc. U. K.* 55, 275–294. doi: 10.1017/S0025315400015940

Johnson, M. P., Frost, N. J., Mosley, M. W. J., Roberts, M. F., and Hawkins, S. J. (2003). The area-independent effects of habitat complexity on biodiversity vary between regions. *Ecol. Lett.* 6, 126–132. doi: 10.1046/j.1461-0248.2003.00404.x

Kawamata, S. (2010). Inhibitory effects of wave action on destructive grazing by sea urchins: a review. *Bull. Fish. Res. Agency* 32, 95–102.

Kemp, K. (ed.) (2007). *Encyclopedia of Geographic Information Science*. Thousand Oaks, CA: SAGE publications, Inc.

Keough, M. J., and Downes, B. J. (1982). Recruitment of marine invertebrates: the role of active larval choices and early mortality. *Oceologia* 54, 348–352. doi: 10.1007/BF00380003

Kim, K., Lecours, V., and Frederick, P. C. (2018). Using 3d micro-geomorphometry to quantify interstitial spaces of an oyster cluster. *PeerJ Prepr.* 7:e27596v1. doi: 10.7287/peerj.preprints.27596v1

Knight-Jones, E. W., and Stevenson, J. P. (1950). Gregariousness during settlement in the barnacle *Elminius modestus* Darwin. *J. Mar. Biol. Assoc. U. K.* 29, 281–297.

Knott, N. A., Underwood, A. J., Chapman, M. G., and Glasby, T. M. (2006). Growth of the encrusting sponge *Tedania anhelans* (Lieberkuhn) on vertical and on horizontal surfaces of temperate subtidal reefs. *Mar. Freshw. Res.* 57, 95–104. doi: 10.1071/MF05092

Komatsu, K., and Tanaka, K. (2017). Swell-dominant surface waves observed by a moored buoy with a GPS wave sensor in Otsuchi Bay, a ria in Sanriku, Japan. *J. Oceanogr.* 73, 87–101. doi: 10.1007/s10872-016-0362-4

Leichter, J. J., and Witman, J. D. (1997). Water flow over subtidal rock walls: relation to distributions and growth rates of sessile suspension feeders in the Gulf of Marine water flow and growth rates. *J. Exp. Mar. Biol. Ecol.* 209, 293–307. doi: 10.1016/S0022-0981(96)02702-5

Leon, J. X., Roelfsema, C. M., Saunders, M. I., and Phinn, S. R. (2015). Measuring coral reef terrain roughness using 'Structure-from-Motion' close-range photogrammetry. *Geomorphology* 242, 21–28. doi: 10.1016/j.geomorph.2015.01.030

Liu, T. L., and Su, D. T. (2013). Numerical analysis of the influence of reef arrangements on artificial reef flow fields. *Ocean Eng.* 74, 81–89. doi: 10.1016/j.oceaneng.2013.09.006

Loke, L. H. L., and Todd, P. A. (2016). Structural complexity and component type increase intertidal biodiversity independently of area. *Ecology* 97, 383–393.

Lozano-Cortés, D. F., and Zapata, F. A. (2014). Invertebrate colonization on artificial substrates in a coral reef at Gorgona Island, Colombian Pacific Ocean. *Rev. Biol. Trop.* 62, 161–168. doi: 10.15517/rbt.v62i0.16273

Menge, B. A., and Lubchenco, J. (1981). Community organization in temperate and tropical rocky intertidal habitats: prey refuges in relation to consumer pressure gradients. *Ecol. Monogr.* 51, 429–450. doi: 10.2307/2937323

Miyamoto, M., Kiyota, M., Murase, H., Nakamura, T., and Hayashibara, T. (2017). Effects of bathymetric grid-cell sizes on habitat suitability analysis of cold-water gorgonian corals on seamounts. *Mar. Geodesy* 40, 205–223. doi: 10.1080/01490419.2017.1315543

Otobe, H., Onishi, H., Inada, M., Michida, Y., and Terazaki, M. (2009). Estimation of water circulation in Otsuchi Bay, Japan inferred from ADCP observation. *Coast. Mar. Sci.* 33, 78–86. doi: 10.15083/00040706

Paine, R. T. (1966). Food web complexity and species diversity. *Am. Nat.* 100, 65–75. doi: 10.1086/282400

Perkol-Finkel, S., Shashar, N., and Benayahu, Y. (2006). Can artificial reefs mimic natural reef communities? The roles of structural features and age. *Mar. Environ. Res.* 61, 121–135. doi: 10.1016/j.marenvres.2005.08.001Get

Phillips, S. J., Anderson, R. P., and Schapire, R. E. (2006). Maximum entropy modeling of species geographic distributions. *Ecol. Modell.* 190, 231–259. doi: 10.1016/j.ecolmodel.2005.03.026

Pizarro, O., Friedman, A., Bryson, M., Williams, S. B., and Madin, J. (2017). A simple, fast, and repeatable survey method for underwater visual 3D benthic mapping and monitoring. *Ecol. Evol.* 7, 1770–1782. doi: 10.1002/ece3.2701

Ponti, M., Perliini, R. A., Ventra, V., Grech, D., Abbiati, M., and Cerrano, C. (2014). Ecological shifts in Mediterranean coralligenous assemblages related to gorgonian forest loss. *PLoS One* 9:e102782. doi: 10.1371/journal.pone.0102782

Robbins, I. J. (1983). The effects of body size, temperature, and suspension density on the filtration and ingestion of inorganic particulate suspensions by ascidians. *J. Exp. Mar. Biol. Ecol.* 70, 65–68. doi: 10.1016/0022-0981(83)90149-1

Robert, K., Huvenne, V. A. I., Georgiopoulou, A., Jones, O. B., Marsh, L., Carter, G. D. O., et al. (2017). New approaches to high-resolution mapping of marine vertical structures. *Sci. Rep.* 7:9005. doi: 10.1038/s41598-017-09382-z

Sanford, E., and Menge, B. A. (2001). Spatial and temporal variation in barnacle growth in a coastal upwelling system. *Mar. Ecol. Prog. Ser.* 209, 143–157. doi: 10.3354/meps209143

Sarà, M. (1986). Sessile macrofauna and marine ecosystem. *Ital. J. Zool.* 53, 329–337. doi: 10.1080/11250008609355518

Smith, F. G. W. (1946). Effect of water currents upon the attachment and growth of barnacles. *Biol. Bull.* 90, 51–70. doi: 10.2307/1538061

Smith, J., O'Brien, P. E., Stark, J. S., Johnstone, G. J., and Riddle, M. J. (2015). Integrating multibeam sonar and underwater video data to map benthic habitats in an East Antarctic nearshore environment. *Estuar. Coast. Shelf Sci.* 164, 520–536. doi: 10.1016/j.ecss.2015.07.036

Speed, T. (2011). A correlation for the 21st century. *Science* 334, 1502–1503. doi: 10.1126/science.1215894

Su, D. T., Liu, T. L., and Ou, C. H. (2007). A comparison of the PIV measurements and numerical predictions of the flow field patterns within an artificial reef. *Paper Presented at the 17th International Offshore and Polar Engineering Conference*, Vol. 1–4, Lisbon, 2239–2245.

Thomason, J. C., Hills, J. M., Clare, A. S., Neville, A., and Richardson, M. (1998). Hydrodynamic consequences of barnacle colonization. *Hydrobiologia* 375/376, 191–201. doi: 10.1023/A:1017088317920

Tong, R., Purser, A., Guinan, J., and Unnithan, V. (2013). Modeling the habitat suitability for deep-water gorgonian corals based on terrain variables. *Ecol. Inf.* 13, 123–132. doi: 10.1016/j.ecoinf.2012.07.002

Weiss, A. D. (2001). "Topographic positions and landforms analysis (poster)," in *Poster at the ESRI International User Conference*, San Diego, CA: ESRI.

Wendt, P. H., Knott, D. M., and Van Dolah, R. F. (1989). Community structure of the sessile biota on five artificial reefs of different ages. *Bull. Mar. Sci.* 44, 1106–1122.

Westoby, M. J., Brasington, J., Glasser, N. F., Hambrey, M. J., and Reynolds, J. M. (2012). 'Structure-from-Motion' photogrammetry: a low-cost, effective tool for geoscience applications. *Geomorphology* 179, 300–314. doi: 10.1016/j.geomorph.2012.08.021

Wilson, M. F. J., O'Connell, B., Brown, C., Guinan, J. C., and Grehan, A. J. (2007). Multiscale terrain analysis of multibeam bathymetry data for habitat mapping on the continental slope. *Mar. Geodesy* 30, 3–35. doi: 10.1080/01490410701295962

Wu, C. (2013). "Towards linear-time incremental structure from motion," in *Proceedings of the 2013 International Conference on 3D Vision – 3DV 2013*, Seattle, WA, 127–134. doi: 10.1109/3DV.2013.25

Wu, C., Agarwal, S., Curless, B., and Seitez, S. M. (2011). "Multicore bundle adjustment," in *Proceedings of the CVPR 2011*, Colorado Springs, CO, 3057–3064. doi: 10.1109/CVPR.2011.5995552

Yanagi, T., and Nakajima, M. (1991). Change of oceanic condition by the man-made structure for upwelling. *Mar. Pollut. Bull.* 23, 131–135. doi: 10.1016/0025-326X(91)90662-C

Young, G. C., Dey, S., Rogers, A. D., and Exton, D. (2017). Cost and time-effective method for multi-scale measures of rugosity, fractal dimension, and vector dispersion from coral reef 3D models. *PLoS One* 12:e0175341. doi: 10.1371/journal.pone.0175341

Conflict of Interest: The authors declare that the research was conducted in the absence of any commercial or financial relationships that could be construed as a potential conflict of interest.

frontiers in Marine Science

ORIGINAL RESEARCH
published: 16 April 2021
doi: 10.3389/fmars.2021.646475

Colony-Level 3D Photogrammetry Reveals That Total Linear Extension and Initial Growth Do Not Scale With Complex Morphological Growth in the Branching Coral, *Acropora cervicornis*

Wyatt C. Million[1], Sibelle O'Donnell[1], Erich Bartels[2] and Carly D. Kenkel[1]*

[1] *Department of Biological Sciences, University of Southern California, Los Angeles, Los Angeles, CA, United States,* [2] *Elizabeth Moore International Center for Coral Reef Research & Restoration, Mote Marine Laboratory, Summerland Key, FL, United States*

OPEN ACCESS

Edited by:
Manuel Gonzalez-Rivero, Australian Institute of Marine Science (AIMS), Australia

Reviewed by:
Aldo Cróquer, The Nature Conservancy, Dominican Republic
Zac H. Forsman, University of Hawaii at Manoa, United States

***Correspondence:**
Wyatt C. Million
wmillion@usc.edu

Specialty section:
This article was submitted to Coral Reef Research, a section of the journal Frontiers in Marine Science

Received: *27 December 2020*
Accepted: *23 March 2021*
Published: *16 April 2021*

Citation:
Million WC, O'Donnell S, Bartels E and Kenkel CD (2021) Colony-Level 3D Photogrammetry Reveals That Total Linear Extension and Initial Growth Do Not Scale With Complex Morphological Growth in the Branching Coral, Acropora cervicornis. Front. Mar. Sci. 8:646475. doi: 10.3389/fmars.2021.646475

The ability to quantify changes in the structural complexity of reefs and individual coral colonies that build them is vital to understanding, managing, and restoring the function of these ecosystems. However, traditional methods for quantifying coral growth *in situ* fail to accurately quantify the diversity of morphologies observed both among and within species that contribute to topographical complexity. Three-dimensional (3D) photogrammetry has emerged as a powerful tool for the quantification of reefscape complexity but has yet to be broadly adopted for quantifying the growth and morphology of individual coral colonies. Here we debut a high-throughput method for colony-level 3D photogrammetry and apply this technique to explore the relationship between linear extension and other growth metrics in *Acropora cervicornis*. We fate-tracked 156 individual coral transplants to test whether initial growth can be used to predict subsequent patterns of growth. We generated photographic series of fragments in a restoration nursery immediately before transplanting to natural reef sites and re-photographed coral at 6 months and 1 year post-transplantation. Photosets were used to build 3D models with Agisoft Metashape, which was automated to run on a high-performance computing system using a custom script to serially process models without the need for additional user input. Coral models were phenotyped in MeshLab to obtain measures of total linear extension (TLE), surface area, volume, and volume of interstitial space (i.e., the space between branches). 3D-model based measures of TLE were highly similar to by-hand measurements made in the field (r = 0.98), demonstrating that this method is compatible with established techniques without additional in water effort. However, we identified an allometric relationship between the change in TLE and the volume of interstitial space, indicating that growth in higher order traits is not necessarily a linear function of growth in branch length. Additionally, relationships among growth

measures weakened when comparisons were made across time points, implying that the use of early growth to predict future performance is limited. Taken together, results show that 3D photogrammetry is an information rich method for quantifying colony-level growth and its application can help address contemporary questions in coral biology.

Keywords: coral, morphology, 3D photogrammetry, *Acropora cervicornis*, TLE, volume, surface area, allometry

INTRODUCTION

The three-dimensional structural complexity of coral is central to the ecological function of reefs (Alvarez-Filip et al., 2009; Zawada et al., 2010). Structurally intricate reefs sustain high biological diversity (Risk, 1972; Graham and Nash, 2013), increase productivity (Szmant, 1997), and reduce hydrodynamic energy (Lugo-Fernández et al., 1998; Monismith, 2007). Colony morphology also influences small scale water flow that controls the size of the diffusion boundary layer, influencing heat and mass transfer (Stocking et al., 2018) and pH of the tissue surface (Chan et al., 2016). These physicochemical processes support key aspects of a coral's biology, including nutrient uptake, and mitigation of acidification and thermal stress (Dennison and Barnes, 1988; Lesser et al., 1994; Jimenez et al., 2011). Consequently, the ability to quantify changes in the structural complexity of reefs and the individual coral colonies that build them is vital to understanding, managing, and restoring the function of these ecosystems.

Traditional methods for measuring coral growth have provided foundational knowledge of extremely fast growth rates in *Acropora cervicornis* compared to other species (Lirman et al., 2014), trade-offs between growth and thermal susceptibility (Jones and Berkelmans, 2010; Cunning et al., 2015) and the capacity for morphological plasticity (Bruno and Edmunds, 1997; Todd, 2008; Drury et al., 2017). However, the type and quality of information that can be obtained from each individual metric is limited. Moreover, many require handling, or even destructive sampling, hindering the potential to investigate temporal changes in growth using repeated measures. Non-invasive methods for measuring growth *in situ* include total linear extension (TLE, Johnson et al., 2011) and estimated ellipsoidal volumes (Kiel et al., 2012). TLE relies on linear measures of branch lengths, typically taken by hand with calipers or a ruler, to quantify skeletal size (Johnson et al., 2011). However, this measure is only applicable to branching species, and can be arduous to complete *in situ* as colonies increase in size (Lirman et al., 2014). Alternatively, colony size can be calculated from the volume of an ellipsoid with the same length, width, and height as a coral colony (Kiel et al., 2012). However, this method is likely unable to resolve changes in the pattern of growth that do not increase the maximum dimensions of a colony. Invasive techniques to measure coral growth include direct measures of surface area (SA) via wax dipping (Stimson and Kinzie, 1991; Veal et al., 2010), volume (V) via water displacement (Jokiel et al., 1978; Herler and Dirnwöber, 2011), and mass via buoyant weighing (Davies, 1989). However, each of these methods requires handling and, for wax dipping, sacrificing the coral completely. Measuring growth in one dimension also ignores structural differences. For example, two colonies may have the same linear extension or ellipsoidal volume but encompass vastly different morphological forms (Pratchett et al., 2015). Therefore, multiple independent methods would be required to gain a comprehensive understanding of colony growth and morphology.

Three-dimensional (3D) photogrammetry, i.e., obtaining measurements from digital, scaled 3D representations of objects, has become a powerful tool for quantifying structural components of coral reefs (Burns et al., 2015; D'Urban Jackson et al., 2020; Hernández-Landa et al., 2020). There has been growing application of this technology to quantify reefscape complexity (McKinnon et al., 2011; Burns et al., 2015; Leon et al., 2015), but 3D photogrammetry has yet to be broadly adopted for quantifying growth and morphology of individual coral colonies, despite several studies validating its application (Figueira et al., 2015; Lavy et al., 2015; Agudo-Adriani et al., 2016; Ferrari et al., 2017; House et al., 2018; Doszpot et al., 2019; Lange and Perry, 2020). One reason for this may be that although model building algorithms and the user-friendliness of applications continue to improve, methodological nuances can result in differences in the required processing time, quality of models produced, and traits measured (Lange and Perry, 2020 compared to Lavy et al., 2015). Similar to open source software that allows for community contribution that drives innovation (Hippel and Krogh, 2003), increasing accessibility and reproducibility of 3D photogrammetry methods can help facilitate broader adoption and advancement of this technique. The information richness of a single 3D model is a major methodological advantage, expanding the range of biological questions that can be investigated. For example, in addition to quantifying coral growth via TLE, SA, or V, quantifying the volume of interstitial space (V_{inter}) can give insights into the ecological function of coral growth by providing an estimate of the amount of resulting habitat space that is created (Coker et al., 2014; Agudo-Adriani et al., 2016). 3D models can also provide digital structures to enable more accurate mapping of the hydrodynamics of flow around colonies (Stocking et al., 2018). Finally, the permanent record of 3D models allows for researchers to revisit historical datasets to verify previous measures or test new hypotheses. This unprecedented access to multiple traits once hard to measure comes without the need to touch or manipulate the coral itself, making it especially useful for conducting repeated measures over time.

The ability to non-invasively quantify changes in key performance traits also has important practical applications, particularly in the context of reef restoration. The structural complexity of Caribbean coral reefs has been altered by dramatic losses of branching acroporids (Miller et al., 2002;

Alvarez-Filip et al., 2009). As a result, *A. cervicornis* and *A. palmata* have been the focus of broad-scale restoration efforts in Florida and the broader Caribbean. Significant effort has been invested in the development of in-water and *ex situ* nurseries in order to generate biological material to outplant to degraded reef sites (Rinkevich, 1995; Young et al., 2012; Lohr et al., 2015). However, the ultimate success of these efforts has been hampered by the inability to predict the performance of coral outplants, given that both genetic and environmental variables can influence survival and growth (Drury et al., 2017; O'Donnell et al., 2017). The ability to use early, non-invasive indicators to quantify outplant success would be beneficial in restoration settings that aim to optimize efforts to repopulate Caribbean reefs (Edmunds and Putnam, 2020; Parkinson et al., 2020).

Reliable predictors of coral performance that can be evaluated before or soon after outplanting can guide restoration programs to strategically enhance efforts. However, prior work suggests that the predictive power of traditional growth metrics may be limited. Early growth rate in TLE for *Acropora cervicornis* was found to be a poor predictor of future growth rate for nursery-grown (O'Donnell et al., 2018) and wild corals (Edmunds, 2017). Similarly, early growth rates for two massive coral species as measured in nurseries explained only a portion of future performance, and the predictive power of these metrics varied over sampling points and traits (Edmunds and Putnam, 2020). The utility of higher order traits, such as SA, V, and V_{inter}, for predicting subsequent growth remains unknown because handling or destructive sampling of outplants is not possible in a restoration context.

Here we apply high-throughput colony-level 3D photogrammetry to fill this knowledge gap. First, we develop an open-access protocol for conducting colony-level 3D photogrammetry that provides guidance for *in situ* image collection, makes high-throughput model building more readily accessible, and creates a repeatable, standardized method for coral phenotyping from 3D models. We then employ this method to address questions regarding the predictive power of higher order morphological traits in *A. cervicornis* by quantifying the growth of outplants at different intervals throughout 1 year. We test to what degree total linear extension (TLE), a commonly used non-invasive metric of growth in *A. cervicornis* (Johnson et al., 2011), can be used to estimate growth in higher order traits, such as surface area (SA), volume (V), and the volume of the interstitial space (V_{inter}), in addition to testing for predictive correlations among these traits.

MATERIALS AND METHODS

Study Design

In April 2018, three ramets of each of ten genotypes of *A. cervicornis* from Mote Marine Laboratory's *in situ* nursery were transplanted in triplicate to nine offshore reef sites throughout the Lower Florida Keys under FKNMS permits 2015-163-A1 and 2018-035 (n = 27 initial ramets/genotype). Triplicate ramets were attached to the reef substrate, with one ramet per genotype assigned to each of 3 randomized arrays within each site. Coral morphology was quantified with 3D photogrammetry at 3 time points: in the *in situ* nursery prior to transplantation (April 2018), and 6 months (October 2018) and 12 months (April 2019) post-transplantation. Of the 270 outplanted coral fragments, 72 died or were lost from the transplant after 12 months. An additional 43 coral fragments, including 40 nursery fragments, 2 fragments at 6 months, and 1 fragment at 12 months were removed from the dataset due to insufficient photographic coverage causing incomplete models, resulting in a final dataset of 156 fragments measured for all traits at all-time points. Additionally in April 2018 and October 2018, TLE was measured by-hand with a flexible ruler following the protocol of Lirman et al. (2014) and these measurements were used to compare with TLE obtained through 3D photogrammetry in order to assess the potential for backward compatibility.

Image Capture

Photographs of outplanted corals were taken by SCUBA divers following the protocol available at dx.doi.org/10.17504/protocols.io.bgdcjs2w. Briefly, photographs were taken from multiple angles using the Olympus Tough TG-4/TG-5 (Olympus America Inc.), maintaining roughly 80% overlap until the entire coral colony was captured with 2D images. The Olympus Tough TG-4/TG-5 was chosen for its low price point, its built-in underwater capabilities which avoids the need for auxiliary underwater housings, and its small size which allowed divers to operate the camera with one hand in high wave-action environments. Cameras were set to "underwater" or "auto" mode with flash turned off, and photos were taken by either manually pressing the shutter or set to capture images automatically at 1 s intervals, depending on photographer preference. In April 2018, coral ramets were photographed in the nursery prior to transplantation in groups of 10 (**Supplementary Figure 1**) requiring 120–383 photos per group. Post-transplantation, in October 2018 and April 2019, a custom-built scaling object incorporating Agisoft Metashape markers was included around each coral to provide a fixed reference for model generation. The number of photos taken for each colony ranged from 7 to 293, with the number of photographs depending on size of the colony and water quality conditions at a given location.

Image Pre-processing and Model Building

Photos were downloaded and sorted into separate photo sets for each group of 10 nursery corals (April 2018) or individual outplanted colony (October 2018, April 2019). Photographs where the coral was out of focus or out of frame were manually removed. Photographs shot in "auto" mode were color corrected in Lightroom (Adobe® Lightroom® software) to remove green tint and enhance contrast of the coral when needed, for example, when model building was hindered by bright white branch tips.

Three-dimensional models were generated from photo sets using Agisoft Metashape (Agisoft LLC, St. Petersburg, Russia).

Metashape is processing intensive so in order to rapidly build 3D models with limited user input, we completed all model building on a Dell PowerEdge R910 with an Intel® Xeon® Processor E7-4850 with Metashape manually limited to 20–40 CPUs and 250 GB of RAM. Due to limited licensing capabilities of Metashape, a custom Python script was used to serially process models and Metashape settings were adjusted when needed for individual models. Models were exported as Wavefront (.OBJ) files which are capable of maintaining color pulled from 2D photos. Models with portions of colonies missing were rebuilt with a modified script that expands the size of the bounding box during the "Align Photos" step to include all calculated tie points. All bioinformatic scripts used to run Metashape on the command line can be found at https://github.com/wyattmillion/Coral3DPhotogram. We assessed the performance of 200 automated Agisoft Metashape runs through the number of tie points found from each photoset (overlapping points found in two or more photos) and the number of faces making up each mesh.

3D Phenotyping

Models generated in Metashape were imported into the free 3D model editing software, Meshlab v2016.12 (Cignoni et al., 2008) to obtain measurements of TLE, SA, V, and Vinter following protocols outlined at dx.doi.org/10.17504/protocols.io.bgbpjsmn. Briefly, models were scaled using Agisoft Metashape markers and scaling accuracy was verified by remeasuring markers. Models were manually trimmed using the *Select vertices* and *Remove current set of selected vertices* tools leaving only living coral in the models. Small holes in the areas of coral tissue were filled prior to phenotyping models using the *Close Holes* filter. To calculate TLE, the lengths of all branches were manually measured and summed using the *Measuring Tool*. Surface area was automatically quantified using MeshLab's *Compute Geometric Measure* filter. The bottom of coral models were then closed using the *Close Holes* filter in order to make the mesh "watertight" for the *Compute Geometric Measure* filter to measure the volume of the coral. The volume of a colony was subtracted from the volume of a convex hull, i.e., a mesh overlaid over the most extreme branch tips (**Supplementary Figure 2**), in order to quantify V_{inter}. Traits such as "proportion occupied" (Doszpot et al., 2019) and "convexity" (Zawada et al., 2019) utilize a convex hull but instead derive morphometric features standardized to coral volume or surface area. Here we used V_{inter} to measure the absolute volume of empty space between coral branches.

Five colonies suffered severe breakage and only a small portion of living tissue remained after 12 months (**Supplementary Figure 3**). 3D models were not built for these colonies and instead, SA was measured in ImageJ (Rasband, 1997–2014) following (Kenkel et al., 2015) and V and V_{inter} were recorded as 0 because the colony tissue represented a 2D area with no living 3D structure beyond the height of a single polyp (**Supplementary Figure 3**). TLE was recorded as 1 mm as this was the average height of the coral polyps on the colonies at the 6-month time point.

Statistical Analysis

All statistical analysis was completed in R 3.6.3 (R Core Team, 2020). One coral was randomly chosen to assess precision of the 3D photogrammetry method. To do this, we determined the coefficient of variation (CV) for each focal trait measure (TLE, SA, V, and V_{inter}) across 6 replicate models built from a reduced photoset where a random 10% of the photographs were removed, similar to Ferrari et al. (2017) and Lange and Perry (2020). The corals used in this study are part of restoration efforts and as such could not be removed from the substrate to measure volume or surface through traditional methods. Instead, TLE measured by-hand *in situ* was used to ground-truth measurements of TLE obtained from 3D models.

Pearson correlations were used to assess the relationship between by-hand and 3D model based measurements of TLE collected at two time points (initial, and 6 months, n = 311) and to assess whether the difference in methods is a function of coral size. To assess the strength of predictive relationships among trait measurements within and across time-points, Kendall's tau correlations were used to relate the change in trait values between 0–6 months and 6–12 months (n = 156). Kendall's tau was used for its ability to handle non-normally distributed data and heteroscedastic residuals, as well as outliers, which here represent true biological variation, and non-linearity (Newson, 2002). Additive polynomial regressions were used to maximize the fit of non-linear relationships observed for TLE and V_{inter}, while adding the fewest polynomial terms.

A. cervicornis naturally reproduces through fragmentation (Tunnicliffe, 1981; Drury et al., 2019). To assess whether natural fragmentation events influenced the predictive relationship among traits, we recorded the number of breakage events experienced by each coral by comparing photographic records across time points. Breakage was coded as a binary with coral experiencing one or more breakage events considered "Broken" and corals experiencing no breakage considered "Unbroken."

RESULTS

Modeling Performance and Precision

3D models of individual colonies (6- and 12-month time points) were built from an average of 91 photos, while as few as 7 photos (for the smallest colonies) and as many as 293 photos (for the largest colonies) were used in successful runs. The number of photos used as input into the model building step was loosely related to the size of the colony following a linear pattern (**Supplementary Figure 4**). We used a subset of 200 models to evaluate our model building pipeline which took about 1.5 h on average to build models of colonies ranging from 0.1 to 74 cm TLE and with 1 to 21 branches. The number of tie points for the 200 model runs ranged from 920 to 151,132, and the number of faces ranged from 137,873 to 5,337,592.

Replicate models of a single coral colony at the 12-month time point were measured to assess the precision of model building and phenotyping steps. This coral represented a relatively large and complex colony, with 21 branches total (TLE = 74 cm,

SA = 261 cm^2, V = 85 cm^3, V_{inter} = 434 cm^3). Replicate 3D models had similar resolution with an average of 2,125,932 faces per model (CV = 1.5%). The replicate models produced very similar trait measurements, once individually scaled, with a CV of 1.3% for TLE, 3.7% for SA, 5.7% for V, and 4.9% for V_{inter}.

Photogrammetry vs. Traditional Methods

A strong correlation was observed between TLE measures made by-hand *in situ* and those obtained from the 3D models (r = 0.98, n = 311, **Figure 1A**). The average absolute difference between the two methods for a single colony was 12.8 mm (**Figure 1A**). Additionally, there was a significant but weak positive correlation between the absolute size of a focal colony and accuracy, as quantified by the difference in the value of TLE, based on how the measurement was made (r = 0.29, $p < 0.001$, **Figure 1B**). A greater agreement between by-hand and 3D model based measurements (i.e., a lower difference value) indicates higher accuracy, suggesting that discrepancies between the two methods increase as colonies increase in size.

TLE as a Proxy for Higher Order Traits

TLE was highly correlated with growth in higher order traits when compared within the same time point (**Figure 2** and **Supplementary Figure 5**). The change in TLE over the first 6 months of outplanting was very strongly correlated with growth of SA, V, and V_{inter} over the same time window (τ = 0.76–0.85). The strength of correlations was slightly reduced in the second 6-month window, but TLE was still strongly correlated with other three-dimensional traits (τ = 0.64–0.8).

Regression plots of individual trait correlations suggest that non-linear dynamics likely influenced trait relationships (**Supplementary Figure 5**). For example, a second order polynomial better explained the relationship between growth in TLE and growth in V_{inter} during the first 6 months (r = 0.922, p = 2.2e-16) and during the second 6 months (r = 0.864, p = 2.2e-16; **Figure 3**), with V_{inter} increasing at a faster rate than TLE.

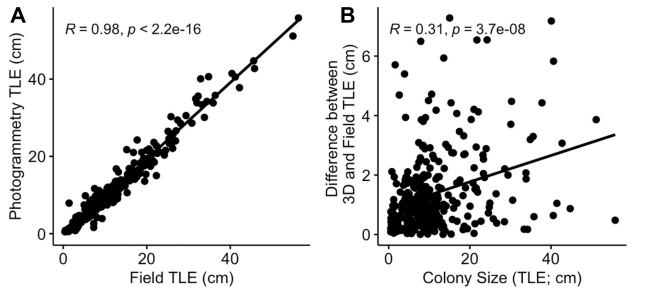

FIGURE 1 | The relationship between **(A)** TLE measured by-hand in the field and from 3D models and **(B)** the absolute difference between by-hand and 3D based measures and the size of the focal coral colony (n = 311).

Relationships Among Growth Traits Over Time

Relationships among growth measurements weakened markedly when comparisons were made across time points (**Figure 2**). Trait growth in the first 6 months post-outplant was weakly correlated with growth of the focal trait over the second 6 months (τ = 0.35–0.45, **Figure 2**). The use of non-linear regressions explained an additional 2.5% of the variation in subsequent TLE growth and an additional 1.7% of the variation in subsequent V_{inter} growth. The relationships between future and subsequent growth in SA and V were not significantly improved by non-linear models (**Supplementary Figure 6**).

Random coral breakage influences the predictive power of initial growth measurements, but relationships remain weaker than for the within time-point correlations even when broken corals are excluded from models (**Figure 4**). For example, the correlation between initial and subsequent V_{inter} growth improved when broken coral were excluded (Broken included: τ = 0.45, p = 5.05e-17; **Figure 2**; Broken excluded: τ = 0.63, p = 3e-9, **Figure 4D**). Similar effects of breakage diminish the power of initial growth to predict future growth in other traits as Kendall's tau coefficients also increased for correlations between initial and subsequent growth in TLE and SA (τ = 0.57 and τ = 0.49, respectively) when broken corals were excluded (**Figures 4A,B**). No significant relationships between initial and subsequent growth were observed for corals that experienced breakage (**Figure 4**).

The change in TLE over the first 6 months of outplanting was generally a poor predictor of future growth. The strongest predictive relationships for an initial measure of growth were observed for V, which had the strongest correlations with subsequent growth in all traits regardless of breakage events (τ = 0.37–0.48, **Figure 2**), and when broken corals were excluded (τ = 0.37–0.49, **Supplementary Figure 7**). Interestingly, initial growth in all traits displayed stronger relationships with subsequent growth in V_{inter}, as evidenced by stronger correlation coefficients in the 6–12 month V_{inter} column, than for other initial to subsequent growth comparisons (TLE, SA, V, **Figure 2**).

DISCUSSION

The complex structure of a coral reef is vital to its function (Alvarez-Filip et al., 2009; Zawada et al., 2010). Consequently, declines in populations of reef building corals dramatically change the topography of these biologically diverse ecosystems (Denis et al., 2017). *Acropora cervicornis* was once a prolific reef builder in the Caribbean and its decline has sparked massive restoration efforts in areas like the Florida Keys (Young et al., 2012). To quantify restoration outcomes, practitioners often desire to track colony growth as a performance metric (Young et al., 2012; Ware et al., 2020) because coral size correlates with fitness-related traits like survival and fecundity (Babcock, 1991; Hughes et al., 1992; Álvarez-Noriega et al., 2016). However, given the scale of

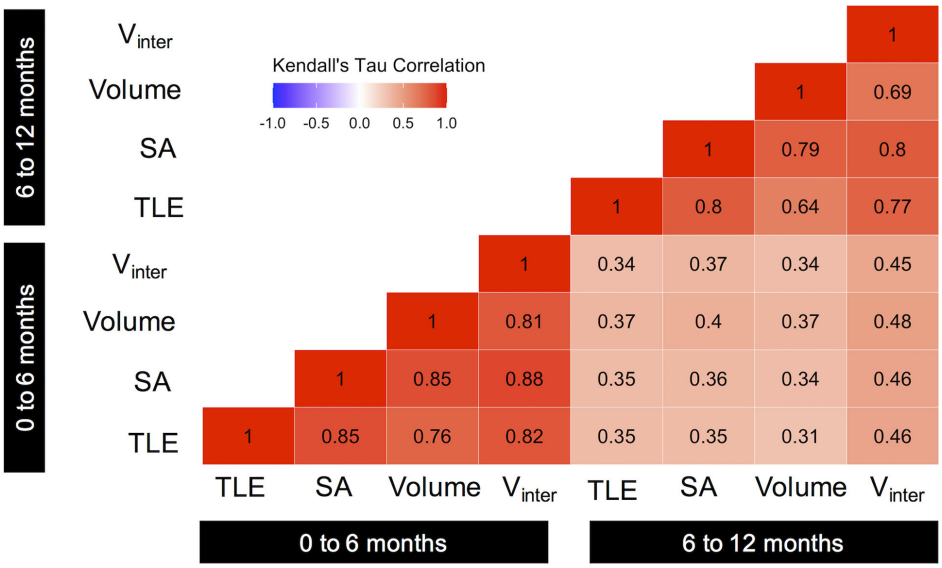

FIGURE 2 | Correlation matrix showing the relationships among growth in traits over time. Values indicate Kendall's tau correlation coefficient. All relationships were significant ($p < 0.05$). Color indicates the magnitude and direction of the correlation.

outplanting efforts, invasive methods to track coral growth are inefficient and counter to the goals of restoration when destructive sampling is necessary (Johnson et al., 2011). Similarly, while non-invasive measurements, such as TLE, are informative (Johnson et al., 2011), they can be painstaking and slow if done by-hand (Lirman et al., 2014). Here we show that 3D photogrammetry can generate accurate measurements of linear growth while simultaneously providing information on higher order traits reflective of an individual coral's condition, like surface area, and volume, as well as its function, such as the volume of interstitial space produced by its branching morphology. We find that linear extension is a strong correlate of growth in higher order traits within a monitoring period. However, predictive relationships across time-points are poor. Moreover, breakage and non-linear relationships among traits present obstacles to predicting future growth in coral colonies. Variation in morphological growth brought on by environmental variation may further complicate projections made from initial growth rates.

Relationships Between TLE and Higher Order Traits

Growth in TLE was a reliable estimator for growth in SA, V, and V_{inter} within a particular monitoring window. Relationships were the strongest within the first 6 months post-outplant suggesting that TLE could be used to approximate higher order traits in smaller, less complex colonies. However, this relationship weakened on average during the second 6-month monitoring window. This decrease in the strength of relationships among traits over time could be due to allometric variation in the growth rates of traits relative to overall colony size.

Allometry broadly describes the scaling of two biological traits (West et al., 1997) but often implies differences in growth rate between these traits. For example, horn length in male rhinoceros beetles showed a positive allometric relationship to prothorax size, meaning that increases in body size resulted in disproportionately large increases in horn size (McCullough et al., 2015). Allometric scaling has also been used to describe size-dependent growth rates in plants that show negative allometry—growth rate decreases as overall biomass increases (Wesselingh et al., 1997; Félix-Burruel et al., 2019). Additionally, allometric relationships can change due to environmental effects, resulting in inconsistent scaling between traits within a species. This phenomenon has been reported in height-stem diameter relationships across environmental gradients for some tree species (Lines et al., 2012). Finally, intraspecific variation in allometric scaling between traits can result in further phenotypic variation, for example, scaling between horn and body size can

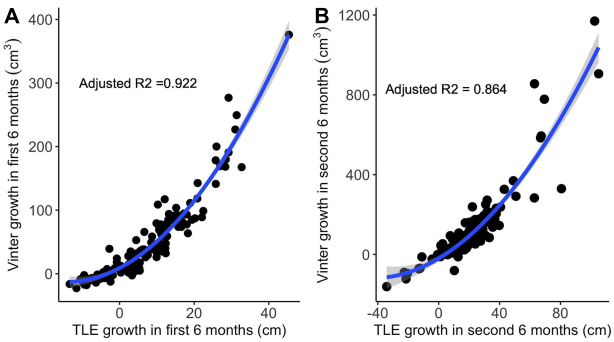

FIGURE 3 | Growth in TLE compared to growth in V_{inter} over the first 6 months **(A)** and over the second 6 months **(B)**. The solid blue line shows the second order polynomial fit to each relationship. Shaded areas around each line represent the 95% confidence intervals ($n = 156$).

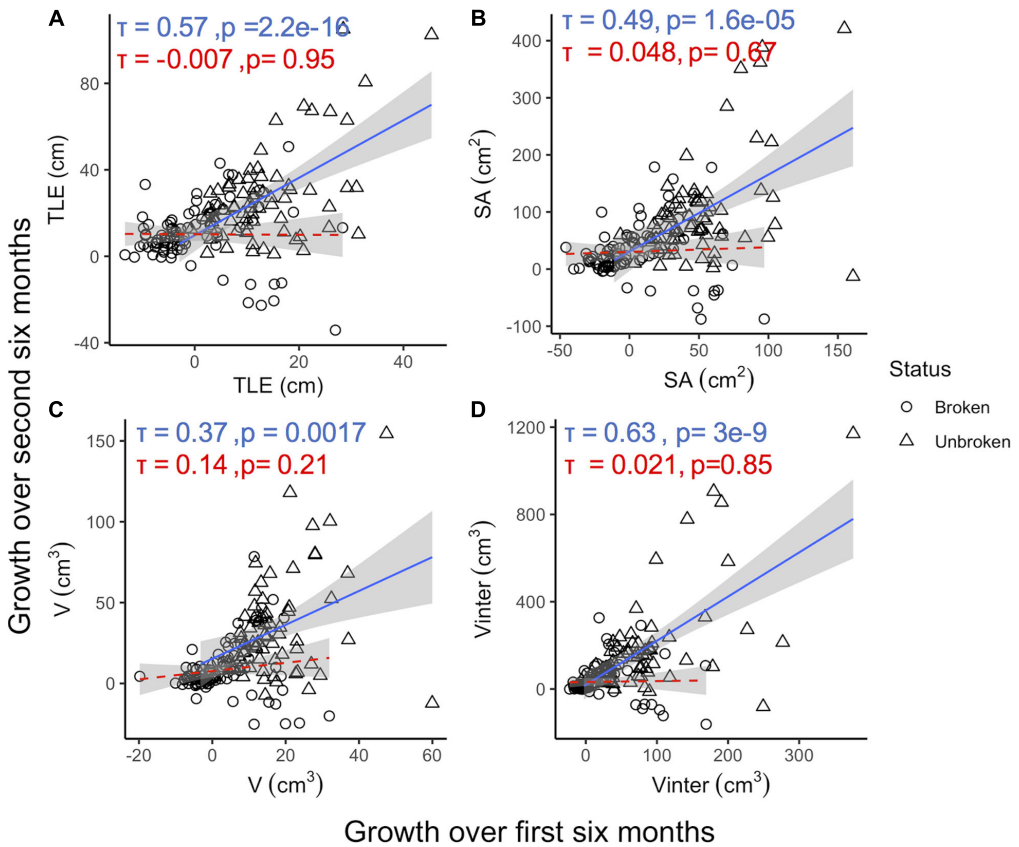

FIGURE 4 | Growth over the first 6 months compared to growth over the second 6 months for TLE **(A)**, SA **(B)**, V **(C)**, and V_{inter} **(D)** colored by whether coral experienced breakage (open circles, dashed red line) or not (open triangles, solid blue line). Kendall's tau coefficients and *p*-values are included for correlations. Shaded areas around each line represent the 95% confidence intervals (n = 156).

vary among competing males of a single rhinoceros species (McCullough et al., 2015).

We uncover an exponential relationship between TLE and V_{inter} where marginal increases in TLE result in larger increases in V_{inter} as corals grow, indicating positive allometry. Similar positive allometry was observed in multiple coral morphotypes for shelter volume-colony diameter and planar area relationships (Urbina-Barreto et al., 2020), and between colony surface complexity and colony volume (Zawada et al., 2019). The allometric relationship observed here between TLE and V_{inter} means that small colonies create interstitial space at a slower rate than larger colonies. This may slow restoration of the ecological function of *A. cervicornis* reefs if colonies are not able to reach large sizes due to natural breakage (Tunnicliffe, 1981; Madin et al., 2014) in addition to intrinsic negative scaling that can limit the overall size of an otherwise healthy coral (Dornelas et al., 2017). Negative allometric relationships can also impact morphological growth. Allometry in colony geometry and volume (Zawada et al., 2019) indicate that growth in higher order traits has the potential to plateau or regress as coral size increases. Changes in colony shape and geometry would result in shifts of ecological functionality over colony size ranges. The complex growth dynamics influenced by positive and negative allometry underscore the need to track various forms of morphological growth to understand the ecological consequences (Lesser et al., 1994; Agudo-Adriani et al., 2016; Chan et al., 2016), a need which can be met by 3D photogrammetry.

The remaining correlations between TLE and SA or V in *A. cervicornis* were explained by linear functions; however, the strength of these relationships decreased over the second 6 months. Explanations for this pattern likely include both environmental or genetic variation in allometric relationships. For example, location-specific variation in the relationship between ellipsoid volume and TLE has been reported in *A. cervicornis* (Huntington and Miller, 2014). Moreover, while intraspecific allometric variation was not found for negative size-dependent growth (Dornelas et al., 2017), an extensive body of work has identified genotypic variation in *A. cervicornis* morphology (Bowden-Kerby, 2008; Kuffner et al., 2017; Lohr and Patterson, 2017; Drury et al., 2019) supporting the potential for intraspecific variation in allometric scaling relationships among traits. Here, colonies representing multiple genotypes were outplanted to multiple reef sites likely to vary in environmental conditions; however, our current dataset lacks the temporal resolution with which to identify patterns of site-specific and intraspecific variation in allometry between TLE and higher order

traits. Tracking individuals with high temporal resolution would help capture site-specific and genotypic growth curves spanning multiple size classes. Allometric variation among colonies can also result in varying trait growth relationships within or between reef sites, which could play a role in the weakened among-trait correlations seen in this study. Ultimately, quantifying the potential for allometric variation among individuals is important for understanding the ecology and evolution of populations and species, especially when that variation arises in fitness-related traits, such as growth in coral (Babcock, 1991; Hughes et al., 1992; Álvarez-Noriega et al., 2016).

Predictive Power of Initial Growth

Coral restoration can benefit from reliable predictors of key performance traits that can be used to guide propagation and outplanting of corals with desired traits (van Oppen et al., 2015). We tested the predictive power of initial growth by relating it to growth in subsequent time intervals. Initial growth was weakly correlated with subsequent growth in each morphological trait (τ = 0.35–0.45). This is significantly higher than the predictive power of growth rates measured in an *in situ* field nursery for growth post-outplant in *A. cervicornis* (O'Donnell et al., 2018). This suggests that post-outplant growth, rather than nursery growth, can more reliably project the performance of *A. cervicornis* transplants. However, the moderate correlations seen here, which are similar to the correlations between initial and subsequent growth previously reported for massive species (Edmunds and Putnam, 2020), imply that colony growth is determined by more than just intrinsic growth rate.

One random factor exerting a negative effect on growth in *A. cervicornis* is fragmentation, or breakage. Breakage is a natural ecological process that can lead to asexual propagation (Tunnicliffe, 1981; Drury et al., 2019), partial mortality, or death (Madin et al., 2014). Breakage was frequent in this study, with 54% of colonies experiencing at least one breakage event over the 1 year monitoring window. The effects of breakage on the predictive power of initial growth in TLE, SA, and V_{inter} were evident as correlations with subsequent growth improved once broken colonies were removed from models. Interestingly, the exclusion of broken coral resulted in no increase in the predictive power of initial growth in V, suggesting that measures of growth in V may be robust to breakage. Initial growth in V was also the best predictor of subsequent growth in TLE, SA, and V_{inter} when broken corals were included which may indicate a consistent relationship between the growth in V and growth in other traits. This is similar to the findings of Zawada et al. (2019) who showed that for a variety of coral morphotypes including branching species, colony volume scaled consistently with many higher order traits as colony size increased (i.e., limited allometric scaling).

Seasonality may also play a role in modulating growth rates over time as unexplained variation in subsequent trait growth remained even after accounting for breakage. Morphological traits that respond to environmental changes can result in differences in growth patterns over time that further reduce the predictive power of initial growth. Our study spanned four seasons in the Florida Keys with the first 6 months occurring during roughly Summer and Fall while the second 6 months occurred during Winter and Spring. Seasonal variation in environmental conditions like wave energy, which is dictated by wind speed in the Florida Keys (Ahn et al., 2020), can result in fluctuating selection on different aspects of colony growth. For example, high wave energy increased the number of smaller branches produced in *A. cervicornis* colonies (Bottjer, 1980), hypothetically increasing TLE, SA, and V but decreasing V_{inter} if new branches did not extend beyond the initial branch length. Similarly, trade-offs between linear growth and skeletal density were evident in *A. cervicornis* grown using two grow-out methods (blocks vs. suspended trees) thought to modulate the amount of force exerted on colonies by water movement (Kuffner et al., 2017). Environmental conditions can therefore cause differences in how colonies grow and if environmental conditions are not constant over time, growth in one time period will not be indicative of growth in another. Moreover, Edmunds and Putnam (2020) also noted that the predictive power of initial growth varied by season, further confirming that projections of future growth are complicated by temporal changes in environmental conditions.

Advantages of 3D Photogrammetry

It has been nearly 20 years since 3D models built from photographs were first used in the study of coral (Bythell et al., 2001) and in that time, technological improvements have made 3D photogrammetry a reliable method for exploring complex features of coral and coral reefs. We show that small-scale colony-level 3D photogrammetry yields measures of TLE that have a near-perfect correlation with measures of TLE made by-hand and this backward compatibility allows for seamless transitions between methods. 3D photogrammetry could be adopted at any time during the course of a study without the need to apply a correction factor. Alternatively, high correlations between by-hand and 3D measures ensure that those unable to adopt 3D techniques, such as small non-profit organizations, can continue to use traditional methods while still being able to compare results with novel techniques. Measures of SA and V from 3D models could not be directly compared to traditional measures due to the nature of this experiment; however, previous efforts have confirmed the accuracy of 3D photogrammetry (Figueira et al., 2015; House et al., 2018). In addition to facilitating meta-analysis through backward compatibility, 3D photogrammetry also offers several advantages over traditional measurements in terms of its accuracy and information rich digital record, and the ability to obtain multiple trait measurements using a single method.

While the difference between 3D photogrammetry and traditional methods does increase as the coral increases in size, this is likely due to error in by-hand measurements rather than error in the models. Repeated, independent measurements of 3D models showed high precision, even for the larger, more complex colonies. Moreover, we were able to identify errors that would have otherwise gone undetected in the by-hand dataset through re-reviewing the extensive photographic

record. For example, two nearby colonies were wrongly identified due to missing identification tags, but we were able to correctly re-identify these individuals using photographs from previous time points. Additionally, although one colony was identified as an outlier for growth in V_{inter} over the second 6 months, the photographic record allowed us to verify that this was the result of true biological variation rather than sampling error (**Supplementary Figure 8**). 3D photogrammetry also allowed us to measure individual colonies even after a dislodged colony became intertwined with the focal colony (**Supplementary Figure 9**), which would have been impossible to accurately measure by-hand. Despite the advantages of 3D photogrammetry, its application in large scale projects remains hampered by hurdles in downstream image and model processing procedures.

Beyond *in situ* image acquisition, 3D photogrammetry requires additional computational effort which can limit the overall adoption of this technology. Model building software, such as Agisoft Metashape, require large amounts of processing power and time. While the graphical user interface of these programs can be straightforward, in the absence of a dedicated computer 3D model building can be difficult to upscale. Agisoft Metashape also has a command line-based interface that can be run remotely on high-power computing (HPC) systems making model building high-throughput for those with coding knowledge and access to such machines. We sought to lower the accessibility barrier to high-throughput 3D photogrammetry by providing directions and scripts for using Agisoft Metashape on remote HPC systems. This experiment relied on a personally managed remote system but increasing availability of pay-as-you-go cloud computing services are viable alternatives for researchers wanting to increase processing power for 3D model building without the need to purchase and maintain a dedicated computing system.

Broader Applications

The advent of 3D photogrammetry has facilitated investigation of new traits without the need for additional effort in the field or destructive sampling. Traits such as "compactness," "top-heaviness" (Zawada et al., 2019), and "proportion occupied" (Doszpot et al., 2019) quantify complex, ecologically relevant aspects of colony morphology that can easily be accessed using digital 3D models. For example, V_{inter} quantifies the absolute amount of space created between the branches of a coral, similar to shelter volume (Urbina-Barreto et al., 2020). Interstitial space provides important habitat for reef fishes (Wilson et al., 2008; Noonan et al., 2012; Urbina-Barreto et al., 2020) helping to maintain populations (Wilson et al., 2008; Graham, 2014). The volume of interstitial space also influences the physical environment of a colony, as it can result in pockets of reduced flow (Reidenbach et al., 2006). This affects tissue boundary-layer conditions for heat transfer and pH buffering, which influence bleaching and calcification rate (Chan et al., 2016; Stocking et al., 2018). Because V_{inter} exponentially increases with TLE, the ecological functions associated with V_{inter} are also amplified by marginal increases in linear extension. Additionally, large scale experiments addressing local adaption, phenotypic plasticity, and trade-offs in these newly accessible traits are now feasible with high-throughput 3D photogrammetry. Studies requiring large sample sizes, such as those exploring genotype and environment relationships in *A. cervicornis* and *A. palmata*, could be implemented immediately and would produce valuable information for restoration programs.

Here, we show that 3D photogrammetry can be applied efficiently to large sample sizes, but we acknowledge that the colonies used in this study were small relative to the maximum size *A. cervicornis* colonies can reach. However, the success in modeling complex structures like those seen in **Supplementary Figure 9** highlight the potential of 3D photogrammetry to capture increasingly complex morphologies by simply taking more photographs *in situ* (**Supplementary Figure 4**). Furthermore, the use of 3D photogrammetry in studies of densely branched species (Doszpot et al., 2019) provide further confidence this technology can maintain accuracy while improving trait accessibility for research and restoration.

Colony-level 3D photogrammetry could also serve restoration practitioners who seek more detailed information on outplant performance. For example, the tracking of individuals can identify reef sites or genotypes that cultivate large interstitial space crucial for fish habitat (Wilson et al., 2008; Noonan et al., 2012; Urbina-Barreto et al., 2020) ultimately helping to strategize restoration efforts. While reef-scape 3D photogrammetry (McKinnon et al., 2011; Burns et al., 2015; Leon et al., 2015) may prove more effective for tracking restoration outcomes in terms of percent cover and ecosystem complexity, colony-level methods could be used to ground-truth the lower resolution photogrammetry that practitioners employ over hundreds of square meters to determine if accurate measures of colony-level phenotype can be obtained from this coarser method. While 3D photogrammetry (at both large and fine-scales) has yet to become a common tool in restoration, its potential for data collection, its methodological simplicity in the field, and recently improved accessibility of post-processing methods have set the stage for its utility. Taken together, colony-level 3D photogrammetry is a powerful tool for investigating organismal processes such as phenotypic plasticity and ecosystem-level patterns that could prove vital for restoration efforts.

DATA AVAILABILITY STATEMENT

The datasets presented in this study can be found in online repositories. The names of the repository/repositories and accession number(s) can be found below: https://github.com/wyattmillion/Frontiers3Dmorphology.

AUTHOR CONTRIBUTIONS

WM and CK conceived, designed the study, and coded the pipeline and built 3D models. WM was responsible for *in situ* coral photography, conducted analysis, and drafted the initial manuscript. EB completed by-hand TLE measurement of coral and coordinated all diving operations. WM and SO'D prepared images for 3D construction and analyzed 3D models for precision

metrics and coral traits. All authors contributed to discussions, interpretations, and writing. All authors read and approved the submitted version.

FUNDING

Funding for this study was provided by the NOAA Coral Reef Conservation Program grant NA17NOS4820084.

ACKNOWLEDGMENTS

We are grateful to Maria Ruggeri, Yingqi Zhang, Hunter Ramo, Cory Walter, Joseph Kuehl, and Cory Krediet for their help photographing coral *in situ*. Phoebe Chang contributed to image preprocessing and Alexandra Stella and Aryana Volk helped with model validation. Elaina Graham generously facilitated access to the Heidelberg Lab high performance computer. All fieldwork was conducted under permits FKNMS-2015-163-A1 and FKNMS-2018-035.

SUPPLEMENTARY MATERIAL

The Supplementary Material for this article can be found online at: https://www.frontiersin.org/articles/10.3389/fmars.2021.646475/full#supplementary-material

REFERENCES

Agudo-Adriani, E. A., Cappelletto, J., Cavada-Blanco, F., and Croquer, A. (2016). Colony geometry and structural complexity of the endangered species acropora cervicornis partly explains the structure of their associated fish assemblage. *PeerJ* 4:e1861. doi: 10.7717/peerj.1861

Ahn, S., Haas, K. A., and Neary, V. S. (2020). Dominant wave energy systems and conditional wave resource characterization for coastal waters of the united states. *Energies* 13:3041. doi: 10.3390/en13123041

Alvarez-Filip, Y., Dulvy, N. K., Gill, J. A., Côté, I. M., and Watkinson, A. R. (2009). Flattening of caribbean coral reefs: region-wide declines in architectural complexity. *Proc. Biol. Sci.* 276, 3019–3025. doi: 10.1098/rspb.2009.0339

Álvarez-Noriega, M., Baird, A. H., Dornelas, M., Madin, J. S., Cumbo, V. R., and Connolly, S. R. (2016). Fecundity and the demographic strategies of coral morphologies. *Ecology* 97, 3485–3493. doi: 10.1002/ecy.1588

Babcock, R. C. (1991). Comparative demography of three species of scleractinian corals using age- and size-dependent classifications. *Ecol. Monogr.* 61, 225–255. doi: 10.2307/2937107

Bottjer, D. J. (1980). Branching morphology of the reef coral acropora cervicornis in different hydraulic regimes. *J. Paleontol.* 54, 1102–1107.

Bowden-Kerby, A. (2008). "Restoration of threatened acropora cervicornis corals: intraspecific variation as a factor in mortality, growth, and self-attachment," in *Proceedings of the 11th International Coral Reef Symposium, 2:1200–1204* (Norfolk, VA: NSU).

Bruno, J. F., and Edmunds, P. J. (1997). Clonal variation for phenotypic plasticity in the coral madracis mirabilis. *Ecology* 78, 2177–2190. doi: 10.2307/2265954

Burns, J., Delparte, D., Gates, R. D., and Takabayashi, M. (2015). Integrating structure-from-motion photogrammetry with geospatial software as a novel technique for quantifying 3D ecological characteristics of coral reefs. *PeerJ* 3:e1077. doi: 10.7717/peerj.1077

Bythell, J., Pan, P., and Lee, J. (2001). Three-dimensional morphometric measurements of reef corals using underwater photogrammetry techniques. *Coral Reefs* 20, 193–199. doi: 10.1007/s003380100157

Chan, N. C., Wangpraseurt, D., Kühl, M., and Connolly, S. R. (2016). Flow and coral morphology control coral surface pH: implications for the effects of ocean acidification. *Front. Mar. Sci.* 16:10.

Cignoni, P., Callieri, M., Corsini, M., Dellepiane, M., Ganovelli, F., and Ranzuglia, G. (2008). "MeshLab: an open-source mesh processing tool," in *Proceedings of the Sixth Eurographics Italian Chapter Conference* (Sweden: Eurographics Association).

Coker, D. J., Wilson, S. K., and Pratchett, M. S. (2014). Importance of live coral habitat for reef fishes. *Rev. Fish Biol. Fish.* 24, 89–126. doi: 10.1007/s11160-013-9319-5

Cunning, R., Gillette, P., Capo, T., Galvez, K., and Baker, A. C. (2015). Growth tradeoffs associated with thermotolerant symbionts in the coral pocillopora damicornis are lost in warmer oceans. *Coral Reefs* 34, 155–160. doi: 10.1007/s00338-014-1216-4

D'Urban Jackson, T., Williams, G. J., Walker-Springett, G., and Davies, A. J. (2020). Three-dimensional digital mapping of ecosystems: a new era in spatial ecology. *Proc. Biol. Sci.* 287:20192383. doi: 10.1098/rspb.2019.2383

Davies, P. S. (1989). Short-term growth measurements of corals using an accurate buoyant weighing technique. *Mar. Biol.* 101, 389–395. doi: 10.1007/bf00428135

Denis, V., Ribas-Deulofeu, L., Sturaro, N., Kuo, C. Y., and Chen, C. A. (2017). A Functional approach to the structural complexity of coral assemblages based on colony morphological features. *Sci. Rep.* 7:9849.

Dennison, W. C., and Barnes, D. J. (1988). Effect of water motion on coral photosynthesis and calcification. *J. Exp. Mar. Biol. Ecol.* 115, 67–77. doi: 10.1016/0022-0981(88)90190-6

Dornelas, M., Madin, J. S., Baird, A. H., and Connolly, S. R. (2017). "Allometric growth in reef-building corals," in *Proceedings of the Royal Society B: Biological Sciences*, 284. doi: 10.1098/rspb.2017.0053

Doszpot, N., McWilliam, M., Pratchett, M., Hoey, A., and Figueira, W. (2019). Plasticity in three-dimensional geometry of branching corals along a cross-shelf gradient. *Diversity* 11:44. doi: 10.3390/d11030044

Drury, C., Greer, J. B., Baums, I., Gintert, B., and Lirman, D. (2019). Clonal diversity impacts coral cover in acropora cervicornis thickets: potential relationships between density, growth, and polymorphisms. *Ecol. Evol.* 9, 4518–4531. doi: 10.1002/ece3.5035

Drury, C., Manzello, D., and Lirman, D. (2017). Genotype and local environment dynamically influence growth, disturbance response and survivorship in the threatened coral, acropora cervicornis. *PLoS One* 12:e0174000. doi: 10.1371/journal.pone.0174000

Edmunds, P. J. (2017). Intraspecific variation in growth rate is a poor predictor of fitness for reef corals. *Ecology* 98, 2191–2200. doi: 10.1002/ecy.1912

Edmunds, P. J., and Putnam, H. M. (2020). Science-based approach to using growth rate to assess coral performance and restoration outcomes. *Biol. Lett.* 16:20200227. doi: 10.1098/rsbl.2020.0227

Félix-Burruel, R. E., Larios, E., Bustamante, E., and Búrquez, A. (2019). Nonlinear modeling of saguaro growth rates reveals the importance of temperature for size-dependent growth. *Am. J. Bot.* 106, 1300–1307. doi: 10.1002/ajb2.1358

Ferrari, R., Figueira, W. F., Pratchett, M. S., Boube, T., Adam, A., Kobelkowsky-Vidrio, T., et al. (2017). 3D photogrammetry quantifies growth and external erosion of individual coral colonies and skeletons. *Sci. Rep.* 7:16737.

Figueira, W. F., Ferrari, R., Weatherby, E., Porter, A., Hawes, S., and Byrne, M. (2015). Accuracy and precision of habitat structural complexity metrics derived from underwater photogrammetry. *Remote Sens.* 7, 16883–16900. doi: 10.3390/rs71215859

Graham, N. A. J. (2014). Habitat complexity: coral structural loss leads to fisheries declines. *Curr. Biol.* 24, R359–R361.

Graham, N. A. J., and Nash, K. L. (2013). The importance of structural complexity in coral reef ecosystems. *Coral Reefs* 32, 315–326. doi: 10.1007/s00338-012-0984-y

Herler, J., and Dirnwöber, M. (2011). A simple technique for measuring buoyant weight increment of entire, transplanted coral colonies in the field. *J. Exp. Mar. Biol. Ecol.* 407, 250–255. doi: 10.1016/j.jembe.2011.06.022

Hernández-Landa, R. C., Barrera-Falcon, E., and Rioja-Nieto, R. (2020). Size-frequency distribution of coral assemblages in insular shallow reefs of the mexican caribbean using underwater photogrammetry. *PeerJ* 8:e8957. doi: 10.7717/peerj.8957

Hippel, E. V., and Krogh, G. V. (2003). Open source software and the 'private-collective' innovation model: issues for organization science. *Organ. Sci.* 14, 209–223. doi: 10.1287/orsc.14.2.209.14992

House, J. E., Brambilla, V., Bidaut, L. M., Christie, A. P., Pizarro, O., Madin, J. S., et al. (2018). Moving to 3D: relationships between coral planar area, surface area and volume. *PeerJ* 6:e4280. doi: 10.7717/peerj.4280

Hughes, T. P., Ayre, D., and Connell, J. H. (1992). The evolutionary ecology of corals. *Trends Ecol. Evol.* 7, 292–295. doi: 10.1016/0169-5347(92)90225-z

Huntington, B. E., and Miller, M. W. (2014). Location-specific metrics for rapidly estimating the abundance and condition of the threatened coral acropora cervicornis. *Restor. Ecol.* 22, 299–303. doi: 10.1111/rec.12057

Jimenez, I. M., Kühl, M., Larkum, A. W. D., and Ralph, P. J. (2011). Effects of flow and colony morphology on the thermal boundary layer of corals. *J. R. Soc. Interface* 8, 1785–1795. doi: 10.1098/rsif.2011.0144

Johnson, M. E., Lustic, C., Bartels, E., Baums, I. B., Gilliam, D. S., Larson, E. A., et al. (2011). *Caribbean Acropora Restoration Guide: Best Practices for Propagation and Population Enhancement*. Arlington, VA: The Nature conservancy.

Jokiel, P. L., Maragos, J. E., and Franzisket, L. (1978). "Coral growth: buoyant weight technique," in *Monographs on Oceanographic Methodology, UNESCO.Coral Reefs: Research Methods*, eds D. R. Stoddart and R. E. Johannes (Paris: UNESCO).

Jones, A., and Berkelmans, R. (2010). Potential costs of acclimatization to a warmer climate: growth of a reef coral with heat tolerant vs. sensitive symbiont types. *PloS One* 5:e10437. doi: 10.1371/journal.pone.0010437

Kenkel, C. D., Setta, S. P., and Matz, M. V. (2015). Heritable differences in fitness-related traits among populations of the mustard hill coral, porites astreoides. *Heredity* 115, 509–516.

Kiel, C., Huntington, B. E., and Miller, M. W. (2012). Tractable field metrics for restoration and recovery monitoring of staghorn coral acropora cervicornis. *Endanger. Species Res.* 19, 171–176. doi: 10.3354/esr00474

Kuffner, I. B., Bartels, E., Stathakopoulos, A., Enochs, I. C., Kolodziej, G., Toth, L. T., et al. (2017). Plasticity in skeletal characteristics of nursery-raised staghorn coral, acropora cervicornis. *Coral Reefs* 36, 679–684. doi: 10.1007/s00338-017-1560-2

Lange, I. D., and Perry, C. T. (2020). A quick, easy and non-invasive method to quantify coral growth rates using photogrammetry and 3D model comparisons. *Methods Ecol. Evol.* 11, 714–726. doi: 10.1111/2041-210x.13388

Lavy, A., Eyal, G., Neal, B., Keren, R., Loya, Y., and Ilan, M. (2015). A quick, easy and non-intrusive method for underwater volume and surface area evaluation of benthic organisms by 3d computer modelling. *Methods Ecol. Evol.* 6, 521–531. doi: 10.1111/2041-210x.12331

Leon, J. X., Roelfsema, C. M., Saunders, M. I., and Phinn, S. R. (2015). Measuring coral reef terrain roughness using 'structure-from-motion' close-range photogrammetry. *Geomorphology* 242, 21–28. doi: 10.1016/j.geomorph.2015.01.030

Lesser, M. P., Weis, V. M., Patterson, M. R., and Jokiel, P. L. (1994). Effects of morphology and water motion on carbon delivery and productivity in the reef coral, pocillopora damicornis (linnaeus): diffusion barriers, inorganic carbon limitation, and biochemical plasticity. *J. Exp. Mar. Biol. Ecol.* 178, 153–179. doi: 10.1016/0022-0981(94)90034-5

Lines, E. R., Zavala, M. A., Purves, D. W., and Coomes, D. A. (2012). Predictable changes in aboveground allometry of trees along gradients of temperature, aridity and competition. *Global Ecol. Biogeogr. J. Macroecol.* 21, 1017–1028. doi: 10.1111/j.1466-8238.2011.00746.x

Lirman, D., Schopmeyer, S., Galvan, V., Drury, C., Baker, A. C., and Baums, I. B. (2014). Growth dynamics of the threatened caribbean staghorn coral acropora cervicornis: influence of host genotype, symbiont identity, colony size, and environmental setting. *PLoS One* 9:e107253. doi: 10.1371/journal.pone.0107253

Lohr, K. E., and Patterson, J. T. (2017). Intraspecific variation in phenotype among nursery-reared staghorn coral acropora cervicornis (Lamarck, 1816). *J. Exp. Mar. Biol. Ecol.* 486, 87–92. doi: 10.1016/j.jembe.2016.10.005

Lohr, K. E., Bejarano, S., Lirman, D., Schopmeyer, S., and Manfrino, C. (2015). Optimizing the productivity of a coral nursery focused on staghorn coral acropora cervicornis. *Endanger. Species Res.* 27, 243–250. doi: 10.3354/esr00667

Lugo-Fernández, A., Roberts, H. H., Wiseman, Jr., and Wj. (1998). Tide effects on wave attenuation and wave set-up on a caribbean coral reef. *Estuar. Coast. Shelf Sci.* 47, 385–393. doi: 10.1006/ecss.1998.0365

Madin, J. S., Baird, A. H., Dornelas, M., and Connolly, S. R. (2014). Mechanical vulnerability explains size-dependent mortality of reef corals. edited by howard cornell. *Ecol. Lett.* 17, 1008–1015. doi: 10.1111/ele.12306

McCullough, E. L., Ledger, K. J., O'Brien, D. M., and Emlen, D. J. (2015). Variation in the allometry of exaggerated rhinoceros beetle horns. *Anim. Behav.* 109, 133–140. doi: 10.1016/j.anbehav.2015.08.013

McKinnon, D., He, H., Upcroft, B., and Smith, R. N. (2011). *Towards Automated and in-Situ, Near-Real Time 3-D Reconstruction of Coral Reef Environments*. Piscataway, NJ: IEEE.

Miller, M., Bourque, A., and Bohnsack, J. (2002). An analysis of the loss of acroporid corals at looe key, Florida, USA: 1983–2000. *Coral Reefs* 21, 179–182.

Monismith, S. G. (2007). Hydrodynamics of coral reefs. *Annu. Rev. Fluid Mech.*. 39, 37–55.

Newson, R. (2002). Parameters behind 'nonparametric' statistics: kendall's tau, somers' d and median differences. *Stata J. Promot. Commun. Stat. Stata* 2, 45–64.

Noonan, S. H. C., Jones, G. P., and Pratchett, M. S. (2012). Coral size, health and structural complexity: effects on the ecology of a coral reef damselfish. *Mar. Ecol. Prog. Ser.* 456, 127–137.

O'Donnell, K. E., Lohr, K. E., Bartels, E., and Patterson, J. T. (2017). Evaluation of staghorn coral (*Acropora cervicornis*, Lamarck 1816) production techniques in an ocean-based nursery with consideration of coral genotype. *J. Exp. Mar. Biol. Ecol.* 487, 53–58. doi: 10.1016/j.jembe.2016.11.013

O'Donnell, K. E., Lohr, K. E., Bartels, E., Baums, I. B., and Patterson, J. T. (2018). Acropora cervicornis genet performance and symbiont identity throughout the restoration process. *Coral Reefs* 37, 1109–1118.

Parkinson, J. E., Baker, A. C., Baums, I. B., Davies, S. W., Grottoli, A. G., Kitchen, S. A., et al. (2020). Molecular tools for coral reef restoration: beyond biomarker discovery. *Conserv. Lett.* 13:e12687. doi: 10.1111/conl.12687

Pratchett, M. S., Anderson, K. D., Hoogenboom, M. O., Widman, E., Baird, A. H., Pandolfi, J. M., et al. (2015). Spatial, temporal and taxonomic variation in coral growth—implications for the structure and function of coral reef ecosystems. *Oceanogr. Mar. Biol.* 53, 215–295.

R Core Team (2020). *R: A Language and Environment for Statistical Computing*. Vienna: R Foundation for Statistical Computing. Available online at: https://www.R-project.org/.

Rasband, W. S, (1997–2014).*ImageJ. U.S. National Institutes of Health*. Bethesda: Maryland.

Reidenbach, M. A., Koseff, J. R., Monismith, S. G., Steinbuckc, J. V., and Genin, A. (2006). The effects of waves and morphology on mass transfer within branched reef corals. *Limnol. Oceanogr.* 51, 1134–1141.

Rinkevich, B. (1995). Restoration strategies for coral reefs damaged by recreational activities: the use of sexual and asexual recruits. *Restor. Ecol.* 3, 241–251.

Risk, M. J. (1972). Fish diversity on a coral reef in the Virgin Islands. *Atoll Res. Bull.* 153, 1–4.

Stimson, J., and Kinzie, R. (1991). The temporal pattern and rate of release of zooxanthellae from the reef coral pocillopora damicornis (Linnaeus) under nitrogen-enrichment and control conditions. *J. Exp. Mar. Biol. Ecol.* 153, 63–74.

Stocking, J. B., Laforsch, C., Sigl, R., and Reidenbach, M. A. (2018). The role of turbulent hydrodynamics and surface morphology on heat and mass transfer in corals. *J. R. Soc. Interface* 15:20180448.

Szmant, A. M. (1997). Nutrient effects on coral reefs: a hypothesis on the importance of topographic and trophic complexity to reef nutrient dynamics. in *Proceedings of the 8th International Coral Reef Symposium*. Panama: Tropical Research Institute

Todd, P. A. (2008). Morphological plasticity in scleractinian corals. *Biol. Rev. Camb. Philos. Soc.* 83, 315–337.

Tunnicliffe, V. (1981). Breakage and propagation of the stony coral acropora cervicornis. *Proc. Natl. Acad. Sci. USA* 78, 2427–2431.

Urbina-Barreto, I., Chiroleu, F., Pinel, R., Fréchon, L., Mahamadaly, V., Elise, S., et al. (2020). Quantifying the shelter capacity of coral reefs using

photogrammetric 3D modeling: from colonies to reefscapes. *Ecol. Indic.* 121:107151.

van Oppen, M. J. H., Oliver, J. K., Putnam, H. M., and Gates, R. D. (2015). Building coral reef resilience through assisted evolution. *Proc. Natl. Acad. Sci. USA* 112, 2307–2313.

Veal, C. J., Carmi, M., Fine, M., and Hoegh-Guldberg, O. (2010). Increasing the accuracy of surface area estimation using single wax dipping of coral fragments. *Coral Reefs* 29, 893–897.

Ware, M., Garfield, E. N., Nedimyer, K., Levy, J., Kaufman, L., Precht, W., et al. (2020). Survivorship and growth in staghorn coral (*Acropora Cervicornis*) outplanting projects in the florida keys national marine sanctuary. *PLoS One* 15:e0231817.

Wesselingh, R. A., Klinkhamer, P. G. L., De Jong, T. J., and Boorman, L. A. (1997). Threshold size for flowering in different habitats: effects of size-dependent growth and survival. *Ecology* 78, 2118–2132.

West, G. B., Brown, J. H., and Enquist, B. J. (1997). A general model for the origin of allometric scaling laws in biology. *Science* 276, 122–126. doi: 10.1126/science.276.5309.122

Wilson, S. K., Burgess, S. C., Cheal, A. J., Emslie, M., Fisher, R., Miller, I., et al. (2008). Habitat utilization by coral reef fish: implications for specialists vs. generalists in a changing environment. *J. Anim. Ecol.* 77, 220–228.

Young, C. N., Schopmeyer, S. A., and Lirman, D. (2012). A review of reef restoration and coral propagation using the threatened genus acropora in the caribbean and Western Atlantic. *Bull. Mar. Sci.* 88, 1075–1098.

Zawada, D. G., Piniak, G. A., and Hearn, C. J. (2010). Topographic complexity and roughness of a tropical benthic seascape. *Geophys. Res. Lett.* 37:L14604.

Zawada, K. J. A., Dornelas, M., and Madin, J. S. (2019). Quantifying coral morphology. *BioRxivi [Preprint]* doi: 10.1101/553453

Conflict of Interest: The authors declare that the research was conducted in the absence of any commercial or financial relationships that could be construed as a potential conflict of interest.

frontiers in Marine Science

ORIGINAL RESEARCH
published: 24 May 2021
doi: 10.3389/fmars.2021.636902

Which Method for Which Purpose? A Comparison of Line Intercept Transect and Underwater Photogrammetry Methods for Coral Reef Surveys

Isabel Urbina-Barreto[1,2], Rémi Garnier[2], Simon Elise[1], Romain Pinel[3], Pascal Dumas[4], Vincent Mahamadaly[2,3], Mathilde Facon[2], Sophie Bureau[1], Christophe Peignon[4], Jean-Pascal Quod[5], Eric Dutrieux[2], Lucie Penin[1,6] and Mehdi Adjeroud[6,7,8]*

[1] UMR 9220 ENTROPIE, IRD, Université de la Réunion, Université de la Nouvelle-Calédonie, IFREMER, CNRS, La Réunion, France, [2] Creocean OI, La Réunion, France, [3] Geolab S.A.S., La Réunion, France, [4] UMR 9220 ENTROPIE, IRD, Université de la Réunion, Université de la Nouvelle-Calédonie, IFREMER, CNRS, Nouméa, New Caledonia, [5] ARVAM-Pareto, c/o Technor, Sainte Clotilde cedex, France, [6] Laboratoire d'Excellence "CORAIL", Paris, France, [7] UMR 9220 ENTROPIE, IRD, Université de la Réunion, Université de la Nouvelle-Calédonie, IFREMER, CNRS, Perpignan, France, [8] PSL Université Paris, USR 3278 CRIOBE - EPHE-UPVD-CNRS, Perpignan, France

The choice of ecological monitoring methods and descriptors determines the effectiveness of a program designed to assess the state of coral reef ecosystems. Here, we comparer the relative performance of the traditional Line Intercept Transect (LIT) method with three methods derived from underwater photogrammetry: LIT on orthomosaics, photoquadrats from orthomosaics, and surface analyses on orthomosaics. The data were acquired at Reunion Island on five outer reef slopes and two coral communities on underwater lava-flows. Coral cover was estimated *in situ* using the LIT method and with LITs and photoquadrats digitized on orthomosaic. Surface analyses were done on the same orthomosaics. Structural complexity of the surveyed sites was calculated from digital elevation models using three physical descriptors (fractal dimension, slope, surface complexity), and used to explore their possible influence in coral cover estimates. We also compared the methods in terms of scientific outputs, the human expertise and time required. Coral cover estimates obtained with *in situ* LITs were higher than those obtained with digitized LITs and photoquadrats. Surfaces analyses on orthomosaics yielded the lowest but most the precise cover estimates (i.e., lowest sample dispersion). Sites with the highest coral cover also had the highest structural complexity. Finally, when we added scientific outputs, and requirements for human expertise and time to our comparisons between methods, we found that surface analysis on the orthomosaics was the most efficient method. Photoquadrats were more time-consuming than both *in situ* and digitized

OPEN ACCESS

Edited by:
Manuel Gonzalez-Rivero, Australian Institute of Marine Science (AIMS), Australia

Reviewed by:
Chris M. Roelfsema, The University of Queensland, Australia
Andrew Robert Halford, Pacific Community (SPC), New Caledonia

***Correspondence:**
Isabel Urbina-Barreto
isabel.urbina-barreto@univ-reunion.fr

Specialty section:
This article was submitted to Coral Reef Research, a section of the journal Frontiers in Marine Science

Received: *02 December 2020*
Accepted: *27 April 2021*
Published: *24 May 2021*

Citation:
Urbina-Barreto I, Garnier R, Elise S, Pinel R, Dumas P, Mahamadaly V, Facon M, Bureau S, Peignon C, Quod J-P, Dutrieux E, Penin L and Adjeroud M (2021) Which Method for Which Purpose? A Comparison of Line Intercept Transect and Underwater Photogrammetry Methods for Coral Reef Surveys. Front. Mar. Sci. 8:636902. doi: 10.3389/fmars.2021.636902

LITs, even though they provided coral cover estimates similar to those of digitized LITs and yielded more than one descriptor. The LIT *in situ* method remains the least time-consuming and most effective for species-level taxonomic identifications but is the most limited method in terms of data outputs and representativeness of the ecosystem.

Keywords: coral cover, LIT, orthomosaic, reef survey methods, structural complexity, underwater photogrammetry

INTRODUCTION

The advent of SCUBA diving in the second part of the twentieth century facilitated direct observations of underwater marine ecosystems and prompted the development of coral reef survey techniques (Goreau, 1959; Loya, 1972; Riedl, 1980; Dahl, 1981). Quantitative methods [i.e., Line Intercept Transect Method (LIT), Point Intercept Transect Method (PIT), photoquadrats, video transect] and semi-quantitative methods [i.e., Dahl quotation, Medium Scale Approach (MSA)] were developed in what became reference studies in benthic reef ecology (Loya, 1978; English et al., 1997). These methods mostly focused on assessing 2D descriptors (e.g., percent coral cover), while few attempted to estimate 3D parameters such as "reef rugosity," with the chain and tape method (Risk, 1972) or to combine 2D and 3D assessments as with the Chain Intercept Transect Method (see Hill and Wilkinson, 2004) and habitat complexity assessment (see Friedlander and Parrish, 1998; Wilson et al., 2007). The LIT method became widespread as it is well suited to acquire long-term monitoring data, as well as relatively easy and cheap (e.g., Global Coral Reef Monitoring Network). This method is one of more adopted worldwide to monitor benthic communities and specially to assess coral cover and provided historical records over the last 60 years (English et al., 1997; Hill and Wilkinson, 2004). Yet, over past two decades, photoquadrats, as a method, was increasingly recommended to standardize regional data as was done by the GCRMN Caribbean node (see Vallès et al., 2019).

Recently, new coral reef descriptors and innovative operational tools for monitoring reefs were developed and made more accessible (e.g., Burns et al., 2015; Hedley et al., 2016; Madin et al., 2016; Elise et al., 2019a). Compared to older, simpler traditional survey methods, these tools aim to enhance the quantity and quality of data (e.g., Lechene et al., 2019) which in turn lead to better understanding reef communities and their ecological functioning (e.g., Elise et al., 2019b; Zawada et al., 2019; Urbina-Barreto et al., 2020). In a recent study, Obura et al. (2019) reviewed and analyzed coral reef monitoring methods, assessment technologies, and short-term management perspectives. Obura et al. (2019) found that while hard coral cover is the single most reported reef parameter, alone it cannot reflect the status of a reef or be the basis for conservation measures. Other essential data needed include functional characteristics upon which coral communities rely, such as the relative abundance of different coral colony structures and descriptors of structural complexity of reefs (Pendleton et al., 2016; González-Barrios and Álvarez-Filip, 2018). Structural complexity supports the ecological functioning of coral reefs, as well as the resilience and the long-term stability of associated biodiversity (Peterson et al., 1998; Alvarez-Filip et al., 2013; Darling et al., 2017; Magel et al., 2019). However, a global review of coral benthic community monitoring methods shows that only three out of 15 methods included a descriptor of structural complexity, namely reef rugosity (Hill and Wilkinson, 2004).

The selection of a given ecological monitoring method to assess the status of reefs should optimally be based on three main factors: (1) observer bias along with standardization of protocols and data (e.g., Caldwell et al., 2016; Flower et al., 2017; Rossi et al., 2021), (2) the ability to conduct assessment at varying spatial and temporal scales (e.g., González-Rivero et al., 2014, González-Rivero et al., 2020; Wedding et al., 2019), and (3) the technical, financial, and social feasibility of the method (e.g., Gilbert and Quod, 2018; Darling et al., 2019). Overly simple descriptors will not capture enough information while overly complicated ones will not be sustainable. The choice of survey methods should be guided by the objectives of the program and their ability to provide data appropriate for answering the question posed, in addition to being sustainable. Over the past 50 years, several studies compared the effectiveness and accuracy of ecological methods and descriptors for benthic reef surveys(e.g., Weinberg, 1981; Ohlhorst et al., 1988; Lam et al., 2006; Dumas et al., 2009; Facon et al., 2015; Storlazzi et al., 2016). Several handbooks were published to support both scientists and managers in selecting the best method corresponding to their specific objectives, including ecological, conservation, and management purposes (e.g., Dahl, 1981; Hill and Wilkinson, 2004; Obura and Grimsditch, 2009; Obura, 2014). Yet comparisons between traditional methods (e.g., LIT) and novel methods such as photogrammetric assessment are lacking.

Current technological advances provide novel tools and methods for reef surveys that can provide more descriptors of reef condition with a minimal increase in effort. Among them, photogrammetry by Structure from Motion (SfM) generates three-dimensional reconstructions of coral reefs as well as 3D models, Digital Elevation Models (DEM, i.e., digital representation of a continuous surface with terrain elevation data) and orthomosaics (i.e., geometrically corrected mosaicked images with a uniform scale). Photogrammetry enables the quantitative monitoring of physical (e.g., structural complexity: slope, fractal dimension, surface complexity) and biological features (e.g., cover of benthic communities, colonies size and abundance) of ecosystems over time (e.g., Storlazzi et al., 2016; Fukunaga et al., 2019; Price et al., 2019; Carlot et al., 2020). These new techniques and methods are likely to become

new standards for reef surveying in the coming years (Obura et al., 2019; D'Urban et al., 2020) notably with new solutions helping to automate image analysis such as the widely used machine-learning CoralNet tool, which estimates of coral cover are highly comparable to those generated by reef experts (Williams et al., 2019) and other artificial intelligence applications (e.g., González-Rivero et al., 2016; Hopkinson et al., 2020; Mohamed et al., 2020).

Here, we compare four reef benthic survey methods to estimate coral cover: the traditional Line Intercept Transect method (LIT) and three methods derived from photogrammetric outputs (LIT on orthomosaics, photoquadrats from orthomosaics, and surface analyses at two different scales on orthomosaics. We also examine three physical descriptors of the structural complexity (fractal dimension, slope and surface complexity) in each study site. Our three main goals were to (1) compare estimates of percent coral cover between methods and explore the possible influence of structural complexity in these estimates; (2) examine whether the LIT and photoquadrats methods can be applied to orthomosaics (photogrammetric outputs); and (3) compare the scientific outputs, required resources (expertise and time), as well as the pros and cons of these methods. We then summarize our comparisons of practical aspects of traditional and novel reef assessment methods with regard to project objectives, available manpower and financial resources.

MATERIALS AND METHODS

Study Sites

The study was conducted at seven coral reef sites around Reunion, an island of the Mascarene Archipelago in the Western Indian Ocean region. We sampled five outer reef slopes sites located on the West coast and two sites with coral communities on underwater lava-flows located on the East coast (**Figure 1**). This allowed us to compare the performance of survey methods in different reef environments. The fieldwork took place from March to August 2018 at depths varying from 8 to 15 m. Depending on the monitoring method and region considered, the size of coral reef study site can range from dozens to several hundreds square-meters (Hill and Wilkinson, 2004). For this study, "a site" was an area of 150 m^2 for coral communities on lava flows and 500 m^2 for those on outer reef slopes. All four reef survey methods were applied to each of these sites.

Coral Cover Estimation Methods

Line Intercept Transects

We conducted the LIT *in situ* while using SCUBA and following the Global Coral Reef Monitoring Network protocol (Obura, 2014; **Figure 2A**). Three replicate transects were set up at each site. They were each 20 m long and spaced apart by at least 5 m. An experienced coral reef ecologist identified all benthic categories and estimated percent hard coral cover (scleractiniam corals) by dividing the total length of occurrence of hard corals by the total length of the transect.

Photogrammetric Methods and Digital Assessments

Reefscapes of the seven sites were modeled in 3D by using photogrammetry. Images collected using SCUBA covered 150 m^2 area on underwater lava-flow sites (C77, CAE) and 500 m^2 on outer reef slope sites (COR, GEN, SAL, SBL, and TRC). The mean overlap between images was ∼70%. For each site, we generated an orthomosaic and a DEM. The mean re projection error was 0.25 pixel, and the mean resolution (i.e., Ground Sampling Distance) was 0.13 cm $pixel^{-1}$. Percent coral cover was estimated from the orthomosaics using digitized LITs (**Figure 2B.1**) and photoquadrats (**Figure 2B.2**). We also assessed percent cover by segmenting surfaces and manually classifying benthic communities on the same orthomosaics (**Supplementary Figure 1**), which were then clipped into two sampling units: 40 m^2 × 3 (**Figure 2B.3**) and 150 m^2 × 3 (**Figure 2B.4**). These methods applied the same benthic classification as for LITs done *in-situ*. Digital assessments were done using: (i) LITs on orthomosaics; (ii) Photoquadrats from orthomosaics; (iii) Surface analyses on orthomosaics; and analyses on DEMs of structural complexity descriptors.

Line Intercept Transects on orthomosaics were done by the same diver who conduct the LITs *in situ* did three 20 m transects (**Figure 2B.1**) using the open source QGIS software (version 3.1). Measurements of the lengths of the segments were done using the QGIS command: *$length* with the field calculator tool. Coral cover was calculated as described in section "Line Intercept Transects."

Ten photoquadrats, each 1 m^2 size and spaced 50 cm apart, were extracted along each of the three transects generated for the LIT orthomosaic method (**Figure 2B.2**). The 30 photoquadrats were exported from the orthomosaic and the CPCe software was applied to conduct a benthic classification (Kohler and Gill, 2006). Following the recommendation in Dumas et al. (2009), a stratified point sampling was done where each photoquadrat was divided into nine cells (three columns and three rows), with one point classified per cell (i.e., 9 total points were classified per photoquadrat). The software then directly calculated the mean total percent coral cover.

For the surface analyses done on orthomosaics, the benthic classification was done manually delineating each coral colony as a polygon in QGIS (**Supplementary Figure 1**). For all sites, the colony layer was clipped in three areas of 40 m^2 (**Figure 2B.3**) and three sampling areas of 150 m^2 for the five outer reef slopes (**Figure 2B.4**) to check for the possible differences between the two total sampling surfaces and optimize sampling (Lechene et al., 2019). The field calculator tool and the *area(*$geometry)* command in QGIS were used to measure the polygonal surfaces of hard corals. Percent coral cover was then estimated by dividing the sum of hard corals by the area of total sampling area (i.e., 40 or 150 m^2). We used the total coral cover for a 150 m^2 area as a possible reference value given that this area is typically used for benthic reef monitoring.

Finally, for the analyses of DEMs, at each site we estimated surface complexity (i.e., the ratio of 2D to 3D surface), slope, and fractal dimension from the DEMs (**Supplementary Figure 2**) running the R code developed by R Core Team (2019); Fukunaga et al. (2019). Importantly we

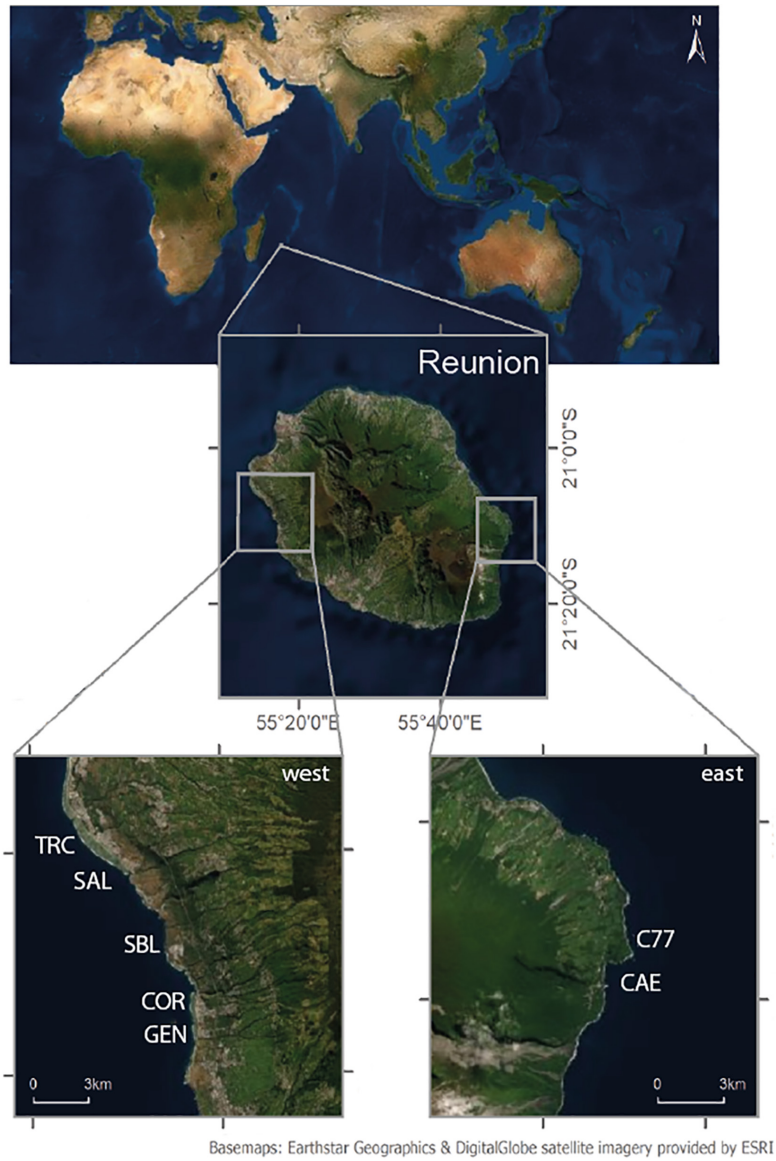

FIGURE 1 | Map of the study sites. On the west coast: TRC, SAL, SBL, COR and GEN. On the east oast (lava-flow reefs): C77 and CAE.

assessed the influence of structural complexity on percent coral cover estimates by each method.

We performed two-way ANOVAs and Tukey multiple mean comparisons to test the effects of site, method, and their interaction on coral cover estimates.

Comparisons of Traditional and Photogrammetric Methods

The methods were compared in terms of data out-put, the human expertise and time required, advantages and limitations, and fields of application. **Table 1** presents the comparison criteria. Importantly all authors contributed to these comparisons which therefore reflects varying experience or approaches to coral reef ecology including fundamental academic research, applied sciences, environmental consultancy, and research and development in coral reef ecology (research directors, senior lecture, PhD in marine ecology, environmental consultancy firm directors and managers, engineers in marine ecology, engineers in geography).

RESULTS

Estimates of percent coral cover were significantly different across sites and methods (two-way ANOVA method × site $p < 0.05$; **Supplementary Table 1**). The LITs done *in situ* resulted in the highest estimates of coral cover. In comparison LITs on orthomosaics and photoquadrats from orthomosaic methods yielded significantly lower coral cover and there was no

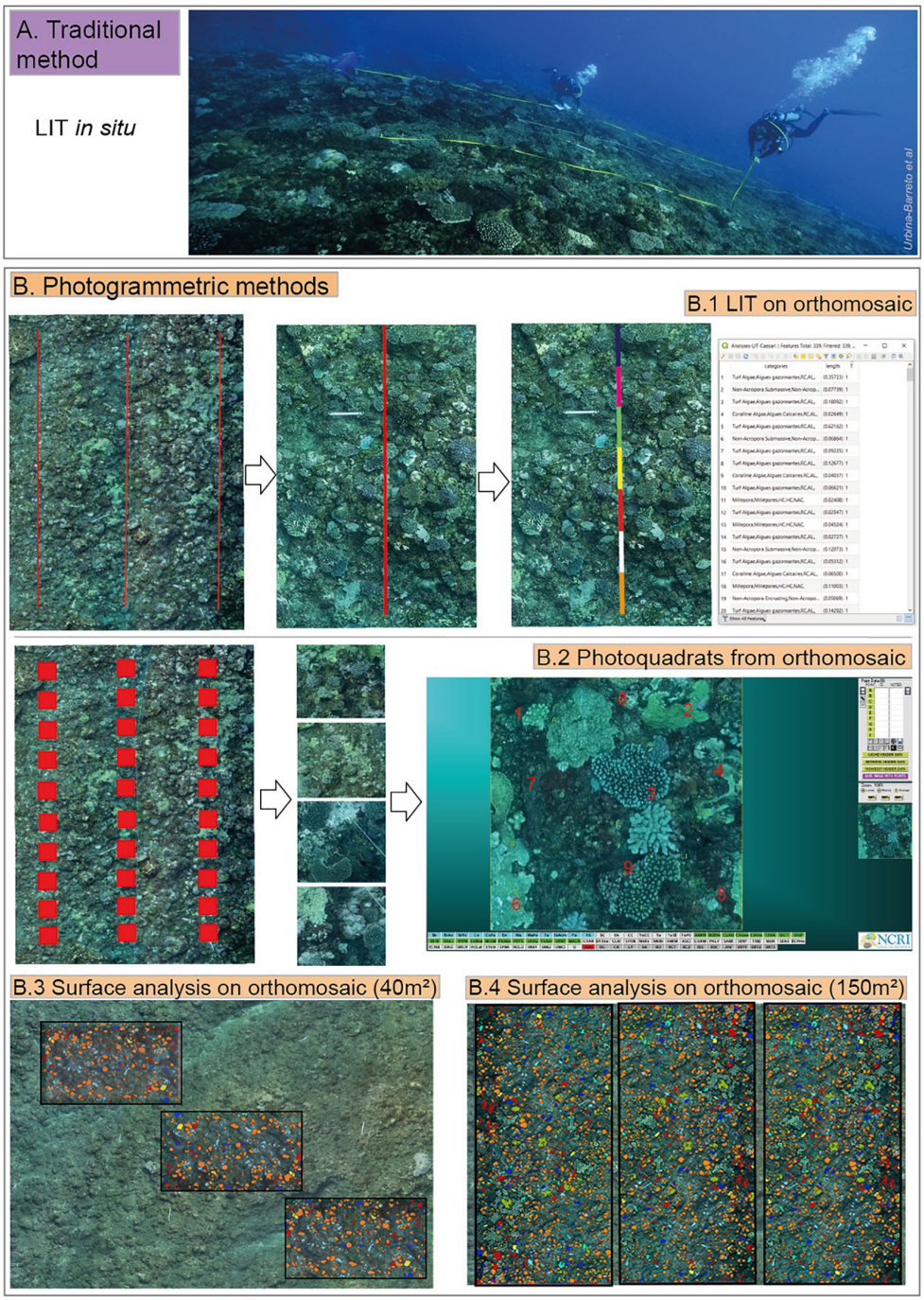

FIGURE 2 | Illustration of the traditional method: LIT *in situ*, sampling distance 20 m × 3 **(A)** and the photogrammetric methods **(B)**: LIT on orthomosaic, sampling distance 20 m × 3 **(B.1)**; photoquadrats from orthomosaic, sampling area 1 m^2 × 10 × 3 **(B.2)**; and surface analyses on orthomosaic: sampling area of 40 m^2 × 3 **(B.3)** and sampling area of 150 m^2 × 3 **(B.4)** colors show different benthic categories.

significant difference in coral cover estimates between these two last methods. The surface analyses on orthomosaics (40 m^2 × 3 and 150 m^2 × 3) generated significantly lower coral cover estimates compared to the three other methods but without any significant differences between the two surfaces analyses (two-way ANOVA $p < 0.001$; **Supplementary Table 1**; Tukey tests $p < 0.01$; **Supplementary Table 2**; **Figure 3**). At each site, these two surface analyses provided the lowest coral cover estimates except for outer ref slope site SBL where photoquadrats and LITs on orthomosaics generated the lowest values, and for the underwater lava-flow site CAE, where LITs on orthomosaic also yielded a lower value compared to surface analyses. Coral cover

TABLE 1 | Definition of each criterion used for the description and comparison of survey methods.

Criterion			Definition
Method description	Type of estimator		Type of measurement used to estimate the descriptor (point, line, polygon)
	Sampling effort		Number and size of the samples used for one site
	Survey dimensions		Number of spatial dimensions represented by the sampling
	Attainable descriptors		List of descriptors possible to obtain from the field data with further analyses
	Limits for the taxonomic identification of scleractinian corals		Maximum level of identification possible for Scleractinian corals. Other benthic organisms e.g., algae, sponges etc. were not considered in this evaluation
	Raw data		Type of data recorded on the field, on which are based all the analyses and which allow their reproduction
	Observer bias in biological analysis		Bias in the analyses due to subjective human observations and assessments
	Underwater equipment		Materials needed to deploy the method
	Computing equipment		Computer resources and software needed for the analyses
	Environmental constraints		Naturals conditions needed to realize fieldwork and collect the data
Human expertise & time required	1. Planning	Protocol design	Evaluation of human expertise and time required for the spatial scale of the present study: – The expert (i.e., experienced coral reef ecologist) and time required (estimated in days; 1 day = 7 h) – The technician (i.e., no specific skills in marine biology but with diver skills if fieldwork is scuba diving) and time required (estimated in days; 1 day = 7 h)
		Sampling plan	
		Field tools	
	2. Fieldwork (for 1 site)	Field Mob/Demob*	
		Field survey**	
	3. Office analyses	Data handling	
		Processing model	
		Ecological analyses	
Review & perspectives	Advantages and disadvantages		Synthesis of identified advantages and disadvantages
	Field of applications		Potential organizations or domains for operational applications and perspectives envisioned

**Field Mob/Demob: overall time of preparation (mobilization and demobilization, including car and boats rides). **Field survey: diving time.*

estimated from surface analyses on orthomosaics was associated with a lower variance compared to the other methods (**Figure 4**). Estimates of single surface sampling (150 m^2) on orthomosaics for each site showed similar trends at underwater lava-flow sites C77 and CAE. Coral cover estimates done at outer reef slope sites SAL, SBL and TRC were higher than the two sampling surfaces ($40m^2 \times 3$ and $150m^2 \times 3$) but lowest than LIT *in situ* method. In contrast estimates for outer reef slopes sites GEN and COR were lower than all other methods (**Figure 4** and **Supplementary Table 3**).

With respect to sites, the percent coral cover was highest on underwater lava-flow sites C77, CAE and on the outer reef slope site GEN, with the lowest percent cover estimated on outer reef slope sites SBL and TRC (two-way ANOVA $p < 0.001$; **Supplementary Table 1**; Tukey tests $p < 0.01$; **Figure 4**; **Supplementary Table 4**).

With the DEMs we quantified structural complexity and examinated its possible influence on coral cover estimates (**Table 2** and **Figure 5**). The differences between LITs done *in situ* and surface analyses on 40 $m^2 \times 3$ were significantly correlated with the slope (Pearson correlation $R^2 = 0.68$; $p < 0.05$) and surface complexity (Pearson correlation $R^2 = 0.66$; $p < 0.05$, **Figure 5**). The same trends were observed for LITs done on orthomosaics, although the slope and surface complexity effects were not significant (**Supplementary Figure 3**). Yet the fractal dimension showed no correlation when examining differences between LITs done *in situ* and photoquadrats from orthomosaics.

Results of the method description and criteria evaluation are shown in **Table 3** with three categories: Method description, Human expertise and Time required, and Review and Perspectives.

DISCUSSION

Estimating Coral Cover

The LITs conducted *in situ* generated higher estimates of coral cover compared to other methods which is consistent with findings of Leujak and Ormond (2007) who compared six methods of coral community surveys and found that LIT and Point Intercept Transect (PIT) methods overestimated principal benthic categories. Lam et al. (2006) also showed that the PIT method overestimates coral cover, particularly at sites with scarce coral colonies. However, Facon et al. (2015) show that the PIT method generates almost the same level of information as for the LIT method. Regarding digital assessments on orthomosaics, no differences were detected between LITs on orthomosaics and photoquadrats from orthomosaics suggesting that the linear and point sampling used (length and number) may be equivalent in terms of representativeness for coral cover and accuracy.

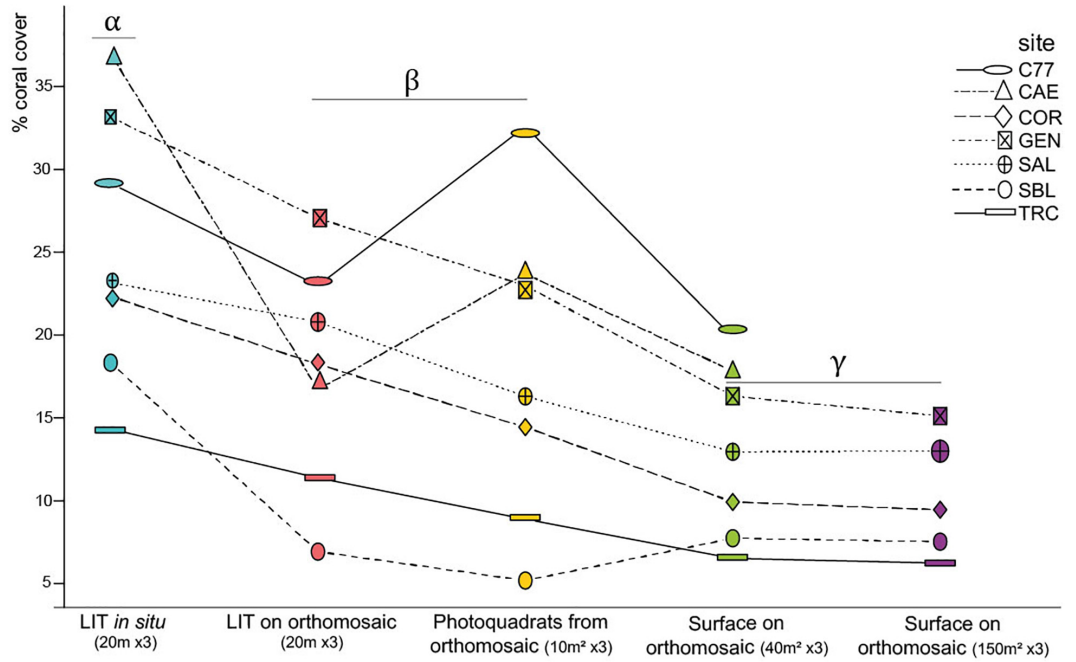

FIGURE 3 | Method x Site interaction plot of percent coral cover estimations. Groups with the same Greek letters (α, β, γ) display no significant difference (two-way ANOVA and Tukey tests, $p < 0.001$). Colors represent survey methods: LIT *in-situ* (turquoise); LIT from orthomosaic (pink), Photoquadrats from orthomosaic (yellow); surface analyses on orthomosaic sampling 40 m^2 × 3 (green); surface analyses on orthomosaic sampling 150 m^2 × 3 (purple).

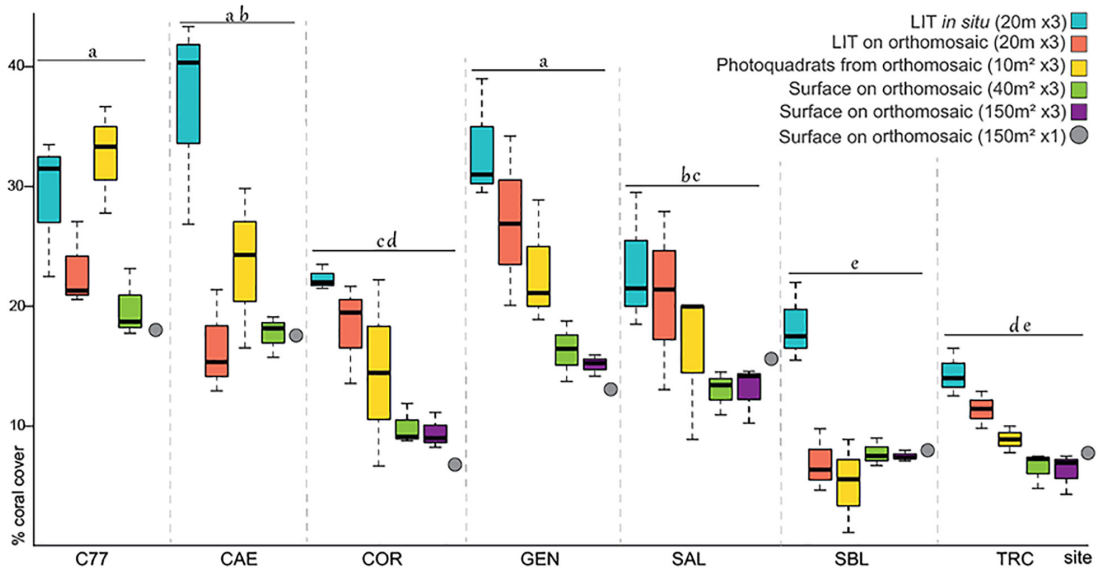

FIGURE 4 | Percent coral cover by method across sites. Same letters (a, b, c, d or e) in top of boxplots/site means no significant differences between groups (two-way ANOVA and Tukey test $p < 0.01$).

Among all methods, surface analyses on orthomosaics resulted the lowest and least variable percent coral cover estimates, and is therefore probably the most accurate methodology. The sampling unit of surface analyses is a polygon (surface estimator) which is more representative than lines or points, despite errors associated with manual delineations on the orthomosaics. The low variances of percent coral cover estimates confirms that a surface analysis based on orthomosaics is comparatively the most accurate and reliable method. Molloy et al. (2013) showed that coral recovery could not be detected using even the most intensive photoquadrats protocols, and suggested a coral surface area as a more sensitive and powerful means to

TABLE 2 | Physical descriptors of the structural complexity: surface complexity, slope, and fractal dimension computed from each study site's DEM.

Site	Surface complexity	Slope (°)	Fractal dimension
CAE	2.05	38.02	2.15
COR	1.73	33.83	2.12
C77	1.73	33.39	2.13
GEN	1.72	34.23	2.13
SBL	1.40	29.37	2.07
SAL	1.40	29.84	2.08
TRC	1.32	24.59	2.07

detect coral recovery. However, a weakness of photogrammetric methods relates to the orthographic projection used to generate orthomosaics. While this does not affect flat sites, sites whit high structural complexity or that steeply slope are more impacted by the orthographic projection resulting in an underrepresentation of the terrain when projected. Consequently, the surface area of colonies is likely underestimated in complex habitats on reef slopes (Urbina-Barreto et al., 2020). Here, the differences found between cover estimates from LITs done *in situ* and surface analyses on orthomosaics increased both with surface complexity and slope. This point to a methodological limitation which could be problematic when comparing sites with large differences in slope or complexity. Here, however, the studied sites had small differences in slope values and surface complexity. Further research is needed on assessing how habitat complexity descriptors affect estimates of coral cover (e.g., surface complexity, slope) when applying innovative photogrammetric methods.

The findings of our study could very well support coral reef conservation. Until now, coral reef studies applied different methods to map reefs as accurately as possible, aiming to improve the descriptors and determine the optimal level of sampling to monitor coral communities (e.g., Goreau, 1959; Weinberg, 1981; Leujak and Ormond, 2007; Casella et al., 2016; Fukunaga et al., 2019; Hernández-Landa et al., 2020). Scientists and managers often overlook the under or overestimation of coral cover, despite this being a crucial aspect when defining targets for resource conservation. Further such targets increasingly require to integrate the variable results of numerous surveys conducted at broad spatial scales (Edmunds and Bruno, 1996; Hoegh-Guldberg et al., 2018). Recently, Lechene et al. (2019) examined levels of sampling using large-area mosaics that optimize coral reef sampling strategies. They concluded that each benthic category has own optimal level of sampling. For instance they required a 60 m^2 area to obtain representative cover estimates of 55% of all benthic features. This points to an essential need for a calibration between survey methods, in particular for LIT and PIT methods since they are widely used to support coral reef conservation. Vallès et al. (2019) studied the transition between the chain intercept transect (a method derived from LIT but using a chain instead of a taut measuring tape) and photoquadrat methods on Caribbean reefs and concluded that switching methods for coral surveys would be complicated, as almost all reef benthic categories would require different conversion procedures (i.e., specific mathematical adjustments). More such comparisons studies between traditional and photogrammetric methods for coral reef surveys are needed to prepare for a likely transition between methods, to ensure more accurate and long-term surveys of reef ecosystems at wide spatial scales without dismissing the fundamental historical data gathered over the last six decades.

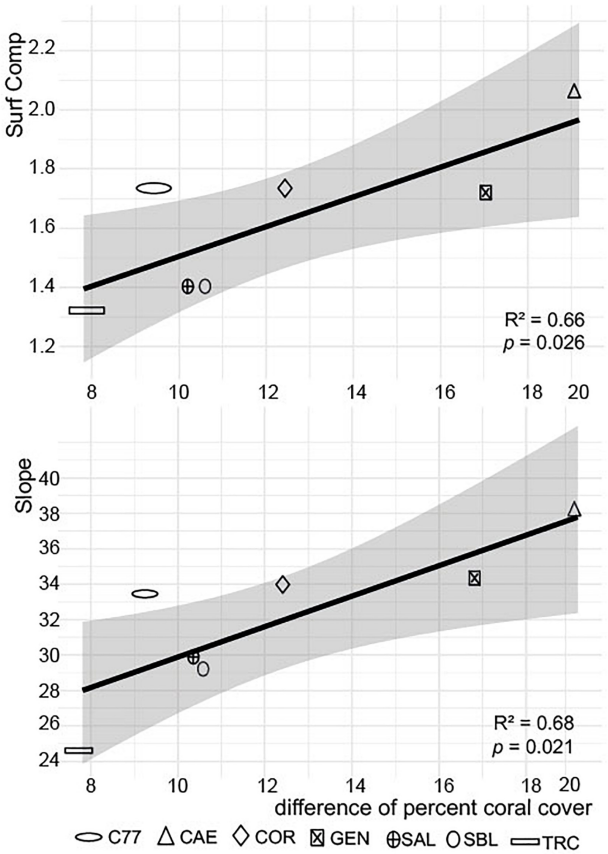

FIGURE 5 | Differences in percent coral cover obtained with LIT *in situ* and surface analysis on 40 m^2 × 3 orthomosaics as a function of the structural complexity descriptors: for surface complexity (top) and slope (bottom).

Comparison of Traditional and Photogrammetric Methods

The LIT *in situ* method generates significantly less data than photogrammetric methods (**Table 3**). Indeed surface analyses can deliver more than eight highly comprehensive and high-quality reef descriptors based on DEM and orthomosaic analyses, not to mention the analyses that could be performed on other photogrammetric outputs such as point clouds and meshes. The photoquadrats from orthomosaics method is a less comprehensive method, delivering only four descriptors, while LITs on orthomosaics only delivers a single descriptor (percent cover of benthic categories), as does LIT *in situ* method. Furthermore, photogrammetric raw field data (i.e., photographs) allow post-dive analysis by different operators or using new tools to automatically annotate underwater imagery (e.g., Beijbom

TABLE 3 | Comparison of the survey methods deployed in this study. Abbreviations: NA = not applicable.

		Traditional method	**Photogrammetric methods**		
	Criterion	**LIT *in situ***	**LIT on orthomosaic**	**Photoquadrats from orthomosaic**	**Surface analyses on orthomosaic and digital elevation model (DEM)**
Method description	Brief description	Method operated by biologist divers recording benthic categories (i.e., corals, algae, sponges, mineral substrate) along transects laid on substratum. Percent cover is obtained by dividing the total category length by the total transect length.	Photogrammetry by SfM is a technique that allows building 3D models from overlapping photographs. The main outputs from photogrammetry are 3D models (as point clouds and meshes), digital elevation models, and orthomosaics. Over the last decade, this technique has been adopted in the underwater domain to conduct quantitative coral reef studies and surveys.		
			Reproduction of LIT *in situ* survey method on an orthomosaic.	Reproduction of the traditional photoquadrat method, though frames are extracted from the orthomosaic. The classification of points allows estimating cover of different benthic categories.	Various spatial or biological analyses can be performed with GIS software, based on the outputs from photogrammetry.
	Estimator	Lines	Lines	Points	Polygons and measurements on elevation grids (DEM)
	Sampling effort	3 × 20 m transects (= 60 m)	3 × 20 m transects (= 60 m)	30 × 1 m^2 photoquadrats along 3 transects (= 30 m^2)	3 × 40 m^2 or 3 × 150 m^2 orthomosaic (= 120 m^2; 450 m^2)
	Survey dimensions	1D	1D	2D	2D (orthomosaic) 2.5D (digital elevation model) 3D (if point cloud or mesh is used)
	Attainable descriptors	• Percent cover of benthic categories	• Percent cover of benthic categories	• Percent cover and frequency of benthic categories • Coral colony size and abundance • Distance between colonies	• Surface area and percent cover of benthic categories • Occurrence and frequency of benthic categories • Coral colony size and abundance • Distance between colonies • Surface complexity • Fractal dimension • Shelter capacity • Mean slope

(Continued)

TABLE 3 | Continued

	Criterion		Traditional method	Photogrammetric methods		
			LIT *in situ*	**LIT on orthomosaic**	**Photoquadrats from orthomosaic**	**Surface analyses on orthomosaic and digital elevation model (DEM)**
	Limits for the taxonomic identification of Scleractinian corals		Species determination possible in most cases	Genus determination possible in most cases		
	Raw data		Length of segments for different benthic categories	Photographs		
	Observer bias in biological analysis		Medium (by the biologist diver)	Medium (by the biologist on computer)		
	Underwater equipment		GPS, measuring tape, Tablet, and pen	Photographic equipment, measuring tape, scale bars, GPS, and georeferencing targets		
	Computing equipment		No specific requirements	Computer with high processing power and photogrammetry software		
				Geographic Information System software	CPCe software and Geographic Information System software	Geographic Information System software
	Environmental constraints		Low swell and current	Sufficient lighting sources (natural or artificial) and low turbidity and swell		
	Criterion		**Traditional Method**	**Photogrammetric methods**		
			LIT *in situ*	**LIT on orthomosaic**	**Photoquadrats from orthomosaic**	**Analyses on orthomosaic and digital elevation model (DEM)**
Human expertise & Time required (1 study site)	1. Planning	Protocol design	NA	0.5 or 1.0 day for highly complex sites		
		Sampling plan	0.2 day-1 person	0.5 day-1 person		
		Field tools	NA	0.3 day-1 person		
		Man-day	0.2 (Technician or expert)	1.3 (technician or expert) or 1.8 (technician or expert) for highly complex sites		
	2. Fieldwork	Mob/Demob	0.8 day-2 persons	0.8 day-2 persons		
		Field survey	0.2 day-2 persons	0.2 day-2 persons		
		Man-day	2.0 (1 technician + 1 expert)	2.0 (1 technician + 1 expert or 2 technicians or 2 experts)		
	3. Office analysis	Data handling	0.1 day-1 person	0.7 day-1 person *(Reproducing transects)*	1 day-1 person *(Exporting frames)*	0.5 day-1 person *(Selecting photographs)*
		Photogram-metry processing	NA	1 day-1 person *(For ∼800 photographs)*		

(Continued)

TABLE 3 | Continued

	Criterion		Traditional method	Photogrammetric methods		
			LIT *in situ*	**LIT on orthomosaic**	**Photoquadrats from orthomosaic**	**Surface analyses on orthomosaic and digital elevation model (DEM)**
				Here, expert (E) requires biology, photogrammetry, and GIS skills		
		Ecological analyses	0.1 day (results handling)	0.4 day-1 person *(1.5 h for ecological GIS analysis + 1 h for length computation and results handling)*	0.3 day-1 person (*0.3 h for CPCe analysis + 2 h for.csv exports and results handling)*	1–5 day(s)-1 person *(According to targeted descriptors and the benthic cover of reef area—high coral cover involves more GIS analysis time)*
		Man-day	0.2 (Technician or expert)	2.1 (1 expert)	2.3 (1 expert)	2.5 to 6.5 (1 expert)
	Total estimation of human resources and time requirement by method E = expert T = technician		**2.4 man-days** (a) 1.2 E + 1.2 T or (b) 1.4 E + 1 T or (c) 2.4 E	**5.4–5.9 man-days** For a standard site: (a) 2.1 E + 3.3 T or (b) 3.1 E + 2.3 T or (c) 3.4 E +2 T or (d) 4.1 E + 1.3 Tor (e) 4.4 E+ 1 Tor (f) 5.4 E	**5.6–6.1 man-days** For a standard site: (a) 2.3 E + 3.3 T or (b) 3.3 E + 2.3 T or (c) 3.6 E +2 T or (d) 4.3 E + 1.3 Tor (e) 4.6 E+ 1 Tor (f) 5.6 E	**5.8–10.3 man-days** For a standard site: (a) 2.5 E + 3.3 T or (b) 3.5 E + 2.3 T or (c) 3.8 E +2 T or (d) 4.5 E + 1.3 Tor (e) 4.8 E+ 1 Tor (f) 5.8 E
Review & perspectives	Advantages		– Minimal equipment required – Less dependence on water conditions – Short time for office analyses	– Field work can be done by non-biologist – Availability of raw data for future analyses and repeatability – More accurate data (cm) and possibility for accurate long-term surveys – Approach allows obtaining numerous descriptors and gaining more information in terms of data quantity and quality – Sampling at a large spatial scale (seascape), which can be more representative – Individual colonies in shallow waters (< 3 m depth) can be sampled and tagged to conduct temporal survey (e.g., monitoring growth or erosion).		
	Disadvantages		– Field work must be done by an expert diver biologist – Only measures percent cover of the benthic categories of interest	– Requires good underwater conditions – Requires a minimum of depth to map large reef areas (ideally > 5 meters depth). The technique is not adapted to map large shallow reef areas (< 3 meters depth). – Requires specific photographic and computing equipment and software – Requires skills or training for the photogrammetry processing and GIS analyses – No direct measurements (the photogrammetry processing must be complete before performing the analyses) – Orthomosaics of sites presenting high structural complexity and/or steep slope likely lead to underestimation of surfaces		
	Fields of application		– Marine area management	– Marine area management & industrial applications – Visually attractive outputs can be used for communication and awareness – Advances in artificial intelligence (AI) to automatize ecological analyses are promising and can promote new applications – Remotely Operated Vehicle and Autonomous Underwater Vehicle developments open perspectives for fieldwork optimization		

et al., 2015; Williams et al., 2019; González-Rivero et al., 2020), whereas raw data collected with the LIT *in situ* method (or in any other *in situ* visually based method) relies on the diver's in situ expertise. However, photogrammetric methods require more equipment (cameras, computer, and software), and are more constrained by environmental conditions. Despite limitations in terms of data output, the LIT *in situ* method allows for a finer taxonomic determination. Then again, compared to the LIT *in situ* method, a significant advantage of photogrammetric methods is the ability to calculate essential habitat descriptors on reefs, i.e., surface complexity, fractal dimension, slope, and rugosity profiles which are closely linked to reef biodiversity and productivity as well as ecological changes in seascapes (e.g., Graham and Nash, 2013; Rees et al., 2018; Price et al., 2019).

In terms of practicality, in contrast to the LIT *in situ* method, photogrammetric methods do not require expert biologists for planning and implementing survey operations and underwater data recording. Then again, an expert is not required for post-acquisition analyses of LIT *in situ* data whereas expertise is mandatory to generate 3D models and photogrammetric outputs, and to conduct ecological and spatial analyses.

As for the time required, the photogrammetric methods and ecological analyses comparatively need more preparation than the LIT *in situ* method, while the time needed for fieldwork is more or less the same. In decreasing order, the total time needed by method for the preparation, fieldwork and analyses was as follow: (1) Analyses on orthomosaics and DEM (5.8–10.3 man-days/site); (2) Photoquadrats from orthomosaics (5.6–6.1 man-days/site); (3) LIT on orthomosaics (5.4–5.9 man-days/site); (4) LIT *in situ* (2.4 man-days/site). As mentioned earlier, results are directly correlated with the quantity and quality of the information produced.

Selection of a Survey Method

Overall, the comparisons made here of coral cover estimates, data outputs, and required technical and human resources point to the method that may more suitable for a given reef monitoring program or resource conservation purpose. When taking into account the results of this study and those by others who compared means, fieldwork and accuracy across different benthic survey methods (e.g., Weinberg, 1981; Ohlhorst et al., 1988; Beenaerts and Berghe, 2007; Dumas et al., 2009; Facon et al., 2015; Lechene et al., 2019), surface analysis on orthomosaics stands out as the most efficient method when considering the quantity and quality of data gathered and time expended. The photoquadrat from orthomosaics method is an intermediate solution. The traditional LIT *in situ* method remains the least time-consuming method, efficient for specific taxonomic identifications, while being the most limited in terms of reef descriptors and representativeness of the ecosystem. The reproduction of traditional methods from photogrammetric outputs (DEMs or orthomosaics), as proposed here, is an innovative alternative to traditional reef survey methods that can be adapted for any coral reef study.

Confronting the global coral reef crisis, challenging conservation targets require the optimization of reef survey methods. New technologies can promote rapid advancements in reef science and support management programs to solve key issues facing coral reefs (Bellwood et al., 2004; Hoegh-Guldberg et al., 2018; Madin et al., 2019. In this context, our study is a first step to launch the likely transition from traditional methods to novel and more efficient ones (Storlazzi et al., 2016). We also provide new information to complement and optimize reef surveys, and enhance the effectiveness of conservation programs. Photogrammetric tools can be of particular interest to coastal planners and decision-makers when it comes to avoidance, reduction, or compensation measures often required by local environmental laws for coastal and seascape works. Improving the efficiency of conservation is likely to promote the recovery of marine life (if major pressures are relieved) and as such is an ethical and smart economic objective to achieve a sustainable future (Kenchington, 2018; Duarte et al., 2020). To this end, new methods adopting the FAIR principles (findability, accessibility, interoperability, and reusability) for stewardship of reef data can improve the monitoring of these ecosystems (Rossi et al., 2021). Among them the development of artificial intelligence for automated analysis of images (Williams et al., 2019; González-Rivero et al., 2020) and photogrammetry outputs (e.g., Hopkinson et al., 2020; Mohamed et al., 2020), multispectral and hyperspectral imagery (e.g., Parsons et al., 2018; Bajjouk et al., 2019; Li et al., 2019), and the improvement of diver-based or automated data acquisition from Remotely Operated Vehicles and Autonomous Underwater Vehicles (Friedman et al., 2012; Obura et al., 2019; Hatcher et al., 2020; Rossi et al., 2021) will likely revolutionize this field. Finally the integration of all existing reef habitat mapping data in common and open source data bases could help to overcome the lack of transferability across systems/scale, provide more accurate and representative assessments of habitats, and generate conservation measures and habitat rehabilitation actions (Madin et al., 2019; Rossi et al., 2021). Together, these efforts will foster the application of these new methods in both research and coral reef conservation programs.

DATA AVAILABILITY STATEMENT

The original contributions presented in the study are included in the article/**Supplementary Material**, further inquiries can be directed to the corresponding author/s.

AUTHOR CONTRIBUTIONS

IU-B, RG, SE, RP, and MA conceived the ideas. IU-B, RG, RP, J-PQ, LP, ED, and MA designed the methodology. IU-B, VM, J-PQ, RG, and SB collected the data. IU-B and RP generated digital elevation models and orthomosaics. IU-B, PD, CP, and SE performed data handling and analyzed the data. IU-B, RG, RP, J-PQ, MF, PD, SE, ED, LP, and MA evaluated the criteria methods. IU-B led the writing of the manuscript with SE, LP, and MA. All authors contributed critically to the drafts and gave final approval for publication.

FUNDING

IU-B was supported by a CIFRE fellowship, from the French Association of Research and Technologies, under the agreement 2017/0322. The project was also supported by Agence de l'Eau Rhône-Méditerranée-Corse (Pierre Boissery).

ACKNOWLEDGMENTS

We are thankful to Henrich J. Bruggemann for the valuable advice of this manuscript. Thank you to Ken Deslarzes and Jane Ballard for the English revision of the manuscript. We thank Ifigenia Urbina-Barreto and Julio A. Urbina for their inputs throughout writing of the manuscript. We also thank the reviewers for the comments that greatly improved this manuscript. Thank you to the Reserve Naturelle Marine de La Réunion for authorizing the work inside the reserve. We are grateful to know that this study was selected by the SCORE-REEF project workshops and reflections, which is supported by FRB/CESAB.

SUPPLEMENTARY MATERIAL

The Supplementary Material for this article can be found online at: https://www.frontiersin.org/articles/10.3389/fmars.2021.636902/full#supplementary-material

REFERENCES

Alvarez-Filip, L., Carricart-Ganivet, J. P., Horta-Puga, G., and Iglesias-Prieto, R. (2013). Shifts in coral-assemblage composition do not ensure persistence of reef functionality. *Scientific Rep.* 3, 1–5. doi: 10.1038/srep03486

Bajjouk, T., Mouquet, P., Ropert, M., Quod, J. P., Hoarau, L., Bigot, L., et al. (2019). Detection of changes in shallow coral reefs status: towards a spatial approach using hyperspectral and multispectral data. *Ecol. Indic.* 96, 174–191. doi: 10.1016/j.ecolind.2018.08.052

Beenaerts, N., and Berghe, E. V. (2007). Comparative Study of Three Transect Methods to Assess Coral Cover, Richness and Diversity. *West. Ind. Ocean J. Mar. Sci.* 4, 29–38. doi: 10.4314/wiojms.v4i1.28471

Beijbom, O., Edmunds, P. J., Roelfsema, C., Smith, J., Kline, D. I., Neal, B. P., et al. (2015). Towards Automated Annotation of Benthic Survey Images: variability of Human Experts and Operational Modes of Automation. *PLoS One* 10:e0130312. doi: 10.1371/journal.pone.0130312

Bellwood, D. R., Hughes, T. P., Folke, C., and Nyström, M. (2004). Confronting the coral reef crisis. *Nature* 429, 827–833. doi: 10.1038/nature02691

Burns, J. H. R., Delparte, D., Gates, R. D., and Takabayashi, M. (2015). Utilizing underwater three-dimensional modeling to enhance ecological and biological studies of coral reefs. *Int. Arch. Photogr.* 5, 61–66. doi: 10.5194/isprsarchives-XL-5-W5-61-2015

Caldwell, Z. R., Zgliczynski, B. J., Williams, G. J., and Sandin, S. A. (2016). Reef fish survey techniques: assessing the potential for standardizing methodologies. *PLoS One* 11:e0153066. doi: 10.1371/journal.pone.0153066

Carlot, J., Rovère, A., Casella, E., Harris, D., Grellet-Muñoz, C., Chancerelle, Y., et al. (2020). Community composition predicts photogrammetry-based structural complexity on coral reefs. *Coral Reefs* 39, 967–975. doi: 10.1007/s00338-020-01916-8

Casella, E., Collin, A., Harris, D., Ferse, S., Bejarano, S., Parravicini, V., et al. (2016). Mapping coral reefs using consumer-grade drones and structure from motion photogrammetry techniques. *Coral Reefs* 36, 1–7. doi: 10.1007/s00338-016-1522-0

Dahl, A. L. (1981). *Coral Reef Monitoring Handbook. South Pacific Comission 1981*. Autralia: Bridge Printery Sidney.

Darling, E. S., Graham, N. A. J., Januchowski-Hartley, F. A., Nash, K. L., Pratchett, M. S., and Wilson, S. K. (2017). Relationships between structural complexity, coral traits, and reef fish assemblages. *Coral Reefs* 36, 561–575. doi: 10.1007/s00338-017-1539-z

Darling, E. S., McClanahan, T. R., Maina, J., Gurney, G. G., Graham, N. A. J., Januchowski-Hartley, F., et al. (2019). Social-environmental drivers inform strategic management of coral reefs in the Anthropocene. *Nat. Ecol. Evol.* 3, 1341–1350. doi: 10.1038/s41559-019-0953-8

Duarte, C. M., Agusti, S., Barbier, E., Britten, G. L., Castilla, J. C., Gattuso, J. P., et al. (2020). Rebuilding marine life. *Nature* 5807801, 39–51.

Dumas, P., Bertaud, A., Peignon, C., Léopold, M., and Pelletier, D. (2009). A 'quick and clean' photographic method for the description of coral reef habitats. *J. Exp. Mar. Biol. Ecol.* 368, 161–168. doi: 10.1016/j.jembe.2008.10.002

D'Urban, J. T., Williams, G. J., Walker-Springett, G., and Davies, A. J. (2020). Three-dimensional digital mapping of ecosystems: a new era in spatial ecology. *Proc. Biol. Sci.* 287:20192383. doi: 10.1098/rspb.2019.2383

Edmunds, P. J., and Bruno, J. F. (1996). The importance of sampling scale in ecology: kilometer-wide variation in cora reef communities. *Mar. Ecol. Prog. Ser.* 143, 165–171.

Elise, S., Bailly, A., Urbina-Barreto, I., Mou-Tham, G., Chiroleu, F., Vigliola, L., et al. (2019a). An optimised passive acoustic sampling scheme to discriminate among coral reefs' ecological states. *Ecol. Indic.* 107:105623. doi: 10.1016/j.ecolind.2019.105627

Elise, S., Urbina-Barreto, I., Pinel, R., Mahamadaly, V., Bureau, S., Penin, L., et al. (2019b). Assessing key ecosystem functions through soundscapes: a new perspective from coral reefs. *Ecol. Indic.* 107:105623. doi: 10.1016/j.ecolind.2019.105623

English, S., Wilkinson, C., and Baker, V. (1997). *Survey Manual for Tropical Marine Resources*, II Edn. Australia: Australian Institute of Marine Science.

Facon, M., Pinault, M., Obura, D., Pioch, S., Pothin, K., Bigot, L., et al. (2015). A comparative study of the accuracy and effectiveness of Line and Point Intercept Transect methods for coral reef monitoring in the southwestern Indian Ocean islands. *Ecol. Indic.* 60, 1045–1055. doi: 10.1016/j.ecolind.2015.09.005

Flower, J., Ortiz, J. C., Chollett, I., Abdullah, S., Castro-Sanguino, C., Hock, K., et al. (2017). Interpreting coral reef monitoring data: a guide for improved management decisions. *Ecol. Indic.* 72, 848–869. doi: 10.1016/j.ecolind.2016.09.003

Friedlander, A. M., and Parrish, J. D. (1998). Habitat characteristics affecting fish assemblages on a Hawaiian coral reef. *J. Exp. Mar. Biol. Ecol.* 224, 1–30. doi: 10.1016/S0022-0981(97)00164-0

Friedman, A., Pizarro, O., Williams, S. B., and Johnson-Roberson, M. (2012). Multi-Scale Measures of Rugosity, Slope and Aspect from Benthic Stereo Image Reconstructions. *PLoS One* 7:e50440. doi: 10.1371/journal.pone.0050440

Fukunaga, A., Burns, J., Craig, B., and Kosaki, R. (2019). Integrating Three-Dimensional Benthic Habitat Characterization Techniques into Ecological Monitoring of Coral Reefs. *J. Mar. Sci. Eng.* 2:27. doi: 10.3390/jmse7020027

Gilbert, D., and Quod, J. P. (2018). *Coral Reef Monotoring Coping with Climate Change, Toward a Social-ecological System Perspective. Communicating Climate Change Information Decision-Making*. Cham: Springer Climate.

González-Barrios, F. J., and Álvarez-Filip, L. (2018). A framework for measuring coral species-specific contribution to reef functioning in the Caribbean. *Ecol. Ind.* 95, 877–886. doi: 10.1016/j.ecolind.2018.08.038

González-Rivero, M., Beijbom, O., Rodriguez-Ramirez, A., Bryant, D. E., Ganase, A., Gonzalez-Marrero, et al. (2020). Monitoring of coral reefs using artificial intelligence: a feasible and cost-effective approach. *Remote Sens.* 12, 1–22. doi: 10.3390/rs12030489

González-Rivero, M., Beijbom, O., Rodriguez-Ramirez, A., Holtrop, T., González-Marrero, Y., Ganase, A., et al. (2016). Scaling up Ecological Measurements of Coral Reefs Using Semi-Automated Field Image Collection and Analysis. *Remote Sens.* 8:30. doi: 10.3390/rs8010030

González-Rivero, M., Bongaerts, P., Beijbom, O., Pizarro, O., Friedman, A., Rodriguez-Ramirez, A., et al. (2014). The Catlin Seaview Survey - kilometre-scale seascape assessment, and monitoring of coral reef ecosystems. *Aquat. Conser* 24, 184–198. doi: 10.1002/aqc.2505

Goreau, T. (1959). The ecology of Jamaican coral reefs. I. species composition and zonation. *Ecology* 40, 67–90.

Graham, N. A. J., and Nash, K. L. (2013). The importance of structural complexity in coral reef ecosystems. *Coral Reefs* 32, 315–326. doi: 10.1007/s00338-012-0984-y

Hatcher, G. A., Warrick, J. A., Ritchie, A. C., Dailey, E. T., Zawada, D. G., Kranenburg, C., et al. (2020). Accurate Bathymetric Maps From Underwater Digital Imagery Without Ground Control. *Front. Mar. Sci.* 7, 1–20. doi: 10.3389/fmars.2020.00525

Hedley, J., Roelfsema, C., Chollett, I., Harborne, A., Heron, S., Weeks, S., et al. (2016). Remote Sensing of Coral Reefs for Monitoring and Management: a Review. *Remote Sens.* 8:118. doi: 10.3390/rs8020118

Hernández-Landa, R. C., Barrera-Falcon, E., and Rioja-Nieto, R. (2020). Size-frequency distribution of coral assemblages in insular shallow reefs of the Mexican Caribbean using underwater photogrammetry. *PeerJ.* 8:e8957. doi: 10.7717/peerj.8957

Hill, J., and Wilkinson, C. (2004). *Methods for Ecological Monitoring of Coral Reefs*. Townsville: Australian Institute of Marine Science, doi: 10.1017/CBO9781107415324.004

Hoegh-Guldberg, O., Kennedy, E. V., Beyer, H. L., McClennen, C., and Possingham, H. P. (2018). Securing a Long-term Future for Coral Reefs. *Trends Ecol. Evol.* 33, 936–944. doi: 10.1016/j.tree.2018.09.006

Hopkinson, B. M., King, A. C., Owen, D. P., Johnson-Roberson, M., Long, M. H., and Bhandarkar, S. M. (2020). Automated classification of three-dimensional reconstructions of coral reefs using convolutional neural networks. *PLoS One* 15:e0230671. doi: 10.1371/journal.pone.0230671

Kenchington, R. (2018). Science and the management of coral reefs. *Mar. Poll. Bull.* 136, 508–515. doi: 10.1016/j.marpolbul.2018.09.046

Kohler, K. E., and Gill, S. M. (2006). Coral Point Count with Excel extensions (CPCe): a Visual Basic program for the determination of coral and substrate coverage using random point count methodology. *Comput. Geosci.* 32, 1259–1269. doi: 10.1016/j.cageo.2005.11.009

Lam, K., Shin, P. K. S., Bradbeer, R., Randall, D., Ku, K. K. K., Hodgson, P., et al. (2006). A comparison of video and point intercept transect methods for monitoring subtropical coral communities. *J. Exp. Mar. Biol. Ecol.* 333, 115–128. doi: 10.1016/j.jembe.2005.12.009

Lechene, M. A. A., Haberstroh, A. J., Byrne, M., Figueira, W., and Ferrari, R. (2019). Optimising Sampling Strategies in Coral Rees Using Large-Areas Mosaics. *Remote Sens.* 11:2907. doi: 10.3390/rs11242907

Leujak, W., and Ormond, R. F. G. (2007). Comparative accuracy and efficiency of six coral community survey methods. *J. Exp. Mar. Biol. Ecol.* 351, 168–187. doi: 10.1016/j.jembe.2007.06.028

Li, J., Schill, S. R., Knapp, D. E., and Asner, G. P. (2019). Object-based mapping of coral reef habitats using planet dove satellites. *Remote Sens.* 11:1445. doi: 10.3390/rs11121445

Loya, Y. (1972). Community structure and species diversity of hermatypic corals at Eilat Red Sea. *Mar. Biol.* 13, 100–123. doi: 10.1007/BF00366561

Loya, Y. (1978). Plotless and transect methods. In D. R. S. and R. E. Johannes (Ed.), Monographs on Oceanic Methodology. *Coral Reefs* 5, 197–218.

Madin, E. M. P., Darling, E. S., and Hardt, M. J. (2019). Emerging Technologies and Coral Reef Conservation: opportunities. Challenges, and Moving Forward. *Front. Mar. Sci.* 6:727. doi: 10.3389/fmars.2019.00727

Madin, J. S., Hoogenboom, M. O., Connolly, S. R., Darling, E. S., Falster, D. S., Huang, D., et al. (2016). A Trait-Based Approach to Advance Coral Reef Science. *Trends Ecol. Evol.* 31, 419–428. doi: 10.1016/j.tree.2016.02.012

Magel, J. M. T., Burns, J. H. R., Gates, R. D., and Baum, J. K. (2019). Effects of bleaching-associated mass coral mortality on reef structural complexity across a gradient of local disturbance. *Scientific Rep.* 9, 1–12. doi: 10.1038/s41598-018-37713-1

Mohamed, H., Nadaoka, K., and Nakamura, T. (2020). Towards Benthic Habitat 3D Mapping Using Machine Learning Algorithms and Structures from Motion Photogrammetry. *Remote Sens.* 12:127. doi: 10.3390/rs12010127

Molloy, P. P., Evanson, M., Nellas, A. C., Rist, J. L., Marcus, J. E., Koldewey, H. J., et al. (2013). How much sampling does it take to detect trends in coral-reef habitat using photoquadrat surveys? *Aquat. Conserv. Mar. Freshw. Ecosyst.* 23, 820–837. doi: 10.1002/aqc.2372

Obura, D. (2014). *Coral Reef Monitoring Manual South-West Indian Ocean islands*. France: Indian Ocean Commission.

Obura, D., Aeby, G., Amornthammarong, N., Appeltans, W., Bax, N., Bishop, J., et al. (2019). Coral Reef Monitoring, Reef Assessment Technologies, and Ecosystem-Based Management. *Front. Mar. Sci.* 6:580. doi: 10.3389/fmars.2019.00580

Obura, D., and Grimsditch, G. (2009). Resilience Assessment of Coral Reefs bleaching and thermal stress. *IUCN Resil. Sci. Group Work. Paper Ser.* 5:70.

Ohlhorst, S. L., Liddell, W. D., Taylor, R. J., and Taylor, J. M. (1988). "Evaluation of reef census techniques," in *Proceedings of the 6th International Coral Reef Symposium*, Vol. 2, (Australia: Townsville), 319–324.

Parsons, M., Bratanov, D., Gaston, K. J., and Gonzalez, F. (2018). UAVs, hyperspectral remote sensing, and machine learning revolutionizing reef monitoring. *Sensors* 18, 1–20. doi: 10.3390/s18072026

Pendleton, L. H., Hoegh-Guldberg, O., Langdon, C., and Comte, A. (2016). Multiple stressors and ecological complexity require a new approach to coral reef research. *Front. Mar. Sci.* 3:36. doi: 10.3389/fmars.2016.00036

Peterson, G., Allen, C. R., and Holling, C. S. (1998). Ecological resilience, biodiversity, and scale. *Ecosystems* 1, 6–18.

Price, D. M., Robert, K., Callaway, A., Lo Iacono, C., Hall, R. A., and Huvenne, V. A. I. (2019). Using 3D photogrammetry from ROV video to quantify cold-water coral reef structural complexity and investigate its influence on biodiversity and community assemblage. *Coral Reefs* 38, 1007–1021. doi: 10.1007/s00338-019-01827-3

R Core Team (2019). *R?: A language and Statistical, Statistical Computing*. Vienna: R Foundation for Computing.

Rees, M. J., Knott, N. A., Neilson, J., Linklater, M., Osterloh, I., Jordan, A., et al. (2018). Accounting for habitat structural complexity improves the assessment of performance in no-take marine reserves. *Biol. Conserv.* 224, 100–110. doi: 10.1016/j.biocon.2018.04.040

Riedl, R. (1980). Marine Ecology a century of changes. *Mar. Ecol.* 1, 3–46.

Risk, M. (1972). Fish diversity on a Coral Reef in the Virgin Island. *Atoll Res. Bull.* 153, 1–4.

Rossi, P., Ponti, M., Righi, S., Castagnetti, C., Simonini, R., Mancini, F., et al. (2021). Needs and Gaps in Optical Underwater Technologies and Methods for the Investigation of Marine Animal Forest 3D-Structural Complexity. *Front. Mar. Sci.* 8, 1–9. doi: 10.3389/fmars.2021.591292

Storlazzi, C. D., Dartnell, P., Hatcher, G. A., and Gibbs, A. E. (2016). End of the chain? Rugosity and fine-scale bathymetry from existing underwater digital imagery using structure-from-motion (SfM) technology. *Coral Reefs* 35, 889–894. doi: 10.1007/s00338-016-1462-8

Urbina-Barreto, I., Chiroleu, F., Pinel, R., Fréchon, L., Mahamadaly, V., Elise, S., et al. (2020). Quantifying the shelter capacity of coral reefs using photogrammetric 3D modelling, from colonies to reefscapes. *Ecol. Indicat.* 121:107151. doi: 10.1016/j.ecolind.2020.107151

Vallès, H., Oxenford, H. A., and Henderson, A. (2019). Switching between standard coral reef benthic monitoring protocols is complicated: proof of concept. *PeerJ.* 2019, 1–24. doi: 10.7717/peerj.8167

Wedding, L. M., Jorgensen, S., Lepczyk, C. A., and Friedlander, A. M. (2019). Remote sensing of three-dimensional coral reef structure enhances predictive modeling of fish assemblages. *Remote Sens. Ecol. Conser* 5, 150–159. doi: 10.1002/rse2.115

Weinberg, S. (1981). A comparison of coral reef survey methods. *Bijdrag. Tot. de Dierk.* 51, 199–218.

Williams, I. D., Couch, C. S., Beijbom, O., Oliver, T. A., Vargas-Angel, B., Schumacher, B., et al. (2019). Leveraging automated image analysis tools to transform our capacity to assess status and trends on coral reefs. *Front. Mar. Sci.* 6, 1–14. doi: 10.3389/fmars.2019.00222

Wilson, S. K., Graham, N. A. J., and Polunin, N. V. C. (2007). Appraisal of visual assessments of habitat complexity and benthic composition on coral reefs. *Mar. Biol.* 151, 1069–1076. doi: 10.1007/s00227-006-0538-3

Zawada, K. J. A., Madin, J. S., Baird, A. H., Bridge, T. C. L., and Dornelas, M. (2019). Morphological traits can track coral reef responses to the Anthropocene. *Funct. Ecol.* 33, 962–975. doi: 10.1111/1365-2435.13358

Conflict of Interest: IU-B, RG, MF, VM, and ED were employed by Crecoean OI; RP and VM were employed by Geolab S.A.S; J-PQ was employed by ARVAM-Pareto.

The remaining authors declare that the research was conducted in the absence of any commercial or financial relationships that could be construed as a potential conflict of interest.

frontiers in Marine Science

ORIGINAL RESEARCH
published: 28 May 2021
doi: 10.3389/fmars.2021.647943

Comparing Coral Colony Surveys From In-Water Observations and Structure-From-Motion Imagery Shows Low Methodological Bias

Courtney S. Couch[1,2], Thomas A. Oliver[2], Rhonda Suka[1,2], Mia Lamirand[1,2], Mollie Asbury[2], Corinne Amir[1,2], Bernardo Vargas-Ángel[1,2], Morgan Winston[1,2], Brittany Huntington[1,2], Frances Lichowski[1,2], Ariel Halperin[1,2], Andrew Gray[1,2], Joao Garriques[1,2] and Jennifer Samson[2]*

[1] Joint Institute for Marine and Atmospheric Research, University of Hawai'i, Honolulu, HI, United States, [2] Pacific Islands Fisheries Science Center, National Marine Fisheries Service, Honolulu, HI, United States

As the threats to coral reefs mount, scientists and managers are looking for innovative ways to increase the scope, scale, and efficiency of coral reef monitoring. Monitoring changes in coral communities and demographic features provides key information about ecosystem function and resilience of reefs. While most monitoring programs continue to rely on in-water visual survey methods, scientists are exploring 3D imaging technologies such as photogrammetry, also known as Structure-from-Motion (SfM), to enhance precision of monitoring, increase logistical efficiency in the field, and generate a permanent record of the reef. Here, we quantitatively compare data generated from in-water surveys to SfM-derived metrics for assessing coral demography, bleaching, and diversity in the main Hawaiian Islands as part of NOAA's National Coral Reef Monitoring Program. Our objectives were to compare between-method error to within-method error, test for bias between methods, and identify strengths and weaknesses of both methods. Colony density, average colony diameter, average partial mortality, prevalence of bleaching, species richness, and species diversity were recorded using both methods within the same survey areas. For all metrics, the magnitude of between-method error was comparable to the within-method error for the in-water method and between method error was significantly higher than within-method error for SfM for one of the seven metrics. Our results also reveal that a majority of the metrics do not vary significantly between methods, nor did we observe a significant interaction between method and habitat type or method and depth. Exceptions include estimates of partial mortality, bleaching prevalence, and *Porites* juvenile density–though differences between methods are generally small. Our study also highlights that SfM offers a unique opportunity to more rigorously quantify and mitigate inter-observer error by providing observers unlimited "bottom time" and the opportunity to work together to resolve difficult annotations. However, the necessary investment in equipment and expertise does present substantial up-front costs, and the time associated with curating imagery, photogrammetric modeling, and manual image annotation can reduce the timeliness of data reporting. SfM provides a powerful tool to reimagine how we study and manage

OPEN ACCESS

Edited by:
Will F. Figueira, The University of Sydney, Australia

Reviewed by:
Randi D. Rotjan, Boston University, United States
Andrea Oliveira Ribeiro Junqueira, Federal University of Rio de Janeiro, Brazil

***Correspondence:**
Courtney Couch
Courtney.s.couch@noaa.gov

Specialty section:
This article was submitted to Coral Reef Research, a section of the journal Frontiers in Marine Science

Received: *30 December 2020*
Accepted: *04 May 2021*
Published: *28 May 2021*

Citation:
Couch CS, Oliver TA, Suka R, Lamirand M, Asbury M, Amir C, Vargas-Ángel B, Winston M, Huntington B, Lichowski F, Halperin A, Gray A, Garriques J and Samson J (2021) Comparing Coral Colony Surveys From In-Water Observations and Structure-From-Motion Imagery Shows Low Methodological Bias. Front. Mar. Sci. 8:647943. doi: 10.3389/fmars.2021.647943

coral reefs, and this study provides the first quantified methodological comparison to validate the transition from standard in-water methods to SfM survey methods for estimates of coral colony-level surveys.

Keywords: coral reef, photogrammetry, structure-from-motion, coral demography, coral diversity, Hawaii, benthic monitoring

INTRODUCTION

Coral reefs are suffering under multiple global threats associated with climate change (Hoegh-Guldberg et al., 2007; Pandolfi et al., 2011; Heron et al., 2016; Hughes et al., 2018) as well as local threats including overfishing, pollution, disease, severe storms, and overuse (Sandin et al., 2008; Ruiz-Moreno et al., 2012; Lamb et al., 2014; Pollock et al., 2014; Vega Thurber et al., 2014). These compounding disturbances are resulting in shifts in coral reef communities (Loya et al., 2001; Munday, 2004; Hughes et al., 2018) and progressive decline in coral reefs (Bruno and Selig, 2007; Miller et al., 2009; De'ath et al., 2012). Percent coral cover is the most widely used metric most widely used metric for detecting these shifts (Bruno and Selig, 2007; Edmunds and Elahi, 2007; Hughes et al., 2018), but this coarse metric often operates on decadal timescales that impede timely management action and does not elucidate the underlying demographic processes contributing to change (Edmunds and Riegl, 2020). Metrics such as colony density, size frequency distribution, partial mortality, colony health, and diversity can provide key information about a population's recovery potential, response to acute and chronic disturbance events, shifts in communities, and ultimately shed light on the underlying mechanisms that cannot be gleaned from cover alone (Edmunds and Elahi, 2007; Riegl et al., 2013, 2017; Baskett et al., 2014; Riegl and Purkis, 2015; Edmunds and Riegl, 2020; García-Urueña and Garzón-Machado, 2020; Kodera et al., 2020).

Over the last five decades, coral reef ecologists have used a broad range of in-water visual and imaging survey methods to quantify various features of benthic communities. Historically, visual methods such as line intercept transects (Loya, 1972), point intercept transects (English et al., 1994), quadrats (Conand et al., 1999), timed swims (Donnelly et al., 2003), and belt transects (Connell et al., 1997) have been widely used. While these methods allow divers to leave the water with data in hand, they can be time consuming to conduct, require specialized training, and visual observations made by a single diver cannot be verified or re-evaluated. Video transects (Carleton and Done, 1995; Houk and Van Woesik, 2006) and photoquadrats (English et al., 1994; Preskitt et al., 2004) have become more widely adopted during the last two decades with the increased accessibility of digital cameras. These methods are more efficient underwater, require less specialized skills in the field, and create a permanent record of the reef. However, they necessitate significant post-processing, are typically only used to quantify benthic cover, only capture a small area of reef which does not allow for accurate colony-level measurements, and usually only captures the reef in two dimensions (Beijbom et al., 2015; Jokiel et al., 2015; Page et al., 2016).

An emerging photogrammetry technology called structure-from-motion (SfM) is gaining popularity in coral reef science (Burns et al., 2015a; Bryson et al., 2017; Casella et al., 2017; Ferrari et al., 2017; Fox et al., 2019; Obura et al., 2019) and offers a potential opportunity to continue collecting population and community metrics beyond coral cover while reducing field costs. SfM uses two dimensional (2D) overlapping images to incorporate every pixel into a 3D point cloud surface. With this 3D point cloud, an orthorectified 2D mosaic of all the 2D images as well as a geometrically accurate 2D projection of the dense point cloud can be generated. This technique provides researchers versatility to study the reef from the coral polyp to reef-scale. To date, a majority of studies on coral reefs utilizing SfM methodology have focused on quantifying structural complexity (Burns et al., 2015a; Figueira et al., 2015; Storlazzi et al., 2016; Bryson et al., 2017; Fukunaga et al., 2020; Torres-Pulliza et al., 2020). Others have used SfM in small-scale studies to quantify disease and bleaching (Fox et al., 2019; Voss et al., 2019; Burns et al., 2020), spatial clustering of corals (Edwards et al., 2017; Pedersen et al., 2019), coral growth (Kodera et al., 2020; Lange and Perry, 2020), and size frequency distributions (Hernández-Landa et al., 2020). SfM can generate high resolution mosaics that facilitate colony-level assessments, but SfM may limit our ability to capture every surface and colony-angle that can be achieved with in-water assessments and significant post processing may impede timely data generation. Thus a comprehensive methodological comparison is needed to assess data comparability and methodological trade-offs. While Burns et al. (2020) conducted a small scale study comparing in-water assessments of coral health to data generated from SfM, no study has tested whether the standard suite of coral metrics (e.g., density, colony size, diversity, partial mortality, prevalence of altered health states, and diversity) extracted from SfM imagery are consistent with in-water observations across gradients of community structure, depth and reef complexity.

In this study, we evaluated the use of SfM as a tool for quantifying seven coral metrics (adult density, juvenile density, colony size, old partial mortality, bleaching prevalence, species richness, and species diversity) in comparison to traditional visual in-water assessments. We conducted this study across eight main Hawaiian Islands where reefs vary considerably in coral abundance, community structure, depth, and structural complexity. To contextualize methodological differences we quantified inter-observer error and compared it to methodological error. To assess the utility of SfM for benthic monitoring, the three objectives of this study are to: (1) compare between-method error to within method observer error, (2) test for methodological bias between SfM

and in-water visual surveys across habitats and depths, and (3) review logistical and technical strengths and weaknesses of both methods.

MATERIALS AND METHODS

In-Water Data Collection

We conducted 104 benthic surveys across eight main Hawaiian Islands between April and July 2019 (**Figure 1**). Sites were randomly selected within hard bottom habitat from 0 to 30 m and distributed across 17 sub-island sectors. These sites represent a broad range of depths (1–25 m), habitat types (aggregate reef, patch reef, pavement, rock and boulder, and rubble), coral cover, and diving conditions. At each site, an 18 m transect line was deployed along the depth contour. Visual observations were recorded within four 1 × 2.5 m segments along the transect (at 0–2.5, 5–7.5, 10–12.5, and 15–17.5 m). When dive time was limited (i.e., depths > 18 m), only three segments were surveyed. For each adult coral colony (>=5 cm in diameter), maximum diameter, ID (to lowest taxonomic level), and estimated percent old partial mortality (denuded skeleton colonized by turf or other organisms and hereafter referred to as "old dead") were recorded. Bleaching extent (% of living tissue with reduced or loss of pigmentation) and severity (1 = slight paling, 2 = significant pigmentation loss, and 3 = stark white) were also recorded. Juvenile coral colonies (<5 cm maximum diameter) were recorded within the first 1 m^2 of the first three segments. For juvenile colonies, only ID and maximum diameter were recorded. At a subset of these 104 sites, 43 haphazardly chosen segments across 28 sites were re-surveyed by a different diver to create replicate in-water observations for assessing within method observer error (**Figure 1**). Data were quality controlled in R with specific queries to identify and correct data entry errors.

Structure-From-Motion Image Collection

Structure-From-Motion image collection was conducted at each site during the in-water visual surveys described above. Scale bar markers, also known as ground control points (GCPs), were placed at the beginning of each segment at least 0.5 m away from the transect line. The depth and relative position of each GCP were recorded. JPEG imagery was collected continuously by the diver depressing the shutter of an entry level digital SLR camera (Canon EOS Rebel SL2, with Ikelite underwater housing with 6" dome port) with an 18–55 mm lens fixed at 18 mm. Prior to conducting the survey the camera was white balanced at depth with an 18% gray card. At depths of 1–20 m (**Figure 2**), SfM imagery was collected over a 3 × 20 m area and at depths > 18 m, a 3 × 13 m area was surveyed, both with the transect line running down the middle of the survey area. This imaged area allowed divers to capture the 3–4 segments discussed above as well and an adequate buffer around the segments to ensure that colonies that extended outside the segments were fully captured in the imagery. Images were taken continuously along the transect by a diver swimming back and forth with 0.5 m spacing between passes, while maintaining a 1 m distance from the seafloor. The photographer swam three passes on each side of the transect line, for a total of six passes, to produce the total image area (**Figure 2**). This swim pattern allowed for >60% side overlap and >80% forward overlap of images. Imagery was manually evaluated to ensure only quality imagery (i.e., no overexposed or blue imagery) were included in the models.

Structure-From-Motion Model Generation and Data Extraction

A 3D model from each site was generated using Agisoft Metashape software (AgiSoft Metashape Professional Version 1.6.1). The workflow sequence included aligning images, and then building and exporting the 3D dense point cloud (DPC) following parameters described by Suka et al. (2019). All DPCs were created using a Supermicro SuperServer with a Dual Xeon E5-2600 64 GB processor with 128 GB memory and eight Quardro P4000 graphics processing units. The DPC was then brought into Viscore, a visualization software (Petrovic et al., 2014), and scaled and oriented using the GCP information. The average ground sample distance (resolution/pixel) of all scaled DPC models was 0.000234 m/pix and ranged 0.000145–0.00031 m/pix. The average error was 1.227 pix and ranged 0.618–2.496 pix. These values are comparable to those reported in other coral reef SfM studies (Burns et al., 2015a,b; Suka et al., 2020). A geometrically accurate 2D/top down projection of the DPC, hereafter referred to as an orthoprojection, and a scale grid were exported from Viscore (**Figure 3**). The orthoprojection and grid were then imported into ArcMap 10.6.1 for manual colony annotation (see Suka et al., 2019 for detailed methods).

In ArcMap, each site was set up for annotation by defining the ratio of the scale of the orthoprojection using the scale grid, manually digitizing the transect and segments as a shapefile using the same sampling design as the in-water surveys, and setting up the attribute table in a geodatabase to mirror the in-water visual survey database. To record and extract data from the orthoprojection, each coral colony was annotated following the in-water visual survey methods. A total of six annotators extracted data from 104 sites. Each colony was measured by digitizing a line across the maximum diameter of the colony. Coral ID (to lowest taxonomic level), estimated percent old mortality, and bleaching extent and severity were recorded. During annotation, the original JPEG imagery was viewed alongside the orthoprojection with the Viscore Image View feature to see fine scale colony details, observe colonies from multiple angles, and locate colonies not visible in the orthoprojection (i.e., under ledges). Annotators were encouraged to speak with each other during the annotation process. In addition to this standard annotation, the subset of 43 segments across 28 sites that were replicated in-water by divers were also annotated twice by different SfM annotators to create replicate data sets for both methods. SfM data were quality controlled using a multi-stage process. Data were first quality controlled in R with specific queries to identify and correct data entry errors. Then data were summarized to the segment-level by

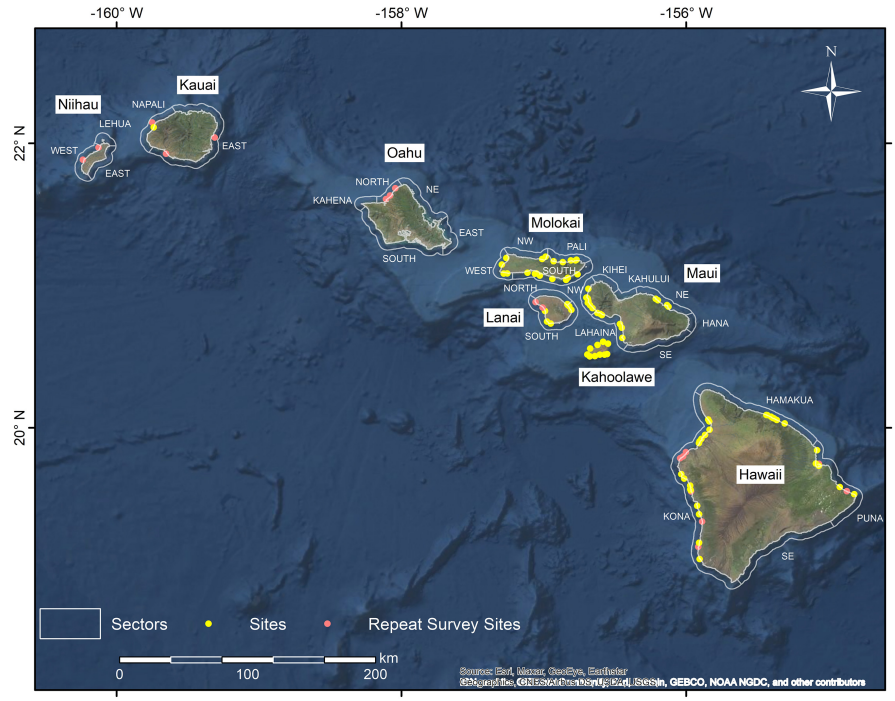

FIGURE 1 | Location of 104 survey sites (pink and yellow), sites with 28 repeated surveys indicated in pink. White outlines and labels indicate sub-island sectors.

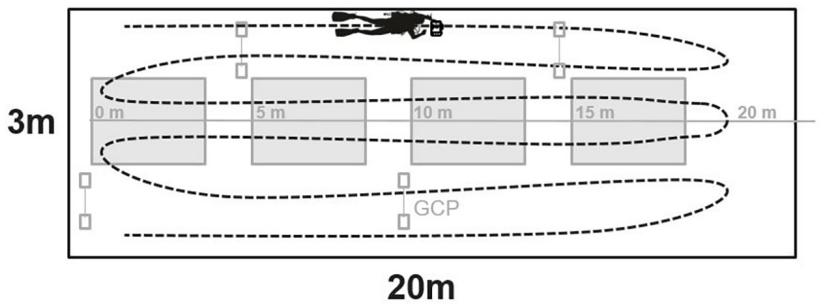

FIGURE 2 | Graphic of benthic survey plot with in-water visual survey segments (in gray). The SfM swim path is indicated by the black dashed line, covering an image area of 3 m × 20 m area. Note, at depths > 18 m, divers reduced the image survey area to 3 × 13 m. GCP, ground control point.

annotator to identify potential issues (i.e., anomalously high or low mean values for specific metrics relative to other annotators). This QC step revealed that all six annotators had issues with at least one metric, the most common being low juvenile density, high adult colony density and low bleaching prevalence. If issues were identified for a given annotator, that annotator reviewed and corrected each site if they did find errors. The third stage involved annotators reviewing a subset (10% of the annotated segments) of randomly selected segments (stratified by annotator) that they did not originally annotate and recording errors to establish individual annotator error rates for each metric. This QC step revealed that one of the annotators had an error rate of >10% for adult density due to missing colonies and four annotators had an error rate of >10% for juvenile density due to missing colonies. All of the sites for the annotators that had error rates >10% were reviewed and corrected for the metric in question by a different annotator.

Data Analysis

All data were analyzed in R v3.6.1 (R Core Team, 2019). Seven metrics were summarized as follows: adult colony density (number of colonies ≥ 5 cm per m^2), juvenile colony density (number of colonies 0.7–4.9 cm per m^2), average maximum adult diameter, average percent old dead, bleaching prevalence (percent of colonies with a bleaching severity ≥ 2), adult species richness (number of species), and adult Shannon-Wiener diversity ($H^{'} = -\sum_{i=1}^{R} p_i \, ln \, p_i$), where p_i is the proportion of individuals belonging to the ith species at a site and R is the total number of species at a site. Colonies with bleaching severity 1 (slight paling) were not included in this analysis due

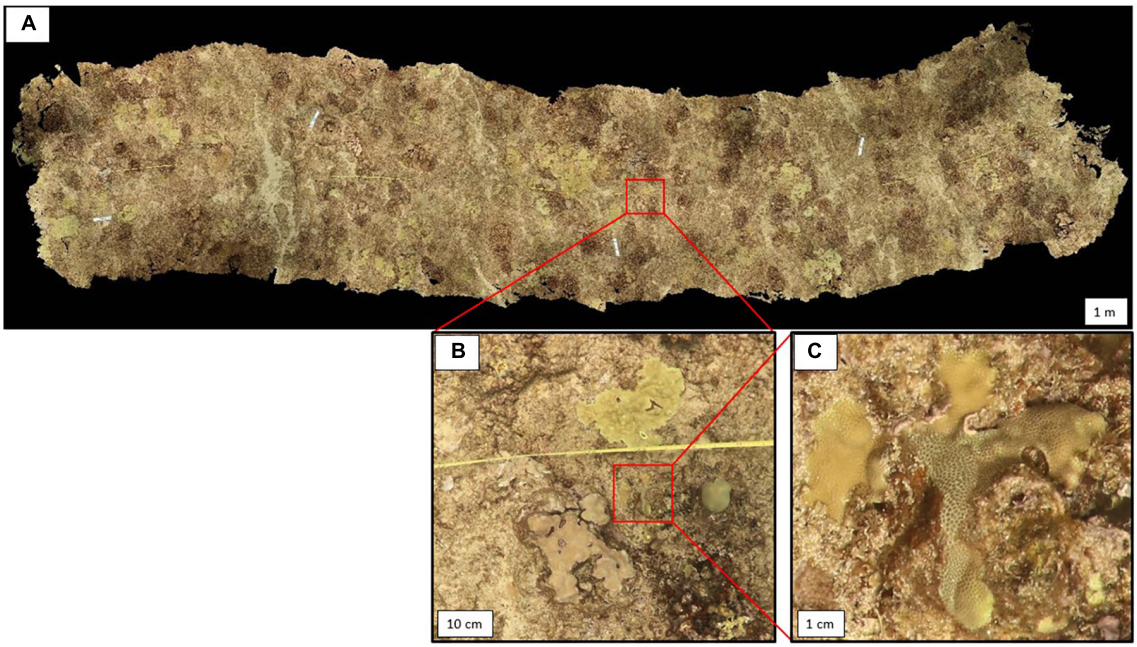

FIGURE 3 | (A) 60 m^2 orthoprojection and associated high resolution imagery **(B,C)** used to both create the orthoprojection and assist with coral colony annotation in ArcMap.

to challenges associated with identifying low levels of bleaching severity consistently across observers regardless of method type. Richness and diversity of juveniles were not calculated due to the challenges of identifying juvenile corals to the species level using either methods.

To compare error between methods to within method observer error for the seven metrics, data were summarized at the segment-level for all scleractinians combined. The identities of observers within each method were randomly assigned to observer "1" or "2" (i.e., Diver 1 vs. Diver 2, SfM 1 vs. SfM 2). Therefore, comparisons between observers within a method highlight general variation among multiple observers, but do not reflect the tendencies of a single, human observer. Error was calculated as the absolute difference in values (between methods or observers) divided by overall mean and then scaled from 0 to 1 so that we could compare the relative level of error across metrics (termed "midpoint scaled mean absolute error"). Error was calculated for three different types of comparisons for the 43 paired segments repeatedly sampled by both SfM and in-water methods. "Diver observer error" represents the difference between divers for a given demographic metric (**Supplementary Figure 1A**). "SfM observer error" represents the difference in error for a given metric between SfM annotators (**Supplementary Figure 1B**). "Method Error" is the difference between methods for all possible combinations of method x observer divided by the mean difference across all method x observer comparisons for a given metric (**Supplementary Figure 1C**). We summarize each of these error distributions using the mean and standard error of the mean. We used nonparametric Kruskal–Wallis tests and Dunn's post hoc tests with Benjamini and Hochberg multiple test corrections to test for differences between the three errors because metrics did not meet assumptions of normality and equal variance.

To test for differences between methods in the coral metrics, data were summarized at the site-level at 104 sites that were surveyed by one diver and one SfM annotator. Data were pooled to the site-level because this is the lowest spatial resolution typically summarized using NCRMP data. Within a site, only segments that were surveyed in both methods were included and then pooled to the site-level. Results are presented for the seven metrics for total scleractinian corals combined and for adult and juvenile density of the three dominant coral genera (*Porites, Montipora,* and *Pocillopora*). Each metric was tested for normality and equal variance. Measures of adult density, juvenile density, and average old partial mortality were square root transformed. Average colony diameter and *Porites* adult and juvenile density were log transformed. Richness and diversity met assumptions of normality and equal variance. 1:1 plots with a linear regressions were used to compare and visualize in-water and SfM-generated estimates for each metric. Root mean squared error (RMSE) was used to evaluate the level of error between methods and was calculated as follows: $\mathrm{RMSE} = \sqrt{\sum_{i=1}^{n} \frac{(y_i - x_i)2}{n}}$; where y_i is the in-water metric value for a given site, x_i is the SfM-generated metric value for a given site and n is the total number of sites. For each of these metrics, we established a series of linear mixed effects models (LMMs) to test effect of: method, method × habitat, and method × maximum depth. These variables were treated as fixed effects and sub-island sector was treated as a random effect. To assess the significance of fixed effects, we refit each model using maximum

likelihood estimation (ML) and applied likelihood ratio tests (LRTs) (Zuur et al., 2009). Fixed effects that were not significant were sequentially dropped from models. The resulting best-fit models were refit using REML in order to estimate the fixed-effects parameters and associated effect sizes. Bleaching prevalence, *Montipora* density, and *Pocillopora* density could not be transformed because standard transformations failed to result in distributions that met assumptions of normality and equal variance and therefore were only tested for overall difference between methods using nonparametric Wilcoxon Rank Tests for each metric.

To determine whether we had adequate sampling to detect significant methodological bias, we ran power analyses for each of the metrics assuming a two-tailed *t*-test, the standard deviation of the untransformed or transformed metric (see transformation type above), power of 0.8, $\alpha = 0.05$, and an N from 3 to 350 samples. On each of the resulting curves, we selected the observed sample size (102–104) and compared it to the calculated mean absolute error (MAE), which is the mean absolute difference between methods.

RESULTS

How Does Methodological Error Compare to Observer Error?

To determine whether the absolute difference between methods is greater or smaller than the difference between observers, we compared the level of method error to both kinds of observer error across the subset of 43 segments surveyed by two in-water divers and two SfM annotators (**Figure 4**). For adult density, diver observer error was significantly higher than SfM error, but was not different from method error (**Figure 4** and **Supplementary Table 1**). Similarly, for average colony diameter, there was no difference between diver error and method error, but SfM observer error was significantly lower than the other

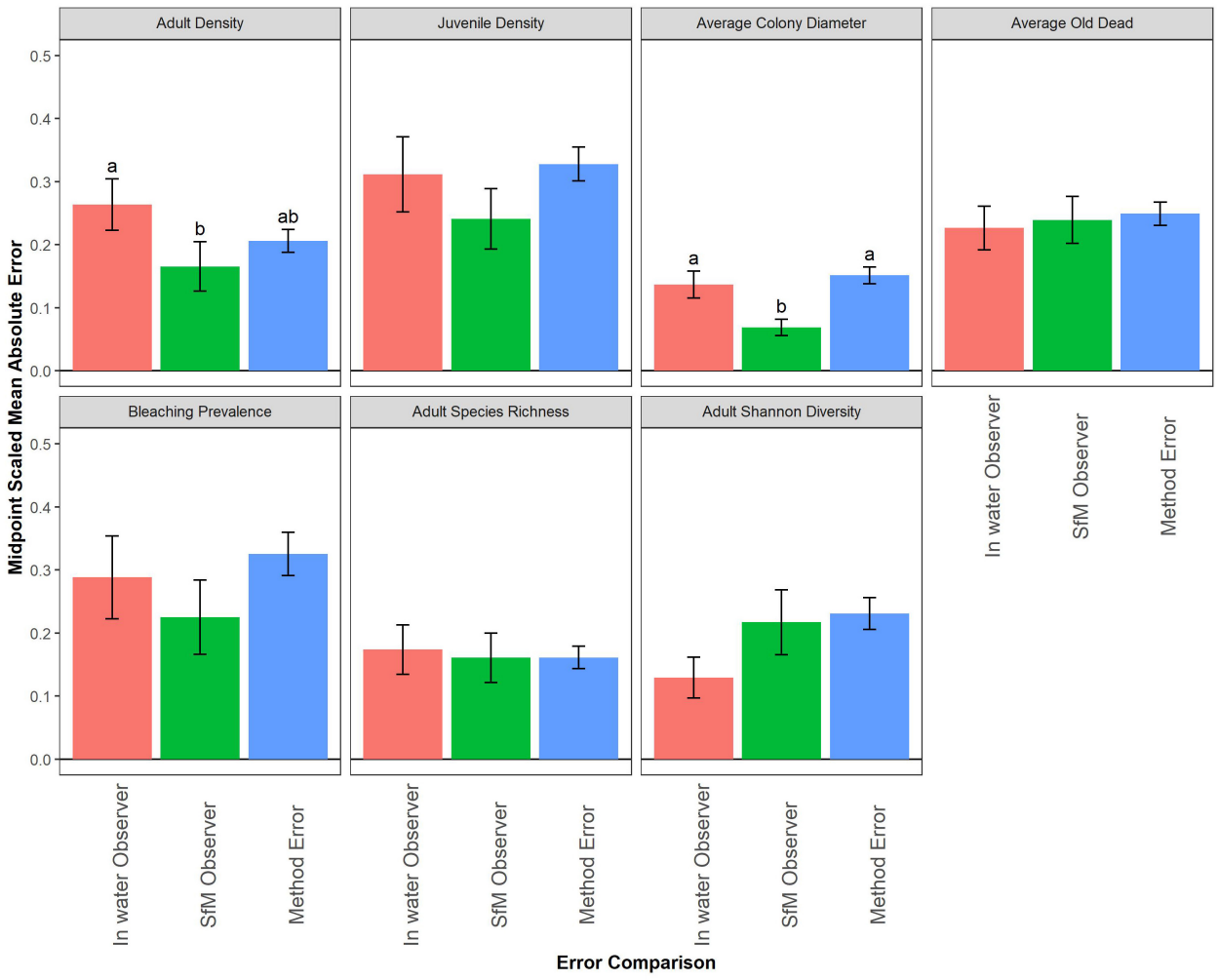

FIGURE 4 | A Comparison of the in-water observer error (difference between divers; red) and structure-from-motion (SfM) observer error (difference between SfM annotators; green) to method error (difference between methods; blue) for each coral demographic metric. *Letters*, when present, denote significant differences among error types based on post hoc tests for each metric using Dunn's tests with Benjamini and Hochberg multiple test corrections (adjusted $\alpha = 0.05$).

error comparisons (**Figure 4** and **Supplementary Table 1**). These results suggest that the difference between methods for adult density and colony diameter were just as variable as what we normally see between divers underwater, but SfM annotators were more consistent in scoring than divers. For the other metrics there was no significant difference between the three error types.

Overall, this suggests that while there may be variability between methods, it is consistent with the level of variability we have between divers. The probability distributions of the metrics show only minor variation (especially for old dead, maximum colony diameter and bleaching prevalence) in the general shape of the distribution among observers/methods across all metrics (**Supplementary Figure 2**). The density metrics and average colony length each show substantial right skew, while average old dead, adult species richness, and adult species diversity all show the least skewed distributions. Bleaching prevalence showed dominance by zero values (i.e., zero-inflation) with a scattering of positive values.

Is There a Methodological Bias in Coral Demographic Metrics at the Site-Level?

At the site-level, adult colony density was strongly correlated between methods with a low root mean square error (RMSE) and more variability above 15 colonies/m^2 (**Figure 5A**). We did not detect a significant methodological difference (**Figure 5B** and **Supplementary Table 2**), nor was there a significant interaction between method and habitat (**Supplementary Figure 3A** and **Supplementary Table 2**), or method and depth (**Supplementary Figure 3B** and **Supplementary Table 2**).

Juvenile colony density was strongly correlated between methods with a low RMSE (**Figure 5C**). It does appear that SfM may be slightly underestimating juveniles relative to in-water surveys at higher densities, although we did not detect a significant methodological difference (**Figure 5D** and **Supplementary Table 2**). More observations are needed at higher densities to resolve this. Juvenile density did not vary significantly as a function of method and habitat (**Supplementary Figure 3C** and **Supplementary Table 2**). While there was no significant interaction of method and depth, SfM annotators recorded slightly higher juvenile density with increasing depth, with predicted SfM juvenile density approximately 6 colonies/m^2 higher than in-water surveys at deep sites (**Supplementary Figure 3D** and **Supplementary Table 2**).

Adult average maximum diameter was strongly correlated with a low RMSE between methods (**Figure 5E**) and we did not detect a significant methodological difference (**Figure 5F** and **Supplementary Table 2**). There was no significant interaction of method and habitat (**Supplementary Figure 3E** and **Supplementary Table 2**), nor was the interaction of method and depth significant (**Supplementary Figure 3F** and **Supplementary Table 2**).

Average percent old dead was only moderately correlated with a high RMSE between methods (**Figure 5G**). SfM percent old partial mortality was significantly higher than in-water (**Figure 5H** and **Supplementary Table 2**). Although SfM percent old dead was higher than diver old dead in patch reef habitats, the interaction of method and habitat was not significant (**Supplementary Figure 3G** and **Supplementary Table 2**). There was no significant interaction between method and depth (**Supplementary Figure 3H** and **Supplementary Table 2**).

Bleaching prevalence was moderately correlated between methods with a higher RMSE (**Figure 5I**). SfM annotators recorded significantly higher bleaching compared to divers (**Figure 5J** and **Supplementary Table 2**). When considering each habitat separately, SfM bleaching prevalence was significantly higher than diver prevalence on aggregate reefs and prevalence did not vary between methods for the other habitats (**Supplementary Figure 3I** and **Supplementary Table 2**). Prevalence was similarly correlated with depth for both SfM (Spearman rho = 0.07) and in-water methods (Spearman rho = 0.08), suggesting that there is no interaction of method and depth (**Supplementary Figure 3J**).

For all three of the dominant coral genera in the main Hawaiian Islands, adult colony density was strongly correlated between methods, with the greatest correlation observed in *Pocillopora* (**Supplementary Figures 4A–C**). Adult density did not vary significantly between methods for any of the dominant genera (**Supplementary Figures 4D–F** and **Supplementary Table 2**). However, it does appear that divers may be underestimating adult *Porites* relative to SfM annotators at densities > 10 colonies/m^2 and there was more variability between methods for *Montipora* densities > 10 colonies/m^2 (**Supplementary Figures 4A,B**).

Juvenile colony density of the three dominant genera were moderately to strongly correlated between methods, with the weakest correlation observed in *Montipora* (**Supplementary Figures 5A–C**). SfM annotators observed significantly more juvenile *Porites* than divers, particularly at sites with low juvenile density (**Supplementary Figure 5D** and **Supplementary Table 2**). While *Montipora* and *Pocillopora* juvenile density was slightly lower for SfM compared to divers, we did not detect a significant difference between methods (**Supplementary Figures 5E,F** and **Supplementary Table 2**).

Adult species richness and Shannon-Wiener species diversity were strongly correlated between methods with a low RMSE (**Figures 6A,C**). It does appear that SfM may be slightly underestimating richness and diversity relative to in-water methods, although we did not detect a significant methodological difference (**Figures 6B,D**). Richness and diversity did not vary significantly by method x habitat (**Supplementary Figures 6A,C** and **Supplementary Table 2**), nor method × depth (**Supplementary Figures 6B,D** and **Supplementary Table 2**).

Differences across methods for five of the seven total scleractinian metrics and five of the six dominant genera metrics showed no significant difference from zero (**Figures 5,6** and **Supplementary Figures 4, 5**) and overall, the between-method error (MAE) was very low for all metrics (**Supplementary Figures 7, 8**). The power analysis (**Supplementary Figures 7, 8**) suggests that we have an adequate sample size to detect a significant difference between methods, especially as six of the seven observed MAEs for total scleractinians and three of the six dominant taxa metrics show non-significant estimates at or above our power analysis effect size. This suggests that the consistent

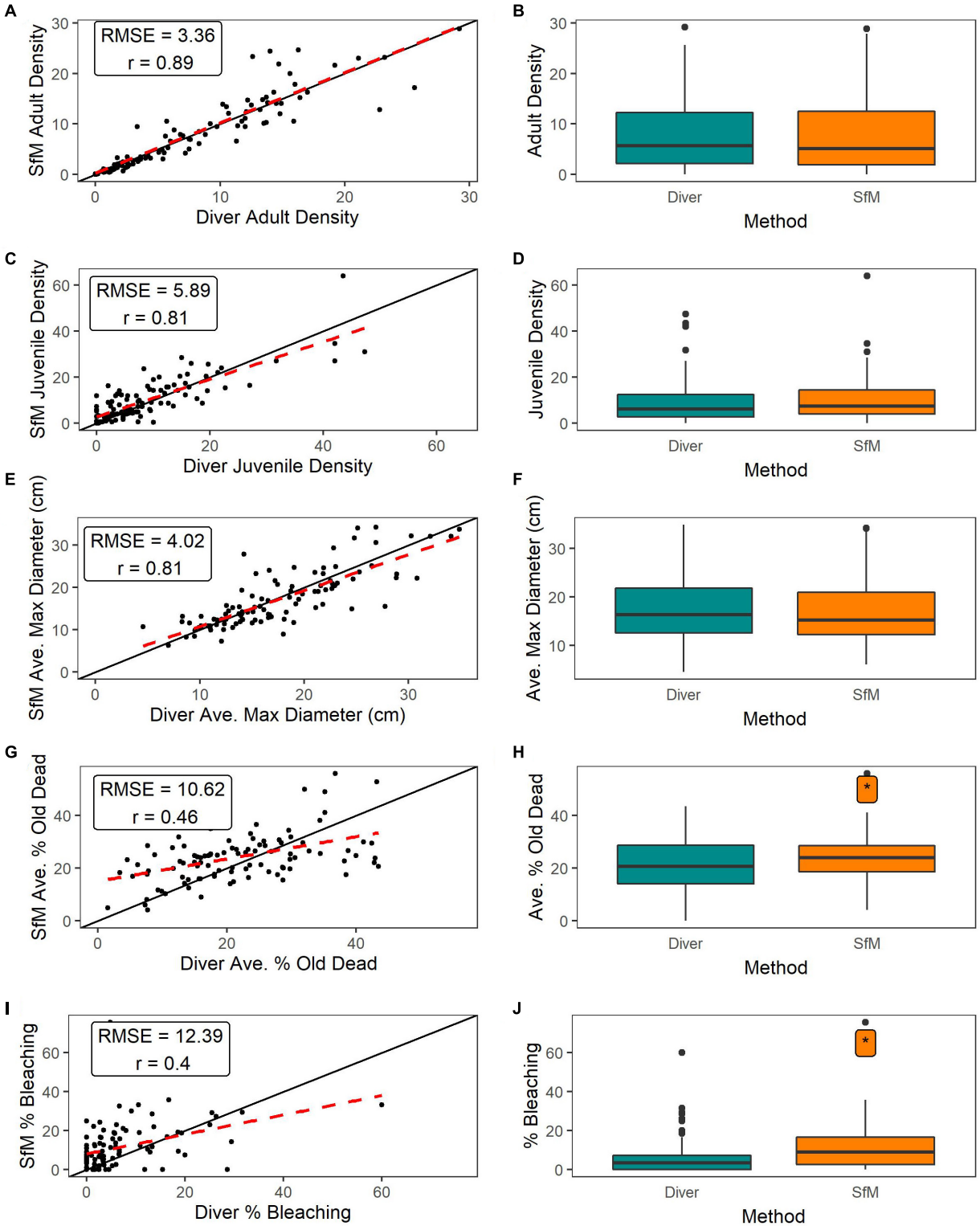

FIGURE 5 | (A,C,E,G,I) 1:1 Plots of the paired site-level SfM versus diver data for adult colony density, juvenile colony density, average adult maximum diameter, average adult colony percent old partial mortality, and bleaching prevalence, respectively (points). Black line is 1:1 line, red dashed line is linear regression line for all 1:1 plots. **(B,D,F,H,J)** Boxplots of site-level data by method type for adult colony density, juvenile colony density, average adult maximum diameter, average adult colony percent old partial mortality, and bleaching prevalence, respectively. Asterisk, when present, indicates significant difference between methods based on LMMs and LRTs **(B,D,F,H)** and nonparametric Wilcoxon Test **(J)** ($\alpha = 0.05$).

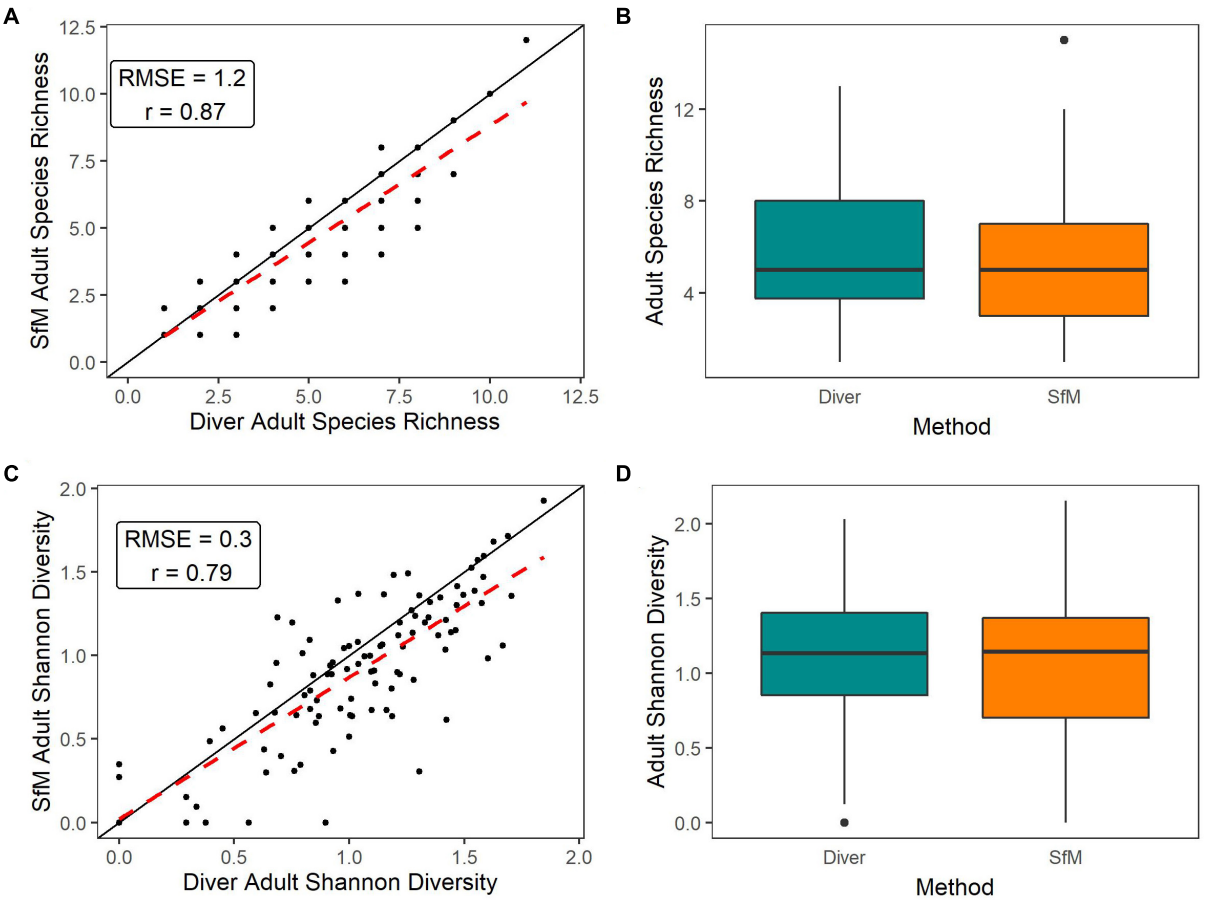

FIGURE 6 | (A,C) 1:1 Plots of the paired site-level (points) SfM versus Diver data for adult species richness and adult Shannon-Wiener diversity, respectively. Black line is the 1:1 line, red dashed line is the linear regression line between methods. **(B,D)** Boxplots of site-level data by method type for adult species richness and adult Shannon-Wiener diversity, respectively. No significant between methods was detected using LMMs and LRTs ($\alpha = 0.05$) **(B,D)**.

pattern of small and non-significant differences between methods is not due to a lack of statistical power, but instead due to well-supported similarities in the results across methodologies.

DISCUSSION

Understanding the scale of threats to coral reefs and implementing timely management strategies to slow degradation has motivated the scientific community to explore SfM as a tool for expanding the scale of reef monitoring and improving the efficiency of field data collection by replacing visual surveys. Our results suggest that there is little evidence of consistent methodological bias between in-water collection and SfM imagery in the metrics included in this study.

Most Metrics Show Low Methodological Bias

Overall, our results suggest that adult colony density, average colony diameter, species richness and species diversity were strongly correlated between methods and did not vary significantly between methods across habitats or depths (**Figures 5**, **6** and **Supplementary Figures 3, 6**). While this is the first study comparing in-water to SfM generated data for these metrics, several studies have conducted similar comparative analysis of density and richness using visual surveys and other imagery based methods. Contrary to our results, Page et al. (2016) found that colony density was inflated in 2D photoquadrat images compared to in-water surveys because colony bases of branching colonies were often obscured in the 2D images and continuity of tissues between branches could not be confirmed, leading annotators to assume that each branch was a physiologically discrete colony. However, similarly to our study, Jokiel et al. (2015) found that coral species richness was similar between in-water visual methods (i.e., point intercept transect and quadrats) and imaging methods such as video and photoquadrats. These studies highlight that while photoquadrat imagery may be appropriate for quantifying diversity in low diversity systems, SfM's ability to capture the reef from a variety of angles provides a significant improvement over standard photoquadrat methods.

Quantifying juveniles can be challenging given their small size and cryptic nature, sometimes preferring crevices and vertical surfaces to exposed substrates (Babcock and Mundy, 1996; Edmunds et al., 2004). For these reasons, we hypothesized that SfM may underestimate juvenile density. However, our results indicate that density was strongly correlated between methods and there was no significant difference for all taxa combined between methods, nor between methods across habitats and depths. These results are not consistent with previous studies that found that photoquadrat methods significantly underestimate juvenile density compared to in-water observations (Edmunds et al., 1998; Burgess et al., 2010), which the authors attribute to juvenile colonies growing in cryptic microhabitats. These conflicting results may be partly due to the fact that Burgess et al. (2010) only quantified juveniles < 0.5 cm diameter where our study quantified juveniles between 0.7 and 4.9 cm. While juveniles < 0.7 cm could often be detected using SfM in our study, we did not include them due to the challenges of consistently identifying these smaller size classes regardless of method. Our results indicate that it is important to consider the size range of juveniles when comparing across studies and methods, but also indicate that SfM is able to capture many of the cryptic habitats that are not visible using two dimensional photoquadrat images commonly used by many monitoring programs. In addition, significant improvements in digital camera technology and image resolution since these earlier studies were conducted may have also contributed to differing results. Juvenile colony density for *Porites* among SfM observers was significantly higher than recorded by divers. *Porites* juveniles tend to be more inconspicuous than other juvenile taxa, often blending in with the substrate due to their muted color and low profile. In fact, when we evaluated the quality of SfM annotations, the most common issue across all annotators was missing juveniles. While we were able to review and correct this in the SfM dataset, we were not able to correct missing juveniles in the in-water dataset.

Metrics that rely on direct counts or measurements (such as colony density and size) were more strongly correlated between methods than metrics that rely on visual estimates of extent (such as percent partial mortality). Specifically, old dead was significantly higher using SfM compared to in-water methods, but did not vary significantly between methods across habitats and depths. However, the absolute difference in old mortality estimates between methods (MAE) was low, i.e., only 1.27% (**Supplementary Figure 7**) relative to the overall mean of 23% averaged across both methods. One possible explanation for the higher levels of partial mortality in SfM is that with unlimited "bottom time", annotators have more time to review colonies and record lower levels of partial mortality (especially below 20%) than divers who may be more likely to miss low levels. SfM annotators may also be underestimating mortality on branching colonies where it is difficult to see the bases of colonies.

Estimating old partial mortality can be challenging due to the coarse nature of this metric (recorded in 5% increments) and the challenges identifying colony boundaries consistently across observers. Identifying the boundaries of colonies is a fundamental challenge of these types of demographic surveys regardless of whether surveys are conducted underwater or behind a computer. As colonial organisms, corals can fragment into tissue patches. Our methods dictate that observers identify colonies by lumping together tissue fragments of a similar color and morphology on the same skeletal structure into one colony (Winston et al., 2020). Enumerating and sizing colonies can also be challenging when partial mortality is not recent and colonies are densely aggregated, likely explaining why we observed higher variability between methods at higher colony densities and larger mean colony diameter (**Figure 4**). Fragmentation is also especially common for taxa such as *Porites* and *Montipora,* resulting in difficulty distinguishing between tissue fragments and sexual recruits. Despite significant diver and annotator training, this variability is likely partially explained by variability between observers. The role of observer error in these patterns is supported by the fact that we reported that variability between divers in adult density and adult maximum diameter is comparable to differences between methods (**Figure 4**). The challenges of identifying colonies and recording demographic information are most certainly not unique to our program. Monitoring programs can continue to improve the quality of their datasets by more rigorous training and quantitative calibration of field staff. In addition, with lower error between observers (**Figure 4**) and the ability to virtually revisit plots, SfM may provide an opportunity to reduce observer error more effectively than visual surveys.

With increasing severity and frequency of mass coral bleaching events, many monitoring programs are looking to quantify coral bleaching over large areas using digital imagery (Lafratta et al., 2017; Levy et al., 2018; Fox et al., 2019; Ritson-Williams and Gates, 2020). In our study, bleaching prevalence was significantly higher in SfM compared to in-water assessments with an MAE of 8.07%. However, care should be taken when interpreting bleaching MAE as data were highly zero-inflated. As this phenomenon was particularly noticeable on aggregate reefs, one possible explanation for this pattern is that aggregate reefs generally have higher colony density, which means that divers, with limited bottom time to conduct surveys, are more task loaded and may be prone to overlooking low to moderate levels of bleaching. It is also possible that imagery from some sites may have appeared slightly overexposed, leading to overestimation of bleaching in SfM. However, we expect the effects of overexposure to be minimal because cameras were white balanced at depth, imagery was rigorous quality controlled, and all SfM annotators used the same monitors and settings. Our results differ slightly from previous studies that found bleaching estimates did not differ between in-water and photoquad (Page et al., 2016) or SfM surveys (Burns et al., 2020). Previous studies were conducted on a very limited number of shallow homogenous sites; therefore, it is unsurprising that our results differ given that we surveyed 104 sites distributed across a large range of depths, turbidity, lighting, and habitats. Our study was also conducted during the early stages of the 2019 Hawaii bleaching event, and although severe bleaching is easy to identify, low to moderate levels that were more common during the time of these surveys

were more challenging to quantify consistently. While SfM annotators could discuss bleaching levels and revise annotations, divers were unable to do this underwater and may have been more conservative.

Strengths and Weaknesses of SfM and In-Water Surveys

Both in-water and SfM survey methods have a variety of strengths and weaknesses for coral demographic and community surveys (**Table 1**), and which method to choose depends on the research question, the timeline for data dissemination, and logistical constraints of the survey. Similar to Burns et al. (2020), our study highlights that there may not be a "gold standard" for colony-level surveys, and observed methodological differences can highlight deficiencies in either method. In-water surveys allow divers to look at corals at the polyp-level from all possible angles, which is important for observing taxa located in crevices, under overhangs, or covered by sand or algae. It also allows scientists to exit the water with data that require minimal post-processing, resulting in summarized data on the order of weeks to months. However, in-water monitoring also has several weaknesses. Surveys generally require more field effort. For example, our program's in-water assessments require 45–60 min with a three-person team to complete one site. Given the longer dive time and the number of metrics collected underwater, it can be more strenuous to survey in poor conditions and diver fatigue can impact data quality. With limited bottom time, measurements of size and habitat complexity are generally measured or estimated at coarse levels, and the reef area that can be surveyed by divers is often reduced or requires two dives when surveying deeper reefs. Lastly, visual survey data does not allow divers to verify or re-evaluate the benthos, which can lead to unmitigated observer error.

TABLE 1 | Comparison of in-water and SfM strengths and weaknesses.

Metric	In-water	SfM
Data extraction	Quick	Lengthy
Permanent visual record	No	Yes
Survey team needed (# of divers)	Moderate (3)	Small (2)
Benthic training needed	Yes	Yes
Survey in poor conditions	Difficult and strenuous	Moderate to easy
Bottom time	30 min to 1 h	10–25 min
Cryptic corals	Often easier to identify	Sometimes difficult to see
Sizing	Accurate	Highly accurate
Species Identification	Relatively easy	More difficult for some species
Visual observation	3D in-water	2D image
Data verification and re-evaluation	No	Yes
Area surveyed	Limited by bottom time	Limited by area imaged by diver
Complexity metrics	Estimated and generalized	Accurate and detailed
Computing requirements	CPU: Intel Core i5	CPU: Dual Xeon E5-2600
	Storage: 500 GB	Storage: 6x2TB
	Memory: 8 GB RAM	Memory: 8x16GB RAM
	Graphics: NA	Graphics: 8x Quardro P4000

The computing hardware listed for SfM is preferred for processing >30 models of 3 × 20 m (four models generated per day). A computer with an Intel Xenon 8 core processor, 1TB of storage, 64 GB of RAM, and dual NVIDIA Quadro P4000 Graphics would be sufficient for processing >30 models of 3 × 20 m (two models generated per day).

Conducting SfM surveys in the field is generally more time efficient depending on the size and shape of the plot, which reduces field costs. For example, our program requires 15–20 min with two divers to complete a 3 × 20 m SfM belt survey, compared to a 45–60 min with three divers for an in-water survey. Overall when comparing the total time needed to collect data during a NCRMP survey mission, SfM reduced field time by 55%. While we did not measure habitat complexity in this study, other studies have found that SfM allows scientists to more accurately quantify reef complexity compared to common in-water methods such as "chain and tape" or visual estimates (Storlazzi et al., 2016; Bayley et al., 2019). Contrary to in-water methods, SfM annotators are not limited by time, can take breaks when fatigued, and the area sampled is only limited by the extent of the reef that is imaged. Annotators also have the opportunity to converse during data recording to improve consistency, thus reducing observer error. The SfM method allows, for the first time, the ability to use a more comprehensive quality control process, produce statistically robust error rates and correct observer error by revisiting the imagery. Finally, with SfM the survey provides a permanent visual record, allowing for additional metrics to be extracted in future projects.

One of the primary weaknesses of SfM for colony-level surveys is the time it takes to extract data from the imagery, which is on the order of months to a year depending on the number of sites, annotators, and access to computational resources, leading to delays in data dissemination. For example, in this study, an average of 9 h of hands-on time was needed to generate 3D and 2D products, manually annotate, and QC data per site (most was manual annotation). In addition to the significant manual annotation time, SfM also requires a substantial investment in hardware such as digital cameras, software, and GPU-accelerated computers to process models efficiently. Another weakness is that annotators are limited by the quality and coverage of the imagery. If the imagery is poor quality or has poor overlap then it may be difficult to achieve polyp-level detail or fully capture all of the colonies. This can make species and coral health identification challenging. Even with good image coverage, SfM cannot capture all of the surfaces that divers can assess in in-water surveys. Therefore, it may also be appropriate to consider a hybrid of in-water and SfM to capture more polyp-level detail and balance in-field and annotation costs. While the time needed to implement each stage of these methods will vary in accordance with the experience of the individual and complexity of the reef, a

comparison of the average time to execute each stage of the *in situ* versus SfM surveys can be found in Couch et al. (2021; see **Table 2**).

Future Directions

Our study provides compelling evidence that with careful consideration to how imagery is collected, SfM may increase efficiency in the field and access to a wealth of other types of data such as habitat complexity, urchin density, and coral growth rates. Our study also highlights that SfM provides an opportunity to more rigorously quantify and mitigate inter-observer error, thus improving our ability to detect smaller changes in the benthos. While SfM provides a powerful tool to reimagine how we study and manage coral reefs, it may not be the best fit for every program and practitioners should carefully weigh the strengths and weaknesses of standard in-water and SfM survey methods. Addressing SfM's weaknesses outlined above and making this approach more broadly accessible will require a series of steps.

To maximize data quality and utility of SfM, it is paramount that divers prioritize the collection of quality imagery using guidelines such as those described by Suka et al. (2019). Collecting properly color balanced and sharp images is the foundation for quality annotations and derived data products. In addition, shooting from more than one angle allows divers to capture colonies on vertical or concave surfaces and reduce gaps in the model. This may be especially important in habitats with high complexity.

One of the largest hurdles to overcome with SfM is the significant annotation and post-processing time/resources necessary to extract data. The rapidly expanding field of artificial intelligence (AI) has the potential to significantly reduce the amount of human interaction time required to extract data from SfM imagery. While AI tools are potentially revolutionary for scaling up coral reef monitoring, they cannot fully replace humans and tools should continue to leverage human expertise by employing "human-in-the-loop" approaches. This challenge is currently being tackled for coral reef monitoring using a variety of approaches such as CoralNet, a widely used machine-learning image analysis tool for point classification (Beijbom et al., 2015); an encoder-decoder convolutional neural network (CNN) for semantic segmentation leveraging human annotated sparse points (Alonso et al., 2017); TagLab, an interactive semantic segmentation tool that integrates CNN results and previous human labeling (Pavoni et al., 2019); the use of bounding boxes to more efficiently identify benthic features for humans to annotate (Mandel et al., 2019; Modasshir and Rekleitis, 2020); NemoNet, a CNN approach with a citizen-scientist videogame to generate training data and segment benthic features (Chirayath and Li, 2019); and AI challenges that invite computer scientists to develop completely novel automated solutions to delineation (Ionescu et al., 2019). While 2D orthoprojections are still the "industry-standard" for SfM work, annotating natively in 3D will provide more accurate assessments of structure, vital rates, and diversity, especially in dense, structurally complex reefs. These advances will help move annotation from a mostly hands-on, time-intensive approach to a semi-automated workflow, and shifts annotation from 2D to 3D space. The hardware and software investment needed to generate the DPCs, 2D products and derived benthic metrics efficiently may exceed the means of most small monitoring programs. To address this challenge, current SfM practitioners should identify opportunities to develop infrastructure for cloud processing, data sharing and data storage.

DATA AVAILABILITY STATEMENT

The datasets presented in this study can be found in online repositories. The names of the repository/repositories and accession number(s) can be found at: https://www.fisheries.noaa.gov/inport/item/36164 and https://www.fisheries.noaa.gov/inport/item/63097.

AUTHOR CONTRIBUTIONS

CC was the project manager and was responsible for all aspects of this study from project inception, data collection, data analysis, data management, and writing. TO and RS contributed to project inception, data collection, data analysis, data management, and writing. ML, MA, CA, FL, and AH were responsible for image post processing/annotation and the manuscript review. BV-Á, MW, BH, and AG assisted with data collection in the field and the manuscript review. JG assisted with data collection in the field. JS assisted with the manuscript review and overall project management. All authors contributed to the article and approved the submitted version.

FUNDING

This work was funded by the NOAA Coral Reef Conservation Program, as part of the Pacific-National Coral Reef Monitoring Program.

ACKNOWLEDGMENTS

We would like to thank Raymond Boland, Noah Pomeroy, and the crew of the NOAA vessel Oscar Elton Sette for providing field support during the main Hawaiian Islands Rapid Assessment and Monitoring Cruise. We would also like to thank Michael Akridge, Brooke Olenski, Kevin Trick, and Annette DesRochers for assistance with development and maintenance of the data management pipeline. We also thank Stuart Sandin, John Burns, Nicole Pederson, Vid Petrovic, and Clinton Edwards for support with field testing, methods development and implementation of SfM.

SUPPLEMENTARY MATERIAL

The Supplementary Material for this article can be found online at: https://www.frontiersin.org/articles/10.3389/fmars.2021.647943/full#supplementary-material

REFERENCES

Alonso, I., Cambra, A., Muñoz, A., Treibitz, T., and Murillo, A. C. (2017). "Coral-segmentation: training dense labeling models with sparse ground truth," in *Proceedings - 2017 IEEE International Conference on Computer Vision Workshops, ICCVW 2017*, (Venice), doi: 10.1109/ICCVW.2017.339

Babcock, R., and Mundy, C. (1996). Coral recruitment: consequences of settlement choice for early growth and survivorship in two scleractinians. *J. Exp. Mar. Bio. Ecol.* 206, 179–201. doi: 10.1016/S0022-0981(96)02622-6

Baskett, M. L., Fabina, N. S., and Gross, K. (2014). Response diversity can increase ecological resilience to disturbance in coral reefs. *Am. Nat.* 184, E16–E31. doi: 10.1086/676643

Bayley, D. T. I., Mogg, A. O. M., Koldewey, H., and Purvis, A. (2019). Capturing complexity: field-testing the use of "structure from motion" derived virtual models to replicate standard measures of reef physical structure. *PeerJ* 7:e6540. doi: 10.7717/peerj.6540

Beijbom, O., Edmunds, P. J., Roelfsema, C., Smith, J., Kline, D. I., Neal, B. P., et al. (2015). Towards automated annotation of benthic survey images: variability of human experts and operational modes of automation. *PLoS One* 10:1–22. doi: 10.1371/journal.pone.0130312

Bruno, J. F., and Selig, E. R. (2007). Regional decline of coral cover in the indo-pacific: timing, extent, and subregional comparisons. *PLoS One* 2:e711. doi: 10.1371/journal.pone.0000711

Bryson, M., Ferrari, R., Figueira, W., Pizarro, O., Madin, J., Williams, S., et al. (2017). Characterization of measurement errors using structure-from-motion and photogrammetry to measure marine habitat structural complexity. *Ecol. Evol.* 7, 5669–5681. doi: 10.1002/ece3.3127

Burgess, S. C., Osborne, K., Sfiligoj, B., and Sweatman, H. (2010). Can juvenile corals be surveyed effectively using digital photography: implications for rapid assessment techniques. *Environ. Monit. Assess.* 171, 345–351. doi: 10.1007/s10661-009-1282-1

Burns, J., Delparte, D., Gates, R., and Takabayashi, M. (2015a). Integrating structure-from-motion photogrammetry with geospatial software as a novel technique for quantifying 3D ecological characteristics of coral reefs. *PeerJ* 3:e1077. doi: 10.7717/peerj.1077

Burns, J. H. R., Delparte, D., Gates, R. D., and Takabayashi, M. (2015b). "Utilizing underwater three-dimensional modeling to enhance ecological and biological studies of coral reefs," in *Proceedings of the International Archives of the Photogrammetry, Remote Sensing and Spatial Information Sciences - ISPRS Archives*, (Piano di Sorrento), doi: 10.5194/isprsarchives-XL-5-W5-61-2015

Burns, J. H. R., Weyenberg, G., Mandel, T., Ferreira, S. B., Gotshalk, D., Kinoshita, C. K., et al. (2020). A comparison of the diagnostic accuracy of in-situ and digital image-based assessments of coral health and disease. *Front. Mar. Sci.* 7:304. doi: 10.3389/fmars.2020.00304

Carleton, J. H., and Done, T. J. (1995). Quantitative video sampling of coral reef benthos: large-scale application. *Coral Reefs* 14, 35–46. doi: 10.1007/BF00304070

Casella, E., Collin, A., Harris, D., Ferse, S., Bejarano, S., Parravicini, V., et al. (2017). Mapping coral reefs using consumer-grade drones and structure from motion photogrammetry techniques. *Coral Reefs* 36, 269–275. doi: 10.1007/s00338-016-1522-0

Chirayath, V., and Li, A. (2019). Next-Generation Optical Sensing Technologies for Exploring Ocean Worlds—NASA FluidCam, MiDAR, and NeMO-Net. *Front. Mar. Sci.* 6:521. doi: 10.3389/fmars.2019.00521

Conand, C., Chabanet, P., Quod, J.-P., and Bigot, L. (1999). *Guidelines for Coral Reef Monitoring in the South-West Region of the Indian Ocean*. Mauritius: commission de l'océan indien.

Connell, J. H., Hughes, T. P., and Wallace, C. C. (1997). A 30-year study of coral abundance, recruitment, and disturbance at several scales in space and time. *Ecol. Monogr.* 67, 461–488.

Couch, C., Suka, R., Oliver, T., Lamirand, M., Asbury, M., Amir, C., et al. (2021). *Comparing Coral Demographic Surveys From in Situ Observations and Structure-From-Motion Imagery Shows Low Methodological Bias. PIFSC Administrative Report, H-21-01*. Honolulu, HI: PIFSC Administrative, doi: 10.25923/307k-fk90

De'ath, G., Fabricius, K. E., Sweatman, H., and Puotinen, M. (2012). The 27–year decline of coral cover on the Great Barrier Reef and its causes. *Proc. Natl. Acad. Sci.U.S.A.* 109, 17995–17999.

Donnelly, R., Neville, D., and Mous, P. (2003). *Report on a rapid ecological assessment of the Raja Ampat islands, Papua, Eastern Indonesia, held October 30 - november 22, 2002*. Bali: The Nature Conservancy Bali Indonesia,

Edmunds, P. J., Aronson, R. B., Swanson, D. W., Levitan, D. R., and Precht, W. F. (1998). Photographic versus visual census techniques for the quantification of juvenile corals. *Bull. Mar. Sci.* 62, 937–946.

Edmunds, P. J., Bruno, J., and Carlon, D. (2004). Effects of depth and microhabitat on growth and survivorship of juvenile corals in the Florida Keys. *Mar. Ecol. Ser.* 278, 115–124. doi: 10.3354/meps278115

Edmunds, P. J., and Elahi, R. (2007). The demographics of a 15-year decline in cover of the Caribbean reef coral *Montastraea annularis*. *Ecol. Monogr.* 77, 3–18.

Edmunds, P. J., and Riegl, B. (2020). Urgent need for coral demography in a world where corals are disappearing. *Mar. Ecol. Prog. Ser.* 635, 233–242. doi: 10.3354/MEPS13205

Edwards, C. B., Eynaud, Y., Williams, G. J., Pedersen, N. E., Zgliczynski, B. J., Gleason, A. C. R., et al. (2017). Large-area imaging reveals biologically driven non-random spatial patterns of corals at a remote reef. *Coral Reefs* 36, 1291–1305. doi: 10.1007/s00338-017-1624-3

English, S., Wilkinson, C., and Baker, V. (1994). *Survey Manual for Tropical Marine Resources*. Townsville AUS: Australian Institute of Marine Science.

Ferrari, R., Figueira, W. F., Pratchett, M. S., Boube, T., Adam, A., Kobelkowsky-Vidrio, T., et al. (2017). 3D photogrammetry quantifies growth and external erosion of individual coral colonies and skeletons. *Sci. Rep.* 7:16737. doi: 10.1038/s41598-017-16408-z

Figueira, W., Ferrari, R., Weatherby, E., Porter, A., Hawes, S., and Byrne, M. (2015). Accuracy and precision of habitat structural complexity metrics derived from underwater photogrammetry. *Remote Sens.* 7, 16883–16900. doi: 10.3390/rs71215859

Fox, M. D., Carter, A. L., Edwards, C. B., Takeshita, Y., Johnson, M. D., Petrovic, V., et al. (2019). Limited coral mortality following acute thermal stress and widespread bleaching on Palmyra Atoll, central Pacific. *Coral Reefs* 38, 701–712. doi: 10.1007/s00338-019-01796-7

Fukunaga, A., Burns, J. H. R., Pascoe, K. H., and Kosaki, R. K. (2020). Associations between benthic cover and habitat complexity metrics obtained from 3d reconstruction of coral reefs at different resolutions. *Remote Sens.* 12:1011. doi: 10.3390/rs12061011

García-Urueña, R., and Garzón-Machado, M. A. (2020). Current status of Acropora palmata and *Acropora cervicornis* in the Colombian Caribbean: demography, coral cover and condition assessment. *Hydrobiologia* 847, 2141–2153. doi: 10.1007/s10750-020-04238-6

Hernández-Landa, R. C., Barrera-Falcon, E., and Rioja-Nieto, R. (2020). Size-frequency distribution of coral assemblages in insular shallow reefs of the Mexican Caribbean using underwater photogrammetry. *PeerJ* 8:e8957. doi: 10.7717/peerj.8957

Heron, S. F., Johnston, L., Liu, G., Geiger, E. F., Maynard, J. A., De La Cour, J. L., et al. (2016). Validation of reef-scale thermal stress satellite products for coral bleaching monitoring. *Remote Sens.* 8:59.

Hoegh-Guldberg, O., Mumby, P. J., Hooten, A. J., Steneck, R. S., Greenfield, P., Gomez, E., et al. (2007). Coral reefs under rapid climate change and ocean acidification. *Science* 318, 1737–1742. doi: 10.1126/science.1152509

Houk, P., and Van Woesik, R. (2006). Coral reef benthic video surveys facilitate long-term monitoring in the commonwealth of the northern mariana islands: toward an optimal sampling strategy. *Pacific Sci.* 60, 177–189. doi: 10.1353/psc.2006.0005

Hughes, T. P., Kerry, J. T., Baird, A. H., Connolly, S. R., Dietzel, A., Eakin, C. M., et al. (2018). Global warming transforms coral reef assemblages. *Nature* 556, 492–496. doi: 10.1038/s41586-018-0041-2

Ionescu, B., Müller, H., Péteri, R., Cid, Y. D., Liauchuk, V., Kovalev, V., et al. (eds) (2019). "ImageCLEF 2019: multimedia retrieval in medicine, lifelogging, security and nature," in *Lecture Notes in Computer Science (including subseries Lecture Notes in Artificial Intelligence and Lecture Notes in Bioinformatics)*, eds F. Crestani, et al. (Cham: Springer), doi: 10.1007/978-3-030-28577-7_28

Jokiel, P. L., Rodgers, K. S., Brown, E. K., Kenyon, J. C., Aeby, G., Smith, W. R., et al. (2015). Comparison of methods used to estimate coral cover in the Hawaiian Islands. *PeerJ* 2015:e954. doi: 10.7717/peerj.954

Kodera, S. M., Edwards, C. B., Petrovic, V., Pedersen, N. E., Eynaud, Y., and Sandin, S. A. (2020). Quantifying life history demographics of the scleractinian coral

genus *Pocillopora* at Palmyra Atoll. *Coral Reefs* 39, 1091–1105. doi: 10.1007/s00338-020-01940-8

Lafratta, A., Fromont, J., Speare, P., and Schönberg, C. H. L. (2017). Coral bleaching in turbid waters of north-Western Australia. *Mar. Freshw. Res.* 68, 65–75. doi: 10.1071/MF15314

Lamb, J. B., True, J. D., Piromvaragorn, S., and Willis, B. L. (2014). Scuba diving damage and intensity of tourist activities increases coral disease prevalence. *Biol. Conserv.* 178, 88–96. doi: 10.1016/j.biocon.2014.06.027

Lange, I. D., and Perry, C. T. (2020). A quick, easy and non-invasive method to quantify coral growth rates using photogrammetry and 3D model comparisons. *Methods Ecol. Evol.* 11, 714–726. doi: 10.1111/2041-210X.13388

Levy, J., Hunter, C., Lukacazyk, T., and Franklin, E. C. (2018). Assessing the spatial distribution of coral bleaching using small unmanned aerial systems. *Coral Reefs* 37, 373–387. doi: 10.1007/s00338-018-1662-5

Loya, Y. (1972). Community structure and species diversity of hermatypic corals at Eilat, Red Sea. *Mar. Biol.* 13, 100–123. doi: 10.1007/BF00366561

Loya, Y., Sakai, K., Yamazato, K., Nakano, Y., Sambali, H., and van Woesik, R. (2001). Coral bleaching: the winners and the losers. *Ecol. Lett.* 4, 122–131.

Mandel, T., Gotshalk, D., Del Moral, N., Wilde, D., Marshall, M., Spengler, A., et al. (2019). "Balancing human and machine performance when analyzing image cover," in *Proceedings of the 6th Annual Conference on Computational Science and Computational Intelligence, CSCI 2019*, (Las Vegas, NV), doi: 10.1109/CSCI49370.2019.00125

Miller, J., Muller, E., Rogers, C., Waara, R., Atkinson, A., Whelan, K. R. T., et al. (2009). Coral disease following massive bleaching in 2005 causes 60% decline in coral cover on reefs in the US Virgin Islands. *Coral Reefs* 28, 925–937. doi: 10.1007/s00338-009-0531-7

Modasshir, M., and Rekleitis, I. (2020). "Enhancing coral reef monitoring utilizing a deep semi-supervised learning approach," in *Proceedings of the 2020 IEEE International Conference on Robotics and Automation (ICRA)*, (Paris), doi: 10.1109/icra40945.2020.9196528

Munday, P. L. (2004). Habitat loss, resource specialization, and extinction on coral reefs. *Glob. Chang. Biol.* 10, 1642–1647. doi: 10.1111/j.1365-2486.2004.00839.x

Obura, D., Aeby, G., Amornthammarong, N., Appeltans, W., Bax, N., Joe, B., et al. (2019). Coral reef monitoring, reef assessment technologies, and ecosystem-based management. *Front. Mar. Sci.* 6:580. doi: 10.3389/fmars.2019.00580

Page, C. A., Field, S. N., Pollock, F. J., Lamb, J. B., Shedrawi, G., and Wilson, S. K. (2016). Assessing coral health and disease from digital photographs and in situ surveys. *Environ. Monit. Assess.* 189:18. doi: 10.1007/s10661-016-5743-z

Pandolfi, J. M., Connolly, S. R., Marshall, D. J., and Cohen, A. L. (2011). Projecting coral reef futures under global warming and ocean acidification. *Science* 333, 418–422. doi: 10.1126/science.1204794

Pavoni, G., Corsini, M., Palma, M., and Scopigno, R. (2019). "A validation tool for improving semantic segmentation of complex natural structures," in *Eurographics*, eds C. Paolo and M. Eder (Ginevra: Eurographics Association), doi: 10.2312/egs.20191014

Pedersen, N. E., Edwards, C. B., Eynaud, Y., Gleason, A. C. R., Smith, J. E., and Sandin, S. A. (2019). The influence of habitat and adults on the spatial distribution of juvenile corals. *Ecography (Cop.)* 42, 1703–1713. doi: 10.1111/ecog.04520

Petrovic, V., Vanoni, D., Richter, A., Levy, T., and Kuester, F. (2014). Visualizing high resolution three-dimensional and two-dimensional data of cultural heritage sites. *Mediterr. Archaeol. Archaeom.* 14, 93–100.

Pollock, F. J., Lamb, J. B., Field, S. N., Heron, S. F., Schaffelke, B., Shedrawi, G., et al. (2014). Sediment and turbidity associated with offshore dredging increase coral disease prevalence on nearby reefs. *PLoS One* 9:e102498. doi: 10.1371/journal.pone.0102498

Preskitt, L. B., Vroom, P., and Smith, C. (2004). A rapid ecological assessment (rea) quantitative survey method for benthic algae using photoquadrats with scuba. *Pacific Sci.* 58, 201–209. doi: 10.1353/psc.2004.0021

R Core Team. (2019). *R: A language and environment for statistical computing*. Vienna: R Foundation for Statistical Computing.

Riegl, B., Berumen, M., and Bruckner, A. (2013). Coral population trajectories, increased disturbance and management intervention: a sensitivity analysis. *Ecol. Evol.* 3, 1050–1064. doi: 10.1002/ece3.519

Riegl, B., Cavalcante, G., Bauman, A. G., Feary, D. A., Steiner, S., and Purkis, S. (2017). Demographic mechanisms of reef coral species winnowing from communities under increased environmental stress. *Front. Mar. Sci.* 4:344. doi: 10.3389/fmars.2017.00344

Riegl, B., and Purkis, S. (2015). Coral population dynamics across consecutive mass mortality events. *Glob. Chang. Biol.* 21, 3995–4005. doi: 10.1111/gcb.13014

Ritson-Williams, R., and Gates, R. D. (2020). Coral community resilience to successive years of bleaching in Kāneʻohe Bay, Hawaiʻi. *Coral Reefs* 39, 757–769. doi: 10.1007/s00338-020-01944-4

Ruiz-Moreno, D., Willis, B. L., Page, A. C., Weil, E., Croquer, A., Vargas-Angel, B., et al. (2012). Global coral disease prevalence associated with sea temperature anomalies and local factors. *Dis Aquat Organ* 100, 249–261.

Sandin, S. A., Smith, J. E., DeMartini, E. E., Dinsdale, E. A., Donner, S. D., Friedlander, A. M., et al. (2008). Baselines and degradation of coral reefs in the Northern Line Islands. *PLoS One* 3:e1548. doi: 10.1371/journal.pone.0001548

Storlazzi, C. D., Dartnell, P., Hatcher, G. A., and Gibbs, A. E. (2016). End of the chain? Rugosity and fine-scale bathymetry from existing underwater digital imagery using structure-from-motion (SfM) technology. *Coral Reefs* 35, 889–894. doi: 10.1007/s00338-016-1462-8

Suka, R., Asbury, M., Gray, A. E., Winston, M., Oliver, T., and Couch, C. S. (2019). *Processing Photomosaic Imagery of Coral Reefs Using Structure-from-Motion Standard Operating Procedures*. Honolulu: U.S. Department of Commerce, National Oceanic and Atmospheric Administration.

Suka, R., Huntington, B., Morioka, J., O'Brien, K., and Acoba, T. (2020). Successful application of a novel technique to quantify negative impacts of derelict fishing nets on Northwestern Hawaiian Island reefs. *Mar. Pollut. Bull.* 157:11O1312. doi: 10.1016/j.marpolbul.2020.111312

Torres-Pulliza, D., Dornelas, M. A., Pizarro, O., Bewley, M., Blowes, S. A., Boutros, N., et al. (2020). A geometric basis for surface habitat complexity and biodiversity. *bioRxiv[Preprint]* doi: 10.1101/2020.02.03.929521

Vega Thurber, R. L., Burkepile, D. E., Fuchs, C., Shantz, A. A., McMinds, R., and Zaneveld, J. R. (2014). Chronic nutrient enrichment increases prevalence and severity of coral disease and bleaching. *Glob. Chang. Biol.* 20, 544–554.

Voss, J., Shilling, E., and Combs, I. (2019). *Intervention and Fate Tracking for Corals Florida, Affected by Stony Coral Tissue Loss Disease in the Northern Florida Reef Tract*. Miami, FL: Florida DEP.

Winston, M., Couch, C., Huntington, B., and Vargas-Ángel, B. (2020). *Ecosystem Sciences Division Standard Operating Procedures: Data Collection for Rapid Ecological Assessment Benthic Surveys, 2019 Update*. Washington, DC: NOAA, doi: 10.25923/ws5s-km69

Zuur, A. F., Ieno, E. N., Walker, N. J., Saveliev, A. A., and Smith, G. M. (2009). *Mixed Effects Models and Extensions in Ecology with R*. Berlin: Springer Science & Business Media, doi: 10.1007/978-0-387-87458-6

Conflict of Interest: The authors declare that the research was conducted in the absence of any commercial or financial relationships that could be construed as a potential conflict of interest.

frontiers in Marine Science

ORIGINAL RESEARCH
published: 02 June 2021
doi: 10.3389/fmars.2021.639359

Characterizing Geomorphology of Mesophotic Coral Reef Ecosystems in the Southwestern Gulf of Mexico: Implications for Conservation and Management

Melissa Mayorga-Martínez[1], Javier Bello-Pineda[1], Héctor Perales-Valdivia[1], Horacio Pérez-España[1] and William D. Heyman[2]*

[1] Instituto de Ciencias Marinas y Pesquerías, Universidad Veracruzana, Boca del Río, Mexico, [2] LGL Ecological Research Associates Inc., Bryan, TX, United States

Coral reefs are the most biodiverse ecosystems on earth and are presently experiencing severe declines globally. Shallow coral reef ecosystems (<30 m) have been studied extensively while mesophotic coral ecosystems (MCE) are poorly studied. As a result, MCE are rarely included in marine reserve design and management, despite their ecological importance and connectivity to shallow reefs. In this study, we assessed the fine-scale topographic complexity, a proxy for structural complexity, for a group of coastal coral reefs in a marine park in the southwestern Gulf of Mexico, in depths between 2 and 49 m. We conducted hydrographic surveys using a semi-portable multibeam echosounder system to produce 3D bathymetry digital terrain models (DTM) with a 2.5 m spatial resolution for three submerged bank reefs and two emerging reefs. From these models, descriptive terrain parameters were calculated for each reef, including slope, aspect, curvature, rugosity and ruggedness. Results show that all reefs are predominantly northeast-southwest oriented, with well-defined leeward and windward sides. For the three submerged bank reefs, structural complexity increased with depth. Estimated mean ruggedness and rugosity were highest at 20–40 m depth range on windward side slopes. Emerging reefs showed high structural complexity, particularly at the 25–40 m depth range. We identified a spur and groove zone with maximum ruggedness (0.26) and rugosity (3.17) values, and four channels with steep slopes (68°) and dispersed mounds. We found that at mesophotic depths (>30 m), southern reefs basements from two distinct reefs merge to form a continuous complex. This has important management implications since presently, only 28.7% of this reef complex (mostly shallow areas) are within the existing limits of the marine park's core zone. Considering the newly recognized importance of MCE, we propose expanding and reshaping the core zone to include the entire reef complex which mostly encompasses MCE with high structural complexity. Our study illustrates the value of semi-portable MBES for marine planning in developing countries and remote poorly studied areas.

Keywords: bathymetry, geomorphology, Gulf of Mexico, mapping, mesophotic coral ecosystem, multibeam echosounder, structural complexity

OPEN ACCESS

Edited by:
Stuart A. Sandin, University of California, San Diego, United States

Reviewed by:
Xinming Lei, South China Sea Institute of Oceanology (CAS), China
Caroline Eve Dubé, Laval University, Canada

****Correspondence:***
Javier Bello-Pineda
jabello@uv.mx

Specialty section:
This article was submitted to Coral Reef Research, a section of the journal Frontiers in Marine Science

Received: *08 December 2020*
Accepted: *05 May 2021*
Published: *02 June 2021*

Citation:
Mayorga-Martínez M, Bello-Pineda J, Perales-Valdivia H, Pérez-España H and Heyman WD (2021) Characterizing Geomorphology of Mesophotic Coral Reef Ecosystems in the Southwestern Gulf of Mexico: Implications for Conservation and Management. Front. Mar. Sci. 8:639359. doi: 10.3389/fmars.2021.639359

INTRODUCTION

Many studies have shown the global loss in live coral cover and critical degradation of coral reef ecosystems due to natural and anthropogenic disturbances (Gardner et al., 2003; Bellwood et al., 2004; Hoegh-Guldberg et al., 2007; Sweatman et al., 2011; De'ath et al., 2012; Gilmour et al., 2019). Evidence that the loss of live coral led to a drastic decline in the reef structural complexity has been shown for a region-wide scale in the Caribbean (Alvarez-Filip et al., 2009; Prachett et al., 2014; Bozec et al., 2015; Medina-Valmaseda et al., 2020). Such degradation trends generate uncertainty about the possible recovery of shallow coral reefs (Gardner et al., 2003) in which biodiversity, productivity and ecosystem services have been compromised (Moberg and Folke, 1999; Prachett et al., 2014). Current global-scale degradation of shallow coral reefs has encouraged the scientific community to study mesophotic coral ecosystems (MCE) (Menza et al., 2008) that typically occur between 30 and 150 m (Hinderstein et al., 2010) to determine if MCE are facing similar threats to those faced by shallow coral reefs (Bak et al., 2005; Reed et al., 2007; Lesser and Slattery, 2011; Bongaerts et al., 2013; Appeldoorn et al., 2015).

MCE are defined as light-dependent communities distributed between the middle and lower depths of the euphotic zone in tropical and subtropical regions (Hinderstein et al., 2010). Mesophotic reef depth limits vary within and between regions (Kahng et al., 2010) depending on water optical properties (Kirk, 2011). MCE occur at depths where downwelling irradiance reaches the 10 and 1% of subsurface irradiance (Jerlov, 1968). The euphotic zone may extend beyond 200 m deep in clear oceanic waters, while reduced to depths below 30 m near the coast because of increased water turbidity (Wright and Colling, 1995). MCE are considered an extension of shallow coral reefs since the distribution range of some species span from the shallow to the mesophotic zone (Kahng et al., 2010). Connectivity between shallow and mesophotic fish (Bejarano et al., 2014; Tenggardjaja et al., 2014; Papastamatiou et al., 2015) and coral species (Van Oppen et al., 2011; Holstein D.M. et al., 2016) suggest that MCE could be important contributors to reef ecosystem recovery.

Shallow coral reef ecosystems have been studied extensively while MCE remain poorly understood. Menza et al. (2008) showed an exponential decline in scientific literature on coral reefs as depth increases, showing the lack of information on MCE. Turner et al. (2017) showed that most of the studies on MCE are concentrated in a few geographic areas including Hawaii and Australia in the Pacific, Israel in the Middle East, the Caribbean and the northern Gulf of Mexico. Only 5.2% of those studies include reef geomorphology (Turner et al., 2017). The information gap on MCE is due in part to the financial and logistical constraints of conducting research in waters deeper than 30 m which requires specialized equipment and training (Locker et al., 2010).

Scleractinian corals are the dominant framework builders that provide the three-dimensional structure and complexity of coral reefs (Jones et al., 1994; Bruno and Bertness, 2001). Higher structural complexity is positively correlated with higher species biodiversity (Risk, 1972), reef fish biomass, and the abundance and size spectra of fish (Bell and Galzin, 1984; Rogers et al., 2014). Corals provide refuge for reef-dwelling species by reducing predation and competition (Almany, 2004) and space for larval settlement (Idjadi and Edmunds, 2006). Also, structural complexity has a positive effect on the provision of ecosystem services (Graham and Nash, 2013) including the important physical role of protecting coastal areas from waves (Harris et al., 2018).

Geomorphology in marine environments is an inherent physical attribute of the seabed. Geomorphic classification, based on maps of the seabed is a fundamental descriptor that provides a synthesis of attributes and information relevant for characterizing habitats (Harris, 2011) in scales from centimeters to kilometers (Greene et al., 1999). Specific geomorphic features are associated with particular suites of benthic habitats (Harris and Baker, 2011) and can be used as a proxy to identify critical life habitats of marine species (Heyman and Wright, 2011).

Benthic habitats are physically distinct areas of seabed associated with species, communities, or assemblages that consistently occur together (Harris and Baker, 2011). The physical structures of habitat, including its surfaces and substrates, are significant components of habitat complexity playing a key role in the function and structure of the marine communities (Bruno and Bertness, 2001). The habitat complexity of the aquatic systems is characterized by at least five different physical traits: (1) spatial scales, (2) diversity of complexity-generating physical elements, (3) elements spatial arrangement, (4) elements size and (5) elements abundance and density (Tokeshi and Arakani, 2012). Topographic variability is a primary component of habitat complexity. Topographic variability is a basic terrain parameter for seafloor characterization and can be used for delimiting regions or boundaries between habitats that in turn could be associated with distinct faunal assemblages (Wilson et al., 2007).

Coral reef structural complexity has been studied at different spatial scales and resolutions, using a variety of methods. The most commonly used field method is the belt chain, i.e., laying a chain directly over the substrate and estimating a rugosity index as a ratio of the actual surface distance relative to linear distance (Luckhurst and Luckhurst, 1978). Optical remote sensing has also been used to study landscape ecology, bathymetry, rugosity and even to assess the structural complexity of coral reefs (Brock et al., 2004; Zawada and Brock, 2009; Ferrari et al., 2016). Nonetheless, the utility of optical remote sensing techniques is restricted to clear shallow waters (Kenny et al., 2003; Wölfl et al., 2019). These techniques detect and measure energy patterns from different portions of the electromagnetic spectrum (Yang, 2009). Only wavelengths of the visible region of the spectrum (0.4–0.7 μm) penetrate the water column and this penetration decreases for longer wavelengths, becoming opaque for the infrared region

Abbreviations: AGDS, Acoustic ground discrimination systems; CC, Coral Cover; DTM, Digital Terrain Model; H1, Holandesa 1; H2, Holandesa 2; H3, Holandesa 3; MBES, Multibeam Echosounder System; MCE, Mesophotic Coral Ecosystems; MPA, Marine Protected Area; ROV, Remotely Operated Vehicle; SARC, Santiaguillo Anegadilla Reef Complex; SAVNP, Sistema Arrecifal Veracruzano National Park; SBES, Single beam echosounders; SoNAR, Sound Navigation and Ranging.

(Green et al., 2000). The precise degree of penetration in a spectral region is influenced by the optical properties of the water, including the concentration of dissolved organic matter and suspended sediments (Mumby et al., 2004).

Acoustic hydrographic methods based on SoNAR (Sound Navigation and Ranging) or echosounders are suitable tools for seafloor mapping, which in turn supports geomorphic features identification and classification. These methods have been used in coral reefs, including the MCE (Locker et al., 2010; Sherman et al., 2010). Single beam echosounders (SBES) measure water depth by timing the period from when the echo is emitted by the SBES to its return from the seabed (Ainslie, 2010). Acoustic ground discrimination systems (AGDS) based upon an SBES, use the strength and character of the echo to provide an indication of the bottom type (Kenny et al., 2003; Walker et al., 2008; Bejarano et al., 2011). Multibeam echosounder systems (MBES) acquire multiple depth measurements simultaneously and are used to map large areas of the seafloor at high resolution up to 0.1 m (Kenny et al., 2003). Multibeam data combined with data gathered with remotely operated vehicles (ROVs) or autonomous underwater vehicles (AUVs) allows a detailed description of geomorphology (Armstrong et al., 2008), terrain variability (Sherman et al., 2010), topographic variability and its relationship with MCE benthic community structure (Bridge et al., 2011). Descriptors such as slope, texture and landforms have been used for benthic characterizations and benthic habitat delimitating (e.g., Wilson et al., 2007; Costa and Battista, 2013).

Seafloor mapping and habitat modeling are essential for marine spatial planning, designing marine protected areas (MPAs), planning and conducting scientific research on benthic ecosystems and marine geology, and assessing economic resources (Harris and Baker, 2011). The main objectives of this study are to: (1) generate fine-scale bathymetric maps for a group of poorly studied coastal coral reefs in a marine park in the southwestern Gulf of Mexico, including both shallow and mesophotic depths; (2) describe the seafloor geomorphology; (3) assess the topographic variability as a proxy for structural complexity to identify potential areas of interest for conservation and management.

MATERIALS AND METHODS

Study Area

The "Sistema Arrecifal Veracruzano" National Park (SAVNP) in the southwestern Gulf of Mexico, includes 45 fringing and platform coral reef structures (Liaño-Carrera et al., 2019). The SAVNP is located in a terrigenous environment influenced by freshwater discharge from three rivers: the Antigua in the North, the Papaloapan to the South and the Jamapa in the middle (Krutak, 1997). Three weather seasons have been described for the region: dry, rainy and northerly (Gutiérrez de Velasco and Winant, 1996). Water turbidity varies seasonally according to weather conditions. Five coral reefs were selected for this study: three from the northern group and two from the southern group (**Figure 1**). The northern reefs, known as the "Holandesas" are three submerged banks located in front of the port of Veracruz which we refer to herein as Holandesa 1 (H1), Holandesa 2 (H2), and Holandesa 3 (H3). The southern reefs, commonly known as Santiaguillo and Anegadilla are emergent platform reefs located offshore of Anton Lizardo village (Liddell and Tunnell, 2011).

Hydrographic Surveys

Hydrographic surveys were carried out during 2015–2017 using a 30 foot Mexican style skiff equipped with an outboard engine and covered a total area of 6.42 km^2. The boat was equipped with a semi-portable MBES consisting of a 400 kHz SONIC 2020 multibeam echosounder (R2Sonic, Texas, United States) pole-mounted port-side, amidship 0.60 m below the surface, a sound velocity Micro X probe (AML Oceanographic, British Columbia, Canada) mounted at the rear of the transducer, a differential GPS Receiver Vector VS131 (Hemisphere GNSS, Scottsdale, Arizona, United States) with two antennas mounted 1 m apart on top of the pole, an Inertial Navigation System Ekinox-E (SBG systems, Carrières-sur-Seine, France) aligned to the center line of the vessel and used as our central reference point, and the 1PPS box (Hypack/Xylem, Middle-town, Connecticut, United States) installed between the GPS and computer. The box was used to improve time-tagging by reducing the clock sync error to less than 1 ms.

The multibeam echosounder was operated at 300 kHz with an emitted fanned arc of 256 equidistant beams per ping through a 130° swath sector, sampled. Samples were recorded every 15 μs and received using a 60 kHz bandwidth. Surveys were conducted following 180 parallel-line transects at ∼2 km/h average speed. Transects were planned to obtain 100% sector coverage. Sound velocity casts were obtained using an SV-Xchange probe (AML Oceanographic, British Columbia, Canada). Calibration transects were conducted for each survey to determine pitch, roll, and yaw offsets.

Bathymetry Data Processing

Bathymetry data were processed using Hypack hydrographic software (version 2015). Sound velocity, tide, pitch, roll and yaw offsets corrections were applied according to the manual (Hypack, 2015). The noise was manually removed from every transect. The highest estimated resolution was 0.71 m; however, all data were scaled down to generate a standard 2.5 m gridded matrix (x, y, z) and exported to ArcMap software (ESRI, United States). A 3D bathymetry digital terrain model (DTM) was created in raster format with 2.5 m spatial resolution and projected to the UTM zone 14N Transverse Mercator Datum.

Topographic Variability Analysis

Topographic variability analysis was performed using the Benthic Terrain Modeler (BTM) tools for ArcMap, calculated using a 3 × 3 moving window (Walbridge et al., 2018). To describe the geomorphology and structural complexity of the reefs, several key terrain parameters and their variation were measured, as described in **Table 1**. A Pearson correlation coefficient was computed to assess the relationship between the depth and the slope, depth and ruggedness, as well as depth and rugosity for the H1, H2, and H3 coral reefs.

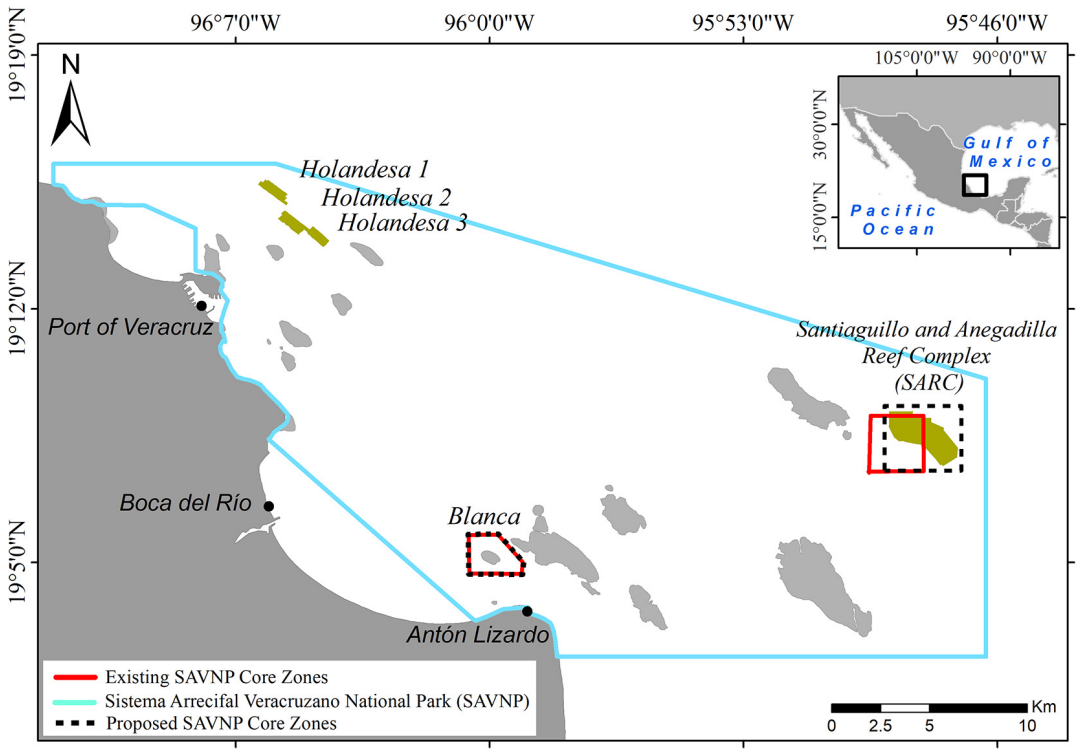

FIGURE 1 | Sistema Arrecifal Veracruzano National Park (SAVNP) located in the southwestern Gulf of Mexico; the two groups of reefs studied are highlighted. Polygons in red indicate core zones; polygons in dashed line indicate the proposed core zone.

RESULTS

Coral Reef Geomorphology

For the Holandesas reef group, the depth ranged from 15 to 44 m (see **Supplementary Material**). Three-dimensional models (**Figure 2**) of those reefs showed three well-defined geomorphologic zones; (1) the leeward side, (2) the reef flat, and (3) the windward side. H1 and H3 present an oval-shape, while H2 is kidney-shaped with a concave bay at the leeward side. H1 is the largest of the northern reef group and has the deepest basement (**Table 2**).

For Santiaguillo and Anegadilla reef group, the depth ranged from 2 to 51 m (see **Supplementary Material**). The reef complex is partially divided by a 0.9 km long channel (Channel-1) oriented northwest to southeast with a width ranging from 0.02 to 0.22 km and depths ranging from 32 to 38 m. Other channels include: Channel-2 which is 0.4 × 0.19 km having depths between 32 to 36 m, Channel-3 is 0.3 × 0.08 km with depths ranging from 33 to 36 m and Channel-4 is 0.7 × 0.07 km with depths ranging from 34 to 43 m. Multiple and well-defined mounds about 0.002–0.008 km^2 area were identified, away from the main reef within sand beds surrounding the leeward side of Anegadilla (**Figure 3A**). Spur and groove were the dominant geomorphological features at depths > 30 m, where the reefs show high structural complexity and are continuous between the two reefs (**Figure 3B**). Our data suggest that Santiaguillo and Anegadilla may constitute a single reef complex, instead of two separate reefs. As such, for the rest of the analyses, these two coral reefs are hereafter referred as the "Santiaguillo and Anegadilla reef complex" (SARC).

Structural Complexity of Holandesas Reef Group

The overall results of the estimated terrain parameters for the Holandesas reef group are summarized in **Table 2** and the DTM of the topographic variability showing the results of the analysis are presented in **Figure 4** in the following order: mean depth, depth standard deviation, slope, aspect, curvature, ruggedness and rugosity. The estimated mean depth ranged from 15 to 42 m and its standard deviation for depth ranged from 0 to 7.2 m. Steepest slopes (**Table 2**) are found in the 25–43 m depth range in specific areas: northeast windward side for H1, southwest leeward side for H2 and southeast windward side for H3. At the reef's flat (within 20–25 m depth), H3 (4.8° ± 2.9°) and H1 (4.5° ± 3.1°) showed moderate mean slope. For the H2 reef flat (15–20 m depth), the mean slope was closer to level (3.2° ± 2.8°). The estimated mean slope increased significantly with depth [H1 $r_{(56,149)} = 0.17$, $p < 0.001$, H2 $r_{(53,039)} = 0.49$, $p < 0.001$, and H3 $r_{(41,894)} = 0.40$, $p < 0.001$; **Figure 6A**].

The bank walls were mainly southwest and northeast oriented for the well-defined leeward and windward sides, respectively. For H1, the northeast surface area was 0.17 km^2 (46.8% of the reef) and the southwest surface area was 0.16 km^2 (46.3% of the reef). For H2, the northeast surface area was 0.18 km^2 (56.2% of the reef); southwest surface area was 0.09 km^2 (29%). For

TABLE 1 | Description of terrain parameters obtained from BTM (Walbridge et al., 2018).

Terrain parameter	Description
Mean depth	Is the average water depth in the 3 × 3 neighborhood (Walbridge et al., 2018).
Standard deviation	It captures the local dispersion (Walbridge et al., 2018).
Slope	It is estimated as the maximum rate of change of the elevation between the site and its surroundings and expressed in degrees. Low values, represent a flat terrain, high values, a steep terrain (Burrough et al., 1998).
Aspect	It measures the surface direction and reflects the orientation of the seabed at any given location. The algorithm uses a 3 × 3 neighborhood, it ranges from 0 to 359.9 degrees, measured clockwise from north, and -1 for locations of no slope (Walbridge et al., 2018).
Curvature	Is the first derivative of the slope (Zevenbergen and Thorne, 1987). Describes the relative position of the terrain features and delimits the regions of distinct habitat by identifying boundaries. Maximum curvature refers to a convex surface, minimum curvature to a concave surface (Walbridge et al., 2018).
Ruggedness	This is calculated using a 3 × 3 moving window, the magnitude of this standardized resultant vector is subtracted from 1 to obtain a dimensionless value that ranges from 0 (no variation) to 1 (complete variation). Typical values are small (≤0.4) in natural data (Walbridge et al., 2018).
Rugosity	Is the ratio of the surface area to the planar area across the neighborhood of 3 × 3 of a central pixel. Flat areas will have a rugosity value near to 1, high relief areas will exhibit higher values (Jennes, 2004).

H3, the northeast surface area was 0.12 km^2 (46.2% of the reef); southwest surface area was 0.09 km^2 (34.6%).

Convex surfaces (curvature range from 100 to 356) delineate the edge of each reef from the Holandesas group. Concave surfaces (curvature range from −100 to −350) revealed notches on the edge of the reefs and depressed areas.

Ruggedness and rugosity analysis revealed highly structurally complex patchy areas that were found at the windward slopes. The H1 showed the maximum ruggedness and H2 showed the highest estimated mean ruggedness among the Holandesas, while H3 presented the lowest ruggedness. Maximum rugosity and estimated mean rugosity were higher for H2, followed for H1 and H3 (**Table 2**). Estimated mean ruggedness [H1 $r_{(56,140)} = 0.080$, $p < 0.001$, H2 $r_{(53,039)} = 0.22$, $p < 0.001$ and H3 $r_{(41,894)} = 0.14$, $p < 0.001$] and rugosity increased significantly with increasing depth [H1 $r_{(59,322)} = 0.11$, $p < 0.001$; H2 $r_{(53,039)} = 0.32$, $p < 0.001$ and H3 $r_{(41,894)} = 0.33$, $p < 0.001$], showing that deeper areas (up to 43 m) are structurally more complex (**Figures 6B,C**).

Structural Complexity of Santiaguillo and Anegadilla Reef Complex

The overall results of the estimated terrain parameters for the SARC are summarized in **Table 2** and the DTM of the topographic variability showing the results of the analysis are presented in **Figure 5** in the following order: mean depth, depth standard deviation, slope, aspect, curvature, ruggedness and rugosity. The estimated mean depth for SARC ranged from 2 to 49 m and its standard deviation ranged from 0 to 7.2 m. The overall estimated mean slope was 10° ± 10.3°. The mean slope was 6.9° ± 5.6° for shallow areas (5–10 m deep), increased up to 18° ± 12.9° between 20–25 m depth and decreased down to 4.4° ± 3.3° between 45 and 49 m depth (**Figure 6A**). The steepest areas were at the channel walls (68°) and the spur and groove areas ranging from 59° to 35°, within 35–49 m depth, respectively.

Aspect analysis showed that leeward and the windward surfaces are both oriented in a southwest-northeast direction, with geomorphologically well-defined slopes. The northeast surface area was ≈1.88 km^2, accounting for 47.2% of the total reef complex. The southwest surface area was approximately 0.97 km^2, accounting for 24.4% of the total reef complex.

The convex surfaces (curvature range 100–356) delineated the channel walls, several mounds dispersed on the sand bed and spur and groove features. Concave surfaces (curvature range from -100 to -350) delineate the edge of the geomorphological features and depressed areas. In shallow areas (2–20 m deep) and the sand bed, the curvature surface ranged from 50 to −50.

The SARC showed the maximum values for slope, ruggedness and rugosity of all reefs (**Table 2**). Channel slopes and spur and groove zones within the 25–40 m depth range of the SARC had the highest structural complexity, considering both, ruggedness and rugosity. The shallow areas (5–10 m) showed the lowest structural complexity with 0.002 ± 0.004 mean ruggedness and 1.016 ± 0.03 mean rugosity. The highest mean ruggedness (0.012 ± 0.016) was observed for the 30–35 m depth range, while the highest mean rugosity (1.107 ± 0.15) was observed for the 20–25 m depth range. Structural complexity was lower for the 45–49 m depth range, with mean ruggedness of 0.002 ± 0.003 and rugosity of 1.017 ± 0.020 (**Figures 6B,C**). For the SARC, the middle depths showed the highest structural complexity, while the shallower and deeper areas showed lower structural complexity.

DISCUSSION

Geomorphological Features

The platform reefs from the SAVPN are characterized by three zones: (1) leeward slope, (2) reef lagoon or reef flat, which shows a crest delimiting the fore reef and (3) windward slope, a surface orientated to the dominant swell (Chávez et al., 2007). For Santiaguillo and Anegadilla, previous descriptions indicated that they are geomorphologically well-formed platform reefs, characterized by relatively steep slopes (Lara et al., 1992), while Santiaguillo is topographically rough with cliffs (Chávez et al., 2007). Gross-scale geomorphological descriptions of Santiaguillo and Anegadilla from Lara et al. (1992) and Chávez et al. (2007) are consistent with our results. Nonetheless, our fine-scale geomorphological description of SARC provided more details than previous studies, demonstrating previously undescribed geomorphological features, including four channels

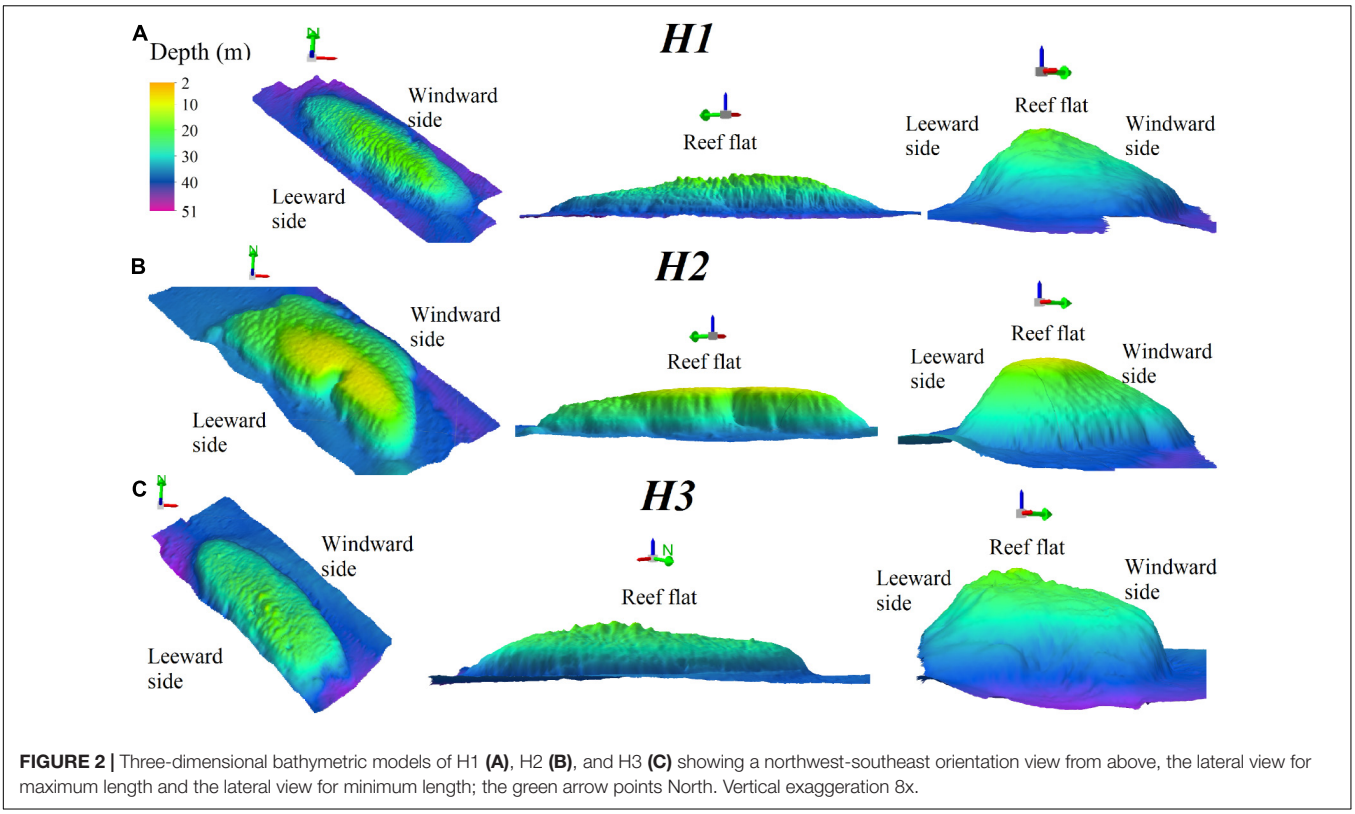

FIGURE 2 | Three-dimensional bathymetric models of H1 **(A)**, H2 **(B)**, and H3 **(C)** showing a northwest-southeast orientation view from above, the lateral view for maximum length and the lateral view for minimum length; the green arrow points North. Vertical exaggeration 8x.

TABLE 2 | Terrain parameters descriptors for each individual reef in the Holandesas group, and the SARC: depth basement (m), depth top (m), reef length (km), reef area (km^2), slope (minimum-maximum), mean slope and standard deviation (SD), ruggedness (minimum-maximum), mean ruggedness (SD) rugosity (minimum-maximum), and mean rugosity (SD).

Terrain parameters descriptors	H1	H2	H3	SARC
Depth top (m)	22	15	23	≤2
Depth basement (m)	43	40	41	49
Reef length (km)	1.13	0.91	0.94	3.6
Reef width (km)	0.41	0.43	0.33	1.2
Reef area (km^2)	0.36	0.32	0.31	3.98
Slope (min-max)	0–37°	0–44°	0–34°	0–68°
Mean slope ± SD	5° ± 3.6°	7° ± 5.8°	5° ± 4°	10° ± 10.3°
Ruggedness (min-max)	0–0.06	0–0.05	0–0.04	0–0.26
Mean ruggedness ± SD	0.0007 ± 0.001	0.0008 ± 0.001	0.0006 ± 0.001	0.0007 ± 0.012
Rugosity (min-max)	1.0–1.317	1.0–1.415	1.0–1.225	1.0–3.176
Mean rugosity ± SD	1.008 ± 0.013	1.015 ± 0.030	1.008 ± 0.014	1.041 ± 0.097

at the windward side with steep slopes (68°) and high structural complexity based on ruggedness (0.26) and rugosity (3.176) and a spur and groove zones that merge at depths > 30 m and sandy flats with patchy mounds at the leeward side (**Figure 3**). Spur and groove features, shore-normal coral ridges separated by shore-normal patches of sediment (grooves) are typically the most prominent features of fore reefs (Storlazzi et al., 2003), which is consistent with results for the SARC. Fine-scale spur and groove geomorphological characterization is fundamental for the study and understanding of coral reef hydrodynamics processes. Rogers et al. (2013) showed that spur and groove formations drive circulation patterns and are linked to debris transportation processes outside the coral reef.

Definition of the windward and leeward side reef slopes was based on the aspect analysis, which reflects the predominant orientation to the northeast of the reef surface. According to Wilson et al. (2007), such an orientation may be the result of the local hydrodynamics. For the Holandesas reefs, which are bank submerged reefs, the aspect analysis revealed a well-defined slope at both leeward and windward sides deeper than 15 m. Aspect analysis includes the estimation of the slope and curvature in one measure (Walbridge et al., 2018), therefore, as a result of this study, we highlight the relevance of the aspect analysis to be used

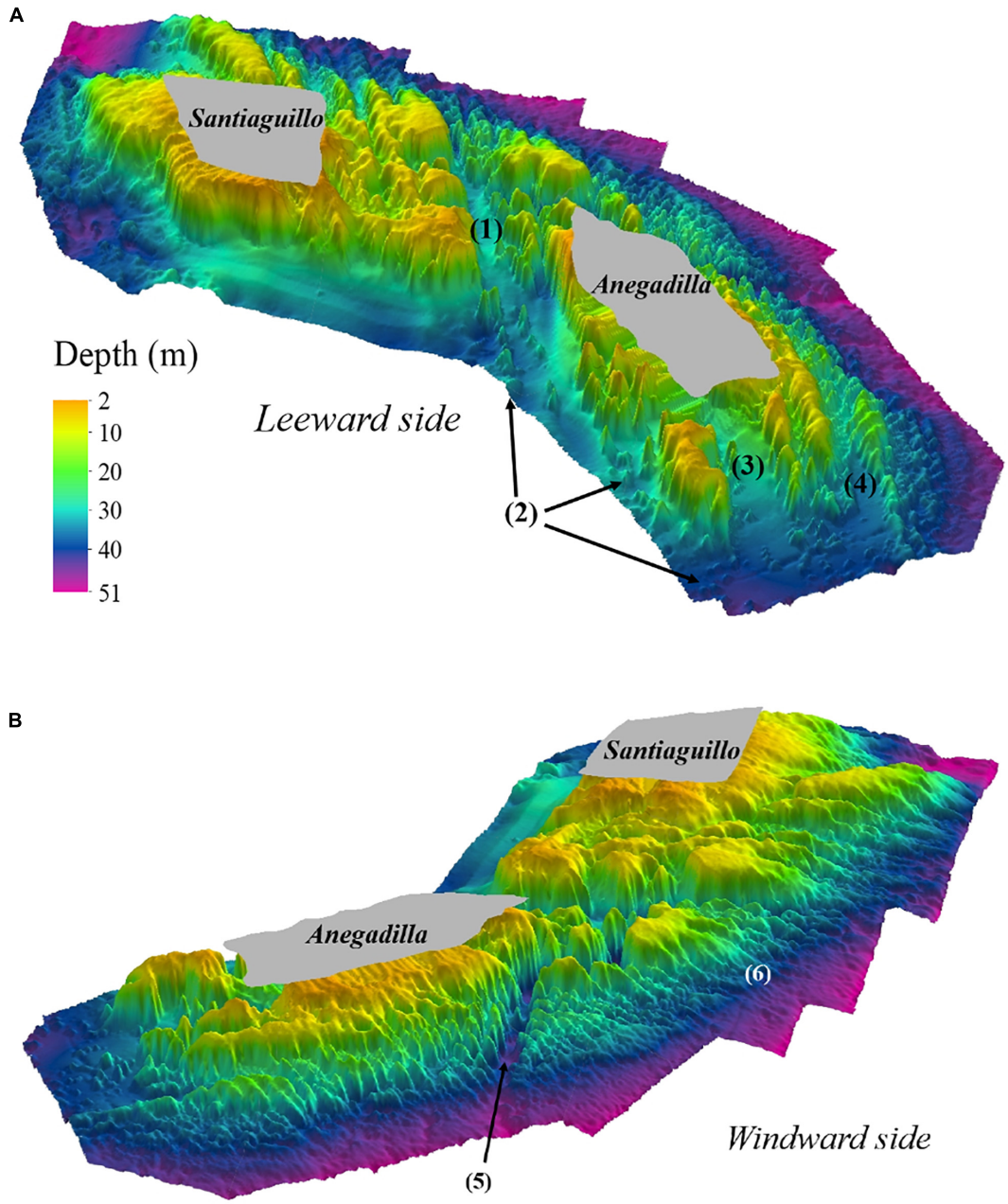

FIGURE 3 | SARC's three-dimensional bathymetric model, showing a leeward side view **(A)**. Remarkable geomorphic features are shown: (1) Channel-1, (2) dispersed mounds, (3) Channel-2 and (4) Channel-3. SARCs' three-dimensional bathymetric model, showing a windward side view **(B)**. Geomorphic features shown are: (5) Channel-4 and (6) spur and grooves. Shallow areas (≤2 m deep) not surveyed are shown in gray. Vertical exaggeration 8x.

for defining zones for different types of reefs in an objective way, including emergent or submerged platform, as well as submerged bank coral reefs.

Surface curvature (concave or convex) is an important geomorphological feature that is liked to ecological processes. Concave surfaces typically accumulate current-carried sediment and foster colonization of sessile organisms (Tokeshi and Arakani, 2012), while convex surfaces favor fish grazing (Bellwood and Choat, 1990). Geomorphological features in coral reefs are related to complex interactions between local oceanographic conditions and ecological functions. Highly complex reef geomorphology is positively correlated to higher biodiversity (Risk, 1972). Analysis of spatial array and complexity of those features can help scientists and decision-makers to identify areas of interest for research, management and conservation, thus, reducing monitoring costs. This is particularly important for developing countries with low budgets, where, having an accurate and detailed bathymetric base

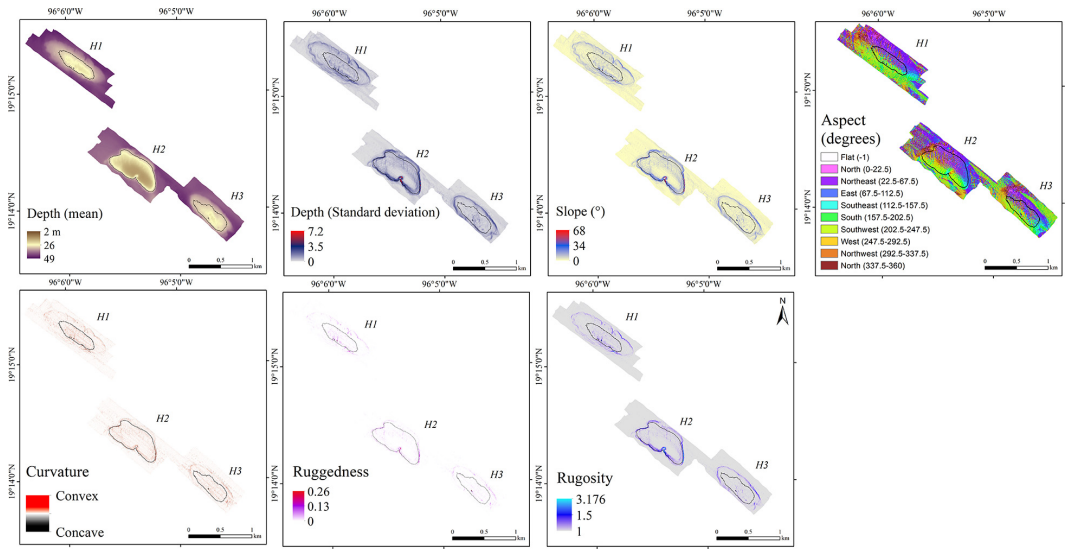

FIGURE 4 | Digital terrain models showing the result of the topographic variability analysis: mean depth, depth standard deviation, slope, aspect, curvature, ruggedness and rugosity for the H1, H2 and H3; 30 m isobath shown in black.

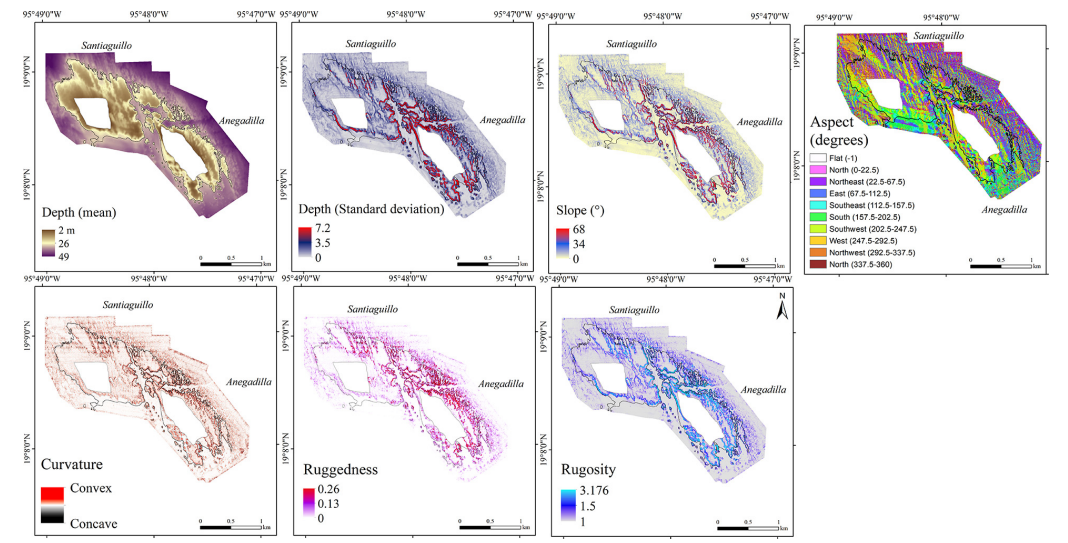

FIGURE 5 | Digital terrain models showing the result of the topographic variability analysis: mean depth, depth standard deviation, slope, aspect, curvature, ruggedness and rugosity for the SARC; 30 m isobath shown in black.

map describing the most conspicuous geomorphologic features can be very cost-effective.

Structural Complexity of MCE in the Southwestern Gulf of Mexico

Our study is one of the first that describes and characterizes the MCE in the Southern Gulf of Mexico in a systematic way and provides the basis for assessing the ecological and economic implications of including MCE explicitly in management strategies for the region. Results presented herein differ from previous studies regarding reef extension and topographic variability. Our detailed results showed that the platform sizes of the Santiaguillo and Anegadilla reefs have been underestimated in previous studies that were based on aerial photographs and Mexican Naval Charts (Lara et al., 1992), single beam (Ortiz-Lozano et al., 2018), and multibeam (Liaño-Carrera et al., 2019). The differences in reef extension and topography previously reported can be attributed to methodological aspects and the spatial resolution used for data acquisition and interpolation (Kenny et al., 2003; Walbridge et al., 2018).

MBES data offers higher resolution and more accurate maps than the techniques used in previous studies and can thus be valuable for both ecological studies and management including

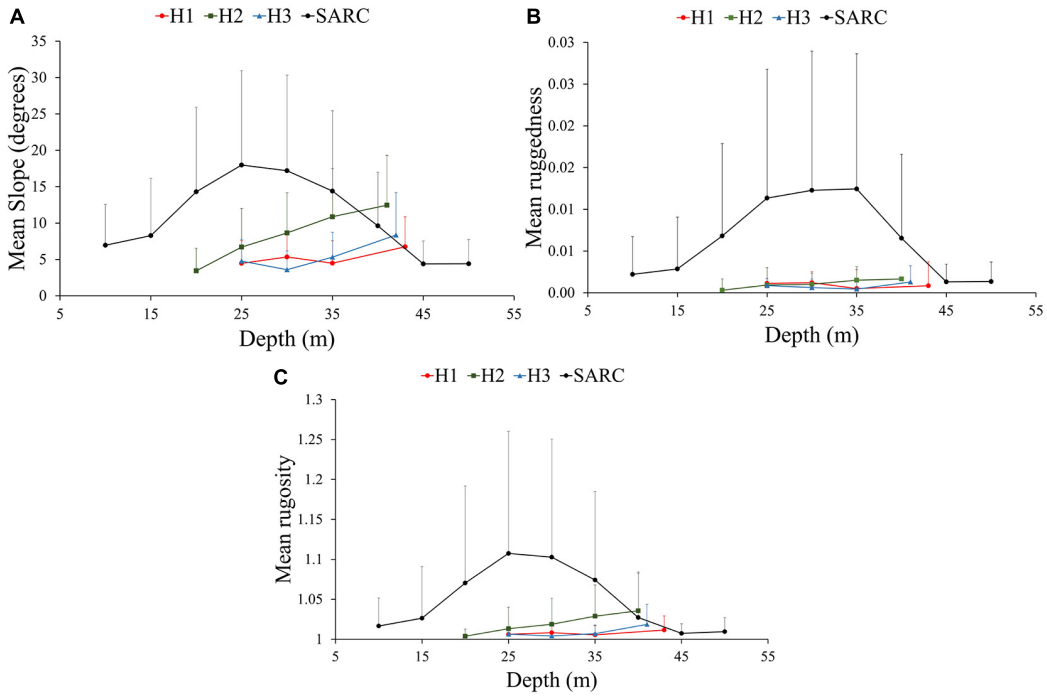

FIGURE 6 | The estimated **(A)** mean slope, **(B)** mean ruggedness and **(C)** mean rugosity, for 5 m depth intervals with standard deviation bars (SD ± 1) for Holandesa group and the SARC.

MPA design. High spatial resolution bathymetric maps, such as those produced in our study, are useful for studying ecological, geological and oceanographic processes. According to Kenny et al. (2003), MBES provide larger seafloor coverage with greater precision (≥0.1 m) and it is a useful technique for studying the MCE spatial distribution (Locker et al., 2010). The 3D bathymetric maps and associated physical characterizations can serve as the basis for carefully designed benthic habitat studies in which replicate sampling sites can be selected from within each of the distinctive geomorphological zones. This can be used to validate the predictions of MCE associations with structural complexity in appropriate depth zones. The technological improvement of acoustic methods has allowed the development and use of semi-portable and relatively affordable equipment for geomorphological sea bottom exploration (Kenny et al., 2003). These improvements are critical for both developing countries and remote and poorly studied areas such as those in the southwestern Gulf of Mexico.

Geomorphology as a Proxy for Benthic Habitat

Our analyses revealed that the highest structural complexity was shown at mesophotic depths (>30 m), for the Holandesas and SARC, which is a remarkably interesting result that needs further study. Structural complexity has been shown to correlate positively with coral cover (Gardner et al., 2003). We are currently assessing the benthic community structure of MCE in the SAVNP and our preliminary results on the relative benthic cover showed that the general pattern of structure community of deeper areas host MCE communities mainly composed of fleshy macroalgae, turf algae, crustose coralline algae and in less proportion sponges, hermatypic coral and other sessile invertebrates (*in preparation*).

There is a well-documented decline in shallow coral cover (CC) and structural complexity in the Caribbean region (Gardner et al., 2003; Alvarez-Filip et al., 2009; Medina-Valmaseda et al., 2020). For the SAVNP, there is also a decline in CC that has been documented since 1970s for shallow areas (<20 m), where the coral cover dropped from 50 to 18% (Chávez et al., 2007; Horta-Puga, 2007; Horta-Puga et al., 2015; Pérez-España et al., 2015). Current CC is similar among the northern and southern coral reefs in the SAVNP (Horta-Puga et al., 2015). In this study, mesophotic areas (>30 m depth) showed high structural complexity for both reef groups, considering slope, ruggedness and rugosity (**Figure 6**). Preliminary results on relative benthic cover for the SARC, show that there is a considerable average of the relative cover of hermatypic coral for mesophotic depths, particularly in spur and groove zones (*in preparation*). Having the fine-scale geomorphological characterization is important for benthic habitat mapping, according to Sherman et al. (2010); the distribution of well-developed MCE can be in the form of patches (Sherman et al., 2010). According to Bridge et al. (2011), community structure distribution depends on small-scale geomorphology. They demonstrated that distinctive functional ecological groups were consistently associated with specific fine-scale habitat types. For example, autotrophs

dominated the submerged reef flat tops while heterotrophs dominated steep slopes.

Management Implications

This study presents evidence of previously undescribed structural complexity and geomorphological continuity in deep SARC reefs (**Figure 3**). Our new data may have implications for the management of the SAVNP. In 1992, SAVNP was declared a National Park with a protected area of 532.38 km^2 (Diario Oficial de la Federación [DOF], 1992). The general boundary of the SAVNP was modified in 2012 and is currently covering 655.16 km^2. Core zone boundaries for both, Santiaguillo and Blanca reefs, cover 11.14 km^2 (Diario Oficial de la Federación [DOF], 2012; **Figure 1**). Activities permitted in the core zone include only monitoring, scientific research and maritime equipment installation for navigation. According to the management plan (Programa de Manejo Parque Nacional Sistema Arrecifal veracruzano, 2017) the Santiaguillo core zone includes 7.12 km^2 of reef area. However, when overlaid onto our bathymetric model using the published coordinates, the polygon covered only 1.84 km^2, equal to only 25.8% of the SARC and includes flat sandy areas with low structural complexity. Based on our results we propose expanding the core zone to 12.2 km^2 to include all of the areas with high structural complexity and associated MCE (**Figure 1**). Marine reserves can enhance the recovery of corals both within and outside the boundaries (Mumby and Harborne, 2010), promote resilience and connectivity by expanding the range of an MPA to include deep reefs (Abelson et al., 2016) since submerged reefs or deep habitats may contribute significantly to larval production (Thomas et al., 2015).

High structural complexity has been related to the provision of ecosystem services, supporting, local culture, tourism and fisheries. MCE provides essential habitat for fish and other species to spawn, shelter, feed and grow to maturity, particularly to important commercial fish (Bejarano et al., 2014; Holstein D. et al., 2016). The more structurally complex are MCE, the greater abundances of fish they have, as they can shelter under steep overhangs and in caves and crevices (Bejarano et al., 2014). In the SAVNP important ecosystem services have been reported: (1) regulation: protection to the coast, protection from erosion processes, (2) support: habitat and biodiversity maintenance, shelter; (3) cultural: recreation, tourism-recreational activities, and academic and research activities; and (4) Provision: fisheries (Arceo et al., 2010; Reyna-González et al., 2014). The structural complexity is an important element that divers take into consideration when selecting diving sites for recreational purposes (Williams and Polunin, 2000). Hence, the highest structural complexity areas are potential sites for recreational diving. However, appropriate regulation is needed for the management of these areas.

We support improved understanding of the MCE and their inclusion in studies, monitoring programs and management strategies (Rooney et al., 2010). The Flower Garden Banks National Marine Sanctuary (FGBNMS) in northwestern Gulf of Mexico, and the Papahānaumokuākea Marine National Monument (PMNM) in northwestern Hawaiian Islands (Papahānaumokuākea Marine National Monument, 2011), are some examples where MCE were included in specific management plans for conservation. FGBNMS includes three separate undersea features, the East and West Flower Garden Banks were designated a National Marine Sanctuary in 1992 and Stetson Bank was added in 1996. Fourteen additional reefs and banks were recently added (Office of National Marine Sanctuaries, 2020), in large part to provide additional protection for sensitive underwater features and marine habitats associated with continental shelf-edge reefs and banks in the northwestern Gulf of Mexico including MCE habitat, as Habitat Areas of Particular Concern (HAPC). HAPCs are high priority areas for conservation, management, or research because they are rare, sensitive, stressed by development, or important to ecosystem function, and they help prioritize and focus conservation effort (U.S. Department of Commerce National Oceanic and Atmospheric Administration, 2012).

CONCLUSION

The present study highlighted the importance of the use of new technologies such as the MBES, which provided accurate fine-scale bathymetric data for the 3D mapping and the assessment of the structural complexity from the shallow reefs to the mesophotic zone. This exploratory study of the geomorphology of a group of poorly studied coral reefs in the Southwestern Gulf of Mexico with a semi-portable MBES offers several novel findings. A striking result was discovering the physical continuity between Santiaguillo and Anegadilla reefs at depths >30 m on the windward side. Previously considered as two separate reefs our study demonstrates that Santiaguillo and Anegadilla are part of a single reef complex (SARC). This finding supports our proposal to expand the SAVNP core zone to include the entire SARC and thus enhance its contribution to coral reef recovery and resilience. In addition, our fine-scale geomorphology analysis revealed a large array of previously undescribed geomorphological features in the deeper areas of both reef groups, the Holandesas and SARC. Features include various channels, spur and grooves and sand flats with intermittent mounds.

DATA AVAILABILITY STATEMENT

The raw data cannot be provided due to size (>100 GB). A downscaled version of data can be provided by contacting first or corresponding author.

AUTHOR CONTRIBUTIONS

MM-M: idea developer, survey designer, data collection, and processing and analysis. JB-P: idea developer, project responsibility, funding administrator, data collection, and processing and analysis. HP-V: data collection and processing and analysis. HP-E and WDH: data analysis. All authors contributed to the article writing and approved the submitted version.

FUNDING

MM-M's Ph.D. scholarship was funded by the Consejo Nacional de Ciencia y Tecnología (CONACyT). This project was funded by CONACyT PN-2015-01-606. Article processing charges were funded by Universidad Veracruzana.

SUPPLEMENTARY MATERIAL

The Supplementary Material for this article can be found online at: https://www.frontiersin.org/articles/10.3389/fmars.2021.639359/full#supplementary-material

REFERENCES

Abelson, A., Nelson, P. A., Edgar, G. J., Shashar, N., Reed, D. C., Belmaker, J., et al. (2016). Expanding marine protected areas to include degraded coral reefs. *Conserv. Biol.* 30, 1182–1191. doi: 10.1111/cobi.12722

Ainslie, M. A. (2010). *Principles Of Sonar Performance Modeling*. Berlin Heildelberg: Springer-Verlag. 2010.

Almany, G. R. (2004). Does increased habitat complexity reduce predation and competition in coral reef fish assemblages? *Oikos* 106, 275–284. doi: 10.1111/j.0030-1299.2004.13193.x

Alvarez-Filip, L., Dulvy, N. K., Gill, J. A., Cote, I. M., and Watkinson, A. R. (2009). Flattening of Caribbean coral reefs: region-wide declines in architectural complexity. *Proc. R. Soc. B Biol. Sci.* 276, 3019–3025. doi: 10.1098/rspb.2009.0339

Appeldoorn, R., Ballantine, D., Bejarano, I., Carlo, M., Nemeth, M., Otero, E., et al. (2015). Mesophotic coral ecosystems under anthropogenic stress: a case study at Ponce, Puerto Rico. *Coral Reefs* 35, 63–75. doi: 10.1007/s00338-0151360-5

Arceo, P., Pérez-España, H., Bello-Pineda, J., Granados-Barba, A., Salas-Monreal, D., and Ortiz-Lozano, L. (2010). "Economic evaluation of fisheries and tourist services of the Veracruz Reef System National Park, Mexico: A spatial approach," in *Proceedings of the 15th Biennial Conference of the International Institute of Fisheries Economics & Trade (iifet). Economics of fish Resources and Aquatic Ecosystems: Balancing uses, Balancing Costs*, (Montpellier: International Institute of Fisheries Economics and Trade), 1–10.

Armstrong, R. A., Singh, H., Rivero, S., and Gilbes, F. (2008). Monitoring coral reefs in optically-deep waters. *Proc. 11th Int. Coral Reef Symp.* 1, 593–597.

Bak, R. P. M., Nieuwland, G., and Meesters, E. H. (2005). Coral reef crisis in deep and shallow reefs: 30 years of constancy and change in reefs of Curacao and Bonaire. *Coral Reefs* 24, 475–479.

Bejarano, I., Appeldoorn, R. S., and Nemeth, M. (2014). Fishes associated with mesophotic coral ecosystems in La Parguera, Puerto Rico. *Coral Reefs* 33, 313–328. doi: 10.1007/s00338-014-1125-6

Bejarano, S., Mumby, P. J., and Sotheran, I. (2011). Predicting structural complexity of reefs and fish abundance using acoustic remote sensing (RoxAnn). *Mar. Bio.* 158, 489–504. doi: 10.1007/s00227-010-1575-5

Bell, J. D., and Galzin, R. (1984). Influence of live coral cover on coral reef fish communities. *Mar. Ecol. Prog. Ser.* 15, 265–274. doi: 10.3354/meps015265

Bellwood, D. R., and Choat, J. H. (1990). A functional analysis of grazing in parrotfishes (family Scaridae): the ecological implications. *Environ. Biol. Fish.* 28:189–214. doi: 10.1007/bf00751035

Bellwood, D. R., Hughes, T. P., Folke, C., and Nyström, M. (2004). Confronting the coral reef crisis. *Nature* 429, 824–833.

Bongaerts, P., Muir, P., Englebert, N., Bridge, T. L. C., and Hoegh-Guldberg, O. (2013). Cyclone damage at mesophotic depths on Myrmidon Reef (GBR). *Coral Reefs* 32:935. doi: 10.1007/s00338-013-1052-y

Bozec, Y. M., Álvarez-Filip, L., and Mumby, P. J. (2015). The dynamics of architectural complexity on coral reefs under climate change. *Glob. Chang. Biol.* 21, 223–235. doi: 10.1111/gcb.12698

Bridge, T. C. L., Done, T. J., Beaman, R. J., Friedman, A., Williams, S. B., Pizarro, O., et al. (2011). Topography, substratum and benthic macrofaunal relationships on a tropical mesophotic shelf margin, central Great Barrier Reef. *Coral Reefs* 30, 143–153. doi: 10.1007/s00338-010-0677-3

Brock, J. C., Wright, C. W., Clayton, T. D., and Nayeghandhi, A. (2004). LIDAR optical rugosity of coral reefs in Biscayne National Park, Florida. *Coral Reefs* 23, 48–59. doi: 10.1007/s00338-003-0365-7

Bruno, J. F., and Bertness, M. D. (2001). "Habitat modification and facilitation in benthic marine communities," in *Marine Community Ecology*, eds M. D. Bertness, S. D. Gaines, and M. E. Hay (Sunderland, Massachusetts: Sinauer Associates, Inc), 201–218.

Burrough, P. A., McDonell, R. A., and Lloyd, C. D. (1998). *Principles of Geographical Information Systems*. New York: Oxford University Press.

Chávez, E. A., Tunnell, J. W., and Whiters, K. (2007). "Coral reef zonation and ecology: Veracruz shelf and Campeche Bank," in *Coral Reefs of the Southern Gulf of Mexico*, eds J. W. Tunnell, E. A. Chávez, K. Withers, and S. Earle (College Station, Texas: Texas A&M University Press). muse.jhu.edu/book/2721.

Costa, B. M., and Battista, T. A. (2013). The semi-automated classification of acoustic imagery for characterizing coral reef ecosystems. *Int. J. Remote Sens.* 34, 6389–6422. doi: 10.1080/01431161.2013.800661

Diario Oficial de la Federación [DOF], (1992). *Decreto Por El Que Se Declara Área Natural Protegida Con Carácter De Parque Nacional La Zona Conocida Como Sistema Arrecifal Veracruzano*. Mexico: Secretariat of the Interior. Lunes 24 de agosto de 1992.

Diario Oficial de la Federación [DOF], (2012). *Decreto Que Modifica Al Diverso Por El Que Se Declara Área Natural Protegida, Con El Carácter De Parque Marino Nacional, La Zona Conocida Como Sistema Arrecifal Veracruzano*. Mexico: Secretariat of the Interior. Jueves 29 de noviembre de 2012.

De'ath, G., Fabricius, K. E., Sweatman, H., and Puotinen, M. (2012). The 27-year decline of coral cover on the Great Barrier Reef and its causes. *PNAS* 109, 17995–17999. doi: 10.1073/pnas.1208909109

Ferrari, R., McKinnon, D., He, H., Smith, R. N., Corke, P., González-Rivero, M., et al. (2016). Quantifying Multiscale Habitat Structural Complexity: a Cost-Effective Framework for Underwater 3D Modelling. *Remote Sens.* 8:113. doi: 10.3390/rs8020113

Gardner, T. A., Côte, I. M., Gill, J. A., Grant, A., and Watkinson, A. R. (2003). Long-term region-wide declines in Caribbean corals. *Science* 301, 958–960. doi: 10.1126/science.1086050

Gilmour, J. P., Cook, K. L., Nicole, M. R., Poutinen, M. L., Green, R. H., Shedrawi, G., et al. (2019). The state of Western Australia's coral reefs. *Coral Reefs* 38, 651–667. doi: 10.1007/s00338-019-01795-8

Graham, N. A. J., and Nash, K. L. (2013). The importance of structural complexity in coral reef ecosystems. *Coral Reefs* 32, 315–326. doi: 10.1007/s00338-012-0984-y

Green, E. P., Mumby, P. J., Edwards, A. J., and Clark, C. D. (2000). *Remote sensing handbook for tropical coastal management. Coastal management sourcebooks 3*. Paris: UNESCO.

Greene, H. G., Yoklavich, M. M., Starr, R. M., O'Connell, V. M., Wakefield, W. W., Sullivan, D. E., et al. (1999). A classification scheme for deep seafloor habitats. *Oceanol. Acta* 22, 663–678. doi: 10.1016/s0399-1784(00)88957-4

Gutiérrez de Velasco, G., and Winant, C. D. (1996). Seasonal patterns of wind stress and wind stress curl over the Gulf. *J. Geophys. Res.* 101, 18127–18140. doi: 10.1029/96jc01442

Harris, D. L., Rovere, A., Casella, E., Power, H., Canavesio, R., Collin, A., et al. (2018). Coral reef structural complexity provides important coastal protection from waves under rising sea levels. *Sci. Adv.* 4:eaao4350. doi: 10.1126/sciadv.aao4350

Harris, P. T. (2011). "Seafloor geomorphology – Coast, shelf, and abyss," in *Seafloor Geomorphology as Benthic Habitat*, eds P. T. Harris and E. K. Baker (Netherlands: ELSEVIER), doi: 10.1016/B978-0-12-385140-6.00001-3

Harris, P. T., and Baker, E. K. (2011). "Why Map Benthic Habitats?," in *Seafloor Geomorphology as Benthic Habitat*, eds P. T. Harris and E. K. Baker (Netherlands: ELSEVIER), 3–22. doi: 10.1016/B978-0-12-385140-6.00001-3

Heyman, W., and Wright, D. J. (2011). Marine geomorphology in the design of marine reserve networks. *Prof. Geog.* 63, 429–442. doi: 10.1080/00330124.2011.585074

Hinderstein, L. M., Marr, J. C. A., Martinez, F. A., Dowgiallo, M. J., Puglise, K. A., Pyle, R. L., et al. (2010). Theme section on Mesophotic Coral Ecosystems: characterization, Ecology, and Management. *Coral Reefs* 29, 247–251. doi: 10.1007/s00338-010-0614-5

Hoegh-Guldberg, O., Mumby, P. J., Hooten, A. J., Steneck, R. S., Greenfield, P., Gomez, E., et al. (2007). Coral reefs under rapid climate change and ocean acidification. *Science* 318, 1737–1742.

Holstein, D. M., Paris, C. B., Vaz, A. C., and Smith, T. B. (2016). Modeling vertical coral connectivity and mesophotic refugia. *Coral Reefs* 35, 23–37. doi: 10.1007/s00338-015-1339-2

Holstein, D., Smith, T. B., and Appeldoorn, R. S. (2016). "Ecosystem services provided by mesophotic coral ecosystems," in *Mesophotic Coral Ecosystems – A Lifeboat For Coral Reefs?*, eds E. K. Baker, K. A. Puglise, and P. T. Harris (Nairobi and Arendal: The United Nations Environment Programme and GRID-Arendal), 98.

Horta-Puga, G. (2007). "Environmental impacts, in Coral reefs of the southern Gulf of Mexico," in *Coral Reefs of the Southern Gulf of Mexico*, eds J. W. Tunnell, E. A. Chávez, K. Withers, and S. Earle (College Station, Texas: Texas A&M University Press). muse.jhu.edu/book/2721.

Horta-Puga, G., Tello-Musi, J. L., Beltrán-Torres, A., Carricart-Ganivet, J. P., Carriquiry, J. D., and Villaescusa-Celaya, J. (2015). "Veracruz Reef System: a hermatypic coral community thriving in a sedimentary terrigenous environment," in *Aportes al conocimiento del Sistema Arrecifal Veracruzano: hacia el Corredor Arrecifal del Suroeste del Golfo de México*, eds A. Granados-Barba, L. Ortiz-Lozano, D. Salas-Monreal, and C. González-Gándara (Campeche: Universidad Autónoma de Campeche), 181–208.

Hypack. (2015). *Hypack hydrographic survey software user manual*. Middletown, CT: HYPACK Inc.

Idjadi, J. A., and Edmunds, P. J. (2006). Scleractinian corals as facilitators for other invertebrates on a Caribbean reef. *Mar. Ecol. Prog. Ser.* 319, 117–127. doi: 10.3354/meps319117

Jennes, J. S. (2004). Calculating landscape surface area from digital elevation models. *Wildl. Soc. Bull.* 32, 829–839. doi: 10.2193/0091-7648(2004)032[0829:clsafd]2.0.co;2

Jerlov, N. G. (1968). *Optical oceanography*. New York: American ELSEVIER publishing company, 194.

Jones, C. G., Lawton, J. H., and Shachak, M. (1994). Organism as ecosystem engineers. *Oikos* 69, 373–386.

Kahng, S. E., Garcia-Sais, J. R., Spalding, H. L., Brokovich, E., Wagner, D., Weil, E., et al. (2010). Community ecology of mesophotic coral reef ecosystems. *Coral Reefs* 29, 255–275.

Kenny, A. J., Cato, I., Desprez, M., Fader, G., Schüttenhelm, R. T. E., and Side, J. (2003). An overview of seabed-mapping technologies in the context of marine habitat classification. *ICES J. Mar. Sci.* 60, 411–418. doi: 10.1016/s1054-3139(03)00006-7

Kirk, J. T. O. (2011). *Light And Photosynthesis In Aquatic Ecosystems*. Cambridge: Cambridge University Press, 665.

Krutak, P. R. (1997). Petrography and provenance of siliciclastic sediments, Veracruz-Anton Lizardo Reefs, Mexico: a hybrid carbonate-siliciclastic system. *Rev. Soc. Mex. Hist. Nat.* 47, 167–177.

Lara, M., Padilla, C., García, C., and Espejel, J. J. (1992). "Coral Reef of Veracruz Mexico I. Zonation and Community," in *Proceedings of the Seventh International Coral Reef Symposium*, (Mangilao, GU: University of Guam Press), 535–544.

Lesser, P., and Slattery, M. (2011). Phase shift to algal dominated communities at mesophotic depths associated with lionfish (*Pterois volitans*) invasion on a Bahamian coral reef. *Biol. Invasions.* 13, 1855–1868. doi: 10.1007/s10530-011-0005-z

Liaño-Carrera, F., Camarena-Luhrs, T., Gómez-Barrero, A., Martos-Fernández, F. J., Ramírez-Macias, J. I., and Salas-Monreal, D. (2019). New coral reef structures in a tropical coral reef system. *LAJAR* 47, 270–281.

Liddell, W. D., and Tunnell, jr. J. W (2011). "Mexican coral reefs," in *Gulf of Mexico, origin, waters, and biota: Volume 3, Geology*, eds N. A. Buster and C. W. Holmes (College Station, Texas: Texas A&M University Press), 354.

Locker, S. D., Armstrong, R. A., Battista, T. A., Rooney, J. J., Sherman, C., and Zawada, D. G. (2010). Geomorphology of mesophotic coral ecosystems: current perspectives on morphology, distribution, and mapping strategies. *Coral Reefs* 29, 329–345. doi: 10.1007/s00338-010-0613-6

Luckhurst, B. E., and Luckhurst, K. (1978). Analysis of the influence of substrate variables on coral reef fish communities. *Mar. Biol.* 49, 317–323. doi: 10.1007/bf00455026

Medina-Valmaseda, A. E., Rodríguez-Martínez, R. E., Álvarez-Filip, L., Jordan-Dahlgren, E., and Blanchon, P. (2020). The role of geomorphic zonation in long-term changes in coral-community structure on a Caribbean fringing reef. *PeerJ* 8:e10103. doi: 10.7717/peerj.10103

Menza, C., Kendall, M., and Hile, S. (2008). The deeper we go the less we know. *Rev. Biol. Trop.* 56, 11–24.

Moberg, F., and Folke, C. (1999). Ecological goods and services of coral reef ecosystems. *Ecol. Econ.* 29, 215–233. doi: 10.1016/s0921-8009(99)00009-9

Mumby, P. J., and Harborne, A. R. (2010). Marine reserves enhance the recovery of corals on Caribbean reefs. *PLoS One* 5:e8657. doi: 10.1371/journal.pone.0008657

Mumby, P. J., Skirving, W., Strong, J., Hardy, E., LeDrew, E., Hochberg, E., et al. (2004). Remote sensing of coral reefs and their physical environment. *Mar. Pollut. Bull.* 48, 219–228.

Office of National Marine Sanctuaries. (2020). *Flower Garden Banks National Marine Sanctuary Expansion Final Environmental Impact Statement. U.S. Department of Commerce, National Oceanic and Atmospheric Administration, Office of National Marine Sanctuaries*. Silver Spring, Maryland: Office of National Marine Sanctuaries.

Ortiz-Lozano, L., Colmenares-Campos, C., and Gutiérrez-Velázquez, A. (2018). Submerged Coral Reefs in the Veracruz Reef System, Mexico, and its implications for marine protected area management. *Ocean. Coast. Manag* 158, 11–23. doi: 10.1016/j.ocecoaman.2018.03.012

Papahānaumokuākea Marine National Monument. (2011). *Maritime Heritage Research, Education, and Management Plan*. Honolulu, Hawai'i: Papahānaumokuākea Marine National Monument, 97.

Papastamatiou, Y. P., Meyer, C. G., Kosaki, R. K., Wallsgrove, N. J., and Popp, B. N. (2015). Movements and foraging of predators associated with mesophotic coral reefs and their potential for linking ecological habitats. *Mar. Ecol. Prog. Ser.* 521, 155–170. doi: 10.3354/meps11110

Pérez-España, H., Ávila-Gutiérrez, P. S., Melo-Merino, S. M., Berumen-Solórzano, P., and Flores-Arévalo, R. R. (2015). "Patrones interanuales e interarrecifales de las comunidades de peces, corales y equinodermos en el Sistema Arrecifal Veracruzano," in *Aportes al conocimiento del Sistema Arrecifal Veracruzano: hacia el Corredor Arrecifal del Suroeste del Golfo de México*, eds A. Granados-Barba, L. D. Ortiz-Lozano, D. Salas-Monreal, and C. González-Gándara (Campeche: Universidad Autónoma de Campeche), 159–178.

Prachett, M., Hoey, A. S., and Wilson, S. K. (2014). Reef degradation and the loss of critical ecosystem goods and services provided by coral reef fishes. *J. Environ. Sustain.* 7, 37–43. doi: 10.1016/j.cosust.2013.11.022

Programa de Manejo Parque Nacional Sistema Arrecifal veracruzano. (2017). *Secretaría de Medio Ambiente y Recursos Naturales*. Mexico: Comisión Nacional de Áreas Naturales Protegidas.

Reed, J. K., Koening, C. C., and Shepard, A. N. (2007). Impacts of bottom trawling on a deep-water Oculina coral ecosystem off Florida. *Bull. Mar. Sci.* 81, 481–496.

Reyna-González, P. C., Bello-Pineda, J., Ortiz-Lozano, L., Pérez-España, H., Arceo, P., and Brenner, J. (2014). Incorporating expert knowledge for development spatial modeling in assessing ecosystem services provided by coral Reefs: a tool for decision-making. *Rev. Biol. Mar. Oceanogr.* 49, 279–292. doi: 10.4067/s0718-19572014000200008

Risk, M. J. (1972). Fish diversity on a coral reef in the Virgin Islands. *Atoll Res. Bull.* 153, 1–7. doi: 10.5479/si.00775630.153.1

Rogers, A., Blanchard, J. L., and Mumby, P. J. (2014). Vulnerability of coral reef fisheries to a loss of structural complexity. *Curr. Biol.* 24, 1000–1005. doi: 10.1016/j.cub.2014.03.026

Rogers, J. S., Monismith, S. G., Feddersen, F., and Stolarzzi, C. D. (2013). Hydrodynamics of spur and groove formations on a coral reef. *J. Geophys. Res. Oceans* 118, 1–15. doi: 10.1002/jgrc.20225

Rooney, J., Donham, E., Montgomery, A., Spalding, H., Parrish, F., Boland, R., et al. (2010). Mesophotic coral ecosystems in the Hawaiian Archipelago. *Coral Reefs.* 29, 361–367.

Sherman, C., Nemeth, M., Ruíz, H., Bejarano, I., Appeldoorn, R., Pagán, F., et al. (2010). Geomorphology and benthic cover of mesophotic coral ecosystems of the upper insolar slope of southwest Puerto Rico. *Coral Reefs* 29, 347–360. doi: 10.1007/s00338-010-0607-4

Storlazzi, C. D., Logan, J. B., and Field, M. E. (2003). Quantitative morphology of a fringing reef tract from high-resolution laser bathymetry: southern Molokai, Hawaii. *Geol. Soc. Am. Bull.* 115, 1344–1355. doi: 10.1130/b25200.1

Sweatman, H., Delean, S., and Syms, C. (2011). Assessing loss of coral cover on Australia's Great Barrier Reef over two decades, with implications for longer-term trends. *Coral Reefs* 30, 521–531. doi: 10.1007/s00338-010-0715-1

Tenggardjaja, K. A., Bowen, B. W., and Bernardi, G. (2014). Vertical and horizontal genetic connectivity in *Chromis verater*, an endemic damselfish found on shallow and mesophotic reefs in the Hawaiian Archipelago and adjacent Johnston Atoll. *PLoS One* 9:e115493. doi: 10.1371/journal.pone.0115493

Thomas, C. J., Bridge, T. C. L., Figueiredo, J., Deleersnijder, E., and Hanert, E. (2015). Connectivity between submerged and near-sea-surface coral reefs: can submerged reef populations act as refuges? Divers. Distrib. 21, 1254–1266. doi: 10.1111/ddi.12360

Tokeshi, M., and Arakani, S. (2012). Habitat complexity in aquatic systems: fractals and beyond. *Hydrobiologia* 685, 27–47. doi: 10.1007/s10750-011-0832-z

Turner, J. A., Babcock, R. C., Hovey, R., and Kendrick, G. A. (2017). Deep thinking: a systematic review of mesophotic coral ecosystems. *ICES J. Mar. Sci* 74, 2309–2320..

U.S. Department of Commerce National Oceanic and Atmospheric Administration, (2012). *Flower Garden Banks National Marine Sanctuary Final Management Plan*. Silver Spring. MD: Createspace Independent.

Van Oppen, M. J. H., Bongaerts, P., Underwood, J. N., Peplow, L. M., and Cooper, T. F. (2011). The role of deep reefs in shallow reef recovery: an assessment of vertical connectivity in a brooding coral from west and east Australia. *Mol. Ecol.* 20, 1647–1660. doi: 10.1111/j.1365-294x.2011.05050.x

Walbridge, S., Slocum, N., Pobuda, M., and Wright, D. J. (2018). Geomorphological Analysis Workflows with Benthic Terrain Modeler. *Geosciences* 8:94. doi: 10.3390/geosciences8030094

Walker, B. K., Riegl, B., and Dodge, R. E. (2008). Mapping coral reef habitats in Southeast Florida using combined technique approach. *J. Coast. Res.* 24, 1138–1150. doi: 10.2112/06-0809.1

Williams, I. D., and Polunin, N. V. C. (2000). Differences between protected and unprotected reefs of the western Caribbean in attributes preferred by dive tourists. *Environ. Conserv.* 27, 382–391. doi: 10.1017/s0376892900000436

Wilson, M. F. J., O'Connell, B., Brown, C., Guinan, J. C., and Grehan, A. J. (2007). Multiscale Terrain Analysis of multibeam bathymetry data for habitat mapping on the continental slope. *Mar. Geod.* 30, 3–35. doi: 10.1080/01490410701295962

Wölfl, A. C., Snaith, H., Amirebrahimi, S., Devey, C. W., Dorschel, B., Ferrini, V., et al. (2019). Seafloor mapping – The challenge of a truly global ocean bathymetry. *Front. Mar. Sci.* 6:283. doi: 10.3389/fmars.2019.00283

Wright, J., and Colling, A. (1995). "Light and sound on seawater," in *Seawater: Its Composition Properties And Behaviour*, ed. G. Bearman (Amsterdam: Elsevier), 61–84. . doi: 10.1016/b978-075063715-2/50006-x

Yang, X. (2009). "Remote sensing, geospatial technologies and coastal ecosystems," in *Remote Sensing And Geospatial Technologies For Coastal Ecosystem*, ed. X. Yang (Berlin Heidelberg: Springer-Verlag), 561.

Zawada, D. G., and Brock, J. C. (2009). A multiscale analysis of coral reef topographic complexity using Lidar-derived bathymetry. *J. Coast. Res.* 53, 6–15.

Zevenbergen, L. W., and Thorne, C. R. (1987). Quantitative analysis of land surface topography. *Earth Surf. Proc. Land.* 12, 47–56.

Conflict of Interest: WDH is employed by the company LGL Ecological Research Associates Inc. which does no business in the study area.

The remaining authors declare that the research was conducted in the absence of any commercial or financial relationships that could be construed as a potential conflict of interest.

frontiers in Marine Science

ORIGINAL RESEARCH
published: 22 June 2021
doi: 10.3389/fmars.2021.669372

High-Resolution Vertical Habitat Mapping of a Deep-Sea Cliff Offshore Greenland

Loïc Van Audenhaege[1,2], Emmeline Broad[1,3], Katharine R. Hendry[4] and Veerle A. I. Huvenne[1]*

[1] National Oceanography Centre, Southampton, United Kingdom, [2] Ifremer, Centre de Bretagne, REM/EEP, Laboratoire Environnement Profond, Plouzané, France, [3] School of Ocean and Earth Science, University of Southampton, Southampton, United Kingdom, [4] School of Earth Sciences, University of Bristol, Bristol, United Kingdom

OPEN ACCESS

Edited by:
Andrew J. Davies, University of Rhode Island, United States

Reviewed by:
Benjamin Misiuk, Memorial University of Newfoundland, Canada
Vanessa Lucieer, University of Tasmania, Australia

***Correspondence:**
Loïc Van Audenhaege
loic.vanaudenhaege@gmail.com

Specialty section:
This article was submitted to Marine Ecosystem Ecology, a section of the journal Frontiers in Marine Science

Received: *18 February 2021*
Accepted: *04 May 2021*
Published: *22 June 2021*

Citation:
Van Audenhaege L, Broad E, Hendry KR and Huvenne VAI (2021) High-Resolution Vertical Habitat Mapping of a Deep-Sea Cliff Offshore Greenland. Front. Mar. Sci. 8:669372. doi: 10.3389/fmars.2021.669372

Recent advances in deep-sea exploration with underwater vehicles have led to the discovery of vertical environments inhabited by a diverse sessile fauna. However, despite their ecological importance, vertical habitats remain poorly characterized by conventional downward-looking survey techniques. Here we present a high-resolution 3-dimensional habitat map of a vertical cliff hosting a suspension-feeding community at the flank of an underwater glacial trough in the Greenland waters of the Labrador Sea. Using a forward-looking set-up on a Remotely Operated Vehicle (ROV), a high-resolution multibeam echosounder was used to map out the topography of the deep-sea terrain, including, for the first time, the backscatter intensity. Navigational accuracy was improved through a combination of the USBL and the DVL navigation of the ROV. Multi-scale terrain descriptors were derived and assigned to the 3D point cloud of the terrain. Following an unsupervised habitat mapping approach, the application of a K-means clustering revealed four potential habitat types, driven by geomorphology, backscatter and fine-scale features. Using groundtruthing seabed images, the ecological significance of the four habitat clusters was assessed in order to evaluate the benefit of unsupervised habitat mapping for further fine-scale ecological studies of vertical environments. This study demonstrates the importance of *a priori* knowledge of the terrain around habitats that are rarely explored for ecological investigations. It also emphasizes the importance of remote characterization of habitat distribution for assessing the representativeness of benthic faunal studies often constrained by time-limited sampling activities. This case study further identifies current limitations (e.g., navigation accuracy, irregular terrain acquisition difficulties) that can potentially limit the use of deep-sea terrain models for fine-scale investigations.

Keywords: marine habitat mapping, deep-water vertical cliff, ROV, multibeam echosounder, terrain point cloud, Greenland glacial trough, suspension-feeding community, underwater exploration

INTRODUCTION

Deep-water vertical and overhanging cliffs are important marine habitats that often host diverse and abundant communities (Huvenne et al., 2011; Johnson et al., 2013; Morris et al., 2013; Robert et al., 2020), including ecosystem engineers such as cold-water corals and deep-sea sponges (Ramirez-Llodra et al., 2010). Vertical cliffs are often associated with broadscale geomorphic features, such as continental margin troughs (Edinger et al., 2011), canyons (Freiwald et al., 2009; Huvenne et al., 2011, 2012; Gori et al., 2013; Brooke and Ross, 2014; Brooke et al., 2017; Robert et al., 2017; Pearman et al., 2020) and fjords (Haedrich and Gagnon, 1991; Gasbarro et al., 2018). Ecological studies usually assume that habitats providing a variety of environmental niches also promote enhanced biodiversity (MacArthur and Wilson, 1967; Kohn and Leviten, 1976). Vertical habitats are known to be hotspots of biodiversity (Robert et al., 2017, 2020) because of a number of interacting processes such as the complex small-scale topography defined by the geomorphology (Althaus et al., 2012; Carter et al., 2018), the depth (Stewart et al., 1985), hydrodynamics (Frederiksen et al., 1992; Mortensen et al., 2001; Kiriakoulakis et al., 2007; Lim et al., 2020; Pearman et al., 2020) and the substrate type (e.g., hard substrate for cold-water coral settlement; Gass and Roberts, 2006; Buhl-Mortensen et al., 2017; Davies et al., 2017).

One of the biggest anthropogenic threats to deep-sea benthic communities is the destructive action of bottom trawling. Deep-sea trawling activities severely damage the biogenic structure formed by epibenthic species such as sponges and cold-water corals (Hall-Spencer et al., 2002; Wheeler et al., 2005; Malecha and Heifetz, 2017). However, these environments are often characterized by increased concentrations of commercial fishes resulting in exploration and active management of Northwest Atlantic areas known to host structure-forming fauna, classified as "Vulnerable Marine Ecosystems" (VMEs, as defined by the United Nations General Assembly (UNGA) resolution 61/105 of 2006) (Costello et al., 2005; Ross and Quattrini, 2007). Crucially, deep-sea trawling activities do not have access to vertical habitats and it has been suggested that deep-water vertical habitats may provide refugia for species under trawling pressure elsewhere (e.g., Huvenne et al., 2011). Therefore, mapping the habitats and identifying the factors driving species distribution on vertical structures are of high importance for defining conservation plans in complex deep-sea environments.

Habitat mapping '*enables to represent or predict biological patterns*' (Brown et al., 2011) as habitats reflect particular physico-chemical conditions that are delineated in space and that influence species distribution (Lamarche et al., 2016). Since the geomorphology and the substrate of the seabed are important proxies for explaining benthic species distribution, the recent advances in acoustic mapping (using multibeam echosounders [MBES] or sidescan sonars) make it a cost-effective remote sensing tool (LaFrance et al., 2014; Lamarche et al., 2016) widely used to map and characterize seafloor habitats (e.g., Greene et al., 1999; Kostylev et al., 2001; Brown and Blondel, 2009; Verfaillie et al., 2009; Brown et al., 2011; Hill et al., 2014; Ismail et al., 2015; Hogg et al., 2016; Vassallo et al., 2018; Zelada Leon et al., 2020). Typically, acoustic surveys are combined with groundtruthing validation of the benthic habitats (Micallef et al., 2012; LaFrance et al., 2014). However, acoustic surveys remain a technical challenge in deep vertical environments.

In many seabed studies, shipboard MBES is used to produce a broad-scale bathymetric map of the seabed that can serve for habitat mapping (Brown and Blondel, 2009; Costello et al., 2010; Harris and Whiteway, 2011). However, the poor resolution of deep-water bathymetry data (∼25–100 m pixel size) overlooks smaller-scale complexity (∼0.1–5 m) of the seabed. In addition to being overlooked by vessel acoustic surveys, vertical marine habitats are historically undersampled and rarely visited (e.g., Haedrich and Gagnon, 1991). Recent advances in remotely operated technology and underwater vehicles have now increased our capability for the exploration of deep-sea vertical environments (Wynn et al., 2014; Huvenne et al., 2018). In particular, Remotely Operated Vehicles (ROVs) offer the potential to map vertical habitats with a fine-scale resolution (Huvenne et al., 2012, 2018; Robert et al., 2017). The selection of the appropriate configuration of the mapping equipment is crucial, as a downward-facing orientation can limit the acquisition of fine-scale features of steep environments in digital terrain models (Huvenne et al., 2016). Outcrops and overhanging features obstruct downward acoustic measurements in complex vertical habitats (Robert et al., 2017) meaning forward-facing data acquisition is optimal for the terrain reconstruction of vertical features (Yoerger et al., 1997).

At centimetric scales, photogrammetry methods integrate biological information with the fine-scale heterogeneity and the complexity of the benthic habitat (Gerdes et al., 2019; Price et al., 2019; Girard et al., 2020; Lim et al., 2020). Acoustic data acquisition can achieve 3D reconstructions of the terrain from a decimeter to a meter resolution over larger areas for the same amount of time than photogrammetry methods (Robert et al., 2017; Huvenne et al., 2018). Recent studies using forward-looking MBES mounted on ROVs have retrieved digital models of near-vertical walls of >60,000 m^2. They have been used to assess the geomorphology of the vertical walls to investigate landslide processes (Huvenne et al., 2016) and in relation to the small-scale distribution of biological communities for ecological studies (Huvenne et al., 2011; Robert et al., 2017).

Substrate properties (e.g., grain size and stability) are important features affecting cold-water coral and sponge community composition and density (Wilborn et al., 2018; De Clippele et al., 2019). MBES offers the opportunity to quantify the backscatter echo intensity as a proxy for substrate roughness, composition and texture. The backscatter corresponds to the overall "inner and micro-scale" material properties of the seabed (Jackson and Briggs, 1992; Brown and Blondel, 2009; Micallef et al., 2012). So far, this aspect of acoustic vertical mapping has not yet been investigated, nor has it been used for the study of substrate characteristics and their distribution at vertical geomorphological features.

This study uses acoustic data collected with a MBES front-mounted onto a ROV at a deep-sea wall located offshore Western Greenland with the aim to (i) improve the workflow to obtain well-navigated vertical bathymetry and retrieve substrate

information, (ii) map out the habitat diversity by applying an unsupervised habitat mapping method based on abiotic terrain variables and (iii) test if the unsupervised abiotic classes contain different benthic communities characterized with ROV photography.

MATERIALS AND METHODS

Study Site

On July 20th 2017, the ROV *Isis* was deployed from the RRS *Discovery* during the DY081 expedition (Dive 333), and explored the terrain of an underwater wall off the Greenland west coast (63°51.9′N, 53°16.9′W) in the Labrador Sea (**Figure 1A**; Hendry, 2017; Hendry et al., 2019). The vertical feature represented a portion of a north-facing cliff which marked the transition between a 900 m-deep glacial trough and the more elevated seabed of the Greenland continental shelf (**Figure 1B**). This site was then selected to investigate habitat characteristics following an unsupervised habitat mapping approach using small-scale descriptors derived from a near-vertical terrain mapped in high resolution during the *Isis* Dive D334 of July 21st 2017.

Unsupervised Habitat Mapping

Digital Terrain Model Acquisition

A portion of the underwater wall was mapped using a Reson7125 multibeam echosounder (MBES; 400 kHz, max. 140° swath angle, 512 beams) front-mounted onto the ROV *Isis* piloted from the RRS *Discovery* (Dive D334). Over 2h40, the ROV performed 7 survey lines at a constant distance (25 m) parallel to the wall. Horizontal survey lines were achieved at three depths, 25 m apart (**Figure 1C**). They were undertaken with two different headings (i.e., 137 and 214°) to ensure better coverage of the different parts of the wall, as the terrain displayed different orientations (**Figure 1C**). In total, seven survey lines were carried out by keeping *Isis*' attitude as constant as possible. The MBES system was operated through the Seabat7K software, while the data were recorded with PDS2000, v.3.9. **Supplementary Figure 1** details the workflow followed to create the vertical terrain point cloud.

The depth of *Isis* was recorded by a Parascientific Digiquartz pressure sensor. The position of the ROV was recorded at a frequency of < 1 Hz with an Ultra Short Baseline acoustic positioning system (Sonardyne USBL) and a Doppler Velocity Log (DVL). The USBL has a positioning error of 1% of the vehicle depth. At great depth, this can result in noisy ROV positioning. The DVL is an inertial system that uses dead-reckoning to calculate the ROV position. Over time, this may result in a gradual drift of the ROV navigation. The DVL positions are therefore characterized by high precision but lower accuracy than the USBL (e.g., **Supplementary Figure 2**). Reconstructing the terrain model therefore required merging of the USBL and DVL navigation to best reconstruct the fine-scale topography (Kwasnitschka et al., 2013; Huvenne et al., 2018). Corrected navigation was acquired by adding the coordinates recorded by the DVL to the average offset between the DVL and the USBL recordings, calculated using a 180-s interval rolling average (e.g., **Supplementary Figure 2**).

Acoustic data files were converted from the .pds format to .s7k files using PDS2000 (version 3.7), and then transferred into the CARAIBES software (Ifremer) for computing of the terrain point cloud of the wall. As established by Huvenne et al. (2016) and Robert et al. (2017), smoothed navigation coordinates were transformed to a metric coordinate reference system (UTM Mercator) for rotation in R (version 3.2.3; R Core Team, 2013) in order to simulate a conventional downward-looking configuration for processing the acoustic data, as to date no acoustic processing software offers the option of processing forward-looking MBES data. Furthermore, attitude data were transformed to comply with the new downward-looking configuration of the navigation (see in Huvenne et al., 2016).

The datasets of the survey lines recorded with similar heading were merged after aberrant soundings were manually removed in CARAIBES. This resulted in two 0.3 m-resolution point clouds, one for each part of the wall, which were exported as point clouds in .txt and back-rotated to their initial reference system in R (Robert et al., 2017). The software CloudCompare (v.2.11; 2019) was used to spatially combine the point clouds collected with different ROV headings. Small lateral adjustments (<10 m) had to be made as slight offsets of latitude and longitude arose between both point clouds, possibly as a result of the smoothing operations of the navigation.

Backscatter intensity was corrected in the Seabat7k software for spherical spreading and absorption losses based on the water temperature and salinity at depth. The acoustic signal amplitudes recorded in the .s7k files did not represent the actual reflectivity in dB, but nominal values (i.e., no unit). The backscatter extraction with the function *Epremo* of CARAIBES simply relays that information while the function *Ereamo* performs the projection in the 3D space. No correction accounting for the true incidence angle on the seafloor was applied. A mosaic was created using the smoothed and rotated navigation coordinates, and further exported in a point cloud with a resolution of 0.3 m. The backscatter was also back-rotated in R, and merged with the bathymetry point cloud by averaging the four nearest backscatter values based on the X,Y,Z coordinates of the bathymetric points.

For further information on the bathymetry and backscatter extraction workflow in CARAIBES, **Supplementary Figure 1** details the complete processing workflow.

Topographic Descriptors

Topographic descriptors were computed using a kernel radius centered on each point of the point cloud using different kernel radii to account for multi-scale variability of the terrain (Ismail et al., 2015). Topographic descriptors were calculated using Kernel radii of 0.9, 3, and 9 m, representing approximately an exponential series starting from the 0.3 m initial resolution of the point cloud. The maximum kernel size was constrained by the average extent of our study area and represented $1/15^{th}$ of the height of the vertical wall (e.g., Robert et al., 2017). Topographic descriptors were chosen to reflect the bathymetry (depth), the steepness (slope), the variability (roughness and Terrain Ruggedness Index, TRI), orientation (northness and eastness), curvature (Gaussian and mean curvatures) and

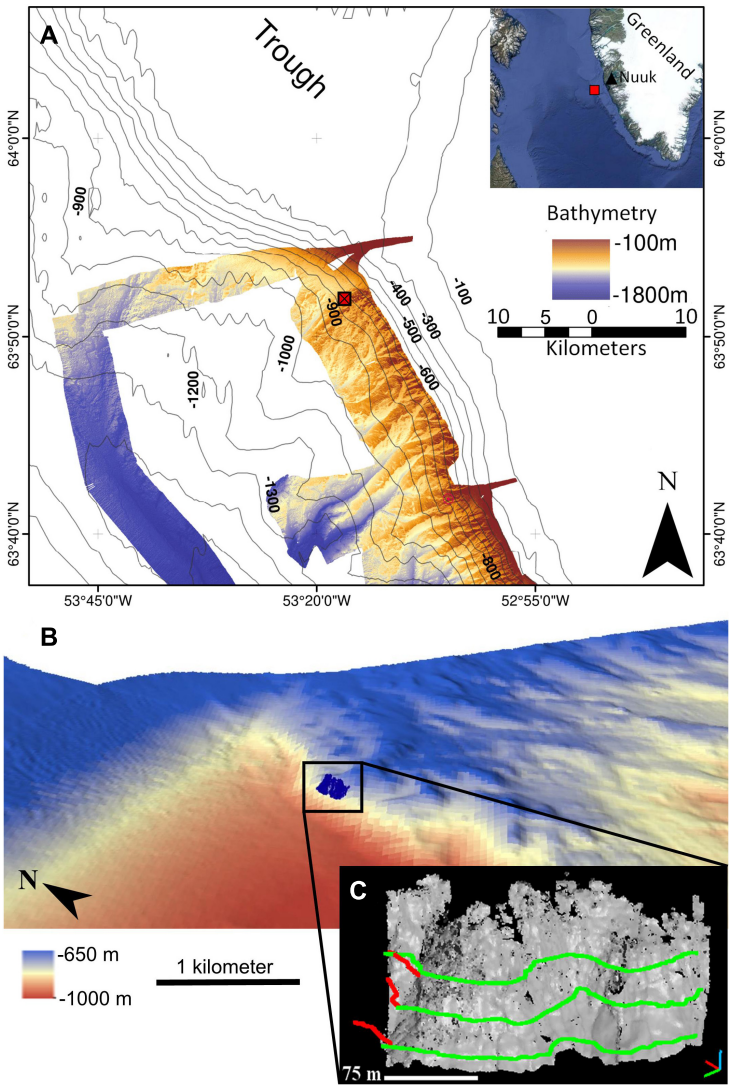

FIGURE 1 | (A) Location map of the study site on the W Greenland continental margin. The red boxes indicate the position of the underwater wall (63°51.9′N, 53°16.9′W) in the Labrador Sea, where the dives D333 and D334 of the ROV *Isis* took place. The bathymetry displayed was acquired on board the RRS Discovery (DY081; Hendry, 2017; Hoy et al., 2018). The background bathymetry (contour lines) was retrieved from ETOPO (NOAA). The wall marks the boundary between a cross-shelf glacial trough and the Greenland continental shelf. **(B)** 3D repositioning of the deep-sea wall according to the shipboard bathymetry (DY081; Hendry, 2017; Hoy et al., 2018). Panel **(B)** was computed on ArcScene (v. 10.8.1). **(C)** The underwater wall with segments representing the ROV tracks carried out at depths of 740, 765, and 790 m with a multibeam echosounder (MBES) front-mounted on the underwater vehicle *Isis*. The ROV was piloted 25 m off the vertical terrain with headings of: 137° (green lines) and 214° (red lines).

relative topographic position (Bathymetric Position Index, BPI) of the terrain in addition to the backscatter values which were used as a proxy for substrate physical characteristics (Wilson et al., 2007; Brown et al., 2011). Normal vectors were computed with a quadric function to derive multi-scale topographic variables (**Table 1**) and were transformed to "dip/dip direction" for computing the slope and the aspect from which the roughness, the mean and the Gaussian curvatures were derived in CloudCompare following Robert et al. (2017). Terrain Ruggedness Index (TRI), Orientation and Topographic Position Index (TPI) were computed in R [R Core Team, 2013; code provided from Robert et al. (2017)]. Abiotic descriptors were calculated for each point of the point cloud. This produced the input dataset for the subsequent clustering: a matrix where each point (i.e., rows) were assigned a specific depth, longitude, latitude, backscatter intensity and its terrain derivatives values (i.e., columns).

Dimensionality Reduction

Unsupervised habitat mapping was achieved following a procedure established by Verfaillie et al. (2009) and modified by Ismail et al. (2015) and Hogg et al. (2016). The distribution of each variable was centered on a zero mean and scaled to a unit variance to give each input variable the same weight in a

TABLE 1 | Variables used for the unsupervised habitat mapping.

Terrain variable	Acquisition	Unit	Scale
Depth	Acoustic data processing	m	0.3
Backscatter	Acoustic data processing	nominal values	0.3, 0.9
Slope	First derivative of the point cloud bathymetry	°	0.9, 3, 9
Bathymetric Position Index (BPI)	Difference between the mean and the average bathymetry	m	0.9, 3, 9
Terrain Ruggedness Index (TRI)	Average difference between the bathymetry of a point and its neighbors	m	0.9, 3, 9
Roughness	Distance between a point and a plane	m	3, 9
Mean curvature	Second derivatives of the point cloud bathymetry	m^{-1}	3, 9
Gaussian curvature	Second derivatives of the point cloud bathymetry	m^{-1}	3, 9
Eastness	cos(aspect)	–	3, 9
Northness	sin(aspect)	–	3, 9

Acquisition information, units and scale of calculation (size of Kernel radius) are listed.

Principal Component Analysis (PCA). PCA is useful to reduce the number of variables into a new set of linearly independent variables called Principal Components (PCs). PCs consist of a linear combination of the initial variables hence discarding collinearity of the variables. Only PCs with eigenvalues > 1 were retained for the clustering analysis following the Kaiser-Guttman criterion (Legendre and Legendre, 1998). Varimax rotation was performed on the retained PCs resulting in Rotated Components (RCs) which were used as input data for the clustering analysis (package 'psych'; Revelle and Revelle, 2015). Orthogonal rotation improves the PCs' independence by maximizing the variance shared among items related to one factor therefore enabling easier interpretation of the factor loading pattern.

Definition of the Number of Clusters

In unsupervised classification, a critical step is to define the optimal number of clusters to consider in the analysis. Typically, indices based on the proportion of variance explained by a given number of clusters are used in order to find a tradeoff between the model output complexity (i.e., number of clusters) and the clusters inertia (i.e., variability of observations in relation to the cluster center indicated by the within-cluster sum of squares; WSS). The Elbow and Caliński-Harabasz (C-H; Caliński and Harabasz, 1974) criteria were calculated over a range from 2 to 15 clusters in order to determine the optimal number of clusters (Milligan and Cooper, 1985; Milligan, 1996). The Elbow criterion aims to identify the optimal number (K) of clusters based on a decrease, or a local maximum in the gradient, of the total WSS when increasing the number of clusters (Legendre and Legendre, 1998). The C-H criterion seeks to find a local maximum in the ratio of the between-cluster sum of squares and the WSS as the number of clusters is increased (package vegan; Oksanen et al., 2013).

K-Means Clustering

The RCs were used as input variables for an unsupervised clustering. The K-means clustering method (Lance and Williams, 1967; MacQueen, 1967) has been extensively used for classifying features of the seabed (e.g., Legendre et al., 2002; Verfaillie et al., 2009). The K-means algorithm first randomly positions K cluster centers (Hartigan, 1975; Hartigan and Wong, 1979; Milligan and Cooper, 1987). Subsequently, (i) every data point is assigned temporarily to the closest center in the Euclidean space defined by the RCs, and (ii) each cluster center is then repositioned to the average coordinates of the temporary cluster. Both operations (i) and (ii) are repeated iteratively until the positions of the cluster centers converge below a chosen threshold.

Clustering Confidence

As the cluster centers converge to fixed coordinates, the distance between each individual sample and each cluster centroid is calculated as a measure of the similarity of the sample to each cluster (Bezdek, 1974). The membership of each point to its cluster can be expressed as a distance ratio (Burrough et al., 1997; Lucieer and Lucieer, 2009) by the following expression adapted by Ismail et al. (2015).

$$\mu_{ik} = \frac{1}{d_{ik}^2} \times \frac{1}{\sum_{k=1}^{n} \frac{1}{d_{ik}^2}}$$

where μ_{ik} is the membership value of the *i*-th data point to cluster k, which results in $\sum_{k=1}^{n} \mu_{ik} = 1$, d_{ik} is the distance between the *i*-th point and the cluster center k in the Euclidean space built by the RCs, n is the number of clusters defined in section 2.4.

An evaluation of the certainty of assigning the point *i* to the cluster *k* and not to another is performed using the confusion index (CI; Burrough et al., 1997). The CI is expressed as the ratio between the data point memberships with the second-closest cluster and the cluster to which it was allocated by the K-means clustering.

$$CI_i = \frac{\mu_{(max-1)_i}}{\mu_{max_i}}$$

Where $\mu_{(max-1)_i}$ is the membership value of the point *i* with the second-closest cluster center in the Euclidean space of the RCs, while $\mu_{(max)_i}$ is the membership value of that same point with the closest cluster center (i.e., to which it was assigned by the K-means clustering algorithm). The CI holds the property to tend to 0 when the membership value for the cluster to which it was allocated is high whereas it tends to 1 when the distance-based allocation of one point to the cluster was not well justified compared to the distance with the second-closest cluster.

Biological Assemblage Characterization

The abiotic clusters represent an unsupervised summary of a combination of environmental factors. Unsupervised clusters therefore describe the multidimensional environmental space that the fauna experiences and that may potentially contribute to driving community differences. Starting from this hypothesis, we tested for significant differences between *a-priori* unsupervised abiotic clusters in terms of community composition metrics derived from photograph annotations. In other words, the null

hypothesis posits that there was no difference of assemblage composition among unsupervised clusters.

Acquisition of Seabed Imagery and Biological Data

The biological data were extracted from seabed images collected during DY081, Dive D333 (Hendry, 2017; Culwick et al., 2020). In total, 159 images were extracted across a depth gradient (715 to 807 m) explored during two vertical transects that crossed the flank of the cross-shelf glacial trough (**Figure 2**; Broad, 2020; see methodology within). The position of the images corresponded to the area mapped using the forward-facing MBES during Dive D334. Images of the wall were collected every 30 s using the ROV *Isis* at an approximate horizontal distance from the wall of 2.5 m. The ROV is equipped with a forward-facing camera "Scorpio" (Insite Pacific Inc.) which is offset from the ROV frame at a down-facing angle of 22.5° and carries parallel lasers spaced 0.1 m apart. Due to the near-vertical orientation of the substrate, estimations of seabed area were calculated as if the images were obtained from a down-facing lens across a flat substrate. Annotation of marine megafauna and estimation of the seabed area within each image were carried out using the online BIIGLE 2.0 platform (Langenkämper et al., 2017). A morphospecies approach was used to characterize the diversity of the epibenthic megafauna, as standardized taxonomic classification of species from deep-sea imagery is not always accurate (Howell et al., 2019).

Generation of Point Cloud Majority Clusters

The area of the point cloud that corresponded with the position of each image was spatially identified by projecting a 2.25 m^2 square in the 3D space, originating from centralized coordinates recorded by the ROV USBL. This area was consistent with the average area captured by seabed images (2.33 m^2). The ROV heading, combined with the sum of the pitch and the inclination of the Scorpio camera, were used to orientate the projection of the 2-dimensional footprint of the initial image squares onto the point cloud, delimiting the estimated field of view recorded by the camera. The terrain points within each field of view did not always display a homogenous affiliation to a particular K-means cluster, therefore we applied a majority filter to create a single assignment of each photograph to a majority cluster.

Community Composition of Majority Clusters

In many cases, individual images of the seabed are not representative of localized species composition, as they sample too small an area (Benoist et al., 2019). Therefore we found it necessary to compile composite replicate samples to accurately account for faunal patchiness over scales larger than captured in single images (Benoist et al., 2019). Individual images were assigned to a majority cluster established by the method described in section "Generation of Point Cloud Majority Clusters." Following Broad (2020), images were then pooled at random within their respective majority cluster and aggregated into composite samples representing a seabed area of 20 m^2 (±SD, 1.30 m^2). The aim was to pool the fauna according to similar conditions they experience within the multivariable environmental space (i.e., environmental proximity) rather than spatial proximity (Benoist et al., 2019; Broad, 2020). Morphospecies abundances were summed in each composite sample. To test for differences in the biological assemblages characterizing each majority cluster, morphospecies abundance data within composite samples were Hellinger transformed and investigated with nonmetric multidimensional scaling plots (nMDS) using a Bray-Curtis dissimilarity matrix calculated in R with the *vegan* package (Oksanen et al., 2013). An Analysis of Similarities (ANOSIM) and Similarity Percentages (SIMPER) were calculated in PRIMER Version 7 to identify significant differences between majority clusters and the morphospecies responsible for pairwise dissimilarity (Anderson et al., 2008).

RESULTS

Cliff Geomorphology in Relation to Terrain Variables

The high-resolution point cloud (0.3 m average resolution, 292,577 points; **Figure 2**) characterized the morphology of the wall. The average topography of the point cloud displayed a slope of 60° (±SD, 18°) oriented north, extending from a depth of 820 to 685 m. The area mapped was ca. 276 m wide with a planar area of 35,880 m^2. Groundtruthing pictures are positioned in the terrain point cloud in **Supplementary Figure 3** to visualize coinciding fine-scale features and different terrain habitat types.

The deepest part of the wall exhibited a smoother slope of ∼50° at 780 to 818 m depth (**Figure 3A**), stretching over the whole width of the wall (>200 m). This illustrated a homogeneous horizontal geomorphic transition within the wall (**Figure 2**). Above that smooth depth band, the underwater cliff displayed areas with steeper slopes reaching on average 60°, but with local gradients up to 90°.

The upper cliff was characterized by a more heterogeneous relief with near-vertical areas (**Figure 3A**) and zones with slopes < 45°, resulting in higher values of the TRI and roughness variables in areas of a few square meters (**Figures 3B,D**). The BPI was rather homogeneous throughout the wall, but it underlined elongated near-horizontal features corresponding to transitions between areas with different slopes presented above (**Figure 3C**). The Gaussian curvature, although it displayed a few localized high values, was generally low (**Figure 3E**), in contrast to the mean curvature (**Figure 3F**) which did not exhibit such a homogeneous pattern.

The underwater cliff was not characterized by a homogeneous orientation (**Figures 3G,H**). Areas with a distinct orientation demonstrated the presence of elongated and protruding features visible (25 m width) in the cliff (**Figure 2**). Lower backscatter values on the upper sections of the point cloud suggested sediment accumulation (**Figure 4**). In fact, lower backscatter intensities are typically associated with finer-grained and well-sorted substrata, while higher backscatter intensities are correlated with coarse or hard substrata. These low-backscatter areas also extended on the sides of the protruding features, appearing like incisions in the backscatter map (**Figure 4**). They may be interpreted as local sediment buildups originating from sediment flow processes.

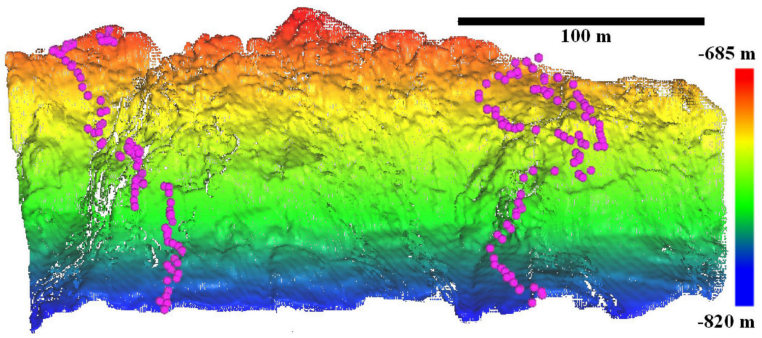

FIGURE 2 | Front view of the high-resolution (0.3 m) terrain point cloud of the underwater wall marking the boundary between a trough and the West Greenland continental shelf (63°51.9′N, 53°16.9′W). The depth ranges from –685 to –820 m and is displayed as a color gradient. The deep-sea cliff terrain was mapped using a forward-looking MBES mounted onto the ROV *Isis* (Dive D334) and is displayed as a point cloud using the software CloudCompare. Pink dots locate the position of the ROV when taking seabed groundtruthing pictures (Dive D333) used to assess for assemblage differences among abiotic clusters.

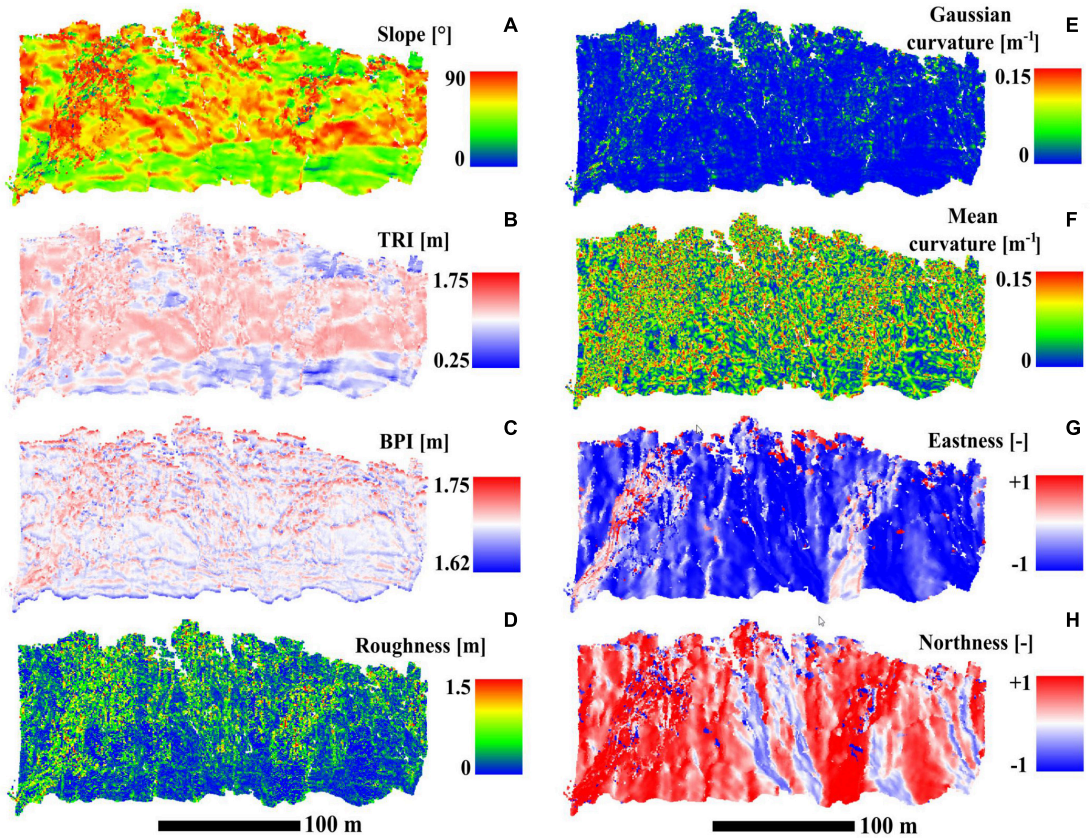

FIGURE 3 | Spatial distribution of terrain derivatives at the finest scale of calculation: **(A)** Slope (0.9 m), **(B)** Terrain Ruggedness Index (0.9 m), **(C)** Bathymetric Position Index (0.9 m), **(D)** Roughness (3 m), **(E)** Gaussian curvature (3 m), **(F)** Mean curvature (3 m), **(G)** Eastness (3 m), **(H)** Northness (3 m).

Artifacts

The point cloud displayed fine-scale vertical stripes or 'ribbing,' perpendicular to the ROV survey tracks. Such across-track artifacts can arise when mapping the terrain, particularly when using high-frequency acoustic sonar and high ping rates, and can be caused by several types of dynamic errors related to the time series recordings of the attitude sensors and the sonar's relative angle (Hugues Clarke, 2003). These regular artificial stripes can also arise from noisy USBL recordings in the case of underwater vehicles (e.g., Robert et al., 2017) and can be removed through post-processing using cosine filters. However, meter-scale 3-dimensional structures were observed in images of bedrock veneer indicating an unsupervised filtering could clean out real terrain features

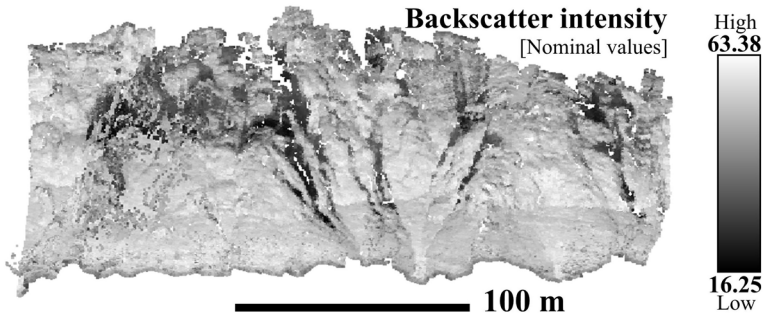

FIGURE 4 | Spatial distribution of the backscatter intensity retrieved from the MBES. The gray scale refers to untransformed, nominal values retrieved from CARAIBES (Ifremer) with darker gray depicting lower backscatter intensity. Low backscatter intensity indicates a substrate characterized by a combination of smooth and/or soft properties of the "inner" material.

that may be important for ecological studies. Hence this was not applied here.

Other artifacts arose when calculating terrain derivatives such as the slope (**Figure 3A**) and the mean curvature (**Figure 3F**) in the form of sections of the cliff displaying highly heterogeneous values. We inferred two different causes for these issues. Firstly, the merging of the two point clouds was not perfect as small-scale offsets (∼m) in the reconstructed point clouds remained. This resulted in higher spatial variability of the terrain derivatives along the section where the two point clouds overlapped. Secondly, many sections exhibiting high local variability in the terrain descriptor values coincided with areas with high eastness (**Figure 3G**) and low northness (**Figure 3H**) but also with low point density (**Supplementary Figure 4**). Therefore, we hypothesize these artifacts to be related to the orientation of the cliff: as the ROV kept a constant heading during survey lines, sections of the cliff that were not locally facing the sonar swath were more overlooked as fewer beams were scanning these areas. This explains a locally poorer resolution of the point cloud, which makes it more sensitive to variability in the data when calculating the terrain descriptors with a given Kernel radius size. Similarly, low backscatter intensity (**Figure 4**) also locally corresponded with low-density areas, and may be caused by the local orientation of the cliff away from the sonar (**Supplementary Figure 4**).

Unsupervised Habitat Mapping

Principal Component Analysis

The Principal Component analysis (PCA) was performed on 10 terrain variables calculated at different scales (**Table 1**). Five RCs with eigenvalues > 1 were retained and explained 58% of the total variance. Factor loads are displayed in the component's matrix (**Table 2**) and allow to investigate the correlation between the terrain variables and the RCs retained. Factor loads (**Table 2**) rarely exceeded a value of 0.5 which indicates a poor one-to-one relationship (Hogg et al., 2016). Terrain variables computed at different scales displayed similar factor loads. Overall, except for the northness and the backscatter, all variables displayed an exclusive relationship with the RCs. The slope and the TRI accounted for the highest factor loads of RC1 (**Table 2**); backscatter for RC2; eastness for RC3; TPI for RC4; backscatter and roughness for RC5. The mean and the Gaussian curvatures did not exhibit high loads in the five RCs retained by the K-means algorithm.

K-Means Clustering

A K-means clustering was performed on 292,557 data points with the five RCs. The Elbow criterion exhibited a decrease in the gradient of the WSS at 4 clusters (**Supplementary Figure 5**). The C-H criterion confirmed this observation with a maximum at 4 and 6 clusters (**Supplementary Figure 5**). We favored the

TABLE 2 | Component matrix showing correlation between the Varimax rotated principal components (RC) and the terrain input variables computed at different scales.

Terrain variable	Resolution [m]	RC1	RC2	RC3	RC4	RC5
Depth	0.3	−0.19	**0.32**	−0.08	0.06	−0.14
Backscatter	0.3	0	**−0.46**	0.17	0.09	**0.4**
	0.9	0	**−0.47**	0.17	0.09	**0.39**
Slope	0.9	**−0.34**	−0.02	0.14	−0.04	−0.06
	3	**−0.41**	−0.05	0.09	−0.04	−0.08
	9	**−0.38**	−0.1	0.11	−0.04	−0.07
TPI	0.9	−0.03	0.03	−0.01	**0.47**	0.1
	3	−0.08	0.06	−0.04	**0.64**	0.08
	9	−0.14	0.13	−0.06	**0.53**	0
TRI	0.9	**−0.32**	0	0.12	−0.07	−0.04
	3	**−0.42**	−0.07	0.11	−0.05	−0.04
	9	**−0.37**	−0.10	0.11	−0.05	−0.03
Roughness	3	−0.11	0.12	−0.22	−0.11	**0.38**
	9	−0.06	0.15	−0.12	−0.09	**0.39**
Mean curvature	3	−0.07	0.08	−0.13	−0.06	0.22
	9	−0.12	0.17	−0.24	−0.12	**0.36**
Gaussian curvature	3	−0.11	0.16	−0.16	0.01	0.07
	9	−0.13	0.18	−0.24	−0.1	0.28
Eastness	3	−0.13	−0.17	**−0.44**	0.05	−0.16
	9	−0.1	−0.23	**−0.45**	0.01	−0.14
Northness	3	0.02	**0.31**	−0.29	−0.01	−0.13
	9	−0.03	**−0.33**	**−0.39**	0.01	−0.12

Factor loads > 0.3 or < −0.3 are highlighted in bold.

least-complex clustering result with a low number of groups (i.e., four clusters).

Terrain Data Partitioning

The four clusters provided by the unsupervised method of data partitioning were mapped in the 3D space as each point of the point cloud was assigned to one of the four clusters (**Figure 5**). Broadly speaking, clusters T1, T2 and T3 were related to different depth bands, also characterized by differences in slope and backscatter. Cluster T4 exhibited a more discontinuous spatial distribution (**Figure 5**), suggesting it was related to variability in terrain characteristics at the scale of the point cloud resolution (i.e., 0.3 m).

The terrain characteristics of each cluster can also be described using violin plots in order to link differences in the data distribution and range of each input variable to each cluster (**Figure 6**). All data in this section are also presented with their mean ± standard deviation in the table in **Supplementary Table 1**. As noted above, depth appeared to be an important variable in constraining the clustering of the point cloud of the underwater cliff. T1 was characterized by the shallowest portion of the vertical wall (−733 ± 19 m) whereas T3 was positioned in the deepest areas (−781 ± 26 m; **Figure 6**) and T2 was located at intermediate depths (−758 ± 22 m). T4 did not occur in a preferential depth range (−751 ± 27 m; **Figures 5**, **6**). Low backscatter values of T1 (36.1 ± 7.2, nominal units) possibly described a different substrate in comparison to T2, T3 and T4 (>50 ± 6, nominal units; **Figure 6**). T3 contained terrain data with smoother slopes (44.7 ± 12.6°) and lower TRI (0.29 ± 0.06 m), while T2 reached the highest values (70.9 ± 12.5° and 0.37 ± 0.04 m; **Figure 6**). The slopes of T1 and T4 were much more variable but still higher in average than those of T3. T4 showed higher and more variable values of roughness (59.83 ± 36.31 10^{-2} m) compared to T1 which exhibited the second-highest roughness (28.69 ± 27.79 10^{-2} m; **Figure 6**). The BPI did not show any clear distinction between clusters notably due to its high variability within clusters. Similarly, the curvatures displayed a relatively similar distribution (**Figure 6**) although the distinction between T1–2–3 and T4 was more pronounced in the case of the Gaussian curvature, with the latter being less positively skewed in the case of T4 (**Figure 6**). Eastness and northness were distributed in an opposite way overall, while no distinct patterns could be observed between clusters (**Figure 6**).

Clustering Confidence

Confusion between clusters can be monitored using the distribution of the CI values (**Table 3**). On average, no clear distinction characterized the CI distribution of the different clusters although T4 reached the highest mean CI and T2 held the lowest mean CI followed by T3 (**Table 3**).

Confidence in the clustering outcome can also be assessed considering the spatial distribution of the CI values (**Figure 7**). The lower part of the cliff displayed very low CI demonstrating a clear distinction between T2 and T3 in this area (**Figure 7**). This deeper depth band also exhibited some small-scale variation of CI (i.e., abrupt increase) coinciding with spatial transitions between T2 and T3 (**Figures 5**, **7**). These features correspond to local changes of the topography suggested by the slope spatial distribution (**Figure 3A**) and other bathymetry derivatives (TRI, BPI, curvatures; **Figure 3**). The upper part of the cliff displayed higher CI values overall (**Figure 7**) coinciding with a mixed spatial arrangement of the clusters in small-scale patches. This supports the interpretation of a more heterogeneous habitat in this area.

Comparison With Biological Communities

The wall supported a diverse community of generalist boreal benthic fauna. Occurring in high abundance were encrusting demosponge morphotypes, crinoids, ophiuroids and soft coral species in the family of Nephtheidae. A number of specialist ecosystem engineers (e.g., the scleractinian cold-water coral *Desmophyllum pertusum*) were observed in isolated patches on rocky outcrops but remained rare in comparison to the generalist community (**Table 4**). **Supplementary Figure 3** illustrates different species and associated habitats found on the wall.

Characterization of epibenthic megafauna observed in the majority clusters showed a general partitioning of the community

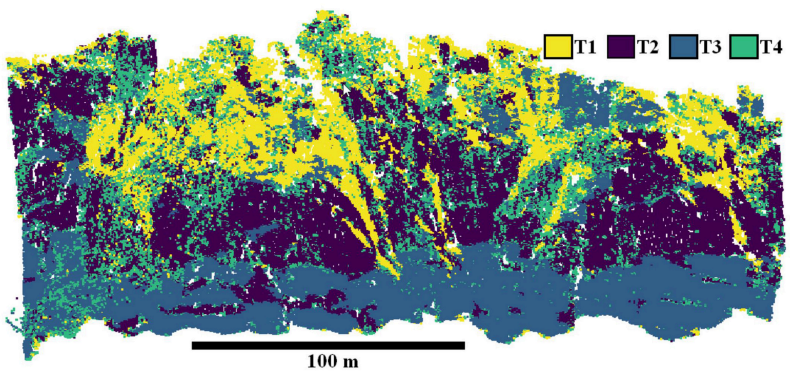

FIGURE 5 | Spatial distribution of the four abiotic clusters computed with a K-means clustering based on depth, backscatter intensity and terrain derivatives. Colors refer to points assigned to one of the habitat clusters (T1–T4).

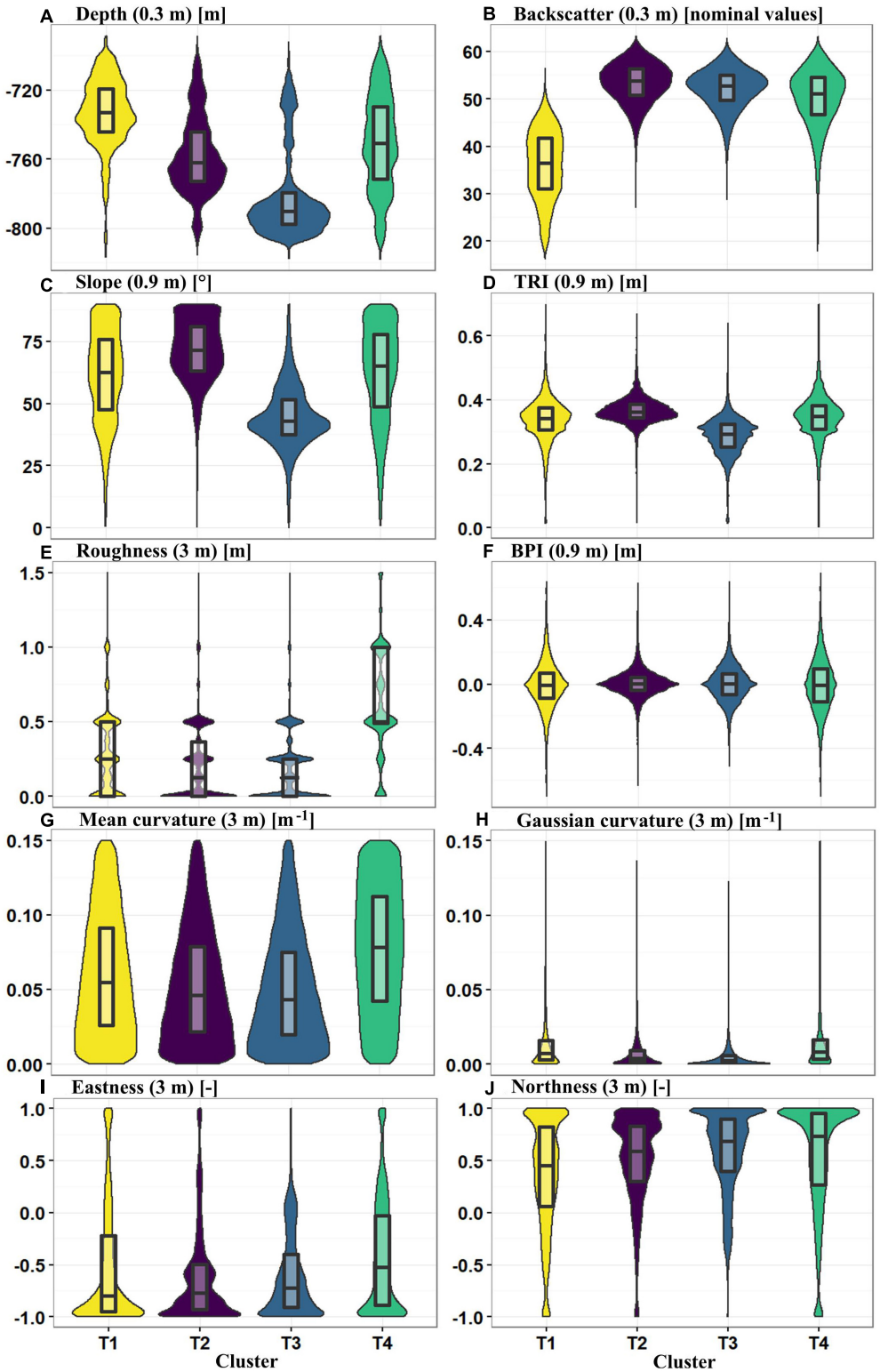

FIGURE 6 | Violin boxplots showing the distribution of terrain variables for each cluster. In the box of the violin boxplot, the middle line is the median, the lower and the upper box boundaries are the first and third quartiles. No statistical outliers are presented. These abiotic variables were used as input variables for the PCA and subsequent K-means clustering that computed the clusters T1–T4. Cluster colors are synchronized with those displayed in **Figure 5**. Terrain variables presented are **A**. Depth (0.3 m) [m], **B**. Backscatter (0.3 m) [nominal values], **C**. Slope (0.9 m) [°], **D**. Terrain Ruggedness Index (TRI, 0.3 m) [m], **E**. Roughness (3 m) [m], **F**. Bathymetric Position Index (BPI, 0.9 m) [m], **G**. Mean curvature (3 m) [m^{-1}], **H**. Gaussian curvature (3 m) [m^{-1}], **I**. Eastness (3 m) [–], **J**. Northness (3 m) [–]. Scales of computation are presented in parentheses and units of the abiotic variable is specified in square brackets as well as in the subtitle of the figure panels.

mapped in the point cloud (**Figure 8**). However, the low ANOSIM global R statistic did not indicate a strong aggregation of the assemblages within the clusters (ANOSIM Global R: 0.54, $p = 0.001$; **Table 4**). The ANOSIM global significance could be attributed to the cluster T4 which was characterized by the exclusive presence of *D. pertusum* and a reduced abundance of *Drifa glomerata*. Pairwise analyses also indicated T1 and T2 and T1 and T3 communities were similar in composition ($p \geq 0.05$, **Table 4**). However, despite the larger distribution of data points within T1 (**Figure 8**), only T2 and T3 were significantly different ($p < 0.01$). The increased abundance of *Acesta* sp. clams (T2, **Table 4**) and of the carnivorous sponge *Asbestopluma pennatula* (T3, **Table 4**) appeared to be contributing the most toward the dissimilarity. Echinoderm morphospecies that contributed to pairwise dissimilarities (**Table 4**) were likely driven by high abundance values promoting their contribution toward dissimilarity.

DISCUSSION

This study successfully mapped and characterized the fine-scale topography of a vertical wall located in deep Greenland waters (760 m). Additionally, our study also extracted the backscatter information from the MBES data and used it together with terrain variables calculated in the 3D space, to create the first habitat map of a deep-sea vertical wall. The subsequent comparison with the faunal communities identified in groundtruthing images indicated that the initial unsupervised classification resulted in habitat categories holding ecological relevance.

Acquisition of High-Resolution Vertical Bathymetry: Advantages and Limitations

Global bathymetry maps are the essential input information for various disciplines such as hazard studies, ocean circulation models, seafloor engineering and marine conservation (Wölfl et al., 2019). However, by 2015 less than 18% of the seabed had been mapped with a resolution of 1 km prompting a global endeavor to acquire, standardize and share bathymetric maps (e.g., Seabed2030; Mayer et al., 2018). Still, most of those mapping initiatives are carried out at fairly coarse resolutions (∼100–500 m pixel size or more). This means that the true heterogeneity of the seabed usually remains underestimated (Costello et al., 2010). At finer scales, terrain characterization at a meter-scale resolution is of importance for ecological investigations. For example, the presence of features increasing seabed roughness can have an influence on ecological modeling output (Robert et al., 2017).

While shipboard bathymetry of the Greenland margin provided a 25 m-pixel map of the area (**Figure 1**; Hendry, 2017; Hoy et al., 2018), the bathymetric and backscatter map supplied by the ROV reached ∼100 times that resolution. A total of 2h40 were needed to map 35,880 m^2 of vertical surface with a resolution of 0.3 m. This is in the same order of magnitude as other studies that mapped deep-sea vertical cliffs with a high resolution (<1 m) using forward-looking acoustic sonar for ecological studies (e.g. 9,000 to 15,000 m^2 per hour in Robert et al., 2017). Fine-scale geomorphological descriptions have applications for studying geohazard events (e.g., Sichi et al., 2005; Huvenne et al., 2016; Carter et al., 2018). This study identified different geomorphic facies over a range of spatial scales (e.g., 2 horizontal bands >200 m wide, with distinct steepness, 25 m protruding features, meter-scale heterogeneity revealed by unsupervised cluster T4) that provide new insights in the geomorphology of the flank of a deep-sea glacial trough, and that could not be mapped from the shipboard MBES data. These geomorphic features result from differential erosion processes affecting on the long term the geomorphology of the bedrock exposed. The terrain will in turn affect the benthic community composition by shaping local dynamics of the sediment and of the currents and by influencing the stability of the terrain (e.g., friability; Edinger et al., 2011; Robert et al., 2017, 2020). Finally, backscatter data acquired together with multibeam bathymetry at a resolution under a meter have potential in ecological modeling studies focusing on fine-scale influences of terrain heterogeneity usually captured with imagery (e.g., Wilborn et al., 2018; Corbera et al., 2019; De Clippele et al., 2019) or in spatial modeling of dynamic sedimentary processes (e.g., Huvenne et al., 2007; Lastras et al., 2011). While understanding of these processes requires combination with larger-scale investigations, this case study demonstrates current abilities for more extensive mapping combined with a decimeter-scale resolution, even if survey time at the study site currently remains a limiting factor in such deep-sea investigation.

Establishing a robust link between backscatter echo intensity and seabed properties usually requires groundtruthing information to establish what property actually drives the relative spatial differences in backscatter response (e.g., by using images, Micallef et al., 2012; Lucieer et al., 2013; using sediment cores, Lo Iacono et al., 2008; De Falco et al., 2010; and geomorphological maps, Lucieer and Lamarche, 2011) since the backscatter response results from a combination of factors that remain difficult to disentangle without groundtruthing validation (i.e., seabed roughness and substrate properties such as grain size and porosity; Jackson and Briggs, 1992). Interpretation of spatial differences in the backscatter at deep underwater cliffs can therefore be challenging since they can result from confounding variables poorly described in these environments. Images of the seabed did show slight differences in seabed type that could affect the acoustic backscatter (e.g., presence of pebbles, thin layers of sediment) while the effect of dense biogenic structures such as *D. pertusum* framework can have an influence on < 1 m resolution backscatter (e.g., Masson et al., 2003, see **Supplementary Figure 3** for localization of the mentioned features). However, calibrating quantitatively the link with the backscatter would have required sampling or a specific groundtruthing investigation as images only picture the superficial layer of the substrate, while backscatter intensity is affected by the substratum characteristics down to a certain depth (the so-called 'volume effect,' depending on acoustic frequency; Lurton and Lamarche, 2015). Nowadays, with improvement of sonar technology, there is a greater interest to integrate backscatter as a substrate surrogate in investigations aiming to characterize the seabed, as shown by recent effort for relating

TABLE 3 | Mean and standard deviation of the CI (Confusion Index) computed for each cluster.

Abiotic cluster	Mean CI ± SD
T1	0.56 ± 0.24
T2	0.45 ± 0.26
T3	0.48 ± 0.25
T4	0.61 ± 0.23

Value of 1/0 (yellow/blue) refers to high/low clustering uncertainty.

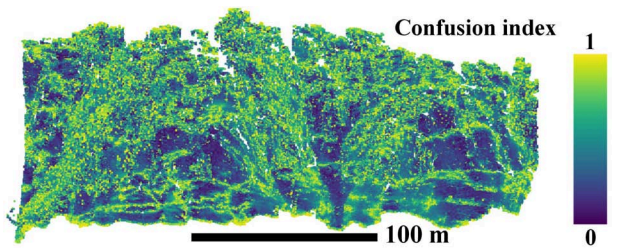

FIGURE 7 | Spatial distribution of CI (Confusion Index) values calculated for the four abiotic clusters. The color gradient refers to uncertainty of clustering based on the membership of a point to the cluster it was assigned by the K-means algorithm. Value of 1/0 (yellow/blue) refers to high/low uncertainty.

quantitatively the backscatter with the seabed properties (Brown and Blondel, 2009; Lucieer and Lamarche, 2011). Backscatter post-processing usually requires geometric and radiometric corrections to remove artifacts produced by the operating device settings (Lamarche et al., 2016; Lurton et al., 2018). While these steps were not tackled in the framework of forward-looking acoustic acquisition at vertical terrains, this work remains a first attempt to aim for backscatter extraction. This study opens space for further development to characterize the backscatter response of vertical features using acquisition and processing tools specifically tailored to vertical mapping configurations (see recommendations in Lurton and Lamarche, 2015; Lamarche and Lurton, 2018).

Other limitations have been identified. In the same way that downward-looking sonar overlooks fine-scale details of steeply sloping terrains, vertical cliffs exhibiting different orientations cannot be evenly mapped using a single ROV heading, as was illustrated by the merging of two sections of the cliff here in this study. To overcome this issue, separate point clouds can be acquired from survey lines with different heading orientations. The data for each survey section are processed separately and back-rotated, after which they can be merged in the overall point cloud. Occasionally small offsets build up between the separate sections. If the point clouds overlap in relatively homogeneous areas displaying only smaller-scale features, these offsets can trigger local inaccuracies in terrain descriptors. This can have an influence on the unsupervised habitat mapping, especially with clustering algorithms relying on variance partitioning methods.

The reason for these small point cloud offsets remains uncertain, but we suggest it may arise from artifacts or inaccuracies occurring in the navigation and attitude recordings. Although pre-processing of underwater vehicle navigation (Rigby et al., 2006; Batista et al., 2012; Kwasnitschka et al., 2013) and attitude (Hugues Clarke, 2003) allows to optimize the quality of fine-scale terrain reconstruction, the latter is intrinsically dependent on the data quality primarily acquired by motion sensors (i.e., spatial accuracy, lower recording time step than acoustic soundings and temporal synchronization). Accuracy and precision of underwater vehicle positioning in the deep sea remains nevertheless a major technological challenge that may particularly affect high-resolution terrain reconstruction efforts. Noisy USBL navigation data of underwater vehicles can create abrupt artifacts in the MBES bathymetry that may lead to inaccurate fine-scale terrain models. In this study, we merged the overall accuracy of the USBL navigation with the precision of the DVL records, to achieve the optimal navigation dataset to avoid terrain artifacts in a vertical reconstruction. To our understanding, this was a necessary step in the workflow of acoustic data processing since the decisions to remove soundings at the manual cleaning stage remain difficult to make, particularly in complex terrain. Meter-scale features such as outcrops could easily be erased from the point cloud which could lead to a reduction of the terrain complexity. Similarly, navigational uncertainty can remain between separate ROV dives (e.g., between the MBES and photography dives), and can cause difficulties in linking groundtruthing data to acoustic datasets.

Unsupervised Habitat Mapping

In this study, we applied an unsupervised clustering method, as proposed by Verfaillie et al. (2009), to partition the terrain descriptors in a reasonable number of categories displaying distinct characteristics based on the computation of RCs. The cluster analysis delineated four abiotic groups or so-called 'potential habitats' characterized by depth, backscatter, slope and roughness. These groups revealed (with high clustering confidence) contiguous zones of the cliff geomorphology even if no information on the spatial autocorrelation of the variables was provided to the cluster algorithm. The habitats included the 'talus' located at the bottom of the cliff, the steepest section of the cliff, the upper, more sedimented parts, and a few large protruding geomorphological features. Mapping such geomorphological features is of importance when characterizing the vertical habitat, particularly of sessile species, as they directly influence other aspects of the abiotic environment (e.g., sedimentation, slope, hydrodynamics). They may also reflect some of the geological processes (e.g., erosion) that shaped the vertical cliff as a result of its geological composition (Edinger et al., 2011).

Some aspects of the K-means partitioning method may constrain the interpretation of the habitat mapping outcome. Firstly, the K-means clustering method is based on spherical partitioning resulting in the computation of clusters of similar size in the multidimensional environmental space. This may not always be useful if delineating terrain groups with different sizes is required (Hogg et al., 2016). Density-based clustering (e.g., DBSCAN; Ester et al., 1996) is an alternative approach as it is capable of identifying patterns with arbitrary sizes in datasets even containing noise and outliers (Khan et al., 2014). Secondly, some clusters did locally exhibit patchy and discontinuous distributions also linked with lower confidence levels nested in

TABLE 4 | Results of ANOSIM and SIMPER analysis on a Bray-Curtis dissimilarity matrix of transformed morphospecies abundance data.

ANOSIM: Global Test		**Sample Statistic**	**Significance**		**SIMPER**				
		***R* = 0.54**	***p* = 0.001*** **						
T_a	**T_b**	**Pairwise R Statistic**	**Pairwise Significance**	**Total Pairwise Dissimilarity (%)**	**Morphospecies**	**Average Abundance (%)**		**Diss/SD**	**Cumulative Contribution to Dissimilarity (%)**
						T_a	**T_b**		
T1	T2	0.48	0.05	–	Not Significant	–	–	–	–
T1	T3	0.41	0.057	–	Not Significant	–	–	–	–
T1	T4	0.5	0.029*	43.79	*Drifa glomerata*	0.26	0.11	1.30	2.88
					Ophiuroidea thick white	0.19	0.33	1.45	5.38
					Desmophyllum pertusum [head]	0.00	0.14	3.03	7.76
T2	T3	0.5	0.006**	37.37	*Acesta* sp.	0.21	0.08	1.52	2.30
					Asbestopluma pennatula	0.03	0.14	2.43	4.18
					Ophiuroidea Hexact pink	0.12	0.15	1.48	5.87
T2	T4	0.57	0.003**	37.44	Ophiuroidea thick white	0.27	0.33	1.44	2.30
					Ophiuroidea indet. pink mix	0.37	0.25	1.55	4.60
					Desmophyllum pertusum [head]	0.02	0.14	2.33	6.84
T3	T4	0.83	0.029*	41.1	Ophiuroidea thick white	0.20	0.33	1.54	2.32
					Desmophyllum pertusum [head]	0.00	0.14	3.18	4.62
					Ophiuroidea Demosponge pink	0.01	0.14	3.92	6.77

*The top three species structuring the dissimilarity between pairwise tests are presented along with their average contribution to pairwise dissimilarity, the ratio between dissimilarity and standard deviation values and cumulative contribution toward total pairwise dissimilarity. See Broad et al. (in prep) for further information on morphospecies characteristics. p-value: * < 0.05, ** < 0.01, *** < 0.001.*

the upper part of the underwater cliff. The clustering algorithm works on examining the best data partitioning according to the input variables' variance but not on their spatial coherence and continuity. Spatial coherence and continuity can be met with a clustering method that accounts for spatial proximity between data points (e.g., ST-DBSCAN; Birant and Kut, 2007). Recurrent terrain patterns could also be investigated using approaches based on signal decomposition (e.g., Empirical Orthogonal Function; Preisendorfer and Mobley, 1988).

Biological Interpretation

As a last step in this study, we tested the ecological relevance of the unsupervised habitat categories summarizing a multivariable environment (i.e., depth, terrain and substrate) with the biological information provided by groundtruthing imagery. Abiotic clusters are regularly used as a proxy to reflect the habitat of certain species or groups of species (Brown et al., 2011), but this assumption requires validation in poorly understood ecosystems such as the deep Greenland waters studied here. Although some terrain descriptors may be greatly affected by biogenic structures (e.g., cold-water coral reefs will affect backscatter at < 1 m resolution, Masson et al., 2003; terrain heterogeneity at 0.1 m resolution, Huvenne et al., 2011), such biogenic structures themselves create habitat for other species, and hence can be considered part of the initial habitat characterization, particularly if it has to be based on remote sensing data, with little or no groundtruthing data available for quantitative validation.

Several clusters did show differences in assemblage composition (**Figure 8**), although sometimes only explained by few species. Being a rare species, *D. pertusum* drove most of the significant differences related to the high-roughness habitat class T4. *D. pertusum* live framework was observed at rocky outcrops which is comparable with previous observations made at steep terrains (Huvenne et al., 2011; Pearman et al., 2020). Patches of *Acesta* sp. grew attached to the hard substrate of vertical features similar to sightings reported in Northeast Atlantic canyons (Johnson et al., 2013; Robert et al., 2017; Pearman et al., 2020). However, community composition differences were not strong, nor was any particular species predominantly contributing to assemblage dissimilarity. For example, on the one hand,

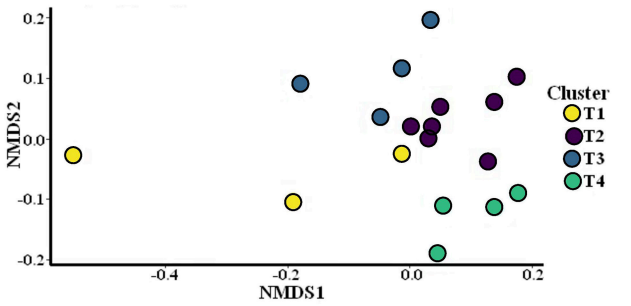

FIGURE 8 | Non-metric MDS ordination of Hellinger transformed Bray-Curtis dissimilarity of assemblage compositions across the wall. Factors T1–T4 refer to the K-means majority clusters. Cluster colors are synchronized with those displayed in **Figure 5**.

D. glomerata showed higher abundances in the high-roughness cluster T4, while on the other hand it still co-occurred with *A. pennatula*, which was more sighted on smoother terrain with low backscatter (T1). Linked together, these results suggest assemblage differences explained by a few rarer species occurring at particular terrain features, whereas the small extent of the study area may have contributed to assemblage similarity as the sessile communities tended to overlap in space. A more extensive characterization of the wall communities is required to confirm these patterns whereas species distribution models may be useful to investigate specific spatial distributions independently from the rest of the community.

Linking abiotic habitats with assemblage composition using unsupervised habitat mapping may not always result in strong delineation of communities, but is one of the only ways to carry out a first-level interpretation of a seabed area if biological data are sparse or non-existent (Hogg et al., 2018). At least 3 additional factors possibly played a role in the outcome of this community analysis. (1) The sampling, which took place before the habitat mapping work was completed, was not designed to collect images according to the spatial arrangement of the abiotic clusters. Vertical ROV tracks aimed to investigate communities across depths, but this can mislead the validity of comparing biological communities across other abiotic terrain categories because of a difference in sampling strategy between both. The terrain investigation resulted in abiotic clusters which did not fully distribute according to depth. Other terrain characteristics, not distributed along depth, also influenced the unsupervised clustering patterns and did influence the presence of a few particular species (e.g., slope, roughness, backscatter intensity). (2) Terrain descriptors that did not strongly explain clustering results may be more important in driving assemblage composition, for example by influencing current exposure through orientation or by positioning the species at keystone structures (e.g., overhangs revealed by BPI (Robert et al., 2017, 2020). Other environmental factors which were not measured may have been at play but remained excluded from the K-means clustering (e.g., hydrodynamics, physical and chemical properties of the water column). Furthermore, at such a fine scale, biological factors act on assemblage structure, such as biotic interactions or the presence of structuring species (Buhl-Mortensen et al., 2010). In ecology, spatial autocorrelation in species distribution is a natural reality triggered not only by the presence of the correct ecological niche, but also by migration of mobile species and dispersion of sessile organisms (Legendre and Legendre, 1998). Therefore, observations may not always reflect the ecological niche a species can occupy. (3) Habitat clusters are discrete categories that may not reflect transitional patterns between communities; especially abiotic clusters were locally patchy and discontinuous. Considering only the majority cluster located within an image area may overlook fine-scale habitat heterogeneity. Local diversity of habitats may influence the presence of a more diverse panel of species than if the seabed habitat were more homogeneous. So-called 'fuzzy classification' approaches that reflect point membership in the point cloud to several clusters may allow a more realistic mapping of transitional habitats or 'ecotones' (Lucieer and Lamarche, 2011).

Application of Unsupervised Vertical Habitat Mapping in Future Surveys

This study presents an application of high-resolution habitat mapping of vertical cliffs in the deep sea. Pre-existing information about deep-water vertical walls in most cases is sparse or non-existent because of their inaccessibility and the difficulties in mapping such terrains with conventional methods. In such cases, an initial unsupervised habitat mapping approach is appropriate to obtain a first-level interpretation of the habitat structure (Hogg et al., 2018). The spatial distribution of clusters will then be useful to objectively and rapidly inform the user regarding the heterogeneity/similarity of the habitat. This initial information can help the definition of a robust sampling design that optimizes habitat representativeness of the area of interest (LaFrance et al., 2014), which is especially useful during exploration activities or in poorly characterized environments such as in deep waters, where sampling time is limited and costly. Defined on that objective information, groundtruth sampling will help to build a refined habitat map by validating the level of (dis)similarity and ecological relevance between habitats delineated by the first seafloor classification.

CONCLUSION

This study demonstrated our ability to capture fine-scale seabed characteristics of vertical habitats in the deep sea using forward-looking acoustic survey methods (bathymetry and backscatter) on underwater platforms. Unsupervised habitat mapping based on K-means clustering was applied to delineate similarities across the vertical seabed and to summarize the multidimensionality of the benthic substrate variables. The latter revealed terrain differences linked with geomorphological

features >200 and >25 m in size, and meter-scale heterogeneity (e.g., roughness). Groundtruthing photographs partitioned among the abiotic clusters indicated dissimilarities of benthic community composition. However, these differences remained attenuated therefore calling for a more representative sampling and characterization of the faunal assemblages based on a better sampling scheme. Simultaneously, this study stresses the need for an investigation into alternative clustering approaches that may describe the environmental conditions in a more adequate way. Furthermore, the extraction of the backscatter intensity at vertical underwater terrain remaining at its infancy, it demonstrates the need for further development to ensure accurate acquisition of this proxy of the substrate properties.

Nevertheless, this investigation demonstrates the need and possibilities of this method for multidisciplinary investigations of vertical features at fine scales in geology, ecology and habitat prediction, especially when adding the backscatter information. Meter-scale unsupervised terrain mapping remains a cost-effective and objective tool to inform relevant and representative field sampling strategies in remote environments where no *a priori* knowledge is available, such as at deep underwater cliffs. However, acquisition of robust groundtruthing data remains necessary to fully characterize the faunal communities, especially in the undersampled deep-sea benthic habitat of Greenland waters. In practice, uncertainties in ROV positioning and attitude recording are still some of the major challenges when working in this type of environment and with high-resolution terrain characterization. While we proposed post-processing methods that help to limit error propagation, positional errors can still affect the habitat mapping outcomes and possibly constrain the spatial accuracy when linking abiotic and biotic datasets. Further investigations and development in vehicle navigation are needed to improve high-resolution habitat mapping in complex deep-sea environments.

DATA AVAILABILITY STATEMENT

The original contributions presented in the study are included in the article/**Supplementary Material**, further inquiries can be directed to the corresponding author/s. Original data (terrain and biotic variables) are provided https://doi.org/10.1594/PANGAEA.931687.

AUTHOR CONTRIBUTIONS

VH conceived the study. VH and KH carried out the field work. LV performed abiotic data analyses and drafted the manuscript. EB conducted biotic data analyses. All authors contributed to editing the final manuscript.

FUNDING

This work was initially part of a thesis supported by the International Master of Science in Marine Biological Resources (IMBRSea; LV). IMBRSea is a Joint Master's Degree under Erasmus Mundus coordinated by Ghent University (FPA 574482-EPP-1-2016-1-BE-EPPKA1-JMD-MOB). Funding for DY081 was from the European Research Council (ERC Starting Grant 678371 ICY-LAB). VH was supported by the NERC National Capability Program CLASS (Grant No. NE/R015953/1). EU H2020 project iAtlantic (Grant No. 818123) also supported VH and LV. Paper publication costs were supported by NERC National Capability funding.

ACKNOWLEDGMENTS

We acknowledge the Captain and the crew of the RRS Discovery as well as the ROV *Isis* technical team of the National Oceanography Centre (NOC). We gratefully thank Tabitha Pearman, Tim Le Bas, Catherine Wardell, Guillem Corbera, Michael Faggetter, David Price, and Pål Buhl-Mortensen for their help and advice and Erik Simon-Lledó for his assistance on the BIIGLE platform. We would like to thank Katleen Robert who provided R scripts for preprocessing and Evan Edinger for reviewing the initial version of our work. We appreciated the constructive feedback of two reviewers who improved the earlier versions of the manuscript.

SUPPLEMENTARY MATERIAL

The Supplementary Material for this article can be found online at: https://www.frontiersin.org/articles/10.3389/fmars.2021.669372/full#supplementary-material

REFERENCES

Althaus, F., Williams, A., Kloser, R. J., Seiler, J., and Bax, N. J. (2012). "Evaluating geomorphic features as surrogates for benthic biodiversity on Australia's western continental margin," in *Seafloor Geomorphology as Benthic Habitat*, eds P. T. Harris and E. K. Baker (Amsterdam: Elsevier), 665–679. doi: 10.1016/B978-0-12-385140-6.00048-7

Anderson, M. J., Gorley, R. N., and Clarke, K. R. (2008). *PERMANOVA+ for PRIMER: Guide to Software and Statistical Methods*. Plymouth: PRIMER-E.

Batista, P., Silvestre, C., and Oliveira, P. (2012). "GES integrated LBL/USBL navigation system for underwater vehicles," in *Proceedings of the 2012 IEEE 51st IEEE Conference on Decision and Control (CDC)*, (Maui, HI: IEEE), 6609–6614. doi: 10.1109/CDC.2012.6426614

Benoist, N. M. A., Morris, K. J., Bett, B. J., Durden, J. M., Huvenne, V. A. I., Le Bas, T. P., et al. (2019). Monitoring mosaic biotopes in a marine conservation zone by autonomous underwater vehicle. *Conserv. Biol.* 33, 1174–1186. doi: 10.1111/cobi.13312

Bezdek, J. C. (1974). Numerical taxonomy with fuzzy sets. *J. Math. Biol.* 1, 57–71. doi: 10.1007/BF02339490

Birant, D., and Kut, A. (2007). ST-DBSCAN: an algorithm for clustering spatial-temporal data. *Data Knowl. Eng.* 60, 208–221. doi: 10.1016/j.datak.2006.01.013

Broad, E. (2020). *The Community Structure of Epibenthic Megafauna on the Continental Slope in Southwest Greenland*, Master's Thesis. Southampton: The University of Southampton, 63.

Brooke, S., and Ross, S. W. (2014). First observations of the cold-water coral Lophelia pertusa in mid-Atlantic canyons of the USA. *Deep. Res. Part II* 104, 245–251. doi: 10.1016/j.dsr2.2013.06.011

Brooke, S. D., Watts, M. W., Heil, A. D., Rhode, M., Mienis, F., Duineveld, G. C. A., et al. (2017). Distributions and habitat associations of

deep-water corals in Norfolk and Baltimore Canyons, Mid-Atlantic Bight, USA. *Deep Res. Part II* 137, 131–147. doi: 10.1016/j.dsr2.2016.05.008

Brown, C. J., and Blondel, P. (2009). Developments in the application of multibeam sonar backscatter for seafloor habitat mapping. *Appl. Acoust.* 70, 1242–1247. doi: 10.1016/j.apacoust.2008.08.004

Brown, C. J., Smith, S. J., Lawton, P., and Anderson, J. T. (2011). Benthic habitat mapping: a review of progress towards improved understanding of the spatial ecology of the seafloor using acoustic techniques. *Estuar. Coast. Shelf Sci.* 92, 502–520. doi: 10.1016/j.ecss.2011.02.007

Buhl-Mortensen, L., Vanreusel, A., Gooday, A. J., Levin, L. A., Priede, I. G., Buhl-Mortensen, P., et al. (2010). Biological structures as a source of habitat heterogeneity and biodiversity on the deep ocean margins. *Mar. Ecol.* 31, 21–50. doi: 10.1111/j.1439-0485.2010.00359.x

Buhl-Mortensen, P., Buhl-Mortensen, L., and Purser, A. (2017). "Trophoic ecology and habitat provision in cold-water coral ecosystems," in *Marine Animal Forests*, eds S. Rossi, L. Bramanti, A. Gori, and C. Orejas (Cham: Springer), 919–944. doi: 10.1007/978-3-319-17001-5

Burrough, P. A., Van Gaans, P. F. M., and Hootsmans, R. (1997). Continuous classification in soil survey: Spatial correlation, confusion and boundaries. *Geoderma* 77, 115–135. doi: 10.1016/S0016-7061(97)00018-9

Caliński, T., and Harabasz, J. (1974). A dendrite method for cluster analysis. *Commun. Stat.* 3, 1–27.

Carter, G. D. O., Huvenne, V. A. I., Gales, J. A., Lo, C., Marsh, L., Ougier-simonin, A., et al. (2018). Ongoing evolution of submarine canyon rockwalls; examples from the Whittard Canyon, Celtic Margin (NE Atlantic). *Prog. Oceanogr.* 169, 79–88. doi: 10.1016/j.pocean.2018.02.001

Corbera, G., Lo, C., Gràcia, E., Grinyó, J., Pierdomenico, M., Huvenne, V. A. I., et al. (2019). Ecological characterisation of a Mediterranean cold-water coral reef: Cabliers Coral Mound Province (Alboran Sea, western Mediterranean). *Prog. Oceanogr.* 175, 245–262. doi: 10.1016/j.pocean.2019.04.010

Costello, M. J., Cheung, A., and De Hauwere, N. (2010). Surface area and the seabed area, volume, depth, slope, and topographic variation for the world's seas, oceans, and countries. *Environ. Sci. Technol.* 44, 8821–8828. doi: 10.1021/es1012752

Costello, M. J., Mccrea, M., Freiwald, A., Lundälv, T., Jonsson, L., Bett, B. J., et al. (2005). "Role of cold-water *Lophelia pertusa* coral reefs as fish habitat in the NE Atlantic," in *Cold-water Corals and Ecosystems*, eds A. Freiwald and J. M. Roberts (Berlin: Springer-Verlag), 771–805.

Culwick, T., Phillips, J., Goodwin, C., Rayfield, E. J., and Hendry, K. R. (2020). Sponge density and distribution constrained by fluid forcing in the deep sea. *Front. Mar. Sci.* 7:395. doi: 10.3389/fmars.2020.00395

Davies, J. S., Guillaumont, B., Tempera, F., Vertino, A., Beuck, L., Ólafsdóttir, S. H., et al. (2017). A new classification scheme of European cold-water coral habitats: implications for ecosystem-based management of the deep sea. *Deep Res. Part II Top. Stud. Oceanogr.* 145, 102–109. doi: 10.1016/j.dsr2.2017.04.014

De Clippele, L. H., Huvenne, V. A. I., Molodtsova, T. N., and Roberts, J. M. (2019). The diversity and ecological role of non-scleractinian corals (Antipatharia and Alcyonacea) on scleractinian cold-water coral mounds. *Front. Mar. Sci.* 6:184. doi: 10.3389/fmars.2019.00184

De Falco, G., Tonielli, R., Di Martino, G., Innangi, S., Simeone, S., and Michael Parnum, I. (2010). Relationships between multibeam backscatter, sediment grain size and *Posidonia oceanica* seagrass distribution. *Cont. Shelf Res.* 30, 1941–1950. doi: 10.1016/j.csr.2010.09.006

Edinger, E. N., Sherwood, O. A., Piper, D. J. W., Wareham, V. E., Baker, K. D., Gilkinson, K. D., et al. (2011). Geological features supporting deep-sea coral habitat in Atlantic Canada. *Cont. Shelf Res.* 31, S69–S84. doi: 10.1016/j.csr.2010.07.004

Ester, M., Kriegel, H. P., Sander, J., and Xu, X. (1996). "A density-based algorithm for discovering clusters in large spatial databases with noise," in *KDD'96: Proceedings of the Second International Conference on Knowledge Discovery and Data Mining*, (Miinche: AAAI), 226–231. doi: 10.1016/B978-044452701-1.00067-3

Frederiksen, R., Jensen, A., and Westerber, H. (1992). The distribution of the scleractinian coral Lophelia pertusa around the Faroe Islands and the relation to internal tidal mixing. *Sarsia* 77, 157–171.

Freiwald, A., Beuck, L., Rüggeberg, A., Taviani, M., and Hebbeln, D. (2009). The white coral community in the central mediterranean sea revealed by ROV surveys. *Oceanography* 22, 58–74. doi: 10.5670/oceanog.2009.06

Gasbarro, R., Wan, D., and Tunnicliffe, V. (2018). Composition and functional diversity of macrofaunal assemblages on vertical walls of a deep northeast Pacific fjord. *Mar. Ecol. Prog. Ser.* 597, 47–64.

Gass, S. E., and Roberts, J. M. (2006). The occurrence of the cold-water coral *Lophelia pertusa* (Scleractinia) on oil and gas platforms in the North Sea: colony growth, recruitment and environmental controls on distribution. *Mar. Pollut. Bull.* 52, 549–559. doi: 10.1016/j.marpolbul.2005.10.002

Gerdes, K., Arbizu, P. M., Schwarz-Schampera, U., Schwentner, M., and Kihara, T. C. (2019). Detailed mapping of hydrothermal vent fauna: a 3d reconstruction approach based on video imagery. *Front. Mar. Sci.* 6:96. doi: 10.3389/fmars.2019.00096

Girard, F., Sarrazin, J., Arnaubec, A., Cannat, M., Sarradin, P.-M., Wheeler, B., et al. (2020). Currents and topography drive assemblage distribution on an active hydrothermal edifice. *Prog. Oceanogr.* 187:102397. doi: 10.1016/j.pocean.2020.102397

Gori, A., Orejas, C., Madurell, T., Bramanti, L., Martins, M., Quintanilla, E., et al. (2013). Bathymetrical distribution and size structure of cold-water coral populations in the Cap de Creus and Lacaze-Duthiers canyons (northwestern Mediterranean). *Biogeosciences* 10, 2049–2060. doi: 10.5194/bg-10-2049-2013

Greene, H. G., Yoklavich, M. M., Starr, R. M., O'Connell, V. M., Wakefield, W. W., Sullivan, D. E., et al. (1999). A classification scheme for deep for seafloor habitats. *Oceanol. Acta* 22, 663–678.

Haedrich, R. L., and Gagnon, J. M. (1991). Rock wall fauna in a deep Newfoundland fiord. *Cont. Shelf Res.* 11, 1199–1207.

Hall-Spencer, J., Allain, V., Fossa, J. H., and Copernic, P. N. (2002). Trawling damage to Northeast Atlantic ancient coral reefs. *Proc. R. Soc. Lond. Ser. B Biol. Sci.* 269, 507–511. doi: 10.1098/rspb.2001.1910

Harris, P. T., and Whiteway, T. (2011). Global distribution of large submarine canyons: geomorphic differences between active and passive continental margins. *Mar. Geol.* 285, 69–86. doi: 10.1016/j.margeo.2011.05.008

Hartigan, J. A. (1975). *Clustering Algorithms*. Hoboken, NJ: John Wiley & Sons, Inc.

Hartigan, J. A., and Wong, M. A. (1979). A K-means clustering algorithm: algorithm AS 136. *Appl. Stat.* 28, 126–130.

Hendry, K. R. (2017). *RRS Discovery cruise DY081, July 6th-August 8th 2017*. Southampton: ICY-LAB.

Hendry, K. R., Huvenne, V. A. I., Robinson, L. F., Annett, A., Badger, M., Jacobel, A. W., et al. (2019). The biogeochemical impact of glacial meltwater from Southwest Greenland. *Prog. Oceanogr.* 176:102126. doi: 10.1016/j.pocean.2019.102126

Hill, N. A., Lucieer, V., Barrett, N. S., Anderson, T. J., and Williams, S. B. (2014). Estuarine, coastal and shelf science filling the gaps: predicting the distribution of temperate reef biota using high resolution biological and acoustic data. *Estuar. Coast. Shelf Sci.* 147, 137–147. doi: 10.1016/j.ecss.2014.05.019

Hogg, O. T., Huvenne, V. A. I., Griffiths, H. J., Dorschel, B., and Linse, K. (2016). Landscape mapping at sub-Antarctic South Georgia provides a protocol for underpinning large-scale marine protected areas. *Sci. Rep.* 6:33163. doi: 10.1038/srep33163

Hogg, O. T., Huvenne, V. A. I., Griffiths, H. J., and Linse, K. (2018). On the ecological relevance of landscape mapping and its application in the spatial planning of very large marine protected areas. *Sci. Total Environ.* 626, 384–398. doi: 10.1016/j.scitotenv.2018.01.009

Howell, K. L., Davies, J. S., Louise Allcock, A., Braga-Henriques, A., Buhl-Mortensen, P., Carreiro-Silva, M., et al. (2019). A framework for the development of a global standardised marine taxon reference image database (SMarTaR-ID) to support image-based analyses. *bioRxiv* [Preprint] doi: 10.1101/670786

Hoy, S. K., Hendry, K. R., and Huvenne, V. A. I. (2018). *North Atlantic EM-122 multibeam swath bathymetry collected during RRS Discovery cruise DY081DY081 (links to raw files and gridded data)*. Bremen: PANGAEA, doi: 10.1594/PANGAEA.892825

Hugues Clarke, J. E. (2003). Dynamic motion residuals in swath sonar data: ironing out the creases. *Int. Hydrogr. Rev.* 4, 6–23.

Huvenne, V. A. I., Georgiopoulou, A., Chaumillon, L., Lo Iacono, C., and Wynn, R. B. (2016). "Novel method to map the morphology of submarine landslide headwall scarps using remotely operated vehicles," in *Advances in Natural and Technological Hazards Research*, eds G. Lamarche, J. Mountjoy, S. Bull, T. Hubble, S. Krastel, E. Lane, et al. (Cham: Springer US), 135–144. doi: 10.1007/978-3-319-20979-1_13

Huvenne, V. A. I., Huenerbach, V., Blondel, P., and Le Bas, T. P. (2007). "Detailed mapping of shallow-water environments using image texture analysis on sidescan sonar and multibeam backscatter imagery," in *Proceedings of the International Conference "Underwater Acoustic Measurements: Technologies & Results*, eds J. S. Papadakis and L. Bjorno (Heraklion: Foundation for Research & Technology), 879–886.

Huvenne, V. A. I., Pattenden, A. D. C., Masson, D. G., and Tyler, P. A. (2012). "Habitat heterogeneity in the Nazaré deep-sea canyon offshore Portugal," in *Seafloor Geomorphology as Benthic Habitat*, eds P. T. Harris and E. K. Baker (Amsterdam: Elsevier), 691–701. doi: 10.1016/B978-0-12-385140-6.00050-5

Huvenne, V. A. I., Robert, K., Marsh, L., Lo Iacono, C., Le Bas, T., and Wynn, R. B. (2018). "ROVs and AUVs," in *Springer Geology*, eds A. Micallef, S. Krastel, and A. Savini (New York, NY: Springer US), 93–108. doi: 10.1007/978-3-319-57852-1_7

Huvenne, V. A. I., Tyler, P. A., Masson, D. G., Fisher, E. H., Hauton, C., Hühnerbach, V., et al. (2011). A picture on the wall: Innovative mapping reveals cold-water coral refuge in submarine canyon. *PLoS One* 6:e28755. doi: 10.1371/journal.pone.0028755

Ismail, K., Huvenne, V. A. I., and Masson, D. G. (2015). Objective automated classification technique for marine landscape mapping in submarine canyons. *Mar. Geol.* 362, 17–32. doi: 10.1016/j.margeo.2015.01.006

Jackson, D. R., and Briggs, K. B. (1992). High-frequency bottom backscattering: roughness versus sediment volume scattering. *J. Acoust. Soc. Am.* 92, 962–977. doi: 10.1121/1.403966

Johnson, M. P., White, M., Wilson, A., Würzberg, L., Schwabe, E., Folch, H., et al. (2013). A vertical wall dominated by *Acesta excavata* and *Neopycnodonte zibrowii*, part of an undersampled group of deep-sea habitats. *PLoS One* 8:e79917. doi: 10.1371/journal.pone.0079917

Khan, K., Rehman, S. U., Aziz, K., Fong, S., and Sarasvady, S. (2014). "DBSCAN: Past, Present and Future. in The fifth international conference on the applications of digital information and web technologies," in *Proceedings of the The Fifth International Conference on the Applications of Digital Information and Web Technologies (ICADIWT 2014)*, (Bangalore: IEEE), 232–238.

Kiriakoulakis, K., Freiwald, A., Fisher, E., and Wolff, G. A. (2007). Organic matter quality and supply to deep-water coral / mound systems of the NW European Continental Margin. *Int. J. Earth Sci.* 96, 159–170. doi: 10.1007/s00531-006-0078-6

Kohn, A. J., and Leviten, P. J. (1976). Effect of habitat complexity on population density and species richness in tropical intertidal predatory gastropod assemblages. *Oecologia* 25, 199–210.

Kostylev, V. E., Todd, B. J., Fader, G. B. J., Courtney, R. C., Cameron, G. D. M., and Pickrill, R. A. (2001). Benthic habitat mapping on the Scotian Shelf based on multibeam bathymetry, surficial geology and sea floor photographs. *Mar. Ecol. Prog. Ser.* 219, 121–137. doi: 10.3354/meps219121

Kwasnitschka, T., Hansteen, T. H., Devey, C. W., and Kutterolf, S. (2013). Doing fieldwork on the seafloor: photogrammetric techniques to yield 3D visual models from ROV video. *Comput. Geosci.* 52, 218–226. doi: 10.1016/j.cageo.2012.10.008

LaFrance, M., King, J. W., Oakley, B. A., and Pratt, S. (2014). A comparison of top-down and bottom-up approaches to benthic habitat mapping to inform offshore wind energy development. *Cont. Shelf Res.* 83, 24–44. doi: 10.1016/j.csr.2014.04.007

Lamarche, G., and Lurton, X. (2018). Recommendations for improved and coherent acquisition and processing of backscatter data from seafloor-mapping sonars. *Mar. Geophys. Res.* 39, 5–22. doi: 10.1007/s11001-017-9315-6

Lamarche, G., Orpin, A. R., Mitchell, J. S., and Pallentin, A. (2016). "Benthic habitat mapping," in *Biological Sampling in the Deep Sea*, eds M. R. Clark, M. Consalvey, and A. A. Rowden (Hoboken, NJ: John Wiley & Sons), 80–102.

Lance, G. N., and Williams, W. T. (1967). A general theory of classificatory sorting strategies: 1. Hierarchical systems. *Comput. J.* 9, 373–380. doi: 10.1093/comjnl/9.4.373

Langenkämper, D., Zurowietz, M., Schoening, T., and Nattkemper, T. W. (2017). BIIGLE 2 . 0 – browsing and annotating large marine image collections. *Front. Mar. Sci.* 4:83. doi: 10.3389/fmars.2017.00083

Lastras, G., Canals, M., Amblas, D., Lavoie, C., Church, I., De Mol, B., et al. (2011). Understanding sediment dynamics of two large submarine valleys from seafloor data: Blanes and La Fonera canyons, northwestern Mediterranean Sea. *Mar. Geol.* 280, 20–39. doi: 10.1016/j.margeo.2010.11.005

Legendre, P., Ellingsen, K. E., Bjørnbom, E., and Casgrain, P. (2002). Acoustic seabed classification: improved statistical method. *Can. J. Fish. Aquat. Sci.* 59, 1085–1089. doi: 10.1139/f02-096

Legendre, P., and Legendre, L. (1998). *Numerical Ecology*, 2 Edn. Amsterdam: Elsevier Science BV.

Lim, A., Wheeler, A. J., Price, D. M., O'Reilly, L., Harris, K., and Conti, L. (2020). Influence of benthic currents on cold-water coral habitats: a combined benthic monitoring and 3D photogrammetric investigation. *Sci. Rep.* 10:19433. doi: 10.1038/s41598-020-76446-y

Lo Iacono, C., Gràcia, E., Diez, S., Bozzano, G., Moreno, X., Dañobeitia, J., et al. (2008). Seafloor characterization and backscatter variability of the Almería Margin (Alboran Sea, SW Mediterranean) based on high-resolution acoustic data. *Mar. Geol.* 250, 1–18. doi: 10.1016/j.margeo.2007.11.004

Lucieer, V., Hill, N. A., Barrett, N. S., and Nichol, S. (2013). Do marine substrates "look" and "sound" the same? Supervised classification of multibeam acoustic data using autonomous underwater vehicle images. *Estuar. Coast. Shelf Sci.* 117, 94–106. doi: 10.1016/j.ecss.2012.11.001

Lucieer, V., and Lamarche, G. (2011). Unsupervised fuzzy classification and object-based image analysis of multibeam data to map deep water substrates, Cook Strait, New Zealand. *Cont. Shelf Res.* 31, 1236–1247. doi: 10.1016/j.csr.2011.04.016

Lucieer, V., and Lucieer, A. (2009). Fuzzy clustering for seafloor classification. *Mar. Geol.* 264, 230–241. doi: 10.1016/j.margeo.2009.06.006

Lurton, X., Eleftherakis, D., and Augustin, J. M. (2018). Analysis of seafloor backscatter strength dependence on the survey azimuth using multibeam echosounder data. *Mar. Geophys. Res.* 39, 183–203. doi: 10.1007/s11001-017-9318-3

Lurton, X., and Lamarche, G. (2015). *Backscatter Measurements by Seafloor – Mapping Sonars. Guidelines and Recommendations*. Eastsound, WA: GEOHAB.

MacArthur, R. H., and Wilson, E. O. (1967). *The Theory of Island Biogeography*. Princeton, NJ: Princeton University Press, 1.

MacQueen, J. (1967). "Some methods for classification and analysis of multivariate observations," in *Proceedings of the Fifth Berkeley Symposium on Mathematical Statistics and Probability*, Vol. 1, eds L. M. Le Cam and J. Neyman (Berkeley, CA: University of California Press), 281–297.

Malecha, P., and Heifetz, J. (2017). Long-term effects of bottom trawling on large sponges in the Gulf of Alaska. *Cont. Shelf Res.* 150, 18–26. doi: 10.1016/j.csr.2017.09.003

Masson, D. G., Bett, B. J., Billett, D. S. M., Jacobs, C. L., Wheeler, A. J., and Wynn, R. B. (2003). The origin of deep-water, coral-topped mounds in the northern Rockall Trough, Northeast Atlantic. *Mar. Geol.* 194, 159–180. doi: 10.1016/S0025-3227(02)00704-1

Mayer, L., Jakobsson, M., Allen, G., Dorschel, B., Falconer, R., Ferrini, V., et al. (2018). The Nippon foundation-GEBCO seabed 2030 project: the quest to see the world's oceans completely mapped by 2030. *Geosci.* 8, 1–18. doi: 10.3390/geosciences8020063

Micallef, A., Le Bas, T. P., Huvenne, V. A. I., Blondel, P., Hühnerbach, V., and Deidun, A. (2012). A multi-method approach for benthic habitat mapping of shallow coastal areas with high-resolution multibeam data. *Cont. Shelf Res.* 39, 14–26. doi: 10.1016/j.csr.2012.03.008

Milligan, G. W. (1996). "Clustering validation: results and implications for applied analyses," in *Clustering and Classification*, eds P. Arabie, L. J. Hubert, and G De Soete (Singapore: World Scientific Publishing), 341–375.

Milligan, G. W., and Cooper, M. C. (1985). An examination of procedures for determining the number of clusters in a data set. *Psychometrika* 50, 159–179. doi: 10.1007/BF02294245

Milligan, G. W., and Cooper, M. C. (1987). Methodology review: clustering methods. *Appl. Psychol. Meas.* 11, 329–354. doi: 10.1177/014662168701100401

Morris, K. J., Tyler, P. A., Masson, D. G., Huvenne, V. A. I., and Rogers, A. D. (2013). Distribution of cold-water corals in the Whittard Canyon,

NE Atlantic Ocean. *Deep Res. Part II* 92, 136–144. doi: 10.1016/j.dsr2.2013.03.036

Mortensen, P. B., Hovland, M. T., Fossa, J. H., and Furevik, D. M. (2001). Distribution, abundance and size of *Lophelia pertusa* coral reefs in mid-Norway in relation to seabed characteristics. *J. Mar. Biol. Assoc.* 81, 581–597.

Oksanen, J., Blanchet, F. G., Friendly, M., Kindt, R., Legendre, P., McGlinn, D., et al. (2013). *Package "vegan". Community Ecology Package, Version 2*.

Pearman, T. R. R., Robert, K., Callaway, A., Hall, R., Lo Iacono, C., and Huvenne, V. A. I. (2020). Improving the predictive capability of benthic species distribution models by incorporating oceanographic data – Towards holistic ecological modelling of a submarine canyon. *Prog. Oceanogr.* 184:102338. doi: 10.1016/j.pocean.2020.102338

Preisendorfer, R. W., and Mobley, C. D. (1988). *Principal Component Analysis in Meteorology and Oceanography*. New York, NY: ScienceOpen.

Price, D. M., Robert, K., Callaway, A., Lo Iacono, C., Hall, R. A., and Huvenne, V. A. I (2019). Using 3D photogrammetry from ROV video to quantify cold-water coral reef structural complexity and investigate its influence on biodiversity and community assemblage. *Coral Reefs* 38, 1007–1021. doi: 10.1007/s00338-019-01827-3

R Core Team (2013). *R: A Language and Environment for Statistical Computing*. Vienna: R Foundation for Statistical Computing, 201.

Ramirez-Llodra, E., Brandt, A., Danovaro, R., De Mol, B., Escobar, E., German, C. R., et al. (2010). Deep, diverse and definitely different: Unique attributes of the world's largest ecosystem. *Biogeosciences* 7, 2851–2899. doi: 10.5194/bg-7-2851-2010

Revelle, W., and Revelle, M. W. (2015). Package "psych.". *Compr. R Arch. Netw.* 337, 338.

Rigby, P., Pizarro, O., and Williams, S. B. (2006). "Towards geo-referenced AUV navigation through fusion of USBL and DVL measurements," in *Proceedings of the Oceans 2006*, (Boston, MA: IEEE), 1–6. doi: 10.1109/OCEANS.2006.306898

Robert, K., Huvenne, V. A. I., Georgiopoulou, A., Jones, D. O. B., Marsh, L., Carter, D. O. G., et al. (2017). New approaches to high-resolution mapping of marine vertical structures. *Sci. Rep.* 7:9005. doi: 10.1038/s41598-017-09382-z

Robert, K., Jones, D. O. B., Georgiopoulou, A., and Huvenne, V. A. I. (2020). Cold-water coral assemblages on vertical walls from the Northeast Atlantic. *Divers. Distrib.* 26, 284–298. doi: 10.1111/ddi.13011

Ross, S. W., and Quattrini, A. M. (2007). The fish fauna associated with deep coral banks off the southeastern United States. *Deep. Res. Part I* 54, 975–1007. doi: 10.1016/j.dsr.2007.03.010

Sichi, O. G., Blondel, P. H., and Gràcia, E. (2005). "Acoustic textures and seafloor characterisation of submarine landslides – an example from the Sw Iberian Margin," in *Boundary Influences In High Frequency, Shallow Water Acoustics*, eds N. G. Pace and P. Blondel (Bath: University of Bath), 271–278.

Stewart, P. L., Pocklington, P., and Cunjak, R. A. (1985). Distribution, abundance and diversity of Benthic Macroinvertebrates on the Canadian continental shelf and slope of Southern Davis Strait and Ungava Bay. *Arctic* 38, 281–291.

Vassallo, P., Bianchi, C. N., Paoli, C., Holon, F., Navone, A., Bavestrello, G., et al. (2018). A predictive approach to benthic marine habitat mapping: efficacy and management implications. *Mar. Pollut. Bull.* 131, 218–232. doi: 10.1016/j.marpolbul.2018.04.016

Verfaillie, E., Degraer, S., Schelfaut, K., Willems, W., and Van Lancker, V. (2009). A protocol for classifying ecologically relevant marine zones, a statistical approach. *Estuar. Coast. Shelf Sci.* 83, 175–185. doi: 10.1016/j.ecss.2009.03.003

Wheeler, A. J., Bett, B. J., Billett, D. S. M., Masson, D. G., and Mayor, D. J. (2005). "The impact of demersal trawling on northeast Atlantic deepwater coral habitats: the case of the Darwin mounds, United Kingdom," in *Proceedings of the American Fisheries Society Symposium*, (Bethesda, MD: American Fisheries Society), 807–818.

Wilborn, R., Rooper, C. N., Goddard, P., Li, L., Williams, K., and Towler, R. (2018). The potential effects of substrate type, currents, depth and fishing pressure on distribution, abundance, diversity, and height of cold-water corals and sponges in temperate, marine waters. *Hydrobiologia* 811, 251–268. doi: 10.1007/s10750-017-3492-9

Wilson, M. F. J., O'Connell, B., Brown, C., Guinan, J. C., and Grehan, A. J. (2007). Multiscale terrain analysis of multibeam bathymetry data for habitat mapping on the continental slope. *Mar. Geod.* 30, 3–35. doi: 10.1080/01490410701295962

Wölfl, A. C., Snaith, H., Amirebrahimi, S., Devey, C. W., Dorschel, B., Ferrini, V., et al. (2019). Seafloor mapping – the challenge of a truly global ocean bathymetry. *Front. Mar. Sci.* 6:283. doi: 10.3389/fmars.2019.00283

Wynn, R. B., Huvenne, V. A. I., Le Bas, T. P., Murton, B. J., Connelly, D. P., Bett, B. J., et al. (2014). Autonomous Underwater Vehicles (AUVs): Their past, present and future contributions to the advancement of marine geoscience. *Mar. Geol.* 352, 451–468. doi: 10.1016/j.margeo.2014.03.012

Yoerger, D. R., Kelley, D. S., and Delaney, J. R. (1997). Fine-scale three-dimensional mapping of a deep-sea hydrothermal vent site using the Jason ROV system. *Int. J. Rob. Res.* 19, 1000–1014.

Zelada Leon, A., Huvenne, V. A. I., Benoist, N. M. A., Ferguson, M., Bett, B. J., and Wynn, R. B. (2020). Assessing the repeatability of automated seafloor classification algorithms, with application in marine protected area monitoring. *Rem. Sens.* 12:1572. doi: 10.3390/rs12101572

Conflict of Interest: The authors declare that the research was conducted in the absence of any commercial or financial relationships that could be construed as a potential conflict of interest.

frontiers in Marine Science

PERSPECTIVE
published: 15 July 2021
doi: 10.3389/fmars.2021.638979

Reefscape Genomics: Leveraging Advances in 3D Imaging to Assess Fine-Scale Patterns of Genomic Variation on Coral Reefs

Pim Bongaerts[1,2], Caroline E. Dubé[1,3†], Katharine E. Prata[1,4†], Johanna C. Gijsbers[1,5†], Michelle Achlatis[1,2,5†] and Alejandra Hernandez-Agreda[1]*

[1] California Academy of Sciences, San Francisco, CA, United States, [2] Caribbean Research and Management of Biodiversity Foundation, Willemstad, Curaçao, [3] Institut de Biologie Intégrative et des Systèmes, Université Laval, Québec, QC, Canada, [4] School of Biological Sciences, The University of Queensland, St Lucia, QLD, Australia, [5] Institute for Biodiversity and Ecosystem Dynamics, University of Amsterdam, Amsterdam, Netherlands

OPEN ACCESS

Edited by:
Manuel Gonzalez-Rivero, Australian Institute of Marine Science (AIMS), Australia

Reviewed by:
Lida Teneva, Independent Researcher, Sacramento, CA, United States
Renata Ferrari, Australian Institute of Marine Science (AIMS), Australia

***Correspondence:**
Pim Bongaerts
pbongaerts@calacademy.org

† These authors have contributed equally to this work

Specialty section:
This article was submitted to Ocean Solutions, a section of the journal Frontiers in Marine Science

Received: *08 December 2020*
Accepted: *16 June 2021*
Published: *15 July 2021*

Citation:
Bongaerts P, Dubé CE, Prata KE, Gijsbers JC, Achlatis M and Hernandez-Agreda A (2021) Reefscape Genomics: Leveraging Advances in 3D Imaging to Assess Fine-Scale Patterns of Genomic Variation on Coral Reefs. Front. Mar. Sci. 8:638979. doi: 10.3389/fmars.2021.638979

Coral reefs across the world are undergoing rapid deterioration, and understanding the ecological and evolutionary processes that govern these ecosystems is critical to our ability to protect them. Molecular ecological studies have been instrumental in advancing such understanding, and while initially focused primarily on broad-scale patterns, they have gradually uncovered the prevalence of local genetic structuring. Genome-wide sequencing approaches have provided new opportunities to understand both neutral and adaptive contributions to this largely unexplained diversity, but fine-scale assessments have been hampered by challenges associated with aquatic environments, in terms of (geo)referencing, seafloor characterization, and *in situ* phenotyping. Here, we discuss the potential of "reefscape genomics," leveraging recent advances in underwater imaging to enable spatially explicit genomic studies on coral reefs. More specifically, we consider how (close-range) photogrammetry approaches enable (1) fine-scale spatial mapping of benthic target organisms, (2) repeatable characterization of the abiotic and biotic reefscape, and (3) simultaneous *in situ* mass-phenotyping. The spatially explicit consideration of genomic data –combined with detailed environmental and phenotypic characterization– opens up the opportunity for fine-scale landscape genomic approaches on coral reefs (and other marine ecosystems). Such approaches enable assessment of the spatio-temporal drivers and adaptive potential of the extensive genetic structuring and cryptic diversity encountered in benthic invertebrates, such as reef-building corals. Considering the threats that coral reefs are facing worldwide, we believe that reefscape genomics represents a promising advancement of our molecular ecological toolkit to help inform how we can most effectively conserve and restore coral reef ecosystems into the future.

Keywords: reefscape genomics, seascape genomics, coral reefs, photogrammetry, structure from motion, landscape genomics

INTRODUCTION

Coral reefs are one of the most biodiverse and economically important ecosystems. Yet, they are undergoing an unprecedented decline due to a wide range of anthropogenic stressors (e.g., increasing sea temperatures, ocean acidification, pollution, and overfishing) (Hoegh-Guldberg et al., 2007; McClenachan et al., 2017). Our ability to manage and conserve these vulnerable ecosystems is contingent on our understanding of the fundamental processes underpinning their resilience. Over the past decades, molecular ecology has played a major role in elucidating these processes for reef-building corals (order Scleractinia) (van Oppen and Gates, 2006), by uncovering patterns of dispersal and connectivity (Ayre and Hughes, 2000; van Oppen et al., 2008), contributions of sexual and asexual reproduction (Miller and Ayre, 2004; Foster et al., 2013; Dubé et al., 2017), the prevalence and nature of hybridization (Vollmer and Palumbi, 2002; Combosch et al., 2008), and the endosymbiotic microbial diversity which is critical to their survival (Baums et al., 2014; Boilard et al., 2020). Importantly, the advent of high-throughput genomic approaches (e.g., reduced representation and whole-genome sequencing) has facilitated increasingly sophisticated assessments for non-model organisms (Riginos et al., 2016; Matz, 2018), including the opportunity to study adaptive variation critical to the persistence of coral reefs (Bay and Palumbi, 2014; Dixon et al., 2015). While these genomic advances hold great promise to address knowledge gaps in ecology and evolution, their true potential is ultimately dependent on our ability to couple their outputs with environmental and/or phenotypic information at the relevant spatial scale (Andrew et al., 2013).

Landscape genetics has provided a powerful framework in terrestrial ecosystems to predict population genomic patterns from landscape attributes and processes (Manel et al., 2003; Balkenhol et al., 2016). By extension, landscape genomics is a more recent discipline that queries similar relationships but across both neutral and adaptive parts of the genome (Balkenhol et al., 2017; Li et al., 2017). As its marine counterpart, seascape genomics shares much of the aforesaid theoretical and analytical framework, but is challenged by physical variability of the oceanic environment and the unique life histories of marine organisms (e.g., high dispersal potential and large effective population sizes) (Riginos et al., 2016; Liggins et al., 2019). Recent studies have demonstrated the potential of seascape genomics in the study of reef-building corals, for example by identifying genes associated with thermal adaptation (Jin et al., 2016; Fuller et al., 2020; Selmoni et al., 2020a,b). Nevertheless, there are several major limitations associated with the application of seascape genomics to coral reef environments. Firstly, due to its reliance on remote sensing methods, the environmental characterization mostly focuses on the (upper) ocean surface (i.e., oceanographic features) rather than the benthic landscape (or "benthoscape"). In addition, the spatial resolution (or "grain") of such remotely sensed methods generally only allows for limited characterization on a within-reef scale. Lastly, spatially explicit, individual-based sampling has been hampered (compared to terrestrial studies) due to the inability of using satellite-based geo-positioning, as radio signals do not propagate sufficiently underwater.

In this perspective, we discuss the potential for "reefscape genomics," leveraging advances in underwater imaging to enable fine-scale landscape genomic studies on coral reefs. The term "reefscape" has been used loosely in the coral reef literature, mostly as an underwater equivalent to the term landscape (e.g., Arias-González et al., 2006; Urbina-Barreto et al., 2020). Inherently connected to seascape genomics, we define reefscape genomics as spatially explicit studies focused on a within-reef scale that use reefscape attributes and processes as statistical predictors of genomic variation. This follows a recent call to expand seascape characterization to specifically include the benthic component (Van Wynsberge et al., 2017), but we argue the additional value of doing so at a high spatial resolution. Such fine-scale characterization of the reefscape has recently been made possible due to advances in computer vision, and further facilitated by the increased accessibility of the underwater environment (e.g., through autonomous underwater vehicles, dive propulsion vehicles, and closed-circuit rebreathers). In particular, we believe that close-range photogrammetry has the potential to transform seascape genomics by enabling (1) fine-scale spatial mapping benthic components, (2) repeatable characterization of both abiotic and biotic features of the benthoscape, and (3) simultaneous mass-phenotyping of target organisms. We begin by explaining why a reefscape genomics approach is relevant in terms of major knowledge gaps (focusing mostly on reef-building corals), we then elaborate on the types of relevant (meta)data that can be acquired through photogrammetry, and we conclude by illustrating how such data can be integrated into genomic assessments to address the outlined knowledge gaps.

WHY REEFSCAPE GENOMICS?

The choice of spatial scale in molecular ecology is critical as it defines the ability to identify the processes underlying genetic variation (Hellberg, 2007). Given the biphasic life cycle of most marine organisms (i.e., pelagic larval and benthic adult phase), it has been traditionally assumed that neutral genetic patterns are governed by broad-scale larval dispersal processes (Kinlan et al., 2005; Liggins et al., 2013). However, studies have since demonstrated the prevalence of local genetic differentiation within both species with internal (brooders) and external (broadcasters) fertilization. For brooding species, such fine-scale population structure can be linked to strongly localized sperm and larval dispersal (Underwood et al., 2007; Ledoux et al., 2010; Warner et al., 2016), while such patterns for broadcasting species contradict with their broad dispersal capability and with observations of high gene flow over large distances (Ayre and Hughes, 2000; van Oppen et al., 2008; Cros et al., 2020). These non-intuitive population structures are likely the result of the complex interplay and spatio-temporal variability in species attributes, pelagic conditions, and benthic features (Liggins et al., 2019). The perceived chaos in reef-building corals is –at least in part– due to a mismatch in spatial

resolution (Cros et al., 2020), a predominance of population-level sampling (Riginos and Liggins, 2013; Liggins et al., 2019), and an almost complete lack of temporal assessments (but see Williams et al., 2014; Underwood et al., 2018). Microsatellite-based studies with exhaustive local sampling have demonstrated the critical relevance of fine-scale, individual-based sampling by revealing the important contributions of clonality and inbreeding (Gorospe and Karl, 2013; Dubé et al., 2017), sperm dispersal and self-fertilization (Warner et al., 2016), co-dispersal of siblings, and self-recruitment (Cros et al., 2020; Dubé et al., 2020). Nonetheless, our understanding of reproduction and dispersal processes in benthic reef organisms is still in its infancy given that spatially explicit, individual-based attempts have been incredibly tedious, and have lacked the ability to characterize and integrate the fine-scale composition and configuration of the reefscape.

Patterns of adaptive variation in marine environments often occur at local scales, with selection contributing to spatial genetic structuring regardless of the extent of gene flow (Liggins et al., 2019). Habitat-specific sampling has demonstrated how local genetic structure in reef-building corals can reflect divergence across environmentally distinct but spatially adjacent reef habitats (Benzie et al., 1995; Bongaerts et al., 2010, 2011; van Oppen et al., 2018), with parallel patterns observed in coral endosymbionts (Frade et al., 2008; Bongaerts et al., 2010; Pantos et al., 2015; Hernandez-Agreda et al., 2018; van Oppen et al., 2018). Such findings highlight the importance of environment-associated selection and the potential for ecological barriers to gene flow. However, substantial genetic and phenotypic diversity in nominal species is being uncovered within reef habitats (Dubé et al., 2017; Gélin et al., 2017; Forsman et al., 2020), with much of that diversity remaining unexplained. While advances in omics-based approaches have shown great potential (Riginos et al., 2016; Matz, 2018), our ability to understand such diversity has been limited by the difficulty of gathering high-resolution data on the corresponding phenotypes and associated environments. Understanding the adaptive potential of this genetic and phenotypic variation (e.g., tolerance to warming or eutrophication) and its nature or origin (e.g., standing genetic variation, hybridization, somatic mutations, or epigenetic), is becoming increasingly important to predict how corals may persist into the future. It is also critical for coral reef conservation and restoration efforts, to ensure that the adaptive potential of protected, translocated, or restored populations is maximized to promote survival under rapidly changing environmental conditions.

REEFSCAPE CHARACTERIZATION THROUGH CLOSE-RANGE PHOTOGRAMMETRY

The logistical difficulty of fine-scale underwater mapping and (geo)referencing has long hampered spatially explicit coral reef studies and thereby direct coupling of genetic data with environmental, ecological, and phenotypic data. However, recent advances in photogrammetry –in particular Structure from Motion (SfM)– now permit fine-scale 3D characterization based on consumer-grade cameras and non-expert software (Figueira et al., 2015; Burns and Delparte, 2017; DeBell et al., 2019). In contrast to stereophotogrammetry that usually relies on calibrated image pairs, SfM can approximate camera position and angle from highly overlapping photographs to generate a "sparse point cloud" (Westoby et al., 2012). This can be further processed using multi-view stereo algorithms into a "dense point cloud" (Iglhaut et al., 2019), from which 2D (orthoprojection/mosaic), 2.5D (digital elevation model), or 3D (textured 3D mesh) products can be generated (**Figure 1**). SfM has been widely adopted in geoscience for topographical surveys (Westoby et al., 2012; Fonstad et al., 2013; Smith et al., 2016), including subaerial forest, wetland and coastal characterization (Kalacska et al., 2017; Iglhaut et al., 2019), but its close-range ability overcomes persistent underwater light attenuation and scattering issues, making SfM particularly suited for fine-scale benthoscape characterization.

SfM has rapidly become a critical tool in benthic ecology studies on coral reefs (Burns et al., 2015; Leon et al., 2015; Ferrari et al., 2016b; Edwards et al., 2017; González-Rivero et al., 2017), where the requirement of a static environment (throughout the imaging process) is largely satisfied by the dominance of reef-building corals. Depending on camera resolution and altitude (i.e., distance to seafloor), current modeling abilities roughly span a grain range of ∼0.1–10 mm and spatial extent range of 0.01–1 ha (**Figure 2**), with a trade-off between grain size and spatial extent. Using scale references, a highly accurate local coordinate system of the generated model can be created (mm to cm accuracy; Ledoux et al., 2010), enabling underwater mapping with unprecedented resolution, efficiency, and repeatability compared to traditional methods using transect tapes, depth gages, and/or compasses (Foster et al., 2013; Gorospe and Karl, 2013; Williams et al., 2014; Gélin et al., 2017; Dubé et al., 2017, 2020). Such local coordinates can be converted to real-world coordinates by georeferencing the model using, e.g., ground control points (GCPs) or by integrating acoustic positioning and orientation sensors on the imaging platform [e.g., ultrashort-baseline (USBL), Doppler velocity log (DVL), and attitude and heading reference systems (AHRS)]. In both cases, the accuracy of georeferencing will be determined by that of the surface-based global navigation satellite system (GNSS) receiver, and the method used to determine positioning relative to that of the receiver (e.g., a simple vertical upline or sophistic multisensory navigation system).

The power of SfM in resolving 3D structure has enabled the study of structural complexity in relation to species diversity, competition, and coexistence. Structural complexity can be characterized through various metrics: linear and surface rugosity (Dustan et al., 2013; Ferrari et al., 2016a, 2018), fractal dimension (Tokeshi and Arakaki, 2012; Leon et al., 2015; Young et al., 2017), crevice or refuge density (González-Rivero et al., 2017; Agudo-Adriani et al., 2019; Oakley-Cogan et al., 2020), viewshed (González-Rivero et al., 2017; Urbina-Barreto et al., 2020), and surface height range (Torres-Pulliza et al., 2020). Broader-scale environmental parameterization (e.g., through the deployment of sensors) has the potential to enable fine-scale modeling of further abiotic variables that cannot be inferred directly from

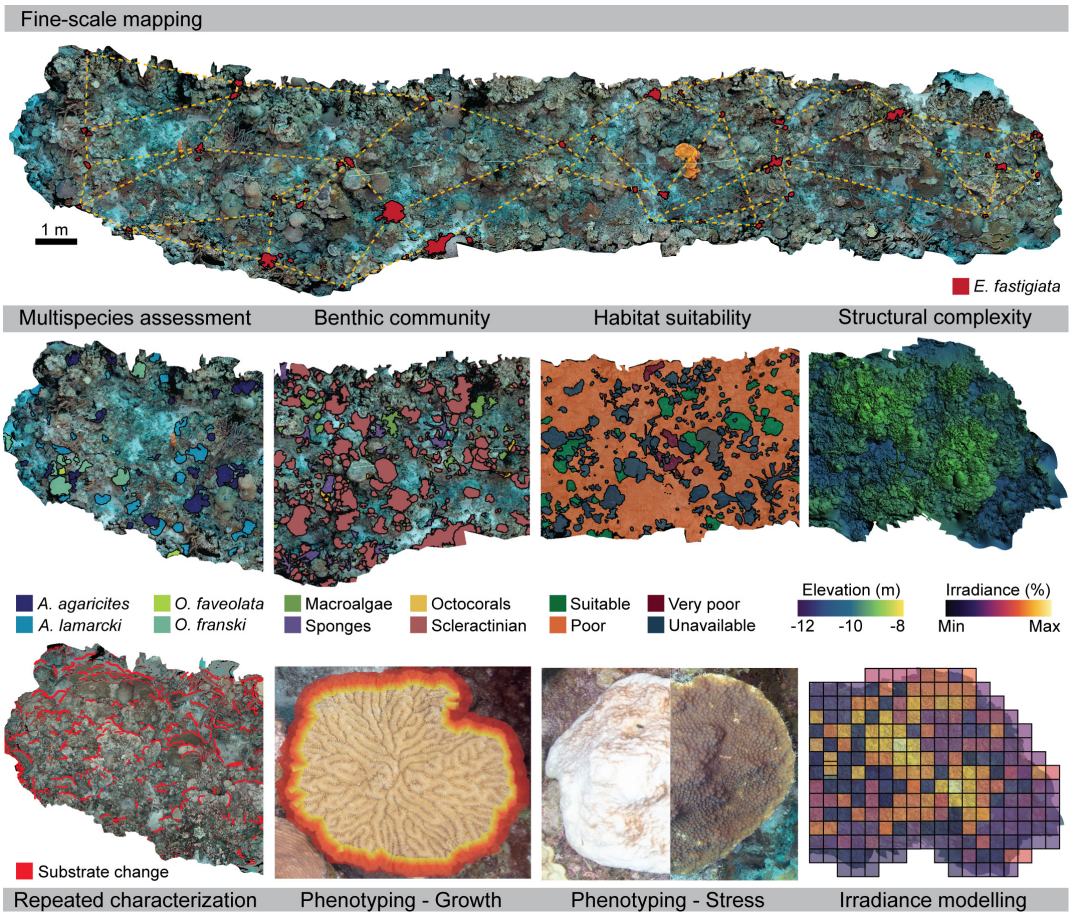

FIGURE 1 | Conceptual diagram summarizing conceptual diagram summarizing different SfM-enabled characterization examples that can be utilized in reefscape genomic studies. The orthoprojection (25 × 4 m) depicts a Caribbean coral reef community at 20 m depth (from the CoralScape project, Curaçao, Southern Caribbean). Fine-scale mapping allows for accurate positioning of target organisms within the reefscape and *a priori* established sampling designs (depicted here for *Eusmilia fastigiata*). It also enables spatially explicit, multi-species assessments (e.g., to characterize broader patterns related to life history or the occurrence and consequences of hybridization). Image-based biotic/abiotic characterization of the reefscape can help elucidate the interaction of dispersal, recruitment, and selection processes with the environment (e.g., considering competitive or mutualistic relationships or habitat suitability). Structural complexity or 3D positioning can be similarly considered or used for environmental or biophysical modeling (e.g., incident irradiance, water flow, sedimentation, or larval dispersal). Repeated characterization allows for spatio-temporal consideration of the reefscape and target organisms, as well as mass-phenotyping of the latter (e.g., growth rates or stress responses).

the imagery, such as temperature, irradiance, water flow, and sedimentation across the reefscape (**Figure 1**). As SfM is imagery-based, detailed characterization (2D/3D) of the seafloor can be undertaken through point-based annotation or semantic segmentation, with promising automation potential through machine learning (Alonso et al., 2019; Williams et al., 2019; Pavoni et al., 2020). Species-level identifications and recruit detection can be facilitated by the pairing of individual points to the original photographs (usually having greater resolution than the constructed dense point cloud), with such characterizations rapidly providing new insights into coral demographics (Edwards et al., 2017; Brito-Millán et al., 2019; Pedersen et al., 2019). The simultaneous documentation of the abiotic and biotic reefscape holds particular promise for landscape community genomic approaches focusing on the interaction of environmental and community effects on genomic variation (Hand et al., 2015).

Another major advantage of SfM characterization is its suitability for repeat surveys, describing how target species populations and interfering biotic and abiotic reefscapes change over time. SfM also opens up the opportunity for simultaneous *in situ* phenotyping of focal organisms through the obtained imagery. Although certain morphological (e.g., gross morphology) and ecological (e.g., symbiotic state) aspects can be extracted from a single time-point, repeated characterization allows for the determination of growth rates (surface or linear expansion; Holmes et al., 2008) or susceptibility to stressors (Chow et al., 2016; Miller et al., 2016; Precht et al., 2016; Page et al., 2017; Gintert et al., 2018; Johnston et al., 2019). The third dimension that photogrammetry adds significantly enhances all aspects of phenotyping; for example, growth traits of corals and other invertebrates are more accurately determined from 3D surface areas and volumes (Lavy et al., 2015;

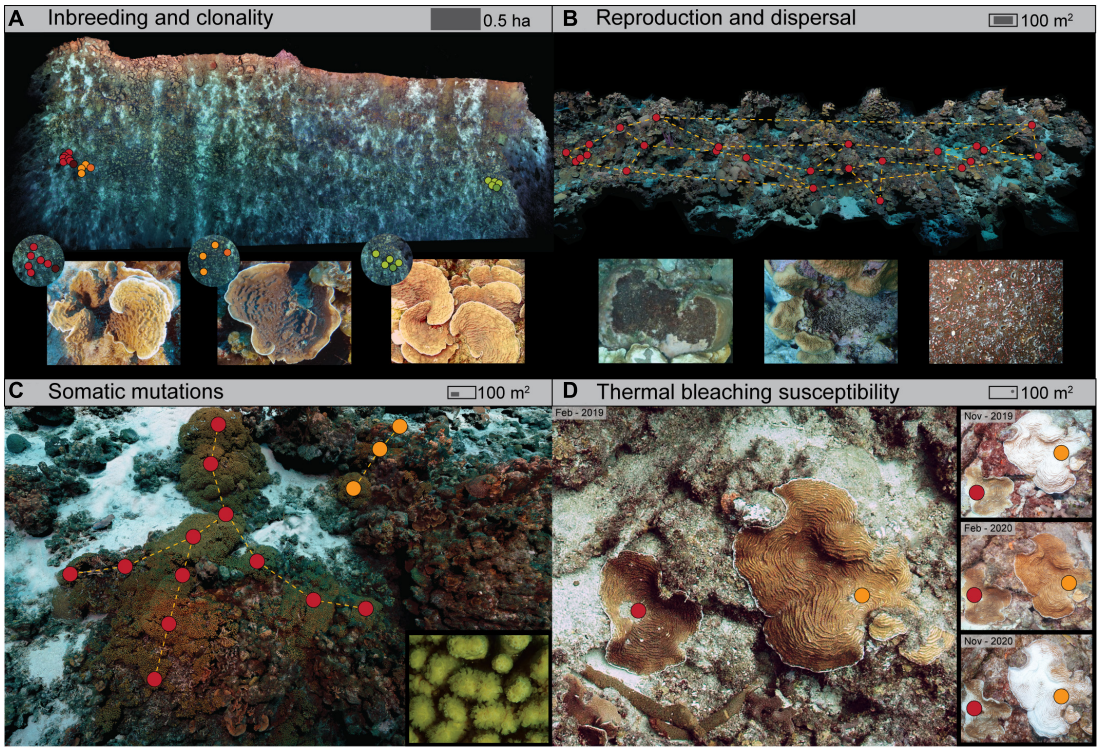

FIGURE 2 | Four example applications of reefscape genomics, conducted as part of the CoralScape project in Curaçao (Southern Caribbean). This project monitors large-area plots (0.5–1 ha per plot) and focal plots (100 m^2) covering a range of 5–60 m depth at eight different locations along the leeward shore. The focal plots are reimaged twice a year (using a Canon 5DsR with an EF 24 mm f1/4 prime lens and four Inon Z330 strobes) and incrementally sampled (for different taxa). Collected samples are referenced to the 3D model using video from a head-mounted camera, with the diver carrying a 96-well rack with numbered 0.5 mL tubes bungee-mounted to their forearm. **(A)** Broad-scale imaging (>0.5 ha per plot) to assess the impact of rapid population decline on the reproduction and genomic variation in the coral *Helioseris cucullata*, and to evaluate extinction risk and appropriate conservation strategies (Hernandez-Agreda et al., unpublished data). **(B)** Medium-scale imaging (100 m^2 per plot) to understand the roles of niche partitioning and asexual reproduction in the fast expansion of coral-eroding sponges in the *Cliona viridis* species complex (Achlatis et al., unpublished data). Inset photographs show different growth forms and a close-up. **(C)** Medium-scale imaging (100 m^2 per plot) to track the spread of somatic mutations in the coral *Madracis mirabilis*, and assess their contributions to genetic diversity in large monospecific stands (Bongaerts et al., unpublished data). **(D)** Medium-scale imaging (100 m^2 per plot) to disentangle the role of environment and genotype in bleaching response and the overall effect of bleaching on population genetic diversity within the coral genus *Agaricia* (Prata et al., unpublished data). Circles represent samples of target organisms (as depicted in close-up photos) colored by genotype (except for in **B**).

Gutiérrez-Heredia et al., 2016; Ferrari et al., 2017; Olinger et al., 2019), as are other colony-level and polyp-level morphological traits (Kruszyński et al., 2007; Gutiérrez-Heredia et al., 2015).

OPPORTUNITIES ENABLED BY REEFSCAPE GENOMICS

Photogrammetric approaches uniquely enable both fine-scale mapping and simultaneous characterization of the focal organism and surrounding reefscape, and will provide a step change in our ability to conduct landscape genomic assessments in marine environments. Such approaches have the potential to overcome pervasive sampling biases associated with underwater population genetic studies (Gorospe et al., 2015; Riginos, 2015) in that rigorous sampling designs can be established based on *a priori* characterized positioning, micro-environment, and phenotypes of organisms across the reefscape (**Figure 1**). As the spatial extent and grain of the reefscape characterization can vary per imaging platform (diver-based or autonomous underwater vehicle) and strategy (low or high altitude), reefscape genomic approaches allow for spatially explicit assessments from fine-scale (e.g., assessing the spread of somatic mutations or distribution of endosymbiotic associations within/between colonies), to medium-scale (e.g., patterns of genetic variation, kinship, and clonality within/across reef habitats), and broad-scale (e.g., in conservation genomics assessments of rare and threatened species at the scale of hectares) (**Figure 2**). Currently, these assessments can be conducted across multiple locations to enable parallel comparisons, or they can be incorporated within a hierarchical seascape genomics framework. Ultimately, they may converge with broader seascape-scale assessments as technologies advance. The explicit consideration of the benthoscape opens up the novel opportunity to assess the effect of the fine-scale biotic and abiotic composition, configuration, and traversability of the underwater landscape on gene flow and dispersal through the use of spatial correlation analyses (e.g., Moran's Eigenvector Maps; Dray et al., 2006) and analyses that identify gene flow

pathways (e.g., resistance-based; McRae, 2006; Petkova et al., 2016). Overall, by enabling repeatable surveys and eliminating constraints on grain size (previously imposed through shipboard, aerial, or orbital characterization), we can now effectively assess the fine-scale spatiotemporal drivers of the extensive unexplained diversity and the hierarchical genetic structuring on coral reefs.

Selection is expected to play a dominant role in shaping the genetic variation of coral reef inhabitants due to the marked environmental heterogeneity occurring between and within reef habitats. Existing approaches investigating adaptive variation can be divided into those that identify genetic signatures of selection resulting from environmental conditions [e.g., outlier tests and genetic-environment association (GEA); Rellstab et al., 2015] and those that identify associations between genotypes and phenotypic traits [e.g., quantitative trait loci (QTL mapping); Stinchcombe and Hoekstra, 2008, genome-wide association studies (GWAS); Korte and Farlow, 2013, and genome-wide selection (GS); Meuwissen et al., 2001]. However, in coral reef invertebrates, GEAs have almost exclusively been explored in relation to either broad-scale oceanographic settings or discrete reef habitats. Characterization of the reefscape now opens the opportunity to investigate the role of fine-scale and biotic selective pressures in population genetic structuring (Gorospe and Karl, 2013), and to explore whether the "sympatric" distribution of morphologically cryptic lineages (Warner et al., 2015) may have overlooked niche partitioning across micro-environments. Moreover, the difficulty of conducting large-scale phenotypic characterization through aquarium-based (due to collection impact concerns) or natural experiments (due to challenges of the underwater environment) has hindered the ability to detect genetic-phenotypic associations. As photogrammetry offers the opportunity of repeated characterization of target organisms, it has the potential to scale up phenotyping efforts of critical traits. Large sample sizes are particularly important for the detection of polygenic signals (i.e., where the phenotype is influenced by more than one locus), such as those identified in relation to thermal bleaching susceptibility (Bay and Palumbi, 2014; Jin et al., 2016; Fuller et al., 2020). Overall, the most promising advance of reefscape genomics is the ability to simultaneously consider the interaction of genotype, (micro-)environment, and phenotype. Disentangling this interaction could elucidate fundamental but poorly understood processes affecting natural evolutionary trajectories, such as cryptic diversification, hybridization, and heritable changes in gene expression (epigenetics). Considering this interaction would also have substantial benefits in terms of restoration and assisted evolution efforts, through more informed identification of resilient natural genotypes and selection of suitable outplanting/transplantation environments (as described in van Oppen et al., 2015; Baums et al., 2019).

CONCLUSION

As advances in genomics have offered the opportunity to transition from few neutral markers to genome-wide assessments, advances in underwater imaging now unlock the full potential of these assessments in benthic marine ecosystems by enabling spatially explicit (individual-based) sampling integrated with fine-scale biotic and abiotic characterization. As discussed in this perspective, this provides the unprecedented potential to apply fine-scale landscape genomics approaches to coral reef environments, allowing us to address fundamental knowledge gaps regarding the role of neutral and adaptive processes in the structuring of coral reef biodiversity. Additional methodological advantages are the opportunities for simultaneous mass-phenotyping (e.g., growth and thermal susceptibility), repeatable surveys (e.g., explaining how demographic changes contribute to changing allele frequencies), cumulative data gathering (e.g., revisit and expand sampling to additional individuals or species), efficient characterization of difficult-to-access environments (e.g., mesophotic habitats), and robust sampling design planning (e.g., based on *a priori* mapped individuals). Although close-range photogrammetry is uniquely suited to document the static structures of reef-building corals, a "benthoscape genomics" approach (to use a more inclusive term) is equally applicable to other marine benthic habitats (e.g., deep-sea bioherms, mangroves, or rocky reefs) where the requirement of a largely static environment can be met. Studying fine-scale patterns and processes in marine ecosystems will be critical in advancing our understanding of contradictory metapopulation structures, our ability to accurately analyze and interpret broader-scale patterns, and ultimately, our capacity to effectively conserve these ecosystems into the future.

AUTHOR CONTRIBUTIONS

PB conceived of the presented idea with input from the other authors. JG created the figures. All authors helped develop the concepts and contributed equally to the writing of the manuscript.

FUNDING

This work was funded by the Hope for Reefs Initiative at the California Academy of Sciences.

ACKNOWLEDGMENTS

We would like to thank the teams of the 100 Island Challenge at Scripps Institution of Oceanography (SIO), the Australian Centre for Field Robotics (ACFR), the Marine Imaging Lab at the University of Haifa, and the Australian Institute of Marine Science (AIMS) for collaborative input on photogrammetry methods. We would also like to thank our Diving Operations team at the California Academy of Sciences for supporting the realization of these ideas in the field.

REFERENCES

Agudo-Adriani, E. A., Cappelletto, J., Cavada-Blanco, F., and Cróquer, A. (2019). Structural complexity and benthic cover explain reef-scale variability of fish assemblages in Los Roques National Park, Venezuela. *Front. Mar. Sci.* 6:690. doi: 10.3389/fmars.2019.00690

Alonso, I., Yuval, M., Eyal, G., Treibitz, T., and Murillo, A. C. (2019). CoralSeg: learning coral segmentation from sparse annotations. *J. Field Robot.* 36, 1456–1477. doi: 10.1002/rob.21915

Andrew, R. L., Bernatchez, L., Bonin, A., Buerkle, A. C., Carstens, B. C., Emerson, B. C., et al. (2013). A road map for molecular ecology. *Mol. Ecol.* 22, 2605–2626. doi: 10.1111/mec.12319

Arias-González, J., Done, T., Page, C., Cheal, A., Kininmonth, S., and Garza-Pérez, J. (2006). Towards a reefscape ecology: relating biomass and trophic structure of fish assemblages to habitat at Davies Reef, Australia. *Mar. Ecol. Prog. Ser.* 320, 29–41. doi: 10.3354/meps320029

Ayre, D. J., and Hughes, T. P. (2000). Genotypic diversity and gene flow in brooding and spawning corals along the Great Barrier Reef, Australia. *Evolution* 54, 1590–1605. doi: 10.1111/j.0014-3820.2000.tb00704.x

Balkenhol, N., Cushman, S. A., Waits, L. P., and Storfer, A. (2016). "Current status, future opportunities, and remaining challenges in landscape genetics," in *Landscape Genetics Concepts, Methods, Applications, First Edition*, eds N. Balkenhol, S. A. Cushman, A. T. Storfer, and L. P. Waits (New York: John Wiley & Sons, Ltd), 247–256. doi: 10.1002/9781118525258.ch14

Balkenhol, N., Dudaniec, R. Y., Krutovsky, K. V., Johnson, J. S., Cairns, D. M., Segelbacher, G., et al. (2017). "Landscape genomics: understanding relationships between environmental heterogeneity and genomic characteristics of populations," in *Population Genomics*, ed. O. Rajora (Cham, CH: Springer), 261–322. doi: 10.1007/13836_2017_2

Baums, I. B., Baker, A. C., Davies, S. W., Grottoli, A. G., Kenkel, C. D., Kitchen, S. A., et al. (2019). Considerations for maximizing the adaptive potential of restored coral populations in the western Atlantic. *Ecol. Appl.* 29:e01978. doi: 10.1002/eap.1978

Baums, I. B., Devlin−Durante, M. K., and LaJeunesse, T. C. (2014). New insights into the dynamics between reef corals and their associated dinoflagellate endosymbionts from population genetic studies. *Mol. Ecol.* 23, 4203–4215. doi: 10.1111/mec.12788

Bay, R. A., and Palumbi, S. R. (2014). Multilocus adaptation associated with heat resistance in reef-building corals. *Curr. Bio.* 24, 2952–2956. doi: 10.1016/j.cub.2014.10.044

Benzie, J. A. H., Haskell, A., and Lehman, H. (1995). Variation in the genetic composition of coral (*Pocillopora damicornis* and *Acropora palifera*) populations from different reef habitats. *Mar. Biol.* 121, 731–739. doi: 10.1007/BF00349309

Boilard, A., Dubé, C. E., Gruet, C., Mercière, A., Hernandez-Agreda, A., and Derome, N. (2020). Defining coral bleaching as a microbial dysbiosis within the coral holobiont. *Microorganisms* 8:1682. doi: 10.3390/microorganisms8111682

Bongaerts, P., Riginos, C., Hay, K. B., van Oppen, M. J. H., Hoegh-Guldberg, O., and Dove, S. (2011). Adaptive divergence in a scleractinian coral: physiological adaptation of *Seriatopora hystrix* to shallow and deep reef habitats. *BMC Evol. Biol.* 11:303. doi: 10.1186/1471-2148-11-303

Bongaerts, P., Riginos, C., Ridgway, T., Sampayo, E. M., van Oppen, M. J. H., Englebert, N., et al. (2010). Genetic divergence across habitats in the widespread coral *Seriatopora hystrix* and its associated *Symbiodinium*. *PLoS One* 5:e10871. doi: 10.1371/journal.pone.0010871

Brito-Millán, M., Werner, B. T., Sandin, S. A., and McNamara, D. E. (2019). Influence of aggregation on benthic coral reef spatio-temporal dynamics. *R. Soc. Open Sci.* 6:181703. doi: 10.1098/rsos.181703

Burns, J., Delparte, D., Gates, R., and Takabayashi, M. (2015). Integrating structure-from-motion photogrammetry with geospatial software as a novel technique for quantifying 3D ecological characteristics of coral reefs. *PeerJ.* 3:e1077. doi: 10.7717/peerj.1077

Burns, J. H. R., and Delparte, D. (2017). Comparison of commercial structure-from-motion photogrammetry software used for underwater three-dimensional modeling of coral reef environments. *Int. Arch. Photogramm. Remote Sens. Spatial Inform. Sci.* XLII-2/W3, 127–131. doi: 10.5194/isprs-archives-xlii-2-w3-127-2017

Chow, M. H., Tsang, R. H. L., Lam, E. K. Y., and Ang, P. Jr. (2016). Quantifying the degree of coral bleaching using digital photographic technique. *J. Exp. Mar. Biol. Ecol.* 479, 60–68. doi: 10.1016/j.jembe.2016.03.003

Combosch, D. J., Guzman, H. M., Schuhmacher, H., and Vollmer, S. V. (2008). Interspecific hybridization and restricted trans−Pacific gene flow in the Tropical Eastern Pacific *Pocillopora*. *Mol. Ecol.* 17, 1304–1312. doi: 10.1111/j.1365-294X.2007.03672.x

Cros, A., Toonen, R. J., and Karl, S. A. (2020). Is post-bleaching recovery of *Acropora hyacinthus* on Palau via spread of local kin groups? *Coral Reefs* 39, 687–699. doi: 10.1007/s00338-020-01961-3

DeBell, L., Duffy, J. P., McKinley, T. J., and Anderson, K. (2019). Species and habitat mapping in two dimensions and beyond. Structure-from-Motion multi-view stereo photogrammetry for the conservation community. *bioRxiv* [Preprint]. doi: 10.1101/2019.12.16.878033

Dixon, G. B., Davies, S. W., Aglyamova, G. V., Meyer, E., Bay, L. K., and Matz, M. V. (2015). Genomic determinants of coral heat tolerance across latitudes. *Science* 348, 1460–1462. doi: 10.1126/science.1261224

Dray, S., Legendre, P., and Peres-Neto, P. R. (2006). Spatial modelling: a comprehensive framework for principal coordinate analysis of neighbour matrices (PCNM). *Ecol. Model.* 196, 483–493. doi: 10.1016/j.ecolmodel.2006.02.015

Dubé, C. E., Boissin, E., Maynard, J. A., and Planes, S. (2017). Fire coral clones demonstrate phenotypic plasticity among reef habitats. *Mol. Ecol.* 26, 3860–3869. doi: 10.1111/mec.14165

Dubé, C. E., Boissin, E., Mercière, A., and Planes, S. (2020). Parentage analyses identify local dispersal events and sibling aggregations in a natural population of *Millepora hydrocorals*, a free−spawning marine invertebrate. *Mol. Ecol.* 29, 1508–1522. doi: 10.1111/mec.15418

Dustan, P., Doherty, O., and Pardede, S. (2013). Digital reef rugosity estimates coral reef habitat complexity. *PLoS One* 8:e57386. doi: 10.1371/journal.pone.0057386

Edwards, C. B., Eynaud, Y., Williams, G. J., Pedersen, N. E., Zgliczynski, B. J., Gleason, A. C., et al. (2017). Large-area imaging reveals biologically driven non-random spatial patterns of corals at a remote reef. *Coral Reefs* 36, 1291–1305. doi: 10.1007/s00338-017-1624-3

Ferrari, R., Figueira, W. F., Pratchett, M. S., Boube, T., Adam, A., Kobelkowsky-Vidrio, T., et al. (2017). 3D photogrammetry quantifies growth and external erosion of individual coral colonies and skeletons. *Sci. Rep.* 7:16737. doi: 10.1038/s41598-017-16408-z

Ferrari, R., Malcolm, H. A., Byrne, M., Friedman, A., Williams, S. B., Schultz, A., et al. (2018). Habitat structural complexity metrics improve predictions of fish abundance and distribution. *Ecography* 41, 1077–1091. doi: 10.1111/ecog.02580

Ferrari, R., McKinnon, D., He, H., Smith, R., Corke, P., González-Rivero, M., et al. (2016b). Quantifying multiscale habitat structural complexity: a cost-effective framework for underwater 3D modelling. *Remote Sens.* 8:113. doi: 10.3390/rs8020113

Ferrari, R., Bryson, M., Bridge, T. C. L., Hustache, J., Williams, S. B., Byrne, M., et al. (2016a). Quantifying the response of structural complexity and community composition to environmental change in marine communities. *Glob. Chang. Biol.* 22, 1965–1975. doi: 10.1111/gcb.13197

Figueira, W., Ferrari, R., Weatherby, E., Porter, A., Hawes, S., and Byrne, M. (2015). Accuracy and precision of habitat structural complexity metrics derived from underwater photogrammetry. *Remote Sens.* 7, 16883–16900. doi: 10.3390/rs71215859

Fonstad, M. A., Dietrich, J. T., Courville, B. C., Jensen, J. L., and Carbonneau, P. E. (2013). Topographic structure from motion: a new development in photogrammetric measurement. *Earth Surf. Process. Landf.* 38, 421–430. doi: 10.1002/esp.3366

Forsman, Z. H., Ritson-Williams, R., Tisthammer, K., Knapp, I. S. S., and Toonen, R. J. (2020). Host-symbiont coevolution, cryptic structure, and bleaching susceptibility, in a coral species complex (Scleractinia; Poritidae). *Sci. Rep.* 10:16995. doi: 10.1038/s41598-020-73501-6

Foster, N. L., Baums, I. B., Sanchez, J. A., Paris, C. B., Chollett, I., Agudelo, C. L., et al. (2013). Hurricane-driven patterns of clonality in an ecosystem engineer: the caribbean coral *Montastraea annularis*. *PLoS One* 8:e53283. doi: 10.1371/journal.pone.0053283

Frade, P. R., De Jongh, F., Vermeulen, F., Van Bleijswijk, J., and Bak, R. P. M. (2008). Variation in symbiont distribution between closely related coral species

over large depth ranges. *Mol. Ecol.* 17, 691–703. doi: 10.1111/j.1365-294X.2007.03612.x

Fuller, Z., Mocellin, V. J. L., Morris, L. A., Cantin, N., Shepherd, J., Sarre, L., et al. (2020). Population genetics of the coral *Acropora millepora*: toward genomic prediction of bleaching. *Science* 369:eaba4674. doi: 10.1126/science.aba4674

Gélin, P., Fauvelot, C., Bigot, L., Baly, J., and Magalon, H. (2017). From population connectivity to the art of striping Russian dolls: the lessons from *Pocillopora* corals. *Ecol. Evol.* 8, 1411–1426. doi: 10.1002/ece3.3747

Gintert, B. E., Manzello, D. P., Enochs, I. C., Kolodziej, G., Carlton, R., Gleason, A. C. R., et al. (2018). Marked annual coral bleaching resilience of an inshore patch reef in the Florida Keys: a nugget of hope, aberrance, or last man standing? *Coral Reefs* 37, 533–547. doi: 10.1007/s00338-018-1678-x

González-Rivero, M., Harborne, A. R., Herrera-Reveles, A., Bozec, Y.-M., Rogers, A., Friedman, A., et al. (2017). Linking fishes to multiple metrics of coral reef structural complexity using three-dimensional technology. *Sci. Rep.* 7:13965. doi: 10.1038/s41598-017-14272-5

Gorospe, K. D., Donahue, M. J., and Karl, S. A. (2015). The importance of sampling design: spatial patterns and clonality in estimating the genetic diversity of coral reefs. *Mar. Biol.* 162, 917–928. doi: 10.1007/s00227-015-2634-8

Gorospe, K. D., and Karl, S. A. (2013). Genetic relatedness does not retain spatial pattern across multiple spatial scales: dispersal and colonization in the coral, *Pocillopora damicornis*. *Mol. Ecol.* 22, 3721–3736. doi: 10.1111/mec.12335

Gutiérrez-Heredia, L., Benzoni, F., Murphy, E., and Reynaud, E. G. (2016). End to end digitisation and analysis of three-dimensional coral models, from communities to corallites. *PLoS One* 11:e0149641. doi: 10.1371/journal.pone.0149641

Gutiérrez-Heredia, L., D'Helft, C., and Reynaud, E. G. (2015). Simple methods for interactive 3D modeling, measurements, and digital databases of coral skeletons. *Limnol. Oceanogr. Methods* 13:178–193. doi: 10.1002/lom3.10017

Hand, B. K., Lowe, W. H., Kovach, R. P., Muhlfeld, C. C., and Luikart, G. (2015). Landscape community genomics: understanding eco-evolutionary processes in complex environments. *Trends Ecol. Evol.* 30, 161–168. doi: 10.1016/j.tree.2015.01.005

Hellberg, M. E. (2007). Footprints on water: the genetic wake of dispersal among reefs. *Coral Reefs* 26, 463–473. doi: 10.1007/s00338-007-0205-2

Hernandez-Agreda, A., Leggat, W., Bongaerts, P., Herrera, C., and Ainsworth, T. D. (2018). Rethinking the coral microbiome: simplicity exists within a diverse microbial biosphere. *mBio* 9, e00812–18.

Hoegh-Guldberg, O., Mumby, P. J., Hooten, A. J., Steneck, R. S., Greenfield, P., Gomez, E., et al. (2007). Coral reefs under rapid climate change and ocean acidification. *Science* 318, 1737–1742. doi: 10.1126/science.1152509

Holmes, G., Ortiz, J., Kaniewska, P., and Johnstone, R. (2008). Using three-dimensional surface area to compare the growth of two Pocilloporid coral species. *Mar. Biol.* 155, 421–427. doi: 10.1007/s00227-008-1040-x

Iglhaut, J., Cabo, C., Puliti, S., Piermattei, L., O'Connor, J., and Rosette, J. (2019). Structure from motion photogrammetry in forestry: a review. *Curr. For. Rep.* 5, 155–168. doi: 10.1007/s40725-019-00094-3

Jin, Y. K., Lundgren, P., Lutz, A., Raina, J. B., Howells, E. J., Paley, A. S., et al. (2016). Genetic markers for antioxidant capacity in a reef-building coral. *Sci. Adv.* 2:e1500842. doi: 10.1126/sciadv.1500842

Johnston, M. A., Hickerson, E. L., Nuttall, M. F., Blakeway, R. D., Sterne, T. K., Eckert, R. J., et al. (2019). Coral bleaching and recovery from 2016 to 2017 at East and West Flower Garden Banks, Gulf of Mexico. *Coral Reefs* 38, 787–799. doi: 10.1007/s00338-019-01788-7

Kalacska, M., Chmura, G. L., Lucanus, O., Bérubé, D., and Arroyo-Mora, J. P. (2017). Structure from motion will revolutionize analyses of tidal wetland landscapes. *Remote Sens. Environ.* 199, 14–24. doi: 10.1016/j.rse.2017.06.023

Kinlan, B. P., Gaines, S. D., and Lester, S. E. (2005). Propagule dispersal and the scales of marine community process. *Divers. Distrib.* 11, 139–148. doi: 10.1111/j.1366-9516.2005.00158.x

Korte, A., and Farlow, A. (2013). The advantages and limitations of trait analysis with GWAS: a review. *Plant Methods* 9:29. doi: 10.1186/1746-4811-9-29

Kruszyński, K. J., Kaandorp, J. A., and van Liere, R. (2007). A computational method for quantifying morphological variation in scleractinian corals. *Coral Reefs* 26, 831–840. doi: 10.1007/s00338-007-0270-6

Lavy, A., Eyal, G., Neal, B., Keren, R., Loya, Y., and Ilan, M. (2015). A quick, easy and non−intrusive method for underwater volume and surface area evaluation of benthic organisms by 3D computer modelling. *Methods Ecol. Evol.* 6, 521–531. doi: 10.1111/2041-210x.12331

Ledoux, J.-B., Garrabou, J., Bianchimani, O., Drap, P., Féral, J.-P., and Aurelle, D. (2010). Fine-scale genetic structure and inferences on population biology in the threatened Mediterranean red coral, *Corallium rubrum*. *Mol. Ecol.* 19, 4204–4216. doi: 10.1111/j.1365-294x.2010.04814.x

Leon, J. X., Roelfsema, C. M., Saunders, M. I., and Phinn, S. R. (2015). Measuring coral reef terrain roughness using 'Structure-from-Motion' close-range photogrammetry. 242, 21–28. doi: 10.1016/j.geomorph.2015.01.030

Li, Y., Zhang, X.-X., Mao, R.-L., Yang, J., Miao, C.-Y., Li, Z., et al. (2017). Ten years of landscape genomics: challenges and opportunities. *Front. Plant Sci.* 8:2138. doi: 10.3389/fpls.2017.02136

Liggins, L., Treml, E. A., and Riginos, C. (2013). Taking the plunge: an introduction to undertaking seascape genetic studies and using biophysical models. *Geogr. Compass* 7, 173–196. doi: 10.1111/gec3.12031

Liggins, L., Treml, E. A., and Riginos, C. (2019). "Seascape genomics: contextualizing adaptive and neutral genomic variation in the ocean environment," in *Population Genomics Marine Organisms. Population Genomics*, eds M. Oleksiak and O. Rajora (Cham, CH: Springer), 171–218. doi: 10.1007/13836_2019_68

Manel, S., Schwartz, M. K., Luikart, G., and Taberlet, P. (2003). Landscape genetics: combining landscape ecology and population genetics. *Trends Ecol. Evol.* 18, 189–197. doi: 10.1016/s0169-5347(03)00008-9

Matz, M. V. (2018). Fantastic beasts and how to sequence them: ecological genomics for obscure model organisms. *Trends Genet.* 34, 121–132. doi: 10.1016/j.tig.2017.11.002

McClenachan, L., O'Connor, G., Neal, B. P., Pandolfi, J. M., and Jackson, J. B. (2017). Ghost reefs: nautical charts document large spatial scale of coral reef loss over 240 years. *Sci. Adv.* 3:e1603155. doi: 10.1126/sciadv.1603155

McRae, B. H. (2006). Isolation by resistance. *Evolution* 60, 1551–1561. doi: 10.1554/05-321.1

Meuwissen, T. H., Hayes, B. J., and Goddard, M. E. (2001). Prediction of total genetic value using genome-wide dense marker maps. *Genetics* 157, 1819–1829. doi: 10.1093/genetics/157.4.1819

Miller, K. J., and Ayre, D. J. (2004). The role of sexual and asexual reproduction in structuring high latitude populations of the reef coral *Pocillopora damicornis*. *Heredity* 92, 557–568. doi: 10.1038/sj.hdy.6800459

Miller, M. W., Karazsia, J., Groves, C. E., Griffin, S., Moore, T., Wilber, P., et al. (2016). Detecting sedimentation impacts to coral reefs resulting from dredging the Port of Miami, Florida USA. *PeerJ.* 4:e2711. doi: 10.7717/peerj.2711

Oakley-Cogan, A., Tebbett, S. B., and Bellwood, D. R. (2020). Habitat zonation on coral reefs: structural complexity, nutritional resources and herbivorous fish distributions. *PLoS One* 15:e0233498. doi: 10.1371/journal.pone.0233498

Olinger, L. K., Scott, A. R., McMurray, S. E., and Pawlik, J. R. (2019). Growth estimates of Caribbean reef sponges on a shipwreck using 3D photogrammetry. *Sci. Rep.* 9:18398. doi: 10.1038/s41598-019-54681-2

Page, C. A., Field, S. N., Pollock, F. J., Lamb, J. B., Shedrawi, G., and Wilson, S. K. (2017). Assessing coral health and disease from digital photographs and in situ surveys. *Environ. Monit. Assess.* 189:18. doi: 10.1007/s10661-016-5743-z

Pantos, O., Bongaerts, P., Dennis, P. G., Tyson, G. W., and Hoegh-Guldberg, O. (2015). Habitat-specific environmental conditions primarily control the microbiomes of the coral *Seriatopora hystrix*. *ISME J.* 9, 1916–1927. doi: 10.1038/ismej.2015.3

Pavoni, G., Corsini, M., and Cignoni, P. (2020). A state of the art technology in large scale underwater monitoring. *ERCIM News* 2020:121.

Pedersen, N. E., Edwards, C. B., Eynaud, Y., Gleason, A. C., Smith, J. E., and Sandin, S. A. (2019). The influence of habitat and adults on the spatial distribution of juvenile corals. *Ecography* 42, 1703–1713. doi: 10.1111/ecog.04520

Petkova, D., Novembre, J., and Stephens, M. (2016). Visualizing spatial population structure with estimated effective migration surfaces. *Nat. Genet.* 48, 94–100. doi: 10.1038/ng.3464

Precht, W. F., Gintert, B. E., Robbart, M. L., Fura, R., and van Woesik, R. (2016). Unprecedented disease-related coral mortality in Southeastern Florida. *Sci. Rep.* 6:31374. doi: 10.1038/srep31374

Rellstab, C., Gugerli, F., Eckert, A. J., Hancock, A. M., and Holderegger, R. (2015). A practical guide to environmental association analysis in landscape genomics. *Mol. Ecol.* 24, 4348–4370. doi: 10.1111/mec.13322

Riginos, C. (2015). Clones in space—how sampling can bias genetic diversity estimates in corals: editorial comment on the feature article by Gorospe et al. *Mar. Biol.* 162, 913–915. doi: 10.1007/s00227-015-2638-4

Riginos, C., Crandall, E. D., Liggins, L., Bongaerts, P., and Treml, E. A. (2016). Navigating the currents of seascape genomics: how spatial analyses can augment population genomic studies. *Curr. Zool.* 62, 581–601. doi: 10.1093/cz/zow067

Riginos, C., and Liggins, L. (2013). Seascape genetics: populations, individuals, and genes marooned and adrift. *Geogr. Compass* 7, 197–216. doi: 10.1111/gec3.12032

Selmoni, O., Rochat, E., Lecellier, G., Berteaux−Lecellier, V., and Joost, S. (2020b). Seascape genomics as a new tool to empower coral reef conservation strategies: an example on north−western Pacific *Acropora digitifera*. *Evol. Appl.* 13, 1923–1938. doi: 10.1111/eva.12944

Selmoni, O., Lecellier, G., Magalon, H., Vigliola, L., Benzoni, F., Peignon, C., et al. (2020a). Seascape genomics reveals candidate molecular targets of heat stress adaptation in three coral species. *bioRxiv* [Preprint]. doi: 10.1101/2020.05.12.090050,

Smith, M. W., Carrivick, J. L., and Quincey, D. J. (2016). Structure from motion photogrammetry in physical geography. *Prog. Phys. Geogr.* 40, 247–275. doi: 10.1177/0309133315615805

Stinchcombe, J. R., and Hoekstra, H. E. (2008). Combining population genomics and quantitative genetics: finding the genes underlying ecologically important traits. *Heredity* 100, 158–170. doi: 10.1038/sj.hdy.6800937

Tokeshi, M., and Arakaki, S. (2012). Habitat complexity in aquatic systems: fractals and beyond. *Hydrobiologia* 685, 27–47. doi: 10.1007/s10750-011-0832-z

Torres-Pulliza, D., Dornelas, M. A., Pizarro, O., Bewley, M., Blowes, S. A., Boutros, N., et al. (2020). A geometric basis for surface habitat complexity and biodiversity. *Nat. Ecol. Evol.* 4, 1495–1501. doi: 10.1038/s41559-020-1281-8

Underwood, J. N., Richards, Z. T., Miller, K. J., Puotinen, M. L., and Gilmour, J. P. (2018). Genetic signatures through space, time and multiple disturbances in a ubiquitous brooding coral. *Mol. Ecol.* 27, 1586–1602. doi: 10.1111/mec.14559

Underwood, J. N., Smith, L. D., van Oppen, M. J. H., and Gilmour, J. P. (2007). Multiple scales of genetic connectivity in a brooding coral on isolated reefs following catastrophic bleaching. *Mol. Ecol.* 16, 771–784. doi: 10.1111/j.1365-294X.2006.03187.x

Urbina-Barreto, I., Chiroleu, F., Pinel, R., Fréchon, L., Mahamadaly, V., Elise, S., et al. (2020). Quantifying the shelter capacity of coral reefs using photogrammetric 3D modeling: from colonies to reefscapes. *Ecol. Indic.* 121:107151. doi: 10.1016/j.ecolind.2020.107151

van Oppen, M. J. H., Bongaerts, P., Frade, P., Peplow, L. M., Boyd, S. E., Nim, H. T., et al. (2018). Adaptation to reef habitats through selection on the coral animal and its associated microbiome. *Mol. Ecol.* 27, 2956–2971. doi: 10.1111/mec.14763

van Oppen, M. J. H., and Gates, R. D. (2006). Conservation genetics and the resilience of reef-building corals. *Mol. Ecol.* 15, 3863–3883. doi: 10.1111/j.1365-294x.2006.03026.x

van Oppen, M. J. H., Lutz, A., De'ath, G., Peplow, L., and Kininmonth, S. (2008). Genetic traces of recent long-distance dispersal in a predominantly self-recruiting coral. *PLoS One* 3:e3401. doi: 10.1371/journal.pone.0003401

van Oppen, M. J. H., Oliver, J. K., Putnam, H. M., and Gates, R. D. (2015). Building coral reef resilience through assisted evolution. *Proc. Natl. Acad. Sci. U. S. A.* 112, 2307–2313. doi: 10.1073/pnas.1422301112

Van Wynsberge, S., Andréfouët, S., Gaertner-Mazouni, N., Tiavouane, J., Grulois, D., Lefèvre, J., et al. (2017). Considering reefscape configuration and composition in biophysical models advance seascape genetics. *PLoS One* 12:e0178239. doi: 10.1371/journal.pone.0178239

Vollmer, S. V., and Palumbi, S. R. (2002). Hybridization and the evolution of reef coral diversity. *Science* 296, 2023–2025. doi: 10.1126/science.1069524

Warner, P. A., van Oppen, M. J. H., and Willis, B. L. (2015). Unexpected cryptic species diversity in the widespread coral *Seriatopora hystrix* masks spatial-genetic patterns of connectivity. *Mol. Ecol.* 24, 2993–3008. doi: 10.1111/mec.13225

Warner, P. A., Willis, B. L., and van Oppen, M. J. H. (2016). Sperm dispersal distances estimated by parentage analysis in a brooding scleractinian coral. *Mol. Ecol.* 25, 1398–1415. doi: 10.1111/mec.13553

Westoby, M. J., Brasington, J., Glasser, N. F., Hambrey, M. J., and Reynolds, J. M. (2012). 'Structure-from-Motion' photogrammetry: a low-cost, effective tool for geoscience applications. *Geomorphology* 179, 300–314. doi: 10.1016/j.geomorph.2012.08.021

Williams, D. E., Miller, M. W., and Baums, I. B. (2014). Cryptic changes in the genetic structure of a highly clonal coral population and the relationship with ecological performance. *Coral Reefs* 33, 595–606. doi: 10.1007/s00338-014-1157-y

Williams, I. D., Couch, C. S., Beijbom, O., Oliver, T. A., Vargas-Angel, B., Schumacher, B. D., et al. (2019). Leveraging automated image analysis tools to transform our capacity to assess status and trends of coral reefs. *Front. Mar. Sci.* 6:222. doi: 10.3389/fmars.2019.00222

Young, G. C., Dey, S., Rogers, A. D., and Exton, D. (2017). Cost and time-effective method for multi-scale measures of rugosity, fractal dimension, and vector dispersion from coral reef 3D models. *PLoS One* 12:e0175341. doi: 10.1371/journal.pone.0175341

Conflict of Interest: The authors declare that the research was conducted in the absence of any commercial or financial relationships that could be construed as a potential conflict of interest.

frontiers in Marine Science

ORIGINAL RESEARCH
published: 19 July 2021
doi: 10.3389/fmars.2021.639309

The Three-Dimensional Structure of Mediterranean Shallow Rocky Reefs: Use of Photogrammetry-Based Descriptors to Assess Its Influence on Associated Teleost Assemblages

Tiffany Monfort[1,2†], Adrien Cheminée[1,3†], Olivier Bianchimani[1], Pierre Drap[4], Arthur Puzenat[1] and Thierry Thibaut[2]*

[1] Septentrion Environnement, Marseille, France, [2] IRD, CNRS, Aix Marseille Univ., Université de Toulon, CNRS, IRD, MIO UM 110, Marseille, France, [3] Faculté des Sciences, Aix Marseille Université, Marseille, France, [4] CNRS, Aix-Marseille Univ., Université de Toulon, LIS UMR 7020, Marseille, France

OPEN ACCESS

Edited by:
Will F. Figueira, The University of Sydney, Australia

Reviewed by:
Mauro Sinopoli, Stazione Zoologica Anton Dohrn Napoli, Italy
Valeriya Komyakova, Norwegian Institute of Marine Research (IMR), Norway

***Correspondence:**
Adrien Cheminée adrien.cheminee@septentrion-env.com

† These authors have contributed equally to this work

Specialty section:
This article was submitted to Marine Ecosystem Ecology, a section of the journal Frontiers in Marine Science

Received: *08 December 2020*
Accepted: *22 June 2021*
Published: *19 July 2021*

Citation:
Monfort T, Cheminée A, Bianchimani O, Drap P, Puzenat A and Thibaut T (2021) The Three-Dimensional Structure of Mediterranean Shallow Rocky Reefs: Use of Photogrammetry-Based Descriptors to Assess Its Influence on Associated Teleost Assemblages. Front. Mar. Sci. 8:639309. doi: 10.3389/fmars.2021.639309

In the Mediterranean Sea, shallow rocky reefs and the associated three-dimensional (3D) structure support rich and abundant communities; they are therefore of functional importance, in particular for the renewal of fish stocks. However, these habitats and their functions are likely to be altered by anthropogenic pressures inducing habitat transformations. It is therefore necessary to assess their 3D structure, their transformations and relationship to communities, especially for management and conservation purposes. In this article we aimed (i) to compare two methods that quantify the metrics of the 3D structure (rugosity) of shallow rocky reefs (chain-and-tape method and photogrammetry), and (ii) to quantify the possible links between this habitat structure and the fish assemblages. We found that photogrammetry and the chain-and-tape method yielded a similar estimate of rugosity, but photogrammetry was the most efficient method in terms of measurement quality and time (when considering in-water acquisition). This method also displayed the best repeatability. The 3D habitat descriptors (mean surface rugosity, variation of surface rugosity, and depth) differed significantly between the studied sites and were therefore included as covariables. Total fish abundance and species richness increased with higher mean surface rugosity. In addition, the composition of fish assemblages was significantly influenced by surface rugosity, although this effect was modulated by depth. When focusing on specific taxa, neither density patterns nor size class distributions displayed clear patterns in relation to rugosity metrics. However, this study demonstrated that spatial variability of teleost fish assemblages can be explained by habitat rugosity which probably increases the number of shelters and food resources, and therefore improves chances of survival. In addition, our study has shown that photogrammetry is an appropriate method to assess 3D structure metrics in a temperate rocky reef.

Keywords: habitat complexity, rugosity, metrics, photogrammetry, benthic fishes, efficiency, repeatability, Mediterranean Sea

INTRODUCTION

The Mediterranean Basin is described as a hotspot of diversity for its various fish species and its specific marine ecosystems (Bianchi and Morri, 2000; Cuttelod et al., 2009). The infralittoral (i.e., subtidal) rocky reef provides various habitats for different species such as teleost fishes. This zone is important because of the strong benthic primary production provided by macrophytes, and because of the associated secondary production (Harmelin, 1987). Many coastal species at different life stages coexist making the subtidal rocky reef an ideal area for fish species. However, climate change and the transformation of habitat due to coastal urbanization are anthropogenic pressures that can impact the 3D structure of these rocky habitats (Thiriet et al., 2014). Therefore it may also affect endemic species (Airoldi et al., 2008; Coll et al., 2012).

The structure of these habitats is defined as the quantity, the composition and the three-dimensional (3D) arrangement of the physical components (biotic and abiotic) at a specific location (Cheminée et al., 2017b; Cuadros et al., 2019). It is constituted of complexity which is the absolute abundance of the individual structural components (Beck, 2000; Byrne, 2007; Bell et al., 2012; Cuadros et al., 2019), and of the heterogeneity of their spatial settings (August, 1983). In order to understand the effects that habitat complexity could have on teleost fish assemblages, it is necessary to define and use metrics (also known as environmental descriptors) of complexity. One widely employed descriptor is rugosity. It can be interpreted as a category of the structural complexity of underwater habitats (Friedman et al., 2012; Burns et al., 2015; Storlazzi et al., 2016; Calders et al., 2020). It has been observed that rugosity is an important ecological parameter for shaping fish and other benthic assemblages (Luckhurst and Luckhurst, 1978; Friedman et al., 2012; Storlazzi et al., 2016). It has been reported that rugosity plays a role in interactions between species such as predation or competition (Harborne et al., 2012).

In the history of marine ecology field work, the chain-and-tape method has been commonly used to quantitatively estimate rugosity (Risk, 1972; Luckhurst and Luckhurst, 1978; McCormick, 1994; Hill and Wilkinson, 2004; Storlazzi et al., 2016). More recent methods exist such as the use of photogrammetry: an approach that requires 2D images to create a 3D model of the environment and can therefore estimate precise measurements (Drap et al., 2013; Bryson et al., 2017; Calders et al., 2020). These methods are mainly used to characterize tropical coral reefs. However little is known regarding their comparative efficiency and precision in temperate waters (Ventura et al., 2020).

Environmental descriptors are known to influence community metrics (Hewitt et al., 2005; Harborne et al., 2012; Komyakova et al., 2013; Figueira et al., 2015). It has been shown that fish abundance is greatly influenced by the quantity and quality of the structure of the coral reef habitat (Messmer et al., 2011; Harborne et al., 2012; Kovalenko et al., 2012). This trend has often been described in tropical waters (Luckhurst and Luckhurst, 1978; Gratwicke and Speight, 2005; Graham and Nash, 2013) but rarely in temperate environments (Charton and Ruzafa, 1998; Meager et al., 2011; Rees et al., 2014). The possible relationships between the 3D structure of the Mediterranean rocky reefs and metrics of nektobenthic species have been little studied, while understanding the role of habitat complexity is to allow better preservation of biodiversity and the function of the ecosystem (Kovalenko et al., 2012; Rees et al., 2018; Sinopoli et al., 2018). To characterize habitat complexity, a precise method is needed in order to adequately comprehend the interactions between species and the environment.

The present study aimed to assess how substrate rugosity may affect fish community on temperate reefs, after previously assessing how good rugosity metrics are derived from photogrammetry as a proxy of the classic chain-and-tape rugosity measurement. Indeed, such comparison has been done in tropical environments (Young et al., 2017) but remains poorly explored in temperate environments of the Mediterranean Sea. However, some specific cases have been studied in this region, such as biogenic reefs bio-constructed by *Sabellaria alveolata* (Ventura et al., 2020). First, we have studied which method (chain-and-tape or photogrammetry-based) can best measure the rugosity metric of Mediterranean rocky reefs. More precisely, it aimed to determine whether the estimation of the mean rugosity of a site and the *in situ* acquisition time (efficiency) are different depending on the method used, the habitat category, and the site studied. It also estimated which method provides a more precise measurement (repeatability). Moreover, this study proposed to verify whether there is a relationship between the complexity of rocky reefs and fish assemblages. It attempted to identify the effects of descriptors of the 3D structure (mean rugosity, variation of the rugosity) on the descriptors of the teleost assemblages linked to the substrate (i.e., benthic taxa).

We predicted that photogrammetry would be the most robust, efficient and should be easier to repeat than the chain-and-tape method. Furthermore, we expected that one or several metrics describing the teleost assemblage would be influenced by habitat rugosity. More specifically, we expected that rocky reefs with higher rugosity mean and/or higher variation of rugosity would host richer, more abundant, and more diversified fish assemblages. Two datasets from the same study area have been analyzed: one dedicated to the method comparison and the other to the understanding of the relation between 3D structure and teleost populations.

MATERIALS AND METHODS

The study was conducted in the north-western Mediterranean Sea, at the Calanques National Park (western Provence, France) where two datasets were sampled in the Riou Archipelago (**Figure 1**) during spring 2017 and 2018. The 2017 dataset was used to compare the two methods (chain-and-tape method and photogrammetry), while the 2018 dataset was used to understand the influence of substrate complexity on teleost assemblages.

Methods Comparison

Background Definitions

Efficiency in our study is defined as the time (in seconds) spent underwater acquiring data, while precision is defined as

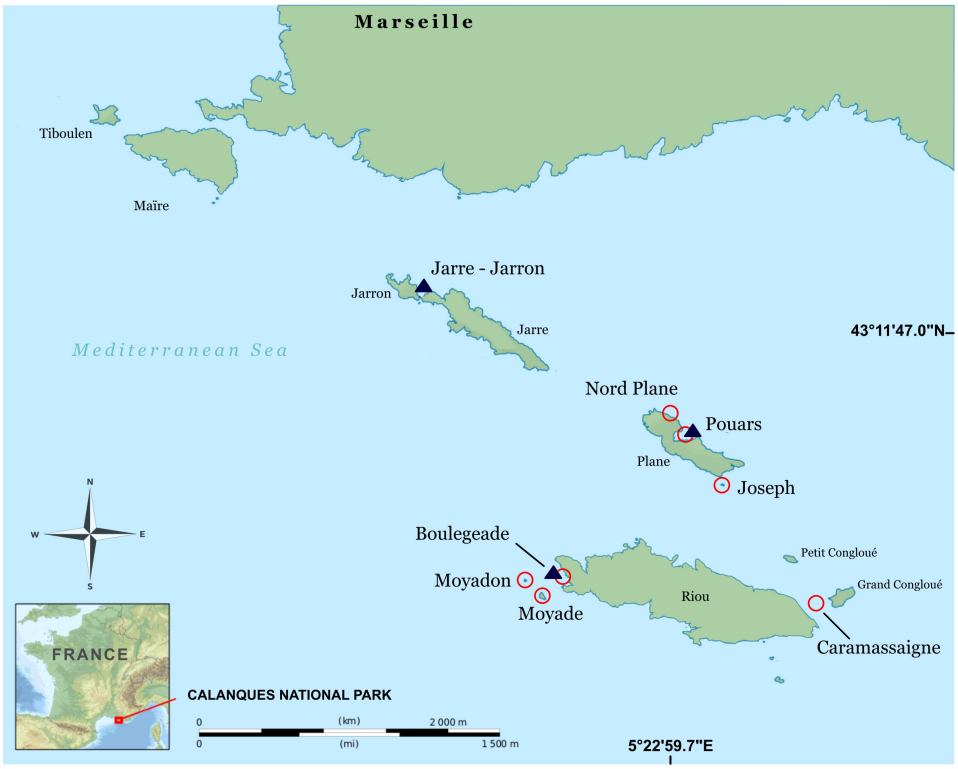

FIGURE 1 | Study area located in the Calanques National Park (France), where sites were sampled in 2017 (dark blue triangles) and in 2018 (red circles). This map was modified from an online source, i.e. from OpenStreetMap data, available on Wikipedia as a public domain image: https://commons.wikimedia.org/wiki/File:Archipel_de_Riou_topographic_map-fr.svg.

"the closeness of agreement between results of independent tests obtained under stipulated conditions (repeatability and reproducibility)" (Arnal, 2017). Repeatability is the part of variability caused by the measuring device in the measurement system studied. Reproducibility is the part of variability induced by the differences between operators. In this study, a single observer managed the data acquisition. For this reason, repeatability was the only concept considered.

Sampling Design and Data Collection

A preliminary sampling design was used to estimate the number of quadrats needed to obtain a reliable measurement of rugosity (sampling effort). Two other sampling designs were used to compare the chain-and-tape method with photogrammetry. The first design evaluated i) the mean rugosity and ii) the efficiency of each method, while the second design was used to study their repeatability. In the first design, sampling effort was evaluated using the cumulative mean rugosity. This procedure was conducted to determine the minimum sampling effort needed to estimate the mean rugosity with both methods. The minimum sampling effort was reached when the cumulative mean rugosity was stabilized. This response variable was studied at one site and in one habitat (at Jarre-Jarron, Infralittoral Rock with Photophilic Algae (IRPA): block facies). In the second design, the responses of mean rugosity and efficiency (time in seconds) were tested as a function of two fixed factors (method: chain-and-tape vs. photogrammetry; and habitat: continuous rocks vs. block fields) and a random factor (site, with 3 levels: Boulegeade, Jarre-Jarron, and Pouars; **Figure 1**). In the third design, repeatability response was tested according to the fixed factor method (same levels: chain-and-tape and photogrammetry). A single site in a single habitat was studied for this design (Pouars, IRPA: block facies).

For all designs, quadrats (3 m × 3 m) were used as the measurement unit. The cumulative mean rugosity was calculated with the mean rugosity of each quadrat added one by one into the calculation of the mean in a delimited area. The quadrats were randomly arranged and placed so that the cumulative mean rugosity was representative of the study area. The minimum sampling effort was reached when the cumulative mean rugosity was stabilized. The mean linear rugosity in each quadrat was estimated with four segments (2 bisectors and 2 medians). The first design was composed of 12 different quadrats (for each habitat-site combinations), whereas the rugosity was estimated by measuring the same quadrat 10 times in a row for each method when precision was evaluated.

When the chain-and-tape method was used to estimate linear rugosity, a diver positioned the chain (link size: 30 mm) along one of the four segments (from A point to A' point, as in Storlazzi et al., 2016; **Supplementary Figures 1A,B**). The same area was created virtually using photogrammetry. Specifically, the diver took pictures zigzagging at a constant distance (1 m) above the quadrat (**Supplementary Figure 1B**).

For each quadrat, an average of 100 pictures were taken to allow satisfactory reconstruction. The same camera handled by the same operator (OB) was used during the entire study: a NIKON D700 protected inside a Nauticam housing, with 14 mm lens and two Ikelite flashes DS 160.

All the photographs were oriented with the Photoscan software (currently Metashape) from the company Agisoft (Royer et al., 2018). A metal square of 50 cm × 50 cm has been placed on the edge of the area to be studied. It was equipped with a buoyancy target for vertical referencing and six coded targets whose distances have been calibrated *a priori*.

The bundle adjustment performed by the photogrammetry software took into account the scaling constraints on the coded targets and offered an accuracy of about 1 mm considering the readable signal on the coded targets (Drap et al., 2015). The vertical referencing was obtained *a posteriori* by introducing the coded target read on the float. In a more recent version of the equipment used, a spirit level has been placed on the bracket as well as three adjustable feet with screws allowing the horizontal adjustment of the reference bracket before the shots. Under these conditions, the coordinates of the coded targets were directly expressed in a vertical reference frame and used as a control point by the bundle adjustment. This had no influence on the overall accuracy obtained. If we took into account on the one hand the short shooting distance and thus the large scale of the photographs and on the other hand the high resolution of the "full frame" sensors of the DSLR (Digital Single Lens Reflex) cameras used, the GSD of the photographs was much smaller than a millimeter (The GSD for Ground Sample Distance is the distance on the ground between two consecutive pixel centers). Such specific parameters (i.e., GSD and RMS error) used to build the quadrat models are compiled in the **Table 1**. Once the orientation of the photographs and the reference systems were validated, a 3D point cloud uniformly distributed on the surface studied was calculated. 3D models were generated using Photoscan software (Royer et al., 2018). In order to obtain a uniformly distributed point cloud with a defined average distance between points the Metashape "Filter Dense Cloud" tool (Tools Dense Cloud) was used. This tool removes or interpolates the necessary points with the colorimetric information to arrive to a dense cloud of the desired spacing. A mesh was then built in Metashape based upon this dense cloud and this was used to assess rugosity. In order to have comparable results with the *in situ* measurements, the average density of the 3D point cloud was adjusted to the chain-link used for the comparison of the methods (3 cm) (e.g., **Supplementary Table 1**). The spacing of vertices in the resulting mesh was verified to be 3 cm by using a small software (coded in JAVA) that analyze the meshes. It produced elementary statistics reliable on the length of the arcs obtained after meshing. It allowed us to validate the two meshes produced and to keep for the production the one generated with Agisoft. This enabled the treatment with the software. It therefore allowed us to verify the spacing of vertices to be 3 cm. We draw reader's attention on the fact that it was necessary to develop a small analysis tool of the meshes because it was not available neither in Agisoft nor in Meshlab.

TABLE 1 | GSD and RMS error of the quadrat models.

Site and quadrat number	GSD (mm)	RMS error (mm)
Pouars 1	0.56	1.0
Pouars 2	0.66	0.7
Pouars 3	0.68	34.9
Pouars 4	0.69	0.9
Pouars 5	0.65	1.2
Pouars 6	0.64	1.8
Pouars 7	0.63	0.6
Pouars 8	0.64	1.5
Pouars 9	0.61	1.6
Pouars 10	0.64	1.1
Pouars 11	0.67	4.6
Pouars 12	0.61	1.9
Jarre 1	0.67	1.9
Jarre 2	0.73	0.9
Jarre 3	0.75	0.4
Jarre 4	0.74	1.5
Jarre 5	0.65	0.3
Jarre 6	0.77	0.8
Jarre 7	0.67	2.1
Jarre 8	0.66	0.9
Jarre 9	0.65	0.5
Jarre 10	0.72	1.6
Jarre 11	0.71	1.5
Jarre 12	0.76	1.0
Boulegeade 1	0.69	1.6
Boulegeade 2	0.75	0.9
Boulegeade 3	0.67	0.8
Boulegeade 4	0.68	1.8
Boulegeade 5	0.73	2.2
Boulegeade 6	0.82	1.1
Boulegeade 7	0.73	2.3
Boulegeade 8	0.74	0.9
Boulegeade 9	0.74	2.1
Boulegeade 10	0.75	0.9
Boulegeade 11	0.70	0.9
Boulegeade 12	0.71	1.9

In each quadrat model, 5–24 measures have been done between several coded targets, using rulers with millimeter accuracy (from 0.071 to 0.6 m).

Finally, it should be noted that the flexibility of the photogrammetric method enabled us to obtain results comparable in quality to those obtained by the chain method. The adjustment of the altitude of the photographs and thus of their GSD, the position of the cameras during the shooting determined the resulting 3D model. For example, the use of photographs with vertical axes only induced a 3D model very close to a DTM or an elevation grid which corresponded to the results obtained with the chain. On the other hand, it would be possible to go further by multiplying the oblique or even quasi-horizontal shots and to integrate into the terrain model the overhangs or even the cavities inaccessible with the chain method.

Once the 3D model was obtained, CloudCompare software was used to perform measurements (CloudCompare, 2018). The

same segments were drawn on the model providing thereby the value of the mean rugosity.

Data Treatment and Statistical Analysis

The mean rugosity and method efficiency data were analyzed by performing PERMutational univariate Analyses Of VAriance (PERMANOVAs) (Anderson et al., 2008), including terms and all interactions. The resemblance matrices were calculated from the initial data matrix containing, for each sample, the response variable (rugosity or time). Analyses were based on Euclidean distances and *p*-values were calculated by 999 residual permutations under a reduced model. When the number of permutations was less than 200, Monte Carlo *p*-values were used (Clarke et al., 2014). The PERMDISP procedure was conducted when it was when necessary to see whether significant differences between levels were due to differences in terms of mean or in terms of dispersion of the data. In addition, this procedure was also used to quantify the proportion of variation of each method, and therefore to determine if they were repeatable. Smaller variation indicates higher repeatability (the method is more precise). Coefficient of variation (CV) was also taken into account in order to measure the relative dispersion.

Teleost Assemblages

Ethics Statement

The observational protocol was submitted to the regional authority *Direction inter-régionale de la mer Méditerranée* (the French administration in charge of Maritime Affairs). No special permit was required since no extractive sampling or animal manipulations were conducted (only visual censuses in natural habitats) and since the surveyed locations were not privately owned.

Sampling Design and Data Collection

Our experimental design was built in order to address the following hypothesis: higher rugosity or variation of rugosity may induce richer, more abundant and more diversified fish assemblages. Additionally, the assemblage of spatial categories (i.e., relative abundances by fish categories as defined by Harmelin (Harmelin, 1987; **Table 2** and **Supplementary Figure 2**) was expected to vary according to substrate rugosity and depth, which are known to shape e.g., food and refuges availability and therefore influence the interactions among taxa (see Introduction for previously cited references). For the same reasons, the size-class distributions of given taxa were expected to be somehow correlated with rugosity, since bottoms with high rugosity may e.g., provide more refuges and be therefore of better "habitat quality"—*sensu* Dahlgren and Eggleston (2000)—for juvenile individual.

In order to test these assumptions, teleost assemblages were inventoried and described according to a predefined list of selected species (nektobenthic and cryptobenthic fishes) (**Table 3**), i.e., species having a way of life related to the bedrock of the rocky infralittoral, therefore likely to be influenced by 3D structuration. Response variables describing teleost assemblages were: (i) total abundance (including all species), (ii) species richness, (iii) Shannon index, (iv) species assemblage (species composition and relative abundances), (v) assemblage of spatial categories. In addition, for a subset of dominant species (see "Results"), we studied: (vi) specific abundance, (vii) size (TL: total length in mm) of each species, and (viii) abundance by size class (small, medium, large). The data were collected using Underwater Visual Census (UVC) (Harmelin-Vivien et al., 1985; Friedlander and DeMartini, 2002; Sala et al., 2012). The size classes were standardized using the work of Louisy (2002). Thresholds of each species size class were defined according to maximum sizes referenced in this work. The predictor variables were: (i) mean surface rugosity, (ii) variation in surface rugosity, (iii) depth, and (iv) site. Photogrammetry was the method used to measure these environmental descriptors.

TABLE 2 | Spatial category assemblage types as described by Harmelin (1987).

Category	Signification
Category 1	Open sea fishes
Category 2	Sedentary schooling fishes found throughout the entire water column
Category 3	Mesophage necto-benthic fishes executing vertical and lateral displacements
Category 4	Necto-benthic fishes with small vertical displacements and more or less important lateral displacements
Category 5	Mesophage and sedentary necto-benthic fishes (with small vertical and lateral displacements)
Category 6	Extreme sedentary necto-benthic fishes (null vertical displacements and rare lateral displacements). During the day: (a) outside, (b) in a shelter.

The relationship between teleost assemblages and substrate rugosity and other factors was investigated in a single habitat, i.e., continuous infralittoral rocky reef (IRPA), using transects (25 m × 5 m) as the unit of measure. 30 transects were randomly distributed among 7 different sites around Riou and Plane islands (fixed factor; **Figure 1**), with a minimum of 3 transects in each site.

The initial transects were divided into four smaller transects (6.25 m × 5 m) to estimate the surface rugosity for each of them using the same photogrammetric method as mentioned previously (**Supplementary Figure 1C**). Subsequently, mean surface rugosity was calculated for the entire initial transect using the mean surface rugosity of these small transects. The variation in surface rugosity was evaluated the same way.

Data Treatment and Statistical Analyses

First, the variability of environmental variables was tested against site factor (fixed). Three transects (20, 22, and 23) were deleted from the database due to environmental conditions (high turbidity/low visibility) as the creation of 3D models was unrealizable. Only 6 sites and 27 transects were taken into account because of this operation. It was observed that environmental variables were not constant between sites (see section "Results"). Consequently, it was justified, in a second analysis, to perceive these environmental descriptors as covariates of the site factor, in order to study the part of environmental variable effects on teleost descriptors.

The analysis model included 3 covariates (mean surface rugosity, variation in surface rugosity and depth: which are

TABLE 3 | Teleost fish assemblage studied: (i) species (ii) spatial category (see **Table 1** and **Supplementary Figure 2**), as described by Harmelin (1987).

Family	Common name	Scientific name	Abbreviation	Spatial category
Apogonidae	Cardinalfish	*Apogon imberbis*	ai	Category 6
Labridae	Mediterranean rainbow wrasse	*Coris julis*	cj	Category 5
Labridae	Brown wrasse	*Labrus merula*	lm	Category 5
Labridae	Green wrasse	*Labrus viridis*	lv	Category 5
Labridae	East Atlantic peacock wrasse	*Symphodus tinca*	st	Category 5
Lophiidae	Anglerfish	*Lophius piscatorius*	lp	Category 6
Mullidae	Striped red mullet	*Mullus surmuletus*	ms	Category 4
Pomacentridae	Damselfish	*Chromis chromis*	cc	Category 2
Sciaenidae	Corb	*Sciaena umbra*	su	Category 5
Scorpaenidae	Small red scorpionfish	*Scorpaena notata*	snot	Category 6
Scorpaenidae	Black scorpionfish	*Scorpaena porcus*	spor	Category 6
Scorpaenidae	Red scorpionfish	*Scorpaena scrofa*	ssco	Category 6
Serranidae	Swallowtail seaperch	*Anthias anthias*	aa	Category 5
Serranidae	Dusky grouper	*Epinephelus marginatus*	em	Category 5
Serranidae	Comber	*Serranus cabrilla*	sc	Category 5
Serranidae	Painted comber	*Serranus scriba*	sscr	Category 5
Sparidae	Zebra sea bream	*Diplodus cervinus*	dc	Category 3
Sparidae	Sharpsnout seabream	*Diplodus puntazzo*	dp	Category 3
Sparidae	Sargo	*Diplodus sargus*	ds	Category 3
Sparidae	Common two-banded seabream	*Diplodus vulgaris*	dv	Category 3
Sparidae	Dreamfish	*Sarpa salpa*	ssal	Category 3
Sparidae	Gilt-head bream	*Sparus aurata*	sa	Category 3

continuous variables) and the site factor (fixed factor with 6 levels). When the size of each species was studied, individuals (fishes) were used as unit of replication instead of transects.

PERMANOVAs were used to compare teleost descriptors between different factor levels, using the same procedure as in the first analysis (method comparisons). However, interactions between the factors were not taken into account. Univariate data were not transformed, and a resemblance matrix was created using Euclidean distance. When multivariate data were involved, modified Gower was used to produce the resemblance matrix after transformation of the data (log base2; Anderson et al., 2008). All three covariates produced a significant response on univariate teleost descriptors when PERMANOVAs were executed (see section "Results"). Therefore, residuals were plotted and calculated using linear model means (in agreement with the establishment of PERMANOVAs).

Since ecological data give rise to inherent variability, significance was considered—for all designs (including in the first analysis to compare methods)—when p-value < 0.1. Each data treatment was carried out using R 3.1.3 (R Core Team, 2017) and PRIMER 6/PERMANOVA + (Clarke and Gorley, 2006; Anderson et al., 2008) software.

RESULTS

Methods Comparison

Sampling Effort

Regardless of the method, the cumulative mean rugosity stabilized around 12 quadrats in the rocky reef habitat (field block facies) (**Figure 2**). It seems that both methods required the same sampling effort. In addition, the two methods obtained an equivalent value of cumulative mean rugosity (cumulative $\bar{x} = 1.32$).

Rugosity Estimation and Methods Efficiency

Habitat type had a significant effect on rugosity: regardless of site and method used, block field habitat consistently exhibited higher rugosity values than continuous rock habitat. This difference was greater at some sites, resulting in a significant habitat × site interaction (PERMANOVA, $P = 0.001$, **Figure 3** and **Table 4**). The habitat × method interaction was also significant (PERMANOVA, $P = 0.024$, **Figure 3** and **Table 4**). In a continuous rocky habitat, the difference between photogrammetry and the chain-and-tape method, although not significant, was closer to the significance levels (PERMANOVA, pair test, $P = 0.153$) than in block field habitat (PERMANOVA, pair test, $P = 0.977$, **Figure 3**). In addition, the method had no effect on the dispersion of the rugosity measurements (PERMDISP, $P = 0.504$). On the other hand, the habitat had a significant effect on this dispersion (PERMDISP, $P = 0.001$): the dispersion of rugosity measurements was greater in block field habitat (from 1.10 to 1.50) than in continuous rocky habitat (1.02–1.15, **Figure 3** and **Table 4**). The acquisition time was longer using the chain-and-tape method than with photogrammetry (**Figure 3** and **Table 5**). It was also more prominent in block field habitat than in continuous rock, regardless of the method used.

Precision/Repeatability

In the second experimental set-up, the dispersion of measurement was greater (low repeatability) with the

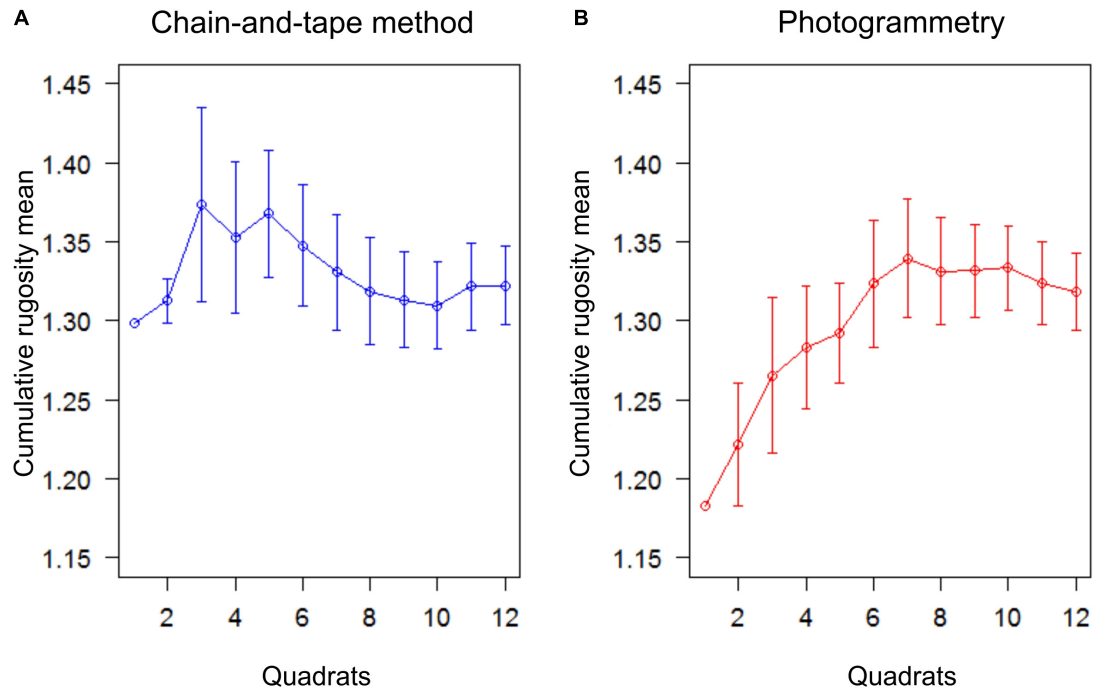

FIGURE 2 | Cumulative rugosity mean obtained according to an increasing number of replicates (quadrats), using alternatively **(A)** the chain-and-tape method or **(B)** the photogrammetry method; the sampling effort required for each method is deduced as the number of quadrats that is necessary to obtain a relative stable measurement of linear rugosity (i.e., when the plot reaches stabilization).

TABLE 4 | PERMANOVA table of results for rugosity; Variation source, degree of freedom (df), mean squares (MS), F statistic (Pseudo-F), *P*-value obtained by permutations [P(perm)] or using the Monte-Carlo test [P(MC)] and numbers of permutations (perms).

Source	Df	MS	Pseudo-F	P(perm)	perms	P(MC)
Habitat (Ha)	1	53.22	27.975	0.108	38	**0.036***
Method (Me)	1	0.22645	0.98803	0.383	38	0.435
Site (Si)	2	1.3949	8.1526	**0.002****	998	0.002
Ha × Me	1	0.21883	28.463	**0.024***	650	0.04
Ha × Si	2	1.9024	11.119	**0.001*****	999	0.002
Me × Si	2	0.22919	1.3395	0.267	998	0.266
Ha × Me × Si	2	7.69E-03	4.49E-02	0.951	999	0.955
Residuals	60	0.1711				
Total	71					

*Significance: ·P ≤ 0.1; *P ≤ 0.05; **P ≤ 0.01; ***P ≤ 0.001. P-values were obtained using 999 residuals permutations under a reduced model.*

chain-and-tape method than with the photogrammetry as shown by the coefficients of variation (CVchain = 1.66%; CVphotogrammetry = 0.62%), and by PERMDISP procedure (P = 0.015; SE (chain) = 4.8931 × 10^{-2} and SE (photogrammetry) = 2.0435 × 10^{-2}; **Figure 4**).

Teleost Assemblages

Environmental Variables According to the Site Factor

The mean surface rugosity, its variation and depth were significantly different according to the site (PERMANOVAs, respectively, P = 0.009; P = 0.002, and P = 0.001; **Supplementary Data Figure 3**). These variables were thus included as covariables in the factorial analysis (see M&M).

Covariables Study: Effects of Mean Rugosity, Its Variation and Depth on Teleost

As the mean surface rugosity increased, the total abundance and species richness were greater once the other variable effects were removed (respectively, PERMANOVA, P = 0.032; P = 0.045; **Figure 5** and **Supplementary Table 2**). These descriptors also had a residual variability when tested in response to the site (independently; **Supplementary Table 2**). When the site effect was exclusively taken into account, the total abundance was greater and more variable at certain sites (e.g., Joseph; **Figure 5**). The species richness was also higher and more variable at certain sites, but the results were different from those of the total abundance (e.g., Moyade; **Figure 5**). The Shannon index was not significantly influenced, either by the site factor or

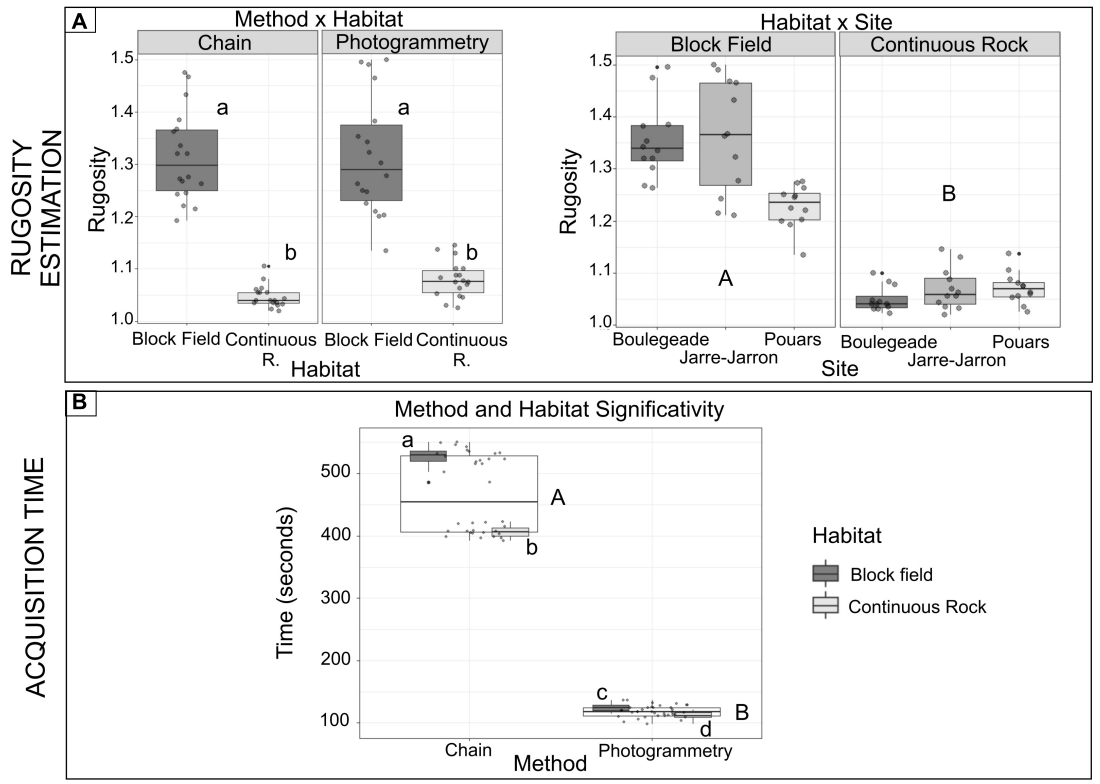

FIGURE 3 | Tukey boxplots of **(A)** rugosity (mean per quadrats) and **(B)** acquisition time per quadrat (seconds)—boxes display levels of treatments. Boxplots indicate the median (bold line near the center), the first and third quartile (the box), the extreme values where distance from the box is at most 1.5 times the inter-quartile range (whiskers), and remaining outliers (dark circles). Pair-wise tests between treatments are given with lower- and upper-case characters for significant terms from tests (**Tables 2**, **3**). Capital letters represent pair-wise tests between method modalities, whilst lowercase letters represent pairwise tests between modalities of the method × habitat treatment.

TABLE 5 | PERMANOVA table of results for time; Variation source, degree of freedom (df), mean squares (MS), F statistic (Pseudo-F), *P*-value obtain by permutations [P(perm)] or using the Monte-Carlo test [P(MC)] and numbers of permutations (perms).

Source	df	MS	Pseudo-F	P(perm)	perms	P(MC)
Habitat (Ha)	1	2.4598	471.87	0.095	38	**0.004****
Method (Me)	1	58.154	212.53	0.09	38	**0.005****
Site (Si)	2	5.10E-03	3.46E-02	0.952	999	0.959
Ha × Me	1	0.48901	2.0337	0.3206	659	0.305
Ha × Si	2	5.21E-03	3.53E-02	0.963	997	0.963
Me × Si	2	0.27363	1.8554	0.142	998	0.172
Ha × Me × Si	2	0.24045	1.6304	0.215	999	0.199
Residuals	60	0.14748				
Total	71					

*Significance: ·P ≤ 0.1; *P ≤ 0.05; **P ≤ 0.01; ***P ≤ 0.001. P-values were obtained using 999 residuals permutations under a reduced model.*

by covariables (**Supplementary Table 2**). Species assemblage (i.e., relative abundances) varied as a function of mean surface rugosity and depth covariables and site factor (**Figure 6** and **Supplementary Table 2**).

The assemblage of spatial categories differed only as a function of the mean surface rugosity and depth (**Supplementary Table 2**).

The specific abundance results differed among the species studied. The mean surface rugosity influenced the abundances of *Apogon imberbis* and *Anthias anthias*. The abundance of the latter species increased when mean surface rugosity was the only effect studied. The variation of surface rugosity only affected the abundance of *Coris julis*: which increased slightly with the increasing variation in surface rugosity. Depth only had an effect

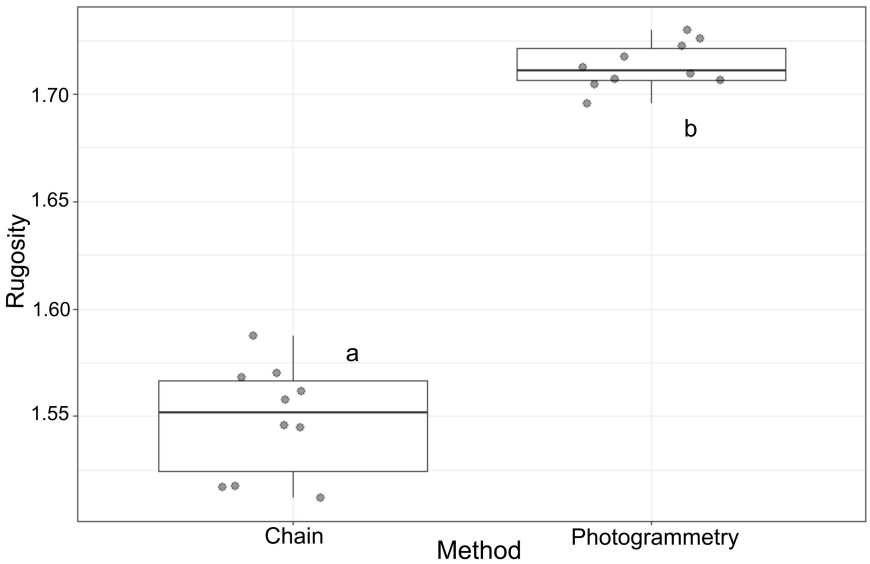

FIGURE 4 | Boxplots evaluating the precision of the chain-and-tape (Chain) and photogrammetry (Photogrammetry) based on the repeatability of each method. Boxes display levels of treatments. Boxplots indicate the median (bold line near the center), the first and third quartile (the box), the extreme values where distance from the box is at most 1.5 times the inter-quartile range (whiskers), and remaining outliers (dark circles).

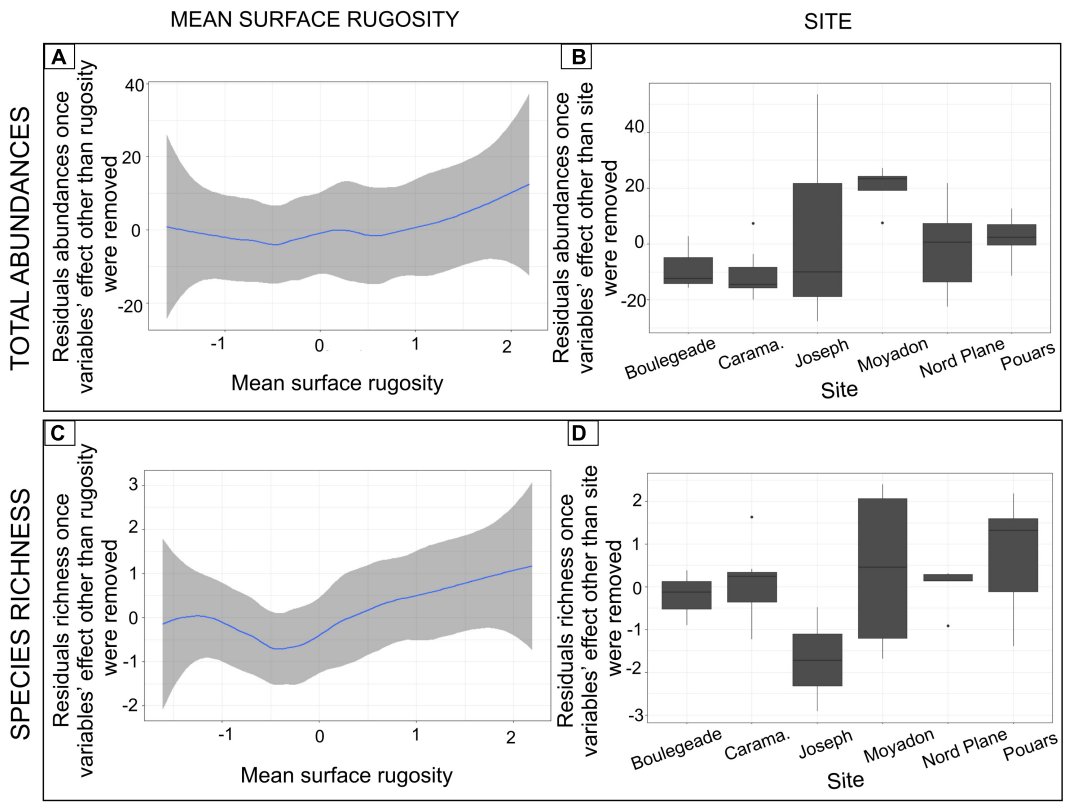

FIGURE 5 | Influence of the mean surface rugosity and the site factor on the total abundances of fish and the fish species richness. More precisely, **(A)** Smoothed curves of residuals of total abundances once the effect of all variables except the mean surface rugosity was removed; **(B)** Boxplots of residuals of total abundances once the effect of all variables except the site factor was removed; **(C)** Smoothed curves of residuals of species richness once the effect of all variables except the mean surface rugosity were removed; **(D)** Boxplots of residuals of species richness once the effect of all variables except the site factor was removed. Graphs show significant terms from tests (**Supplementary Table 2**).

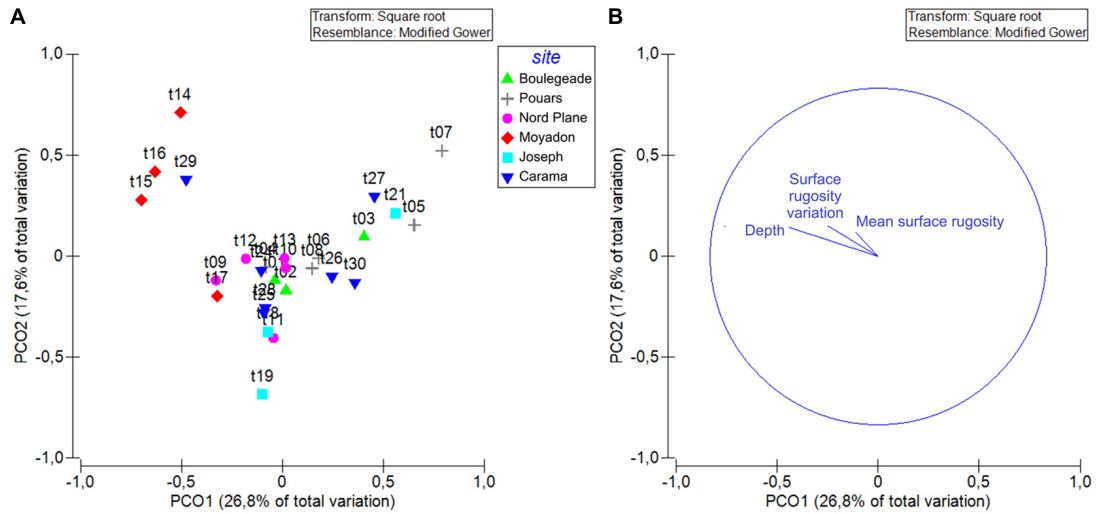

FIGURE 6 | Principal coordinate analysis (PCO) ordinations plot of species assemblage samples (transects) according to the site factor (fixed). **(A)** Each dot corresponds to a single transect attributed to one of the 6 sites (Boulegeade, Pouars, Nord Plane, Moyadon, Joseph and Camara for Camarassaigne). **(B)** Correlation vectors (Spearman) of the mean surface rugosity, the variation of surface rugosity and depth covariables are plotted.

on the abundance of *A. anthias*, in particular its abundance increased with increasing depth. The site factor simultaneously influenced the abundance of *Diplodus vulgaris, A. anthias*, *Serranus cabrilla,* and *A. imberbis*. The abundance of *D. vulgaris* was significantly different from one site to another (when the effects of covariate were removed): it was greater at the Joseph site (**Supplementary Figure 4**). The abundance of other species did not differ in function of the factors (**Supplementary Table 2**).

The size variation results (TL: total length in mm) of each species differed according to the species studied. The mean surface rugosity only influenced the sizes of *A. anthias* and *S. cabrilla*. The size of this latter species increased with increasing mean surface rugosity. The variation in surface rugosity only affected the sizes of *C. julis* and *D. sargus*. The size of *C. julis* decreased as the variation in surface rugosity variation increased (once all other variable effects were removed). Depth influenced the sizes of *C. julis*, *C. chromis,* and *D. vulgaris*. As the depth increased, the size of these three species decreased, and this tendency was more pronounced for *C. chromis*. The site had a significant effect on the size of *C. julis*, *C. chromis*, *D. vulgaris*, *A. anthias,* and *S. cabrilla*. When the site effect was exclusively represented, the sizes of *C. julis* and *C. chromis* did not differ as much between sites as the sizes of *D. vulgaris* and *A. anthias*. In this analysis, *A. imberbis* and *Sarpa salpa* were not taken into account because only a few individuals of each size were sampled. The other species sizes did not vary according to these factors (**Supplementary Table 2**).

The results of abundance by size-class were different depending on the species studied. The mean surface rugosity only influenced *C. julis*, *A. anthias, and A. imberbis* distribution of abundance by size-class. The variation in surface rugosity did not influence the abundance of a single species by size-class. The depth significantly affected the abundance by size-class of *C. julis*, *A. anthias*, *A. imberbis,* and *S. salpa*. The site factor modalities influenced the distribution of *A. anthias* and *A. imberbis* abundances by size-class. *S. cabrilla* was excluded from this analysis because too few individuals were observed, resulting in a negative *p*-value.

DISCUSSION

Methods Comparison

The chain-and-tape method was compared to photogrammetry to determine which approach was the most robust for characterizing habitat complexity. On one hand, we observed that the two methods gave similar estimates of the mean rugosity. More precisely, on a small sample (second experimental set-up), the mean rugosity estimate differed slightly from one method to another. However, on a larger scale (first experimental set-up) this difference was not significant according to the method. It should be noted that in continuous rocky habitat the difference between the methods was closer to the significance level, which might suggest that photogrammetry can detect rugosity more finely than the chain-and-tape method.

The methods differed considerably in terms of acquisition time. Specifically, the time was longer when the chain-and-tape method was used, while photogrammetry was much faster. This contrast is probably due to the manual *in situ* positioning of the chain, a phase that is not necessary with photogrammetry as data acquisition is carried out from pictures. It is interesting to identify which method is the most time-consuming *in situ*, because underwater fieldwork is expensive. It should be, however, noted that photogrammetry could require expensive equipment such as computers, specific software, and cameras. The time post-processing (e.g., the time needed to create 3D models)—which is not considered here—could be substantial according to the material available.

The dispersion of rugosity measurement (i.e., the dispersion around the median of the rugosity) was not significantly different in the first experimental device. However, when repeatability was studied, the dispersion was greater using the chain-and-tape method. In addition, the values of the coefficient of variation—quantifying precision—remained low but, in the case of photogrammetry the coefficient was close to zero. The chain-and-tape method therefore seems less reliable in terms of repeatability, and therefore less precise than photogrammetry. However, it would be interesting in future studies to consider a larger sample in order to verify this tendency. It is to be noted that previous studies highlighted that the chain-and-tape method has the disadvantage of needing many samples to give a robust estimation of rugosity (Storlazzi et al., 2016).

The lack of efficiency and precision of the chain-and-tape method is probably explained by the subjective placement of the chain along the segments (Storlazzi et al., 2016). It is possible that it imperfectly fits and follows the contour of the seabed, leading to an erroneous estimation of rugosity. If the chain links are small, it is possible to characterize the rugosity on a small scale and increase the measurement precision. These complications do not apply using photogrammetry, although it should be noted that one of the weaknesses of photogrammetry resides in the potential lack of pictures in an area, which can lead to an incomplete 3D representation (Ferrari et al., 2016). Photogrammetry could also be affected by the site conditions such as water turbidity (poor visibility). Under these circumstances, it might become very difficult to create models from the photos taken. On the other hand, the chain-and-tape method could still be used and give an acceptable result. Environmental conditions could therefore influence the quality of the images incidentally by reducing the precision of photogrammetry and adding noise in the models (Troisi et al., 2015; Urbina-Barreto, 2020). In addition, photogrammetry is known to cover larger areas than the chain-and-tape method (Leon et al., 2015; Bryson et al., 2017). The software used to create the 3D representation may also have a minimal influence on the results (e.g., Burns and Delparte, 2017).

Overall, photogrammetry appears as the most efficient method since it estimates rugosity more finely and more quickly than the chain-and-tape method during field acquisition. It is also the more repeatable method that estimates rugosity non-invasively (Friedman et al., 2012; Bridge et al., 2014).

Teleost Assemblages

Our work highlights the significant and independent effect of rugosity and other predictors on teleost fish assemblages. To do this, we first studied environmental variables (i.e., mean rugosity, variation of rugosity, and depth) as a function of the site factor and we observed that the site had a significant effect on these three variables. This result was not surprising because no site has strictly similar environmental specificities.

Then, through the factorial analysis, it has been shown that the total abundance and species richness of fish increased with a higher mean surface rugosity (effects of other factors removed). These results reinforce the conclusions from previous studies since they reported the same trends (Gratwicke and Speight, 2005; Komyakova et al., 2013). The abundance results for each species were taxon specific. Some species such as *C. julis* and *A. imberbis* were influenced by an increase of, respectively, the variation of rugosity and the mean surface rugosity, leading to the increase of their abundance.

High rugosity implies a greater quantity of food because the available surface is diversified: the algal cover can further develop and extend, and invertebrates can be more present (Luckhurst and Luckhurst, 1978; Vigliola et al., 1998; Gratwicke and Speight, 2005; Verges et al., 2011; Sinopoli et al., 2015). With more resources available, more species can coexist. It is likely that the number of available niches (Hutchinson niche: theoretical niche) will increase and species that are habitat specialists could then inhabit and occupy these spaces (Johnson et al., 2003; Willis et al., 2005; Bryson et al., 2017; Sinopoli et al., 2017). In addition, high rugosity implies high complexity leading to a greater number of shelters (Harborne et al., 2011, 2012; Ménard et al., 2012; Ferrari et al., 2016; Ferrari, 2017). Species such as nektobenthic and cryptobenthic fishes can easily find refuge. Through the use of these refuges, species can live in high-flow environments (Johansen et al., 2008).

Complexity can play a part in interactions such as predator-prey dynamics. Prey can use these shelters to escape predators (Hixon, 1991; Cheminée et al., 2017b), which improves their chances of survival, while predators can use habitat complexity to their advantage as hiding places to search or pursue prey, depending on their predation tactic (Thiriet et al., 2014; Chacin and Stallings, 2016; Mercader et al., 2019). Prey could be disadvantaged by complexity since it could reduce their visual field and therefore force them, to either risk predation by feeding outside their refuge or to remain in their shelter and risk starvation, and have difficulty in finding reproductive partners (Rilov et al., 2007). The trophic interactions can then depend on the refuges provided by habitat complexity to the predator-prey component (Grabowski, 2004). All these aspects could increase the reproduction of a species or a component but also its growth rate, depending on the interactions that take place, and therefore improve survival. Better habitat provides a given species at a given phase of its life cycle with the best trade-off between growth rate and predation-induced mortality (Dahlgren and Eggleston, 2000); therefore, a complex and heterogeneous seascape can offer various configurations, well-suited to fulfill the diverse needs of different species in terms of habitat quality.

Behavioral strategies can be responsible for specific abundance trends (Almany, 2004). For instance, *A. imberbis*—which has a strong specialization for rocky habitat—exhibits during the day a high degree of fidelity to its resting sites, likely to escape predators (Hoban, 2012). This could possibly illustrate the influence of the mean surface rugosity on the abundance of this species. As for *C. julis*, it is known to compete for the size of its territory (Lejeune, 1987), which could explain why its abundance varied according to the variation in rugosity. In addition, habitat complexity could favor interactions between species leading to specific behaviors. For example, *C. julis* can be a facultative cleaner at its first stage of life by feeding on other species if they are present, such as *S. salpa* (Neto, 2018), making habitat an important selection factor. The link between predator identity and habitat complexity influences the intensity

of the behavioral interactions by affecting trophic cascades (Grabowski et al., 2008).

Furthermore, our results indicated that depth, in interaction with surface rugosity, also had a significant effect on species assemblage and spatial category assemblage. Size patterns (the size of each species and the abundance in each size class) were taxon specific, but in general were also influenced by depth. The effect on spatial category assemblage was not particularly surprising since this variable separates species by their lifestyle (Harmelin, 1987), which can be directly linked to this environmental variable. However, it should be noted that this response variable was created from the spatial organization of diurnal species. The results could therefore differ significantly if we consider the nocturnal activity.

The depth effect has been demonstrated in previous studies (Friedlander and Parrish, 1998; Letourneur et al., 2003; Anderson and Millar, 2004; Milazzo et al., 2011, 2016; Schultz et al., 2014; Ferrari et al., 2018). More recently, works on rocky reefs have shown the significant and independent effect of depth and complexity of canopy-forming algae (Cheminée et al., 2017b; Cuadros et al., 2019), or the cumulative effects of depth and the complexity of habitat (Ferrari et al., 2018).

It could be interesting to integrate algal cover, which can be a proxy of complexity (Cuadros et al., 2019), such as the cover of *Cystoseira sensu lato*, in order to simultaneously consider the complexity of the inert substrate but also the complexity built by species such as in macrophytes forests or biogenic reefs, as well as with the depth factor. In addition, it is known that many fishes graze on epilithic algae (Gratwicke and Speight, 2005; Hinz et al., 2019), and that *Cystoseira* may provide preferred habitats for coastal fishes throughout their life stages (Lejeune, 1987; Rodrigues, 2010; Cheminée et al., 2013; Thiriet et al., 2014, 2016; Thibaut et al., 2017; Hinz et al., 2019).

The depth preference can be linked to the food requirements of the studied species (Bell, 1983) but also to the need to find a suitable habitat (with low temperature and/or reduced light for example Malcolm et al., 2011). The last assumption mainly applies to great depths, which is not the case in our study. In addition (Bell, 1983) demonstrated that some species preferred shallow to deep habitats. In our sample, some species classified as preferring deep conditions by this author were observed in shallow water (e.g., *C. chromis*), and so may have influenced our results.

Several other reasons could explain why species are seen at different depths, such as: avoidance strategy (i.e., species could be using several space-sharing mechanisms; Luckhurst and Luckhurst, 1978), behavior linked to a species' history traits, interactions between species (e.g., competition; Malcolm et al., 2011), trophic interactions, or ontogeny. These last three hypotheses could also coincide with rugosity. For instance, opposed gradients of densities according to depth were observed in the Mediterranean for the labrids *C. julis* and *Thalassoma pavo* (Milazzo et al., 2011; Sinopoli et al., 2017). Milazzo et al. (2011, 2016) highlighted the partitioning of these two species according to both vertical and horizontal gradients as a function of their affinities to colder (*C. julis*) vs. warmer waters (*T. pavo*). These studies underline the shifting trends of this partitioning as a result of global change and the rise of sea surface temperatures in the Mediterranean.

In the case of ontogeny, different ecological processes could be taking place including recruitment, settlement, and post-settlement (Vigliola et al., 1998; De La Morinière et al., 2002; Malcolm et al., 2011). It also must be noted that trophic interactions are intricate, difficult to describe and must be considered on the basis of specific factors, for instance relative to the species' behavior and habitat complexity (Grabowski, 2004). The literature reveals that sizes of some species are smaller in shallow water, concluding that this zone plays a role as nursery habitats (Bell, 1983; Cheminée et al., 2011, 2013, 2016, 2017a, 2020; Cuadros et al., 2017a,b, 2018). Our results do not support this hypothesis, but it is possible that we have omitted a key environmental variable influencing size patterns and masking an influence of depth on size. This could be a consequence of species-specific association: when juveniles of some species could prefer a particular habitat with specific characteristics, while in adulthood they might tend to favor another type of habitat structure (Bonin, 2012; Komyakova et al., 2018). Besides, some of our response variables such as total abundance and species richness were influenced by the site factor (e.g., total abundance was greater at Moyadon than at Caramassaigne). The differences between sites may be due to environmental characteristics that were not considered in the study such as currents (influencing for example the settlement of juveniles) (Friedlander and Parrish, 1998). In fact, this was the purpose of incorporating the site factor: to integrate a set of environmental variables that can take into account heterogeneity and spatial variability relating to the natural environment (Anderson and Millar, 2004; Cheminée et al., 2017b).

Moreover, in our study, the species are considered to be associated with the characteristics of the transects. It is unlikely that all species will stay their entire lifespan in a single isolated habitat, and it is more rational to assume that they move from one habitat to another. Habitats close to the transects could have an influence on the studied assemblages (Schultz et al., 2012). Different spatial scales should then be examined to fully understand the interactions between different life stages and shallow rocky reef habitats, and the movement of species and their interactions (Cheminée, 2012; Kovalenko et al., 2012; Thiriet et al., 2014). For a smaller scale example, Friedlander and Parrish (1998) noted that hole variables can be powerful predictors in describing fish biomass and number of individuals.

Studies on habitat complexity are mainly tropical. The number of metrics characterizing the complexity of Mediterranean shallow rocky reefs is more limited than in tropical environments. For instance, in the literature, coral species are classified according to their structural type (bushy vs. massive) (McCormick, 1994; Bridge et al., 2014), which could hardly be done in temperate waters. New metrics are therefore necessary to quantify the complexity of habitat in this area. Additional studies are also crucial to identify the links between habitat structuration and teleost assemblages. To this end, a larger dataset involving a greater number of species, habitats and sites should be developed and processed.

CONCLUSION

To measure 3D complexity, several methods exist; we demonstrated that photogrammetry is the most efficient and rapid especially when compared to the chain-and-tape method. Using new technologies to characterize 3D complexity is a promising way to acquire data. Photogrammetry offers new perspectives to quantify the habitat's three-dimensional structure (e.g., Urbina-Barreto, 2020), because of its capacity to provide precise and time-efficient measures.

Understanding how habitat complexity operates on species assemblage is essential for understanding key processes and therefore adapting conservation measures, notably in the context of global change. We saw in our study that our environmental variables had a real effect on communities. Specifically, increased rugosity appears to stimulate and promote the abundance and diversity of fish especially when known to provide shelter, food and facilitate interactions and reproduction, which can increase the chances of survival and explain the patterns encountered. Unsurprisingly, depth also had an impact on our biological variables, which has already been described in the literature. Yet, some of our data variability was omitted but described by the site factor. To go further, it could be interesting to consider new environmental descriptors such as currents or, on a smaller scale, hole variables.

Combined with biological data, the study of 3D complexity can be an exploration of the entire marine environment, quantifying horizontal zonation, where vertical zonation can be related to depth. Even though habitat complexity has a strong impact on teleost fish assemblage structure, it should be borne in mind that all habitats are important in maintaining regional fish diversity (Gratwicke and Speight, 2005). On the basis of this knowledge, it could be interesting to study on a larger spatial scale these aspects at the 3D level by means of photogrammetry.

DATA AVAILABILITY STATEMENT

The raw data supporting the conclusions of this article will be made available by the authors, without undue reservation.

ETHICS STATEMENT

Ethical review and approval was not required for the animal study because the study was non-lethal. More precisely, we only used Underwater Visual Census (UVC) to count teleost individuals.

AUTHOR CONTRIBUTIONS

AC, PD, and OB designed the experiments. AC and OB managed the funding acquisition. AP and OB performed the field work. TM and AC compiled and analyzed output data, and designed and wrote the first version of the manuscript. TM, AC, PD, and TT prepared the revised version of the manuscript. All authors discussed the results and implications and commented on the manuscript at all stages and contributed extensively to the work presented in this manuscript.

FUNDING

This work was part of TM's Ph.D. thesis and was conducted within the scope of the THALIA Project. Part of the data was collected within the framework of the project "Contribution à la surveillance des biocénoses littorales selon l'approche paysagère" funded by the *Agence de l'Eau Rhône Méditerranée Corse, Délégation PACA et Corse-AGAF*. TM received a Ph.D. scholarship EJD n°2020_03366 funded by the *Conseil Régional de la Région SUD-PACA*.

ACKNOWLEDGMENTS

We wish to thank Pierre Thiriet for his scientific advises, Pierre Boissery from the Agence de l'Eau Rhône Méditerranée Corse, Renata Ferrari and Will F. Figueira for a preliminary discussion on the topic, Holly Monfort and Michael Paul for proofreading of the English text, and both reviewers for their advice.

SUPPLEMENTARY MATERIAL

The Supplementary Material for this article can be found online at: https://www.frontiersin.org/articles/10.3389/fmars.2021.639309/full#supplementary-material

Supplementary Figure 1 | Schematization of the sampling methods. **(A)** Calculation of linear rugosity of a rocky reef habitat using the chain-and-tape method as presented by Hill and Wilkinson (2004). **(B)** *In situ* data acquisition corresponding to the method comparison. **(C)** *In situ* data acquisition to measure on the one hand, the fish assemblage descriptors and on the other hand, the environmental variables (mean surface rugosity, surface rugosity variation and depth) corresponding to the second analysis to determine the relation between the habitat complexity and the Teleost assemblages.

Supplementary Figure 2 | Spatial organization of ichthyofauna in Mediterranean shallow rocky reef bottoms. The numbers refer to the spatial categories (see **Table 1**). In this study, no distinction was made between category 6.a and 6.b. Modified from Harmelin (1987).

Supplementary Figure 3 | Mean and standard error of each environmental variable [**(A)** surface rugosity mean, **(B)** surface rugosity variation and **(C)** depth] according to the site factor (6 sites: Boulegeade, Carama for Caramassaigne, Joseph, Moyadon, Nord Plane, Pouars).

Supplementary Figure 4 | Influence of the mean surface rugosity, the surface rugosity variation, depth, and the site factor on the specific abundances. More precisely, **(A)** Smoothed curves of residuals of *Coris julis* abundance once the effect of all variables expect surface rugosity variation was removed. **(B)** Boxplots of residuals of *Diplodus vulgaris* once the effect of all variables except the factor site was removed. **(C)** Boxplots and smoothed curves of residuals of *Anthias anthias* once the effect of all variables except mean surface rugosity, depth or the site factor were removed. Graphs show significant terms from tests (**Supplementary Table 2**). Sites abbreviations: B, Boulegeade; C, Caramassaigne; J, Josepth; M, Moyadon; N-P, Nord Plane; P, Pouars.

Supplementary Table 1 | Processing parameters used to create the 3D models with Agisoft Metashape. These parameters refer to the third quadrat model in Pouars site (Pouars 3) as for an example.

Supplementary Table 2 | PERMANOVA table of results for all response variables tested (corresponding to the Teleost assemblage, including the ones that are taxon specific); Variation source, degree of freedom (df), mean squares (MS), F statistic (Pseudo-F), *P*-value obtain by permutations [P(perm)] or using the Monte-Carlo test [P(MC)] and numbers of permutations (perms). Significance: $\cdot P \leq 0.1$; $^{*}P \leq 0.05$; $^{**}P \leq 0.01$; $^{***}P \leq 0{,}001$. *P*-values were obtained using 999 residuals permutations under a reduced model.

REFERENCES

Airoldi, L., Balata, D., and Beck, M. W. (2008). The gray zone: relationships between habitat loss and marine diversity and their applications in conservation. *J. Exper. Mar. Biol. Ecol.* 366, 8–15. doi: 10.1016/j.jembe.2008.07.034

Almany, G. R. (2004). Does increased habitat complexity reduce predation and competition in coral reef fish assemblages? *Oikos* 106, 275–284. doi: 10.1111/j.0030-1299.2004.13193.x

Anderson, M. J., Gorley, R. N., and Clarke, K. R. (2008). *Plymouth: primer-E; 2008. PERMANOVA+ for PRIMER: Guide to software and statistical methods*. 214.

Anderson, M. J., and Millar, R. B. (2004). Spatial variation and effects of habitat on temperate reef fish assemblages in northeastern New Zealand. *J. Exper. Mar. Biol. Ecol.* 305, 191–221. doi: 10.1016/j.jembe.2003.12.011

Arnal. (2017). *Répétabilité & Reproductibilité d'une méthode*. France: Université de Bordeaux.

August, P. V. (1983). The role of habitat complexity and heterogeneity in structuring tropical mammal communities. *Ecology* 64, 1495–1507. doi: 10.2307/1937504

Beck, M. W. (2000). Separating the elements of habitat structure: independent effects of habitat complexity and structural components on rocky intertidal gastropods. *J. Exper. Mar. Biol. Ecol.* 249, 29–49. doi: 10.1016/S0022-0981(00)00171-4

Bell, J. D. (1983). Effects of depth and marine reserve fishing restrictions on the structure of a rocky reef fish assemblage in the north-western Mediterranean Sea. *J. Appl. Ecol.* 20, 357–369. doi: 10.2307/2403513

Bell, S. S., McCoy, E. D., and Mushinsky, H. R. (2012). *Habitat structure: the physical arrangement of objects in space*. Berlin: Springer Science & Business Media.

Bianchi, C. N., and Morri, C. (2000). Marine biodiversity of the Mediterranean Sea: situation, problems and prospects for future research. *Mar. Pollut. Bull.* 40, 367–376. doi: 10.1016/S0025-326X(00)00027-8

Bonin, M. C. (2012). Specializing on vulnerable habitat: Acropora selectivity among damselfish recruits and the risk of bleaching-induced habitat loss. *Coral Reefs* 31, 287–297. doi: 10.1007/s00338-011-0843-2

Bridge, T. C., Ferrari, R., Bryson, M., Hovey, R., Figueira, W. F., Williams, S. B., et al. (2014). Variable responses of benthic communities to anomalously warm sea temperatures on a high-latitude coral reef. *PloS One* 9:e113079. doi: 10.1371/journal.pone.0113079

Bryson, M., Ferrari, R., Figueira, W., Pizarro, O., Madin, J., Williams, S., et al. (2017). Characterization of measurement errors using structure-from-motion and photogrammetry to measure marine habitat structural complexity. *Ecol. Evol.* 7, 5669–5681. doi: 10.1002/ece3.3127

Burns, J. H. R., and Delparte, D. (2017). Comparison of commercial structure-from-motion photogrammety software used for underwater three-dimensional modeling of coral reef environments. *Int. Arch. Photogramm. Remote Sens. Spatial Inf. Sci.* 42, 127–131. doi: 10.5194/isprs-archives-XLII-2-W3-127-2017

Burns, J. H. R., Delparte, D., Gates, R. D., and Takabayashi, M. (2015). Integrating structure-from-motion photogrammetry with geospatial software as a novel technique for quantifying 3D ecological characteristics of coral reefs. *PeerJ.* 3:e1077. doi: 10.7717/peerj.1077

Byrne, L. B. (2007). Habitat structure: a fundamental concept and framework for urban soil ecology. *Urban Ecosyst.* 10, 255–274. doi: 10.1007/s11252-007-0027-6

Calders, K., Phinn, S., Ferrari, R., Leon, J., Armston, J., Asner, G. P., et al. (2020). 3D imaging insights into forests and coral reefs. *Trends Ecol. Evol.* 35, 6–9. doi: 10.1016/j.tree.2019.10.004

Chacin, D. H., and Stallings, C. D. (2016). Disentangling fine-and broad-scale effects of habitat on predator–prey interactions. *J. Exper. Mar. Biol. Ecol.* 483, 10–19. doi: 10.1016/j.jembe.2016.05.008

Charton, J. G., and Ruzafa, A. P. (1998). Correlation between habitat structure and a rocky reef fish assemblage in the southwest Mediterranean. *Mar. Ecol.* 19, 111–128. doi: 10.1111/j.1439-0485.1998.tb00457.x

Cheminée, A. (2012). *Ecological functions, transformations and management of infralittoral rocky habitats from the Northwestern Mediterranean: the case of fish (Teleostei) nursery habitats*. France: Université Nice Sophia Antipolis.

Cheminée, A., Francour, P., and Harmelin-Vivien, M. (2011). Assessment of Diplodus spp.(Sparidae) nursery grounds along the rocky shore of Marseilles (France, NW Mediterranean). *Sci. Mar.* 75, 181–188. doi: 10.3989/scimar.2011.75n1181

Cheminée, A., Le Direach, L., Rouanet, E., Astruch, P., Goujard, A., Blanfuné, A., et al. (2020). *Typology of fish nurseries in shallow Mediterranean coastal zones: all habitats matter*. doi: 10.21203/rs.3.rs-118728/v1

Cheminée, A., Merigot, B., Vanderklift, M. A., and Francour, P. (2016). Does habitat complexity influence fish recruitment? *Mediter. Mar. Sci.* 17, 39–46. doi: 10.12681/mms.1231

Cheminée, A., Pastor, J., Bianchimani, O., Thiriet, P., Sala, E., Cottalorda, J.-M., et al. (2017a). Juvenile fish assemblages in temperate rocky reefs are shaped by the presence of macro-algae canopy and its three-dimensional structure. *Sci. Rep.* 7, 1–11. doi: 10.1038/s41598-017-15291-y

Cheminée, A., Rider, M., Lenfant, P., Zawadzki, A., Mercière, A., Crec'Hriou, R., et al. (2017b). Shallow rocky nursery habitat for fish: spatial variability of juvenile fishes among this poorly protected essential habitat. *Mar. Pollut. Bull.* 119, 245–254. doi: 10.1016/j.marpolbul.2017.03.051

Cheminée, A., Sala, E., Pastor, J., Bodilis, P., Thiriet, P., Mangialajo, L., et al. (2013). Nursery value of Cystoseira forests for Mediterranean rocky reef fishes. *J. Exper. Mar. Biol. Ecol.* 442, 70–79. doi: 10.1016/j.jembe.2013.02.003

Clarke, K. R., and Gorley, R. N. (2006). *PRIMER v6: user manual/tutorial, Primer E: Plymouth*. Plymouth, UK: Plymouth Marine Laboratory.

Clarke, K. R., Gorley, R. N., Somerfield, P. J., and Warwick, R. M. (2014). *Change in marine communities: an approach to statistical analysis and interpretation*. Alban: Primer-E Ltd.

CloudCompare (2018). Available Online at: http://cloudcompare.org/ (accessed April 12, 2021).

Coll, M., Piroddi, C., Albouy, C., Ben Rais Lasram, F., Cheung, W. W. L., Christensen, V., et al. (2012). The Mediterranean Sea under siege: spatial overlap between marine biodiversity, cumulative threats and marine reserves: The Mediterranean Sea under siege. *Global Ecol. Biogeogr.* 21, 465–480. doi: 10.1111/j.1466-8238.2011.00697.x

Cuadros, A., Basterretxea, G., Cardona, L., Cheminée, A., Hidalgo, M., and Moranta, J. (2018). Settlement and post-settlement survival rates of the white seabream (Diplodus sargus) in the western Mediterranean Sea. *PloS One* 13:e0190278. doi: 10.1371/journal.pone.0190278

Cuadros, A., Cheminée, A., Thiriet, P., Moranta, J., Vidal, E., Sintes, J., et al. (2017a). The three-dimensional structure of Cymodocea nodosa meadows shapes juvenile fish assemblages at Fornells Bay (Minorca Island). *Regional Stud. Mar. Sci.* 14, 93–101. doi: 10.1016/j.rsma.2017.05.011

Cuadros, A., Moranta, J., Cardona, L., Thiriet, P., Pastor, J., Arroyo, N. L., et al. (2017b). Seascape attributes, at different spatial scales, determine settlement and post-settlement of juvenile fish. *Estuarine Coastal Shelf Sci.* 185, 120–129. doi: 10.1016/j.ecss.2016.12.014

Cuadros, A., Moranta, J., Cardona, L., Thiriet, P., Francour, P., Vidal, E., et al. (2019). Juvenile fish in Cystoseira forests: influence of habitat complexity and depth on fish behaviour and assemblage composition. *Mediter. Mar. Sci.* 20, 380–392. doi: 10.12681/mms.18857

Cuttelod, A., García, N., Malak, D. A., Temple, H. J., and Katariya, V. (2009). "The Mediterranean: a biodiversity hotspot under threat," in *Wildlife in a Changing World–an analysis of the 2008 IUCN Red List of Threatened Species*, eds J.-C. Vié, C. Hilton-Taylor, and S. N. Stuart (Gland, Switzerland: IUCN), 180.

Dahlgren, C. P., and Eggleston, D. B. (2000). Ecological processes underlying ontogenetic habitat shifts in a coral reef fish. *Ecology* 81, 2227–2240. doi: 10.1890/0012-9658(2000)081[2227:EPUOHS]2.0.CO;2

De La Morinière, E. C., Pollux, B. J. A., Nagelkerken, I., and Van der Velde, G. (2002). Post-settlement life cycle migration patterns and habitat preference of coral reef fish that use seagrass and mangrove habitats as nurseries. *Estuarine Coastal Shelf Sci.* 55, 309–321. doi: 10.1006/ecss.2001.0907

Drap, P., Merad, D., Hijazi, B., Gaoua, L., Nawaf, M. M., Saccone, M., et al. (2015). Underwater photogrammetry and object modeling: a case study of Xlendi Wreck in Malta. *Sensors* 15, 30351–30384. doi: 10.3390/s151229802

Drap, P., Merad, D., Mahiddine, A., Seinturier, J., Peloso, D., Boï, J.-M., et al. (2013). Underwater Photogrammetry for Archaeology. What will be the next step? *Int. J. Herit. Digital Era* 2, 375–394. doi: 10.1260/2047-4970.2.3.375

Ferrari, R. (2017). The hidden structure in coral reefs. *Coral Reefs* 36, 445–445. doi: 10.1007/s00338-017-1540-6

Ferrari, R., Bryson, M., Bridge, T., Hustache, J., Williams, S. B., Byrne, M., et al. (2016). Quantifying the response of structural complexity and community

composition to environmental change in marine communities. *Global Change Biol.* 22, 1965–1975. doi: 10.1111/gcb.13197

Ferrari, R., Malcolm, H. A., Byrne, M., Friedman, A., Williams, S. B., Schultz, A., et al. (2018). Habitat structural complexity metrics improve predictions of fish abundance and distribution. *Ecography* 41, 1077–1091. doi: 10.1111/ecog.02580

Figueira, W., Ferrari, R., Weatherby, E., Porter, A., Hawes, S., and Byrne, M. (2015). Accuracy and precision of habitat structural complexity metrics derived from underwater photogrammetry. *Remote Sens.* 7, 16883–16900. doi: 10.3390/rs71215859

Friedlander, A. M., and DeMartini, E. E. (2002). Contrasts in density, size, and biomass of reef fishes between the northwestern and the main Hawaiian islands: the effects of fishing down apex predators. *Mar. Ecol. Prog. Ser.* 230, 253–264. doi: 10.3354/meps230253

Friedlander, A. M., and Parrish, J. D. (1998). Habitat characteristics affecting fish assemblages on a Hawaiian coral reef. *J. Exper. Mar. Biol. Ecol.* 224, 1–30. doi: 10.1016/S0022-0981(97)00164-0

Friedman, A., Pizarro, O., Williams, S. B., and Johnson-Roberson, M. (2012). Multi-scale measures of rugosity, slope and aspect from benthic stereo image reconstructions. *PloS One* 7:e50440. doi: 10.1371/journal.pone.0050440

Grabowski, J. H. (2004). Habitat complexity disrupts predator–prey interactions but not the trophic cascade on oyster reefs. *Ecology* 85, 995–1004. doi: 10.1890/03-0067

Grabowski, J. H., Hughes, A. R., and Kimbro, D. L. (2008). Habitat complexity influences cascading effects of multiple predators. *Ecology* 89, 3413–3422. doi: 10.1890/07-1057.1

Graham, N. A. J., and Nash, K. L. (2013). The importance of structural complexity in coral reef ecosystems. *Coral Reefs* 32, 315–326. doi: 10.1007/s00338-012-0984-y

Gratwicke, B., and Speight, M. R. (2005). The relationship between fish species richness, abundance and habitat complexity in a range of shallow tropical marine habitats. *J. Fish Biol.* 66, 650–667. doi: 10.1111/j.0022-1112.2005.00629.x

Harborne, A. R., Mumby, P. J., and Ferrari, R. (2012). The effectiveness of different meso-scale rugosity metrics for predicting intra-habitat variation in coral-reef fish assemblages. *Environ. Biol. Fishes* 94, 431–442. doi: 10.1007/s10641-011-9956-2

Harborne, A. R., Mumby, P. J., Kennedy, E. V., and Ferrari, R. (2011). Biotic and multi-scale abiotic controls of habitat quality: their effect on coral-reef fishes. *Mar. Ecol. Prog. Ser.* 437, 201–214. doi: 10.3354/meps09280

Harmelin, J.-G. (1987). Structure et variabilité de l'ichtyofaune d'une zone rocheuse protégée en Méditerranée (Pare national de Port-Cros, France) Structure and Variability of the Ichthyo-fauna in a Mediterranean Protected Rocky Area (National Park of Port-Cros, France). *Mar. Ecol.* 8, 263–284. doi: 10.1111/j.1439-0485.1987.tb00188.x

Harmelin-Vivien, M. L., Harmelin, J. G., Chauvet, C., Duval, C., Galzin, R., Lejeune, P., et al. (1985). Evaluation visuelle des peuplements et populations de poissons méthodes et problèmes. *Rev. Ecol.* 40, 1–72.

Hewitt, J. E., Thrush, S. F., Halliday, J., and Duffy, C. (2005). The importance of small-scale habitat structure for maintaining beta diversity. *Ecology* 86, 1619–1626. doi: 10.1890/04-1099

Hill, J. J., and Wilkinson, C. C. (2004). *Methods for ecological monitoring of coral reefs: a resource for managers*. Townsville, MC: Australian Institute of Marine Science.

Hinz, H., Reñones, O., Gouraguine, A., Johnson, A. F., and Moranta, J. (2019). Fish nursery value of algae habitats in temperate coastal reefs. *PeerJ.* 7:e6797. doi: 10.7717/peerj.6797

Hixon, M. A. (1991). "Predation as a process structuring coral reef fish communities," in *The ecology of fishes on coral reefs*, ed. P. F. Sale (San Diego: Academic Press), 475–508. doi: 10.1016/B978-0-08-092551-6.50022-2

Hoban, M. (2012). *Habitat specialization in the Mediterranean cardinalfish, Apogon imberbis*.

Johansen, J. L., Bellwood, D. R., and Fulton, C. J. (2008). Coral reef fishes exploit flow refuges in high-flow habitats. *Mar. Ecol. Prog. Ser.* 360, 219–226. doi: 10.3354/meps07482

Johnson, M. P., Frost, N. J., Mosley, M. W., Roberts, M. F., and Hawkins, S. J. (2003). The area-independent effects of habitat complexity on biodiversity vary between regions. *Ecol. Lett.* 6, 126–132. doi: 10.1046/j.1461-0248.2003.00404.x

Komyakova, V., Jones, G. P., and Munday, P. L. (2018). Strong effects of coral species on the diversity and structure of reef fish communities: A multi-scale analysis. *PloS One* 13:e0202206. doi: 10.1371/journal.pone.0202206

Komyakova, V., Munday, P. L., and Jones, G. P. (2013). Relative importance of coral cover, habitat complexity and diversity in determining the structure of reef fish communities. *PloS One* 8:e83178. doi: 10.1371/journal.pone.0083178

Kovalenko, K. E., Thomaz, S. M., and Warfe, D. M. (2012). Habitat complexity: approaches and future directions. *Hydrobiologia* 685, 1–17. doi: 10.1007/s10750-011-0974-z

Lejeune, P. (1987). The effect of local stock density on social behavior and sex change in the Mediterranean labrid Coris julis. *Environ. Biol. Fish* 18, 135–141. doi: 10.1007/BF00002601

Leon, J. X., Roelfsema, C. M., Saunders, M. I., and Phinn, S. R. (2015). Measuring coral reef terrain roughness using 'Structure-from-Motion'close-range photogrammetry. *Geomorphology* 242, 21–28. doi: 10.1016/j.geomorph.2015.01.030

Letourneur, Y., Ruitton, S., and Sartoretto, S. (2003). Environmental and benthic habitat factors structuring the spatial distribution of a summer infralittoral fish assemblage in the north-western Mediterranean Sea. *J. Mar. Biol. Assoc. UK.* 83, 193–204. doi: 10.1017/S0025315403006970h

Louisy, P. (2002). *Guide d'identification des poissons marins: Europe de l'ouest et Méditerranée*. Paris: Editions Eugen Ulmer.

Luckhurst, B. E., and Luckhurst, K. (1978). Analysis of the influence of substrate variables on coral reef fish communities. *Mar. Biol.* 49, 317–323. doi: 10.1007/BF00455026

Malcolm, H. A., Jordan, A., and Smith, S. D. (2011). Testing a depth-based habitat classification system against reef fish assemblage patterns in a subtropical marine park. *Aquatic Conserv. Mar. Freshwater Ecosyst.* 21, 173–185. doi: 10.1002/aqc.1165

McCormick, M. I. (1994). Comparison of field methods for measuring surface topography and their associations with a tropical reef fish assemblage. *Mar. Ecol. Prog. Ser.* 112, 87–96. doi: 10.3354/meps112087

Meager, J. J., Schlacher, T. A., and Green, M. (2011). Topographic complexity and landscape temperature patterns create a dynamic habitat structure on a rocky intertidal shore. *Mar. Ecol. Prog. Ser.* 428, 1–12. doi: 10.3354/meps09124

Ménard, A., Turgeon, K., Roche, D. G., Binning, S. A., and Kramer, D. L. (2012). Shelters and their use by fishes on fringing coral reefs. *PloS One* 7:e38450. doi: 10.1371/journal.pone.0038450

Mercader, M., Blazy, C., Di Pane, J., Devissi, C., Mercière, A., Cheminée, A., et al. (2019). Is artificial habitat diversity a key to restoring nurseries for juvenile coastal fish? Ex situ experiments on habitat selection and survival of juvenile seabreams. *Restor. Ecol.* 27, 1155–1165. doi: 10.1111/rec.12948

Messmer, V., Jones, G. P., Munday, P. L., Holbrook, S. J., Schmitt, R. J., and Brooks, A. J. (2011). Habitat biodiversity as a determinant of fish community structure on coral reefs. *Ecology* 92, 2285–2298. doi: 10.1890/11-0037.1

Milazzo, M., Palmeri, A., Falcón, J. M., Badalamenti, F., Garcìa-Charton, J. A., Sinopoli, M., et al. (2011). Vertical distribution of two sympatric labrid fishes in the Western Mediterranean and Eastern Atlantic rocky subtidal: local shore topography does matter. *Mar. Ecol.* 32, 521–531. doi: 10.1111/j.1439-0485.2011.00447.x

Milazzo, M., Quattrocchi, F., Azzurro, E., Palmeri, A., Chemello, R., Di Franco, A., et al. (2016). Warming-related shifts in the distribution of two competing coastal wrasses. *Mar. Environ. Res.* 120, 55–67. doi: 10.1016/j.marenvres.2016.07.007

Neto, J. N. (2018). *Facultative cleaner species in marine temperate waters: The ecological role of juvenile Diplodus sargus (Sparidae)*. Portugal: ISPA Instituto universitário.

R Core Team. (2017). *R: A language and environment for statistical computing. Vienna, Austria. R Foundation for Statistical Computing*. Available Online at: http://www.R-project.org/

Rees, M. J., Jordan, A., Price, O. F., Coleman, M. A., and Davis, A. R. (2014). Abiotic surrogates for temperate rocky reef biodiversity: implications for marine protected areas. *Diver. Distrib.* 20, 284–296. doi: 10.1111/ddi.12134

Rees, M. J., Knott, N. A., Neilson, J., Linklater, M., Osterloh, I., Jordan, A., et al. (2018). Accounting for habitat structural complexity improves the assessment of performance in no-take marine reserves. *Biol. Conserv.* 224, 100–110. doi: 10.1016/j.biocon.2018.04.040

Rilov, G., Figueira, W. F., Lyman, S. J., and Crowder, L. B. (2007). Complex habitats may not always benefit prey: linking visual field with reef fish behavior and distribution. *Mar. Ecol. Prog. Ser.* 329, 225–238. doi: 10.3354/meps329225

Risk, M. J. (1972). Fish diversity on a coral reef in the Virgin Islands. *Atoll Res. Bull.* 153, 1–4. doi: 10.5479/si.00775630.153.1

Rodrigues, D. D. (2010). *Habitat associations and behaviour of wrasses of the genus Symphodus (Rafinesque, 1810) at the Arrábida Marine Park, Portugal*. Lisbon, Portugal: Faculdade De Ciências Da Universidade De Lisboa.

Royer, J.-P., Nawaf, M. M., Merad, D., Saccone, M., Bianchimani, O., Garrabou, J., et al. (2018). Photogrammetric surveys and geometric processes to analyse and monitor red coral colonies. *J. Mar. Sci. Eng.* 6:42. doi: 10.3390/jmse6020042

Sala, E., Ballesteros, E., Dendrinos, P., Di Franco, A., Ferretti, F., Foley, D., et al. (2012). The structure of Mediterranean rocky reef ecosystems across environmental and human gradients, and conservation implications. *PloS One* 7:e32742. doi: 10.1371/journal.pone.0032742

Schultz, A. L., Malcolm, H. A., Bucher, D. J., Linklater, M., and Smith, S. D. (2014). Depth and medium-scale spatial processes influence fish assemblage structure of unconsolidated habitats in a subtropical marine park. *PloS One* 9:e96798. doi: 10.1371/journal.pone.0096798

Schultz, A. L., Malcolm, H. A., Bucher, D. J., and Smith, S. D. (2012). Effects of reef proximity on the structure of fish assemblages of unconsolidated substrata. *PloS One* 7:e49437. doi: 10.1371/journal.pone.0049437

Sinopoli, M., Cattano, C., Chemello, R., Timpanaro, A., Milisenda, G., and Gristina, M. (2018). Nest-mediated parental care in a marine fish: Are large-scale nesting habitats selected and do these habitats respond to small-scale requirements? *Mediter. Mar. Sci.* 19, 248–255. doi: 10.12681/mms.14993

Sinopoli, M., Cattano, C., Chemello, R., Timpanaro, A., Timpanaro, V., and Gristina, M. (2015). Nest building in a Mediterranean wrasse (S ymphodus ocellatus): are the algae used randomly chosen or actively selected? *Mar. Ecol.* 36, 942–949. doi: 10.1111/maec.12187

Sinopoli, M., Chemello, R., Vaccaro, A., and Milazzo, M. (2017). Food resource partitioning between two sympatric temperate wrasses. *Mar. Freshwater Res.* 68, 2324–2335. doi: 10.1071/MF16363

Storlazzi, C. D., Dartnell, P., Hatcher, G. A., and Gibbs, A. E. (2016). End of the chain? Rugosity and fine-scale bathymetry from existing underwater digital imagery using structure-from-motion (SfM) technology. *Coral Reefs* 35, 889–894. doi: 10.1007/s00338-016-1462-8

Thibaut, T., Blanfuné, A., Boudouresque, C. F., Personnic, S., Ruitton, S., Ballesteros, E., et al. (2017). An ecosystem-based approach to assess the status of Mediterranean algae-dominated shallow rocky reefs. *Mar. Pollut. Bull.* 117, 311–329. doi: 10.1016/j.marpolbul.2017.01.029

Thiriet, P., Cheminée, A., Mangialajo, L., and Francour, P. (2014). *"How 3D complexity of macrophyte-formed habitats affect the processes structuring fish assemblages within coastal temperate seascapes?," in Underwater Seascapes*. Cham: Springer, 185–199. doi: 10.1007/978-3-319-03440-9_12

Thiriet, P. D., Di Franco, A., Cheminée, A., Guidetti, P., Bianchimani, O., Basthard-Bogain, S., et al. (2016). Abundance and diversity of crypto-and necto-benthic coastal fish are higher in marine forests than in structurally less complex macroalgal assemblages. *PloS One* 11:e0164121. doi: 10.1371/journal.pone.0164121

Troisi, S., Del Pizzo, S., Gaglione, S., Miccio, A., and Testa, R. L. (2015). 3D Models Comparison of Complex Shell in Underwater and Dry Environments. *Int. Arch. Photogr. Remote Sens. Spatial Inform. Sci.* XL, 215–222. doi: 10.5194/isprsarchives-XL-5-W5-215-2015

Urbina-Barreto, I. (2020). *Nouveaux indices quantitatifs pour le suivi des récifs coralliens issus de modélisation 3D par photogrammétrie*. Réunion: Université de La Réunion.

Ventura, D., Dubois, S. F., Bonifazi, A., Jona Lasinio, G., Seminara, M., Gravina, M. F., et al. (2020). Integration of close-range underwater photogrammetry with inspection and mesh processing software: a novel approach for quantifying ecological dynamics of temperate biogenic reefs. *Remote Sens. Ecol. Conserv.* 7, 169–186. doi: 10.1002/rse2.178

Verges, A., Vanderklift, M. A., Doropoulos, C., and Hyndes, G. A. (2011). Spatial patterns in herbivory on a coral reef are influenced by structural complexity but not by algal traits. *PloS One* 6:e17115. doi: 10.1371/journal.pone.0017115

Vigliola, L., Harmelin-Vivien, M. L., Biagi, F., Galzin, R., Garcia-Rubies, A., Harmelin, J.-G., et al. (1998). Spatial and temporal patterns of settlement among sparid fishes of the genus Diplodus in the northwestern Mediterranean. *Mar. Ecol. Prog. Ser.* 168, 45–56. doi: 10.3354/meps168045

Willis, S. C., Winemiller, K. O., and Lopez-Fernandez, H. (2005). Habitat structural complexity and morphological diversity of fish assemblages in a Neotropical floodplain river. *Oecologia* 142, 284–295. doi: 10.1007/s00442-004-1723-z

Young, G. C., Dey, S., Rogers, A. D., and Exton, D. (2017). Cost and time-effective method for multi-scale measures of rugosity, fractal dimension, and vector dispersion from coral reef 3D models. *PloS One* 12:e0175341. doi: 10.1371/journal.pone.0175341

Conflict of Interest: The authors declare that the research was conducted in the absence of any commercial or financial relationships that could be construed as a potential conflict of interest.

frontiers in Marine Science

METHODS
published: 03 August 2021
doi: 10.3389/fmars.2021.660846

A Non-destructive Method to Create a Time Series of Surface Area for Coral Using 3D Photogrammetry

Daniel D. Conley[1,2]* *and Erin N. R. Hollander*[2]

[1] *Mitchell Laboratory, Scripps Institution of Oceanography, University of California, San Diego, San Diego, CA, United States,* [2] *Smith/Sandin Laboratory, Scripps Institution of Oceanography, University of California, San Diego, San Diego, CA, United States*

The wax dip method typically used to determine the surface area of corals for data normalization is destructive, rendering the collection of time series for such data impossible. With recent advancements in photogrammetric technology, it is now possible to collect these data in a non-destructive manner at very high levels of accuracy. This photogrammetric method using Agisoft's Metashape is compared to the standard wax-dip method using both objects of known surface area and objects of unknown surface area. Objects of known surface area (i.e., objects that have surface areas that can be calculated using geometrical formulas) were estimated with a similar degree of accuracy with the Photogrammetry (PG) method (R^2 = 0.9922, slope = 0.9835) as with the wax-dip method (R^2 = 0.9872, slope = 1). A single factor ANOVA confirmed that there was no significant difference between measurements from the three methods of geometrical calculation, wax dipping, or photogrammetry for objects of known surface area. This paper describes the methods for rapidly collecting surface area data of small to moderately sized coral nubbins in a laboratory setting and characterizes the relationship between buoyant weight and surface area over time for the coral species *Stylophora pistillata*. Finally, two predictive models are proposed to estimate surface area from weight in air measurements.

Keywords: surface area, buoyant weight, wax dip, *Stylophora pistillata*, photogrammetry, coral physiology

OPEN ACCESS

Edited by:
Christian Robert Voolstra, University of Konstanz, Germany

Reviewed by:
Matthew R. Nitschke, University of Aveiro, Portugal
Charles Alan Jacoby, St. Johns River Water Management District, United States

***Correspondence:**
Daniel D. Conley
D1conley@ucsd.edu

Specialty section:
This article was submitted to Coral Reef Research, a section of the journal Frontiers in Marine Science

Received: *29 January 2021*
Accepted: *29 June 2021*
Published: *03 August 2021*

Citation:
Conley DD and Hollander ENR (2021) A Non-destructive Method to Create a Time Series of Surface Area for Coral Using 3D Photogrammetry. Front. Mar. Sci. 8:660846. doi: 10.3389/fmars.2021.660846

INTRODUCTION

Surface area (SA) is an extremely important parameter in benthic coral ecology (Dahl, 1973), and it is commonly used as a metric to normalize oxygen production and consumption measurements, and other biomass-dependent data. This is due to photosynthesis and respiration occurring in the surface tissues of the coral. The higher the SA of a coral the more potential it has to perform photosynthesis and respire (Hoegh-Guldberg, 1988; Jones et al., 2008; Holmes et al., 2008; Laforsch et al., 2008; Naumann et al., 2009; Veal et al., 2010). Most hermatypic corals have a thin layer of tissue that closely corresponds to the shape of the coral's skeleton (Veal et al., 2010). For these reasons, SA is a better normalizing parameter than one like buoyant weight (BW_t) (Dodge et al., 1984). BW_t is measured by suspending the coral nubbin in a basket in seawater of

a known density to estimate the weight of the calcium carbonate without the coral tissue as the BW_t method operates on the assumption that tissue and mucus are neutrally buoyant (Jokiel and Maragos, 1978). While BW_t is a good parameter for estimating health, growth, and calcification, due to the complex growth forms and differences in density exhibited by many corals, BW_t may not be indicative of the SA and thus is not the preferred normalizing parameter (Dodge et al., 1984).

There have been many methods used to estimate the SA of corals, each with its specific pros and cons. In 1962, Harrod and Hall were of the first to consider the implications of measuring actual SA. They attempted to glean the SA of leaves by precisely measuring the difference in weight of *Hydrangea* leaves before and after being submerged in water (Harrod and Hall, 1962). One of the first ways SA was estimated for corals was by simply taking the planar area of the corals projected from 2D images taken from the normal of the coral surface (Kanwisher and Wainwright, 1967). This method is not sufficient for most growth forms of corals as it does not consider the three-dimensionality of coral structures and would therefore grossly underestimate the SA (Hoegh-Guldberg, 1988). For this reason, a method like this would only be applicable in cases where there is virtually zero rugosity to the growth form of the coral.

More recently, prior to 1991, the most common way of collecting coral SA was the foil method (Hoegh-Guldberg, 1988). This method was used in many studies including Davies (1980); Szmant-Froelich and Pilson (1980); Hawkins and Lewis (1982); Burris et al. (1983); Muscatine et al. (1984), as well as several others. The coral samples are either covered in pieces of foil of known SA and tallied, or the coral is covered in foil, then the foil is removed and measured. Another method performed by Meyer and Schultz (1985) used a liquid latex rubber to coat the skeleton after being sealed in paraffin wax. The latex was removed after it dried and placed between plates of glass and traced on a transparent film. This film was then digitized to estimate the SA. While these methods were relatively easy to perform and produced reasonably accurate results, they were only appropriate for corals with simple growth forms or individual branches of more complex growth forms.

In 1988, Hoegh-Guldberg developed a new method to estimate the SA of more complex growth forms particularly that of *Pocillopora damicornis*. The corals were coated in up to 5 layers of "Verathane" plastic varnish with a thickness range of 0.03–0.05 mm then the corals were dipped in an aqueous Methylene Blue dye/detergent solution. The SA was directly proportional to the amount of dye that clung to the coral specimens and was easily estimated using this technique. While this method was successful in estimating the SA of *P. damicornis*, it was noted that this method consistently underestimated the SA of objects with known geometries, so this was most likely occurring with the corals as well. Also, due to the added thickness of the varnish, this method was not attempting to estimate the absolute SA, the SA of the naked skeleton of the corals, but the "primary" SA of the corals, defined as the SA occupied by the coral polyps while extended (Hoegh-Guldberg, 1988). It is critical to know what space your selected method of measurement is measuring. Due to the thickness of the Verathane, it was impossible to get a true measurement of the skeleton itself. This concept is also important to take into account when measuring corals with or without living tissue intact.

In 1991, Stimson and Kinzie developed a new method where corals were double dipped in Paraffin wax and the weight of the added wax was used as a proxy for SA. In 2010, Veil et al. further refined this method to make it more practical and more accurate using a single dip method. The wax dip method has proven to be extremely robust and has become a standard method to estimate the SA of corals in the lab and the field. All the methods described above share a common negative, being that they are all destructive and cannot be performed *in vivo*. Here "destructive" is defined as an action or procedure that kills the coral and not merely stresses the coral. To calculate the change in SA over time, a non-destructive method must be used to collect the data.

In the past decade, computer-aided tools have been used to estimate the SA of corals *in vivo*. In 2008, Jones et al. used a simple freeware 3D animation program called GMAX to create simple wire-frames that were very accurate at estimating the SA of objects with a known SA and small simple coral branches compared to the wax dip method. Others have used medical-grade X-ray computed tomography scan (CT) to measure coral SA with extremely high accuracy (Laforsch et al., 2008; Naumann et al., 2009; House et al., 2018). Unfortunately, CT scanners are expensive to operate and one would need access to special facilities to make the measurements needed, which adds another layer of difficulty to measuring the corals' SA.

Photogrammetry (PG) is the creation of 3D models from an array of 2D images and can be used to estimate SA without sacrificing the corals. The PG method allows for the creation of a time series for SA, as well as a more accurately normalized time series for SA dependant measurements. Ferrari et al. (2017) used the PG method in the field to measure coral growth and contraction with PG-derived SA estimates for the first time, but with only two time points. Since then, House et al. (2018), compared the PG method directly to CT by measuring the same objects or corals with both methods and analyzing them for differences. While they found that PG was reasonably accurate when compared to the CT method with best fit models with adjusted R^2 ranging from 0.70 to 0.97, they also found that PG-derived SA was significantly different from the CT-derived SA (p = 0.008) (House et al., 2018). It is notable, however, that House et al. (2018) used a relatively small number of photos (only 39 for their smallest specimens) for the size of their specimens. PG is highly dependant on the number of photos and view angles that are input into the system to construct the 3D models. The larger and more complex a specimen is, the more images and angles are needed to accurately construct the 3D model. In the House et al.'s (2018) study, they relied more on varying the camera view angle and did not take as many images. This potential under-sampling of camera views would lead to a reduced accuracy for the models created by reducing the amount of overlap for each image. In this study due to the simple morphology of the nubbins, we will rely on

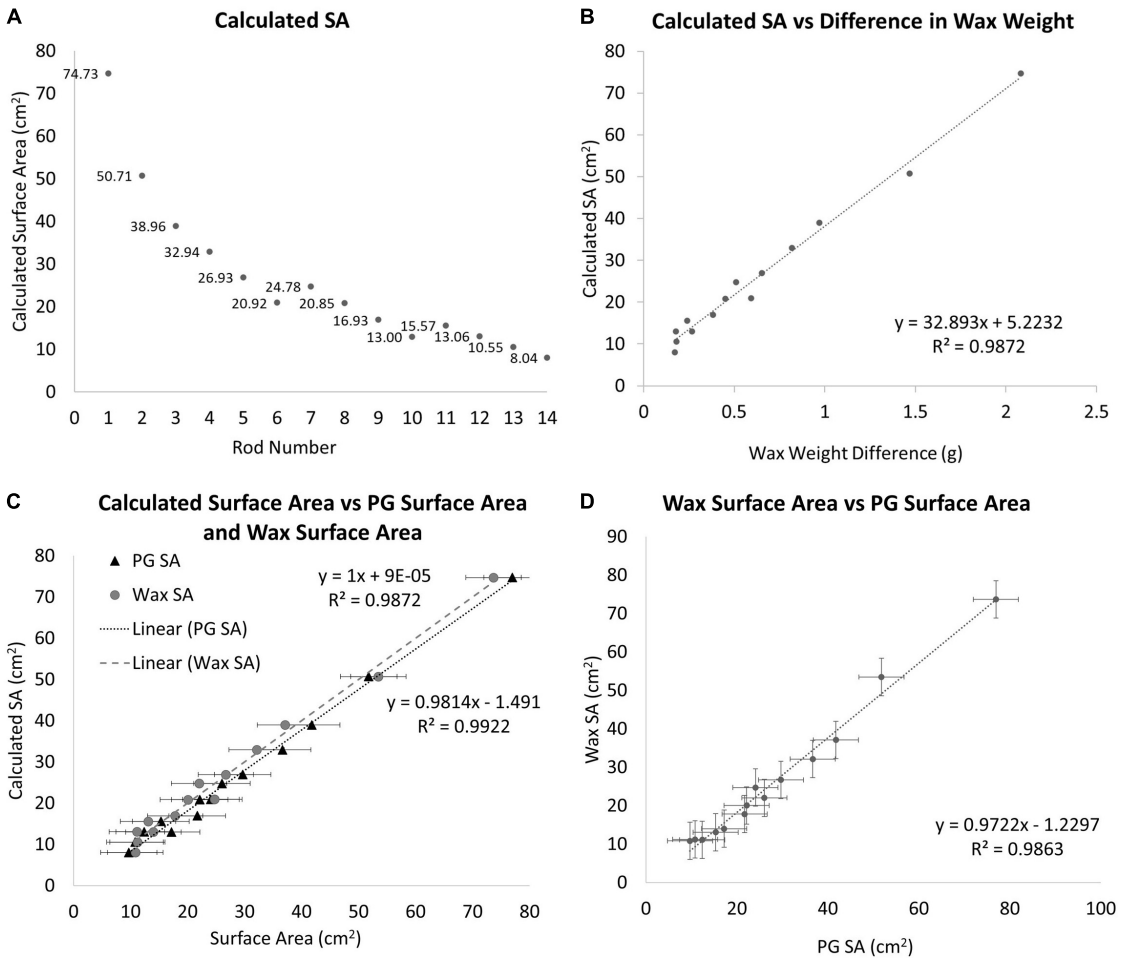

FIGURE 1 | (A) The geometrically calculated SAs of the standards. The standards are a series of doweling rods of different diameters and lengths. SA is the SA of the side and the top excluding the bottom using the equation SA = (πr2)+ (hπD). **(B)** The geometrically calculated SA of the standard rods vs. the difference in pre and post-wax dipped standard rods. A best-fit line is fit to the data points with the equation y = 32.893x+ 5.2232. **(C)** A comparison between the geometrically calculated SA and the wax-dip derived SA, gray circles (R^2 = 0.9872, Slope = 1) and the PG derived SA, black triangles (R^2 = 0.9814, Slope = 0.9922). **(D)** A comparison of wax dip derived SA and PG derived SA (R^2 = 0.9863, Slope = 0.9722).

saturation of photo overlaps and use a single camera angle to streamline photo collection and minimize the time in air for the coral nubbins.

The goal of this study is to use one of the latest software platforms, Agisoft Metashape, to create many 3D models of the same corals over time to create a time series of growth based on SA instead of BW_t. Agisoft Metashape was chosen because it allows for the end-to-end creation of 3D models from 2D images with little to no specialized knowledge and thus is extremely easy to allow even the most novice operators to build these models after a short tutorial. Other studies, like House et al. (2018), that use the PG method use an array of open-source software that would take some time to master. The creation of this time series will allow for new questions about SA to be asked. For example, "is SA growth linear over time?" and "how does SA change with BW_t over time?" With the previous methodologies, these types of questions were out of reach. This software provides a simple method of creating time series for the growth of coral based on SA. Also, a strict and consistent imaging protocol that oversamples the specimen to ensure saturation of camera views makes it possible to increase the accuracy of the 3D models produced. Due to the very small size and lack of complexity of the specimens used in this study, we rely on an oversampling of a single camera view angle.

METHODS

Coral Acquisition and Preparation

Corals were sourced from Aqua SD, a local online coral distributor in San Diego, CA. A single head of *Stylophora pistillata* (approximately 30 cm in diameter) was purchased, fragmented, and grown at an average temperature of 27°C under the light of 150 μE/s/m^2 on average, with a 12 h/12 h day-night schedule. Each newly fragmented coral was attached to a pure aragonite coral plug that was 20 mm in diameter (Ocean Wonders,

United States). The corals were attached to the plugs using Reef Glue (Ocean Wonders, United States). The seawater system was a pass-through system receiving new water pumped in from the ocean at the end of Scripps Pier (La Jolla Shores, La Jolla, CA). The water was passed through a four-stage sand filter system and heated to the temperature of 27°C. After fragmentation, the corals were acclimated for 4 weeks before any measurements were taken. Eighty nubbins were selected and tagged. The corals were then randomly subdivided into two groups of 40. Corals 1–40 (group 1) were measured weekly on a specific day, while corals 41–80 (group 2) were measured weekly on a different day.

Buoyant Weight Data Collection

The BW_t of 80 coral nubbins were collected weekly over 14 weeks using a Mettler Toledo scale (Mettler Toledo, United States) with a hanging basket attachment accurate to 0.001 g. The basket was placed into a 9.46 L tank with a 50-watt titanium tube water heater (Finnex, United States). The water temperature was controlled within a range of 25.5–27.5°C. The salinity was measured using a refractometer accurate to 1 ppt (ADE Advanced Optics, United States). The salinity and temperature data for each BW_t measurement were used to calculate the density of the water at the time of each measurement. The density of the water was then calculated using the water density formulas provided by UNESCO (Massel, 2015). The air weight (W_a) of the coral nubbins were calculated using the equation from Jokiel and Maragos (1978):

$$W_a = \frac{W_w}{1 - \left(\frac{D_w}{D_a}\right)} \quad (1)$$

Where W_w is the measured BW_t, D_w is the density of the water the nubbin is weighed in, and D_a is the density of the nubbin. For this study D_a (the average density of *Stylophora pistillata*) is assumed to be 2.5 g/cm^3 as measured by Ferrier-Pagès et al. (2003).

Wax Dipping Data Collection

Wax dip-derived SA data can only be collected from a coral that has been sacrificed (Stimson and Kinzie, 1991). Before data can be collected from corals, a calibration curve must be constructed from a series of objects with SAs that can be calculated. These SAs must be calculated using basic geometric equations. Wooden cylindrical rods of varying diameters and heights were used to create this calibration curve (**Figure 1A**). Where SA is the SA of the side and the top excluding the bottom of the rod using the equation:

$$SA = (\pi r2) + (h\pi D) \quad (2)$$

Diameters and lengths of the rods were measured using a pair of Husky digital calipers accurate to 0.01 mm (Husky, United States). After the SAs have been calculated, each standard is weighed using a Mettler Toledo scale (Mettler Toledo, United States; accurate to 0.001 g), and their masses are recorded. Each standard is then dipped in paraffin wax using the single dip method as in Veal et al. (2010), at a wax temperature of 70°C. The wax temperature was maintained using a Fisher scientific hotplate with a built-in magnetic stirrer and measured with a Fisher Scientific digital thermometer accurate to 0.1°C (Thermo Fisher Scientific, United States). A two-inch stir bar was used at the lowest setting to keep the wax at a homogeneous temperature. The stir bar was turned off while dipping and on between treatments. All specimens were at room temperature (25°C) at the time of dipping. The standards were dipped for 3 s and then pulled out and twisted back and forth for 10 s to ensure an even coating of the wax. The wax-dipped standards were set aside to dry for no less than 15 min after which time they were weighed and their masses were recorded again. The difference between the pre and post-wax weights was calculated and compared to the calculated dimensions of the rods (**Figure 1B**). From this comparison a best-fit line is placed giving us the following equation:

$$y = 32.893x + 5.2232 \quad (3)$$

Where y is the estimated SA of the unknown object and x is the difference in weight between the unknown object before and after being dipped in wax. From this equation, it is possible to estimate any objects' SA when dipped into the same wax at the same temperature. Corals skeletons from group 1 were wax-dipped using the same method outlined above at the end of the experiment for comparison to PG-derived SA.

Photogrammetric Surface Area Data Collection

SA was measured by taking an average of 60 photos of each nubbin in air from a single camera view angle (approximately 25–30 degrees) using a custom-built motorized turntable and a

TABLE 1 | This table shows all the steps in the workflow and the relevant settings needed to create a single model.

Workflow step	Relevant settings	Approximate time per model (min)
Import images	Create chunk for each subfolder	1
Align images (build sparse point cloud)	Accuracy—High Generic; Preselection—Yes; Key Point Limit—0; Tie Points–5,000	1–5
Build dense point cloud	Quality—High; Depth Filtering—Mild; Reuse Depth Maps—Yes	10–30
Build mesh	Depth Maps Quality—High; Face Count—Custom; Custom Face Count–500,000	5–15
Build texture	Mapping Mode—Generic; Texture Size—4096; Hole Filling—Yes	2–10
Scaling	Create markers and scale bars	1
Model clean up	Remove all non-coral portions of the model	3

The estimated time for completing each step for a single model is included. A range indicates the difference in times for a high-end system and an average system, respectively, per model completed. A batch file with all appropriate settings preset has been included in ***Supplementary Material****.*

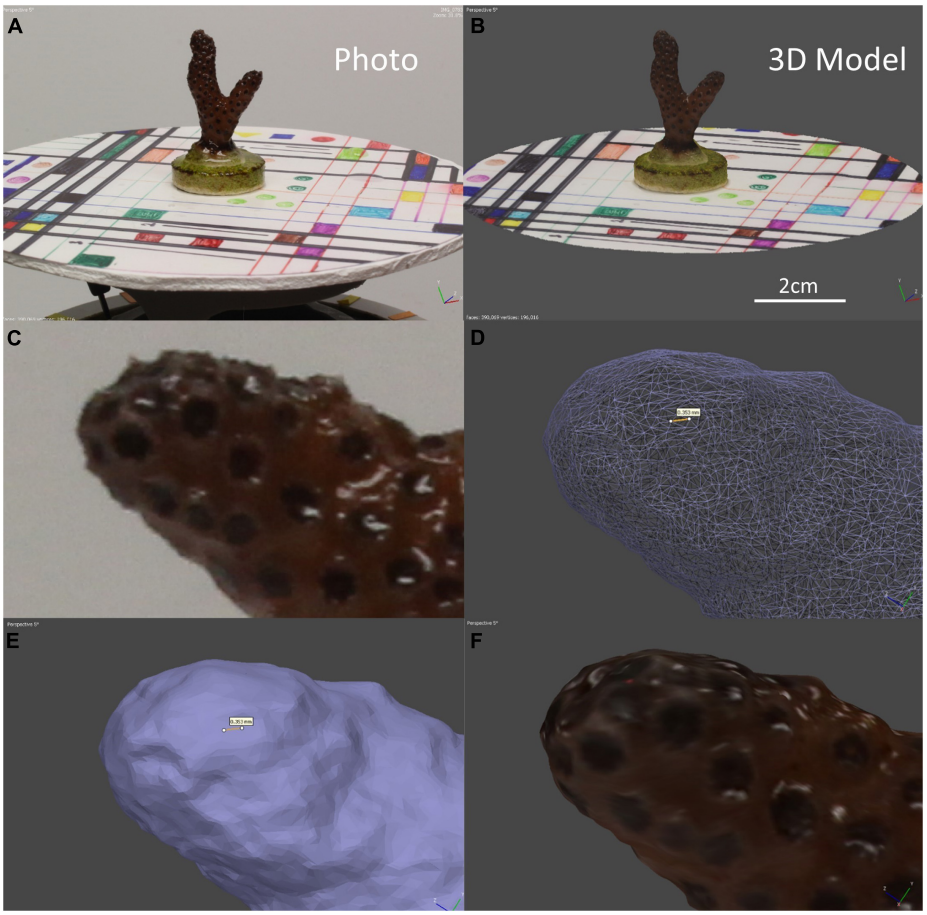

FIGURE 2 | (A) A photo of coral nubbin 4–01 from week 3 on the motorized turntable with the scaling disk. **(B)** An example of a fully rendered 3D model for the coral in A with reference disc and scale bar. **(C)** A close-up photo of coral 4–08 from week 8. **(D)** Close up of the wireframe mesh for the coral in C, the yellow line represents 0.353 mm. **(E)** Close up of the solid mesh of the coral in C, the yellow line represents 0.353 mm. **(F)** Close up of the final render of the coral in **(C)**.

Canon T3i DSLR Camera with an 18MP CMOS sensor capturing images with a resolution of 5184 × 3456 pixels (Canon, JP). The camera was operated with an infrared remote control to eliminate having to physically touch the camera after it was positioned. The motorized turntable had a wired button that turned the platform approximately 6 degrees for every press of the button. The corals were placed on a scaling disc with an arbitrary pattern of lines and geometric shapes as well as 4 scale bars. This disc allows for manual scaling of the models after the full render is completed, and also gives the computer software the necessary geometric reference patterns to properly align the photos. The nubbins were photographed in front of a contrasting blank backdrop in the ambient light condition of the lab. For live corals, a white backdrop was used and a black backdrop was used for coral skeletons.

Each set of images were then imported to the program (AgiSoft Metashape Professional, 2020). The program aligns the images, creates tie points, builds a sparse point cloud and depth maps for each image, builds the dense point cloud, builds mesh, builds texture. The model then is scaled using the aforementioned scale bars and trimmed so that only the coral remains in the model. Finally, SA is estimated using the Mesh Tool in the drop down menu entitled "tools". In between each step, it is necessary to perform minor adjustments of the models to ensure the most accurate final model. For example, after photos are aligned, the model range, the 3D space in which the model is constructed, may not be properly set. If this is ignored, it would lead to portions of the coral not being incorporated into the final model creating holes in the model. Also, once the dense point cloud is created it is usually necessary to remove any points allocated from the background of the images. If this step is ignored, it is possible to get non-coral incorporated into the final model and it would have to be rerendered. Once a clean dense point cloud was created, the last two steps were run using a script that automatically created the mesh and texture. The average passive processing time (not including any active steps in between computer processing steps) to create one completed model was approximately 10 min. **Table 1** shows each step with the relevant setting parameters to create a singe coral nubbin model.

A custom-built computer running a Threadripper 2990wx 32 core 64 thread processor with 128 GB of RAM and two Radeon VII graphics cards with 60 compute units each was used to

process the models in Windows 10 Pro. The processing time for models will vary depending on the specifications of the computer used and the number of photos per model. For 40 corals with 60 photos each, the total passive processing time was just under 12 h for this system. A lower-powered system would take significantly longer to perform these tasks. For example, a system running a Threadripper 1950 × 12 core 24 thread processor with 32 GB of RAM and a single Radeon VEGA 56 graphics card with 56 compute units would have a total passive processing time (for 40 models with 60 photos each) of approximately 33 h. It is possible to complete this entire workflow on a computer system that does not have a graphics card, but again the process would take an extremely long time comparatively. This would only be practical for a project with relatively few models that needed to be constructed. An example comparison between a photo, solid model, wireframe mesh, and a finished model with the scaling disk and a close-up of the wireframe can be seen in **Figure 2**. During preliminary investigations of this method, it was determined that one angle and 60 photos produced models with the same surface area as 2 angles and 120 photos. For this reason, only 60 photos and one angle were used as this practice takes half the time and limits the corals' "in air" time. If corals with more complex growth forms, are used, more camera angles and photos would be necessary to created accurate models.

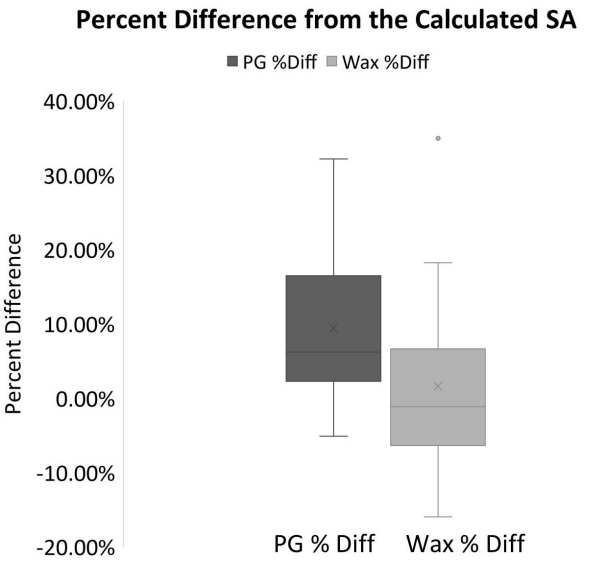

FIGURE 3 | Box plots for the percent difference from the geometrically calculated SA for both the PG and the wax derived SA measurements. The mean is indicated x and the median is represented by the line bisecting each plot. The dark gray plot represents the PG percent difference data, and the light gray represents the data for the Wax percent difference. Dots outside the plot represent outliers in the data.

Statistical Methods

Standard *t*-tests were used to compare the difference between geometrically calculated, wax-derived, and PG-derived SA estimates of standards. Regression analyses were used to determine the R^2 and slope of the wax and PG-derived SA's relationship to the geometrically calculated SA of the standards. To determine if there was a significant difference between the results of the 3 methods on the standards an ANOVA analysis was conducted. A single factor ANOVA compared the difference between wax derived another regression analysis compared the growth rates produced by W_a and SA measurements. Additionally, to establish whether the initial size of the coral affected its growth rate a regression analysis was conducted comparing the growth rates for both methods to their respective initial measurements. A single factor ANOVA was conducted to determine the difference between both methods of calculating growth rates. To determine if there was a significant difference

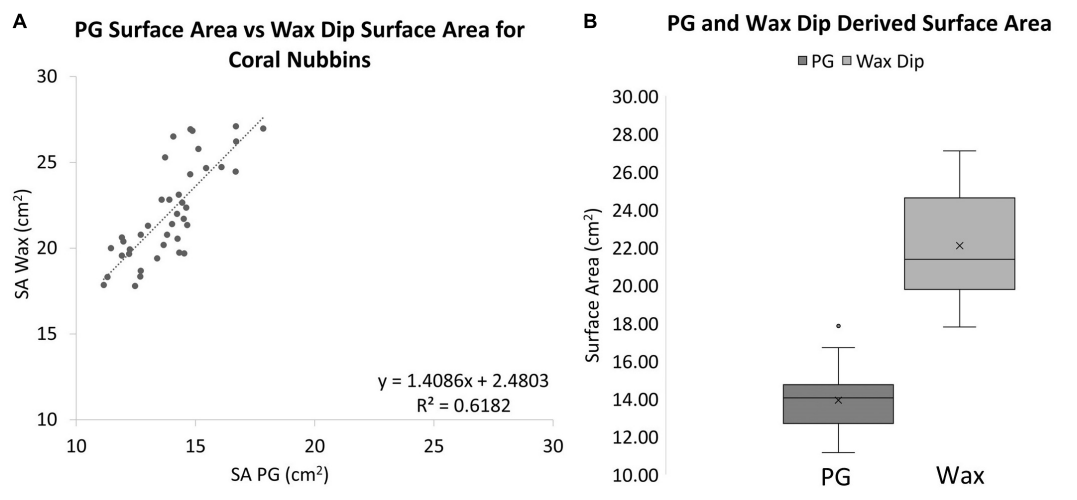

FIGURE 4 | (A) A comparison of wax dip-derived SA and PG-derived SA for coral nubbins (R^2 = 0.6182, Slope = 1.4086). **(B)** Box plots for PG and wax dip-derived SA measurements of coral nubbins. The wax-dip method was on average 58.9% higher than the PG method. The mean is indicated x and the median is represented by the line bisecting each plot. Dots outside the plot represent outliers in the data.

between the SA "simple" and "complex" prediction models and the PG-derived SA data, a regression analysis and single-factor ANOVA were conducted. Power rule models were applied to the data to create the predictive models reported here. All statistics and modeling were performed using Microsoft Excel (Microsoft, United States).

RESULTS

Wax Dipping Comparison

A one-to-one relationship was observed between the geometrically calculated and the wax-derived SAs with an R^2-value of 0.9872 (Slope = 1) (**Figure 1C**). The wax dip method overestimates SA when compared to the geometrically calculated SA, especially for smaller objects. On average, this method overestimated the SA of standard objects by approximately 1.61% when compared to the calculated values.

The SAs for all standards also were estimated using PG in Metashape. When the estimates were compared to the calculated values, a 1:1 relationship was observed with an R^2 of 0.9922 (Slope = 0.9814) (**Figure 1C**). The relationship between the PG method of estimating SA and the calculated SA was slightly stronger but was not significantly different from the wax-derived method (Paired t-test, $p = 0.5000$).

When the wax-dipped SAs were compared directly to the PG SAs, a marginally weaker relationship is observed with an R^2-value of 0.9869 (Slope = 0.9746) (**Figure 1D**). When the results were compared for the measurements of the standards, the PG method had higher overall values. However, the results of a single factor ANOVA showed no significant difference between geometrically calculated, wax-dipped, and PG measurements [$F(2, 39) = 0.056$, $p = 0.945$]. **Figure 3** shows the box plots for the percent difference from the geometrically calculated SA for both the wax dip method and the PG method.

When these methods were applied to corals, a significantly different result was observed. The wax-dipped method of measuring SA of coral nubbins yielded significantly higher results than did the PG method. On average the wax dip method estimated SA 58.9% higher than did the PG method for the same coral (**Figure 4**). A single factor ANOVA showed a very significant difference between the two groups of wax dipped and PG measurements [$F(1, 78) = 252.53$, $p \leq 0.001$].

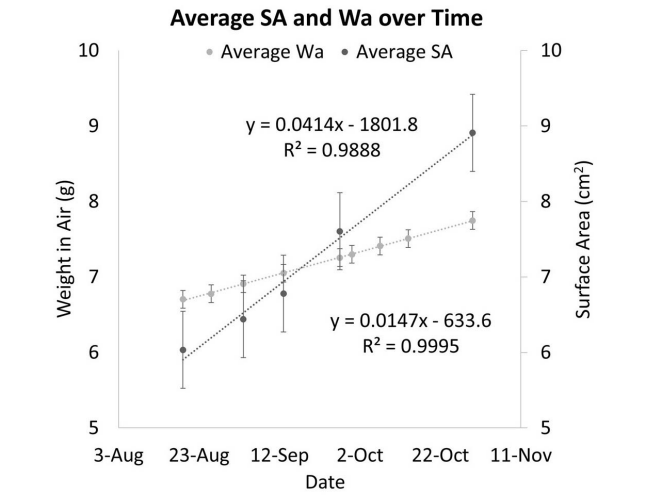

FIGURE 5 | A comparison of W_a over time and SA over time for the same corals. Dark circles represent the average change in PG SA over time. Light circles represent the change in W_a over time. The error bars represent the standard error.

Surface Area's Relationship to Buoyant Weight

The two methods of determining growth rates also were significantly different with SA on average growing 0.69% per day for a total of 49.55% between August 19th, 2019 and October

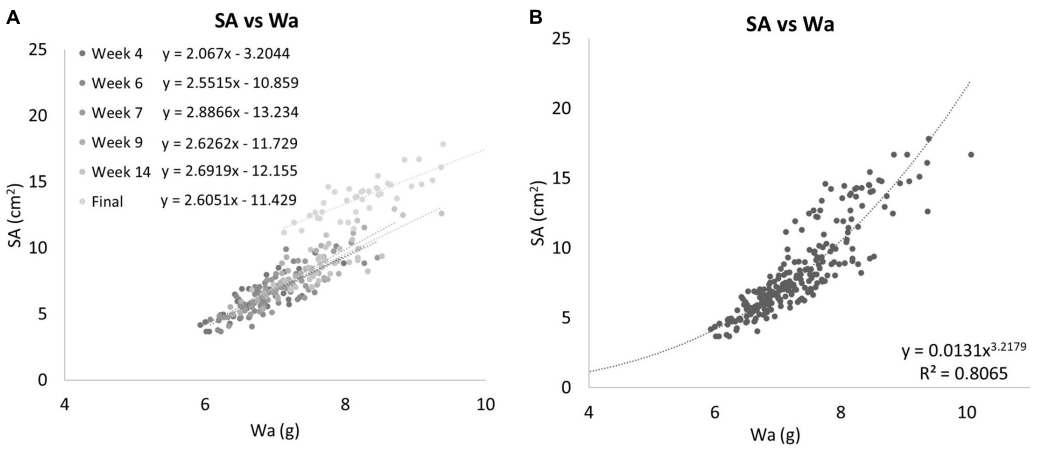

FIGURE 6 | (A) Surface area campared to W_a for all Group 1 corals separated into individual weeks. The equations for the best fit lines of each weeks data can be found in the legend. Each time point's data exhibit linear relationships on their own. **(B)** All Group 1 coral data are treated as a single group. When all data is compared together, a nonlinear relationship emerges. SA is related to W_a by the equation $y = 0.0131x^{3.170}$, $R^2 = 0.8065$.

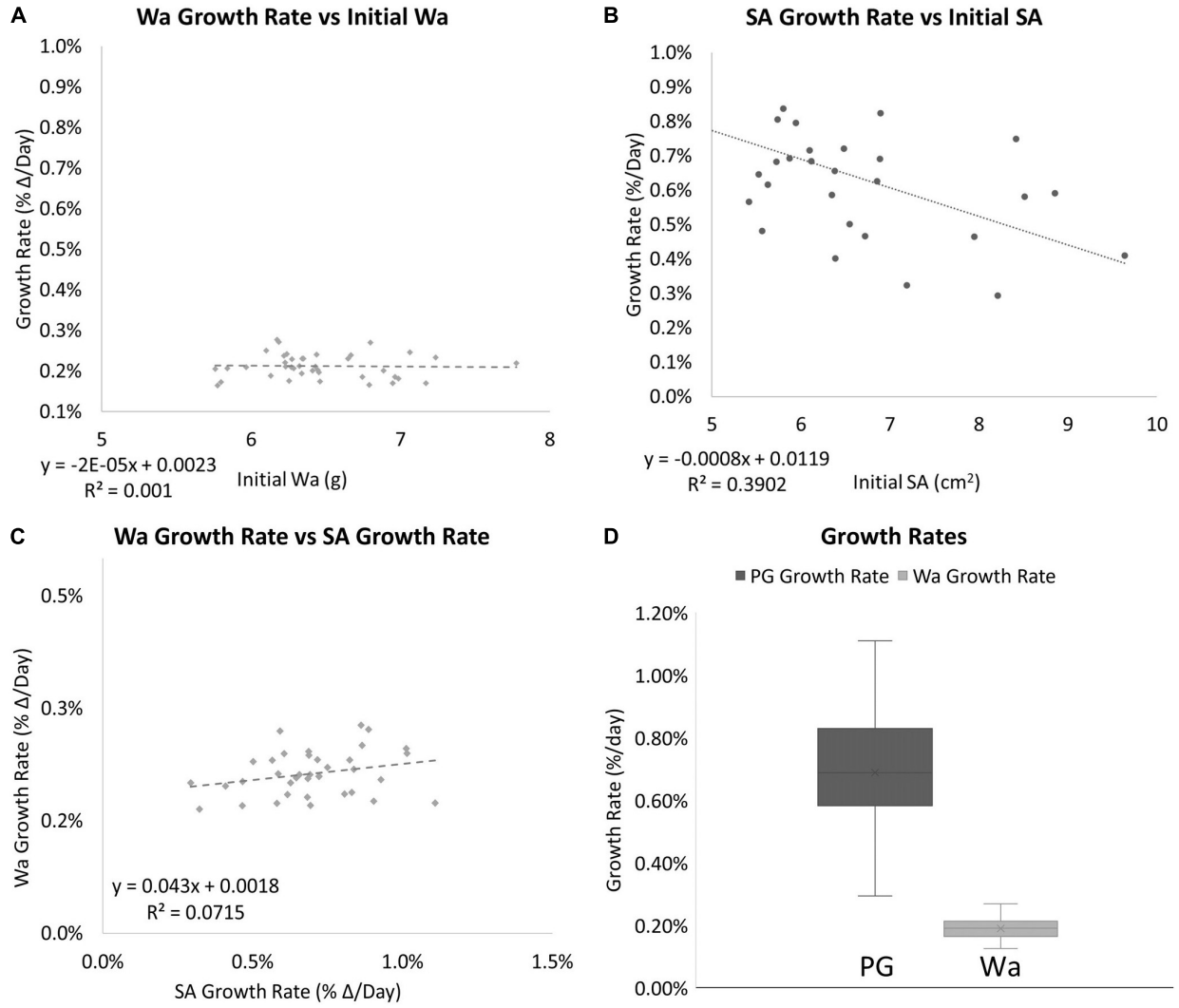

FIGURE 7 | (A) The relationship between the initial W_a and the growth rate of individual nubbins. No correlation was observed. **(B)** The relationship between the initial SA vs. and the growth rate of individual nubbins. A slight negative correlation was observed **(C)** The relationship between the growth rate (percent Δ/Day) of W_a and the growth rate (percent Δ/Day) of SA. No correlation was observed between the two factors with an R^2 = 0.0715 and Slope = 0.043. **(D)** Box plots for the growth rates for corals based on different methods of measurement. Dark gray is the growth rate as measured by SA and light gray is the growth rate as measured by W_a. The mean is indicated x and the median is represented by the line bisecting each plot. Dots outside the plot represent outliers in the data.

30th, 2019, and W_a on average growing 0.21% per day for a total of 19.93% between July 29th, 2019, and October 30th, 2019. On average, measuring the growth rate with SA would yield a growth rate that was 69.8% higher than if the corals used. **Figure 5** shows that while both SA and W_a increase over time, the slope of the best fit line for SA is 2.82 times steeper than the line for W_a. When compared directly, a similar relationship is observed with the average slope of the best fit lines for each week's cluster of coral measurements being 2.57 (**Figure 6A**). When the W_a-derived growth rate was compared to the initial W_a weight, no correlation was observed, R^2 = 0.001 (Slope = 0.000) (**Figure 7A**). When the SA-derived growth rate was compared to the initial SA, a slight negative correlation was observed, R^2 = 0.3902 (Slope = –0.0008) (**Figure 7B**). When both growth rates are directly compared, we find that there is no relationship between the two methods, R^2 = 0.0715 (Slope = 0.043) (**Figure 7C**). A single factor ANOVA showed a very significant difference between the growth rates estimated with the two methods [$F(1, 78) = 272.92$, $P = 0.001$]. The box plots in **Figure 7D** illustrate that there is a much larger range in values for PG-derived growth rate when compared to W_a-derived growth rate.

The ratio between W_a and SA is shown to decrease over time as the coral grows (**Figure 8**). When this ratio is compared to W_a, there is a negative correlation that begins to asymptote in the 0.5–0.6 range (**Figures 9A,C**). This relationship is made much clearer when this ratio is compared to SA. The same asymptote can be observed in the same range as the previous example (**Figures 9B,D**).

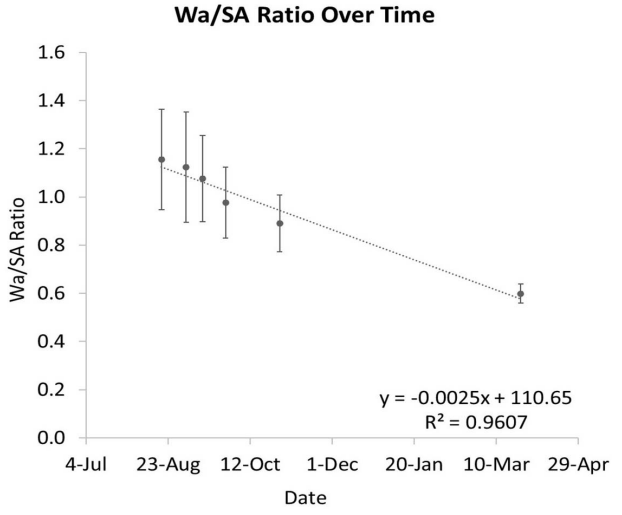

FIGURE 8 | The ratio of W_a to SA over time. As the coral grows, this ratio decreases. The error bars represent one standard deviation from the mean on any given date.

When the SA data was directly compared to the W_a data for all dates, a nonlinear relationship was observed. This is because the SA of the corals grew much faster than the W_a (**Figure 6B**). If we apply a power rule model to this data, we get the equation:

$$y = 0.0131x^{3.2179} \quad (4)$$

This simple equation gives the SA for any *S. pistillata* W_a within the range of this data set, $R^2 = 0.8065$. It can be rewritten as:

$$SA = 0.0131 {W_a}^{3.2179} \quad (5)$$

Comparing SA to W_a/BW_t of the same corals over time showed that the nubbins of *S. pistillata* on average grew significantly faster if measured by SA instead of by W_a with 0.69% per day and 0.21% per day average growth, respectively. This relationship provides another non-linear relationship that can be calculated when the ratio of the W_a and SA is compared to the W_a. If a power-law model is applied to these data, we get **Figure 9C** and the equation:

$$y = 76.604x^{-2.218} \quad (6)$$

This equation estimates the W_a/SA ratio for any *S. pistillata* W_a measurements within the range of our data or approximately from 6 to 10 grams, $R^2 = 0.6644$. To determine the relationship outside this range would require additional data. Now that we can estimate the W_a/SA ratio from a given W_a with the equation:

$$\frac{W_a}{SA} = 76.604 {W_a}^{-2.218} \quad (7)$$

We can simply solve for SA yielding the equation:

$$SA = \frac{W_a}{76.604 {W_a}^{-2.218}} \quad (8)$$

Again, these equations can only be used within the range of the data that we have available. Now we have two equations for estimating SA from W_a. A "simple" model, Eq. 5, and a more "complex" model, Eq. 8. If we apply these two equations to the real W_a data and compare the results to the PG SA data, it produces SA data that are almost identical to each other and very close to the PG measured SA data (**Figure 10**). The best fit lines for both data sets are almost identical with the simple model estimating 0.33% more SA than the complex model for every data point. When compared to the actual SA data, the simple model on average overestimated the SA by 1.55%, while the complex model on average overestimated the SA by only 1.22%. A single factor ANOVA showed that there was no significant difference between the two models and the PG measured SA data [$F(2, 705) = 0.5492$, $P = 0.93897$]. A regression analysis for the complex model and the PG SA indicated a very strong relationship between the two data sets [$F(1, 235) = 786.836$, $R^2 = 0.7708$. $p \leq 0.001$].

DISCUSSION

It has been shown that various techniques for determining SA can result in significantly different measurements in SA for the same coral (Naumann et al., 2009). In this study, the single wax-dip method was shown to significantly overestimate the value of SA for coral skeletons while relatively accurately estimating the SA of wooden objects of a known dimension. This indicates that the coral skeleton holds the wax differently enough to produce discrepancies upwards of 58.9%. This is similar to what Naumann et al. (2009) found. The wax dip estimates of branching corals similar to the ones in this study were only 57% accurate compared to the CT method (Naumann et al., 2009). An important next step would be to compare the PG technique to other techniques that use optics to estimate SA, like the CT method. If the PG method is sufficiently accurate to a highly precise method like CT scanning, it would lend credence to this method. The use of optics is advantageous here because there is no reliance on how a fluid adheres or does not adhere to various objects and substrates. If the fluid being used only adheres well to standard objects but not to corals, or has a higher adherence to corals than it does to standards, this will create discrepancies in data that can lead to gross under and overestimations of SA. The fact that there was no significant difference between the three estimations of SA for the standards means that the 59% difference seen in the wax data is most likely an overestimation. When Naumann et al. (2009) compared surface areas for various species of coral derived with different methods, the wax dip method did not compare favorably with the CT method, which was assumed to produce the true value (Naumann et al., 2009). This further suggests that the differences in how the wax is held by different coral species are most likely the reason there are discrepancies between wax-derived SA, and PG and CT-derived SA. Another consideration is the fact that the wax dipping is taking an absolute SA measurement, as mentioned before, and the practical application of this method is for live corals. While camera resolution limitations prevented the collection of fine-scale information on a live coral, this information would already be obscured by the coral tissue itself.

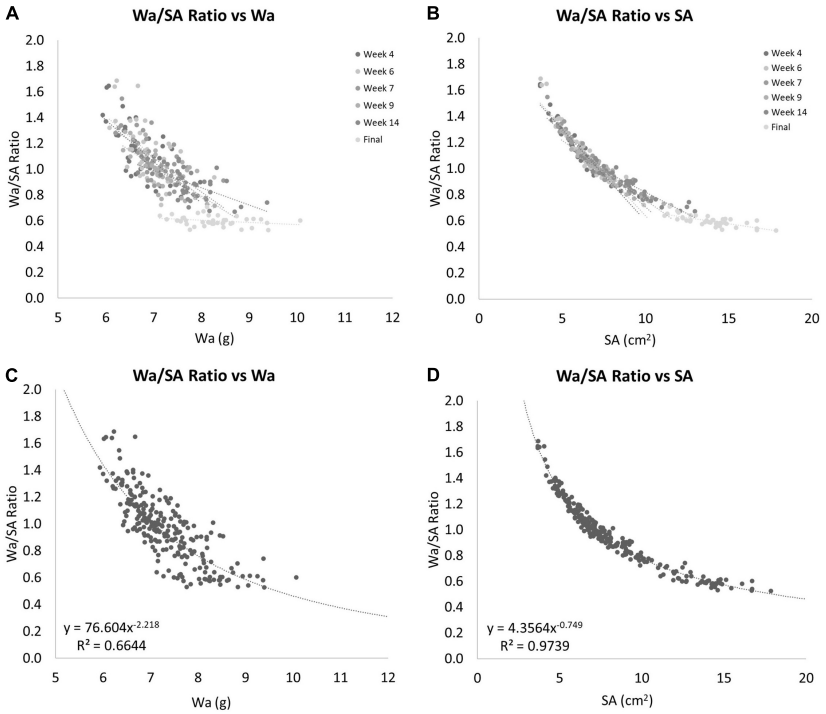

FIGURE 9 | (A) The ratio of W_a to SA compared to W_a. This shows that as the W_a increases this ratio decreases, but seems to have a limit as this ratio never drops below 0.5. **(B)** The ratio of W_a to SA compared to SA. This shows that as the SA increases this ratio decreases. This example shows a clear nonlinearity to this relationship. **(C)** Gives the equation for the relationship between the ratio of W_a to SA vs. W_a for nubbins of S. pistillata between 6 and 10 grams in weight. **(D)** Gives the equation for the relationship between the ratio of W_a to SA vs. SA for nubbins of S. pistillata between 4 and 18 cm^2 in size.

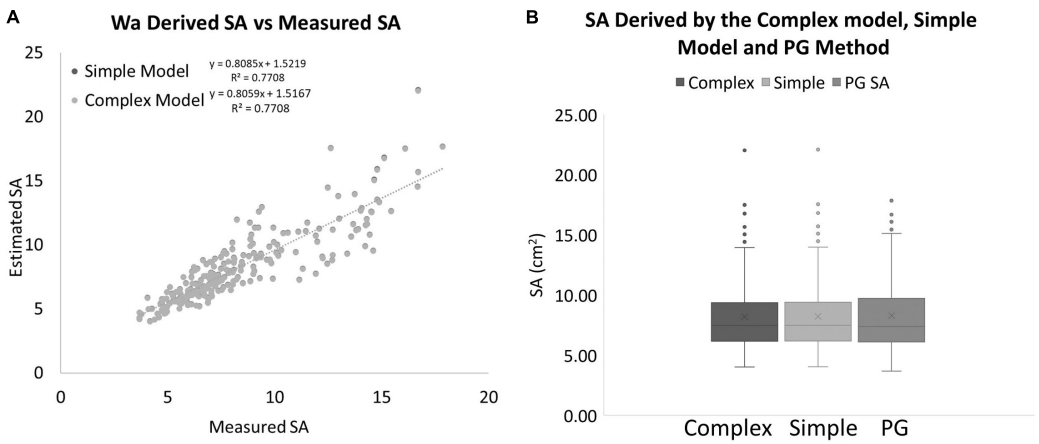

FIGURE 10 | (A) SA values estimated with two different models using only a measurement of W_a compared to SA values that were measured with the PG method for the same coral nubbins. **(B)** Box plots showing the range and averages for the complex model, simple model, and PG measured SA of corals. The mean is indicated by x and the median is represented by the line bisecting each plot. Dots outside the plot represent outliers in the data.

The wax dip method has been shown to over or underestimate the actual SA due to a variety of factors (Naumann et al., 2009). In this study, wax dipping overestimated the SA by 58.9% on average when compared to the PG method detailed here. Now with the complex model developed here, we can estimate SA from W_a measurements within approximately 1.22% of a measured value for an accuracy of 101.22% on average when compared to the PG method. This approximation is a reasonable estimate if we are comparing it to 77.3% accuracy for the branching corals in Naumann et al.'s (2009) study. Further work needs to be done to further tune the equations. For example, in this study, the D_a of 2.5 g /cm^3 was used as an estimation of the density of *Stylophora pistillata*. While this is a reasonable assumption, it is possible that small variations in the density of various specimen accounted for

some of the error seen in the models and correlations. A longer time series study may clear up any uncertainty that is found outside of the range of the current data. Also, the PG photos to construct 3D models were all taken in air which may introduce artifacts into the models like light shimmer that may lower the overall accuracy of the models. Taking the photos in water to create the 3D models could improve the accuracy of this metric. Estimates of the SA of corals with polyps extended and contracted also could be attempted. Throughout all of the data, it can be seen that as the corals become larger, more noise is apparent in the data. Even with the estimation models, it is apparent that at smaller weights the models are more accurate with the average percent difference from the PG SA for the complex model being only 4.92% for corals with a PG SA under 9 cm^2 and −7.21% for corals with a PG SA over 9 cm^2.

Any accuracy estimates in this study are in reference to another form of measurement, so they are only relative to that measurement. Therefore, if a more accurate reference measurement is selected, for example, X-ray CT scanning, it would only allow for more accurate estimation models to be created and honed. Thus far, there has only been a few studies that directly compare surface area methods to the CT method (Naumann et al., 2009; House et al., 2018), but these studies are missing either the PG method or the wax dip method. For this reason, a study comparing the latest PG methods outlined here and in Ferrari et al., 2017 and the wax dip method to X-ray CT scanning data would help confirm the accuracy of this very effective method of determining SA and its direct comparison to the wax dip method with the CT method serving as a highly accurate reference. More research is needed to increase the efficacy of this very promising emerging method of estimating coral SA of live coral specimens.

DATA AVAILABILITY STATEMENT

The original contributions presented in the study are publicly available. This data can be found here: https://zenodo.org/record/5126449#.YPpd9ehKiUk.

AUTHOR CONTRIBUTIONS

DC designed and implemented all protocols for this study and performed all analysis and authored the manuscript. EH collected and assisted in the collection of all the data necessary to perform the study, performed data management tasks to keep all the data organized and available for use. Both authors contributed to the article and approved the submitted version.

FUNDING

This study was funded in part by a grant provided by the UC San Diego Academic Senate grant number BG079912 at Scripps Institution of Oceanography. The grant provided funds for the computer system necessary to conduct this study in a timely fashion.

ACKNOWLEDGMENTS

We would like to acknowledge B. Greg Mitchell for his advising support on this project. We would also like to acknowledge the Smith/Sandin Laboratory at Scripps Institution of Oceanography for the use of wet lab and general lab space during this study. This study was funded in part by the UC San Diego Academic Senate that provided funds for the computer equipment necessary to conduct this study in a timely fashion. We would also like to acknowledge Aqua SD for providing us with the coral specimens necessary to conduct this study.

SUPPLEMENTARY MATERIAL

The Supplementary Material for this article can be found online at: https://www.frontiersin.org/articles/10.3389/fmars.2021.660846/full#supplementary-material

REFERENCES

AgiSoft Metashape Professional (2020). *AgiSoft Metashape Professional (Version 1.6.2) (Software)*. Available online at: http://www.agisoft.com/downloads/installer/ (accessed March 01, 2020)

Burris, J. E., Porter, J. W., and Laing, W. A. (1983). Effects of carbon dioxide concentration on coral photosynthesis. *Mari. Biol.* 75.2-3, 113–116. doi: 10.1007/bf00405992

Dahl, A. L. (1973). Surface area in ecological analysis: quantification of benthic coral-reef algae. *Mari. Biol.* 23.4, 239–249. doi: 10.1007/bf00389331

Davies, P. S. (1980). Respiration in some Atlantic reef corals in relation to vertical distribution and growth form. *Biol. Bull.* 158.2, 187–194. doi: 10.2307/1540930

Dodge, R. E., Wyers, S. C., Frith, H. R., Knap, A. H., and Smith, S. R. (1984). "Coral calcification rates by the buoyant weight technique: effects of alizarin staining". *J. Exp. Mari. Biol. Ecol.* 75. 3, 217–232. doi: 10.1016/0022-0981(84)90167-9

Ferrari, R., Figueira, W. F., Pratchett, M. S., Boube, T., Adam, A., et al. (2017). 3D photogrammetry quantifies growth and external erosion of individual coral colonies and skeletons. *Sci. Rep.* 7.1, 1–9.

Ferrier-Pagès, C., Witting, J., Tambutte, E., and Sebens, K. P. (2003). Effect of natural zooplankton feeding on the tissue and skeletal growth of the scleractinian coral Stylophora pistillata. *Coral Reefs* 22.3, 229–240. doi: 10.1007/s00338-003-0312-7

Harrod, J. J., and Hall, R. E. (1962). A method for determining the surface areas of various aquatic plants. *Hydrobiologia* 20.2, 173–178. doi: 10.1007/bf00046315

Hawkins, C. M., and Lewis, J. B. (1982). Benthic primary production on a fringing coral reef in Barbados, West Indies. *Aquat. Bot.* 12, 355–363. doi: 10.1016/0304-3770(82)90027-4

Hoegh-Guldberg, O. (1988). A method for determining the surface area of corals. *Coral Reefs* 7.3, 113–116. doi: 10.1007/bf00300970

Holmes, G., Ortiz, J., Kaniewska, P., and Johnstone, R. W. (2008). Using three-dimensional surface area to compare the growth of two Pocilloporid coral species. *Mari. Biol.* 155.4, 421–427. doi: 10.1007/s00227-008-1040-x

House, J. E., Brambilla, V., Bidaut, L. M., Christie, A. P., Pizarro, O., Madin, J. S., et al. (2018). Moving to 3D: relationships between coral planar area, surface area and volume. *PeerJ* 6:e4280. doi: 10.7717/peerj.4280

Jokiel, P. L., and Maragos, J. E. (1978). Coral growth: buoyant weight technique. *Coralreefs Res. Methods* 41, 529–541.

Jones, A. M., Berkelmans, R., Cantin, N. E., Negri, A. P., and Sinclair, W. (2008). A 3D modeling method to calculate the surface areas of coral branches. *Coral Reefs* 27.3, 521–526. doi: 10.1007/s00338-008-0354-y

Kanwisher, J. W., and Wainwright, S. A. (1967). Oxygen balance in some reef corals. *Biol. Bull.* 133.2, 378–390. doi: 10.2307/1539833

Laforsch, C., Christoph, E., Glaser, C., Naumann, M., Wild, C., and Niggl, W. (2008). A precise and non-destructive method to calculate the surface area in living scleractinian corals using X-ray computed tomography and 3D modeling. *Coral Reefs* 27.4, 811–820. doi: 10.1007/s00338-008-0405-4

Massel, S. R. (2015). *Internal Gravity Waves in the Shallow Seas*. Poland: Springer International Publishing.

Meyer, J. L., and Schultz, E. T. (1985). Tissue condition and growth rate of corals associated with schooling fish 1. *Limnol. Oceanogr.* 30.1, 157–166. doi: 10.4319/lo.1985.30.1.0157

Muscatine, L., Falkowski, P., Porter, W. J., and Dubinsky, Z. (1984). Fate of photosynthetic fixed carbon in light-and shade-adapted colonies of the symbiotic coral Stylophora pistillata. *Proc. R. Soc. London Series B. Biol. Sci.* 222.1227, 181–202. doi: 10.1098/rspb.1984.0058

Naumann, M. S., Niggl, W., Laforsch, C., Glaser, C., and Wild, C. (2009). Coral surface area quantification–evaluation of established techniques by comparison with computer tomography. *Coral Reefs* 28.1, 109–117. doi: 10.1007/s00338-008-0459-3

Stimson, J., and Kinzie, R. A. III (1991). The temporal pattern and rate of release of zooxanthellae from the reef coral Pocillopora damicornis (Linnaeus) under nitrogen-enrichment and control conditions. *J. Exp. Mari. Biol. Ecol.* 153.1, 63–74. doi: 10.1016/s0022-0981(05)80006-1

Szmant-Froelich, A., and Pilson, M. E. (1980). The effects of feeding frequency and symbiosis with zooxanthellae on the biochemical composition of *Astrangia danae* Milne Edwards & Haime 1849. *J. Exp. Mar. Biol. Ecol.* 48, 85–97. doi: 10.1016/0022-0981(80)90009-X

Veal, C. J., Carmi, M., Fine, M., and Hoegh-Guldberg, O. (2010). Increasing the accuracy of surface area estimation using single wax dipping of coral fragments. *Coral Reefs* 29, 893–897. doi: 10.1007/s00338-010-0647-9

Conflict of Interest: The authors declare that the research was conducted in the absence of any commercial or financial relationships that could be construed as a potential conflict of interest.

Publisher's Note: All claims expressed in this article are solely those of the authors and do not necessarily represent those of their affiliated organizations, or those of the publisher, the editors and the reviewers. Any product that may be evaluated in this article, or claim that may be made by its manufacturer, is not guaranteed or endorsed by the publisher.

frontiers in Marine Science

ORIGINAL RESEARCH
published: 30 August 2021
doi: 10.3389/fmars.2021.639334

3D Photogrammetry Modeling Highlights Efficient Reserve Effect Apparition After 5 Years and Stillness After 40 for Red Coral *(Corallium rubrum)* Conservation in French MPAs

Justine Richaume[1], Adrien Cheminée[1], Pierre Drap[2], Patrick Bonhomme[3], Frederic Cadene[4], Bruno Ferrari[5], Virginie Hartmann[4], Noëmie Michez[5] and Olivier Bianchimani[1]*

[1] Septentrion Environnement, Marseille, France, [2] CNRS, Aix-Marseille Université, Université De Toulon, LIS UMR 7020, Marseille, France, [3] Parc National des Calanques, Marseille, France, [4] Réserve Naturelle Marine de Cerbère Banyuls, Département des Pyrénées-Orientales, Banyuls-sur-Mer, France, [5] Parc Naturel Marin du Golfe du Lion/Office Français de la Biodiversité, Argelès-sur-Mer, France

Imaging the marine environment is more and more useful to understand relationships between species, as well as natural processes. Developing photogrammetry allowed the use of 3D measuring to study populations dynamics of sessile organisms at various scales: from colony to population. This study focuses on red coral *(Corallium rubrum),* as known as precious coral. Metrics measured at a colony scale (e.g., maximum height, diameter and number of branches) allowed population understanding and a comparison between an old (Cerbère-Banyuls reserve) vs. a new (Calanques National Park) MPA. Our results suggested a 5-year time step allows the appearance of a significant difference between populations inside vs. outside the Calanques National Park no-take zones. Red coral colonies were taller and had more branches inside no-take zones. A significant difference was still observable for the populations inside the Cerbère-Banyuls reserve after 40 years of protection, reflecting the sustainability and effectiveness of precautionary measures set by the reserve. The impacts at the local level (mechanical destruction) and those presumed to occur *via* global change (climatic variations) underline the need to develop strategies both to follow the evolutions of red coral populations but also to understand their resilience. Photogrammetry induced modeling is a time and cost effective as well as non-invasive method which could be used to understand population dynamics at a seascape scale on coralligenous reefs.

Keywords: MPAs, photogrammetry, *Corallium rubrum*, reserve effect, BACI design

OPEN ACCESS

Edited by:
John H. R. Burns,
University of Hawai'i at Hilo,
United States

Reviewed by:
Atsuko Fukunaga,
University of Hawai'i at Mānoa,
United States
Kailey Pascoe,
University of Hawai'i at Hilo,
United States

***Correspondence:**
Adrien Cheminée
adrien.cheminee@septentrion-env.com

Specialty section:
This article was submitted to Marine Conservation and Sustainability, a section of the journal Frontiers in Marine Science

Received: *08 December 2020*
Accepted: *29 July 2021*
Published: *30 August 2021*

Citation:
Richaume J, Cheminée A, Drap P, Bonhomme P, Cadene F, Ferrari B, Hartmann V, Michez N and Bianchimani O (2021) 3D Photogrammetry Modeling Highlights Efficient Reserve Effect Apparition After 5 Years and Stillness After 40 for Red Coral (Corallium rubrum) Conservation in French MPAs. Front. Mar. Sci. 8:639334. doi: 10.3389/fmars.2021.639334

INTRODUCTION

Marine protected areas (MPAs) efficiency is a great question when one species conservation is at stake. Conserving marine biodiversity through a "good environmental status" by 2020 was the initial aim of the Marine Strategy Framework Directive (2008/CE/56, DCSMM). Over the past decade, more and more interest has grown for marine conservation policies and assessing MPAs efficiency for fish (Lester et al., 2009), as well as sessile organisms (Linares et al., 2012).

Some Mediterranean MPAs have shown efficiency to protect sessile species such as endangered red coral (*Corallium rubrum*). Mediterranean red coral *Corallium rubrum* (Linnaeus, 1758) is a long-lived suspensivorous colonial octocoralliary belonging to the Corallidae family. Adult individuals are polyps living in clonal colonies that can bring together several hundred individuals (Torrents, 2007). This species is found in low light, strong hydrodynamic and low temperature conditions (Torrents, 2007; Linares et al., 2010) mainly colonizing overhangs, anfractuosities and cave entrances on hard substrates (Gibson et al., 2006).

Ocean acidification (Bramanti et al., 2013) and extreme climatic events endanger red coral (Perez et al., 2000; Garrabou et al., 2001; Crisci et al., 2011) as well as commercial exploitation (Lo Basso and Raveux, 2018) and anthropogenic disturbances (Garrabou et al., 2001; Crisci et al., 2011; Bramanti et al., 2013; Linares et al., 2013; Zapata-Ramírez et al., 2013). Population decrease could result in a general loss of ecological functionality in Mediterranean coastal ecosystems (Santangelo et al., 1993; Bruckner, 2009) as the red coral contributes to the consolidation of coralligenous substrate and structures the habitat of many species including algae, invertebrates, fish and microorganisms (Gibson et al., 2006).

However red coral conservation is a major challenge for policy makers wishing to both preserve natural habitats and maintain a traditional economic activity (Bonhomme et al., 2015). Conservation initiatives already exist and are being reinforced: in France, several Marine Protected Areas (MPAs) wishing to manage and maintain the populations of red coral have prohibited harvest from all [Cerbère-Banyuls Marine Natural Reserve (1974), Scandola Natural Reserve (1975), Côte Bleue Marine Park (1982), Bouches de Bonifacio Natural Reserve (1999)], or part of their perimeter [Calanques National Park (2012)].

Evolution of local conservative measures reflects existing conflicts of interest with successive changes in laws (Cau et al., 2013). These issues concern all the precious corals exploited (Bruckner, 2009; Santangelo et al., 2012). Nowadays after 30 years of protection in French and Spanish MPAs, the size of red coral colonies still does not reach the values of the primary populations suggesting that full recovery will require centuries of protection (Garrabou and Harmelin, 2002; Tsounis et al., 2006; Linares et al., 2010).

Red coral height growth rate is estimated at 1.78 ± 0.7 mm/year (Garrabou and Harmelin, 2002). Basal diameter growth is estimated around 0.62 ± 0.19 mm/year (Bramanti et al., 2005). Growth rates are influenced by environmental condition within the habitat as well as factors specific to the genetics and biology of individuals (Ledoux et al., 2010).

Moreover the study of these fragile sessile organisms is complex and was recently allowed by photogrammetry techniques (Drap et al., 2014). Photogrammetry has been used for more than 50 years in the fields of archeology and more recently in marine biology (Drap et al., 2013b) in order to collect various metrics describing an object of study, at scales ranging from the millimeter to hundred meters. It is an indirect and non-invasive measurement technique (Bythell et al., 2001; Burns and Delparte, 2017) that has been validated in various studies on long-lived benthic species (Linares et al., 2010). It also reduces the time spent underwater, thus reducing the constraints and risks associated with diving. Despite a long post-processing time, this technique provides reusable raw data for additional measurements and a posteriori parameter analysis. Photogrammetry is based on the construction of 3D models of an object from a set of 2D photos using the principle of triangulation (Ludvigsen et al., 2006). Under ideal conditions, these models allow measurements to be made with an accuracy of around 1/10 of a millimeter. Once the models have been reconstructed, it is then possible to carry out measurements with suitable software tools such as Arpenteur, developed for the study of red coral (Royer et al., 2018).

The present paper presents a comparison between two marine protected areas in the Mediterranean and their implication in red coral conservation: the 40 years old Cerbère-Banyuls Reserve (CB reserve) and the 5 years old Calanques National Park (Calanques NP). Using photogrammetry-born biometrics of the red coral populations, collected in various levels of protection of both MPAs, we constructed a Before-After-Control-Impact design (BACI) in order to test the following hypothesis: we hypothesize that there is a significant effect of the interaction between year and protection in the case of the Calanques NP but not in the case of the CB reserve, revealing the apparition of a reserve effect between sites outside (i.e., Control) vs. inside (i.e., Impact) no-take zones of the young Calanques NP between 2013 (i.e., before) and 2019 (i.e., after), while (ii) such reserve effect would be already present and maintain itself in the old CB reserve.

MATERIALS AND METHODS

Study Sites

The study sites are located inside and outside the protected no-take zones of two MPAs located along the Western Mediterranean French rocky coast, respectively, between Cap Bear and Cap Cerbère for the Cerbère-Banyuls Reserve populations, and between west of Marseille and La Ciotat for the Calanques National Park populations (**Figure 1**), located 350 km from each other. Cerbère-Banyuls Reserve (42°28′18″N, 3°9′53″E) covers 650 ha and encompasses 2 zones, a central no-take zone (i.e., "full reserve"), where all activities are prohibited except for scientific surveys and a peripheral "partial reserve" zone where small-scale and recreational fishing and diving are permitted with some restrictions. Red coral harvesting as well as other fishing activities have been banned inside the

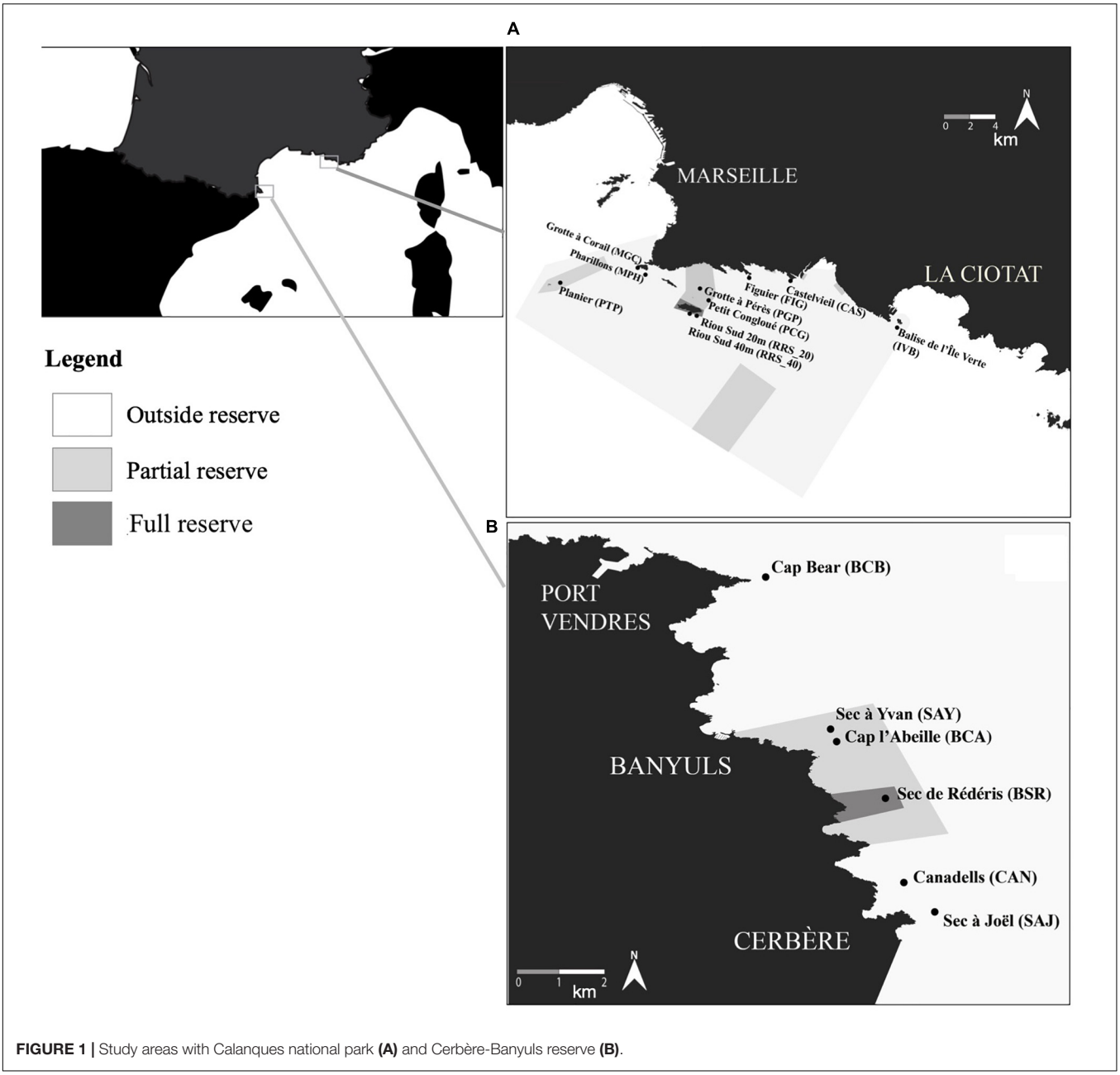

FIGURE 1 | Study areas with Calanques national park **(A)** and Cerbère-Banyuls reserve **(B)**.

Cerbère-Banyuls marine reserve since 1974. The substrate is mostly schist stone and detrital sediments (Flemming, 1972). Calanques National Park (43°12′34″ N, 5°26′57″ E) covers 43,500 ha and encompasses 2 zones as well: several no-take zones (i.e., "full reserves") where any fishing or harvesting activities are prohibited since 2013 and a surrounding "partial reserve" where fishing and recreational diving and fishing are still partly permitted. The substrate in the Calanques National Park is mostly limestone (Flemming, 1972). In both MPAs, these zones displaying full and partial protection are surrounded by unprotected "outside reserve" zones (**Figure 1**).

The red coral settlements in these regions are characterized by a frequent occurrence in shallow overhangs and cavities on hard substrate (Torrents, 2007). We studied shallow red coral populations settled at depths ranging from 19 to 25 m.

Sample Collection and Photogrammetric Protocol

Corallium rubrum populations of the Calanques National Park and Cerbère-Banyuls reserve were studied using photogrammetry, an indirect and non-invasive method previously validated in a study on long-lived benthic species (Linares et al., 2010).

In the Calanques National Park, photogrammetric surveys were done at the studied sites during sampling campaigns

performed in December 2013 (i.e., when the MPA was created) and in December 2019: five sites were located outside no-take zones (Bonhomme et al., 2015) [Castelviel (CAS), Figuier (FIG), Balise de l'Île Verte (IVB), Grotte à Corail (MGC), and Pharillons de l'Île Maïre (MPH)], three sites were located in the partial reserve [Petit Congloué (PCG), Grotte Pérès (PGP), Le Planier (PTP)]; and finally 2 sites were located inside the full reserve zone [South Riou 20 m (RRS_20) and South Riou 40 m (RRS_40)].

In Cerbère-Banyuls, photogrammetric surveys were done in December 2012 and December 2020 during sampling campaigns at three sites located outside the no-take zones [Sec à Joël (SAJ), Canadells (CAN), and Cap Béar (BCB)]; two sites located inside partial reserve [Sec à Yvan (SAY) Cap Abeille (BCA)]; and one site located inside the full reserve [Sec de Rédéris (BSR)].

In each MPAs, at both occasions, in each site, the surveys were done in the same populations i.e., patches of red coral colonies : in each site, red coral populations were haphazardly sampled using 20 cm × 20 cm quadrats (0.04 m^2). For each site, between 19 and 41 quadrats were modeled (**Table 1**). For each quadrat, 3 photographs were taken with a Nikon D700 DSLR (sensor pixel density = 1.41 Mp/cm^2) and a 20 mm lens, Nauticam housing with hemispherical window and two pairs of Ikelite DS160 flashes.

The pictures were taken from slightly different angles in order to build the corresponding photogrammetric model with the Arpenteur software (Drap et al., 2013a, 2014). An angle of approximately 20° allows a high overlap of the pixels between the two images (50–70%) for a reliable 3D reconstruction (Royer et al., 2018). More than 20 coded targets, uniformly distributed on the quadrat, are measured automatically by the software. Each quadrat is previously calibrated and the targets are known in the reference system of the quadrat in which the measurements of the colonies were to be made. Orientation of the photos was done by bundle adjustment using the measures on the coded targets. The accuracy obtained on the targets is usually less than 1 mm (Drap et al., 2013a). Once the 3D model was obtained, the acquisition of the metrics describing the populations and colonies was carried out for each quadrat by selection of the homologous points so that the resulting 3D point is calculated by triangulation (Bythell et al., 2001; Drap et al., 2014, p. 2014; Royer et al., 2018). Resolution inside the quadrats was around 0.1 mm/px.

Metrics were measured at the scale of the colony. In each quadrat and for each colony three metrics were measured: number of branches, basal diameter, and maximum height (maximum distance between base and apex of a branch).

TABLE 1 | Number of quadrats modeled for each site in Cerbère-Banyuls reserve (A) and Calanques National Park (B) in each protection status (FR, Full Reserve; PR, Partial Reserve; OR, Outside Reserve.

(A) Population	Protection	Number of quadrats modeled in 2012	Number of quadrats modeled in 2020
BCA	PR	21	26
BCB	OR	20	43
BSR	FR	31	29
CAN	OR	20	41
SAJ	OR	19	35
SAY	PR	15	42
(B) Population	**Protection**	**Number of quadrats modeled in 2014**	**Number of quadrats modeled in 2019**
PTP	PR	19	20
PGP	OR	31	45
PCG	PR	17	24
RRS_20	FR	22	73
RRS_40	FR	18	20
CAS	OR	9	20
FIG	PR	23	31
IVB	OR	18	23
MGC	OR	15	17
MPH	OR	26	29

Data Processing, Statistical Design, and Analysis

Data considered as aberrant given the literature were excluded: this was the case for colonies exceeding 220 mm for their maximum size and 15 mm in basal diameter (Garrabou and Harmelin, 2002; Marschal et al., 2004). The aberrant data came from model distorsions due to underwater constraints in some quadrats which were removed from the analysis. Precision is around one pixel and the calculated mean distance error with Arpenteur tool was less than 0.5 mm (Royer et al., 2018).

We were interested in the descriptors of *C. rubrum* measured on colonies: (i) maximum height (ii) basal diameter, and (iii) number of branches, in order to test their responses to the following explanatory factors: protection, site and year. For both MPAs separately (Cerbère-Banyuls Reserve and Calanques National Park), we carried out permutational multi- or univariate analysis of variance (PERMANOVA) (Anderson et al., 2008) in order to determine the effect of the factors studied (site, year and protection and their interaction) on the descriptors of *C. rubrum* populations. The resemblance matrices were calculated from the initial data matrix containing, for each sample (i.e., the colony) a row displaying the response variable(s). The response variable was alternatively a multivariate set of data containing the combination of (i) maximum height (ii) basal diameter, and (iii) number of branches or a univariate data (i.e., each descriptor separately). Indeed, independently of potential differences in the multivariate combination of descriptors, understanding the population dynamics requires a further inspection of the individual behavior of each descriptor. In order to study the effect of explaining factors, two designs were used. A first design was set to assess the spatio-temporal variability of these descriptors, testing the effect of both the year and the site. Year was a two-level fixed factor (respectively, 2013 and 2019 for Calanques NP and 2012 and 2020 for Cerbère-Banyuls Reserve). Site was a random factor with 6 modalities for Cerbère-Banyuls reserve and 10 modalities for Calanques national park. A second design was set to test the effect of year and protection on the same response variables. Protection was a three-level fixed factor (Outside reserve, partial reserve and full reserve), while year was set as previously.

This BACI design (design 2) allowed us to test the hypothesis that there is an interaction between year and protection in the case of the Calanques NP but not in the case of the CB marine reserve; indeed it would reveal the apparition of a reserve effect between samples from outside (i.e., Control) vs. inside (i.e., Impact) no-take zones of the young Calanques NP between 2013 (i.e., before) and 2019 (i.e., after), while (ii) such reserve effect would be already present and maintain itself in the old Cerbère-Banyuls reserve. Such approaches are used in particular to detect significant changes indicative of the effect of ecosystem management (Underwood, 1981, 1992). In addition, the first design also allowed us to address the natural spatio-temporal variability of population descriptors.

For this inferential approach, Euclidean distance matrices were calculated from standardized data measured on all colonies (normalization by sum function on PRIMER). *P*-values were calculated by 999 residual permutations under a reduced model. When the number of permutations was below 200, Monte Carlo *p*-values were used (Clarke et al., 2014).

Since ecological data give rise to intrinsic inherent variability, significance was considered—for all designs—when p-value < 0.1. Data treatment and graphical representations were carried out using R 3.1.3 programming freeware (R Core Team, 2017) and PRIMER 6 software with PERMANOVA + add-on (Anderson, 2001; Clarke and Gorley, 2006; Anderson et al., 2008).

RESULTS

Red Coral Populations in Cerbère-Banyuls Reserve

In 2020, in Cerbère-Banyuls reserve on all 6 sites studied, a total of 1,186 arborescent colonies was found within the 217 quadrats (**Table 2**). In addition, a small number of individuals ($n = 28$) had

TABLE 2 | Number of colonies measured, mean and standard deviation of each metric for each site of Cerbère-Banyuls reserve and Calanques national park: maximum size, basal diameter, and number of branches for each site of each year in each protection status (FR, Full Reserve; PR, Partial Reserve; OR, Outside Reserve).

	Sites	Number of colonies measured	Protection	Maximum height (mm)		Basal diameter (mm)		Number of branches	
				Mean	SD	Mean	SD	Mean	SD
2020 Cerbère-Banyuls reserve	BCA	114	PR	53.86	35.53	10.22	6.11	5.03	4.27
	BCB	119	OR	48.34	27.96	11.32	6.85	2.75	3.21
	BSR	98	FR	87.49	45.88	11.77	5.34	6.86	6.25
	CAN	90	OR	56.45	28.73	9.21	5.25	5.25	3.77
	SAJ	113	OR	36.18	20.98	7.95	3.82	2.31	2.16
	SAY	90	PR	62.07	32.10	10.64	6.59	8.56	6.24
2012 Cerbère-Banyuls reserve	BCA	101	PR	39.59	28.08	6.21	3.42	4.89	2.20
	BCB	97	OR	27.76	18.01	6.45	4.59	2.75	1.89
	BSR	172	FR	51.34	33.80	8.25	5.63	6.07	2.78
	CAN	44	OR	55.58	26.35	7.81	4.05	4.93	3.12
	SAJ	78	OR	21.99	11.60	6.05	2.14	2.31	1.45
	SAY	32	PR	59.29	29.90	6.77	2.52	8.10	3.26
2019 Calanques national park	CAS	75	OR	29.05	14.37	6.81	3.71	2.85	2.15
	FIG	69	OR	53.12	22.51	6.00	2.85	7.29	5.01
	IVB	102	OR	41.92	15.37	6.71	3.76	4.39	2.68
	MGC	95	OR	49.60	20.71	6.19	3.38	5.26	3.27
	MPH	110	OR	43.25	20.05	6.23	3.30	4.78	3.58
	PCG	114	PR	35.58	16.04	6.57	3.16	3.45	2.27
	PGP	98	PR	40.02	14.65	7.05	3.25	4.10	2.54
	PTP	80	PR	50.60	27.13	7.91	3.85	4.51	3.09
	RRS_20	84	FR	84.18	21.48	7.23	2.80	8.93	5.22
	RRS_40	94	RI	47.53	18.23	6.54	3.76	4.66	2.78
2013 Calanques national park	CAS	82	OR	36.62	21.40	5.61	2.09	5.69	4.48
	FIG	100	OR	29.63	14.20	4.90	1.87	4.42	3.03
	IVB	100	OR	20.31	12.91	4.36	1.85	2.31	1.96
	MGC	90	OR	38.72	18.63	7.61	3.94	5.88	4.87
	MPH	97	OR	25.94	16.37	6.06	3.26	3.06	3.04
	PCG	93	PR	30.88	15.99	6.01	2.70	3.54	2.38
	PGP	100	PR	32.43	18.20	5.29	2.67	3.39	2.55
	PTP	99	PR	27.10	17.52	5.72	2.93	2.82	2.05
	RRS_20	99	FR	37.61	21.24	5.93	2.38	4.54	3.27
	RRS_40	108	FR	21.63	15.80	4.28	1.62	2.34	2.09

abnormal measurements and were therefore removed from the dataset. The complete set presented a total of 1,158 individuals distributed over the 6 Cerbère-Banyuls studied populations.

Differences in population structure between sites were highlighted by a significant effect of the factor "site" as well as a significant interaction between year and site on the multivariate combination of metrics (PERMANOVA, p-value = 0.004, **Table 3**). In 2020, large disparities in the distributions of the three descriptors from one site to another were observed (**Figures 2–4**). The distributions of populations in site BCA and site BCB were similar and centered toward small values, whatever the descriptor. Some populations had an unimodal distribution (BCA, BCB, SAJ) while others had nearly uniform probability densities for maximum height, indicating that individuals were distributed more evenly. The colonies of BSR (in full reserve) were on average larger (μ = 87.49 $\pm$ 45.88 mm, **Table 2**) than in the other populations (**Figure 2**). For the populations of sites CAN and SAY, a second density peak was observed around 100 mm. The distributions in basal diameter were more homogeneous between populations than the maximum height distributions. Some populations showed a unimodal peak followed by an increase in probability density at higher values of basal diameter: CAN, BCA, SAJ, SAY. The distribution of BSR probability densities is the most homogeneous, with a peak around 7 mm of basal diameter. Finally, the number of branches per colony was distributed relatively differently from one population to another.

Red Coral Populations in Calanques National Park

In 2019, in the Calanques National Park, 1,809 colonies of the "arborescent" type were found (**Table 2**). A small number of individuals (n = 59) had abnormal measurements and were therefore removed from the dataset. The complete set presented a total of 1,750 individuals distributed over the 10 Calanques sites.

In 2019, we observed large disparities in the distribution from one population to another when representing probability density of each site as a function of size classes for maximum height (**Figure 5**). Populations of sites CAS, PCG, PGP, and MPH showed decreasing distributions concentrated toward small values of height (between 29 $\pm$ 14.37 and 43.25 $\pm$ 20.05 mm, **Table 2**). Some populations had a unimodal height distribution (MPH, PCG, PGP) while others displayed bimodal (RRS_20, FIG) or even almost uniform (PTP) height probability densities indicating that individuals are distributed more evenly according to their maximum height. Basal diameter density probabilities were more homogeneous between populations (**Figure 6**). Some sites showed an unimodal peak followed by a resurgence in probability density of diameter at higher values: IVB, MGC, MPH, PCG, RRS_40. The distribution of PTP diameter probability densities is the most homogeneous, with a slight peak around 7 mm. The number of branches per colony is distributed relatively differently from one population to another (**Figure 7**). All sites displayed populations with an unimodal distribution of number of branches but with some disparities.

When we observe the evolution of each metric between 2013 and 2019 by site, we observed various dynamic between populations, which was reflected in a significant effect of year * site interaction on the multivariate dataset (PERMANOVA, p-value = 0.001, **Table 3**). The maximum size increased between 2013 and 2019 for all Calanques NP populations regardless of whether or not they are located inside the protection of the Calanques national park except for site Castelvieil (CAS) (**Table 2**).

TABLE 3 | Results of permutation analyzes of variance (PERMANOVA) in the Cerbère-Banyuls reserve and the Calanques national park MPAs *via* a design incorporating the "site" and "year" factors, applied for the multivariate matrix (maximum size; basal diameter; number of branches) and each univariate matrix.

Area	Variable	Factor	P-perm	Number of permutations
Calanques national park	Multivariate matrix			
		Year	0.002***	998
		Site	0.001***	996
		Year * site	0.001***	999
Cerbère-Banyuls reserve	Multivariate matrix			
		Year	0.311	996
		Site	0.001***	998
		Year * site	0.004**	999

*Sources of variation are: "year", a fixed factor with 2 modalities; "site", a random factor with 6 modalities for Cerbère-Banyuls reserve and 10 modalities for Calanques national park; and the interaction "year * site". Significance: P ≤ 0.1; *P ≤ 0.05; **P ≤ 0.01; ***P ≤ 0.001. P-values were obtained using 999 residuals permutations under a reduced model.*

Protection Effect in Cerbère-Banyuls Reserve and Calanques National Park

Cerbère-Banyuls Reserve

In Cerbère-Banyuls reserve we observed a significant interaction between year and protection for the multivariate matrix (PERMANOVA, p-value = 0.022, **Table 4**), as well as for the univariate maximum height (PERMANOVA, p-value = 0.001, **Table 4** and **Figure 8**) and the number of branches (PERMANOVA, p-value = 0.001, **Table 4** and **Figure 8**). In 2020, the multivariate matrix revealed a significant difference between the populations of the full reserve and those located in the partial reserve (PERMANOVA Pair-wise comparison, p-value = 0.012, **Table 5**), which did not appear in 2012 (PERMANOVA Pair-wise comparison, p-value = 0.23, **Table 5**). Moreover the gap widens between population located outside reserve and inside full reserve from 2012 to 2020 (**Figure 8**). The one-to-one comparison of the three colony-scale metrics between 2012 and 2020 showed a significant effect of the interaction year * protection status for maximum height (PERMANOVA, p-value = 0.001, **Table 4**) and number of branches (PERMANOVA p_value = 0.001, **Table 4**). It was confirmed when we observed graphically (**Figure 8**) a clearer increase from 2012 to 2020 of the difference in the maximum size and number of branches (than for basal diameter) when

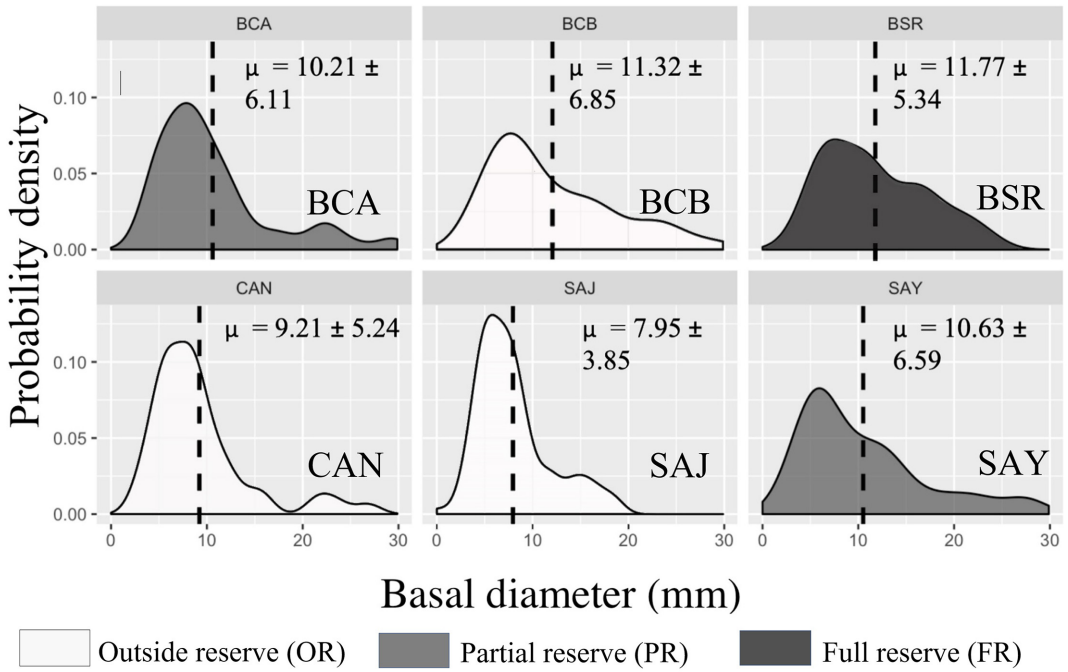

FIGURE 2 | Cerbère-Banyuls reserve: representation of probability density functions by population of each site for the basal diameter variable (mm) in 2020. The values indicated correspond to the means followed by the standard deviations. In dark the population in full reserve (BSR), in medium the populations in partial reserve (BCA, SAY), in clear the populations outside the reserve (BCB, CAN, SAJ).

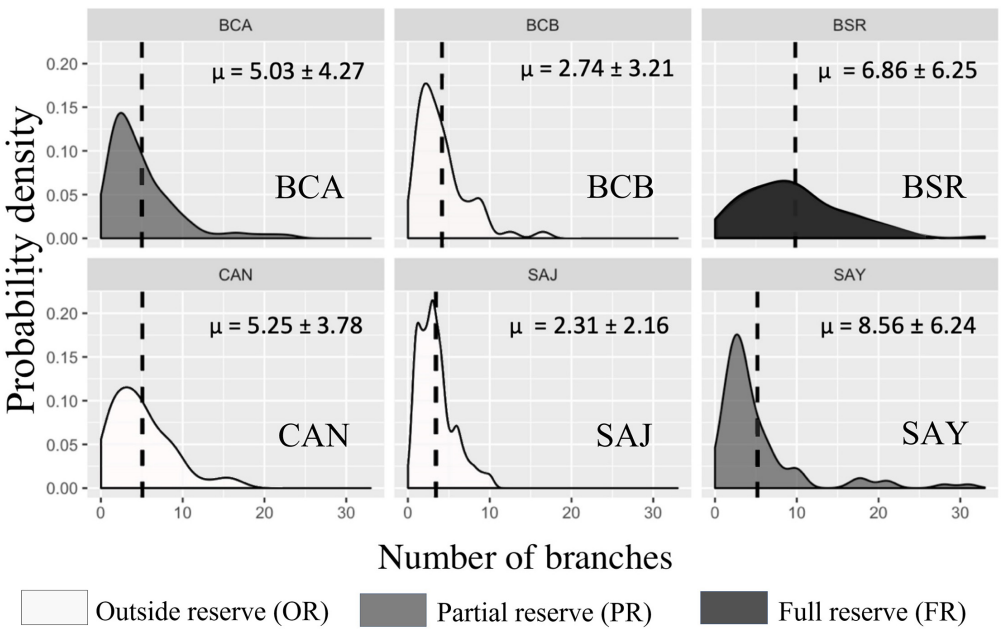

FIGURE 3 | Cerbère-Banyuls reserve: representation of probability density functions by population of each site for the variable number of branches in 2020. The values indicated correspond to the means followed by the standard deviations. In dark the population in full reserve (BSR), in medium the populations in partial reserve (BCA, SAY), in clear the populations outside the reserve (BCB, CAN, SAJ).

comparing full reserve vs. others levels. In 2012, the density functions (**Figure 8**) showed an almost total overlap within the Cerbère-Banyuls reserve (partial reserve and outside reserve) for the basal diameter. In 2020, there was an overlap between partial reserve and full reserve for the basal diameter distribution, considering a slight shift to the right for the full reserve modality.

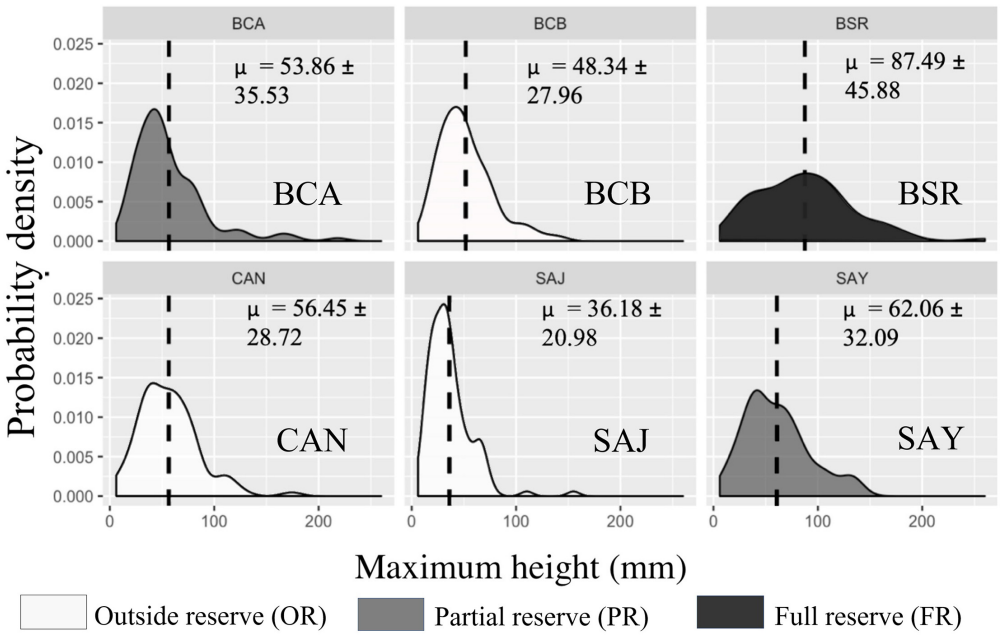

FIGURE 4 | Cerbère-Banyuls reserve: representation of probability density functions by population of each site for the variable maximum height (mm) in 2020. The values indicated correspond to the means followed by the standard deviations. In dark the population in full reserve (BSR), in medium the populations in partial reserve (BCA, SAY), in clear the populations outside the reserve (BCB, CAN, SAJ).

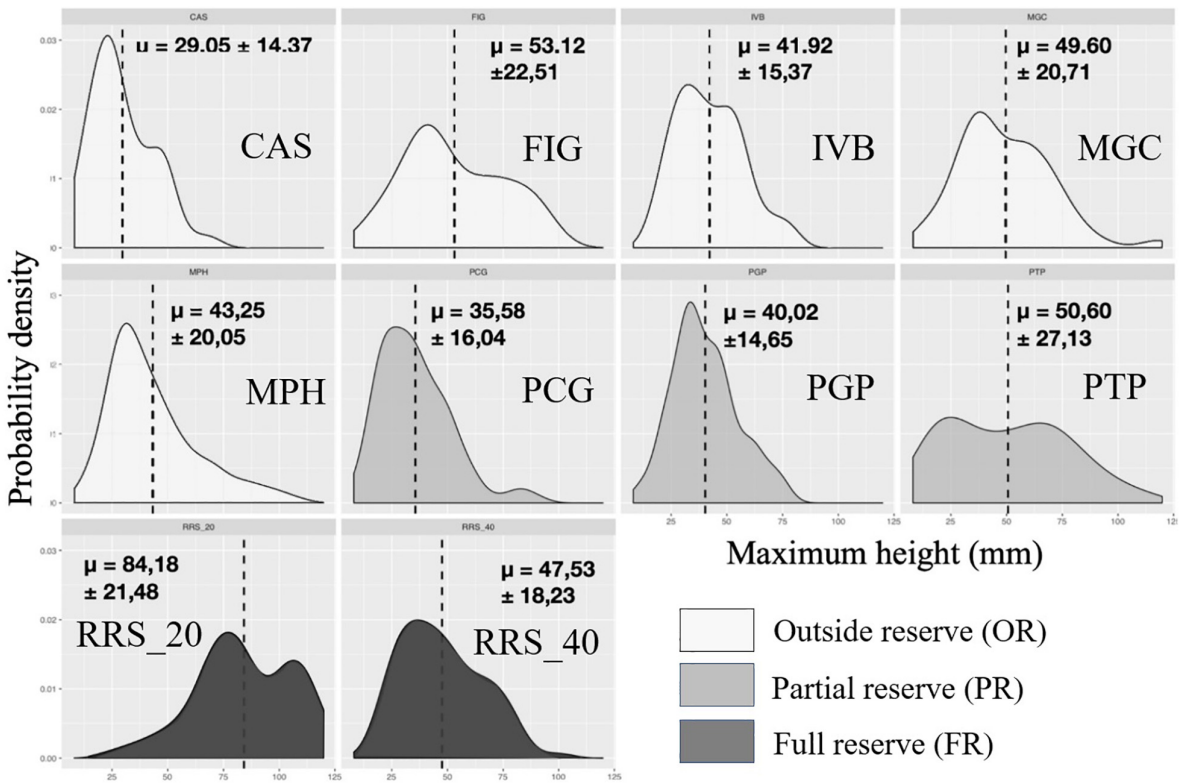

FIGURE 5 | Calanques national park: representation of probability density functions by population of each site for maximum height (mm) in 2020. The values indicated correspond to the means followed by the standard deviations. In dark the populations in full reserve (RRS_20; RRS_40), in medium the populations in partial reserve (PTP, PGP, PTP), in clear the populations outside the reserve (MPH, CAS, FIG, IVB, MGC).

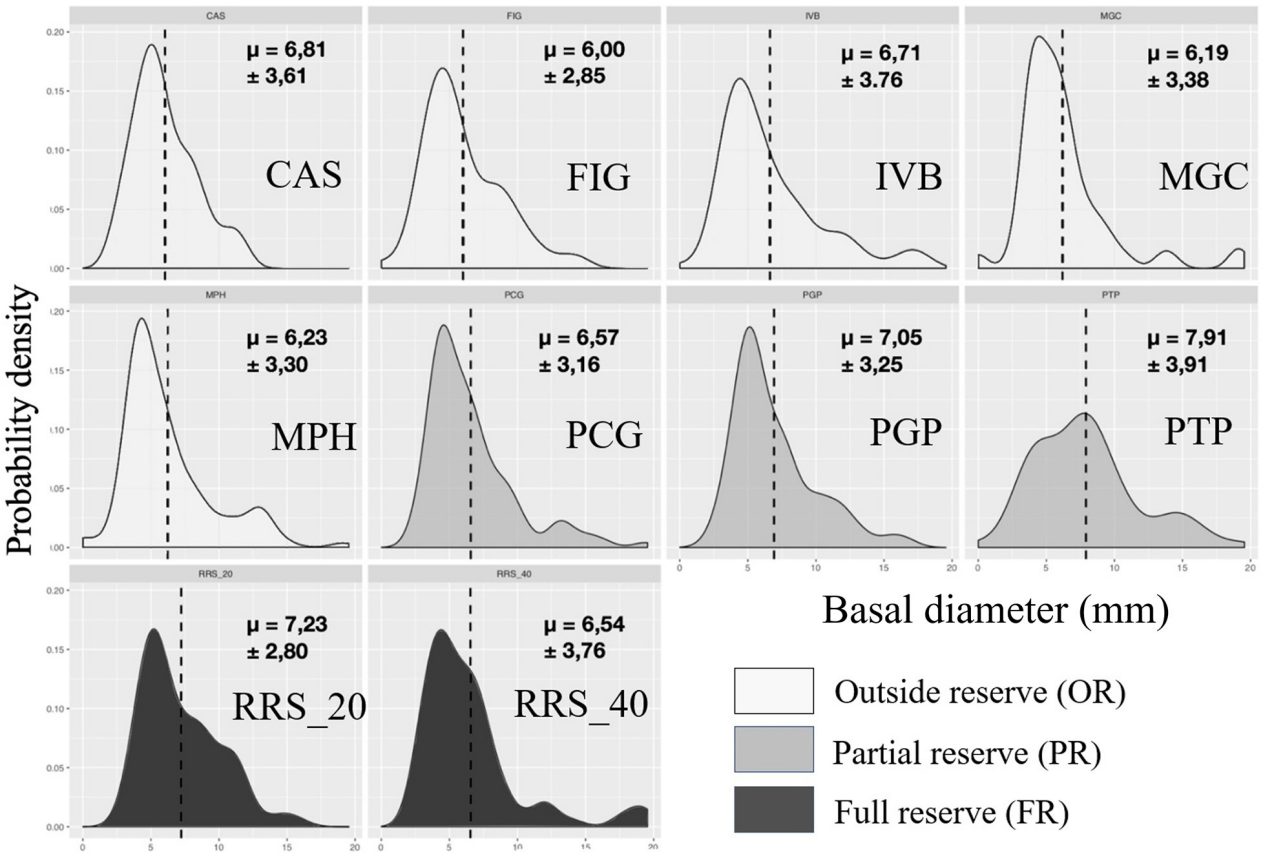

FIGURE 6 | Calanques national park: representation of probability density functions by population of each site for basal diameter (mm) in 2020. The values indicated correspond to the means followed by the standard deviations. In dark the populations in full reserve (RRS_20; RRS_40), in medium the populations in partial reserve (PTP, PGP, PTP), in clear the populations outside the reserve (MPH, CAS, FIG, IVB, MGC).

In 2020 for the maximum height there was a clearer shift toward higher values (**Figure 8**), as already confirmed by the results of the PERMANOVA (PERMANOVA *p*-value = 0.001, **Table 4**).

Calanques National Park

We observed a significant effect of the interaction between year and protection for the multivariate matrix (PERMANOVA, *p*-value = 0.001, **Table 4**), and univariate maximum height (PERMANOVA, *p*-value = 0.001, **Table 4**), basal diameter (PERMANOVA, *p*-value = 0.038, **Table 4**) and number of branches (PERMANOVA, *p*-value = 0.001, **Table 4**). The gap widens between outside the reserve and full reserve: in 2013 there was no significant difference in the number of branches between full reserve and outside reserve (PERMANOVA Pair-wise comparison, *p*-value = 0.649, **Table 5**), while there was a significant difference in 2019 (PERMANOVA Pair-wise comparison, *p*-value = 0.001 In the Calanques NP there was also a significant interaction between protection and year for maximum height (PERMANOVA Pairwise comparison, *p*-value = 0.001). Indeed in 2013 there was no significant difference of maximum height between outside reserve, partial reserve and full reserve (respectively, PERMANOVA Pairwise comparison, *p*-value = 0.8; *p*-value = 0.535; and *p*-value = 0.467, **Table 5**). Meanwhile in 2019 there was a significant difference between outside reserve and partial reserve (PERMANOVA Pairwise comparison, *p*-value = 0.032), outside reserve and full reserve (PERMANOVA Pairwise comparison, *p*-value = 0.001) and between partial reserve and full reserve (PERMANOVA Pairwise comparison, *p*-value = 0.001). These results highlighted the appearance of a reserve effect between 2013 and 2019 for maximum height and number of branches. Graphically (**Figure 9**) in 2013, the density functions showed almost total overlap between the sites located outside reserve and inside full reserve for number of branches and maximum height. In 2019, for the number of branches, a slight shift to the right of the density function was observed for the colonies in full reserve vs. the colonies inside partial and outside reserve. For the maximum height there was a clearer shift toward higher values for the colonies inside full reserve in 2019. Finally, concerning basal diameter, although the trend was not so clear, we still observed that in 2013 there was no significant difference between outside reserve and partial reserve (PERMANOVA, *p*-value = 0.923) whereas there was a significant difference in 2019 (PERMANOVA, *p*-value = 0.008): in 2019, the density functions showed a slight shift of the basal diameter to the right for the colonies in full reserve.

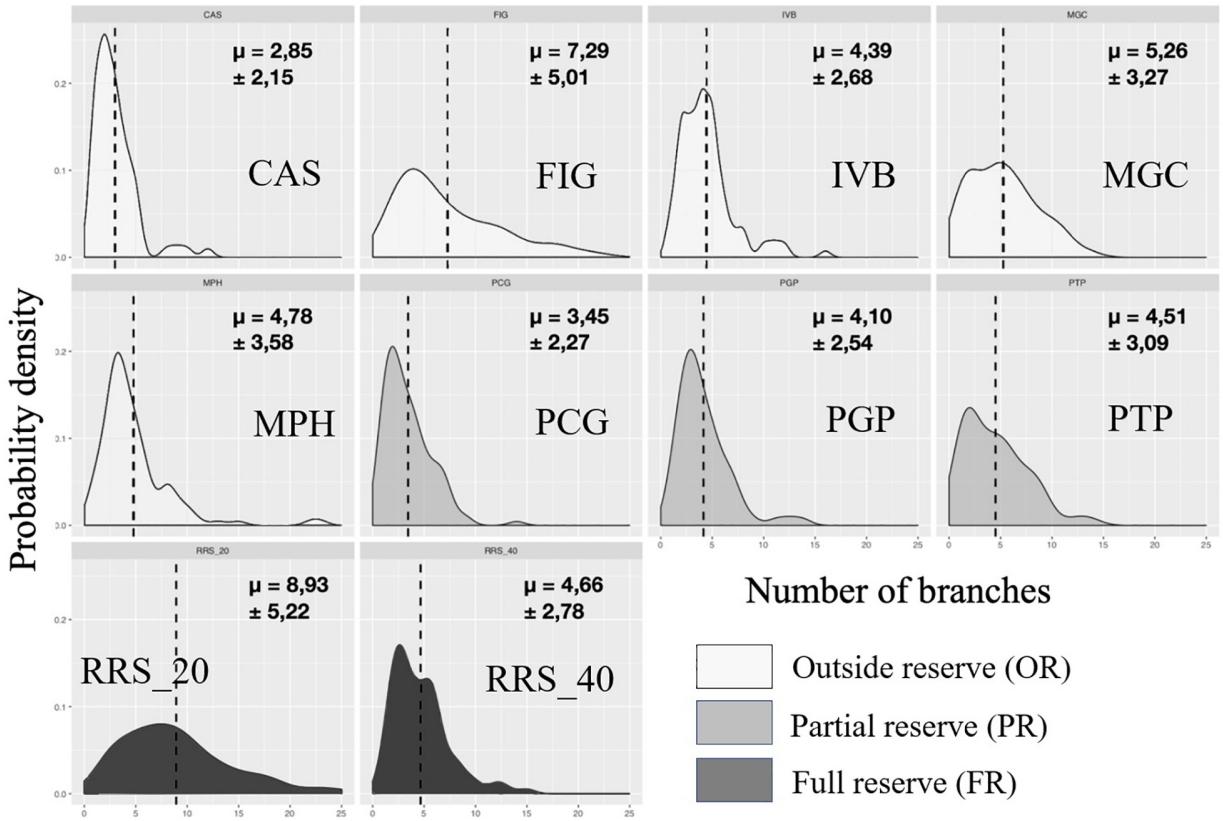

FIGURE 7 | Calanques national park: representation of probability density functions by population of each site for the variable number of branches in 2020. The values indicated correspond to the means followed by the standard deviations. In dark the populations in full reserve (RRS_20; RRS_40), in medium the populations in partial reserve (PTP, PGP, PTP), in clear the populations outside the reserve (MPH, CAS, FIG, IVB, MGC).

DISCUSSION

This study provides valuable demographic data obtained through photogrammetry to help infer the long-term effects of effective protection on red coral populations in 2 Mediterranean MPAs, which encompass an important geographic scale (up to about 450 km).

Protection Strategies Impact Red Coral Populations Locally

In Calanques National Park

In our BACI design, for the Calanques National Park, we highlighted a significant interaction between protection and year on colony scale metrics (for the multivariate matrix, for maximum height, basal diameter, and for number of branches) reflecting the apparition of a reserve effect in 2019 whereas it was absent in 2013. Indeed in 2013, right after the MPA was created, no significant differences existed between colonies located outside reserve and inside reserve regarding maximum height and number of branches. However in 2019 the mean number of branches as well as the maximum height were significantly higher inside. Additionally we have seen that probability densities had changed between 2013 and 2019 for the 3 metrics at the colony scale with distinct patterns for those inside vs. outside no-take zones. These results seem to reflect the effectiveness of no-take zones where impacts are limited (coral harvesting interdiction, as well as regulated fishing) and the conditions are thus favorable to red coral. These results provide evidence for reinforced protection zones effectiveness for red coral conservation and therefore of its habitat in the Calanques National Park. Establishment of no-take zones has benefited red coral populations by limiting exploitation as well as accidental destruction by fishing gear and overall enhanced conservation conditions.

South Riou populations (RRS_20 and RRS_40) showed growth rates overpassing what is known in the wild. Previous studies already shown very high fertility on this site (Garrabou and Harmelin, 2002) and equivalent growth rates have already been obtained in a controlled environment (Goff et al., 2017). Local environmental conditions might explain these observed growth rates: little light and low temperatures [around 13°C in February; and 20°C in August (Vielzeuf et al., 2013)], proximity to a major coastal upwelling zone (Millot and Wald, 1980), influencing the diversity of organisms on the substrate (*Oscarella* spp., *Reniera fulva*, *Crella mollior*, *Aplysina cavernicola* as well as overpulids and bryozoa), lack of competition (Montero-Serra et al., 2018) as well as the composition of the microbiome

TABLE 4 | Results of permutation analyzes of variance (PERMANOVA) in the Cerbère-Banyuls reserve (A) and the Calanques national park (B) via a design incorporating the year and protection factor (year as a fixed factor with 2 modalities; protection as a fixed factor with three modalities; interaction protection * year) for the multivariate matrix (maximum size; basal diameter; number of branches) and each univariate matrix.

Variable	Factor	P-perm	Number of permutations
(A) Cerbère-Banyuls reserve Multivariate matrix			
	Protection	0.001***	999
	Year	0.003***	999
	Protection * year	0.022*	999
(A) Cerbère-Banyuls reserve Univariate			
Maximum height	Protection	0.001***	998
	Year	0.001***	997
	Protection * year	0.001***	997
Basal diameter	Protection	0.945	999
	Year	0.704	997
	Protection * year	0.883	998
Number of branches	Protection	0.001***	998
	Year	0.001***	997
	Protection * year	0.001***	999
(B) Calanques national park Multivariate matrix	Protection	0.287	338
	Year	0.001***	998
	Protection * year	0.001***	999
(B) Calanques national park Univariate			
Maximum height	Protection	0.001**	997
	Year	0.001**	998
	protection * year	0.001***	999
Basal diameter	Protection	0.051	336
	year	0.01*	999
	Protection * year	0.038*	995
Number of branches	Protection	0.001***	339
	Year	0.001***	998
	Protection * year	0.001***	999

*Significance: P ≤ 0.1; *P ≤ 0.05; **P ≤ 0.01; ***P ≤ 0.001. P-values were obtained using 999 residuals permutations under a reduced model.*

(Van de Water et al., 2018). Castelvieil (CAS) observed a still different dynamic. A decrease in the maximum size was observed between 2013 and 2019 (36.62 ± 21.4–29.05 ± 14.37 mm) and in the number of branches (5.7 in 2013; 2.85 in 2019). These results reflect a mechanical destruction that was also detected by image analysis. This illustrates the effectiveness of the photogrammetric monitoring method to detect one-off events.

In the Cerbère-Banyuls Reserve

Concerning Cerbère-Banyuls reserve, descriptors differed from 2012 to 2020, illustrating a global natural growth of colonies. Moreover, a strong protection effect is present whatever the year, suggesting conservation measures maintain its efficiency to protect red coral.

We have highlighted a significant difference between protection levels: there is a significant effect of the protection status on maximum height and number of branches. We have also highlighted a significant effect of the interaction between year and protection status for the number of branches and maximum height, which reveals that between 2012 and 2020 the gap widens between populations from different protection statuses and in particular between partial and full reserve.

Thus, the forty years of protection carried out by the Cerbère-Banyuls reserve have significantly influenced the populations of red coral. The colonies within the full reserve are larger and more tree-like than those located in the partial reserve and outside the reserve (where both professional fishing and recreational diving are allowed). In fact, a maximum size gradient is observed according to the protection gradient: it has been observed that the maximum size is significantly greater in the full reserve, decreases in the partial reserve and was even smaller outside the reserve.

Given the current state of populations within the reserve, it seems conservation measures set by the Cerbère-Banyuls reserve such as limited use, security and guarding measures show efficiency. This is consistent with the conclusions of many authors who highlight the effectiveness of strengthened measures such as no-take zones for marine ecosystems conservation (Sala et al., 2018; Zupan et al., 2018). Our results are thus arguments encouraging perpetuating or even strengthening these measures. In addition, it should be reminded that deep populations may be able to constitute a genetic refuge for populations (Priori et al., 2013; Cannas et al., 2016) and therefore could also be the subject of conservatory measures.

Comparison Between Calanques National Park and Cerbère-Banyuls Reserve

Thus, our results are consistent with the conclusions of many authors who emphasize the effectiveness of enhanced measures such as no-take zones for the conservation of marine ecosystems (Sala et al., 2018; Zupan et al., 2018). The old CB reserve still show efficiency to conserve its red coral populations, and a 5-year step allowed the appearance of a reserve effect in the recently settled Calanques national park. Our study sets a comparative data baseline and thus makes it possible to follow the dynamics of red coral which is essential: understanding the life cycle of long-lived species subjected to both exploitation and natural disturbances is an essential prerequisite for conservation (Garrabou and Harmelin, 2002).

Implications for Red Coral Conservation Across the Mediterranean

Red coral is endemic to the Mediterranean but subject to various regulations depending on the area considered, which can sometimes be a source of conflict (Cau et al., 2013; Bruckner, 2014; Cannas et al., 2016; Cattaneo-Vietti et al., 2016). It appears to be a need for harmonization of management practices at the species range level because public authorities do not seem to follow: in 2020, red coral was still not listed under the CITES (Convention on International Trade in Endangered Species of Wild Fauna and Flora).

Achieving red coral conservation and broadly coralligenous habitats in the Mediterranean needs an adaptation of managers to local needs for conservation at the range scale (Giakoumi et al., 2013; Vassallo et al., 2018). Enhanced protection measures

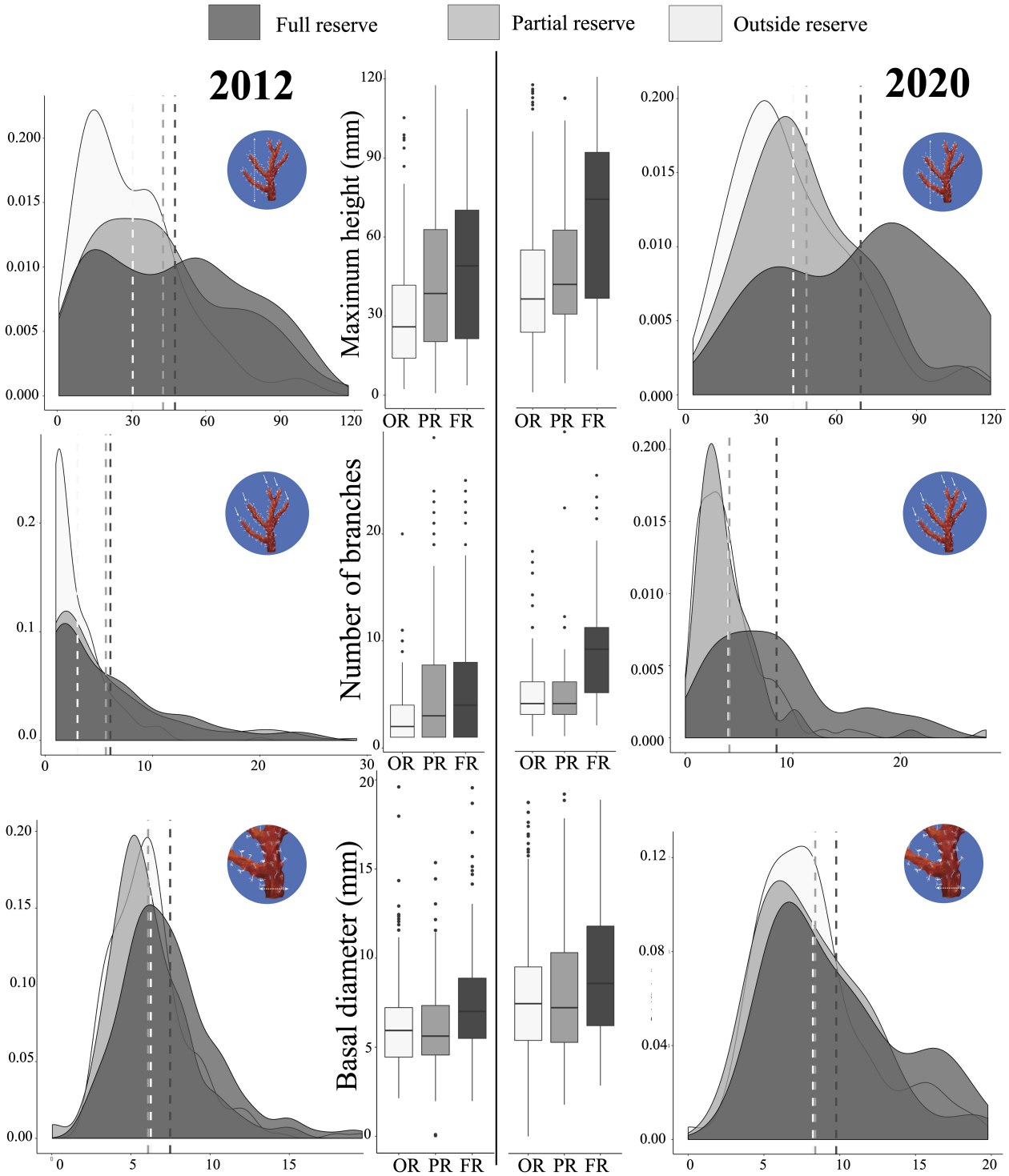

FIGURE 8 | For Cerbère-Banyuls Reserve, representation of probability density functions and Tuckey boxplots by protection levels for each year for the variables (i) Maximum height (mm), (ii) Number of branches, and (iii) Basal diameter (mm). Sites outside reserve (in clear), in partial reserve (in medium gray), in full reserve (in dark). On density functions, mean are shown in a dotted line; Boxplots indicate the median (bold line near the center), the first and third quartile (the box), the extreme values where distance from the box is at most 1.5 times the inter-quartile range (whiskers), and remaining outliers (dark circles).

such as no-take zones and full reserves have been demonstrated to be the most effective in protecting marine biodiversity and new initiatives need to be taken (Casale et al., 2018; Sala et al., 2018). However only 0.04% of the Mediterranean Sea is affected by such measures to date (PISCO., 2016). Investigating the socio-economic impacts of management measures and governance perception by users appears to be a good way to better understand the territory in order to manage it. Finally, such work could provide a global vision of both management and conservation of red coral in the Mediterranean and act in favor of the species and its habitat (Costantini and Abbiati, 2016).

Facing Global Changes

Connectivity

Aurelle et al. (2011) showed that the genetic structures of red coral populations corresponded to the habitat gaps available between Marseille and Catalonia as well as in the Adriatic. This highlights the need of reinforced conservation measures across the range. Some authors emphasize the need to include the conservation of genetic variation and population structure as one of the goals of red coral management (Santangelo et al., 2012; Cattaneo-Vietti et al., 2016) while others recall its functionality within the coralligenous (Ballesteros, 2006). This

TABLE 5 | Pair-Wise test result corresponding to the interaction between year and protection for the 3 descriptors.

Area	Variable	Year	Protection modality	Pairwise *p*_value
Cerbère-Banyuls reserve	*Multivariate matrix*	**2012**	PR vs. OR	0.001***
			PR vs. FR	0.23
			OR vs. FR	0.013 **
		2020	PR vs. OR	0.029
			PR vs. FR	0.012 **
			OR vs. FR	0.001***
Cerbère-Banyuls reserve	*Number of branches*	**2012**	PR vs. OR	0.206
			PR vs. FR	0.667
			OR vs. FR	0.06*
		2020	PR vs. OR	0.222
			PR vs. FR	0.364
			OR vs. FR	0.001***
	Maximum height	**2012**	PR vs. OR	0.001***
			PR vs. FR	0.07
			OR vs. FR	0.001***
		2020	PR vs. OR	0.001***
			PR vs. FR	0.001***
			OR vs. FR	0.001 ***
Calanques national park	Multivariate matrix	2013	PR vs. OR	0.274
			PR vs. FR	0.002***
			OR vs. FR	0.002***
		2019	PR vs. OR	0.032**
			PR vs. FR	0.001***
			OR vs. FR	0.001***
Calanques national park	Maximum height	2013	PR vs. OR	0.8
			PR vs. FR	0.535
			OR vs. FR	0.467
		2019	PR vs. OR	0.032**
			PR vs. FR	0.001***
			OR vs. FR	0.01**
	Basal diameter	2013	PR vs. OR	0.923
			PR vs. FR	0.043*
			OR vs. FR	0.035*
		2019	PR vs. OR	0.008***
			PR vs. FR	0.288
			OR vs. FR	0.25
	Number of branches	2013	PR vs. OR	0.002***
			PR vs. FR	0.011**
			OR vs. FR	0.649
		2019	PR vs. OR	0.001***
			PR vs. FR	0.002***
			OR vs. FR	0.001***

*Pairwise comparisons of the 3 modalities of the protection factor (FR, Full Reserve; PR, Partial Reserve; OR, Outside Reserve) for each modality of the year factor (2012 and 2020 for Cerbère-Banyuls reserve, 2013 and 2019 for Calanques NP). Significance: P ≤ 0.1; *P ≤ 0.05; **P ≤ 0.01; ***P ≤ 0.001. P-values were obtained using 999 residuals permutations under a reduced model. The multivariate matrix includes the 3 morphometrics (Basal diameter, Number of branches and Maximum height).*

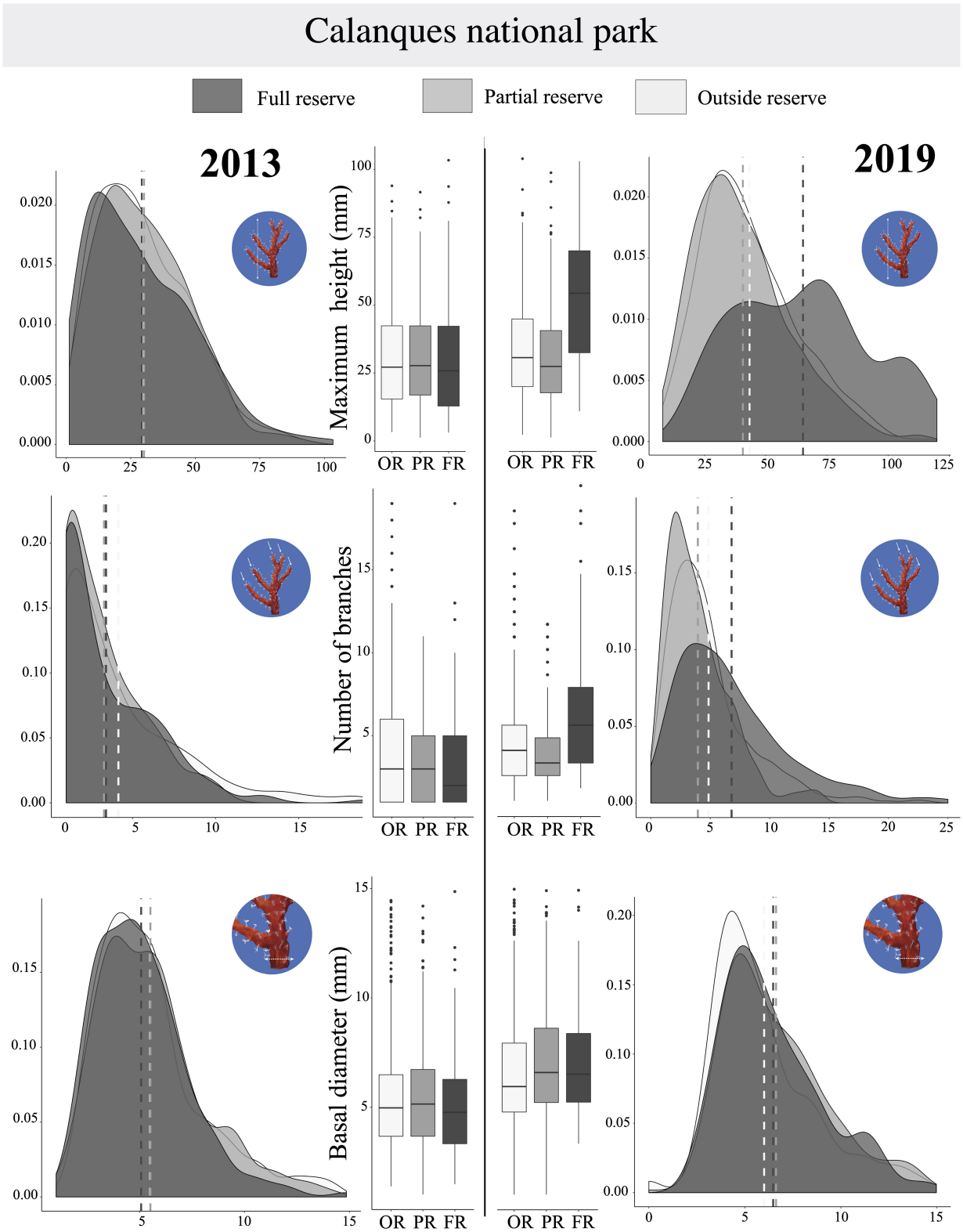

FIGURE 9 | For Calanques National Park, representation of probability density functions and Tuckey boxplots by protection levels for each year for the variables (i) Maximum height (mm), (ii) Number of branches, and (iii) Basal diameter (mm). Sites outside reserve (in clear), in partial reserve (in medium gray), in full reserve (in dark). On density functions, mean are shown in a dotted line; Boxplots indicate the median (bold line near the center), the first and third quartile (the box), the extreme values where distance from the box is at most 1.5 times the inter-quartile range (whiskers), and remaining outliers (dark circles).

induces the need to take local initiatives to conserve the species and in particular shallow perennial populations such as those of Cerbère-Banyuls and Calanques national park when global warming and extreme climatic events are a growing threat in the face of thermo-tolerance of 25°C (Torrents, 2007).

Extreme Climatic Events

Our study populations are located at the edge of the range of the French Mediterranean, in areas whose hydrogeographic conditions explain why they are the least impacted by massive mortality episodes due to extreme weather events (Bally and Garrabou, 2007; Garcia-Rubies et al., 2009; Calvo et al., 2011; Crisci et al., 2011).

Climate Change

However, the evolving risk minimization strategy (Stearns, 1992; Bramanti et al., 2005; Torrents, 2007; Linares et al., 2010; Torrents and Garrabou, 2011) that red coral seems to follow is adapted to species in habitats where environmental conditions are stable but could pose serious challenges for the conservation of shallow populations in the current context of climate change (Linares et al., 2013). It could therefore be interesting to study population genetics by comparing Calanques national park and Cerbère-Banyuls populations to understand their resilience to future disruptions such as the introduction of invasive species, major climate events similar to those of 1999 or 2003 and more broadly global climate change.

However, if shallow populations are the most resistant due to their exposure to significant seasonal variations in temperature (Ledoux et al., 2010; Haguenauer et al., 2013), deep populations might be able to repopulate shallower ones (Bongaerts et al., 2017), reflecting the importance of implementing conservation measures for the latter. Thus, global strategies appear capital while defining management measures at the local level, particularly through MPA managers networking (e.g., MedPAN). This highlights a real need for a monitoring network for vulnerable ecosystems (Danovaro et al., 2017; Montero-Serra et al., 2018) and more, the need to involve MPA managers and stakeholders in conservation and not only surveillance. Subsequently, an interest could be focused on implementing measures to restore populations in the Mediterranean (Aurelle et al., 2011; Montero-Serra et al., 2018).

Perspectives

In the present study, photogrammetry tools were used at the scale of the quadrats. However, it might be interesting to think about the scale of the underwater landscape. Seascape as indeed been proven to be an adequate study scale to better understand marine life mechanisms (Cuadros et al., 2017; Smeltz et al., 2019). In this context, modeling *via* photogrammetry can provide information on species coverage and in particular the spatial dynamics of sessile species over time (Burns et al., 2015; Casella et al., 2017; Ferrari et al., 2017a,b). Indeed, if the image processing takes longer than for a study using photoquadrats, the information that can be extracted from them is unprecedented. During a study using photoquadrats, biases may appear, especially if the field operator is different between the field campaigns: the exact location of the sites can be tricky. This study allows to minor human bias in comparison to *in situ* study: site localization might not be easy in turbid waters context such as in Cerbère-Banyuls.

Representing a site at the scale of the seascape helps limit these bias. 3D modeling of seascapes allows to locate the distribution of red coral patches on a landscape scale and thus realize their position within the coralligenous habitat: overhanging rocks. Modeling can make it possible to take account of changes in the distribution of fixed fauna and it could be interesting to develop these tools for the conservation of red coral populations in MPAs. These tools might give better insight of population dynamics of sessile organisms throughout time (Burns et al., 2015; Ferrari et al., 2016, 2017b). Besides, the use of photogrammetry still lacks to study coralligenous habitats and particularly relations between coralligenous 3D structure and its associated vagile fauna and communities.

CONCLUSION

Finally, our results underlined once more the need to engage conservation efforts in the Mediterranean to conserve sessile fauna. All of these data highlighted the effectiveness of MPAs and the real need to structure a monitoring network for these vulnerable ecosystems (Danovaro et al., 2017; Montero-Serra et al., 2018) and in particular of these populations of indicator species. In this sense, initiatives exist to use coralligenous species (gorgonians, corals) as indicators. Such indicators are the subject of current discussions within the framework of the European framework directives and it is desirable that these consultations lead to the long-term support and sustainability of such large-scale spatial surveillance networks. With this long-term objective, we highlighted in our study the usefulness of photogrammetry and 3D metrics as efficient and cost-effective methods allowing large-scale and long term monitoring based on reliable tools.

DATA AVAILABILITY STATEMENT

The raw data supporting the conclusions of this article will be made available by the authors, without undue reservation.

AUTHOR CONTRIBUTIONS

AC, PD, and OB designed the experiments. AC and OB managed the funding acquisition and performed the field work. JR and AC compiled and analyzed output data and designed and wrote the first version of the manuscript. JR, AC, and PD prepared the revised version of the manuscript. All authors discussed the results and implications and commented on the manuscript at all stages and contributed extensively to the work presented in this manuscript.

FUNDING

This study was funded within the framework of the long term monitoring program of both MPAs: In the Calanques of Marseilles by the Calanques National Park and in the Cerbère-Banyuls Natural Marine Reserve by the Conseil Départemental des Pyrénées Orientales and the Parc Naturel Marin du Golfe du Lion (OFB).

ACKNOWLEDGMENTS

The authors thank the numerous collaborators that contributed to the research on red coral ecology. The authors are also grateful to AF and KP for reviewing the manuscript.

SUPPLEMENTARY MATERIAL

The Supplementary Material for this article can be found online at: https://www.frontiersin.org/articles/10.3389/fmars.2021.639334/full#supplementary-material

REFERENCES

Anderson, M. J. (2001). Permutation tests for univariate or multivariate analysis of variance and regression. *Can. J. Fish. Aquat. Sci.* 58, 626–639. doi: 10.1139/f01-004

Anderson, M. J., Gorley, R. N., and Clarke, K. R. (2008). *PERMANOVA+ for PRIMER: Guide to software and statistical methods*. Plymouth: Primer-E, 214.

Aurelle, D., Ledoux, J.-B., Rocher, C., Borsa, P., Chenuil, A., and Féral, J.-P. (2011). Phylogeography of the red coral (*Corallium rubrum*): inferences on the evolutionary history of a temperate gorgonian. *Genetica* 139:855. doi: 10.1007/s10709-011-9589-6

Ballesteros, E. (2006). Mediterranean coralligenous assemblages: a synthesis of present knowledge (PhD Thesis). thesis of present knowledge. *Oceanogr. Mar. Biol.* 44, 123–195. doi: 10.1201/9781420006391.ch4

Bally, M., and Garrabou, J. (2007). Thermodependent bacterial pathogens and mass mortalities in temperate benthic communities: a new case of emerging disease linked to climate change. *Glob. Change Biol.* 13, 2078–2088. doi: 10.1111/j.1365-2486.2007.01423.x

Bongaerts, P., Riginos, C., Brunner, R., Englebert, N., Smith, S. R., and Hoegh-Guldberg, O. (2017). Deep reefs are not universal refuges: reseeding potential varies among coral species. *Sci. Adv.* 3:e1602373. doi: 10.1126/sciadv.1602373

Bonhomme, P., Berman, L., Le Direach, L., Bianchimani, O., Rouanet, E., Bonhomme, D., et al. (2015). *Réalisation de l'état zéro des zones de non-prélèvement du Parc national des Calanques - Année 2013-2014*. Marseille: GIS Posidonie Publisher.

Bramanti, L., Magagnini, G., De Maio, L., and Santangelo, G. (2005). Recruitment, early survival and growth of the Mediterranean red coral *Corallium rubrum* (L 1758), a 4-year study. *J. Exp. Mar. Biol. Ecol.* 314, 69–78. doi: 10.1016/j.jembe.2004.08.029

Bramanti, L., Movilla, J., Guron, M., Calvo, E., Gori, A., Dominguez-Carrió, C., et al. (2013). Detrimental effects of ocean acidification on the economically important Mediterranean red coral (*Corallium rubrum*). *Glob. Change Biol.* 19, 1897–1908. doi: 10.1111/gcb.12171

Bruckner, A. (2014). Advances in management of precious corals in the family Corallidae: are new measures adequate? *Curr. Opin. Environ. Sustain.* 7, 1–8. doi: 10.1016/j.cosust.2013.11.024

Bruckner, A. W. (2009). Rate and extent of decline in Corallium (pink and red coral) populations: existing data meet the requirements for a CITES Appendix II listing. *Mar. Ecol. Prog. Ser.* 397, 319–332. doi: 10.3354/meps08110

Burns, J., and Delparte, D. (2017). Comparison of commercial structure-from-motion photogrammety software used for underwater three-dimensional modeling of coral reef environments. *Int. Arch. Photogramm. Remote Sens. Spat. Inf. Sci.* 42:127. doi: 10.5194/isprs-archives-xlii-2-w3-127-2017

Burns, J., Delparte, D., Gates, R., and Takabayashi, M. (2015). Integrating structure-from-motion photogrammetry with geospatial software as a novel technique for quantifying 3D ecological characteristics of coral reefs. *PeerJ* 3:e1077. doi: 10.7717/peerj.1077

Bythell, J., Pan, P., and Lee, J. (2001). Three-dimensional morphometric measurements of reef corals using underwater photogrammetry techniques. *Coral Reefs* 20, 193–199. doi: 10.1007/s003380100157

Calvo, E., Simó, R., Coma, R., Ribes, M., Pascual, J., Sabatés, A., et al. (2011). Effects of climate change on Mediterranean marine ecosystems: the case of the Catalan Sea. *Clim. Res.* 50, 1–29. doi: 10.3354/cr01040

Cannas, R., Sacco, F., Cau, A, Cuccu, D., Follesa, M. C., and Cau, A. (2016). Genetic monitoring of deep-water exploited banks of the precious Sardinia coral *Corallium rubrum* (L., 1758): useful data for a sustainable management. *Aquat. Conserv. Mar. Freshw. Ecosyst.* 26, 236–250. doi: 10.1002/aqc.2522

Casale, P., Broderick, A. C., Camiñas, J. A., Cardona, L., Carreras, C., Demetropoulos, A., et al. (2018). Mediterranean sea turtles: current knowledge and priorities for conservation and research. *Endanger. Species Res.* 36, 229–267. doi: 10.3354/esr00901

Casella, E., Collin, A., Harris, D., Ferse, S., Bejarano, S., Parravicini, V., et al. (2017). Mapping coral reefs using consumer-grade drones and structure from motion photogrammetry techniques. *Coral Reefs* 36, 269–275. doi: 10.1007/s00338-016-1522-0

Cattaneo-Vietti, R., Bo, M., Cannas, R., Cau, A., Follesa, C., Meliadò, E., et al. (2016). An overexploited Italian treasure: past and present distribution and exploitation of the precious red coral *Corallium rubrum* (L., 1758) (Cnidaria: Anthozoa). *Ital. J. Zool.* 83, 443–455. doi: 10.1080/11250003.2016.1255788

Cau, A., Cannas, R., Sacco, F., and Follesca, M. (2013). *Adaptive management plan for red coral (Corallium rubrum) in the GFCM competence area*. Rome: FAO.

Clarke, K., and Gorley, R. (2006). *Primer*. Plymouth: Primer-E.

Clarke, K. R., Gorley, R. N., Somerfield, P. J., and Warwick, R. M. (2014). *Change in marine communities: an approach to statistical analysis and interpretation*. Plymouth: Primer-E Ltd.

Costantini, F., and Abbiati, M. (2016). Into the depth of population genetics: pattern of structuring in mesophotic red coral populations. *Coral Reefs* 35, 39–52. doi: 10.1007/s00338-015-1344-5

Crisci, C., Bensoussan, N., Romano, J.-C., and Garrabou, J. (2011). Temperature anomalies and mortality events in marine communities: insights on factors behind differential mortality impacts in the NW Mediterranean. PL*oS One* 6:e23814. doi: 10.1371/journal.pone.002381

Cuadros, A., Moranta, J., Cardona, L., Thiriet, P., Pastor, J., Arroyo, N. L., et al. (2017). Seascape attributes, at different spatial scales, determine settlement and post-settlement of juvenile fish. *Estuar. Coast. Shelf Sci.* 185, 120–129. doi: 10.1016/j.ecss.2016.12.014

Danovaro, R., Aguzzi, J., Fanelli, E., Billett, D., Gjerde, K., Jamieson, A., et al. (2017). An ecosystem-based deep-ocean strategy. *Science* 355, 452–454. doi: 10.1126/science.aah7178

Drap, P., Merad, D., Mahiddine, A., Seinturier, J., Gerenton, P., Peloso, D., et al. (2014). In situ underwater measurements of red coral: non-intrusive approach based on coded targets and photogrammetry. *Int. J. Herit. Digit. Era* 3, 123–139. doi: 10.1260/2047-4970.3.1.123

Drap, P., Merad, D., Mahiddine, A., Seinturier, J., Gerenton, P., Peloso, D., et al. (2013a). "Automating the measurement of red coral in situ using underwater photogrammetry and coded targets," in *Proceedings of the XXIV International CIPA Symposium*, Strasbourg, France.

Drap, P., Merad, D., Seinturier, J., Mahiddine, A., Peloso, D., Boï, J.-M., et al. (2013b). Underwater programmetry for archaeology and marine biology: 40 years of experience in Marseille, France, in *Proceedings of the Digital Heritage International Congress (DigitalHeritage)*, (France: IEEE), 97–104.

Ferrari, R., Figueira, W. F., Pratchett, M. S., Boube, T., Adam, A., Kobelkowsky-Vidrio, T., et al. (2017a). 3D photogrammetry quantifies growth and external erosion of individual coral colonies and skeletons. *Sci. Rep.* 7:16737.

Ferrari, R., Malcolm, H. A., Byrne, M., Friedman, A., Williams, S. B., Schultz, A., et al. (2017b). Habitat structural complexity metrics improve predictions of fish abundance and distribution. *Ecography* 41, 1077–1091 doi: 10.1111/ecog.02580

Ferrari, R., McKinnon, D., He, H., Smith, R. N., Corke, P., González-Rivero, M., et al. (2016). Quantifying Multiscale Habitat Structural Complexity: A Cost-Effective Framework for Underwater 3D Modelling. *Remote Sens.* 8:113. doi: 10.3390/rs8020113

Flemming, N. C. (1972). Relative chronology of submerged Pleistocene marine erosion features in the western Mediterranean. *J. Geol.* 80, 633–662. doi: 10.1086/627793

Garcia-Rubies, A., Mateo, M. A., Hereu, B., Coma, R., Teixidó, T., Garrabou, Q., et al. (2009). "Preliminary assessment of the impact of an extreme storm on Catalan Mediterranean shallow benthic communities," in *Poster at the 11th Plinius Conference on Mediterranean Storms*, Barcelona.

Garrabou, J., and Harmelin, J.-G. (2002). A 20-year study on life-history traits of a harvested long-lived temperate coral in the NW Mediterranean: insights into conservation and management needs. *J. Anim. Ecol.* 71, 966–978. doi: 10.1046/j.1365-2656.2002.00661.x

Garrabou, J., Perez, T., Sartoretto, S., and Harmelin, J. G. (2001). Mass mortality event in red coral *Corallium rubrum* populations in the Provence region (France, NW Mediterranean). *Mar. Ecol. Prog. Ser.* 217, 263–272. doi: 10.3354/meps217263

Giakoumi, S., Sini, M., Gerovasileiou, V., Mazor, T., Beher, J., Possingham, H. P., et al. (2013). Ecoregion-Based Conservation Planning in the Mediterranean: Dealing with Large-Scale Heterogeneity. *PLoS One* 8:e76449. doi: 10.1371/journal.pone.0076449

Gibson, R., Atkinson, R., and Gordon, J. (2006). Mediterranean coralligenous assemblages: a synthesis of present knowledge. *Oceanogr. Mar. Biol. Annu. Rev.* 44, 123–195.

Goff, C. L., Tambutté, E., Venn, A. A., Techer, N., Allemand, D., and Tambutté, S. (2017). *In vivo* pH measurement at the site of calcification in an octocoral. *Sci. Rep.* 7:11210. doi: 10.1038/s41598-017-10348-4

Haguenauer, A., Zuberer, F., Ledoux, J.-B., and Aurelle, D. (2013). Adaptive abilities of the Mediterranean red coral *Corallium rubrum* in a heterogeneous and changing environment: from population to functional genetics. *J. Exp. Mar. Biol. Ecol.* 449, 349–357. doi: 10.1016/j.jembe.2013.10.010

Ledoux, J.-B., Garrabou, J., Bianchimani, O., Drap, P., Féral, J.-P., and Aurelle, D. (2010). Fine-scale genetic structure and inferences on population biology in the threatened Mediterranean red coral, *Corallium rubrum*. *Mol. Ecol.* 19, 4204–4216 doi: 10.1111/j.1365-294x.2010.04814.x

Lester, S. E., Halpern, B. S., Grorud-Colvert, K., Lubchenco, J., Ruttenberg, B. I., Gaines, S. D., et al. (2009). Biological effects within no-take marine reserves: a global synthesis. *Mar. Ecol. Prog. Ser.* 384, 33–46. doi: 10.3354/meps08029

Linares, C., Bianchimani, O., Torrents, O., Marschal, C., Drap, P., and Garrabou, J. (2010). Marine Protected Areas and the conservation of long-lived marine invertebrates: the Mediterranean red coral. *Mar. Ecol. Prog. Ser.* 402, 69–79. doi: 10.3354/meps08436

Linares, C., Cebrian, E., Kipson, S., and Garrabou, J. (2013). Does thermal history influence the tolerance of temperate gorgonians to future warming? *Mar. Environ. Res.* 89, 45–52. doi: 10.1016/j.marenvres.2013.04.009

Linares, C., Garrabou, J., Hereu, B., Diaz, D., Marschal, C., Sala, E., et al. (2012).Assessing the Effectiveness of Marine Reserves on Unsustainably Harvested Long−Lived Sessile Invertebrates. *Conserv. Biol.* 26, 88–96. doi: 10.1111/j.1523-1739.2011.01795.x

Linnaeus, C. (1758). *Systema naturae*. Stockholm: Laurentius Salvius.

Lo Basso, L., and Raveux, O. (2018). *Introduction. Le Corail, un Kaléidoscope Pour L'étude de la Méditerranée Dans le Temps Long. Rives Méditérannéennes* 7–15. doi: 10.4000/rives.5566

Ludvigsen, M., Eustice, R., and Singh, H. (2006). Photogrammetric models for marine archaeology. *Paper Presented at the OCEANS 2006, IEEE*, Boston, MA.

Marschal, C., Garrabou, J., Harmelin, J., and Pichon, M. (2004). A new method for measuring growth and age in the precious red coral *Corallium rubrum* (L.). *Coral Reefs* 23, 423–432. doi: 10.1007/s00338-004-0398-6

Millot, C., and Wald, L. (1980). *The effect of Mistral wind on the Ligurian current near Provence*. Amsterdam: Elsevier.

Montero-Serra, I., Garrabou, J., Doak, D. F., Figuerola, L., Hereu, B., Ledoux, J.-B., et al. (2018). Accounting for life-history strategies and timescales in marine restoration. *Conserv. Lett.* 11:e12341. doi: 10.1111/conl.12341

Perez, T., Garrabou, J., Sartoretto, S., Harmelin, J., Francour, P., and Vacelet, J. (2000). Massive mortality of marine invertebrates: an unprecedented event in northwestern Mediterranean. *C. R. Acad. Sci. III* 323, 853–865.

PISCO. (2016). *La Science des aires marines protégées (3ème édition, Méditerranée)*. France: University of Nice Sophia Antipolis.

Priori, C., Mastascusa, V., Erra, F., Angiolillo, M., Canese, S., and Santangelo, G. (2013). Demography of deep-dwelling red coral populations: age and reproductive structure of a highly valued marine species. *Estuar. Coast. Shelf Sci.* 118, 43–49. doi: 10.1016/j.ecss.2012.12.011

R Core Team (2017). *R: A Language and Environment for Statistical Computing*. Vienna: R Foundation for Statistical Computing.

Royer, J.-P., Nawaf, M., Merad, D., Saccone, M., Bianchimani, O., Garrabou, J., et al. (2018). Photogrammetric Surveys and Geometric Processes to Analyse and Monitor Red Coral Colonies. *J. Mar. Sci. Eng.* 6:42. doi: 10.3390/jmse6020042

Sala, E., Lubchenco, J., Grorud-Colvert, K., Novelli, C., Roberts, C., and Sumaila, R. (2018). Assessing real progress towards effective ocean protection. *Mar. Policy* 91, 11–13. doi: 10.1016/j.marpol.2018.02.004

Santangelo, G., Abbiati, M., Giannini, F., and Cicogna, F. (1993). Red coral fishing trends in the western Mediterranean Sea during the period 1981-1991. *Sci. Mar.* 57, 139–143.

Santangelo, G., Cupido, R., Cocito, S., Bramanti, L., Tsounis, G., and Iannelli, M. (2012). "Demography of long-lived octocorals: survival and local extinction," in *Proceedings of the 12th International Coral Reef Symposium*, Cairns, 9–13.

Smeltz, T. S., Harris, B. P., Olson, J. V., and Sethi, S. A. (2019). A seascape-scale habitat model to support management of fishing impacts on benthic ecosystems. *Can. J. Fish. Aquat. Sci.* 76, 1836–1844. doi: 10.1139/cjfas-2018-0243

Stearns, S. C. (1992). *The evolution of life histories*. Oxford: Oxford University Press.

Torrents, O. (2007). *Biologie des populations du corail rouge Corallium rubrum (L. 1758) de Méditerranée nord-occidentale*. PhD Thesis. Marseille: Université de la Méditerraneé Aix-Marseille II.

Torrents, O., and Garrabou, J. (2011). Fecundity of red coral *Corallium rubrum* (L.) populations inhabiting in contrasting environmental conditions in the NW Mediterranean. *Mar. Biol.* 158, 1019–1028. doi: 10.1007/s00227-011-1627-5

Tsounis, G., Rossi, S., Gili, J.-M., and Arntz, W. (2006). Population structure of an exploited benthic cnidarian: the case study of red coral (*Corallium rubrum* L.). *Mar. Biol.* 149, 1059–1070. doi: 10.1007/s00227-006-0302-8

Underwood, A. (1992). Beyond BACI: the detection of environmental impacts on populations in the real, but variable, world. *J. Exp. Mar. Biol. Ecol.* 161, 145–178. doi: 10.1016/0022-0981(92)90094-q

Underwood, A. (1981). Techniques of analysis of variance in experimental marine biology and ecology. *Oceanogr. Mar. Biol. Annu. Rev.* 19, 513–605.

Van de Water, J. A. J. M., Voolstra, C. R., Rottier, C., Cocito, S., Peirano, A., Allemand, D., et al. (2018). Seasonal Stability in the Microbiomes of Temperate Gorgonians and the Red Coral *Corallium rubrum* Across the Mediterranean Sea. *Microb. Ecol.* 75, 274–288. doi: 10.1007/s00248-017-1006-y

Vassallo, P., Bianchi, C. N., Paoli, C., Holon, F., Navone, A., Bavestrello, G., et al. (2018). A predictive approach to benthic marine habitat mapping: efficacy and management implications. *Mar. Pollut. Bull.* 131, 218–232. doi: 10.1016/j.marpolbul.2018.04.016

Vielzeuf, D., Garrabou, J., Gagnon, A., Ricolleau, A., Adkins, J., Günther, D., et al. (2013). Distribution of sulphur and magnesium in the red coral. *Chem. Geol.* 355, 13–27. doi: 10.1016/j.chemgeo.2013.07.008

Zapata-Ramírez, P. A., Scaradozzi, D., Sorbi, L., Palma, M., Pantaleo, U., Ponti, M., et al. (2013). Innovative study methods for the Mediterranean coralligenous habitats. *Adv. Oceanogr. Limnol.* 4, 102–119. doi: 10.4081/aiol.2013.5339

Zupan, M., Bulleri, F., Evans, J., Fraschetti, S., Guidetti, P., Garcia-Rubies, A., et al. (2018). How good is your marine protected area at curbing threats? *Biol. Conserv.* 221, 237–245. doi: 10.1016/j.biocon.2018.03.013

Conflict of Interest: The authors declare that the research was conducted in the absence of any commercial or financial relationships that could be construed as a potential conflict of interest.

Publisher's Note: All claims expressed in this article are solely those of the authors and do not necessarily represent those of their affiliated organizations, or those of the publisher, the editors and the reviewers. Any product that may be evaluated in this article, or claim that may be made by its manufacturer, is not guaranteed or endorsed by the publisher.

Advantages of publishing in Frontiers

OPEN ACCESS
Articles are free to read for greatest visibility and readership

FAST PUBLICATION
Around 90 days from submission to decision

HIGH QUALITY PEER-REVIEW
Rigorous, collaborative, and constructive peer-review

TRANSPARENT PEER-REVIEW
Editors and reviewers acknowledged by name on published articles

Frontiers
Avenue du Tribunal-Fédéral 34
1005 Lausanne | Switzerland

Visit us: www.frontiersin.org
Contact us: frontiersin.org/about/contact

REPRODUCIBILITY OF RESEARCH
Support open data and methods to enhance research reproducibility

DIGITAL PUBLISHING
Articles designed for optimal readership across devices

FOLLOW US
@frontiersin

IMPACT METRICS
Advanced article metrics track visibility across digital media

EXTENSIVE PROMOTION
Marketing and promotion of impactful research

LOOP RESEARCH NETWORK
Our network increases your article's readership